CÉLINE DUPUIS

Pétrologie et géochimie des provinces mésozoïques téthysiennes reliées à la zone de suture Yarlung Zangbo, Tibet

Thèse présentée
à la Faculté des études supérieures de l'Université Laval
dans le cadre du programme de doctorat interuniversitaire en sciences de la Terre
pour l'obtention du grade de PhilosophiæDoctor, (Ph.D.)

Faculté des sciences et de génie
UNIVERSITÉ LAVAL

Février 2005

Résumé

Dans une problématique de réinterprétation géodynamique de la zone de suture Yarlung Zangbo (ZSYZ) au sens large, la pétrographie, la chimie minérale et la lithogéochimie ont été effectuées sur des roches mafiques, ultramafiques et sédimentaires provenant de trois unités géologiques situées immédiatement au sud des ophiolites de la ZSYZ : le mélange ophiolitique crétacé précoce, le mélange de Yamdrock mésozoïque et le flysch triasique tardif. La majorité des roches mafiques du mélange ophiolitique montrent des caractéristiques géochimiques typiques d'un bassin d'arrière-arc, certaines d'un arc intra-océanique. De même, les roches ultramafiques possèdent des caractéristiques géochimiques qui suggèrent une origine dans un environnement de supra-subduction. Ces caractéristiques varient selon le taux de fusion partielle et le degré d'interaction magma-manteau enregistrés par les péridotites. Une analogie peut être faite avec des systèmes océaniques modernes de type arc-bassin. Le mélange ophiolitique résulte bien de la désagrégation des massifs ophiolitiques sus-jacents. Les roches mafiques du mélange de Yamdrock montrent une affinité géochimique avec le magmatisme intraplaque océanique (de type *OIB*). Les roches mafiques du flysch triasique montrent une signature géochimique *double* qui suggère qu'elles dérivent d'une même source magmatique intraplaque enrichie, mais qu'elles ont subi des processus d'assimilation et de cristallisation fractionnée (ACF). Cette contamination crustale continentale semble résulter de la dislocation de la Plaque Indienne lors de l'ouverture de l'Océan Néo-Téthys. Une analogie peut être faite avec le point chaud de la Réunion, dans l'Océan Indien, et les Trapps de Deccan, à l'ouest de l'Inde. Les roches sédimentaires de ces deux unités possèdent une signature géochimique qui concorde avec un environnement de déposition le long d'une marge passive et avec une source au niveau de la croûte continentale supérieure ancienne de l'Inde. Les blocs mafiques d'affinité intraplaque induiraient une contribution mafique et les batholites granitiques démembrés une contribution felsique à la source de ces turbidites. L'évolution paléozoïque du bassin néo-téthysien a ainsi été reconstituée en fonction de l'environnement tectonique défini pour chaque unité géologique associée à la ZSYZ.

Avant-propos

Je tiens tout d'abord à remercier mon directeur de thèse, le Dr Réjean Hébert, qui m'a donné la possibilité de travailler sur une problématique tibétaine et qui a su me guider et m'encourager tout au long de mes travaux de doctorat. Le projet de recherche dans cette région géographiquement, culturellement et politiquement isolée qu'est le Tibet a été possible grâce au support financier du CRSNG (subvention no 1253 au Dr R. Hébert) et à l'appui chinois du Dr C.S. Wang (Prix de Recherche Remarquable de Chine). Je tiens aussi à remercier personnellement le CRSNG et le FQRNT pour les bourses de doctorat octroyées. Je remercie Marc Choquette, du département de géologie et de génie géologique de l'Université Laval, pour les analyses à la microsonde électronique, R. Gosselin, de l'INRS-ETE Québec, et *Activation Laboratories Inc.* pour les analyses par *ICP-AES* et *ICP-MS*. Je suis reconnaissante envers Marc Richer La Flèche de ses discussions fructueuses sur l'interprétation des résultats et envers Thomas Feninger de ses révisions consciencieuses des manuscripts rédigés en anglais. Ces trois dernières années m'ont été très agréables grâce à la camaraderie et l'entraide des membres du département de géologie et de génie géologique, particulièrement les membres du Groupe GÉO (François Huot, Viviane Dubois-Côté, Carl Guilmette et autres étudiants de passage au PFÉ). Un merci tout particulier à ma famille et à Éric pour leur soutien continu, surtout en fin de parcours.

Pour les trois articles formant le corps de la thèse, les auteurs sont présentés par ordre d'importance de leur contribution. Je, C. Dupuis, suis donc l'auteure principale de ces trois articles, et les résultats qui y sont présentés découlent tous de mes travaux de recherche doctorale. Le deuxième auteur de chaque article est mon directeur de thèse, le Dr Réjean Hébert, qui a su me guider et m'encourager dans l'interprétation des résultats, la préparation et la rédaction de ces articles scientifiques. Les coauteurs suivants, Viviane Dubois-Côté et/ou Carl Guilmette du département de géologie et de génie géologique de l'Université Laval, sont des collègues étudiants à la maîtrise qui travaillent aussi sur la zone de suture Yarlung Zangbo. En plus de leur aide sur le terrain, les discussions constructives avec ces derniers m'ont été fort utiles dans l'interprétation de mes résultats. Enfin, la collaboration avec les coauteurs chinois était indispensable

au bon déroulement des campagnes de terrain au Tibet, une province de la R.P. de Chine dont l'accès aux étrangers est restreint. Le Dr. C.S. Wang, en tant que recteur de l'Université de Technologie de Chengdu, était notre contact diplomatique, alors que les géologues Y.L. Li et Z.J. Li nous ont accompagnés au Tibet lors des campagnes de 2001 et 2002, respectivement.

Le 1er article, intitulé *Petrology and Geochemistry of Mafic Rocks from Mélange and Flysch Units Adjacent to the Yarlung Zangbo Suture Zone, Southern Tibet*, a été soumis à la revue *Chemical Geology* le 25 juillet 2003 et accepté pour publication le 25 octobre 2004. Le 2e article, intitulé *The Yarlung Zangbo Suture Zone ophiolitic mélange (southern Tibet) : New insights from geochemistry of ultramafic rocks*, a été soumis à la revue *Journal of Asian Earth Sciences* le 6 mars 2004 et accepté pour publication le 12 septembre 2004. Le 3e article, intitulé *Geochemistry of sedimentary rocks from mélange and flysch units south of the Yarlung Zangbo Suture Zone, southern Tibet*, a été soumis à la revue *Journal of Asian Earth Sciences* le 20 octobre 2003 et accepté pour publication le 11er novembre 2004. Le contenu des articles incorporés à la thèse n'a pas été modifié, seules les sections décrivant le contexte géologique et les méthodes analytiques ont été supprimées pour éviter des répétitions trop fréquentes.

Table des matières

Liste des tableaux

Table des figures

Liste des acronymes

BABB = *back-arc basin basalt* (basalte de bassin d'arrière-arc)
CAB = *calk-alkaline basalt* (basalte calco-alcalin)
CAMB = *Chilean-type active margin basalt* (basalte de marge active de type chilien)
CB = *continental basalt* (basalte continental)
CC = *continental crust* (croûte continentale)
CFB = *continental flood basalt* (basalte de plateau continental)
CWPAB = *continental within-plate alkaline basalt* (basalte alcalin intraplaque continental)
DM = *depleted mantle* (manteau appauvri)
E-MORB = *MORB* enrichi
GLOSS = *global subductiong sediment* (sédiment subducté global)
HREE = *heavy rare Earth elements* (éléments des terres rares lourdes)
IAB = *intermediate arc basalt* (basalte d'arc intermédiaire)
IAT = *island-arc tholeiite* (tholéiite d'arc)
ICP-AES = *inductively-coupled plasma - atomic emission spectrometry* (ICP - spectrométrie d'émissions atomiques)
ICP-MS = *inductively-coupled plasma - mass spectrometry* (ICP - spectrométrie de masse)
LCC = *lower continental crust* (croûte continentale inférieure)
LREE = *light rare Earth elements* (éléments des terres rares légères)
MORB = *mid-ocean ridge baasalt* (basalte de dorsale médio-océanique)
N-MORB = *MORB* normal
OIAB = *ocean-island alkaline basalt* (basalte alcalin d'île océanique)
OIB = *ocean-island basalt* (basalte d'île océanique)
OIT = *ocean-island tholeiite* (tholéiite d'île océanique)
OPB = *oceanic plateau basalt* (basalte de plateau océanique)
OUC = *old upper crust* (croûte supérieure ancienne)
PM = *primitive mantle* (manteau primitif)
REE = *rare Earth elements* (éléments des terres rares)
SZB = *subduction-zone basalt* (basalte de zone de subduction)
TR = terres rares
UCC = *upper continental crust* (croûte continentale supérieure)

VAB = *volcanic-arc basalt* (basalte d'arc volcanique)
WPAB = *within-plate alkaline basalt* (basalte alcalin intraplaque)
WPB = *within-plate basalt* (basalte intraplaque)
WPT = *within-plate tholeiite* (tholéiite intraplaque)

Chapitre 1

Introduction

Le programme global du groupe GÉO (Genèse et Évolution des Ophiolites), supervisé par le Dr Réjean Hébert, traite des problèmes complémentaires de l'évolution de la lithosphère océanique moderne et des terrains océaniques anciens préservés le long de zones de suture sous forme d'ensembles de roches ultramafiques et mafiques, i.e. les ophiolites. La compréhension des terrains satellites à la formation et à la mise en place des ophiolites fait partie intégrante de ce programme de recherche. En ce sens, plusieurs projets de recherche complémentaires portant sur la chaîne ophiolitique et les unités voisines de la zone de suture Yarlung Zangbo (ZSYZ), dans le sud du Tibet, ont été achevés ces dernières années ou sont actuellement en cours. Ce projet particulier du groupe GÉO touche à plusieurs volets de la géologie, soit l'analyse pétrographique et géochimique des diverses roches mafiques, ultramafiques et sédimentaires des différentes unités, l'analyse structurale et métamorphique de ces unités, l'établissement d'un modèle géodynamique pouvant expliquer la mise en place des unités adjacentes aux ophiolites et la cartographie numérique tri-dimensionnelle de la région d'étude. Le présent projet de doctorat consiste principalement à caractériser les blocs ignés métamorphisés se trouvant au niveau du mélange ophiolitique et des provinces sédimentaires mésozoïques, situées au sud des massifs ophiolitiques, et d'établir leur contexte géodynamique par rapport à celui des ophiolites sensu stricto.

1.1 Problématique et objectifs

Le projet de doctorat s'inscrit dans une problématique de réinterprétation géodynamique du dispositif ZSYZ-arc de Gangdese, au Tibet. La chaîne ophiolitique de la ZSYZ avait

été partiellement cartographiée en 1980 et les principales conclusions indiquaient que cette chaîne représentait des fragments du bassin de la Néo-Téthys formés en contexte de dorsale en expansion (Nicolas et al., 1981 ; Xiao, 1984 ; Girardeau et al., 1984 ; 1985). Les résultats récents menés depuis 1998 suggèrent que l'histoire géologique soit beaucoup plus complexe. Actuellement, les fragments océaniques préservés sont réinterprétés à l'aide de la géochimie dans un contexte de supra-subduction (Hébert et al., 2000 ; 2001 ; 2003 ; Aitchison et al., 2000 ; Dubois-Côté et al., 2003 ; 2004) ; une hypothèse initialement proposée par Wu et Deng (1979) sur la base de la chimie des éléments majeurs. Ces complexes ophiolitiques et d'autres ensembles rocheux provenant du bassin océanique néo-téthysien ont été démembrés et incorporés dans des mélanges tectoniques et sédimentaires. Les blocs mafiques contenus dans ces mélanges, particulièrement ceux à matrice sédimentaire, sont présentement d'origine inconnue car hors contexte. Le présent projet de doctorat vise à caractériser ces blocs mafiques et ultramafiques, ainsi que les roches sédimentaires encaissantes, à proposer des sources pour ces roches et à établir un modèle géodynamique expliquant leur formation et leur incorporation aux mélanges d'âge mésozoïque.

Il est bon de noter que les travaux antérieurs portant sur le sujet sont peu nombreux ou difficilement accessibles car publiés en chinois. Le présent projet de doctorat vise donc aussi à informer la communauté scientifique internationale des phénomènes géologiques observés dans cette région isolée géographiquement, culturellement et politiquement du reste de la planète.

Plus précisément, la région d'étude est située dans la partie centrale de la ZSYZ, le long d'une section de plus de 250 km de long, entre Lhaze et Zedong (Figs. 1.1 and 1.2). Les trois unités géologiques principales à l'étude affleurent immédiatement au sud des massifs ophiolitiques. Elles sont, du nord au sud, le mélange ophiolitique du Crétacé précoce, le mélange de Yamdrock mésozoïque et le flysch triasique (Fig. 1.2). Des blocs mafiques et ultramafiques ont été échantillonnés dans le mélange ophiolitique, alors que des blocs mafiques et des roches sédimentaires encaissantes l'ont été dans les unités sédimentaires, i.e. le mélange de Yamdrock et le flysch triasique. Les analyses géochimiques ont montré que les roches mafiques et ultramafiques échantillonnées dans des zones cartographiées comme des *serpentinites* sont indifférenciables de celles provenant du mélange ophiolitique ; ces unités seront donc traitées comme faisant toutes partie du mélange ophiolitique. Il en va de même pour quelques fragments mafiques tirés du Conglomérat de Liuqu, lequel est intercalé aux mélanges. La provenance géographique et la nomenclature des roches échantillonnées sont données au Tab. A.1, les régions étant localisées sur la Fig. 1.2.

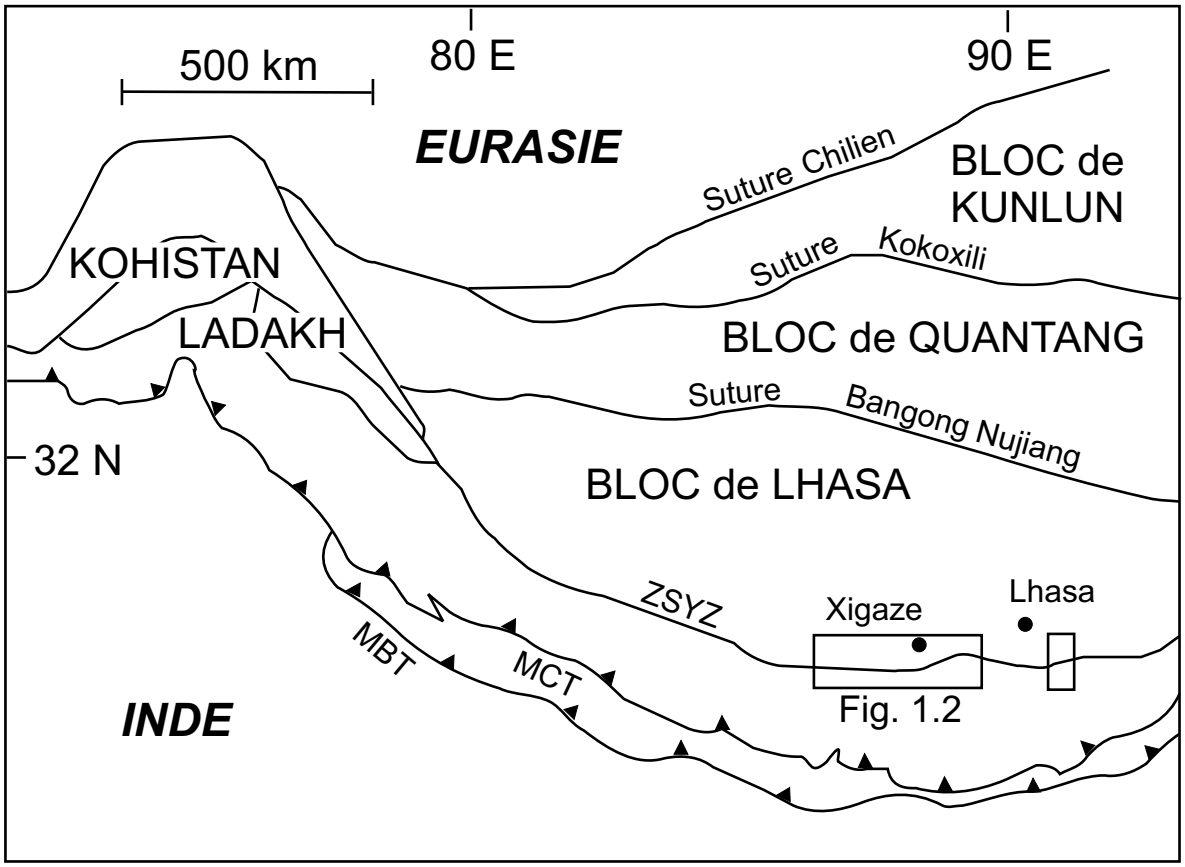

FIG. 1.1 – Carte tectonique schématisée de la chaîne himalayenne, du Plateau tibétain et des régions avoisinantes montrant les blocs crustaux et les zones de sutures (d'après Coulon et al., 1986). Les encadrés délimitent la région d'étude. MBT = *Main Boundary Thrust*, MCT = *Main Central Thrust*, ZSYZ = Zone de Suture Yarlung Zangbo.

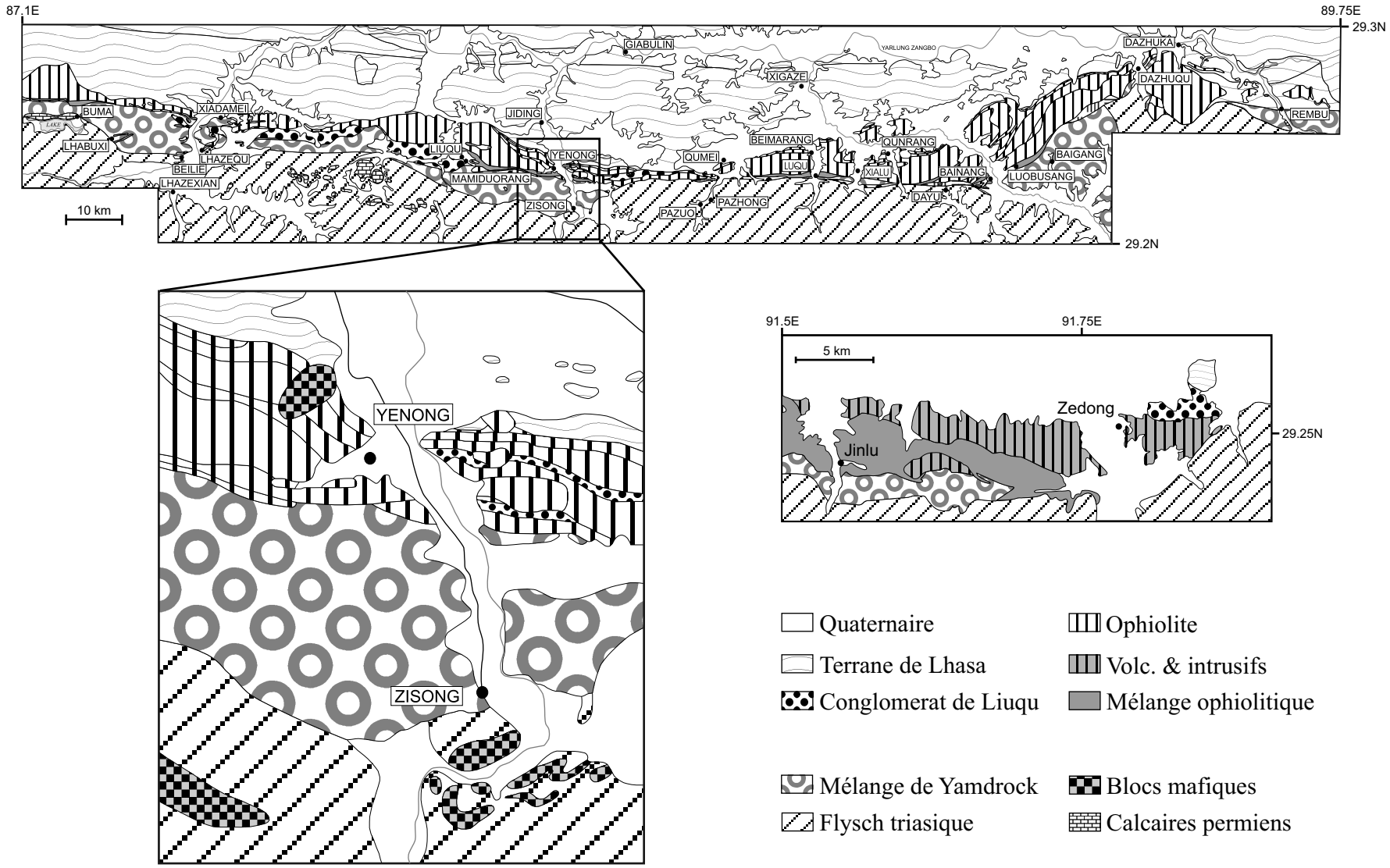

FIG. 1.2 – Carte géologique de la zone de suture du Yarlung Zangbo montrant les régions échantillonnées (d'après Wang et al., 1984). La région de Jiding/Zisong élargie présente toutes les unités qui ont été visitées pour les besoins du présent projet de doctorat. Une version grand format et en couleur sur laquelle tous les échantillons étudiés ont été localisés est jointe à la thèse (Fig. A.1).

Le projet de doctorat avait pour objectifs spécifiques de répondre aux interrogations suivantes :

1. Quelles sont les caractéristiques pétrologiques et géochimiques des blocs mafiques et ultramafiques provenant des unités de type *mélange* au sud des ophiolites de la ZSYZ ?
2. Quelles sont les caractéristiques géochimiques des roches sédimentaires encaissantes du mélange de Yamdrock et du flysch triasique ?
3. Quel est le modèle pétrogénétique le plus compatible avec les caractéristiques pétrologiques et géochimiques des blocs de chaque unité géologique et tient compte de la nature des sédiments encaissants ?
4. Comment les résultats de ces unités se comparent-ils entre-eux et aux séquences ophiolitiques sus-jacentes ?
5. Quel est le nouveau modèle géodynamique d'évolution du bassin néo-téthysien au Mésozoïque qui intègre les caractéristiques sédimentologiques, pétrologiques et géochimiques des ensembles étudiés, et quelles sont les implications pour la ZSYZ ?

Le terme *mélange* employé dans la présente thèse peut être défini au sens large comme un ensemble de terrains, d'origine tectonique ou sédimentaire, montrant, en grand désordre, des blocs de dimensions variées (du cm à plusieurs km) et de natures diverses (Foucault et Raoult, 2000). Bien que plusieurs classifications des mélanges existent (voir Raymond, 1984), les mélanges étudiés dans la thèse sont définis selon les critères de Pini (1999).

Dans le but de répondre à ces objectifs, la pétrographie, la chimie minérale et la lithogéochimie des roches mafiques, ultramafiques et sédimentaires provenant des différentes unités géologiques ont tout d'abord été effectuées, afin de déterminer la pétrogenèse et/ou la source de ces roches. Grâce à une série de diagrammes discriminants utilisant les résultats géochimiques obtenus, l'environnement tectonique de formation le plus compatible pour chaque unité a par la suite été déterminé. Les caractéristiques obtenues pour les trois unités à l'étude ont été comparées entre elles, ainsi que par rapport aux séquences ophiolitiques sus-jacentes, afin d'établir leurs similitudes et leurs divergences, et par le fait même leur signification pour la ZSYZ. Enfin, tous ces résultats ont été regroupés afin d'étendre la reconstruction de l'évolution géodynamique du bassin néo-téthysien tout au long du Mésozoïque.

1.2 Méthodologie

La cartographie et l'échantillonnage ont été effectués lors de deux campagnes de terrain d'une durée approximative de cinq semaines chacune, au début des étés 2001 et 2002, le long de la ZSYZ. Les roches mafiques et ultramafiques ont toutes subi un examen pétrographique détaillé au moyen de lames mines et d'un microscope polarisant. Les résultats sont présentés à l'annexe B.

La chimie minérale des roches mafiques et ultramafiques a été déterminée à l'aide de la microsonde électronique CAMECA SX-100 à cinq spectromètres de l'Université Laval. Les conditions analytiques étaient de 15 kV, 20 nA pour un temps de comptage de 20 s sur les pics et de 10 s sur le bruit de fond. Les standards de calibration utilisés étaient généralement des oxydes simples (*GEO Standard Block* de *P&H Developments*), ou des minéraux lorsque nécessaire (*Mineral Standard Mount MINM25-53* de *Astimex Scientific Limited* ; échantillons de référence provenant de Jarosewich et al., 1980). Les données ont été réduites suivant le modèle *PAP*. L'olivine, l'orthopyroxène et le clinopyroxène non serpentinisés, de même que le spinelle, ont été analysés pour les péridotites, alors que le plagioclase, le clinopyroxène, l'amphibole, la chlorite, l'épidote, la prehnite, l'ilménite, la titanite et autres minéraux opaques ont été analysés pour les roches mafiques. Les résultats sont présentés à l'annexe C.

La préparation des échantillons pour les analyses sur roche totale incluait le broyage et la pulvérisation à l'aide d'un concasseur à mâchoires et d'un broyeur à bols d'agathe. Ces manipulations ont été effectuées à l'Université Laval. Les données de lithogéochimie pour les roches mafiques et sédimentaires ont été déterminées sur fusions alcalines, par spectrométrie d'émissions atomiques *ICP-AES* pour les éléments majeurs et les métaux de transition, et par spectrométrie de masse *ICP-MS* (VG Turbo Plasma Quad^{2+}) pour les éléments traces, incluant les terres rares, au Laboratoire INRS-ETE, Ste-Foy, Québec, Canada. La dissolution des échantillons a été accomplie par fusion dans un fluxeur Claisse. Pour les éléments majeurs, la précision de l'appareil est de $\pm 5\%$, bien que la précision analytique acceptable soit fixée inférieure à $\pm 2.5\%$. Pour les éléments traces, la précision analytique est inférieure à $\pm 1\%$ pour le La, Ce, Pr, Nd, Eu, Tb, Lu et Ba, $\pm 2\%$ pour le Sm, Gd, Dy, Ho, Er, Tm, Yb, Th, Zr, Rb et Sr, $\pm 4\%$ pour le Cs, Y et U, et $\pm 10\%$ pour le Nb (La Flèche et al., 1998). Les données standards d'un basalte et d'une andésite de l'*USGS* analysés avec la même méthode dans le même laboratoire sont rapportées par La Flèche et al. (1998).

Les données de lithogéochimie pour les éléments majeurs et les métaux de transition des roches ultramafiques ont été déterminées par *ICP* sur fusion avec métaborate/tétraborate

de lithium (Code 4B de *Activation Laboratories Ltd*). Les limites de détection sont de 0.001% pour TiO_2 et MnO, et 0.01% pour tous les autres oxydes et la perte au feu. Des analyses de standards basaltiques sont rapportées au Tab. 1.1. Les TR ont été analysées par *ICP-MS* de haute résolution selon une nouvelle méthode développée chez *Activation Laboratories Ltd* qui permet de mieux détecter les concentrations ultra-traces des péridotites. Les péridotites ont subi une fusion avec métaborate/tétraborate de lithium et les TR ont été extraites de la matrice à l'aide d'une résine à échanges ioniques. L'Er a été utilisé pour contrôler la récupération suite à la séparation et ne peut être rapporté. Les limites de détection sont données au Tab. 1.2.

Les compositions utilisées dans les graphiques pour tous les types de roches sont normalisées sur une base anhydre. Le Fe_2O_3 calculé est présumé représenter 10% du fer total analysé en Fe_2O_3. Les résultats sont présentés à l'annexe D.

TAB. 1.1 – Compositions certifiées (CERT) et mesurées de standards basaltiques (*Activation Laboratories Ltd*). Concentrations en % et ppm pour les élélements majeurs et traces, respectivement.

	Diabase		Dolérite		Basalte	
	W-2 CERT	W-2/156	DNC-1 CERT	DNC-1/11	BE-N CERT	BE-N/B31
SiO_2	52.44	52.91	47.04	47.01	38.20	38.11
TiO_2	1.06	1.075	0.48	0.486	2.610	2.645
Al_2O_3	15.35	15.40	18.30	18.48	10.07	10.00
Fe_2O_3	10.74	10.83	9.93	9.92	12.84	12.78
MnO	0.163	0.167	0.149	0.148	0.200	0.197
MgO	6.37	6.37	10.05	10.12	13.15	13.18
CaO	10.87	10.92	11.27	11.25	13.87	13.84
Na_2O	2.14	2.26	1.87	1.95	3.18	3.24
K_2O	0.627	0.55	0.229	0.23	1.39	1.39
P_2O_5	0.131	0.15	0.085	0.08	1.05	1.05
Sc	35	36	31	31	22	23
V	262	265	148	147	235	237
Sr	194	195	145	142	1370	1390
Y	24	21	18	17	30	29
Zr	94	81	41	34	265	242
Ba	182	173	114	104	1025	1050

Tab. 1.2 – Limites de détection (ppm) des terres rares dans les péridotites analysées par *HR-ICP/MS Ion Exchange df 600* (*Activation Laboratories Ltd*).

La	Ce	Pr	Nd	Sm	Eu	Gd	Tb	Dy	Ho	Tm	Yb	Lu
0.015	0.015	0.005	0.025	0.007	0.003	0.008	0.001	0.004	0.002	0.002	0.004	0.004

∗Les limites sont calculées pour chaque élément comme le blanc plus 3 fois l'écart-type de 9 blancs mesurés.

1.3 Contexte géologique

Le sous-continent indien est entré en collision de manière diachronique avec le Tibet au Crétacé tardif-Tertiaire précoce ($\sim$ 70-40 Ma [ex. Patriat et Achache, 1984 ; Pozzi et al., 1984 ; Jaeger et al., 1989 ; Gaetani et Garzanti, 1991 ; Klootwijk et al., 1992 ; 1994 : Beck et al., 1995 ; Lee et Lawver, 1995 ; Le Fort, 1996 ; Rowley, 1996 ; 1998 ; Willems et al., 1996 ; Matte et al., 1997 ; voir revue par Yin et Harrison, 2000 ; Guillot et al., 1999 ; de Sigoyer et al., 2000 ; Corfield et al., 2001]), amorçant la formation de l'orogène himalayen et le soulèvement du Plateau tibétain. Le Plateau tibétain est constitué de plusieurs terranes (ou blocs), le Bloc de Lhasa étant la plus au sud et la dernière à s'être accrétée au continent asiatique grandissant (Fig. 1.1). La marge sud du Bloc de Lhasa a subi un événement de distension au Trias tardif, lequel marque la séparation initiale du Bloc de Lhasa du continent indien et l'ouverture de l'Océan Néo-Téthys (Gaetani et Garzanti, 1991). Durant le Crétacé, le Néo-Téthys a graduellement disparu sous la terrane de Lhasa, par subduction vers le nord, menant à la collision Inde-Asie au Crétacé tardif-Tertiaire précoce. Au moins deux zones de subduction ont été nécessaires pour éliminer le Néo-Téthys (ex. Aitchison et al., 2000 ; Wang et al., 2000 ; Mahéo et al., 2000 ; 2004 ; Hébert et al., 2004 ; Guilmette et al., en préparation).

La zone de suture Yarlung Zangbo (ZSYZ) (aussi appelée Indus-Tsangpo) est principalement composée de reliques du plancher océanique néo-téthysien. Elle marque une suture majeure séparant la Plaque Indienne, au sud, de la terrane de Lhasa (Tibet), au nord. La suture est caractérisée par une chaîne ophiolitique plus ou moins continue. Les ophiolites de la ZSZY, de même que les formations sédimentaires adjacentes, ont d'abord été chevauchées (obductées) vers le sud sur le continent indien, puis rétrochevauchées vers le nord et finalement affectées par du décrochement et de l'extension tardive longitudinale (Gansser, 1974 ; Molnar et Tapponnier, 1975 ; Tapponnier et al., 1981a ; 1981b ; Allègre et al., 1984 ; Burg et Chen, 1984 ; Mercier et al, 1984 ; Ratschbacher et Chen, 1994 ; Yin et al, 1994 ; Harrison et al., 2000 ; Hodges, 2000 ; Yin et Harrison, 2000). Le long de la suture, des discontinuités majeures de la croûte (des systèmes de failles de chevauchement mésozoïques et cénozoïques) délimitent trois unités tectoniques principales ayant subi des histoires géologique, tectonique et métamorphique différentes. Elles sont, du nord au sud, la paléomarge active (terrane de Lhasa), le domaine océanique (composantes du plancher océanique néo-téthysien) et la paléomarge passive (composantes de la marge nord de la Plaque indienne) (Burg et al., 1987 ; Hodges, 2000). Une coupe schématique de la ZSYZ est présentée à la Fig. 1.3.

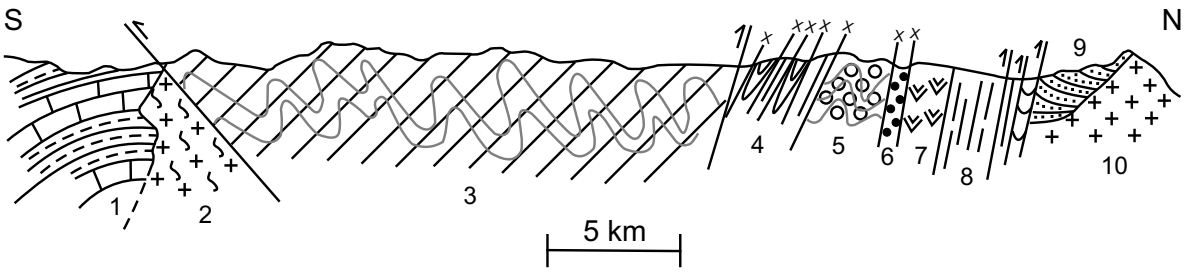

FIG. 1.3 – Coupe schématisée de la zone de suture du Yarlung Zangbo (tirée de Chang et al., 1984). 1) Calcaires permo-carbonifères et ardoises triasiques de la marge passive indienne ; 2) Granite gneissique ; 3) Flysch triasique ; 4) Argiles siliceuses rouges exotiques du mélange de Yamdrock ; 5) Mélange de Yamdrock du Crétacé tardif ; 6) Conglomérat de Liuqu ; 7) Tectonites à harzburgite du manteau ophiolitique avec des lentilles de dunite ; 8) Gabbro et diabase en sill et en filon et radiolarite supra-ophiolitique ; 9) Flysch crétacé du Groupe de Xigaze ; 10) Granitoïdes du Gangdese.

1.3.1 La paléomarge active

Le Bloc de Lhasa est composée de roches sédimentaires et ignées, d'âge Paléozoïque à Crétacé, variablement déformées et métamorphisées. La subduction vers le nord sous la terrane a résulté en un magmatisme calco-alcalin volumineux, aujourd'hui représenté par le batholite du Gangdese situé principalement le long de la marge sud de la terrane (Allègre et al., 1984 ; Harrison et al., 1992). Le Groupe de Xigaze, d'âge Crétacé tardif, au sud du Bloc de Lhasa, est composé de turbidites silicoclastiques interprétées comme des dépôts de bassin d'avant-arc (Einsele et al., 1994 ; Dürr, 1996 ; Wang et al., 2000). L'analyse des lithologies et des données de paléocourant indique la terrane de Lhasa comme source probable.

1.3.2 Le domaine océanique

Des ophiolites, des mélanges ophiolitiques et des roches sédimentaires d'eaux profondes (radiolarites) se trouvent de façon discontinue le long de la ZSYZ. Deux successions ophiolitiques d'âge, de pétrographie et d'affinité géologique différentes ont été décrites dans la littérature. Le premier groupe, le plus commun, inclut les ophiolites de la région de Buma, à l'ouest, à la région centrale de Dazhuqu, alors que le deuxième groupe est restreint à la région de Zedong/Jinlu, à l'est (Fig. 1.2). Bien que des travaux antérieurs aient mené à l'interprétation de toutes les ophiolites de la ZSYZ comme étant dérivées d'une dorsale médio-océanique (Nicolas et al., 1981 ; Prinzhofer et al., 1984), les données récentes de chimie minérale et de lithogéochimie révèlent que ces ophio-

lites tirent leur origine d'un environnement de supra-subduction, avec des signatures superposées d'arc et d'arrière-arc (voir la section suivante ; Zhou et al., 1996 ; Hébert et al., 2000 ; 2001 ; 2003 ; 2004 ; Aitchison et al., 2000 ; McDermid et al., 2001 ; 2002 ; Dubois-Côté et al., 2003 ; 2004).

Pour le premier groupe, l'ophiolite de la région de Xigaze et l'ophiolite de Yungbwa à l'ouest indiquent la formation de la croûte ophiolitique il y a 120±10 Ma (datations U-Pb ; Göpel et al., 1984) et entre 152±33 et 123 Ma (datations $^{40}Ar/^{39}Ar$; Miller et al., 2003), respectivement. La biostratigraphie détaillée de radiolaires (Girardeau et al., 1984 ; Zyabrev et al., 1999 ; Ziabrev et al., 2003 ; Aitchison et al., 2003) indique le dépôt de sédiments pélagiques supra-ophiolitiques du Barrémien tardif à l'Aptien tardif ($\sim$ 123-117 Ma). Par contraste, des datations $^{40}Ar/^{39}Ar$ et des analyses U-Pb à la microsonde ionique sur des ophiolites du deuxième groupe donnent des âges variant de 152,2±3,3 à 161±2,3 Ma (McDermid et al., 2002). Ainsi, les données géochronologiques disponibles indiquent que le(s) système(s) de subduction intra-océanique(s) duquel proviennent probablement les ophiolites de la ZSYZ était au moins actif du Jurassique tardif à la fin du Crétacé précoce.

Le contact sud de la chaîne ophiolitique est marqué par un mélange ophiolitique tectonique fait d'une matrice de serpentinite grandement cisaillée, de blocs de serpentinite, de blocs de diabase et gabbro partiellement rodingitisés, et de blocs composites de serpentinite et d'intrusions diabasiques (Fig. 2.1A). Des foliations métamorphiques définies par l'orientation préférentielle d'amphiboles ont été observées dans les blocs. Les données pétrographiques et géochimiques obtenues du mélange de Beimarang suggèrent que les roches ultramafiques soient similaires à des péridotites du manteau supérieur appauvri (Huot et al., 2002). Ces péridotites ont par la suite été percolées par des magmas d'arrière-arc dont la source mantellique modérément appauvrie avait été affectée par une composante de subduction. Ces données géochimiques corrèlent très bien avec celles des ophiolites sus-jacentes, ce qui suggère fortement une origine magmatique similaire pour les ophiolites et les mélange ophiolitique sous-jacent.

Immédiatement au sud des séquences ophiolitiques affleure un mélange distinctif d'histoire complexe. Il a tout d'abord été décrit comme un *wildflysch à blocs exotiques* par Tapponnier et al. (1981a) et interprété comme un mélange sédimentaire (Shackleton, 1981). Il contient des unités antérieurement appelées *nappes de chevauchement infra-ophiolitiques* (Burg et Chen, 1984) ou *radiolarites rouges du Jurassique tardif au Crétacé précoce* (Girardeau et al., 1984). Il a par la suite été décrit comme le mélange de Yamdrock et interprété comme un mélange tectonique (Searle et al., 1987). Récemment, Aitchison et al. (2000) a renommé cette unité la terrane de Bainang (voir aussi Zyabrev et al., 2000 ; Ziabrev et al., 2000 ; 2001 ; 2004). Cependant, l'étendue et

les caractéristiques géochronologiques, tectoniques, métamorphiques et géochimiques de cette terrane, de même que d'autres terranes compartimentées et renommées le long de la ZSYZ, sont faiblement contraintes, ne justifiant pas, pour l'instant, l'utilisation de cette nomenclature redéfinie. Puisque le terme wildflysch est souvent considéré désuet, j'adhère au terme défini par Searle et al. (1987) pour cette unité, i.e. le mélange de Yamdrock.

Ce mélange consiste en une zone de chevauchement imbriquée contenant plusieurs écailles tectoniques à vergence sud, et qui préserve une stratigraphie de plancher océanique (Aitchison et al., 2000). Des écailles tectoniques de shale rouge siliceux et de chert à radiolaires, et localement des basaltes alcalins, dominent la portion nord du mélange (Chang, 1984 ; Searle, 1987). Vers le sud, la quantité de chert diminue et l'unité est caractérisée par des shales marines d'eaux profondes finement litées. Les blocs exotiques déformés, décimétriques à kilométriques, montrent des âges et des faciès différents (Mercier et al., 1984 ; Lin, 1984 ; Searle et al., 1987) : des calcaires permiens à crétacés, des micrites rouges ou vertes du Campanien-Maestrichtien, des cherts rouges, verts, ou gris du Jurassique moyen au Crétacé précoce (Aptien selon Wu, 1993 ; Matsuoka et al., 2001 ; 2002), et des blocs composés d'une association primaire de laves coussinées. Le style structral et les assemblages de terrain rappellent un complexe de subduction intra-océanique (Mercier et al., 1984, Searle et al., 1987 ; Aitchison et al., 2000) et l'unité a été interprétée comme consistant principalement en du matériel râclé de la plaque téthysienne en subduction (Chang, 1984 ; Ziabrev et al., 2001). La matrice du mélange est principalement composée de couches de roches pélitiques contenant des fossiles *Globotruncana* sénoniens, lesquels indiquent un âge minimum Crétacé tardif pour le mélange (Chang, 1984 ; Mercier et al., 1984). De plus, la stratigraphie détaillée de radiolaires indique que l'accrétion s'est produite au minimum de l'Aptien tardif au Campanien (Zyabrev et al., 2000 ; Ziabrev et al., 2000 ; 2001), alors que les fossiles les plus jeunes retrouvés dans les blocs exotiques et dans la matrice sont du Maestrichtien au Paléocène (Burg et Chen ; 1984), étendant peut-être l'âge de cette unité au Tertiaire précoce.

1.3.3 La paléomarge passive

Les sédiments de la marge passive indienne (d'âge Permien à Crétacé) ont été chevauchés vers l'avant-pays indien, au sud, durant le Paléocène précoce et sont aujourd'hui représentés par trois unités tectoniques majeures allochtones imbriquées (Burg et Chen., 1984 ; Burg et al., 1987 ; Liu et Einsele, 1996 ; 1999). Du nord au sud, ces trois unités consistent en des turbidites (marge continentale), des flyschs carbonatés (sédiments téthysiens du nord) et une séquence de plate-forme (sédiments téthysiens

du sud). L'assemblage se trouve en contact de faille au-dessus de la nappe cristalline du Haut Himalaya et représente des dépôts d'eaux progressivement plus profondes, jusqu'aux flyschs de la ZSYZ au nord. Les flyschs sont localement intercalés avec des roches calcaires et des roches volcaniques mafiques à intermédiaires probablement associées à de la distension continentale et à la formation d'une marge continentale passive (Chang, 1984), tout comme les basaltes continentaux tholéiitiques à légèrement alcalins des Trapps de Panjal au nord-ouest de l'Inde, le long de la marge nord de la plaque indienne (Searle et al., 1987).

Les conditions tectoniques menant à la formation des flyschs ont été rencontrées au Trias (Gansser, 1980 ; Gaetani et Garzanti, 1991). De plus, la séquence de flysch triasique au sud de la ZSYZ contient des fossiles (*Daonella sp., Halobia sp.*) datant du Trias moyen au Jurassique précoce (Mercier et al., 1984). Cette séquence atteint plusieurs kilomètres d'épaisseur et est structuralement complexe. Elle est fortement plissée, à vergence sud, et est affectée par du métamorphisme variant du faciès des schistes verts au faciès des amphibolites (Chang, 1984 ; Burg et al., 1987). Aucune association minérale de haute pression n'y a été trouvée. La section centrale (correspondant à la région d'étude sur la Fig. 1.1) représente probablement la section rocheuse de la marge continentale passive indienne la moins déformée de toute la chaîne himalayenne (Searle et al., 1987). La déformation augmente tout de même vers le nord, alors que le flysch triasique passe de mélange sédimentaire au mélange tectonique, soit le mélange de Yamdrock. Le contact entre le flysch métamorphisé et la séquence sédimentaire de plate-forme généralement non métamorphisée est marqué par une zone tectonisée, le long de laquelle de nombreuses petites intrusions granitiques datant de l'Ordovicien précoce sont observées.

1.3.4 Le conglomérat de Liuqu

Plusieurs zones de sédiments clastiques grossiers, de déposition rapide, affleurent en une série de bassins de décrochement oblique tectoniquement perturbés, à l'intérieur et en marge des terrains intra-océaniques. Ces sédiments, connus sous le nom de Conglomérat de Liuqu, sont les témoins d'une phase paléogène dans l'évolution tectonique du Tibet (Davis et al., 2002, Aitchison et al., 2000). Ils proviennent de l'extrémité nord de la marge indienne et d'un arc intra-océanique dans le Néo-Téthys (Davis et al., 2002). Ils sont interprétés comme des preuves de la convergence oblique et de la translation d'unités le long de la ZSYZ. L'absence de fragments dérivés des unités au nord de la ZSYZ suggère que les bassins associés au dépôt du Conglomérat de Liuqu se sont développés avant la collision finale entre l'Inde et l'Asie, bien que les conglomérats soient principalement peu déformés.

1.3.5 Blocs mafiques et granitiques dans les unités sédimentaires

Des roches mafiques se retrouvent dans le mélange de Yamdrock et dans le flysch triasique, soit dans des zones mafiques cartographiables (Figs. 1.2 et 4.1E), soit en tant que blocs métriques dans la matrice sédimentaire (Fig. 4.1F). Localement à Lhaze, quelques intrusions gabbroïques recoupent le flysch. Les roches, spécialement les laves, sont généralement altérées et démembrées. Des veines et des amygdules de carbonates, quartz, chlorite et épidote sont fréquentes. La spilitisation des laves coussinées est commune. Fait intéressant, les roches gabbroïques des zones mafiques des régions de Zisong et Pazhong montrent une couleur verdâtre à bleuâtre particulière, laquelle semble être causée par un mélange de chlorite et de pumpellyite. Plusieurs auteurs mentionnent la présence, dans les unités sédimentaires de la ZSYZ, de roches volcaniques alcalines provenant d'atolls intra-océaniques (ex. Mercier et al., 1984 ; Searle et al., 1987 ; Liu et Einsele, 1999 ; Aitchison et al., 2000), mais aucune donnée géochimique justifiant leur interprétation n'est fournie ou référée.

Un granite porphyrique a aussi été échantillonné d'un bloc granitique (d'environ 10m de largeur) observé dans le flysch triasique. Le granite est composé à 95% de quartz, de phénocristaux feldspathiques et de phlogopite. La roche est recoupée par de minces veines de carbonates. Le granite échantillonné correspond probablement à une relique des batholites cambro-ordoviciens résultant d'une subduction sous le continent indien et le Bloc de Lhasa accolé, durant le Protérozoïque très tardif et le Paléozoïque très précoce (Yin et Harrison, 2000).

1.4 Caractéristiques des massifs ophiolitiques de la ZSYZ

Les caractéristiques générales des ophiolites de la ZSYZ incluent : 1) une mince croûte ophiolitique de 2 à 4 km ; 2) une composante gabbroïque mineure, souvent manquante ; et 3) plusieurs dykes et sills gabbroïques et diabasiques recoupant les sections mantellique et crustale (Nicolas et al., 1981 ; Mercier et al., 1984 ; Chang, 1984 ; Girardeau et al., 1985a ; Nicolas, 1989 ; Hébert et al., 2003). Comme mentionné précédemment, les basaltes et les diabases de la croûte se subdivisent en deux groupes selon leur pétrographie et lithogéochimie (Dubois-Côté et al., 2003 ; 2004). Le premier groupe à l'ouest, le plus commun, consiste en des roches d'affinité d'arrière-arc, en accord avec des patrons de terres rares (TR) de type *N-MORB* et de faibles anomalies négatives en Nb-Ta et Ti. Les roches du second groupe à l'est sont généralement

porphyritiques et montrent une affinité d'arc intra-océanique, tel que le démontre un enrichissement en TR légères et d'importantes anomalies négatives en Nb-Ta et Ti.

Les roches du manteau sont principalement des harzburgites, partiellement à complètement serpentinisées. Dubois-Côté et al. (2003 ; 2004) ont démontré que les roches les mieux préservées peuvent aussi être subdivisées en deux groupes. La composition du spinelle du premier groupe, à l'ouest, est bien définie et typique d'une composition harzburgitique. La géochimie des TR donne des profils appauvris en TR légères, (rapport $(La/Sm)_N$ moyen de 0.3 ± 0.2). La modélisation pétrogénétique suggère que ces harzburgites se soient formées suite à 7-12% de fusion d'un manteau de type *N-MORB*. Par contraste, le spinelle du second groupe, à l'est, est de composition très variable. Les harzburgites sont caractérisées par des profils enrichis en TR légères, (rapport $(La/Sm)_N$ moyen de 2.8 ± 0.8). La modélisation pétrogénétique suggère 30-40% de fusion d'une source mantellique appauvrie, jumelée à un épisode de métasomatisme du manteau par un fluide ou un magma pauvre en Ti. De plus, la zonation chimique régionale suggère que ces ophiolites de supra-subduction aient été générées en réponse à une augmentation vers l'est de la quantité de fluide métasomatique dérivé de la plaque subductante.

1.5 Prolongement vers l'ouest de la suture

Le prolongement vers l'ouest de la ZSYZ, dans les régions du Kohistan et du Ladakh (Fig. 1.1) est dominé par une séquence d'îles-en-arc de très grandes dimensions, la séquence d'arc du Kohistan-Dras (ex. Searle et al., 1987 ; Mahéo et al., 2004). Cet arc est bordé par deux sutures, la Zone de Suture du Shyok (ZSS), au nord, et la Zone de Suture de l'Indus Tsangpo (ZSIT, équivalante à la ZSYZ), au sud. Associés à la ZSIT, deux groupes d'ophiolites et de mélanges ophiolitiques associés sont reconnus (e.g. Mahéo et al., 2004 qui présente une revue récente des ophiolites du Ladakh sud). Le premier groupe, situé au nord de la ZSIT et associé au batholite du Ladakh, est représenté par la suite volcanique calco-alcaline de l'arc de Dras (ex. Robertson et Degnan, 1994). Ce groupe est l'équivalent ouest du batholite du Gangdese. Le deuxième groupe représente les ophiolites du Sud Ladakh et est constitué de trois ophiolites (Spontang, Nidar, Karzog) et de leur mélange ophiolitique associé (Mahéo et al., 2000). La géochimie similaire des roches mafiques et ultramafiques des ophiolites du Sud Ladakh indique que les trois ophiolites ont été dérivées d'une même source mantellique par des processus similaires (Mahéo et al., 2004). Cette source était de type *N-MORB*, légèrement enrichie en éléments lithophiles à gros rayon ionique (*LILE*) lors d'un événement métasomatique dans une zone de supra-subduction. Les ophiolites du Sud Ladakh seraient donc les témoins d'un arc intra-océanique tholéiitique dans le

Néo-Téthys. Par contre, la modélisation des TR a démontré que les roches mafiques de Spontang et de Nidar ne résultent pas de la fusion partielle des lherzolites associées (Mahéo et al., 2004).

La présence de deux mélanges différents associés à deux groupes distincts d'ophiolites suggèrent l'existence de deux paléo-zones de subduction actives durant le Crétacé tardif (Mahéo et al., 2000 ; 2004 ; Corfield et al., 2001). La zone de subduction la plus au sud était intra-océanique et associée à la formation de l'arc tholéiitique du Sud Ladakh il y a environ 110-130 Ma (datations $^{40}Ar/^{39}Ar$ sur des amphiboles ; Mahéo et al., 2004). La subduction plus au nord, active depuis environ 110 Ma, était proche de la marge asiatique et a produit le magmatisme de type andin du batholite du Ladakh et de l'arc de Dras. Enfin, il découle de corrélations effectuées sur la base de données sédimentaires (Beck et al., 1996 ; Robertson, 2000), de données géochronologiques (Gnos et al., 1998 ; 2000 ; Pederson et al., 2001 ; Corfield et al., 2001 ; Mahéo et al., 2004 ; Guilmette et al., en préparation) et de données géochimiques (Mahéo et al., 2004 ; Dubois-Côté et al., 2003), que les deux zones de subduction à pendage nord devaient avoir accommodé la fermeture du Néo-Téthys de l'Oman jusqu'au Tibet.

1.6 Analyse structurale

Même si l'analyse structurale détaillée des unités étudiées ne constitue pas un des objectifs du projet de doctorat, cette section présente une synthèse de la littérature, jumelée aux observations de terrain et aux interprétations de F. Huot et Li Y.L. (communication personnelle). Les déformations et les mouvements les plus importants le long de la ZSYZ se sont produits lors des premières phases tectoniques responsables du chevauchement des unités néo-téthysiennes vers le sud, i.e. la compression N-S (Ratschbacher et al., 1994 ; Yin et al., 1994 ; 1999 ; Harrison et al., 2000). Le flysch triasique, en particulier, a enregistré quatre phases de déformation régionale. Le métamorphisme au faciès des schistes verts est contemporain de la phase initiale. Les phases tectoniques sont ici décrites de la plus vieille à la plus jeune.

La première phase (φ_1) est caractérisée par des plis isoclinaux à grande échelle et des chevauchements ductiles. Les plis affectent le litage (S_0), tandis que les flancs et les plans axiaux de ces plis sont parallèles à la schistosité régionale (S_1) (voir aussi Lee et al., 2000). Au niveau des horizons de radiolarites légèrement métamorphisées de la semelle infra-ophiolitique, les axes de plis orientés à 150-220° sont aussi parallèles à une linéation d'étirement L_1 définie par des fibres de quartz dans la schistosité S_1 et par des surfaces de friction (miroirs de faille) dans les plans de chevauchement (Burg

et Chen, 1984 ; Mercier et al., 1984). Le flysch triasique est affecté par des plis kilométriques d'orientation N-S à NO-SE et couchés vers le sud ou l'ouest présentent aussi une schistosité fluidale horizontale et une linéation d'étirement d'orientation grossière N-S (Mercier et al., 1984). Les chevauchements ductiles (T_1) ont généralement une vergence sud. Cette phase φ_1 est associée à l'obduction des unités néo-téthysiennes vers le sud au Crétacé. Entre autres, des âges Ar/Ar avoisinant 127 Ma pour des blocs d'amphibolite provenant probablement de la semelle amphibolitique associée aux ophiolites de la ZSYZ pourraient représenter le détachement initial de ces ophiolites (Guilmette et al., en préparation). La majorité des structures à vergence sud sont compatibles avec la déformation normalement observée dans les prismes d'accrétion. Les failles de chevauchement à vergence nord, de plus faible importance, peuvent être reliés à des chevauchements inverses mineurs dans l'assemblage de subduction.

La deuxième phase (φ_2), omniprésente dans toutes les unités, est l'événement de déformation intense dominant. Cette phase est caractérisée par deux types de plis affectant la schistosité S_1. Le premier événement de plissement correspond à des plis serrés (F_{2a}) d'orientation NE-SO à vergence NO et associés à une crénulation orientée à 039°. Ces plis ont été repris par des plis ouverts (F_{2b}) d'orientation E-O caractérisés par des plans et clivages axiaux sub-verticaux associés à une crénulation orientée à 099°. Des plis en chevron orientés à 030-150° et à vergence sud (Burg et Chen, 1984) sont particulièrement caractéristiques de cette phase. Les failles inverses associées à la phase φ_2 ont une vergence nord. Les plis et les failles inverses se sont probablement développés dans le domaine fragile-ductile. Cet événement est donc interprété comme un épisode de rétrochevauchement qui a affecté les structures de déformation φ_1 de même orientation E-O. Le système de chevauchement de Renbu Zedong à pendage sud (Yin et al., 1994 ; 1999 ; Harrison et al., 2000 ; aussi appelé le système de rétrochevauchement par Ratschbacher et al., 1994), actif entre 19 et 10 Ma, délimite la ZSYZ dans le sud du Tibet. Les caractéristiques structurales le long de la suture de part et d'autre de ce chevauchement indiquent un mouvement vers le nord (Yin et al., 1994).

La troisième phase (φ_3) représente l'événement de déformation en coulissage. Cette phase a développé des failles de décrochement et des cisaillements dans le domaine fragile-ductile, quoique, dans la région de Zedong, le flysch triasique montre une déformation plastique intense. Les zones déformées d'orientation E-O sont caractérisées par la présence de fabriques C-S et de plis dont les charnières plongent à fort angle vers le NO et le SE. Les mouvements de décrochement sont majoritairement dextres, avec quelques phases mineures senestres (ex. Armijo et al., 1989 ; Yin et al., 1994). Enfin, la quatrième phase (φ_4) est associée à un épisode de glissement gravitaire qui a développé des failles normales à pendage nord. La déformation associées à ces failles est à l'origine du plissement irrégulier dans le toit des failles et des plis d'entraînement dans le mur des failles.

Ces deux phases φ_3 et φ_4 tardives, datant du Miocène à aujourd'hui, représentent l'événement d'extension, dominant E-O et mineur N-S, associé à l'étirement E-O du Tibet sud et à la flexion oroclinale le long de l'arc himalayen, et sont probablement rattachées au détachement sud tibétain miocène (ex. Mercier et al., 1984 ; Armijo et al., 1986 ; 1989 ; Ratschbacher et al., 1994 ; Yin et al., 1994 ; Hodges, 2000).

Chapitre 2

«Petrology and Geochemistry of Mafic Rocks from Mélange and Flysch Units Adjacent to the Yarlung Zangbo Suture Zone, Southern Tibet »

C. Dupuis[a], R. Hébert[a], V. Dubois-Côté[a], C.S. Wang[b], Y.L. Li[b], Z.J. Li[b]

[a] *Département Géologie et génie géologique, Université Laval, Ste-Foy, Québec, Canada, G1K 7P4*

[b] *Université de Technologie de Chengdu, Chengdu, Sichuan, 610059, R.P. Chine*

Soumis à *Chemical Geology* le 25 juillet 2003 ; accepté le 25 octobre 2004

Cet article traite de la pétrographie et de la géochimie des blocs mafiques des trois unités à l'étude. Pour le mélange ophiolitique, les patrons de TR sont appauvris en TR légères. De légères anomalies négatives en Nb-Ta et Ti suggèrent que ces roches se soient formées dans un bassin d'arrière-arc, comme les roches mafiques du Bassin de Lau. Pour le mélange de Yamdrock, les patrons de TR sont enrichis en TR légères. Ces roches sont d'affinité intraplaque et sont similaires aux roches volcaniques du point chaud de la Réunion. Pour le flysch triasique, les patrons de TR sont très enrichis en TR légères, alors que de légères anomalies négatives en Nb-Ta et Ti sont aussi observées. Ces roches sont similaires aux roches volcaniques des Trapps de Deccan (Inde) et sont

interprétées comme étant dérivées d'une source mantellique intraplaque enrichie, avec assimilation crustale continentale résultant de la dislocation de la Plaque indienne lors de l'ouverture du Néo-Téthys.

Note : Les données géochimiques des roches mafiques ont été tracées dans une série de diagrammes discriminants afin de déterminer leur environnement tectonique de formation. Dans l'article, seuls quelques-uns de ces diagrammes sont présentés et discutés. Un tableau synthèse des résultats obtenus à l'aide de ces diagrammes pour chaque unité géologique à l'étude est donné à l'annexe E.

2.1 Introduction

The Yarlung Zangbo Suture Zone (YZSZ), in Southern Tibet, is a major suture between India and Asia, and marks the location where the Neotethyan oceanic domains have been consumed by northward subduction under the Lhasa terrane during the Cretaceous. The present work is part of a Sino-Canadian project initiated in 1998 and devoted to the geodynamic reinterpretation of the Tibetan ophiolitic massifs located in the central part of the YZSZ, along a 250 km-long portion between Lhaze and Zedong (Figs. 1.1 and 1.2). Recently, Aitchison et al. (2000) renamed the units within, and bounding, the YZSZ, into six lithotectonic units (terranes) bounded by thrust faults. They are, from north to south, the Lhasa terrane, the Xigaze terrane (fore-arc basin), the Zedong terrane (intra-oceanic volcanic arc), the Dazhuqu terrane (ophiolites), the Bainang terrane (subduction complex) and the Indian terrane (see also McDermid et al., 2000 ; 2001 ; 2002 ; Zyabrev et al., 2000 ; Ziabrev et al., 2000 ; 2001 ; 2004). However, the extension, geochronological, tectonic, metamorphic and geochemical characteristics of these terranes are poorly constrained, precluding use of this nomenclature. More work is needed to achieve a new view of the lithostratigraphic picture and mutual relationships between the proposed terrane mosaic.

Oceanic fragments along the suture have been recently reinterpreted in a supra-subduction zone context (Hébert et al., 2000 ; 2001 ; 2003 ; Aitchison et al., 2000 ; Huot et al., 2002 ; Dubois-Côté et al., 2003 ; in press). Previous studies have shown a large compositional diversity among the ophiolitic massifs in the study area (Xigaze, Girardeau et al., 1984, 1985 ; Hébert et al., 2000 ; 2003 ; Dubois-Côté et al., 2003 ; in press). These ophiolitic complexes and spatially associated igneous rock suites coming from the Tethyan basin were dismembered and incorporated into tectonic mélange, turbidite and flysch sedimentary formations. Mafic blocks and intrusions within these moderately deformed sedimentary formations are of unknown origin since their original context has

been disturbed.

The scope of this contribution is part of a complete study that aims to extend the geodynamic interpretation of the YZSZ to the three main geological units lying immediately south of the ophiolitic chain. These are, from north to south, the Early Cretaceous ophiolitic mélange, the Triassic-Cretaceous Yamdrock mélange and the Triassic flysch (Fig. 1.2). Petrography, mineral chemistry and whole-rock geochemistry were performed on ultramafic, mafic and sedimentary rocks of the ophiolitic mélange and sedimentary units in order to assess their tectonic settings. Sampling regions are located on Fig. 1.2. Some ultramafic and mafic rocks were sampled from zones mapped as serpentinites. Analyses revealed that these rocks are very similar to rocks in the ophiolitic mélange and will therefore be treated as part of it. The same applies for three mafic rocks sampled in the Paleogene Liuqu Conglomerate. The particular characteristics of two additional samples obtained from dykes in the Zedong area will be discussed in connection with rocks of the ophiolitic mélange. The present paper aims to compare the petrographic and geochemical characteristics of mafic rocks sampled in the three geological units of interest, and to assess their petrogenesis. Subsequent papers, in press, will deal with the characteristics of ultramafic and sedimentary rocks sampled in the ophiolitic mélange and the sedimentary units, respectively.

2.2 Geological framework

Le contexte géologique est présenté à la section 1.3.

2.3 Mineral chemistry

2.3.1 Analytical method

La méthode analytique est décrite à la section 1.2 et les données complètes sont présentées à l'«Annexe C ».

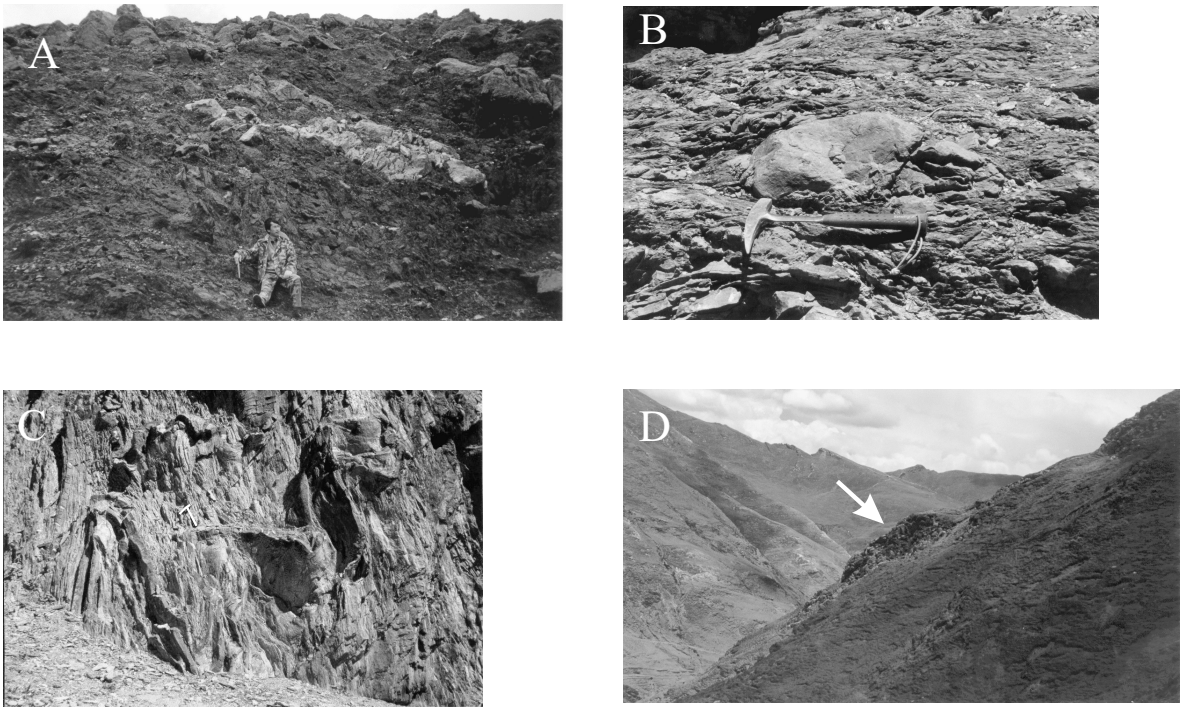

FIG. 2.1 – Field photographs of the three geological units. A) Peridotite blocks and whitish rodingitized mafic blocks within the sheared serpentinite matrix of the ophiolitic mélange. B) Block-in-matrix aspect of the Yamdrock mélange, Dazhuqu area. C) Folded sequence within the Triassic flysch, Beilie area (geological hammer redrawn in white for scale). D) Mafic zone (arrow) within the Yamdrock mélange, Baigang area.

2.3.2 Mineral assemblages

All gabbroic and basaltic rocks experienced metamorphism severely overprinting primary mineral compositions. Relicts of igneous phases are plagioclase, clinopyroxene and ilmenite. Prismatic plagioclase and/or euhedral to subhedral clinopyroxene occur as phenocrysts in many samples and form an ophitic texture (Fig. 2.2A). Basalts, particularly abundant in the Yamdrock mélange, are commonly porphyritic (with plagioclase and clinopyroxene phenocrysts) and/or amygdaloidal. A reddish brown primary amphibole is preserved locally. A few samples from the Liuqu and Qumei areas contain euhedral pseudomorphs of serpentine and chlorite after olivine. One even contains spinel and chromite elsewhere associated with primary olivine. Interstitial quartz (10 vol.% on average) is present in gabbroic rocks of the Triassic flysch (Fig. 2.2B). Accessory apatite is present only in a few samples containing magmatic brown amphibole (Fig. 2.2C). Mafic rocks of the ophiolitic mélange are affected by medium-grade to very low-grade metamorphism. For mafic rocks of the sedimentary units, metamorphism is pervasive but restricted to the low grade facies. It is more typical of low-grade hydrothermal metamorphism than high-grade metamorphism. Metamorphic phases include amphibole, magnetite, titanite, leucoxene, chlorite, epidote, calcite, quartz, prehnite and pumpellyite.

2.3.3 Feldspar

Generally, plagioclase is the most abundant phase, and is albitized and greatly altered, replaced by kaolinite, sericite and/or hydrogrossular (Fig. 2.2). Albite twinning is often visible (Fig. 2.2D). Plagioclase ranges from almost pure albite to An_{84}, the more calcic compositions (An_{37} and higher) being restricted to mafic rocks from the ophiolitic mélange. Plagioclase in the granite has an intermediate composition, falling in the range An_{22-17}. Albitization of plagioclase is an evidence of retrogressive hydrothermal metamorphism. Fresh K-feldspar is observed only in a cataclasite gabbro (sample 2002-BAG-03) and in the granite. K-feldspar are almost pure orthoclase (Or_{98}) in the cataclasite gabbro, but are more sodic in the granite (Or_{71} Ab_{28} An_1). They occur as phenocrysts and coronas growing on plagioclase.

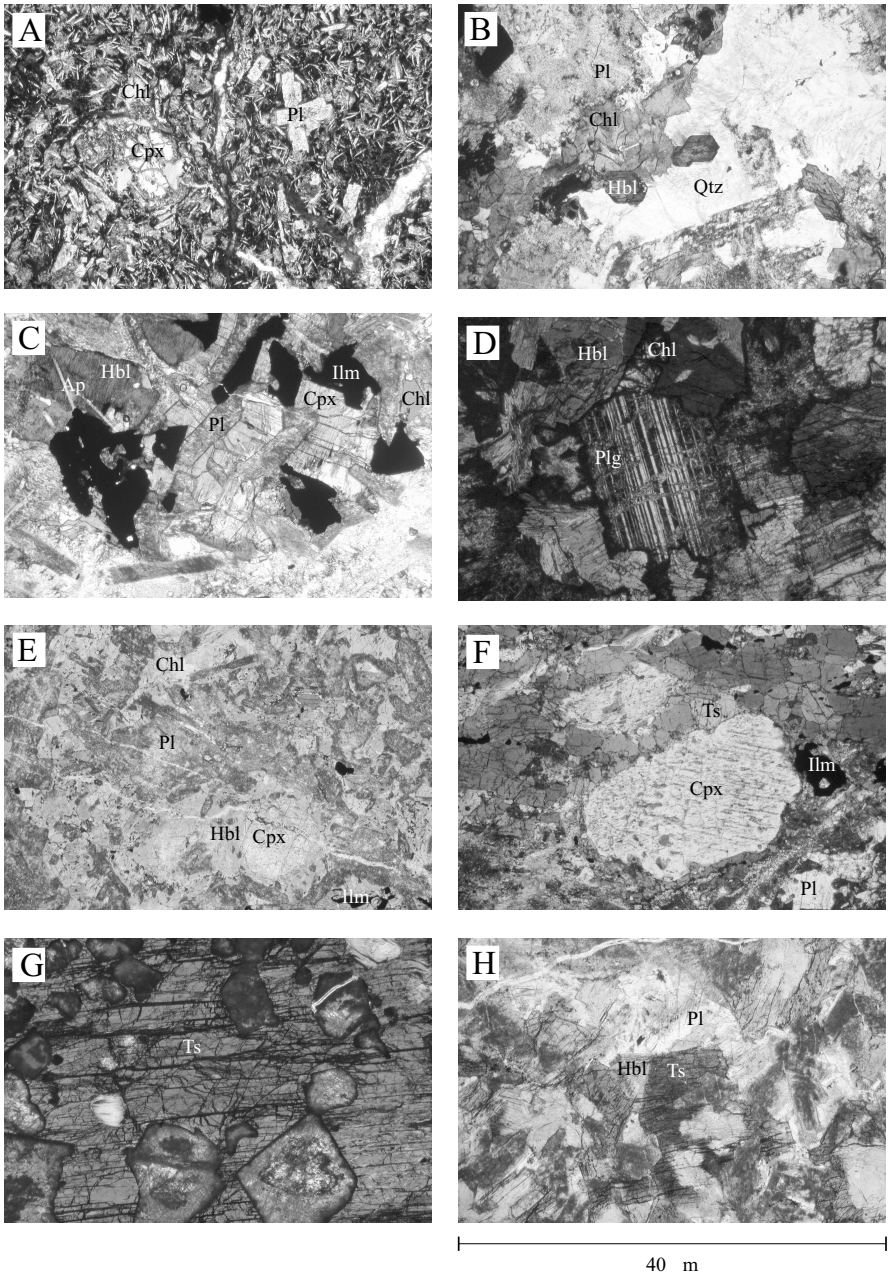

Fig. 2.2 – Microphotographs of various mafic rocks of the three geological units. A) 2001-LHA-05 : Typical porphyritic basalt of the Yamdrock mélange. B) 2002-ZIS-10 : Euhedral crystals of brown magmatic magnesiohornblende and interstitial quartz in a gabbro from the flysch. C) 2002-ZIS-08 : Accessory apatite and brown hornblende in a typical gabbro from the flysch. D) 2002-QUM-15 : Albite twinning of a primary plagioclase (An_{55}) in a coarse-grained gabbro from the ophiolitic mélange. E) 2001-LHA-16 : Green hornblende rimming a clinopyroxene in gabbro from the ophiolitic mélange. F) 2002-LIU-06 : Symplectite of magmatic tschermakite and Cpx in a coarse-grained gabbro from the ophiolitic mélange. G) 2002-QUM-15 : Magmatic brown tschermakite in a coarse-grained gabbro from the ophiolitic mélange. H) 2002-DAZ-02 : Magmatic brown tschermakite rimmed by metamorphic green hornblende in a gabbro from the ophiolitic mélange. Chl, chlorite ; Cpx, clinopyroxene ; Hbl, hornblende ; Ilm, ilmenite ; Pl, plagioclase ; Ts, tschermakite.

2.3.4 Clinopyroxene

Colorless interstitial clinopyroxene ranges from augite to diopside. Its compositional variation reflects sub-solidus re-equilibration. Re-equilibrated diopside compositions are generally restricted to clinopyroxene from the ophiolitic mélange, which is affected by relatively higher-grade metamorphism. Compositional contrasts between the ophiolitic mélange and sedimentary units are reflected by TiO_2, Cr_2O_3 and Al_2O_3 contents vs. Mg# (Fig. 2.3). Although in general, clinopyroxenes have Mg# ranging from 0.60 to 0.94, only clinopyroxene from the ophiolitic mélange shows high values. Clinopyroxene compositions from the ophiolitic mélange fit the general trend for progressive crystal fractionation processes reported in Constantin (1999), whereas those from the sedimentary units show an important enrichment in TiO_2, Al_2O_3 and to a lesser extent Cr_2O_3.

2.3.5 Amphibole

Partial to complete amphibolitization of clinopyroxene is common in the ophiolitic mélange, as is the presence of coronitic textures with amphibole rimming clinopyroxene (Fig. 2.2E). Amphiboles display several habits and can be grouped into three main types : brown tschermakite to magnesiohornblende, green magnesiohornblende, and late pale green actinolite. Based on mineral association (Fig. 2.2F-G), their generally euhedral crystal shape, their reddish brown color, and their chemical composition, the first group of amphibole is considered of magmatic origin (e.g. Coogan et al., 2001). Metamorphic green amphiboles replace primary phases such as brown amphiboles, clinopyroxene and rarely plagioclase. Samples from the Beimarang and Dazhuqu areas are commonly zoned, from brown hornblende at the center to green hornblende to actinolite at the edge (Fig. 2.2H). The actinolite generally exhibits a fibrous habit.

Amphibole compositions define a trend from high-temperature brown magmatic tschermakite ($Al^{iv} > 1.0$; Ti > 0.13) to low-temperature pale green metamorphic actinolite ($Al^{iv} < 0.5$; Ti < 0.06) (Fig. 2.4A). Brown to green magnesiohornblende is intermediate. A porphyritic basalt from Zedong contains phenocrysts of brown magnesiohastingsite and a xenolith composed of green magnesiohornblende. Another sample from the ophiolitic mélange, 2002-BUM-03, contains brown prismatic magnesiohastingsite. These amphiboles have higher alkali (Na + K) contents and therefore plot closer to the pargasitic substitution line (Fig. 2.4B). Amphiboles from mafic blocks within the flysch are richer in Fe, even containing some ferro-hornblende, and plot closer to the edenitic substitution line. Finally, two main samples from the Liuqu (2002-LIU-03) and

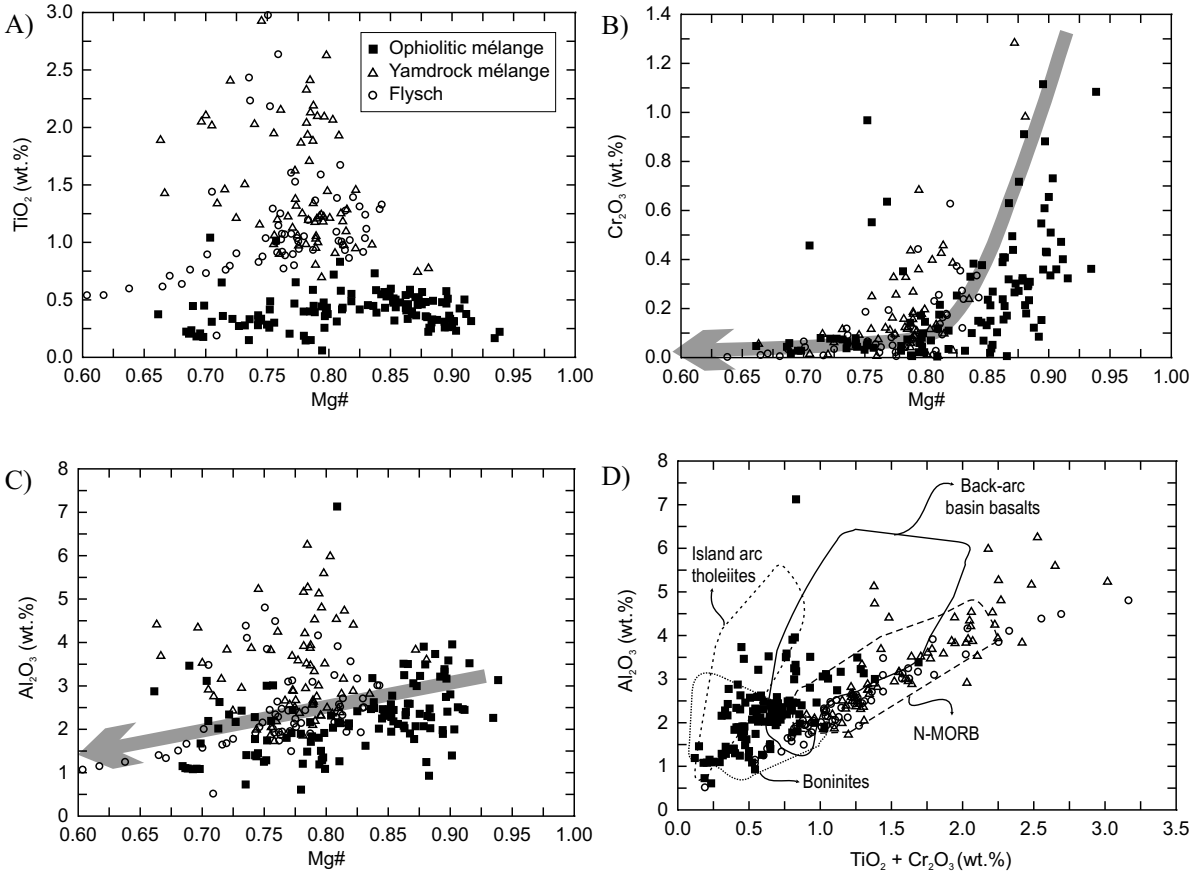

FIG. 2.3 – Compositional variations of clinopyroxenes from mafic rocks of the three geological units. A) TiO_2 vs Mg# ; B) Cr_2O_3 vs Mg# ; C) Al_2O_3 vs Mg#. The arrow in B and C shows a fractional crystallization trend (Constantin, 1999). D) Al_2O_3 vs TiO_2 + Cr_2O_3. Fields outline clinopyroxene compositions in boninites (van der Laan et al., 1992), island arc tholeiites and back-arc basin basalts (Hawkins and Allan, 1994), and N-MORB (Stakes and Franklin, 1994).

Qumei (2002-QUM-15) area also contain accessory gedrite and anthophyllite, possibly replacing original orthopyroxene.

Samples of the ophiolitic mélange containing both brown and green amphiboles, especially those showing coronas of green amphibole around a brown core, have been selected to constrain more closely the compositional variations between the different amphibole types. Euhedral reddish brown amphiboles from two coarse-grained gabbros (2002-LIU-06 and 2002-QUM-15) are used as a reference for magmatic amphiboles. Representative magmatic amphibole compositions from oceanic gabbros (Coogan et al., 2001) are shown for comparison. From the core to the rim, i.e. from primary brown amphibole to late pale green actinolite, silica content increases whereas Ti, Al^{iv} and total alkali decrease (e.g. Fig. 2.4C). These interrelated trends reflect a gradual decrease in temperature. The Mg# varies from 0.59 to 0.96, independently of the Ti, Al or alkali contents, but it is fairly constant for samples coming from the same rock. A few calcic amphiboles from various host rocks have an unusual Mg# of 1 as their total amount of iron has been attributed, according to stoechiometric formulae, to Fe_2O_3. Finally, all types of amphiboles have low chlorine contents (generally less than 0.15 wt.%) but reach slightly higher fluorine levels (generally less than 0.26 wt.%).

2.3.6 Late stage assemblages

Chloritization is pervasive, especially in the sedimentary units. Chlorite replaces chiefly clinopyroxene. In places, it is partially replaced by retrograde blue-green pumpellyite. Prehnite is observed only in rocks of the ophiolitic mélange and is particularly abundant in samples from the Beimarang area (up to 60 vol.%), as previously observed by Huot et al. (2002). It either displays a radial crystallizing growth or an equant allotriomorphic shape. Prehnite is commonly related to rodingitization of metabasites (Rice, 1983). Most of the Yamdrock mélange samples contain veins and/or amygdules filled with secondary chlorite, epidote, albite, quartz and carbonates. Veins are much less common in the generally coarser-grained samples of the ophiolitic mélange and Triassic flysch. Ilmenite and titanite crystals are completely to partially altered to leucoxene.

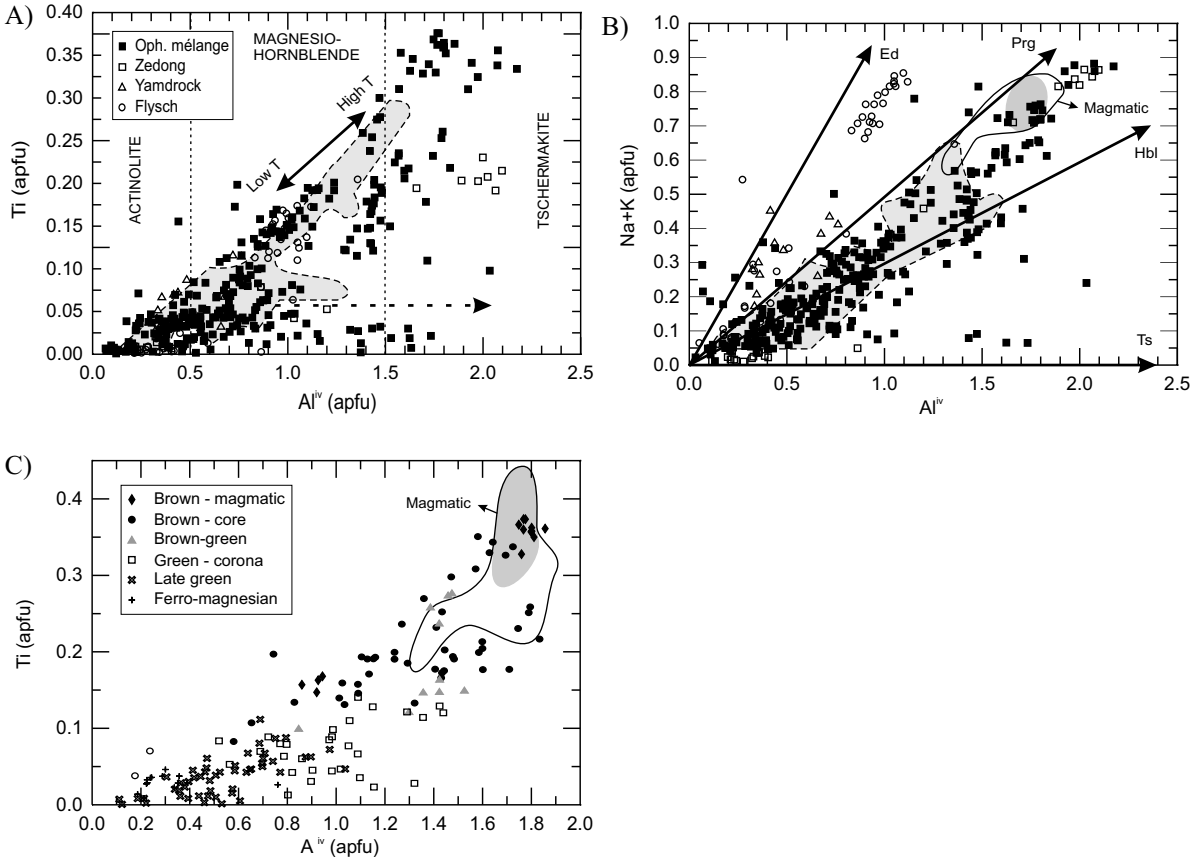

FIG. 2.4 – Compositional variations of amphibole from mafic rocks of the three geological units. A) Ti vs. Al^{iv}. The continuous arrow represents the temperature-dependent compositional variation of amphiboles replacing plagioclase and possibly garnet. Subdivisions in terms of Al^{iv} are from Leake et al. (1997). B) Na + K vs. Al^{iv}. Edenitic (Ed), pargasitic (Prg), and tschermakitic (Ts) substitutions are indicated along with an idealized hornblende (Hbl) substitution (Hietanen, 1974). Dashed light grey field outlines compositions in mafic rocks from the Beimarang serpentinite mélange (Huot et al., 2002). C) Ti vs. Al^{iv} for mafic rocks showing a temperature trend from brown magmatic amphibole to greenish metamorphic amphibole. Field outlines magmatic amphibole compositions from oceanic gabbros, with main compositions shaded in grey (Coogan et al., 2001).

2.4 Whole-rock chemistry

2.4.1 Analytical methods

Compositions of representative mafic rocks of the three geological units are given in Table 2.1.

La méthode analytique est décrite à la section 1.2 et les données complètes sont présentées à l'«Annexe D ».

TAB. 2.1 – Original compositions of representative mafic rocks. Values in wt.% (oxides and LOI) and ppm (minor and trace elements).

	Ophiolitic mélange		Intermediate		Yamdrock mélange		Flysch		Intrusion	Intra-oceanic arc		
	LIU-09	QUM-01	MAM-01	MAM-02	XIA-04	BAG-05	PAZ-06	ZIS-08	LHA-31	JNL-01	LHA-18	BUM-03
SiO_2	51.18	50.51	47.41	47.64	46.27	47.94	47.97	55.90	47.57	56.38	55.81	58.67
TiO_2	1.15	0.67	1.15	2.45	4.18	2.15	2.49	2.01	1.40	0.83	0.37	0.87
Al_2O_3	16.64	14.47	16.15	15.43	12.43	13.02	13.85	12.35	14.49	16.98	18.37	16.52
Fe_2O_3	9.56	8.13	10.50	11.24	16.54	13.91	11.85	11.21	13.10	6.86	3.50	4.38
MnO	0.16	0.11	0.16	0.21	0.20	0.27	0.16	0.18	0.21	0.20	0.07	0.06
MgO	3.98	7.85	6.09	7.29	4.29	6.47	6.50	2.15	6.78	4.04	2.55	1.76
CaO	7.64	8.33	9.40	5.30	7.98	7.68	8.81	5.54	10.22	4.69	10.48	4.85
Na_2O	6.60	3.36	4.05	4.89	4.06	3.60	2.48	3.02	2.78	3.99	5.91	4.65
K_2O	0.18	0.70	0.34	0.23	0.43	0.12	0.90	2.26	0.05	3.32	0.04	3.17
P_2O_5	0.11	0.05	0.09	0.27	0.58	0.29	0.33	0.63	0.11	0.37	0.03	0.40
LOI	2.70	3.42	3.85	3.69	2.36	2.68	3.28	1.92	2.24	2.06	1.99	2.09
Total	99.99	97.69	99.33	98.77	99.55	98.33	98.80	97.36	99.09	99.98	99.19	97.88
Cr	36.20	203.50	332.60	124.20	24.90	104.30	139.10	<10.9	167.20	55.90	36.60	11.10
V	241.80	200.10	234.20	373.80	419.30	361.70	264.30	125.70	330.90	167.50	96.60	92.90
Y	35.39	18.06	23.93	42.60	54.30	39.84	28.83	66.76	30.93	17.40	19.61	9.25
Zr	108.48	41.50	65.80	173.70	346.05	172.41	220.14	509.60	84.96	133.96	150.72	133.30
Nb	1.35	0.26	1.21	6.62	46.53	23.82	16.26	36.20	2.33	6.05	0.90	5.42
La	3.59	0.85	2.22	6.58	35.30	15.17	22.20	68.56	4.31	22.01	3.59	60.24
Ce	11.36	3.56	7.67	20.10	82.96	35.18	52.21	154.56	12.06	48.29	9.35	131.58
Pr	1.85	0.68	1.32	3.17	10.98	4.39	6.71	19.22	1.96	6.03	1.30	15.72
Nd	9.65	3.97	7.41	16.53	47.87	20.26	30.05	79.02	10.40	23.96	5.91	61.63
Sm	3.28	1.57	2.61	5.25	11.22	4.70	7.03	17.00	3.55	4.52	1.72	9.51
Eu	1.22	0.60	0.99	1.52	3.38	1.59	2.30	4.03	1.43	1.41	0.63	2.14
Gd	4.48	2.18	3.51	6.67	11.35	5.92	6.86	15.80	4.96	3.94	2.37	5.34
Tb	0.82	0.43	0.66	1.22	1.74	0.92	1.04	2.26	0.82	0.50	0.42	0.51
Dy	5.18	2.70	4.13	7.71	9.53	5.93	5.64	11.83	5.83	3.00	2.94	1.92
Ho	1.26	0.66	0.97	1.87	2.05	1.27	1.22	2.55	1.20	0.57	0.64	0.34
Er	3.52	1.80	2.68	5.17	5.21	3.58	3.02	6.38	3.51	1.56	2.00	0.77
Tm	0.53	0.27	0.41	0.78	0.73	0.51	0.43	0.90	0.49	0.22	0.30	0.10
Yb	3.61	1.81	2.66	5.28	4.62	3.23	2.75	5.63	3.16	1.37	2.09	0.63
Lu	0.51	0.26	0.38	0.76	0.64	0.51	0.39	0.77	0.46	0.21	0.33	0.09
Hf	2.61	1.11	1.86	4.55	8.21	3.55	6.13	12.05	2.28	2.92	3.60	3.75
Ta	0.11	0.02	0.10	0.49	3.27	1.33	1.30	2.44	0.17	0.38	0.09	0.37
Th	0.20	<0.06	0.10	0.65	5.00	2.07	4.93	19.52	0.96	5.05	0.62	22.32
U	0.09	0.02	0.09	0.24	1.43	0.56	1.10	3.39	0.19	1.33	0.28	5.70

2.4.2 Rock classification

Mafic rocks from the ophiolitic mélange and the sedimentary units were plotted on a series of discrimination diagrams for rocks of basaltic to andesitic composition (not shown) in order to distinguish between possible tectonic environments [see reviews by Rollinson (1993) and Pearce (1996)]. The distinction between these three units is revealed by the diagrams and clearly suggest different tectonic settings (see the following discussion). Note that coarser-grained gabbros and diabases were plotted together with basalts since they do not show cumulus textures. They fit very well the compositional criteria proposed by Pearce (1996). Moreover, we observed that the majority of samples from one unit have very similar geochemical characteristics, independently of their grain size.

The Zr/Ti vs Nb/Y diagram of Winchester and Floyd (1977), revised by Pearce (1996), classifies rocks by their alkalinity and stage of differentiation (Fig. 2.5). Most samples from the ophiolitic mélange show an intermediate level of differentiation, they have compositions transitional between basalt and basaltic andesite, generally at the alkaline-poor end-member of this large field. Samples from Qumei containing olivine pseudomorph are among the most tholeiitic, while samples from Buma/Lhabuxi and Zedong/Jinlu regions containing brown prismatic magmatic amphibole are more alkaline. A gabbro (2001-LHA-16) of average composition is intruded by a more basic diabase intrusion (2001-LHA-17) and cut by a more evolved granodiorite vein (2001-LHA-18). Samples from the Yamdrock mélange are basaltic and generally alkaline. A few samples are subalkaline and probably represent intermediate compositions. Samples from the flysch show a trend from compositions similar to those of the Yamdrock mélange (alkali basalt) towards more evolved and subalkaline andesitic compositions.

2.4.3 Trace-element geochemistry

Normalized to chondrites, rocks of the ophiolitic mélange have flat REE patterns typical of N-MORB with a slight depletion in the most incompatible LREE (Fig. 2.6). However, on multi-element patterns normalized to the primitive mantle, slight negative anomalies in Nb-Ta and Ti diverge from the typical N-MORB signature (Sun and McDonough, 1989) and indicate a subduction component. Our data correlates particularly well with basalts from the Lau Basin, the back-arc basin of the Tonga Arc (Ewart et al., 1994a ; 1994b). Our data also show some correlation with basaltic to andesitic rocks from particular islands of intra-oceanic arcs, such as the Tonga-Kermadec arc (Turner et al., 1997 ; Regelous et al., 1997 ; Ewart et al., 1998), the Izu-Bonin-Mariana arc

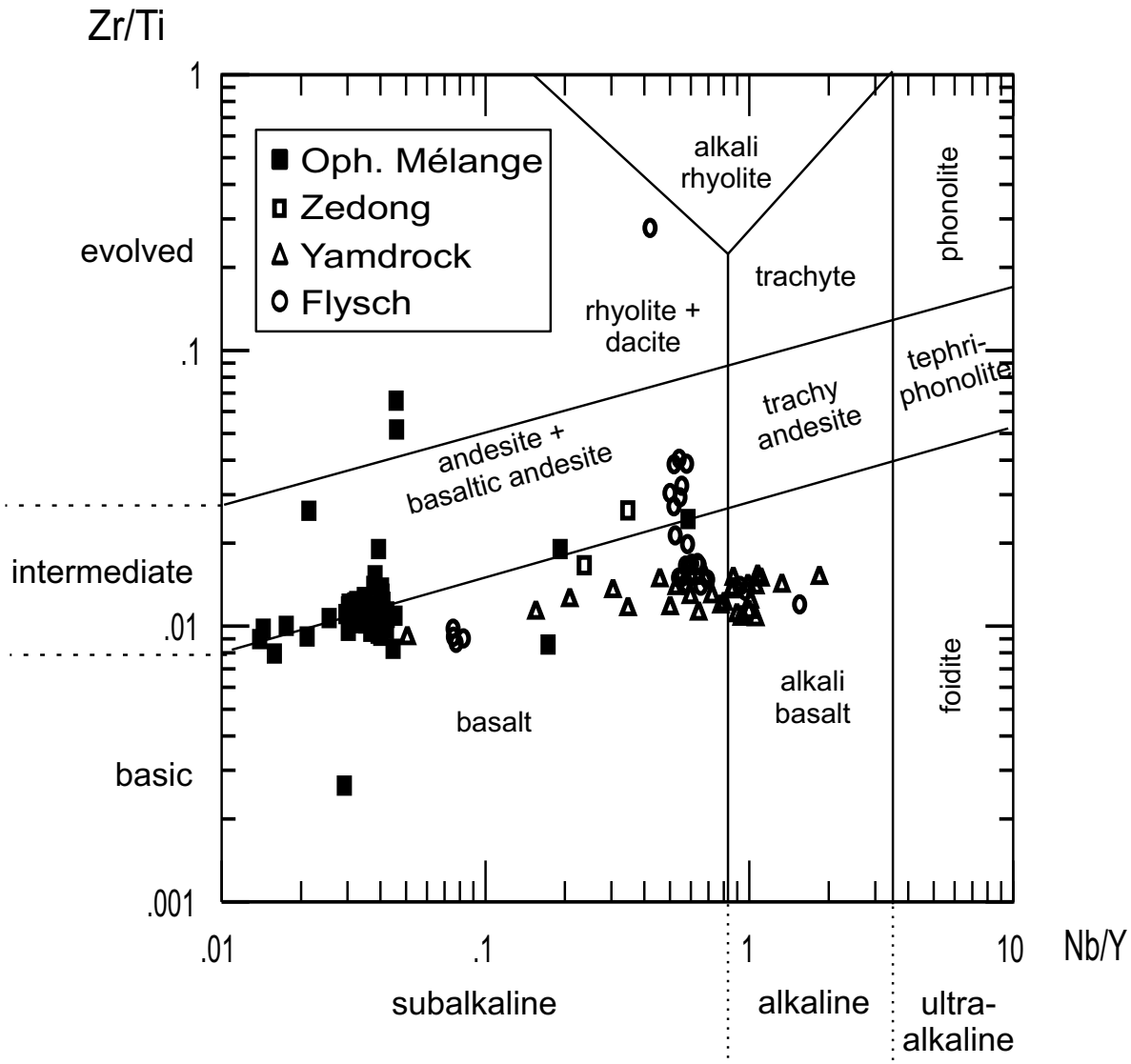

FIG. 2.5 – Zr/Ti vs. Nb/Y diagram of Winchester and Floyd (1977) with fields revised by Pearce (1996).

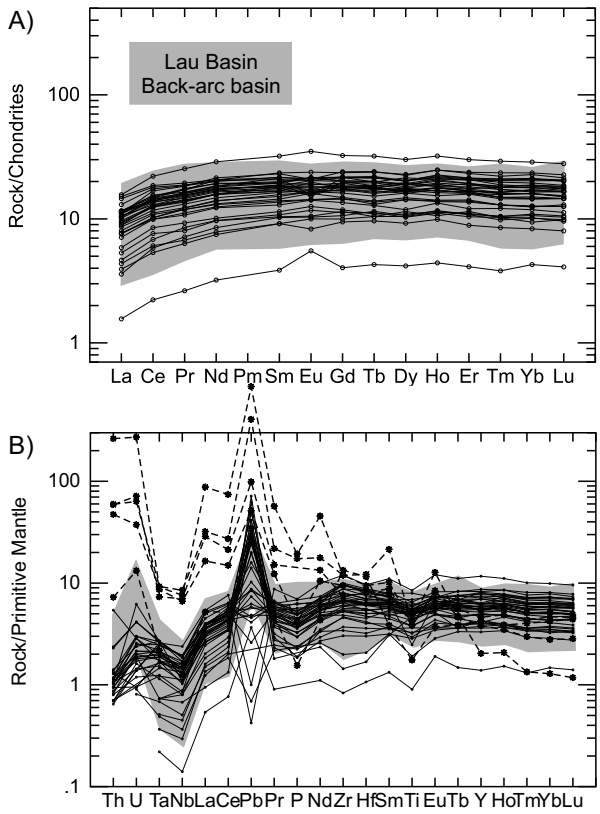

FIG. 2.6 – Geochemistry of mafic rocks from the ophiolitic mélange. A) REE patterns normalized to chondrites ; B) multi-element patterns normalized to primitive mantle. The grey fields outline the compositional range of mafic rocks from the back-arc basin of the Tonga arc (Ewart et al., 1994a ; 1994b). Dashed lines in B represent individual samples from the Buma/Lhabuxi and Zedong/Jinlu areas with more evolved intra-oceanic arc signatures.

(Hawkesworth et al., 1977 ; Elliott et al., 1997 ; Taylor and Nesbitt, 1998 ; Pearce et al., 1999), and the South Sandwich arc (Hole et al, 1984 ; Pearce et al., 1995). Overall trace-element patterns are similar, the main differences being the nearly flat REE profiles (no LREE-depletion) and the strong enrichment in U-Th observed on the intra-oceanic arc patterns. Individual samples from the Buma/Lhabuxi and Zedong/Jinlu regions are LREE-enriched and show strong Nb-Ta and Ti negative anomalies (Fig. 2.6), characteristics observed in ophiolitic lavas from the Jinlu (Zedong) area (Dubois-Côté et al, 2003 ; in press). These samples correlate well with more evolved volcanic rocks of the previously mentioned intra-oceanic arcs.

By contrast, rocks of the Yamdrock mélange have patterns that are LREE-enriched and show slight positive Nb-Ta anomalies (Fig. 2.7). This geochemical signature is typical of ocean-island basalt (OIB) (Sun and McDonough, 1989). Furthermore, our

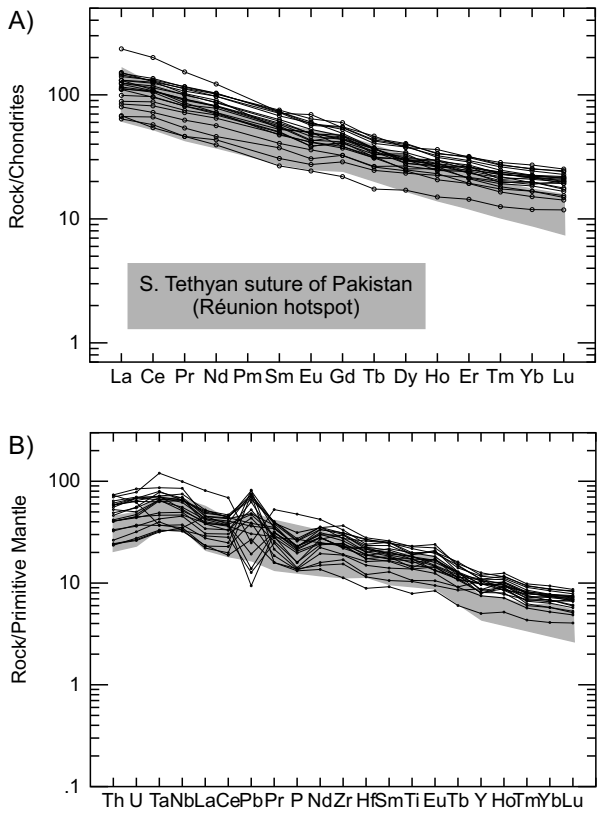

FIG. 2.7 – Geochemistry of mafic rocks from the Yamdrock mélange. A) REE patterns normalized to chondrites ; B) multi-element patterns normalized to primitive mantle. The grey fields outline the compositional range of marine volcanic rocks from the South Tethyan suture zone (STSZ) of Pakistan (Mahoney et al., 2002).

data correlate well with data from the South Tethyan suture zone (STSZ) of Pakistan, the western equivalent of the YZSZ (Mahoney et al., 2002). Marine volcanic rocks of STSZ of Pakistan are believed to be products of the Réunion hotspot located in the Indian Ocean (Mahoney et al., 2002). The overall REE geochemical signature of rocks from the flysch is similar to that of the Yamdrock mélange, but a closer look at multi-element patterns reveals some important differences (Fig. 2.8). LREE are slightly more enriched, while slight negative Nb-Ta and Ti anomalies are observed. Positive Pb and negative P anomalies are also more prominent. All these geochemical characteristics are also observed on patterns of basaltic lavas from the western Deccan Traps of India (Peng and Mahoney, 1995 ; Peng et al., 1994), all of which suggest some extent of crustal contamination. Intrusive rocks from the flysch appear to have no relation to the older rocks found in the mafic blocks. Indeed, they show nearly flat patterns with slight negative Nb-Ta and Ti anomalies.

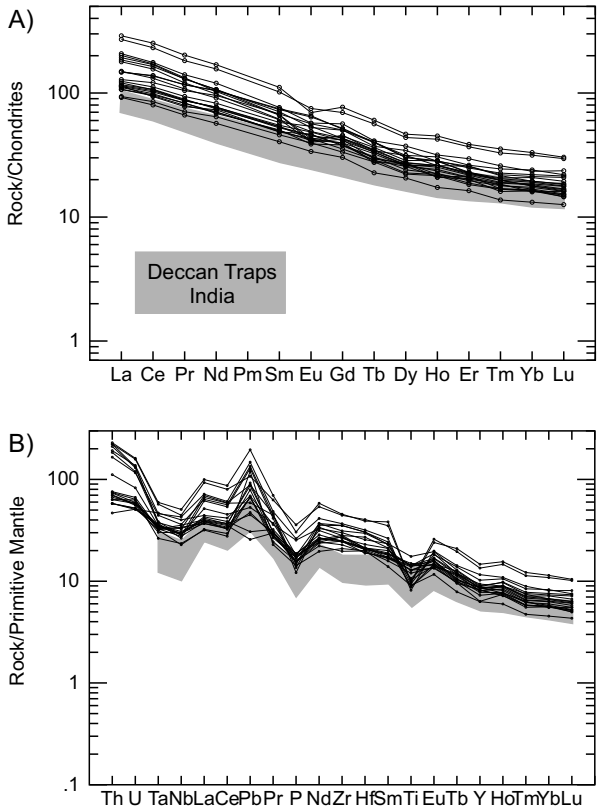

FIG. 2.8 – Geochemistry of mafic rocks from the Triassic flysch. A) REE patterns normalized to chondrites ; B) multi-element patterns normalized to primitive mantle. The grey fields outline the compositional range of basaltic lavas from the western Deccan Traps of India (Peng et al., 1994 ; Peng and Mahoney, 1995).

2.5 Geodynamic implications

2.5.1 Ophiolitic mélange

Compared to diverse modern-day geodynamic settings, clinopyroxene compositions from the ophiolitic mélange are generally most similar to those of clinopyroxenes from back-arc basin basalts and boninites, although some plot in the fields for clinopyroxenes from island-arc tholeiites and N-MORB (Fig. 2.3D). Scattering of the data is reminiscent of the large array of magma compositions found in any supra-subduction-zone setting, and in particular that from back-arc regions (Hawkins and Melchior, 1985 ; Hawkins and Allan, 1994). The occurrence of TiO_2-rich aluminous brown amphibole of probable magmatic origin is also in agreement with a supra-subduction-zone origin, an environment richer in volatiles than mid-ocean ridges (Hawkins and Melchior, 1985). On whole-rock discrimination diagrams, all samples classify as tholeiitic rocks. They generally plot in the overlapping fields for N-MORB and volcanic-arc basalts (VAB) (Fig. 2.9) or in the adjacent fields for N-MORB and island-arc tholeiites (IAT) (Fig. 2.10). The trace-element patterns indicate a strong N-MORB component, while the slight negative Nb-Ta and Ti anomalies on multi-element patterns suggest the influence of an arc component (Fig. 2.6). Such patterns are characteristic of marginal basins (Pearce, 1996). Hence, mafic rocks from the ophiolitic mélange are interpreted as having crystallized from tholeiitic magmas derived from a moderately depleted mantle source affected by a subduction component. Trace-element comparison with modern-day oceanic settings reveals that the majority of our samples correlate better with back-arc basin mafic rocks (e.g. Lau Basin) than with intra-oceanic islands arcs (e.g. Tonga-Kermadec, Izu-Bonin-Mariana and South Sandwich arcs), although some samples show strong arc-related characteristics. This suggest a supra-subduction-zone origin, in agreement with the conclusions reached for the previously studied Beimarang mélange (Huot et al., 2000) and associated YZSZ ophiolites (Hébert et al., 2000 ; 2001 ; 2003 ; Dubois-Côté et al., 2003 ; in press). This study thus confirms that mafic rocks from the ophiolitic mélange all along the central YZSZ are derived from tectonic disruption of the ophiolites. Furthermore, it is now recognized that many of the best-developed ophiolites have the geological and geochemical characteristics of supra-subduction environments (see reviews by Hawkins (2003), and Pearce (2003)), and the YZSZ ophiolites are no exception.

Sample from the ophiolitic mélange in the adjacent regions of Buma and Lhabuxi, including the granodiorite sample, and in the Zedong/Jinlu area, generally fall in the field for volcanic-arc basalts, extending from island-arc tholeiites (IAT) to calc-alkaline basalts (CAB) (Fig. 2.10). Moreover, as observed for Eastern ophiolites (Dubois-Côté

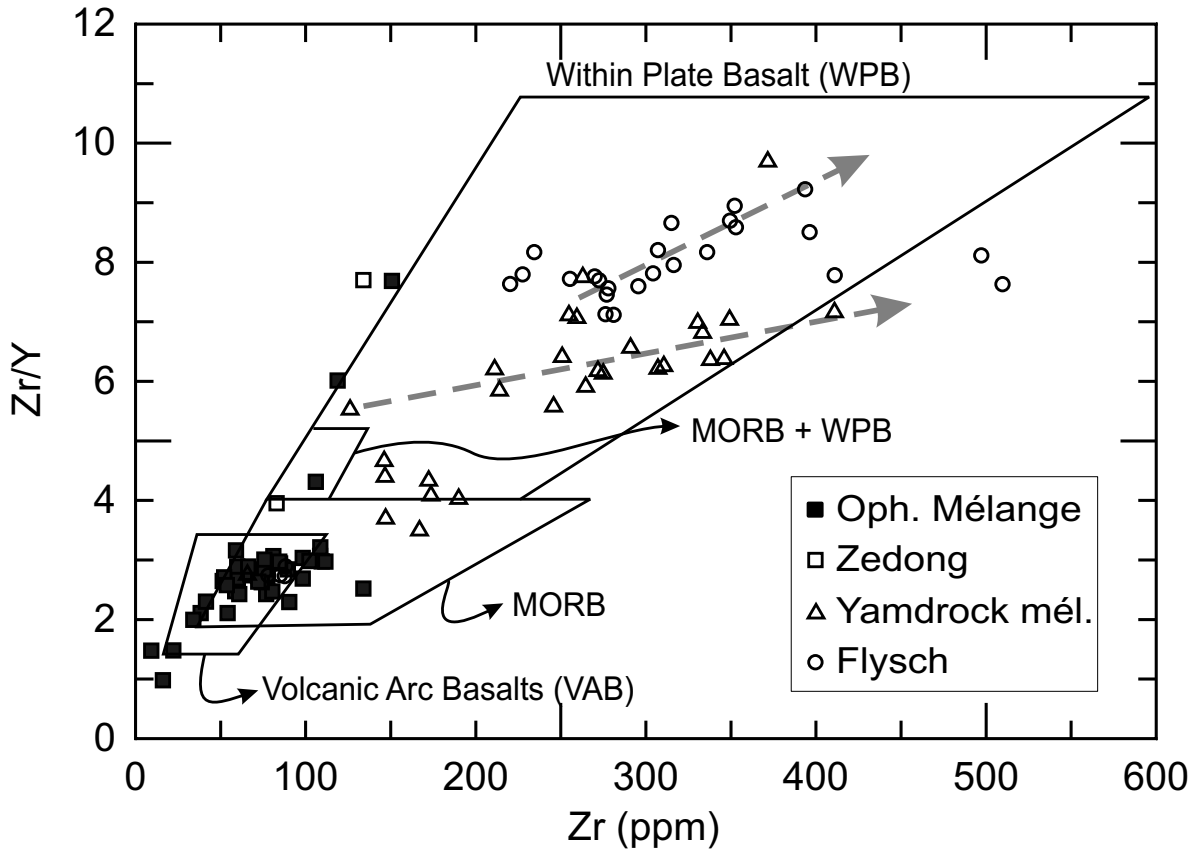

FIG. 2.9 – Zr/Y-Zr discrimination diagram for basalts (Pearce and Norry, 1979).

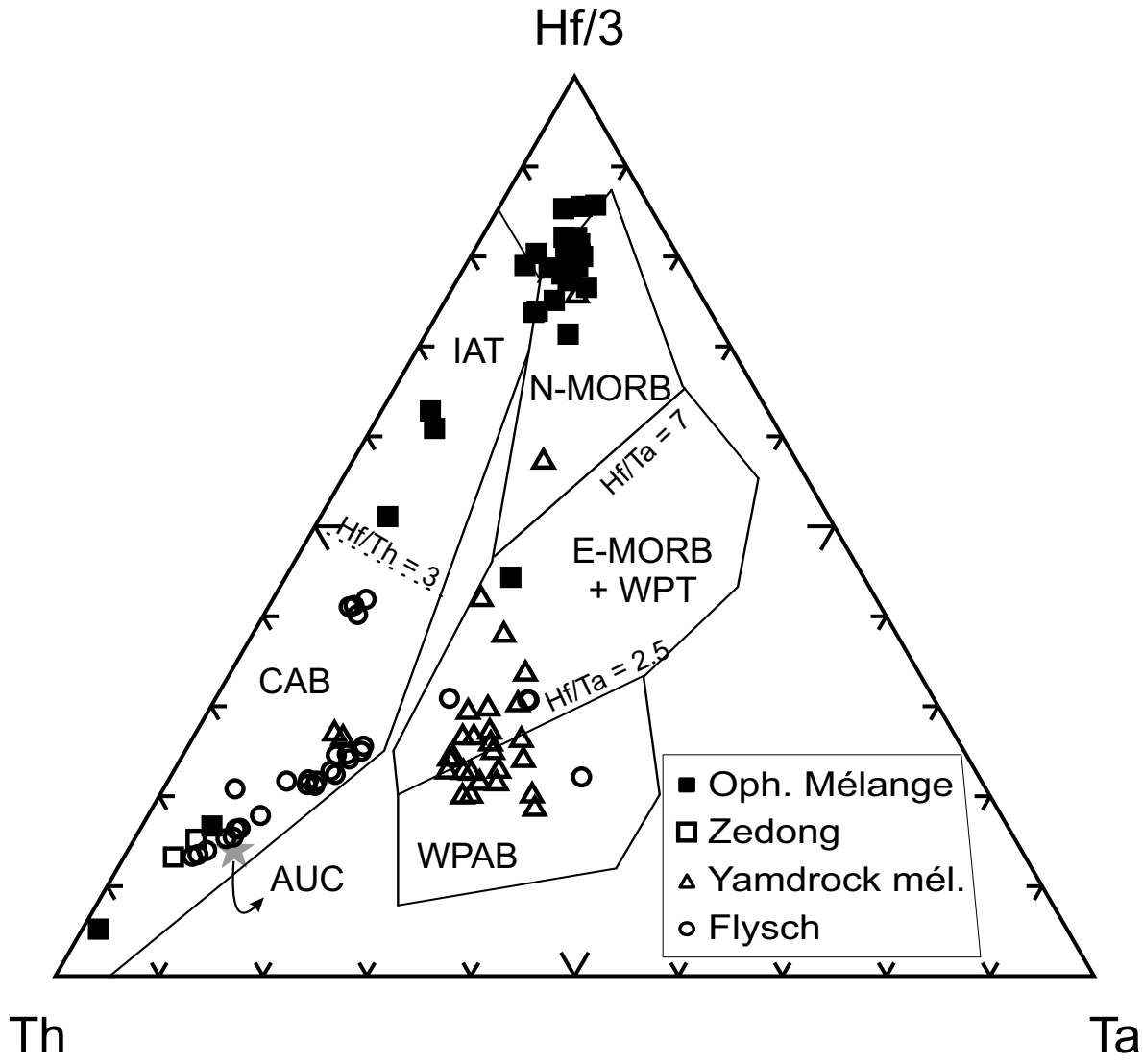

FIG. 2.10 – Th-Hf-Ta discrimination diagram for basalts (Wood, 1980). Key : MORB = mid-ocean ridge basalt ; WPT = within plate tholeiite ; WPAB = within plate alkaline basalt ; IAT = island-arc tholeiite ; CAB = calk-alkaline basalt ; and AUC = average upper crust.

et al., 2003 ; in press), their trace-element patterns are LREE-enriched and show strong negative Nb-Ta and Ti anomalies, and are characteristic of evolved oceanic arc to continental arc (e.g. Pearce, 1996). Based on field observations, McDermid et al. (2000, 2001, 2002) proposed that gabbros, diorites, basaltic-andesite volcanics and volcaniclastics in the Zedong area may represent relicts of a Late Jurassic to Early Cretaceous intra-oceanic magmatic arc within the Neotethys. In agreement with brown magmatic amphibole chemistry, these particular samples are alkali-rich (Na_2O + K_2O reaching 7.8 wt.%), and we suggest that they follow a shoshonitic trend.

2.5.2 Sedimentary units

By contrast, clinopyroxene from the sedimentary units fall mainly in the field of N-MORB, with a few plotting in the fields of back-arc basin basalts and boninites (Fig. 2.3D). The general trend towards an Al-(Ti+Cr)-enriched end-member (outside the outlined fields) suggests crystallization from an enriched mantle source. On whole-rock discrimination diagrams, samples from the Yamdrock mélange generally classify as alkaline rocks, whereas those from the flysch seems to be intermediate, classifying as both alkaline and tholeiitic. On the Zr/Y vs. Zr diagram (Fig. 2.9), samples from both sedimentary units generally plot in the field for within-plate basalts (WPB), although they define two distinct trends. Furthermore, on the Th-Hf-Ta ternary diagram (Fig. 2.10), samples from the Yamdrock mélange generally fall in the fields for WPB, while those from the flysch fall in the field for calc-alkaline basalts (CAB). Similarly, trace-element geochemistry for both units is similar to that of ocean-island basalts (OIB), but slight negative Nb-Ta and Ti anomalies again suggest that a continental subduction or crustal contamination component may be involved in the formation of mafic rocks found in the flysch.

Mafic rocks from the Yamdrock mélange most probably represent alkaline magmas derived from an enriched mantle source of intraplate type, such as a mantle plume, contrasting with the ophiolite geochemistry. Comparison with modern-day oceanic settings further illustrates the great similarity between our data and data from ocean islands or seamounts. Our data correlate especially well with data from the STSZ of Pakistan (Fig. 2.7). According to Mahoney et al. (2002), most STSZ samples have Nd-Pb-Sr isotopic ratios close to those expected for modern-type Réunion source in the Late Cretaceous, and their incompatible element patterns resemble those of recent Réunion shield lavas. However, the 65-66 Ma Deccan Traps of India are commonly believed to represent the initial, plume-head stage of the Réunion hotspot development (e.g. Duncan and Richards, 1991 ; Campbell, 1998). Mahoney et al. (2002) have shown that a Late Cretaceous pre-Deccan marine phase of Réunion hotspot activity on the Tethyan

side of Greater India, as recorded by the marine volcanic rocks of the STSZ of Pakistan, can be accomodated within the framework of the plume-head model. The presence of oceanic seamounts has previously been noted on a paleogeographic reconstruction of the Early Jurassic in southern Tibet (Liu and Einsele, 1999), but linking them to an early stage of the Réunion hotspot is hazardous considering the data at hand. Nevertheless, mafic rocks from the Yamdrock mélange can be interpreted as plume-related intraplate alkaline mafic rocks of OIB-type. The Yamdrock mélange is reminiscent of a subduction complex and consists mostly of material off-scraped from the down-going slab (Ziabrev et al., 2001). Hence our conclusion that mafic blocks from this unit are intraplate igneous products is consistent.

By comparison, the geodynamic interpretation of mafic rocks from the Triassic flysch involves more than one process. Although the geochemical characteristics generally indicate a similar enriched mantle source of intraplate type, they also strongly suggest the influence of a continental subduction or crustal contamination component. On the Zr/Y vs. Zr diagram (Fig. 2.9), the rocks define a linear trend whose slope is intermediate between that of an enriched-mantle trend (high increase in Zr/Y with respect to Zr) and a fractional-crystallization trend (no change in Zr/Y with respect to Zr). This suggests that an originally enriched source coupled with further enrichment through crustal assimilation may be involved. On the Th-Hf-Ta ternary diagram (Fig. 2.10), the same samples define a linear trend starting from an enriched source (WPB, as shown for samples of the Yamdrock mélange) and leading toward an average upper crust (AUC) reservoir.

The comparison of multi-element geochemistry with modern-day oceanic settings (Fig. 2.8) is particularly instructive. Our data correlate with neither typical intraplate-type rocks, which show none to small positive Nb-Ta and Ti anomalies, nor calc-alkaline rocks, which on the contrary show strong negative anomalies in these elements be trapped in the subducting slab. On the other hand, a very satisfactory correlation exists with volcanic rocks of the western Deccan Traps of India, as mentioned earlier. According to Peng et al. (1994), and Peng and Mahoney (1995), age-corrected Nd-Pb-Sr isotopic ratios of these lavas define different trends which reflect mixing between a mantle end-member very similar to that of Réunion Island and at least four different Indian Archean continental lithospheric end-members possessing more negative ϵ_{Nd} but highly variable $^{87}Sr/^{88}Sr$ and $^{206}Pb/^{204}Pb$. If we assume that mafic rocks from the flysch are similar, we can also assume that their trace-element geochemistry reflects mixing between a plume-related intraplate alkaline mantle end-member and a continental lithospheric end-member.

By analogy with the Deccan Traps, the component of crustal contamination is pro-

bably derived from the Indian continental lithosphere, and the contamination process may be related to opening of the Neotethys ocean during Late Triassic time (Gaetani and Garzanti, 1991). The higher modal abundance of quartz in mafic rocks from the flysch, compared to those from the Yamdrock mélange, indicates SiO_2 supersaturation that could have resulted from assimilation of a felsic component. A granitic rock, analogous to the granite sample taken from a granitic block in the flysch, is a good candidate. It is characterized by a very fractionated REE pattern (strong negative slope and LREE-enrichment) and a multi-element pattern which shows strong negative Nb-Ta and Ti anomalies, even where compared to average upper continental crust (Taylor and McLennan, 1981). The extremely fractionated geochemistry of the granite indicates that it has experienced at least one episode of remelting and represents a highly evolved end-member.

2.5.3 AFC modelling

To constrain better the contribution of the granitic contamination on the geochemistry of mafic rocks, assimilation and fractional crystallization (AFC) modelling was performed using the program MIXNFRAC (Nielsen, 1988 ; 1990). We modelled major- and trace-element concentrations. Since mafic rocks from both the flysch and Yamdrock mélange units are believed to have a common intraplate source, rock compositions falling close to the OIB end-member, for both units, have been used as starting compositions, whereas the granite composition was used as the assimilant composition. The same starting composition was crystallized for assimilation factors of 0 to 1, where the assimilation factor is tied to the increment of crystallization. For example, an assimilation factor of 1 represents the case where for each fraction of mineral removed, an equal mass of the contaminating magma is added to the system (Nielsen, 1988). For each assimilation step, we considered the resulting composition at the onset of apatite crystallization as the most representative of our rocks' mineral composition, i.e. plagioclase, augite and spinel, probably subsequently replaced by oxydes. The best fit with our data indicates that the geochemical compositions of mafic rocks from the flysch reflect mixing between an intraplate mantle source end-member and a granitic end-member (Fig. 2.11). Most compositions can be obtained with an assimilation factor around 0.05, although some need an assimilation factor of almost 0.3, after 67-73% fractional crystallization. An assimilation factor value of 0.3 is arguably the maximum allowable if heat balance is to be maintained (Grove and Kinzler, 1986).

2.5.4 Summary

The $(Ta/Th)_N$ and $(La/Sm)_N$ ratios summarize very efficiently the different general chemical behavior, as well as the related tectonic setting and evolution, of mafic rocks from the three geological units (Fig. 2.11). On this diagram, samples from the ophiolitic mélange plot on the N-MORB pole but extend towards the IAT end-member, confirming their back-arc basin affinity (Huot et al., 2002). They are not affected by important fractional crystallization processes. Samples from the Buma/Lhabuxi and Zedong/Jinlu areas extend towards the CAB and global subducting sediments (GLOSS) end-members, except for the unique diabase 2002-BUM-03 which has a much smaller $(Ta/Th)_N$ ratio extending towards the granite composition. They fall close to a modelled AFC trend using a typical ophiolitic mélange gabbro composition as the starting composition and the GLOSS pole as the assimilant. The results confirm the presence of an intra-oceanic arc within the Neotethys. The unique diabase sample is more felsic (see its major element composition in Table 2.1) and may have experienced some continental contamination.

Samples from the Yamdrock mélange define a trend from the primitive mantle (PM) pole through E-MORB and OIB, slightly extending towards the lower continental crust (LCC) pole, although most sample compositions are intermediate between OIB and E-MORB. The fairly constant $(Ta/Th)_N$ ratio along this trend reveals that the rocks have been affected solely by fractional crystallization (FC) processes. Samples from the Triassic flysch define a trend from compositions similar to those of the Yamdrock mélange towards compositions falling between the calc-alkaline basalts (CAB) and upper continental crust (UCC) poles. These last compositions fall in the field for sedimentary rocks sampled in the matrix of the Yamdrock mélange and flysch. The large decrease in the $(Ta/Th)_N$ ratio with increasing $(La/Sm)_N$ ratio along this trend reveals that the rocks have been affected by processes of both assimilation and fractional crystallization (AFC). Moreover, this trend points directly toward the extremely differentiated granite end-member and can realistically be reproduced by calculated AFC processes using the granite as a contaminant analogue. The AFC trend defined by mafic rocks from the flysch confirms that they are derived from intraplate-type alkaline magmas which have assimilated Indian continental lithosphere containing Cambro-Ordovician granitic batholiths during opening of the Neotethys Ocean. Intrusive samples from the flysch fall very close to the IAT end-member, and their geochemistry probably reflects a younger intra-oceanic arc setting, rather than the Late Triassic rifting event.

2.6 Conclusion

The petrography, the mineral chemistry and the whole-rock chemistry of mafic rocks from the ophiolitic mélange, the Yamdrock mélange and the Triassic flysch, along the Yarlung Zangbo Suture Zone of Southern Tibet, revealed a distinct origin and/or evolution for the three units. Although rocks from all three units have a similar primary mineral composition, the secondary mineral assemblages indicate that rocks of the ophiolitic mélange have been affected by relatively higher grade metamorphism. The compositions of clinopyroxene and primary amphibole clearly indicate that mafic rocks from the sedimentary units are more fractionated and crystallized from an alkali-enriched source in comparison with rocks from the ophiolitic mélange. Clinopyroxene also records a supra-subduction-zone signature for rocks of the ophiolitic mélange. The whole-rock chemistry, especially the trace elements, confirms these observations and further confirms that the mafic rocks from the ophiolitic mélange represent tholeiitic rocks of supra-subduction-zone affinity (back-arc basin to intra-oceanic island arc), whereas those from the sedimentary units represent alkaline rocks derived from an enriched mantle source of intraplate type. Superimposed processes of fractional crystallization and partial assimilation of Cambro-Ordovician granitic batholiths of the Indian crust, associated with the magmatism resulting from the opening of the Neotethys basin, overprint the intraplate signature of mafic rocks from the Triassic flysch by producing slight LREE-enrichment and negative Nb-Ta and Ti anomalies. A good analogy can be made with volcanic rocks of the Réunion hotspot and the western Deccan Traps of India. Individual samples of the ophiolitic mélange from the Buma/Lhabuxi and Zedong areas confirm the presence of an intra-oceanic arc within Neotethys during the Late Jurassic to the end of the Early Cretaceous. The heterogeneous mélange-type units south of the YZSZ ophiolites thus record the entire history of the Neotethys oceanic basin, from its opening in the Late Triassic to the India-Asia collision in the Early Tertiary, resulting in the obduction of the ophiolites and the destruction of the passive Indian paleomargin.

Acknowledgments

We would like to thank the funding organization (NSERC/Grant no. 1253 to R. Hébert) for financial support of the Tibet project. We are also grateful for the Chinese contribution by Dr. C.S. Wang (Outstanding Research Award of China). The first author also thanks the NSERC (scholarship PGS B) and FCAR for financial support. We are also thankful to M. Choquette for microprobe analyses and to R. Gosselin for ICP-AES and ICP-MS analyses. The manuscript was kindly reviewed by Dr. T. Feininger (U. Laval), and has further benefited from critical comments by R. Rudnick, S.L. Chung and G.P. Yumul.

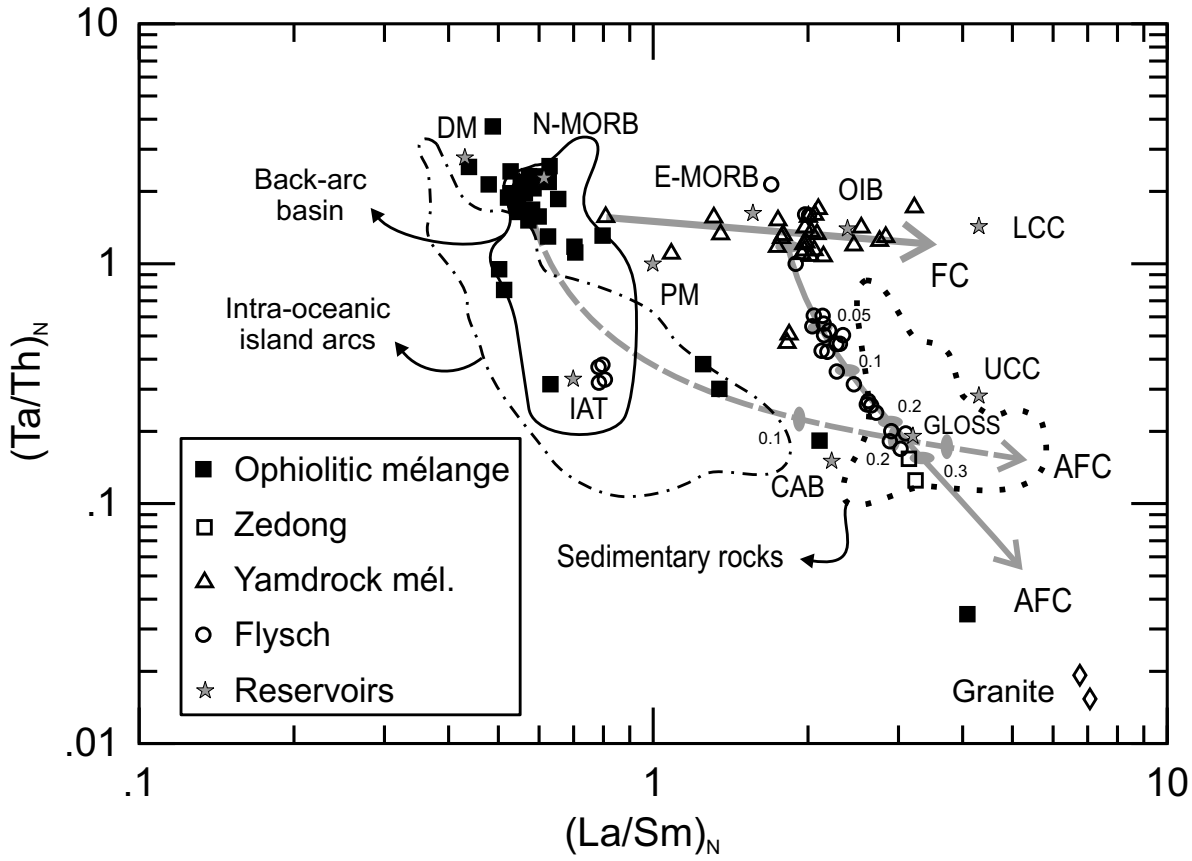

FIG. 2.11 – $(Ta/Th)_N$ vs. $(La/Sm)_N$ for mafic rocks from the three geological units. DM (depleted mantle) from Mckenzie and O'Nions (1991) except for Ta and Th from Chauvel et al. (1992). PM (primitive mantle), N-MORB, E-MORB and OIB from Sun and McDonough (1989). IAT (island-arc tholeiite) and CAB (calc-alkaline basalt) from Sun (1980). LCC (lower continental crust) from Weaver and Tarney (1984). UCC (upper continental crust) from Taylor and McLennan (1981). GLOSS (global subducting sediment) from Plank and Langmuir (1998). FC = fractional crystallization and AFC = assimilation and fractional crystallization. The continuous field outlines basalt compositions from the Lau Basin, the back-arc basin of the Tonga Arc (Ewart et al., 1994a ; 1994b). The dashed-stippled field outlines basaltic to andesitic compositions from particular islands of intra-oceanic arcs, such as the Tonga-Kermadec arc (Turner et al., 1997 ; Regelous et al., 1997 ; Ewart et al., 1998), the Izu-Bonin-Mariana arc (Hawkesworth et al., 1977 ; Elliott et al., 1997 ; Taylor and Nesbitt, 1998 ; Pearce et al., 1999), and the South Sandwich arc (Hole et al, 1984 ; Pearce et al., 1995). The stippled field represents compositions of sedimentary rocks sampled in the Yamdrock mélange and flysch units.

Chapitre 3

«The Yarlung Zangbo Suture Zone ophiolitic mélange (southern Tibet) : New insights from geochemistry of ultramafic rocks »

C. Dupuis[a], R. Hébert[a], V. Dubois-Côté[a], C. Guilmette[a], C.S. Wang[b], Y.L. Li[b], Z.J. Li[b]

[a] *Département Géologie et génie géologique, Université Laval, Ste-Foy, Québec, Canada, G1K 7P4*

[b] *Université de Technologie de Chengdu, Chengdu, Sichuan, 610059, R.P. Chine*

Soumis à *Journal of Asian Earth Sciences* le 6 mars 2004 ; accepté le 12 septembre 2004

Cet article traite de la pétrographie et de la géochimie des roches ultramafiques du mélange ophiolitique. Les péridotites peuvent être subdivisées en trois groupes. Les lherzolites et harzburgites à Cpx correspondent à des péridotites abyssales fertiles avec des profils lisses appauvris en TR légères. Les harzburgites transitionnelles correspondent à des péridotites abyssales appauvries ou de zone de supra-subduction, les TR montrant un appauvrissement continu des TR lourdes aux TR médianes et un léger enrichissement des TR légères résultant d'interactions avec un magma. Les harzburgites et dunites montrent des profils en forme de U caractéristiques d'interactions entre des résidus mantelliques appauvris en TR et un magma enrichi en TR légères. La modélisation de la fusion fractionnée, en accord avec les Mg# et Cr# du spinelle, indique que les harzburgites à Cpx pourraient être les résidus de 5-15% de fusion, les harzburgites transitionnelles de 15-23% et les harzburgites et dunites de 22-29%. Le

système arc-bassin des Sandwichs Sud est considéré comme un analogue moderne de l'environnement géodynamique initial.

3.1 Introduction

Le contexte géologique est présenté à la section 1.3.

Previous studies have shown the heterogeneity of the lithological units found along the YZSZ (see the review in Huot et al., 2002). Here we present new observations and geochemical data on ultramafic blocks of the ophiolitic mélange along a 500km-long section of the central YZSZ, from Lhaze to Zedong (south of Lhasa), and including the Beimarang area (Figs 1.1-1.2). Our aim is to enlarge the restricted data set of Huot et al. (2002), to estimate the nature and degree of partial melting and melt-mantle interactions experienced by mantle blocks prior to their disruption and emplacement, and to determine if there is a spatial variability in the characteristics of the ultramafic blocks along the central YZSZ, as observed for the ophiolitic massifs (Dubois-Côté et al., 2003 ; Dubois-Côté, 2004 ; in press).

3.2 Characteristics of the ophiolitic massifs

Les caractéristiques des massifs ophiolitiques sont présentées à la section 1.4.

3.3 Field observations on the ophiolitic mélange

The ophiolitic mélange is exposed nearly continuously, but unevenly in the studied area (Fig. 1.2). It is fault-bounded to the north by ophiolitic upper mantle and to the south by Mesozoic sedimentary units (mostly turbidites). The latest movements on these two sub-vertical fault zones are related to backthrusting and dextral strike-slip (Huot et al., 2002). Backthrusting explains why some early north-dipping thrust faults associated with the obduction of the ophiolites on the Indian margin are now south-dipping, giving an abnormal mélange-over-mantle structural relationship. In addition, some serpentinite zones within the sedimentary units are observed at a few locations in the studied area, e.g. at Lhabuxi and Rembu. Petrography and geochemistry presented

in this paper reveal that ultramafic rocks from these serpentinite zones are similar to those of the ophiolitic mélange. The serpentinite zones could represent slices of the ophiolitic mélange tectonically incorporated into the sedimentary units during obduction or collision.

The matrix of the mélange is composed of a sheared and flaky black to dark-green serpentinite. No terrigenous or calcareous sedimentary matrix has been observed. The nature of blocks and the gradient of deformation vary across the mélange exposure. The blocks are ultramafic or mafic in composition (Fig. 3.1). Ultramafic blocks are intensely serpentinized. Mafic blocks are often rodingitized, as shown by their white weathered surfaces (Fig. 3.1 ; Dupuis et al., 2004 ; in press), and most of the time strongly foliated. The structural lower part, i.e. adjacent to the sedimentary units, is highly deformed and has a chaotic block-in-matrix aspect. The higher section, i.e. towards the ophiolitic mantle, shows decametric undeformed zones made up of massive serpentinites and crosscutting diabases and bounded by serpentinite shear zones (Chang, 1980 ; Huot et al., 2002). Petrography and geochemical data from the Beimarang area suggest that the ultramafic components are moderately depleted upper mantle peridotites (Huot et al., 2002). These peridotites were intruded by batches of back-arc magma (Huot et al., 2002 ; Dupuis et al., 2003 ; 2004 ; in press). The YZSZ ophiolitic mélange is purely tectonic and is similar to ophiolitic mélanges associated with the South Ladakh ophiolites (Robertson, 2000 ; Mahéo et al., 2004). Mafic blocks from the ophiolitic mélange have geochemical signatures very similar to that of mafic rocks of the ophiolitic crust, which suggest the blocks originally formed in a supra-subduction zone setting (Huot et al., 2002 ; Dupuis et al., 2003 ; 2004 ; in press).

3.4 Petrography

Peridotites are extensively serpentinized. Only two samples from the Zedong area have a near primary composition, affected only by late serpentine veins. Serpentine polymorphs include mesh-texture lizardite, fibrous chrysotile and platy antigorite. Lizardite is the main polymorph replacing granular olivine (mesh-texture) and elongated orthopyroxene (bastite). Textural differences between mesh-texture and bastite (Fig. 3.2A), suggest that most serpentinites were porphyroclastic harzburgites, with 10 to 40 vol% of orthopyroxene. Partially serpentinized samples contain relic olivine in a lizardite mesh, orthopyroxene (Fig. 3.2B) and, in some cases, clinopyroxene (Cpx) (Fig. 3.2C). Opx grains commonly contain Cpx exsolution lamellae and olivine inclusions (Fig. 3.2D). Two peridotites containing 10 and 5 vol.% Cpx are classified as lherzolites, peridotites containing Cpx only as inclusions within Opx (<5 vol.%) are classified as

FIG. 3.1 – Ophiolitic mélange made up of a sheared flaky serpentinite matrix and blocks of serpentinized peridotite and white rodingitized gabbro and diabase.

Cpx-harzburgites. Pyroxene is deformed, Opx frequently shows kink-bands and undulatory extinction (Fig. 3.2D).

Most peridotites contain reddish spinel, which generally has a highly irregular shape and is intergrown with Opx and lined by magnetite (Fig. 3.2E). Samples containing Cpx contain a more aluminous brown spinel (Fig. 3.2F). Micro-granular secondary magnetite associated with serpentinization is common. Magnetite-Opx symplectites are common. Some samples from the Lhabuxi and Dayu areas have been affected by hydrothermal fluids. Sample 2002-LHA-05 is completely amphibolitized, while samples 2002-LHA-07 and 2002-DAY-05 are extensively carbonatized. These samples have not been used for geochemical analyses.

3.5 Mineral chemistry

3.5.1 Analytical method

La méthode analytique est décrite à la section 1.2 et les données complètes sont présentées à l'«Annexe C ».

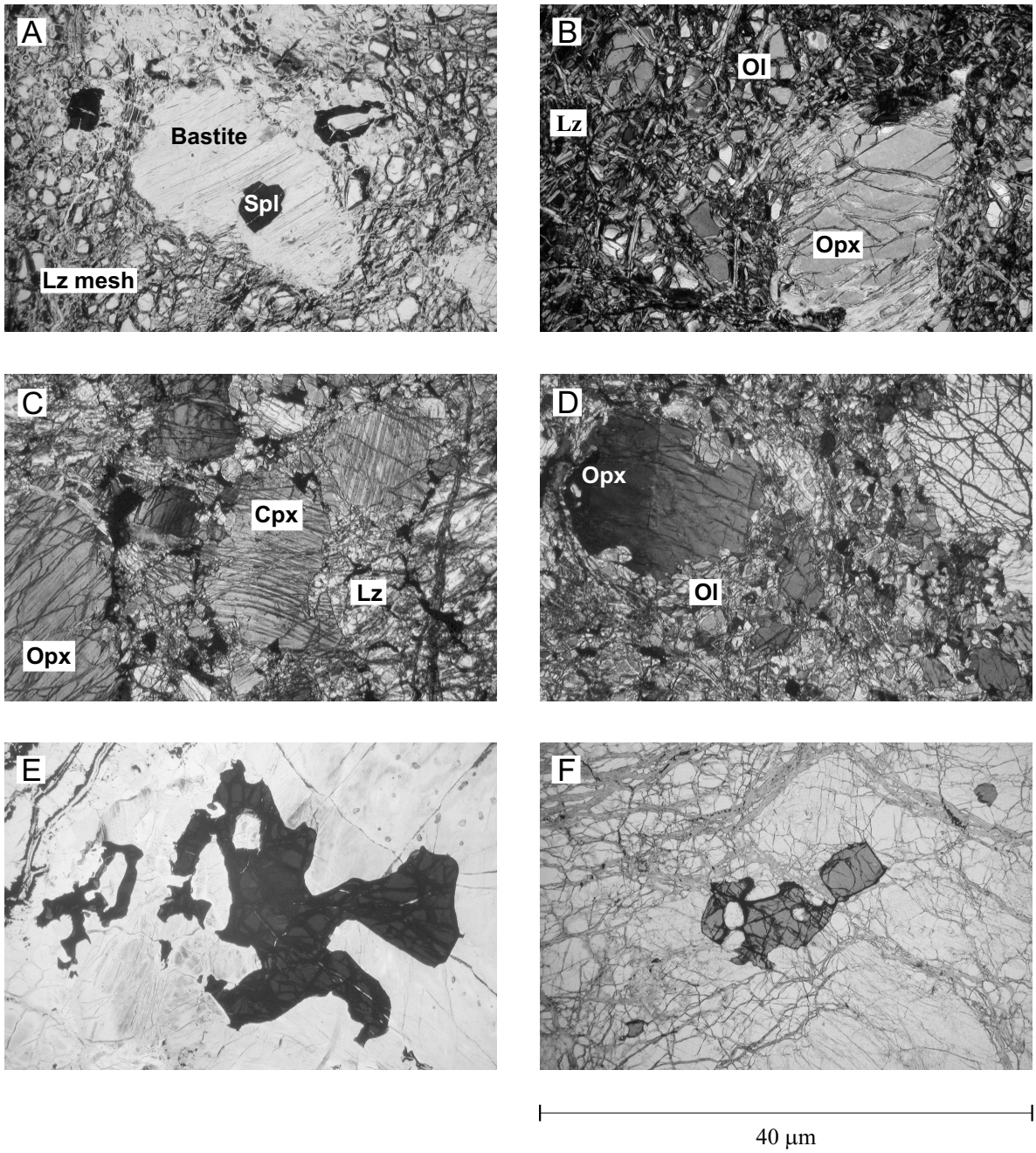

Fig. 3.2 – Microphotographs of peridotites from the ophiolitic mélange. A) Serpentinized harzburgite (2002-QUM-13) with the different lizardite replacement textures. B) Partially serpentinized harzburgite (2002-QUM-14) with primary Opx phenocrysts and olivine crystals. C) Partially serpentinized lherzolite (2002-BUM-08) with primary Opx and Cpx. D) Partially serpentinized Cpx-harzburgite (2002-BUM-02) with a kinked Opx phenocryst containing inclusions of olivine. E) Primary reddish spinel in serpentinized harzburgite (2002-QUM-07). F) Primary aluminous brown spinel in Cpx-harburgite. Cpx, clinopyroxene ; Lz, lizardite ; Ol, olivine ; Opx, orthpyroxene ; Spl, spinel.

3.5.2 Olivine and pyroxenes

In the peridotites, olivine compositions are in the range Fo_{89-91}, with a NiO content between 0.33 and 0.46 wt% (Fig. 3.3). Opx compositions fall in the range En_{90-93} (Fig. 3.4), with Al_2O_3 and Cr_2O_3 contents of 2.3-5.7 wt% and 0.3-0.9 wt%, respectively (Fig. 3.5). Opx was partially re-equilibrated at temperatures ranging from 1100 ° to 500°C (Fig. 3.4). Cpx are diopside (Fig. 3.4), with Mg# ranging from 0.98 to 0.86. The Al_2O_3 content is in the range of 1.4-6.4 wt%, Cr_2O_3 in the range of 0.5-1.3 wt%, and TiO_2 in the range of 0-0.4 wt%. These compositions are inversely proportional to the Mg#, but proportional to the degree of partial melting and the related abundance of Cpx in the peridotite (Fig. 2.3). Cpx was partially re-equilibrated at temperatures ranging from 800°C to <500°C (Fig. 3.4). These chemical compositions are generally similar to those of harzburgites of the YZSZ ophiolitic mantle (Hébert et al., 2003 ; Dubois-Côté, 2004 ; Dubois-Côté et al., in press).

3.5.3 Spinel

In most peridotites, spinel has undergone complex alteration transforming it into a porous and heterogenous amalgamation of secondary silica-bearing ferritchromite with SiO_2 values as high as 20%. Where fresh, brown to red spinels fall into three groups according to corresponding peridotites. Brown spinel in lherzolites and Cpx-harzburgites are relatively Al-rich, with Cr# 0.15-0.27 and Mg# 0.75-0.7. The Cr# increases as the Mg# decreases in reddish spinel of transitional harburgites (Cr# 0.35-0.46 and Mg# 0.66-0.57), and in dark red spinel of harzburgites and chromite dunites (Cr# 0.40-0.63 and Mg# 0.68-0.47) (Fig. 3.7A). The plot along a trend, defined by a large increase in Cr# for a small decrease in Mg#, parallels the array given by Hirose and Kawamoto (1995) for spinel in variously depleted mantle rocks. They also follow the "Luobusa trend" defined by spinel of YZSZ ophiolites (Hébert et al., 2003 ; Dubois-Côté et al., 2004 ; in press) and caused by different degrees of partial melting of the host peridotites. Altered opaque spinels are highly oxidized and tend to follow the Fe^{2+}-enriched trend toward ferritchromite compositions. Spinels aligned along the Luobusa trend have a low TiO_2 content (<0.14 wt%). The trend is generally characterized by a small decrease in TiO_2 for a larger increase in Cr#, except for some harzburgite spinel which show an increase in TiO_2 for a constant Cr# (Fig. 3.7B).

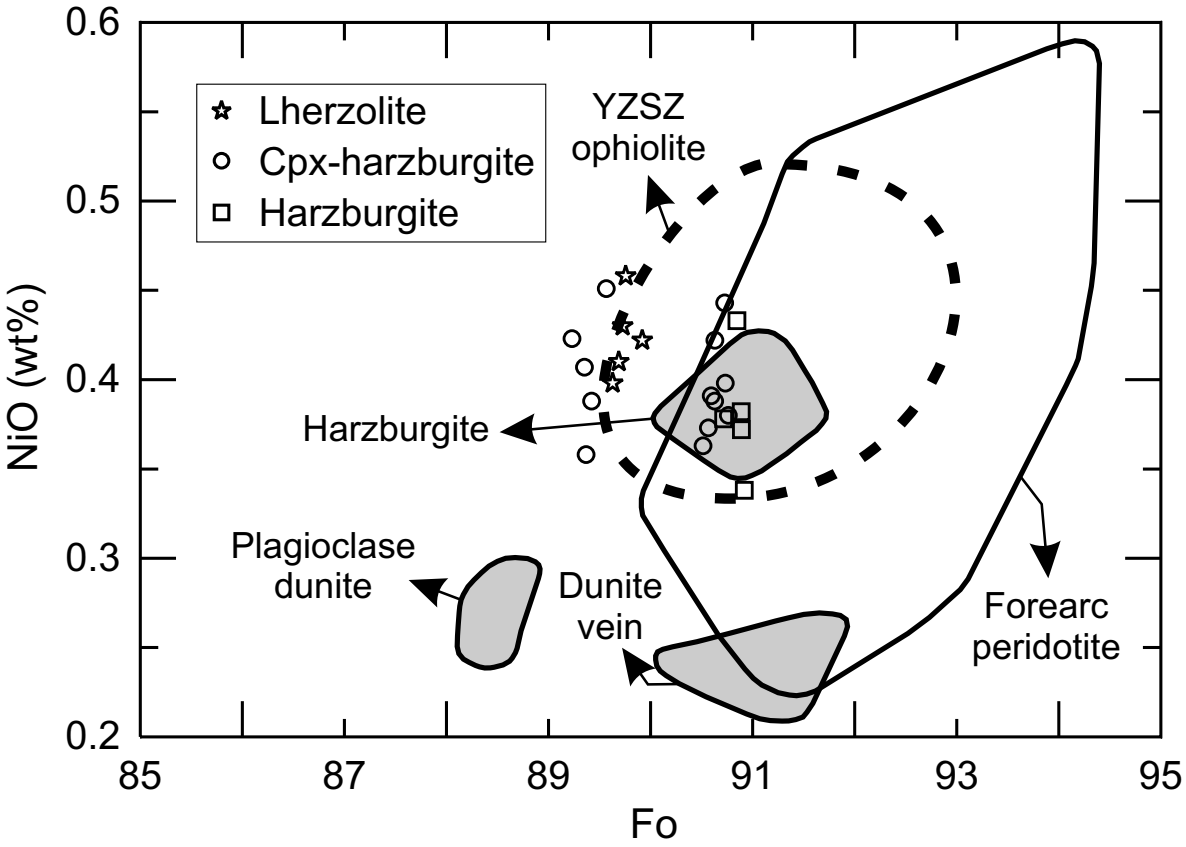

FIG. 3.3 – Variation of NiO vs. Fo in olivine from peridotites. Fields outline olivine compositions in forearc peridotites (Ishii et al., 1992) and various mantle peridotites from the oceanic domain (grey fields ; Constantin et al., 1995). Dashed field outlines compositions in peridotites from the YZSZ ophiolites (Hébert et al., 2003 ; Dubois-Côté et al., 2004 ; in press).

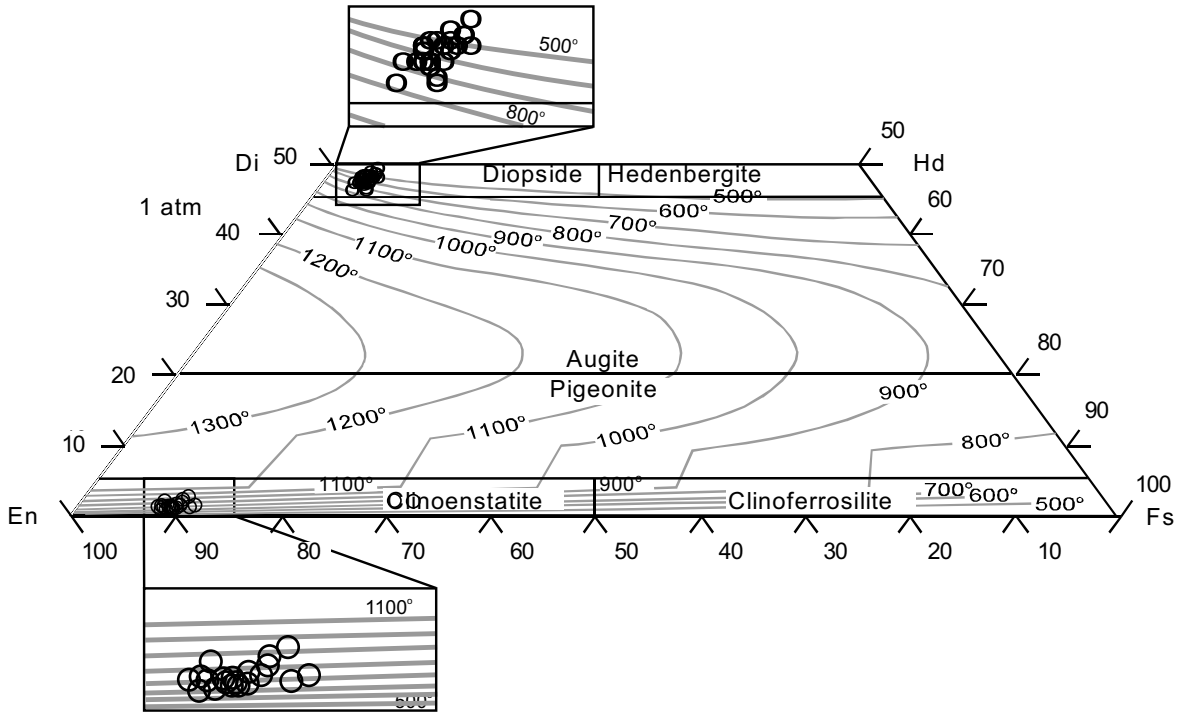

FIG. 3.4 – Compositional variations of orthopyroxene and clinopyroxene projected in the Di-En-Hd-Fs quadrilateral for ultramafic rocks from the ophiolitic mélange. Temperature curves (at 1 atm.) are taken from Lindsley (1983) and the nomenclature is from Morimoto et al. (1989).

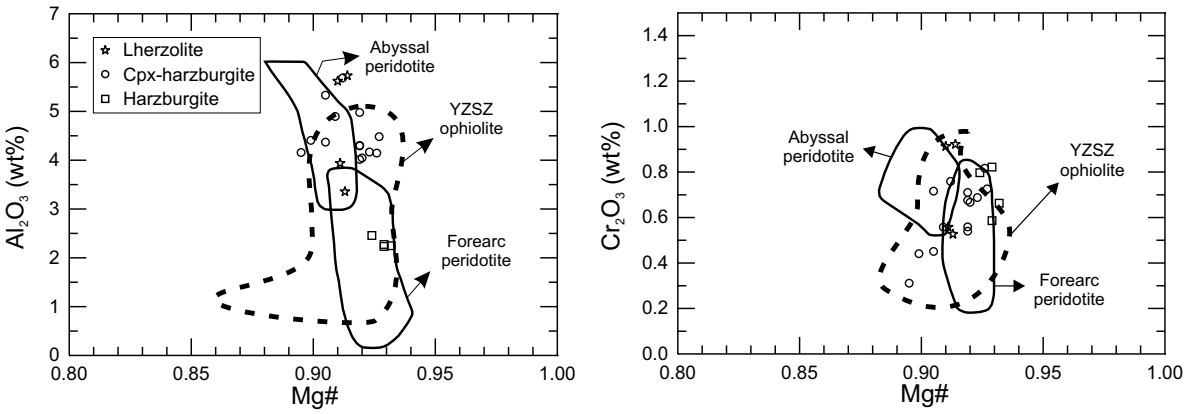

FIG. 3.5 – Compositional variation of orthopyroxene from peridotites. Al_2O_3 and Cr_2O_3 vs Mg#. Fields outline Opx compositions in abyssal peridotites (Johnson et al., 1990) and forearc peridotites (Ishii et al., 1992). Dashed field outlines compositions in peridotites from the YZSZ ophiolites (Hébert et al., 2003 ; Dubois-Côté, 2004 ; Dubois-Côté et al., in press).

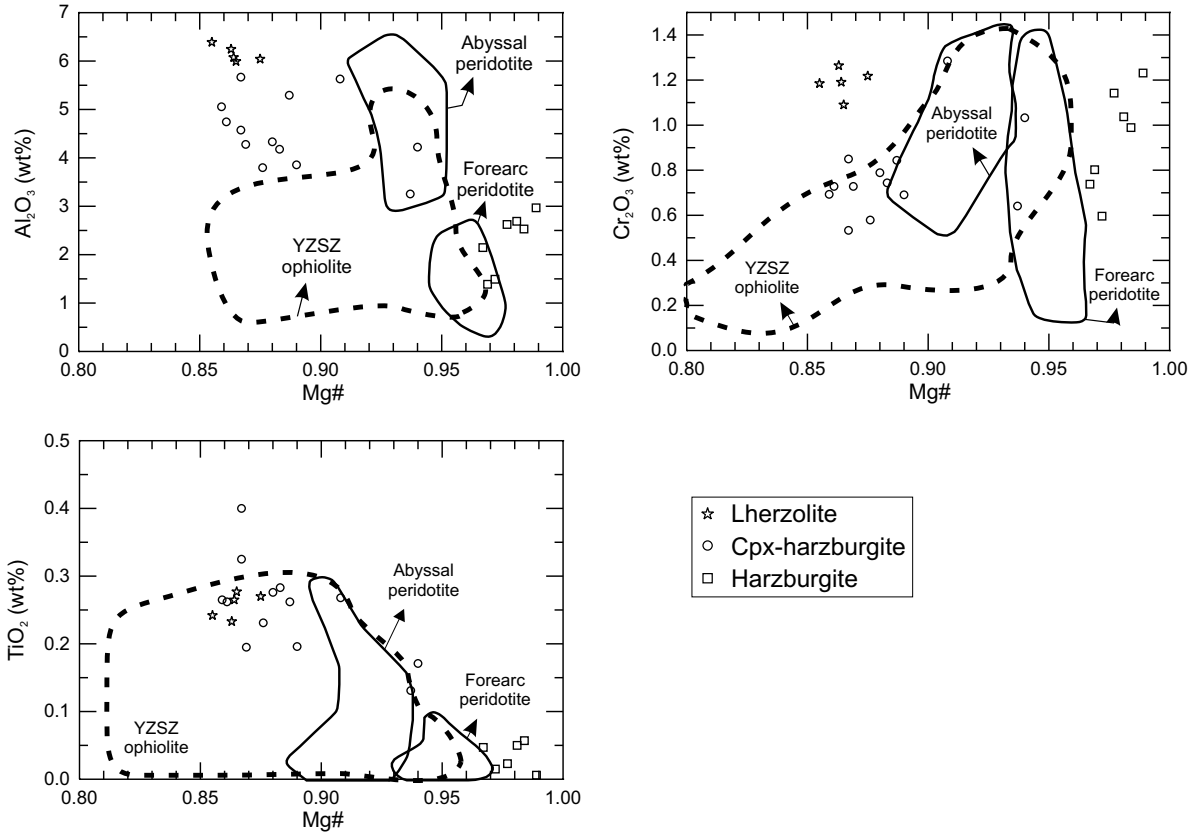

FIG. 3.6 – Compositional variation of clinopyroxene from peridotites. Al_2O_3, Cr_2O_3 and TiO_2 vs Mg#. Fields outline Cpx compositions in abyssal peridotites (Johnson et al., 1990) and forearc peridotites (Ishii et al., 1992). Dashed field outlines compositions in peridotites from the YZSZ ophiolites (Hébert et al., 2003 ; Dubois-Côté, 2004 ; Dubois-Côté et al., in press).

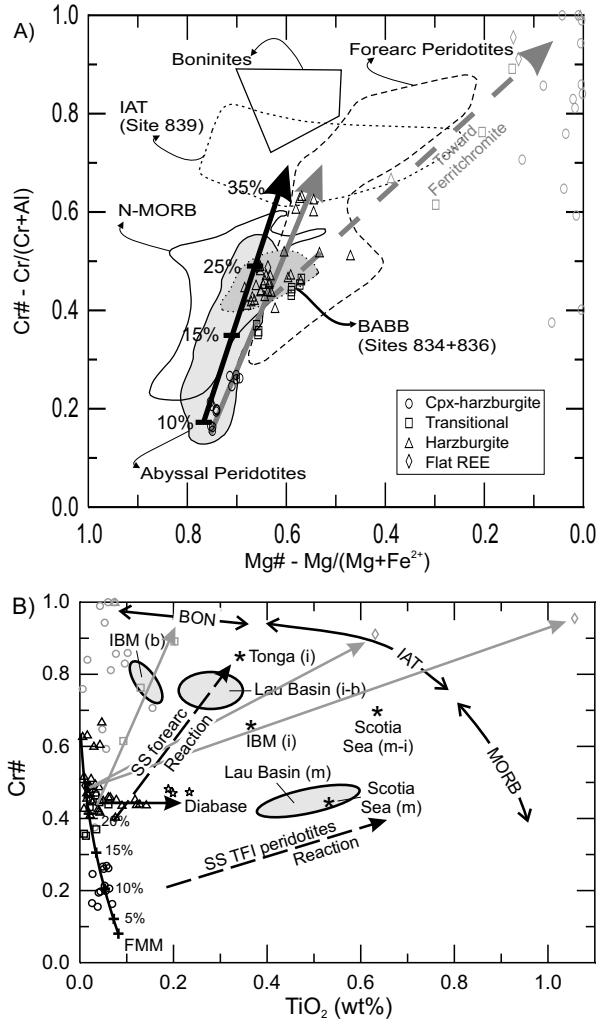

FIG. 3.7 – Compositional variations of spinels in peridotites. A) Cr# vs. Mg#. Fields for spinels in abyssal peridotites, N-MORB and boninites are taken from Dick and Bullen (1984). Others have been drawn from data for spinels in forearc peridotites (Ishii et al., 1992), island-arc tholeiites and back-arc basin basalts (Allan, 1994), and ferrogabbro veins in peridotites and peridotite wall-rock of ferrogabbro veins (Constantin et al., 1995). The arrow with ticks represents the percentage of melting of the host peridotite (Hirose and Kawamoto, 1995). B) Cr# vs TiO_2 for spinels (black) and ferrichromite (grey) (modified from Pearce et al., 2000). The diagram discriminates between partial melting trends (modelled) and melt-mantle interaction trends (drawn empirically). FMM refers to fertile MORB mantle, SS to South Sandwich and IBM to Izu-Bonin-Mariana. Subscripts m, i and b refer to the MORB, island arc tholeiite (IAT) and boninite (BON) chemistries, respectively, of the arc-basin lava spinel reference data.

3.6 Whole-rock chemistry

3.6.1 Analytical methods

La méthode analytique est décrite à la section 1.2 et les données complètes sont présentées à l'«Annexe D ».

3.6.2 Whole-rock compositions

Loss-on-ignition (LOI) values are high (> 10%), reflecting the extensive serpentinization. The effects of serpentinization and post-serpentinization alteration are highly variable. Several peridotites have high abundances of LILE and K indicative of low-temperature alteration (Pearce et al., 2000). By contrast, Ti, Al, HFSE and HREE, known to be relatively insensitive to alteration, and LREE do not show any significant covariation with LOI, Sr, or Ba, indicating that these elements were not fractionated by serpentinization or seawater processes.

All peridotites are strongly depleted in basaltic major elements ($Al_2O_3 < 3.27$ wt%, $CaO < 0.19$ wt%, $Na_2O < 0.23$ wt% when detected, $TiO_2 < 0.06$ wt%), and enriched in ultramafic transition elements (Ni in the range 1240-2740 ppm and Cr 1915-4150 ppm). Mg# varies between 0.69 and 0.82. Al_2O_3 and TiO_2 are highest in lherzolites and Cpx-harzburgites and decrease in transitional harzburgites to reach their lowest values in harzburgites and dunites (Fig. 3.8). Incompatible, immobile trace elements such as Y and Zr covary sympathetically.

The chondrite-normalized rare earth element patterns are illustrated in Fig. 3.9 and compared with patterns of peridotites from the South Sandwich arc-basin system (Pearce et al., 2000). The YZSZ lherzolites and Cpx-harzburgites are characterized by generally smooth LREE-depleted patterns and fairly flat MREE-HREE profiles (Fig. 3.9A). The YZSZ transitional harzburgites are characterized by MREE-HREE profiles with positive slopes indicative of high degrees of partial melting (Fig. 3.9B). LREE profiles vary from depleted to slightly enriched, consistent with some trapped or interacting melt or aqueous fluids. The YZSZ harzburgites and dunites have U-shaped REE profiles characteristic of interaction between LREE-enriched melt and REE-depleted mantle residues (Fig. 3.9C). Two harzburgites show flat REE patterns (Fig. 3.9). Sample 2002-DAY-04 has HREE abundances, as well as Al_2O_3 and TiO_2 contents, that fall at the boundary between Cpx-bearing and transitional harzburgites, while sample 2001-

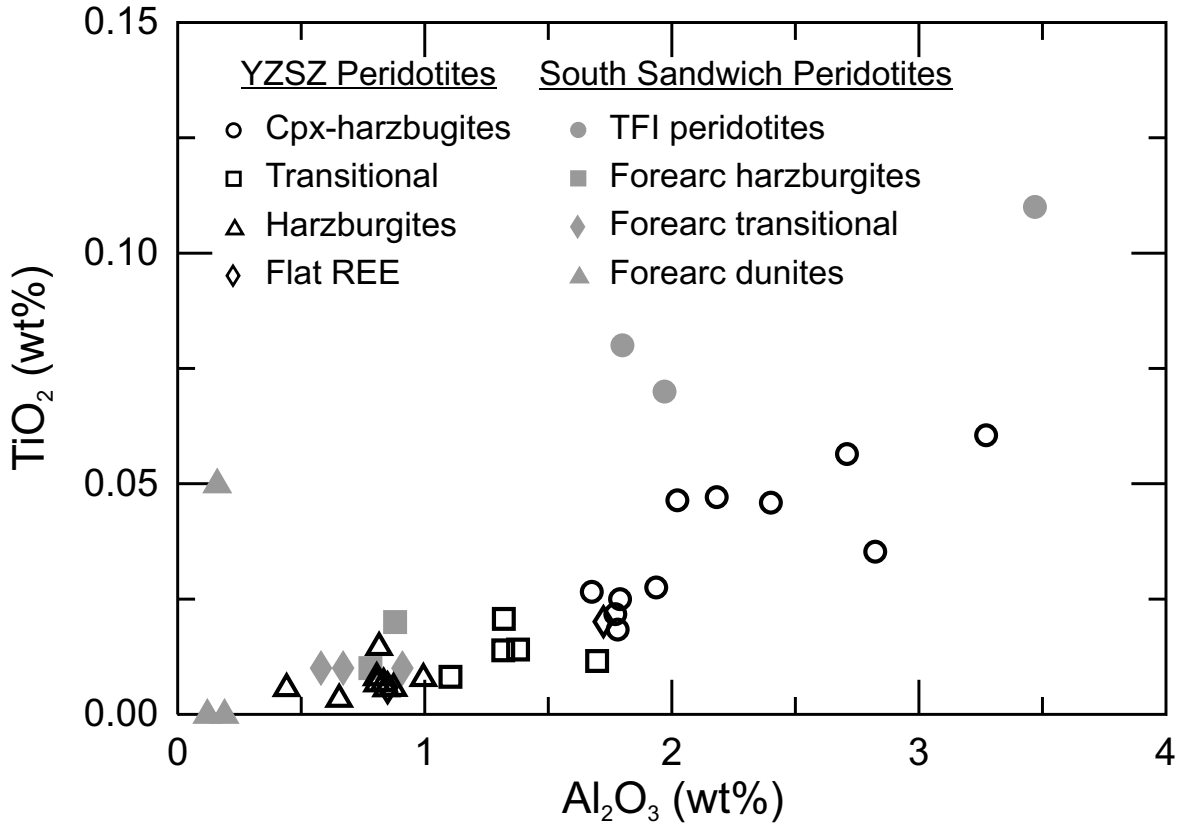

FIG. 3.8 – Variation of TiO_2 vs Al_2O_3 in peridotites of the YZSZ ophiolitic mélange, compared with peridotites from the South Sandwich arc-basin system (Pearce et al., 2000).

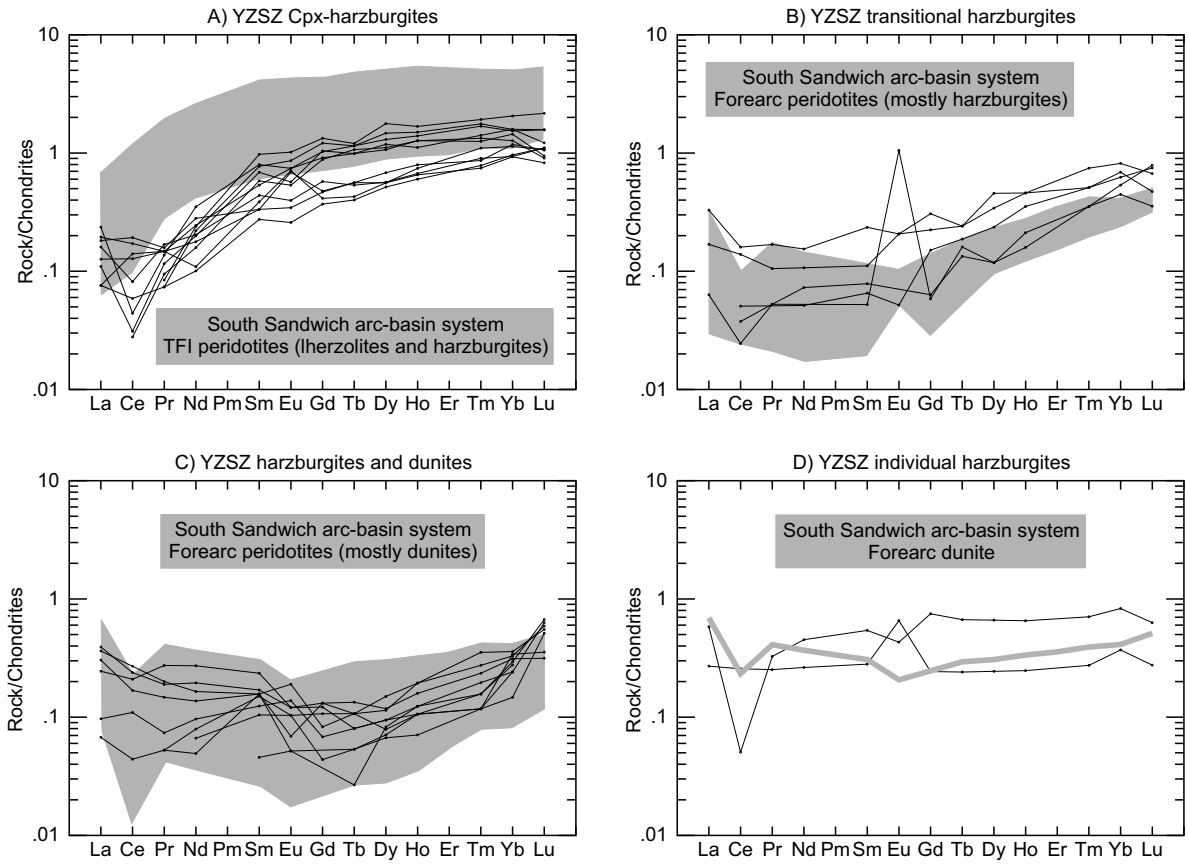

FIG. 3.9 – Chondrite-normalized REE patterns for the YZSZ Cpx-harburgites (A), transitional peridotites (B), harburgites and dunites (C), and particular peridotites (D). Normalizing values are from Sun and McDonough (1989). Compositions of peridotites from the South Sandwich arc-basin system are taken from Pearce et al. (2000).

LHA-39 falls in the field of harzburgites and dunites. A distinctive feature of all REE patterns is the variable and sometimes large Ce anomalies, also observed in some South Sandwich peridotites. Eu anomalies are also variable.

3.7 Petrogenesis

The petrography and geochemistry provide clear evidence that the peridotites of the YZSZ ophiolitic mélange have a multi-process history. The porphyroclastic textures are consistent with an origin of most samples as mantle rocks that have undergone high-temperature deformation at a divergent plate boundary or other geodynamically active region. As melting proceeds, Fo and NiO contents of olivine, Mg# and Cr_2O_3 content of pyroxenes, and Cr# of spinel increase, while Al_2O_3 and TiO_2 contents of pyroxenes and

whole-rock decrease, defining melting lines. In addition, the harzburgites and dunites, in particular, provide evidence for reactions between melt and mantle. Similar petrological and geochemical observations are reported in upper mantle peridotites of the YZSZ (Hébert et al., 2003 ; Dubois-Côté et al., 2003 ; 2004 ; in press) and the Nidar (Ladakh ; Sachan, 2001) ophiolitic sequences, in mantle xenoliths of the Kerguelen archipelago (Mattielli et al., 1996 ; Grégoire et al., 1997), and in peridotites of the South Sandwich arc-basin system (Pearce et al., 2000) and the Mariana Trough (Ohara et al., 2002).

The fertility (enriched fusible incompatible element content) of the peridotites, which is controlled by partial melting in the mantle, versus LREE enrichment, which originates from metasomatic melt-mantle interactions, can be distinguished by plotting representative REE against Al_2O_3 (Fig. 3.10). These diagrams show covariations of HREE with Al_2O_3 that are consistent with igneous processes, i.e. concentrations decrease according to the degree of partial melting. On the other hand, LREE do not seem to show, at first glance, any significant covariations with Al_2O_3. However, if we take only Cpx- and transitional harzburgites that have probably not been affected by significant fluid- or melt-mantle interactions, we can define a similar trend that is consistent with igneous processes. The samples falling off this trend all have higher LREE abundances for a given Al_2O_3 concentration, indicating LREE enrichment by late metasomatism, i.e. interactions between a LREE-enriched melt and a LREE-depleted (refractory) mantle residue. Ce abundances define two *igneous* trends, one that includes negative Ce anomalies and the other that has a steeper slope and includes the *normal* Ce values. The Ce anomaly may be attributed to the mobility of the trivalent LREE during secondary alteration (Gruau et al., 1998 ; Pearce et al., 2000). Ce values could then provide the best indications of the primary LREE concentrations or enrichments in the peridotites (Pearce et al., 2000). Positive Eu anomalies have no obvious explanation since YZSZ peridotites are devoid of textural features indicating melt percolation, such as undeformed interstitial poikilitic clinopyroxene and plagioclase (Hébert et al., 2003).

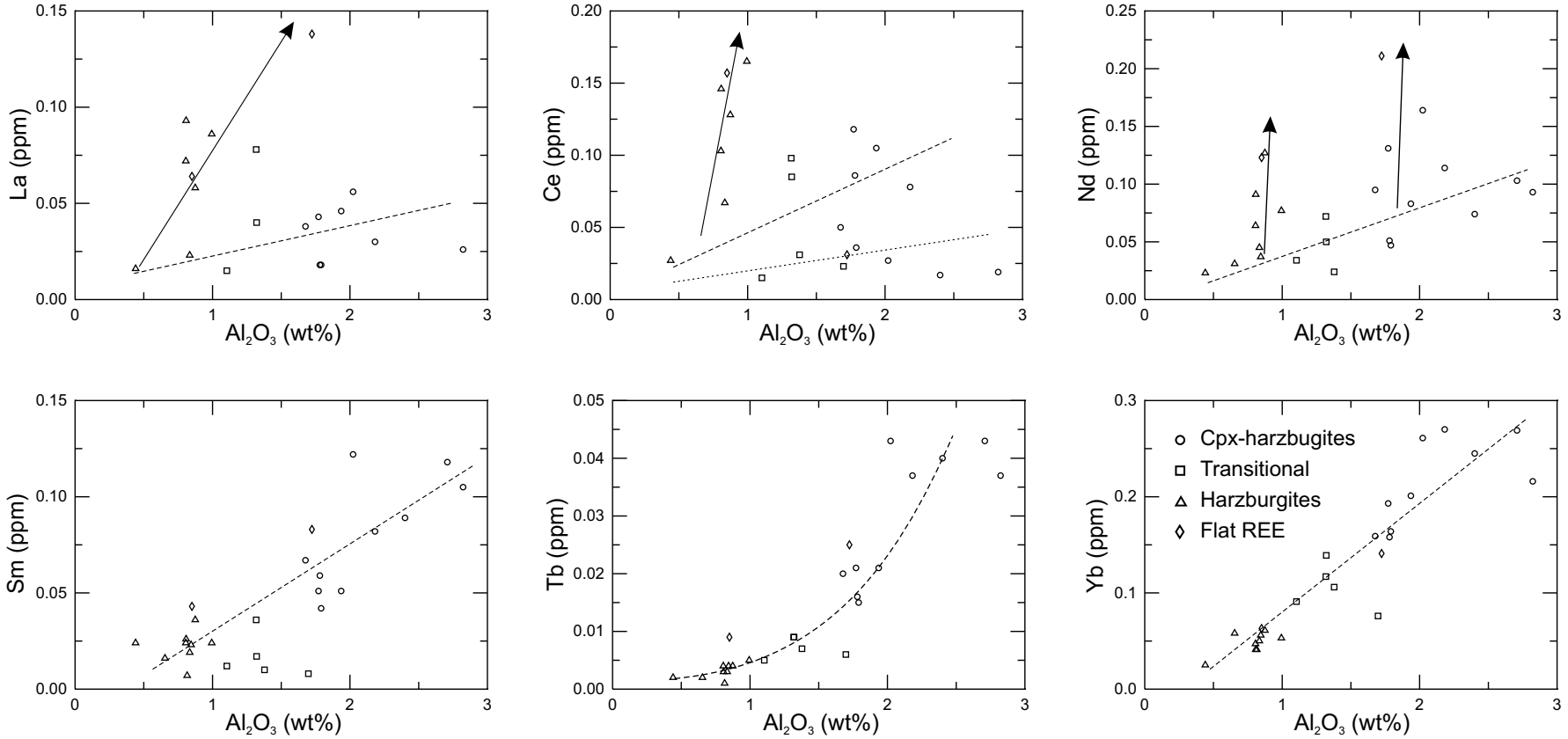

FIG. 3.10 – Representative REEs vs Al_2O_3 in peridotites of the YZSZ ophiolitic mélange. Dashed lines indicate estimated igneous trends. Dotted line in plot of Ce is estimated from rocks showing an apparent negative Ce anomaly on the REE pattern (see text). Arrows indicate LREE enrichment by late metasomatism.

TAB. 3.1 – Values used for modelling fractional melting.

	Congruent melting (Jonhson et al., 1990)		Incongruent melting (Niu, 1997)	
Phase	X_α	p_α	X_α	p_α
Olivine	0.57	0.10	0.52	-0.17
Orthopyroxene	0.26	0.20	0.34	0.65
Clinopyroxene	0.15	0.68	0.14	0.47
Spinel	0.02	0.02	0.02	0.05

Harzburgite 2002-DAY-04 that is characterized by a nearly flat REE pattern and a negative Ce anomaly falls in the field of the least HREE-enriched Cpx-harzburgites when looking at HREE abundances, but indicate slight MREE enrichment and very high LREE enrichment. Interestingly, its Ce abundance falls directly on the igneous trend following Ce negative anomalies. This supports the idea that the apparent Ce anomaly values could indicate the primary LREE concentration in the peridotite and that the sample represents a highly metasomatized harzburgite. The other harzburgite with a flat REE pattern (2001-LHA-39) falls in the field of LREE-metasomatized harburgites and dunites.

3.7.1 Partial melting

Since LREE, and sometimes MREE, were to some extent affected by mantle metasomatism (see the next subsection), the degree of partial melting was estimated based on HREE abundances, which are less affected by this process (Bodinier et al., 1988 ; 1990). We modelled the melting of the depleted mantle (DM ; McCulloch and Bennett, 1994), a fertile MORB mantle, which contains the four-phase assemblage of olivine-Opx-Cpx-spinel (partition coefficients are from a compilation of Bédard (1994)). Two extreme sets of parameters were used : the congruent melting parameters of Johnson et al. (1990) and the incongruent melting parameters (and high Opx contents) of Niu (1997). Values are listed in Table 3.1. Both modal and non-modal fractional melting were used for calculations of REE abundances. Modeling results are given in Table G.19.

Using Yb as reference, the percentages of partial melting obtained for the peridotites are summarized in Table 3.2. The results show that all melting models give similar results for small percentages of melting (<10%) but diverge as the degree of melting increases. Congruent and incongruent melting models give similar results, although the

incongruent melting model of Niu (1997) indicates slightly higher degrees of partial melting. Significant differences in the depletion of REE for similar melting degrees are observed between modal and non-modal fractional melting models. Since modal fractional melting models suggest unrealistically high degrees (reaching more than 35%) of partial melting for the harzburgites and dunites, the non-modal fractional melting model is more realistic. The results suggests that lherzolites and Cpx-harzburgites may be the residues from 5-15% melting, transitional harzburgites from 15-23% melting, and harzburgites and dunites from 22-26% melting with dunite 2002-DAY-08B from maximum 27-29% melting (Table 3.2 and Fig. 3.11). Degrees of partial melting obtained from spinel, based on calculations made by Hirose and Kawamoto (1995), give similar results : melting increases from less than 10% for lherzolites and Cpx-harzburgites to more than 25% for harzburgites and more than 30% for the dunite (Fig. 3.7A).

Tab. 3.2 – Percentage of partial melting of the YZSZ peridotites calculated from Yb abundances.

Melting model	Cpx-harz.	2002-DAY-04	trans.	2001-LHA-39	harz.	dunite
Congruent modal fractional (Johnson et al., 1990)	5-16	17	17.5-25	28	27.5-32	>35
Incongruent modal fractional (Niu, 1997)	5-18	19.5	20-28	30	31-35	$\gg$35
Congruent non-modal fractional (Johnson et al., 1990)	4.5-14	15	15-20	21.5	21.5-24	26.5
Incongruent non-modal fractional (Niu, 1997)	5-15	16.5	17-23	23	23.5-26	29

3.7.2 Melt-mantle interaction

Because our samples represent blocks out of their original geological context, chronological and geological constraints for quantitative modelling of melt-mantle interaction are absent, but some semi-quantitative interpretations can be made. The diagram of Cr# vs. TiO_2 in spinels (Fig. 3.7B) is particularly effective in distinguishing partial melting from melt-rock interaction (e.g. Arai, 1992 ; Zhou et al., 1996). It is apparent from this diagram that YZSZ peridotites spinels mostly follow the melting curve of a fertile MORB-type mantle (FMM) with 0.18 wt% TiO_2 (Pearce et al., 2000). The degrees of partial melting given by this curve for each peridotite set are in agreement with those calculated previously with different methods. Harzburgite and dunite spinels, especially those of sample 2002-QUM-11, define a second trend that deviates from the melting trend, i.e. they show a slight increase in TiO_2 at a constant Cr#. This enrichment in Ti is most probably the result of melt-mantle interaction (Dick and Bullen, 1984 ; Kelemen et al., 1995 ; Edwards and Malpas, 1996 ; Edwards et al., 1996 ; Zhou et al., 1996 ; Cannat et al., 1997). Thus, we can infer that lherzolites and Cpx-harzburgites, and transitional harzburgites, which lie close to residual mantle compositions defined by the melting curve, have undergone relatively little reaction with melt, while some harburgites and dunites, which deviate from the melting curve have experienced some.

Secondary magnetites show an expected increase in Cr# for a given Ti concentration since Al is selectively removed from the spinel structure during alteration (Houlé, 2000). On the other hand, chromites indicate significant and different melt-mantle interactions, one defined by transitional harzburgites and the other by the harzburgite 2002-DAY-04. The simplest explanation of the Ti-enrichment reaction trends is that spinels of harzburgite 2002-QUM-11 and chromites have equilibrated with an interacting melt with a TiO_2 content higher than that of the harzburgite. As a consequence, the spinel (chromite) deviates from the melting trend towards compositions of spinels from some primitive MORB, island arc tholeiites (IAT) and boninites (BON) (see the compilation by Arai, 1992). Examples plotted in Fig. 3.7B include spinels from lavas of the South Sandwich-Scotia Sea arc-basin system (Pearce et al., 2000)), the Izu-Bonin-Mariana arc system (van der Laan et al., 1992) and the Lau-Tonga arc-basin system (Allan, 1994 ; Sobolev and Danyushevsky, 1994).

The Cr# vs. TiO_2 plot (Fig. 3.7B) does not discriminate between reaction and impregnation. The plot of Ti in whole rock (Ti_{wr}) vs. Ti in spinel (Ti_{spl}) (Fig. 3.12) demonstrates that, whereas melt-mantle interaction causes Ti_{spl} to increase and Ti_{wr} to decrease, impregnation causes both Ti_{wr} and (Ti_{spl}) to increase (Pearce et al., 2000). With respect to FMM, variations in Ti_{wr} of YZSZ peridotites suggest that reaction took place, but not impregnation.

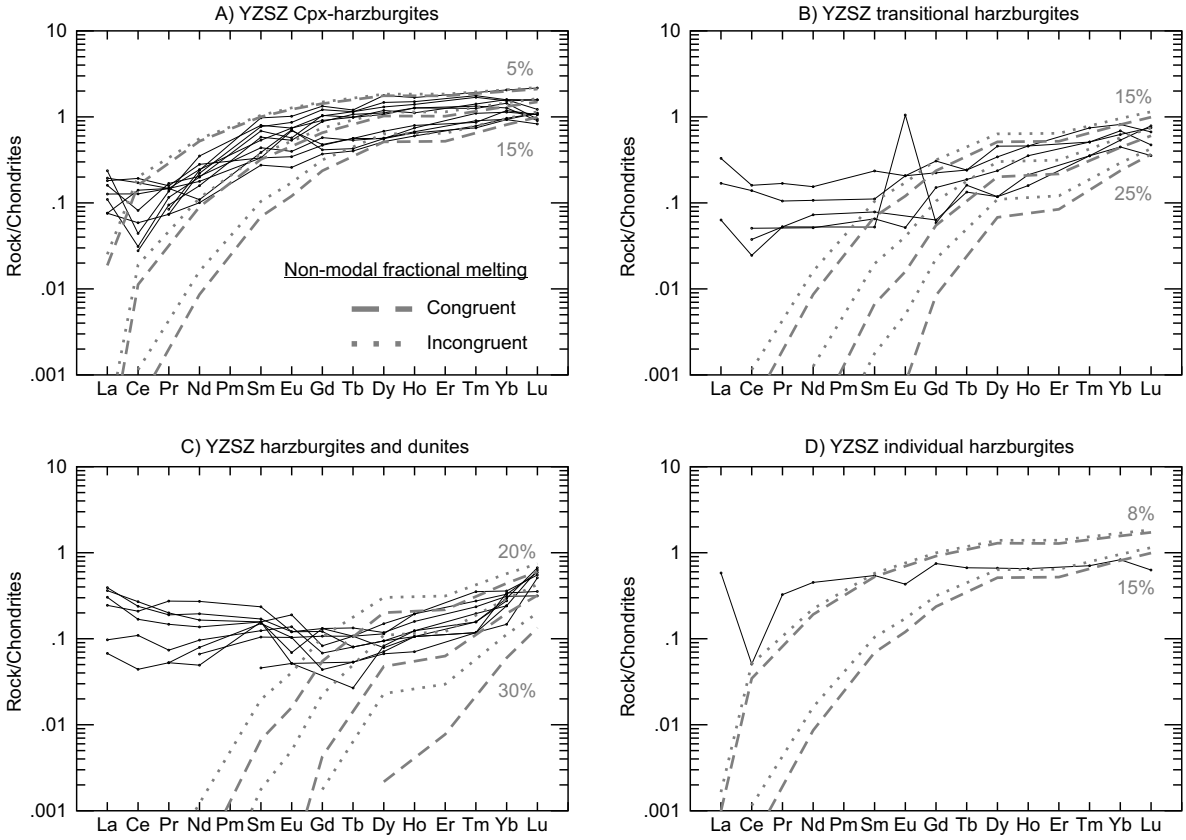

FIG. 3.11 – Calculated fractional melting curves compared to chondrite-normalized REE patterns for the YZSZ Cpx-harburgites (A), transitional peridotites (B), harburgites and dunites (C), and particular peridotites (D). Normalizing values are from Sun and McDonough (1989). Congruent melting model is from Johnson et al. (1990) and incongruent model is from Niu (1997).

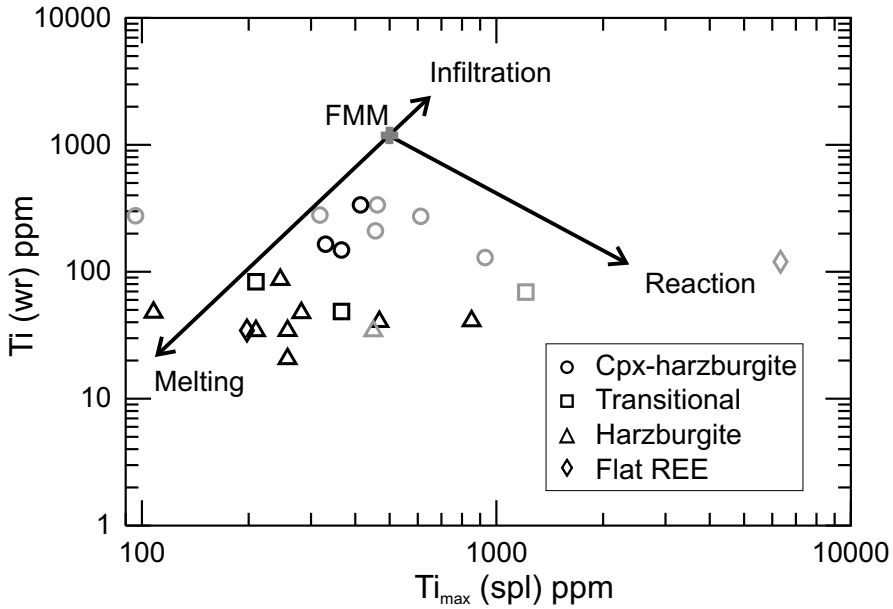

FIG. 3.12 – Variations of whole-rock Ti against maximum spinel (and ferrichromite) Ti (modified from Pearce et al., 2000).

By looking at variations of Sc, Al, Ti and Ni with contrasting partitioning behaviour (Pearce et al., 2000 ; Fig. 3.13), the nature of melt-mantle interactions that took place can be better defined. Even though the majority of peridotites follow the partial melting trend *sensu stricto*, two trends of subsequent interaction can be highlighted. The first, defined by harburgites and dunites, is an enrichment in Ni coupled with a depletion of Sc, Al and Ti that partition into pyroxene. Harzburgites and dunites following this trend can be interpreted as the product of reactions between the mantle residue and a melt saturated in olivine, such as $Opx + melt_1 = olivine + melt_2$ (Kelemen, 1990 ; Pearce, 2000). The second trend also involves enrichment in Ni, but coupled with little or no depletion in Sc, Al and Ti. Cpx-bearing harburgites following this trend can thus be interpreted as the product of reaction between the mantle residue and a melt saturated in olivine + Cpx, such as $Opx + melt_1 = olivine + Cpx + melt_2$ (Kelemen, 1990 ; Pearce, 2000). These melt-mantle interactions are consistent with the presence of several inclusions of olivine and/or Cpx within the Opx phenocrysts. Impregnation, which should produce a depletion in Ni coupled with an enrichment in Sc, Al and Ti, is not observed in the YZSZ peridotites. The YZSZ peridotites contain no or little Cpx (generally less than 5 vol%) and no plagioclase. Cpx crystals of the two lherzolites, like Opx, are deformed (Fig. 3.2C) and thus of original mantle composition.

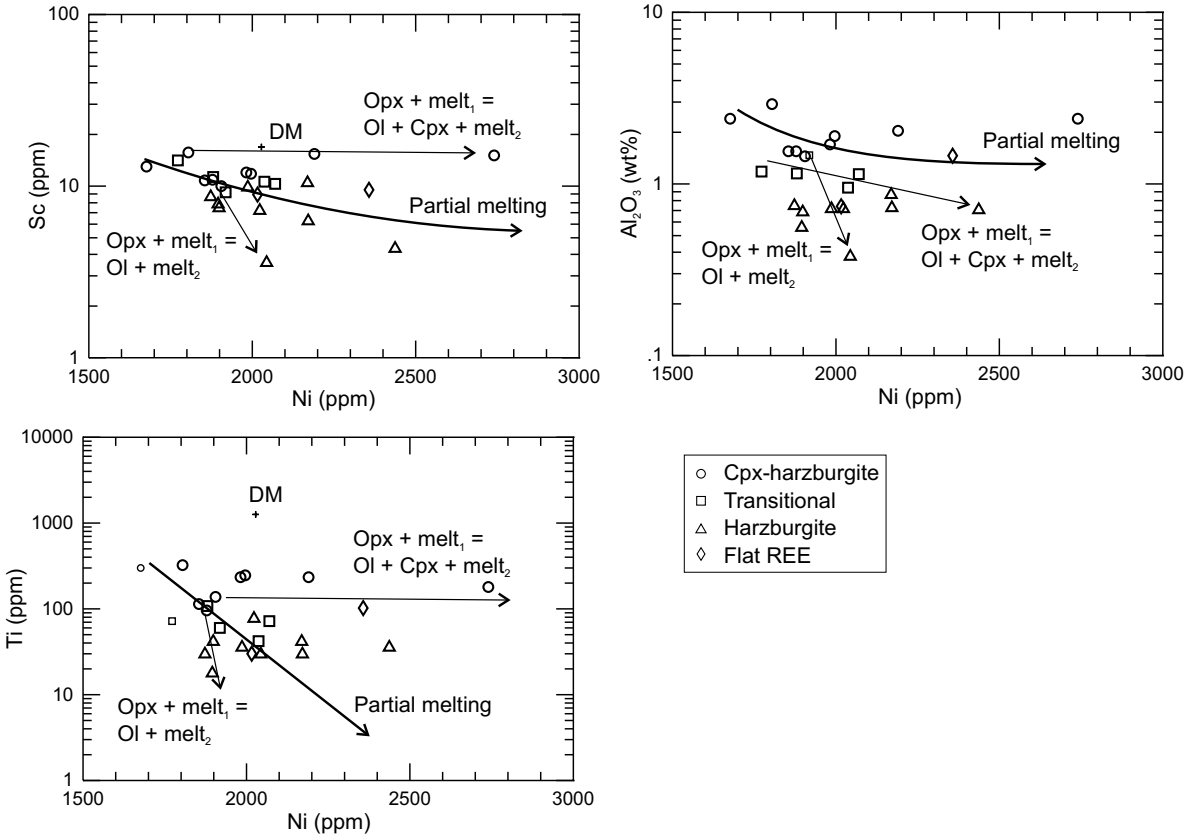

FIG. 3.13 – Variation of Sc, Al_2O_3 and Ti against Ni for peridotites from the YZSZ ophiolitic mélange with partial melting trends for reference (after Pearce et al., 2000). The diagram discriminates between partial melting and different melt-mantle interactions.

3.7.3 Tectonic setting

The results of this study illustrate the complexity of ophiolitic peridotite genesis. Pyroxene chemistry shows that Opx and Cpx were partially re-equilibrated at temperatures ranging from 1100 ° to 500°C, and from 800°C to <500°C, respectively (Fig. 3.4). Subsequent metamorphic conditions lead to secondary antigorite to replace primary minerals at temperatures ranging from 250 to 550°C at a relatively low pressure (e.g. Winkler, 1967 ; Bucher et Frey, 1994). Therefore, mineral assemblages of ultramafic rocks, as well as those of mafic rocks (Huot et al., 2002 ; Dupuis et al., 2004 ; in press), suggest that the rocks have recorded retrogressive metamorphism, from the amphibolite facies to the prehnite-pumpellyite facies, under hydrous low P/T conditions. This thermal regime is characteristic of hydrothermal conditions prevailing at an intra-oceanic divergent zone, such as a mid-oceanic ridge or a back-arc basin. Moreover, YZSZ peridotites have olivine, Opx and Cpx compositions similar to those from both abyssal and forearc peridotites (Figs. 3.3 to 3.6). Most spinels from the metasomatized harzburgites and dunites fall in the field of spinels from back-arc basin basalts, but overlap fields of spinels from abyssal peridotites and N-MORB, as well as forearc peridotites (Fig. 3.7A). By contrast, lherzolite and Cpx-harzburgite spinels plot exclusively in the field of spinels from abyssal peridotites. Hence, the petrology and mineral chemistry of YZSZ ophiolitic mélange peridotites is characterized by interaction between magma and pre-existing oceanic lithosphere, typical of supra-subduction zone settings.

Whole-rock REE signatures (Fig. 3.9) also suggest formation of the YZSZ peridotites in a supra-subduction zone setting, similarly to peridotites of the South Sandwich arc-basin system. Pearce et al. (2000) divided the latter peridotites into two main groups : the South Sandwich TFI (Trench-Fracture Zone intersection) peridotites and the South Sandwich forearc peridotites. Lherzolites and Cpx-harzburgites resemble fertile abyssal peridotites with generally smooth LREE-depleted patterns and fairly flat MREE-HREE profiles. They show good correlation with the South Sandwich TFI harzburgite and with the TFI lherzolite that has the lowest REE abundances. According to Pearce et al. (2002), the TFI lherzolites with the highest REE abundances have the highest modal plagioclase and CPX abundances, i.e. the greatest degree of melt impregnation. As just discussed, YZSZ peridotites were not affected by significant melt impregnation. Transitional harzburgites resemble depleted abyssal peridotites or supra-subduction zone peridotites in that MREE-HREE profiles have positive slopes indicative of high degrees of fractional melting. LREE profiles vary from depleted to slightly enriched, consistent with some trapped or interacting melt or aqueous fluids. They show good correlation with South Sandwich forearc harzburgites and fall within the range of forearc peridotites transitional between harzburgites and dunites. YZSZ harburgites and dunites have U-shaped REE profiles characteristic of interaction between LREE-enriched melt, pro-

bably derived from the subducting slab, and LREE-depleted mantle residues. They fall within the range of South Sandwich forearc dunites and also show good correlation with forearc transitional peridotites with REE patterns similar to forearc dunites. A dunite from the South Sandwich forearc has a mean REE abundance similar to harzburgite 2001-LHA-39, but it is not as flat, showing a slight U shape.

As for the interacting melts, it is apparent that the three YZSZ peridotite interaction trends observed on Fig. 3.7B point to different melt end-members. The harzburgite 2002-QUM-11 trend does not extend far, but it is interesting to note that its end-member lie close to spinel compositions in an intrusive diabase of the same area. This diabase has a back-arc basin basalt (BABB) affinity (Dupuis et al., 2004 ; in press). The trend also points towards MORB to BABB spinel compositions, such as those from the Scotia Sea and the Lau basin. We can thus best explain this trend by interaction between a harzburgite residual mantle and diverse types of magmas generated in a supra-subduction zone context. The transitional harzburgite chromite end-member lies close to boninite spinel compositions, such as those from the Izu-Bonin-Mariana, whereas the 2002-DAY-04 high-Cr# Ti-rich chromites have compositions similar to island arc tholeiite spinels. We can best explain these trends by interaction between an already depleted mantle and various proportions of magmas of boninite to island arc tholeiite compositions, respectively. No obvious boninite signature has been observed in the lavas of the YZSZ ophiolitic mélange, but a few samples have a clear arc signature (Dupuis et al., 2003 ; 2004 ; in press).

A plot of variations in Ti against Yb summarizes the results obtained so far (Fig. 3.14A). The peridotites define a trend from Ti- and Yb-rich lherzolites and Cpx-harzburgites to Ti- and Yb-depleted harzburgites and dunites. The trend is parallel to the calculated non-modal fractional melting trend, but displaced to slightly lower Ti abundances, except for the most REE-depleted samples of the Qumei area which show a slight enrichment in Ti with respect to the overall peridotite suite. This relative Ti enrichment may be correlated with the slight Ti enrichment observed in spinels of Qumei harzburgites (Fig. 3.7B), which was attributed due to melt-mantle interaction. A small negative Ti anomaly was also observed on most multi-element patterns of the YZSZ peridotites, a signature characteristic of supra-subduction zone settings. The trend is also parallel to a trend that encompasses the South Sandwich TFI peridotites, at the fertile end, and the peridotites of the South Sandwich, Mariana and Izu-Bonin forearcs, at the depleted end. This further suggests that the YZSZ ophiolitic mélange peridotites are of supra-subduction zone origin.

Variations of V against Yb can be used to estimate oxygen fugacities and better discriminate between the oxidation conditions in the mantle from supra-subduction

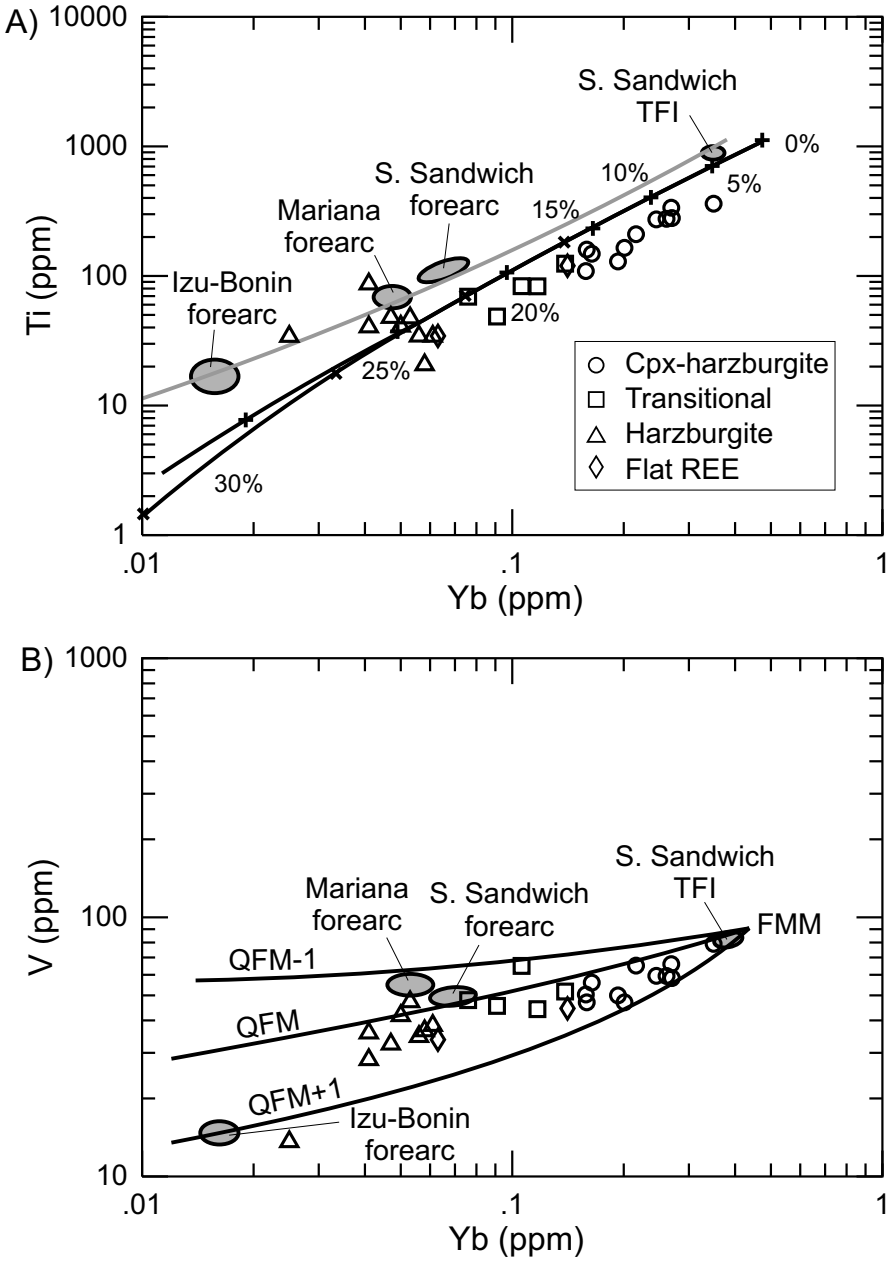

FIG. 3.14 – Modelled degrees of melting and oxygen fugacities using Ti-Yb (A) and V-Yb (B) covariations in mantle peridotites from the YZSZ ophiolitic mélange. Fields for peridotites from the South Sandwich arc-basin and the Izu-Bonin-Mariana forearcs, shown for comparison, were taken from Pearce et al. (2000).

zone settings (Pearce and Parkinson, 1993 ; Pearce et al., 2000 ; Canil, 2002). Peridotites falling close to the QFM melting curve represent transitional lithosphere (e.g. South Sandwich forearc), those falling close to the more reduced QFM-1 melting regime represent MORB lithosphere (e.g. Mariana forearc), while those close to the more oxidizing QFM+1 melting regime represent arc lithosphere (Izu-Bonin forearc) (Fig. 3.14B). The majority of the YZSZ peridotites fall between the QFM and QFM+1 melting curves, with the harzburgites and dunites closer to the QFM melting curve. Such fO_2 values are concordant with an origin at a back-arc ridge with superimposed supra-subduction zone reaction. In this case, fluxed water derived from slab dehydratation causes higher oxygen fugacities.

YZSZ ophiolitic mélange peridotites show geochemical characteristics very similar to those of peridotites from the adjacent ophiolite massifs, suggesting a common origin within a supra-subduction zone for peridotites of both formations. A similar relation was observed for mafic rocks of the two formations (Dupuis et al., 2003 ; 2004 ; in press). However, although there is a variability in the characteristics of ultramafic blocks in the mélange, this variability does not appear to be systematically related to the rock geographical positions along the YZSZ central portion. This contrasts with the spatial variability observed for the ophiolites (Dubois-Côté et al., 2003 ; in press ; Dubois-Côté, 2004), but can be explained by the tectonic nature of the mélange and its strike-slip motion resulting from the oblique convergence (Pozzi et al., 1984). The data presented here are in agreement with the model of magmatic evolution of the YZSZ ophiolite and ophiolitic mélange proposed by Huot et al. (2002). This model involves at least two main distinct stages in the formation of ultramafic and mafic lithologies, separated in time by the development of Late Jurassic-Early Cretaceous intra-oceanic subduction systems. The ultramafic rocks, dated at 404 Ma by Göpel et al. (1984), may thus represent the vestiges of a Tethyan lithophere, which was later affected by melt-mantle interaction within at least two intra-oceanic supra-subduction zones. The first intra-oceanic subduction system (177-152 Ma) generated tholeiitic-, calk-alkaline-, and boninite-type ophiolites, while the second intra-oceanic subduction system (130-120 Ma) involved arc- and back-arc-type ophiolites. The studied mélange is thus considered as the results of tectonic reworking of the second subduction system. A few calk-alkaline blocks derived from the first subduction system might have been incorporated during the mélange formation.

Initiation of the decoupling probably occurred in the region of the back-arc thinned lithosphere (Huot et al., 2002) along thrust faults initiated on previously existing transform faults (Girardeau et al., 1985b). Such a decoupling might be associated with the development of the dynamothermal amphibolite sole now represented by blocks within the ophiolitic mélange of foliated garnet-bearing amphibolites, Cpx-bearing amphibo-

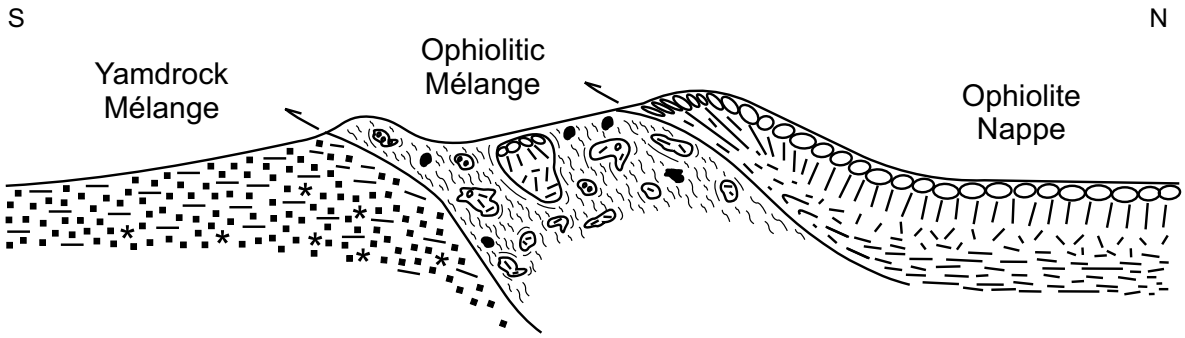

FIG. 3.15 – Schematic section showing the tectonic formation of the ophiolitic mélange during obduction of the ophiolite onto Indian sedimentary units, resulting in mafic and ultramafic ophiolitic blocks mantled in a sheared serpentinite matrix (modified from Saleeby, 1984).

lites and amphibolites (Nicolas et al., 1981 ; Nicolas, 1989 ; Guilmette and Hébert, 2003). Obduction processes of ophiolite emplacement onto the Indian sedimentary units lead to the formation of the tectonic ophiolitic mélange (Huot et al., 2002), in which deformed (Fig. 3.2B-D) serpentinized peridotite blocks are mantled in a mechanically-produced and sheared serpentinite matrix (Fig. 3.15). Similar obduction and metamorphic sole development processes have been proposed for the Albanian and Greek ophiolites (Bortolotti et al., 2004). A mechanism of mélange formation was suggested by Cloos (1982, 1984) for the Californian serpentinite Franciscan mélange belt and by Ishii et al. (1992) for diapiric serpentinite seamounts in the Izu-Ogasawara-Mariana Forearc. This mechanism involves diapiric motion of serpentinite as a prominent factor. However, the petrological and geochemical correspondence between ultramafic and mafic blocks in the mélange and the overlying ophiolitic sequences, the tectonic nature of the ophiolitic mélange, the sheared serpentinite matrix, and the vestiges of the dynamothermal amphibolite sole at the base of the ophiolites all preclude formation of the ophiolitic mélange as a serpentinite diapir.

3.8 Conclusions

The YZSZ ophiolitic mélange peridotites range from lherzolites and Cpx-harzburgites, through transitional harzburgites to harzburgites and dunites. Most peridotites are extensively serpentinized but preserved complex initial characteristics. Chemistry of primary minerals, whole-rock chemistry, and oxygen fugacity between QFM+1 and QFM indicate that their geochemical characteristics may be inherited from multi-stage processes within a complex supra-subduction zone tectonic setting. Lherzolites and Cpx-

harzburgites contain brownish aluminous spinels with Mg# 0.7-0.75 and Cr# 0.15-0.27. These peridotites are characterized by generally smooth LREE-depleted profiles and fairly flat MREE-HREE profiles. Spinel compositions and fractional melting modelling indicates that they may be the residues from 5-15% melting of a depleted mantle source. They are analogous to fertile abyssal peridotites and do not seem to have been affected by a subduction component.

Transitional harzburgites contain reddish spinels with Mg# 0.57-0.66 and Cr# 0.35-0.46. They are characterized by MREE-HREE profiles with positive slopes indicative of high degrees of partial melting. LREE profiles vary from depleted to slightly enriched, consistent with some trapped or interacting melt or aqueous fluid. Spinel compositions and fractional melting modelling indicates that they may be the residues from 15-23% of melting. They correspond to depleted abyssal or supra-subduction zone peridotites. Harzburgites and dunites contain dark reddish spinels with Mg# 0.47-0.68 and Cr# 0.40-0.63. They have U-shaped profiles characteristic of interaction between LREE-enriched melt and REE-depleted mantle residues. Spinel compositions and fractional melting modelling indicate that they may be the residues from 22-29% of melting. They correspond to supra-subduction zone peridotites. Transitional harzburgites and particularly harzburgites and dunites were clearly affected by melt-mantle interactions overprinting their original geochemical signatures. Interacting melts have geochemical compositions ranging from MORB to IAT, suggesting a variable input of subduction components.

YZSZ ophiolitic mélange peridotites show some geochemical characteristics similar to peridotites from the modern South Sandwich arc-basin system, reinforcing their proposed formation in a supra-subduction zone setting. No chemical zonation was observed along the studied 500 km-long portion of the central YZSZ. The geochemical characteristics of ultramafic blocks of the ophiolitic mélange presented in this study, as well as the association with dynamothermal aureole blocks, confirm that all these blocks are mostly derived from tectonic disruption of the YZSZ ophiolites associated with the 130-120 Ma subduction system.

Acknowledgments

We would like to thank the funding organization NSERC (Grant no. 1253) for financial support of the Tibet project. We are also grateful for the Chinese contribution by Dr. C.S. Wang (Outstanding Research Award of China). The first author also thanks the NSERC (scholarship PGS B) and FCAR for financial support. We are also thankful to M. Choquette for microprobe analyses and to R. Gosselin for ICP-AES and ICP-MS analyses. The manuscript was kindly reviewed by T. Feininger (U. Laval), and has

further benefited from critical comments by A.J. Barber, C. Miller and E. Garzanti.

Chapitre 4

«Geochemistry of sedimentary rocks from mélange and flysch units south of the Yarlung Zangbo Suture Zone, southern Tibet »

C. Dupuis[a], R. Hébert[a], C. Guilmette[a], C.S. Wang[b], Z.J. Li[b]

[a] *Département Géologie et génie géologique, Université Laval, Ste-Foy, Québec, Canada, G1K 7P4*

[b] *Université de Technologie de Chengdu, Chengdu, Sichuan, 610059, R.P. Chine*

Soumis à *Journal of Asian Earth Sciences* le 20 octobre 2003 ; accepté le 1er novembre 2004

Cet article traite de la géochimie des roches sédimentaires du mélange de Yamdrock et du flysch triasique. La signature géochimique des grès, des argiles rouges et des argiles noires ne présente pas de variations significatives selon le type de roches ou l'unité et concorde avec un environnement de marge continentale passive. Malgré une altération chimique passablement importante, cette signature n'a pas été affectée de façon significative par du recyclage sédimentaire ou par l'accumulation de minéraux lourds. Les patrons de TR montrent un enrichissement en TR légères typique des argiles et indiquent que les turbidites néo-téthysiennes proviennent de la croûte continentale supérieure felsique ancienne. De légers enrichissements en Ti et Sc suggèrent une contribution mafique qui semble tirer son origine des blocs mafiques d'affinité géochimique intraplaque enrichie retrouvés dans les unités sédimentaires. Les roches sédimentaires

des deux unités dériveraient donc de la croûte continentale indienne archéenne, y compris des blocs granitiques et mafiques intraplaques. L'homogénéité des données de la ZSYZ, lesquelles couvrent l'ensemble du bassin néo-téthysien, et la bonne corrélation avec les données himalayennes sont en accord avec la formation de toutes les unités lithotectoniques himalayennes le long de l'ancienne marge passive indienne.

4.1 Introduction

The Yarlung Zangbo Suture Zone (YZSZ), in Southern Tibet, is a major tectonic feature between India and Asia, and marks the location where the Neo-Tethyan oceanic domains have been consumed by northward subduction under the Lhasa Terrane during the Cretaceous (Tapponnier et al., 1981a ; Allègre et al., 1984 ; see review by Searle et al., 1987). The present work is part of a Sino-Canadian project initiated in 1998 and devoted to the geodynamic reinterpretation of the central YZSZ ophiolitic massifs (Hébert et al., 2000 ; 2001 ; 2003 ; Huot et al., 2002 ; Dubois-Côté et al., 2003 ; 2004), and the mélange and flysch units lying immediately south of the ophiolitic chain, i.e. the Early Cretaceous ophiolitic serpentinite mélange, the Mesozoic Yamdrock mélange and the Triassic flysch (Figs. 1.1 and 1.2). The YZSZ is one the six main tectonic units forming the Himalayan chain, which are from north to south, the Trans-Himalayan zone (Andean-type northern margin of Tethys), the YZSZ, the Tibetan Sedimentary Series, the High Himalayan Crystalline Series, the Lesser Himalayan Series, and the sub-Himalaya comprising sediments eroded from the Himalayan orogen (e.g. Hodges, 2000 ; Najman et al., 2000).

Several authors have used Nd and Sr isotopic data to differentiate between the Greater Himalaya (GH), the Lesser Himalaya (LS) and the Tethyan Himalaya (TH ; including the Tibetan Sedimentary Series and YZSZ sedimentary units), and to determine Tertiary Himalayan foreland basin provenance (e.g. France-Lanord et al., 1993 ; Galy et al., 1996 ; Najman et al., 2000). However, the TH standard values were derived from only six samples (France-Lanord et al., 1993) and little observations have been added since. The lack of new data from the TH sequence has led to an intense debate between Myrow et al. (2003) and DeCelles et al. (2000) on whether these three Himalayan lithotectonic units can be clearly distinguished on the grounds of isotopic values and detrital zircon ages. In that sense, three models have been proposed to explain the stratigraphic differences between the three Himalayan lithotectonic zones : the 'continuous margin' model, in which the three zones represent parts of a single ancient passive margin, the 'crystalline axis' model, in which the GH represent a basement high separating the LH depositional basin from the TH passive margin, and the 'accreted

terrane' model, in which the GH represents the basement of an exotic terrane overlain by the TH sedimentary sequence (Myrow et al., 2003 and references therein). Although each model predicts a unique set of stratigraphic, biogeographic, and geochronologic patterns (Myrow et al., 2003), only the first two models (continuous margin and crystalline axis) would predict a common source for the three Himalayan zones based on geochemical data.

The aim of the present paper is not to define the stratigraphic characteristics of these units, a work thoroughly done by Liu and Einsele (1996 ; 1999) for example, but to fill an important gap in our geochemical knowledge of these units. Several isotopic studies have been conducted on rocks of the Himalayan Series, including the YZSZ (e.g. compilation by Najman et al., 2000), but few trace element data are available for sedimentary rocks of the same area. We present new major- and trace-element geochemical data on sandstones and shales from the Mesozoic Yamdrock mélange and Triassic flysch. The geochemistry of these sedimentary rocks provides unprecedented information on their formation, depositional mode and provenance. It can even help constrain the geodynamic significance of alkaline mafic and granitic rocks incorporated into these sedimentary units.

4.2 Geological setting

Le contexte géologique est présenté à la section 1.3.

4.3 Field observation

At first sight, the Yamdrock mélange and the Triassic flysch appear similar. They consist principally of flysch sequences of pelagic shales with siliciclastic turbidites. The Triassic flysch is dominated by black shales interbedded by sandstones/siltstones and local limestones (Fig 4.1A). Sandstone and limestone beds, locally boudinaged, are generally centimeter to decimeter wide (Fig 4.1B), although meter-thick sequences of beach-like pure sandstones were observed locally. Intercalated grey chert is scarce. Black shales are graphitic, locally containing up to 5% oxidized pyrite crystals, usually on coating adjacent to limestones. Late quartz veins, millimeter to centimeter wide, are frequent. By contrast, the Yamdrock mélange is more heterogeneous. In addition to interbedded black shales and sandstones, this unit is composed of widespread sequences of red and tuffaceous green shales, as well as green and red radiolarian cherts. Red and

green shales and cherts are generally thinly interstratified. Blocks of sandstone, limestone, basalt and chert, of all sizes, are commonly found within or between mudstone sequences. In that case, the unit displays a block-in-matrix aspect (Fig. 4.1C) characteristic of a sedimentary mélange (olistostrome ; Pini, 1999). However, it also locally displays some structural order by parallel orientation of blocks and matrix features and boudinage, which is more characteristic of a tectonic mélange (tectonosome ; Pini, 1999). Both sedimentary units have been affected by greenschist metamorphism, grading from shales to slates to sericite schists. They are highly tectonized, having recorded the four deformation stages mentioned earlier (Fig. 4.1A, B, D). Exotic blocks and nappes of Permian limestones (to marbles) are found within the predominantly siliciclastic units (Fig. 1.2).

Mafic rocks were found in the Yamdrock mélange and in the Triassic flysch, either within mappable mafic zones (Figs. 1.2 and 4.1E) or as meter-size blocks (Fig. 4.1F) within the sedimentary matrix. A granitic block (about 10m wide) was also found within the Triassic flysch. It probably corresponds to a remnant of Cambrian-early Ordovician granites generated by subduction dipping beneath northern Gondwana, including both the future Indian continental lithosphere and the Lhasa Terrane, during the latest Proterozoic and the earliest Paleozoic (Yin and Harrison, 2000). Mafic rocks from the Yamdrock mélange have alkaline intraplate geochemical signatures (Dupuis et al., 2003 ; 2004) and are interpreted as remnants of intra-oceanic seamounts (e.g. Mercier et al., 1984 ; Searle et al., 1987 ; Liu and Einsele, 1999 ; Aitchison et al., 2000). Mafic rocks from the flysch are interpreted to have been derived from an enriched intraplate mantle source, with additional crustal assimilation resulting from disaggregation of the Indian Plate during the opening of the Neo-Tehys ocean (Dupuis et al., 2003 ; 2004). AFC modelling strongly suggests a felsic component analogous to Cambro-Ordovician granites as the major contaminant.

Sandstones (5), red shales (5) and black shales (20) were collected in the Mesozoic Yamdrock mélange and Triassic flysch from the western Buma region to the eastern Rembu region (regions shown on Fig. 1.2). Between Buma and Lhabuxi, 1 sandstone, 1 red shale and 2 black shales were collected in the Yamdrock mélange. In the Lhaze area, 2 sandstones and 2 black shales (north of Beilie), and 1 red shale (south of Xiadamei) were collected in the Yamdrock mélange, respectively. South of Lhaxezian, 2 black shales were collected in the flysch. South of Mamiduorang (Liuqu), 1 sericite schist and 1 red shale were collected in the Yamdrock mélange. In the Zisong area, 1 red shale and 3 black shales were collected in the Yamdrock mélange and the flysch, respectively. South of Qumei, 1 sericite schist and 3 black shales were collected in the Yamdrock mélange and the flysch (near Pazuo/Pazhong), respectively. Near Dayu (east of Bainang), 2 black shales and 1 sericite schist were collected in the flysch, whereas 1 red shale was

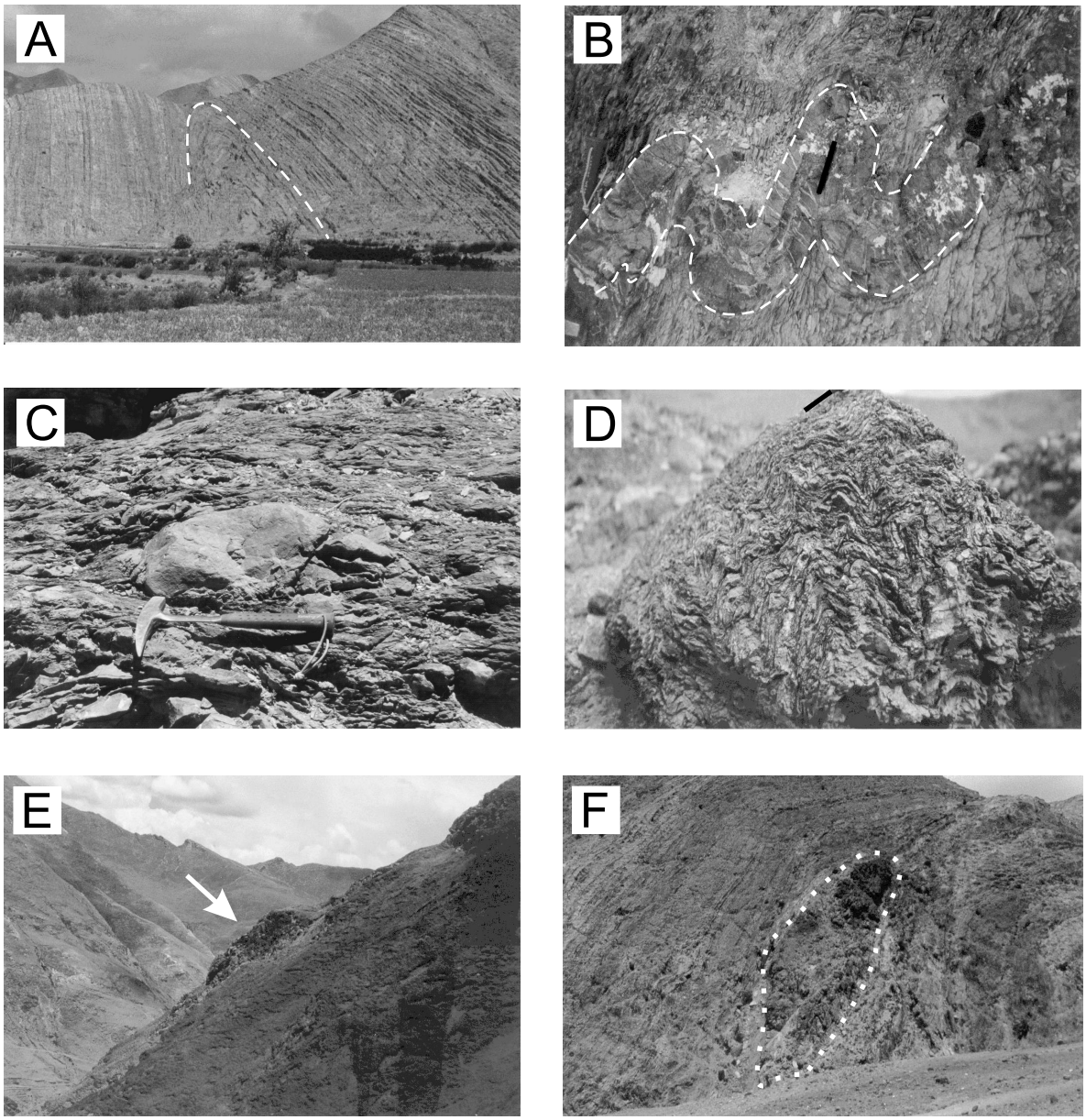

FIG. 4.1 – Field photographs of the sedimentary units. A) Outlined first-order fold in the Triassic flysch, Pazuo. B) Outlined second-order folded sandstone bed in the Triassic flysch, Pazuo region (redrawn black pen shown for scale). C) Block-in-matrix aspect in the Yamdrock mélange, Lhabuxi area (hammer shown for scale). D) Third-order chevron folds in red cherts of the Yamdrock mélange, Lhabuxi area (redrawn black pen shown for scale). E) Kilometer-size mafic zone within the Yamdrock mélange, Baigang area, as indicated by the white arrow. D) Outlined meter-size mafic block within the flysch, Pazuo region.

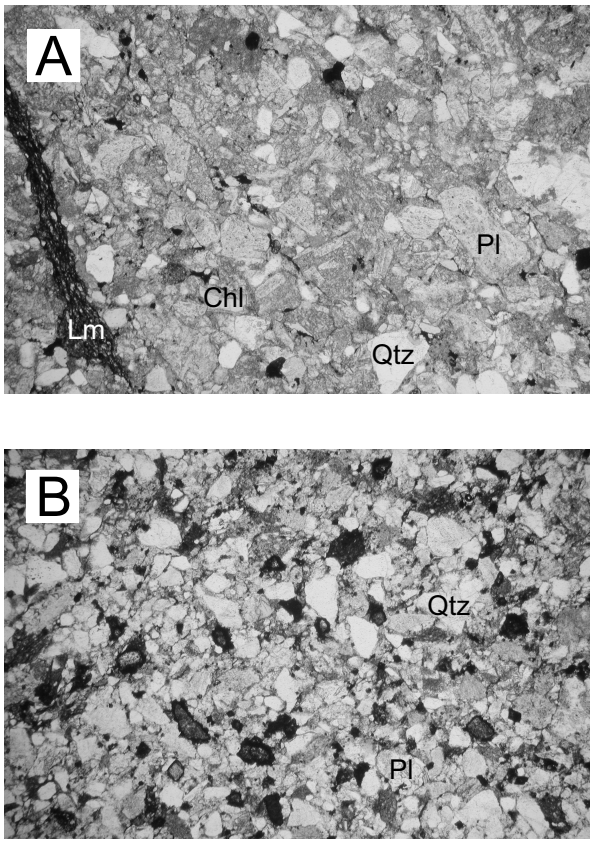

FIG. 4.2 – Microphotographs of sandstones from the Yamdrock mélange. A) Greywacke ; B) Lithic wacke. Chl = chlorite, Lm = limonite, Pl = plagioclase, and Qtz = quartz.

collected in the Yamdrock mélange, to the east. South of Dazhuqu, 1 sandstone and 1 black shale were collected in the Yamdrock mélange, and 1 black shale in the flysch. Finally, south of Rembu, 1 black shale was collected in the Yamdrock mélange.

4.4 Petrographic description of sandstones

On a petrographic basis, sandstones correspond to wackes with 45-55 wt.% of argillaceous matrix, around 20 wt.% of feldspar altered to clay, 5-25 wt.% quartz, generally less than 5 wt.% of diagenetic calcite, and some chlorite, mica, opaque minerals and rocks fragments (Fig. 4.2A). An individual sample contains abundant quartz (45 wt.%) and some altered feldspar grains (Fig. 4.2B). Sandstones are generally non metamorphic, but affected by late hydrothermal circulation. Highly carbonatized samples are not considered in this study. Red shales, usually associated with cherts, contain abundant siliceous fragments, which have been selectively removed for the geochemical analyses.

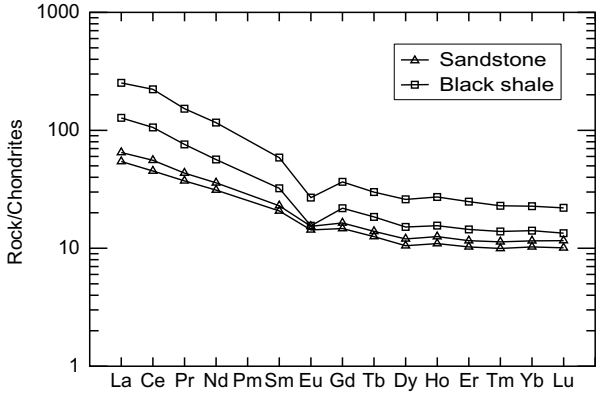

FIG. 4.3 – REE patterns normalized to chondrites for sandstones and black shales from the Mesozoic Yamdrock mélange, in the Beilie and Dazhuqu areas. Normalizing values are from Sun and McDonough (1989).

4.5 Whole-rock chemistry

4.5.1 Analytical methods

La méthode analytique est décrite à la section 1.2 et les données complètes sont présentées à l'«Annexe D ».

4.5.2 Sandstones vs. shales : a compositional test

The geochemical behavior of nearby sandstones and shales, in the Beilie and Dazhuqu regions, has been compared by using chondrite-normalized REE diagrams (Fig. 4.3). The shales are more REE-enriched, especially in the LREE, than the sandstones. These slight differences are attributable to their different clay content. The shales are richer in incompatible elements, especially the most incompatible LREE, which are strongly partitioned in, or absorbed on, clay minerals (e.g. Nesbitt and Young, 1989). Nevertheless, the similar overall distribution of trace elements in the sandstones and shales allows us to plot them together on discrimination diagrams. Moreover, black shales from the Yamdrock mélange and Triassic flysch are chemically undistinguishable and will be treated as a whole in the following discussion.

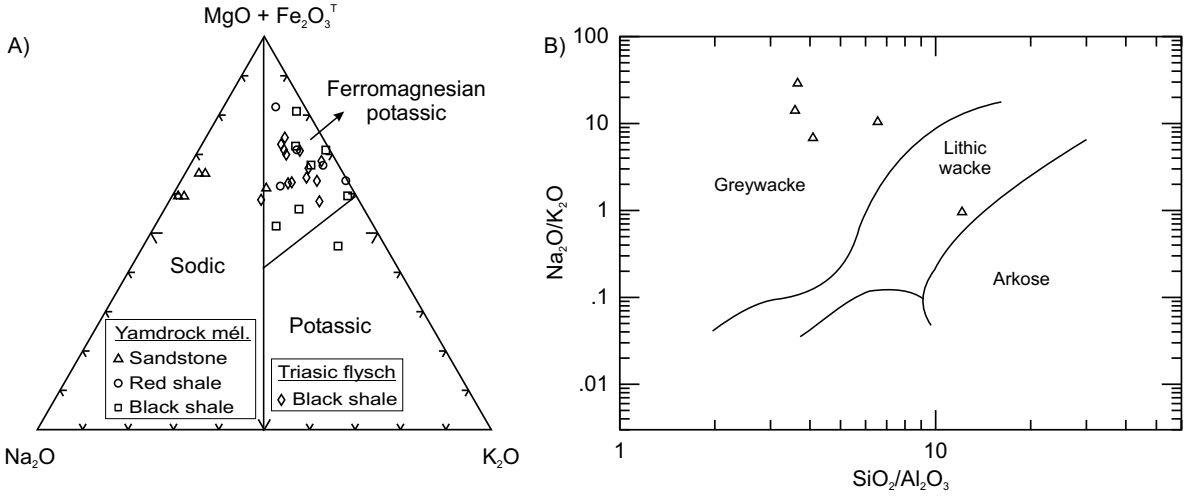

FIG. 4.4 – A) Classification of sandstones according to Blatt *et al.* (1980). B) $\mathrm{Log}(Na_2O/K_2O)$ vs. $\log(SiO_2/Al_2O_3)$ discriminating among greywacke, lithic wacke and arkose (after Pettijohn et al., 1973).

4.5.3 Major elements

On the $(Fe_2O_3{}^T + MgO)$-Na_2O-K_2O triangular diagram of Blatt et al. (1980), four sandstones classify as sodic, whereas the quartz-rich sandstone classifies as ferromagnesian potassic (Fig. 4.4A). On the $\log(Na_2O/K_2O)$-$\log(SiO_2/Al_2O_3)$ diagram of Pettijohn et al. (1973), the same rocks classify as greywackes ($K_2O/Na_2O < 1$) and lithic wacke ($K_2O/Na_2O = 1$), respectively (Fig. 4.4B). The shales, both red and black, almost all classsify as ferromagnesian potassic on the $(Fe_2O_3{}^T + MgO)$-Na_2O-K_2O triangular diagram. One black shale classifies as potassic. However, this shale is one of the most siliceous (SiO_2 of 80.3 wt.%), and other major elements, especially ferromagnesian elements, are correspondingly diluted. The shale composition is thus more representative of a relative depletion in ferromagnesian rather than an enrichment in potassium. Shales have $K_2O/Na_2O > 1$. The less siliceous rocks have SiO_2 lower than 60 wt.% and Al_2O_3 slightly higher than 24 wt.%, whereas the more siliceous have SiO_2 as high as than 86 wt.% and Al_2O_3 as low as 6.6 wt.%, expressing quartz/clays feldspar ratio. SiO_2/Al_2O_3 ratios range from 2.4 to 13.

Most major elements are negatively correlated with SiO_2, reflecting the quartz dilution effect. For the sandstones, SiO_2 strongly correlates with Al_2O_3, MgO, TiO_2 and Na_2O (r of -0.97 to -0.95 at a significance level (α) of 0.5 and 1%, respectively), and correlates well with P_2O_5, MnO and Fe_2O_3 (r of -0.81 to -0.72 at α of 5 to 10%) (Table 4.1). The absence of significant covariation for CaO ($r = +0.26$ at $\alpha >>10\%$) and K_2O ($r = +0.62$ at $\alpha > 10\%$) may be explained by the mobility of these elements during

TAB. 4.1 – Correlation coefficients between major elements and SiO_2 for the sandstones.

	Correlation coefficient r	Student's correlation test t	Significance level α (%)
SiO_2-TiO_2	-0.95	-5.40	1
SiO_2-Al_2O_3	-0.97	-7.24	0.5
SiO_2-Fe_2O_3	-0.72	-1.78	10
SiO_2-MnO	-0.81	-2.40	5
SiO_2-MgO	-0.97	-6.71	0.5
SiO_2-CaO	+0.26	+0.46	>>10
SiO_2-Na_2O	-0.95	-5.14	1
SiO_2-K_2O	+0.62	+1.35	>10
SiO_2-P_2O_5	-0.80	-2.31	10

weathering, diagenesis and regional metamorphism. Correlations are generally much weaker for the shales (r ranging from -0.85 to -0.13 ; Table 4.2). Nevertheless, at α = 0.1%, Al_2O_3 (r = -0.85), K_2O (r = -0.65) and Fe_2O_3 (r = -0.65) show good negative correlations with SiO_2.

4.5.4 Trace elements

REE patterns are LREE-enriched : La abundances vary from 7 to 35 and from 60 to 256 times chondrite for the sandstones and shales, respectively. The same way Yb abundances vary from 4 to 12 and from 54 to 86 times chondrite, respectively (Fig. 4.5). An individual shale has a lower La abundance of 32 times chondrite, but a "normal" Yb abundance of 14 times chondrite, resulting in a U-shape-like pattern. All rocks show a significant negative Eu anomalie. When normalized to the Post-Archean average Australian shale (PAAS, Taylor and McLennan, 1985), REE patterns are generally flat (Fig. 4.6). La abundances vary from 0.3 to 0.5 times PASS and from 0.4 to 1.5 times PASS for the sandstones and shales, respectively. The same way Yb abundances vary from 0.25 to 0.7 and from 0.4 to 1.4, respectively. The individual shale is LREE-depleted ($(La/Yb)_N$ of 0.2). Similarly, on multi-element patterns normalized to the average upper continental crust, the only deviations from the average trend are represented by slight positive Ti anomalies (especially on patterns of sandstones), and slight negative Zr-Hf anomalies on the patterns of shales.

There is moderate but significant correlation between LREE, HREE and Al_2O_3

TAB. 4.2 – Correlation coefficients between major elements and SiO_2 for the shales.

	Correlation coefficient r	Student's correlation test t	Significance level α (%)
SiO_2-TiO_2	-0.55	-3.24	0.5
SiO_2-Al_2O_3	-0.85	-8.05	0.1
SiO_2-Fe_2O_3	-0.65	-4.19	0.1
SiO_2-MnO	-0.19	-0.93	>10
SiO_2-MgO	-0.49	-2.77	1
SiO_2-CaO	-0.36	-1.86	5
SiO_2-Na_2O	-0.28	-1.43	10
SiO_2-K_2O	-0.65	-4.21	0.1
SiO_2-P_2O_5	-0.13	-0.65	>>10

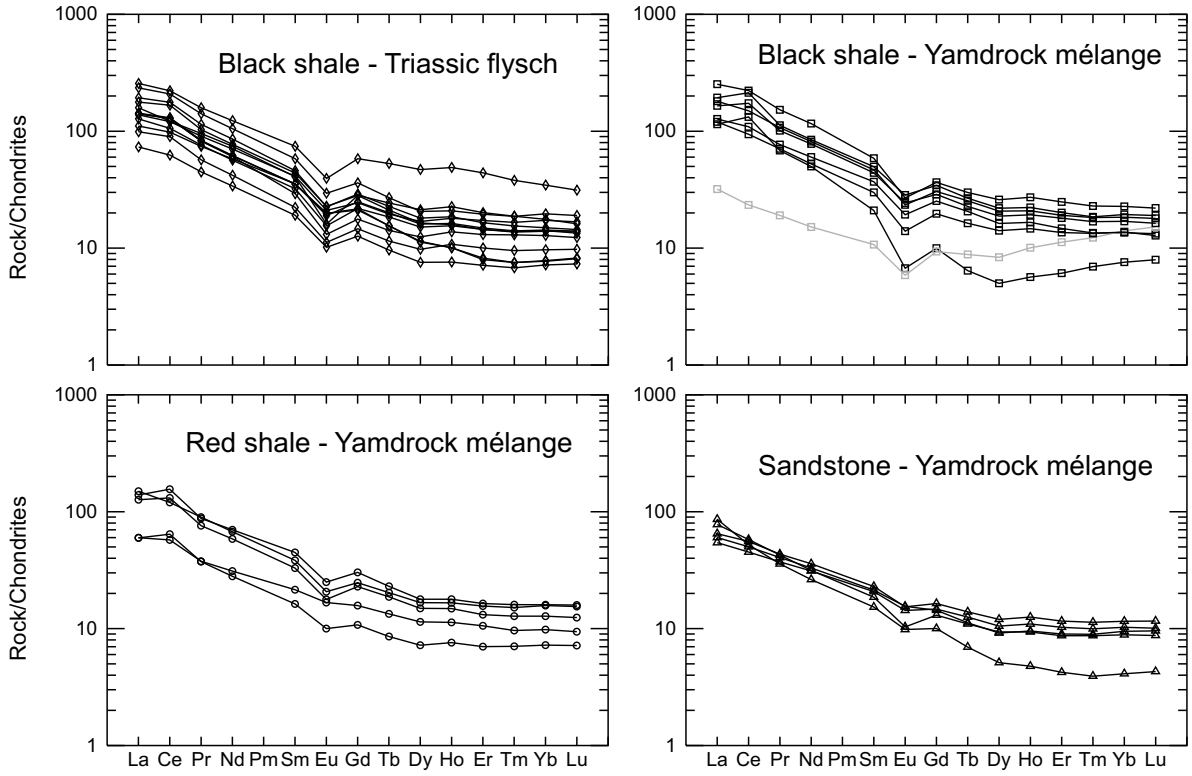

FIG. 4.5 – REE patterns normalized to chondrite for sedimentary rocks from the Mesozoic Yamdrock mélange and the Triassic flysch. Normalizing values are from Sun and McDonough (1989).

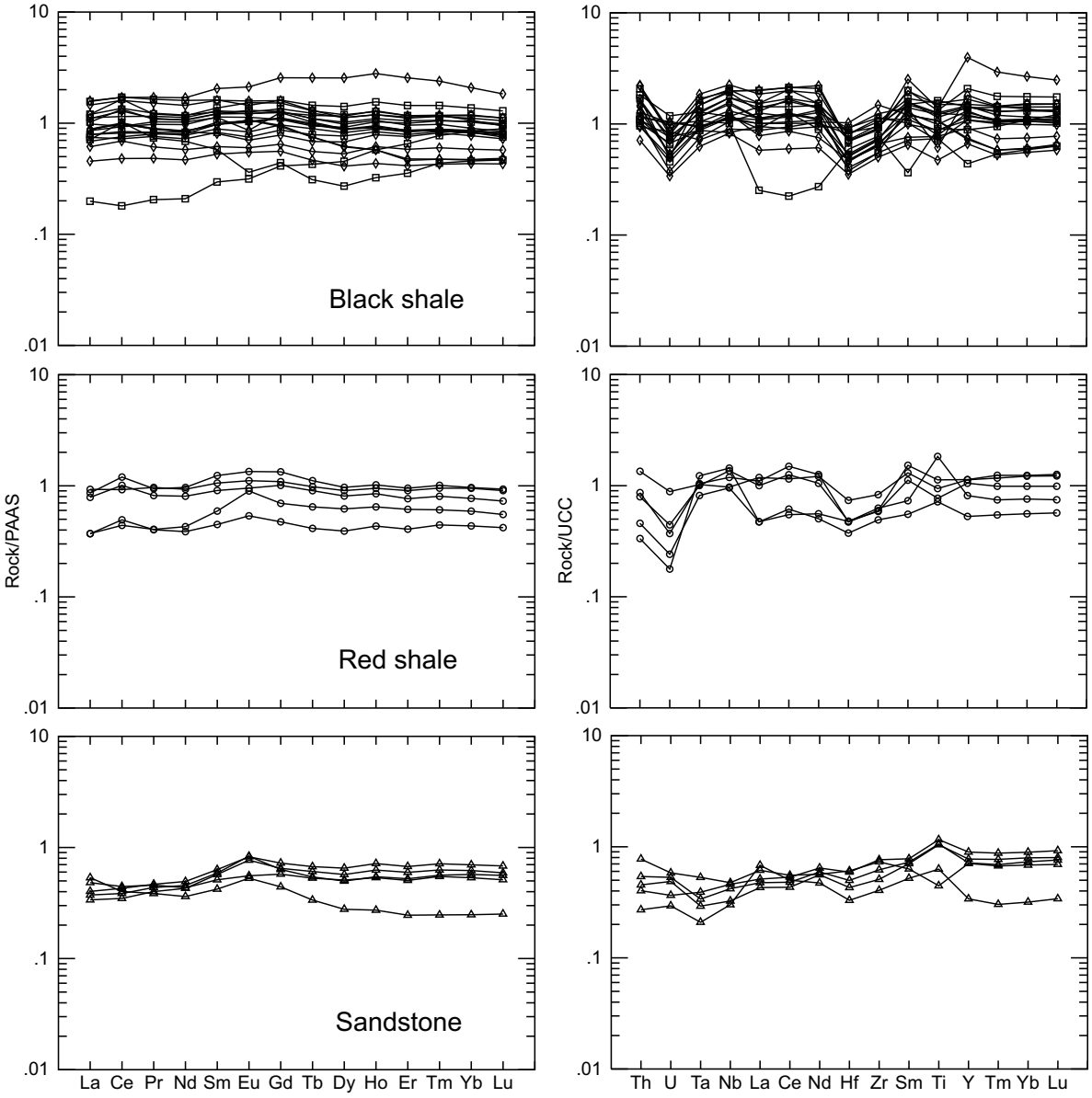

FIG. 4.6 – REE patterns normalized to Post-Archean average Australian shale (PAAS) (left column) and multi-element patterns normalized to the average upper continental crust (UCC) (right column) for sedimentary rocks from the Mesozoic Yamdrock mélange and the Triassic flysch. Normalizing values are from Taylor and McLennan (1985), except Nb, Ta and Ti that are from McLennan (2001).

($r_{Al_2O_3\text{-La}} = +0.62$ and $r_{Al_2O_3\text{-Yb}} = +0.61$ at $(\alpha) = 0.1\%$), as REE are preferentially incorporated into clay minerals. There are moderate to strong positive correlations (α of 0.1%) between the mobile elements Ba, Rb, and Th, and Al_2O_3 ($r_{Al_2O_3\text{-Rb}} = +0.66$; $r_{Al_2O_3\text{-Th}} = +0.73$) and K_2O ($r_{K_2O\text{-Ba}} = +0.65$; $r_{K_2O\text{-Rb}} = +0.89$; $r_{K_2O\text{-Th}} = +0.74$), as these elements are also preferentially incorporated into clay minerals. Not surprisingly, correlation between Al_2O_3 and Rb-Th is much stronger for the shale population alone ($r_{Al_2O_3\text{-Rb}} = r_{Al_2O_3\text{-Th}} = +0.91$ at $\alpha = 0.1\%$). On the other hand, there is no correlation between Rb and Sr ($r_{Rb\text{-Sr}} = +0.07$); this is expected for detrital material derived from source rocks having undergone chemical weathering (Nesbitt and Young, 1989) due to the different behavior of Rb and Sr during weathering processes. Rb/Sr ratios range from 0.3 to 10.6 for the shales, and from 0.05 to 0.6 for the sandstones. The strong positive correlations between Th and LREE ($r_{La\text{-Th}} = +0.89$ at $\alpha = 0.1\%$) further suggests that Th was partitioned among the felsic detrital material. As a consequence, Th/U ratios are very fractionated in the shales (average of 7.7 ± 2.3, maximum of 13).

In a broad manner, Th, U, Ta and Hf are moderately to weakly negatively correlated with SiO_2, indicating that heavy-mineral fraction is not strongly accumulated in these sedimentary rocks. On the other hand, the moderate correlation between Zr and Yb ($r_{Zr\text{-Yb}} = +0.50$ at $\alpha = 0.5\%$) suggests that the distribution of HREE may be controlled to a certain extent by Zr-rich phases, such as detrital zircon. Possible accumulation of detrital titanate minerals (e.g. rutile, titanite) is further indicated by the moderate correlation between Ta and TiO_2 ($r_{TiO_2\text{-Ta}} = +0.66$ at $\alpha = 0.1\%$). It seems however that the distribution of REE was not controlled by that of detrital apatite, as there is no correlation between P_2O_5 and REE ($r_{P_2O_5\text{-Yb}} = +0.03$; $r_{P_2O_5\text{-La}} = -0.17$).

4.6 Discussion

4.6.1 Effects of weathering, heavy-mineral accumulation, diagenesis, and metamorphism on the composition of sedimentary rocks

As will be detailed for each of the following processes, major and trace elements can be subject to important mobilization and fractionation during weathering, mineral accumulation, diagenesis and metamorphism. Hence, in order to properly identify the source characteristics of the studied sedimentary rocks, some control tests must be performed on the geochemical data prior to interpretations.

Source weathering

Weathering involves the conversion of volcanic glass and unstable minerals, mainly feldspars and mica, to clay, as well as oxidization of ferromagnesian components. Degradation to clay coupled with dissolution reactions induce mobilization and fractionation of many elements in weathering profiles, including rare earth elements (e.g. Morey and Setterholm, 1997). Along with progressive weathering, soils are increasingly depleted in soluble cations such as Ca^{2+} and Sr^{2+} ($\pm Mg^{2+}$), while relatively enriched in insoluble primary minerals like zircon, and Fe, K, Rb, Th and REE, which are strongly partitioned in, or absorbed on, clay minerals, iron oxides and hydroxides (e.g. Nesbitt and Young, 1989). The consequent increase in the Rb/Sr ratio of most rocks during weathering is a good indicator of the degree of weathering. As observed by the low argillization of feldspars, the sandstones have relatively low Rb/Sr ratios ranging from 0.04 to 0.57. By comparison, mafic blocks within the Yamdrock mélange and flysch give average values of 0.04 and 0.15, respectively. As expected, the shales reach much higher Rb/Sr ratios of 0.3 - 4.8 (with an exceptional value of 10.6) and 2.4 - 7.3 for the black and red shales, respectively.

The Chemical Index of Alteration (CIA) of Nesbitt and Young (1982) quantitatively expresses the degree of weathering of feldspars to clays. The CIA has been established as a general guide of the degree of weathering of source rocks. Using molecular proportions :

$$\mathrm{CIA} = \mathrm{Al_2O_3}/(\mathrm{Al_2O_3} + \mathrm{K_2O} + \mathrm{Na_2O} + \mathrm{CaO_{Sil}}) * 100, \tag{4.1}$$

where $\mathrm{CaO_{Sil}}$ represents calcium bound in silicate mineral structure. CIA varies from less than 50 for unweathered igneous rocks to near 100 for residual clays ; typical shales average about 70-75. Shales of the Yamdrock mélange and flysch have CIA values ranging from 62 to 79, with an average of 72.5 $\pm$ 6. Three shales have unrealistic low CIA of 39, 50 and 57. Their CaO content is too high to be structurally enclosed in silicate minerals, which suggests, together with high LOI of 7-14 wt.%, that diagenetic or low-T hydrothermal carbonates may be present in a significant amount in these shales. Corrected CIA values of 73, 74 and 70 are obtained by using an average CaO content. Such CIA, in addition with very low CaO/MgO of 0.21 ± 0.11 and fractionation between Rb and Sr (Rb/Sr generally > 0.5), suggest that moderate to strong weathering occurred in the source areas of the shales.

The average CIA of the four greywackes is 51.5 $\pm$ 3.5, whereas that of the more potassic lithic wacke is 32. However, as observed for the shales, CIA values may also depend on the alteration state of the rock. Hydrothermal alteration tends, in a broad

manner, to lower the calculated CIA values of altered greywackes due mainly to relative CaO (and CO_2) gains and Al_2O_3 losses associated with carbonate alteration (La Flèche and Camiré, 1996). The sampled greywackes do contain small amounts of calcite, with LOI ranging between 2.4 and 5.1 wt.%. The very low CIA value of the lithic wacke is due to the relative Al_2O_3 (6.7 wt.%) depletion with respect to other elements (CaO + Na_2O + K_2O = 8.3 wt.%), probably as the result of clays being flushed away by a strong current. Nevertheless, the CIA of greywackes are significantly lower than those of the shales, which suggests, in addition to the slightly higher CaO/MgO of 0.95 ± 0.27 and the lower Rb/Sr values, that they are less weathered. This is to be expected from greywackes, which are considered to have undergone high erosion rates, rapid sedimentation, and therefore a weak to moderate degree of chemical weathering in the source area (La Flèche and Camiré, 1996).

Sedimentary sorting and heavy-mineral accumulation

Heavy-mineral accumulation during sedimentary sorting can considerably complicate interpretations of sediment provenance by producing irregular chemical variations in some trace elements (McLennan et al., 1993). For instance, Zr and Hf may be concentrated in the coarser fraction of the sediment due to zircon accumulation in the latter. In the same manner, REE and Th abundances may depend on accumulation of monazite, apatite, zircon or titanite (e.g. Crichton and Condie, 1993). Although the moderate correlation observed between the pairs Zr-Yb and Ti-Ta suggests some accumulation of zircon and titanite, it appears, nevertheless, that heavy-mineral accumulation did not have a significant effect on the whole-rock geochemical signature of the Neo-Tehyan sediments, as only weak and not systematic covariations are observed between LREE and Th (Fig. 4.7A), HREE and Hf (Fig. 4.7B), and Ta/La and Ti (Fig. 4.7C). Accumulation of apatite and allanite is counterindicated by the weak fractionation of La/Sm, Tb/Yb and Ta/La ratios (Fig. 4.7). Accumulation of monazite is further counterindicated by an average $(Gd/Yb)_N$ ratio of 1.7 ± 0.4, typical of post-Archean sediments and most upper crustal igneous rocks (even small amounts of monazite result in significant increases in the $(Gd/Yb)_N$ ratio ; McLennan, 1989 ; McLennan and Taylor, 1991). Although some samples tend to align along the accumulation trends of zircon and titanite (Fig. 4.7A-B), accumulation of these heavy minerals is probably not significant since the Ta/La ratio is not really fractionated (Fig. 4.7C).

The effect of heavy-mineral accumulation and hydraulic sorting on the geochemical signature of a sediment can also be evaluated by comparing the relative abundances of insoluble elements, such as Al_2O_3 and TiO_2, which are generally unaffected by weathering processes and which are preferentially incorporated in clay particles of argillaceous

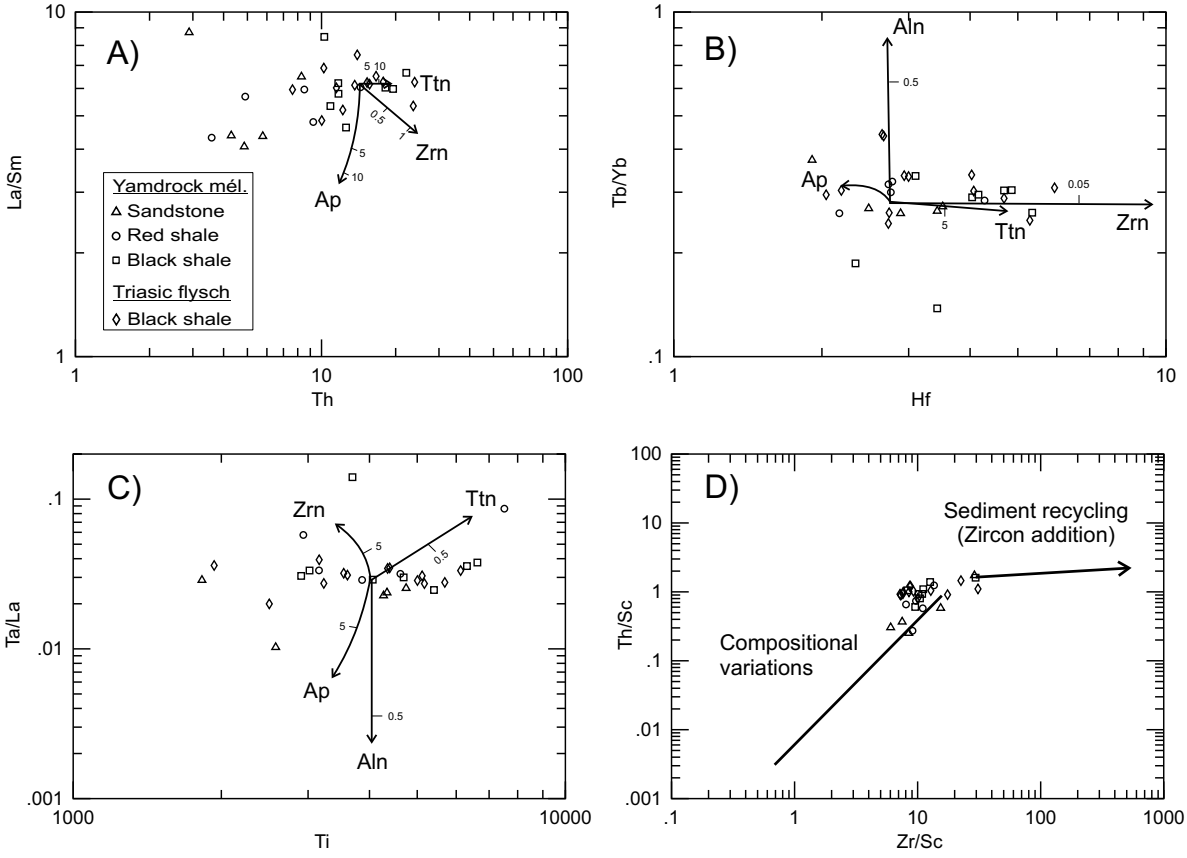

FIG. 4.7 – Calculated accumulation trends of detrital apatite (Ap), allanite (Aln), titanite (Ttn) and zircon (Zrn) showing the effects of heavy-mineral accumulation on selected trace elements and trace element ratios (from La Flèche and Camiré, 1996). A) La/Sm vs. Th ; B) Tb/Yb vs. Hf ; C) Ta/La vs. Ti. D) Plot of Th/Sc vs. Zr/Sc showing enrichments of zircon as opposed to compositional variations of the provenance ; trends of compositional variations and sediment recycling from McLennan et al. (1993).

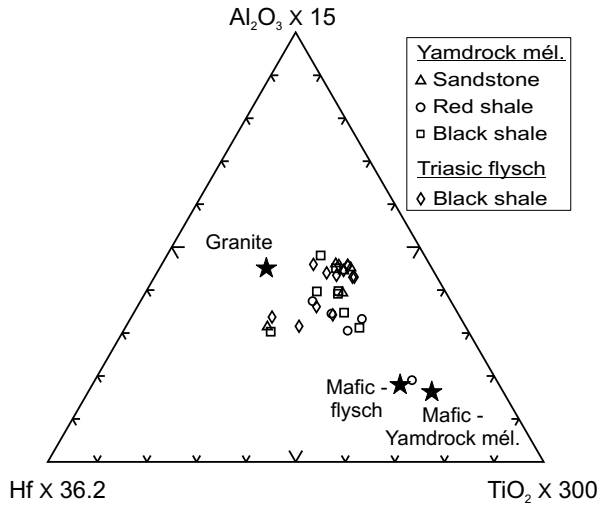

FIG. 4.8 – (Hf × 36.2)-(Al_2O_3 × 15)-(TiO_2 × 300) triangular diagram of Garcia et al. (1994) modified by La Flèche and Camiré (1996). Increasing maturity of sedimentary rocks is indicated by the arrow. The filled stars indicate the average composition of mafic blocks and one granitic block in the sedimentary units (Dupuis et al., 2003 ; 2004).

beds, and Zr and Hf, commonly partitioned in coarser grained zircon of sandy beds. This is schematized in the (Hf × 36.2)-(Al_2O_3 × 15)-(TiO_2 × 300) triangular diagram of Garcia et al. (1994), where close grouping of Neo-Tehyan sedimentary rocks away from the Hf pole indicates that Hf abundances were not controlled by zircon accumulation and that the rocks are fairly juvenile (Fig. 4.8). Finally, on a graph of Th/Sc vs. Zr/Sc (Fig. 4.7D), the sandstones and shales fall on the trend defined by active margin turbidites, a trend consistent with igneous chemical differentiation, i.e. provenance, being the primary control (McLennan et al., 1993). Our sedimentary rocks show high Th/Sc and Zr/Sc ratios similar to those of passive margin turbidites, but do not show a substantial increase in Zr/Sc with respect to Th/Sc indicative of zircon enrichment. These results confirm that the Neo-Tehyan sandstones and shales are passive margin sediments derived from highly chemically differentiated igneous rocks, but not affected by significant sedimentary recycling such as zircon accumulation. Intermediate SiO_2/Al_2O_3 ratios further suggest absence of significant sedimentary reworking (McLennan et al., 1993).

Diagenesis and metamorphism

Significant albitization, illitization, feldspar dissolution, as well as carbonate, quartz and limonite diagenetic cementation, accompanied by important chemical changes, are

well documented in some reservoir sandstones (e.g. Land et al., 1987). Albitization of feldspars may explain why the greywackes have low K_2O/Na_2O ratios. However, in finer grained siliciclastic sediments, the concentrations of most major components are not significantly changed during diagenesis (Wintsch and Kvale, 1994). Among the many reactions occurring during diagenesis, only illitization of smectite and dissolution of calcite appear to have significant effects (K_2O gains and CaO losses, respectively) on the bulk composition of mudstones (La Flèche and Camiré, 1996). Other elements like REE, Hf, Ta, Th, Zr, Cr, Co and Sc are transported in the terrigenous components or carried largely as suspended rather than dissolved loads during erosion, transfer, transport and sedimentation because they are relatively insoluble in most natural waters. They may be massively transferred from source to sediment, and therefore used as reliable provenance indicators (Taylor and McLennan, 1985). Diagenetic and metamorphic reactions (up to upper amphibolite grade) appear to redistribute these elements among various diagenetic and metamorphic minerals without significant remobilization of the elements into or out of the system (Ohr et al, 1991 ; Bau, 1991 ; Totten and Blatt, 1993). Accordingly, neither diagenesis nor metamorphism (up to partial melting reactions) appear to significantly affect bulk-rock REE and mutli-element patterns. Geodynamic interpretations made from such trace-element patterns are therefore more significant and reliable than those obtained from major element compositions.

4.6.2 Geodynamic interpretation

The parameters that are known and should be taken into consideration before chemical constraints can be placed further on the provenance of sedimentary rocks south of the YZSZ are as follows. (1) The Yamdrock mélange and flysch units contain blocks of mafic rocks. (2) A very evolved granitic block was also found in the Triassic flysch. (3) Limited sedimentary reworking and low Hf/TiO_2 and Hf/Al_2O_3 (Fig. 4.8) indicate that the sandstones and shales are immature and most likely monocyclic. (4) Moderate to strong chemical weathering of the source areas suggests, nevertheless, that the sediments were not simply unconsolidated debris eroded from active volcanoes, but probably derive from a continental passive margin.

On the basis of whole-rock chemistry, sedimentary rocks of the Yamdrock mélange and flysch mostly have an old upper continental crustal (OUC) provenance, according to the terrane classification of McLennan et al. (1993). The rocks, especially the shales, generally have evolved major element compositions (e.g. moderately high CIA, $SiO_2/Al_2)_3$, $K_2)/Na_2O$), which reflect a dominance of upper crustal granitic sources and a relatively severe weathering history. The rocks also have substantial negative Eu anomalies (average Eu/Eu* of 0.6 $\pm$ 0.1 and 0.8 $\pm$ 0.04 for the shales and grey-

wackes, respectively), which reflect intracrustal geochemical differentiation involving considerable separation of plagioclase (Taylor and McLennan, 1985). Enrichment of incompatible over compatible elements, such as LREE enrichment (Fig. 4.5) and high Th/Sc ratios (Fig. 4.7D), reflects felsic component provenance compositions, whereas high Rb/Sr (> 0.5) and Th/U (> 3.8) reflect weathering. The different REE pattern of one individual black shale (smaller LREE enrichment) corresponds more to the young differentiated arc (YDA) terrane type of McLennan et al. (1993). The YDA provenance component represents young (mantle derived) volcanic and plutonic igneous rocks of island and continental arcs that were affected by intracrustal differentiation such that they possess significant negative Eu anomalies (Eu/Eu* of 0.6 in this case). However, the shale was significantly affected by weathering processes, a feature not expected for a YDA provenance. As a matter of fact, the shale has a low, but not abnormal, CIA of 65 and a fairly high Rb/Sr of 4.8. A mixture of young undifferentiated arc (YUA) and OUC, such as observed in mature arc environments (McLennan et al., 1990), is probably a more realistic provenance. Moreover, apart from the REE pattern, chemical compositions and ratios of this individual shale are very similar to those of our total turbiditic shale population.

The high Th/U ratios observed in the Yamdrock mélange and sedimentary rocks could also indicate the contribution of granulitic felsic gneisses, i.e. the contribution of deeply eroded cratonic areas. However, low Rb/Cs ratios (average of 25 ± 10) suggest that such a contribution was not significant (La Flèche and Camiré, 1996). Low Y/Ni ratios (<1) rather indicate the contribution of a mafic to ultramafic component to the Neo-Tethyan turbidites. Low Cr/Ti (<0.04) and Cr/V (<1.2) ratios further reflect the probable absence within the turbidites of chromite and ultramafic components characteristic of the ophiolitic sequences lying north of the flysch and Yamdrock mélange sequences. The contrasting geochemistry of mafic blocks within the sedimentary units and the overlying ophiolitic units have already shown that these distinct geological units also come from different tectonic environments (Dupuis et al., 2003 ; 2004).

Examples of sedimentary rocks dominated by OUC include abundant cratonic shales, most passive margin turbidites and foreland basin sediments derived from the older exposed continental crust (McLennan et al., 1993). For the Yamdrock mélange and flysch sedimentary rocks, flat REE patterns averaging 1, when normalized to average Post-Archean Australian Shale (PAAS) and upper continental crust (UCC ; Fig. 4.6), are typical of sedimentary rocks derived from a passive margin. By using the Hf-Al_2O_3-TiO_2 ternary diagram (Fig. 4.8), we can see that the sedimentary rocks may be obtained from mixing of detrital material derived from mafic and felsic rocks of the Indian passive margin, onto which the flysch and Yamdrock mélange units have been deposited. In fact, LREE of the Neo-Tethyan turbiditic sedimentary rocks are strongly fractionated

with $(La/Sm)_{CN}$ ratios falling in between those of the mafic rocks and the granitic value (Fig. 4.9). Low $(Ta/Th)_{CN}$ ratios further indicate that genesis of the igneous source involved subduction and (or) crustal recycling processes (Fig. 4.9A). This signature is most probably derived from a granitic component similar to the granitic block of the flysch, which has a very evolved geochemical signature, and because the mafic rocks rather have an intraplate geochemical signature (Dupuis et al., 2003 ; 2004).

Th/Sc and Hf/Sc ratios are especially sensitive to fluctuations in mafic vs. felsic sources, Sc being preferentially concentrated in the former, while Th and Hf in the latter (La Flèche and Camiré, 1996). Sedimentary rocks of the Yamdrock mélange and flysch have Th/Sc and Hf/Sc ratios closer to those of the average mafic rocks than the granitic one, especially for Hf, indicating that the contribution of mafic intraplate components in the source was probably more important than that of granitic components (Fig. 4.9B-C). However, we have to keep in mind that the chemistry of mafic rocks from the Triassic flysch has itself been partly overprinted by partial crustal assimilation of the Indian Plate associated with magmatism resulting from opening of the Neo-Tehys basin (Dupuis et al., 2003 ; 2004). While the upper continental crust is usually believed to have a granodiorite composition, slight positive Ti anomalies (when normalized to UCC) are reminiscent of enriched mafic blocks of intraplate affinity found in the sedimentary units.

Based solely on their geochemistry, sedimentary rocks of the Triassic flysch and Yamdrock mélange thus seem both to have been deposited on a continental passive margin setting, and to be derived from a similar OUC source. However, based on other geological observations, the Triassic flysch and Mesozoic Yamdrock mélange are representative of distinct specific geodynamic settings (Fig. 4.10). Our results confirm that the Triassic flysch is composed of turbidite sequences deposited on the Indian passive margin and extending on the growing Neo-Tehys basin, as previously illustrated by Nicolas (1989) (Fig. 4.10A). The flysch is the result of erosion of igneous and sedimentary rocks of the Indian upper continental crust (UCC). Contemporaneously with initial rifting, mafic dykes were produced by partial melting of the lower continental crust (LCC) by an continental intraplate alkaline magma source below the Indian Plate (Dupuis et al., 2003 ; 2004). Together with remnants of Cambrian granite batholiths (Yin and Harrison, 2000), they were eroded and incorporated within the flysch unit.

As mentioned in the geological setting description, during the opening of the Neo-Tehys basin in the Late Triassic-Early Jurassic, compression caused by the Indian Block approaching from the south resulted in the initiation of a north-dipping intra-oceanic subduction zone, active from at least Late Jurassic to the end of Early Cretaceous times (Girardeau et al., 1984 ; Göpel et al., 1984 ; Miller et al., 2003 ; Zyabrev et al., 1999 ;

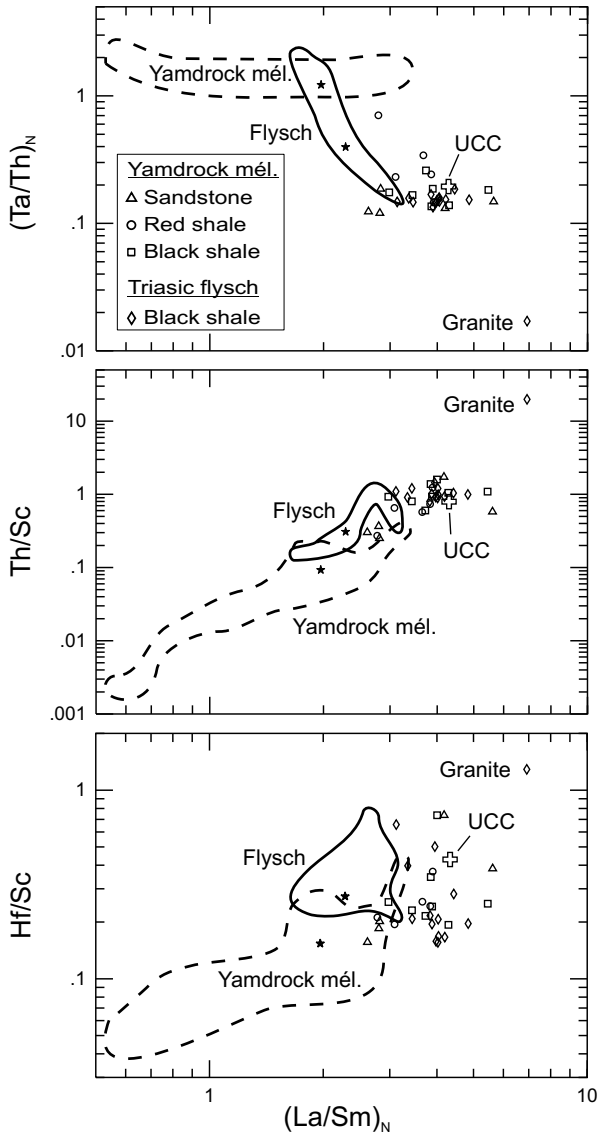

FIG. 4.9 – $(Ta/Th)_N$ (A), Th/Sc (B) and Hf/Sc (C) vs. $(La/Sm)_N$. Chondrite normalizing (N) values from Sun and McDonough (1989). Fields represent mafic blocks found in the sedimentary units with average values represented by the black stars (Dupuis et al., 2003 ; 2004). Upper continental crust (UCC) values from Taylor and McLennan (1985), expect Ta and Sc from McLennan (2001).

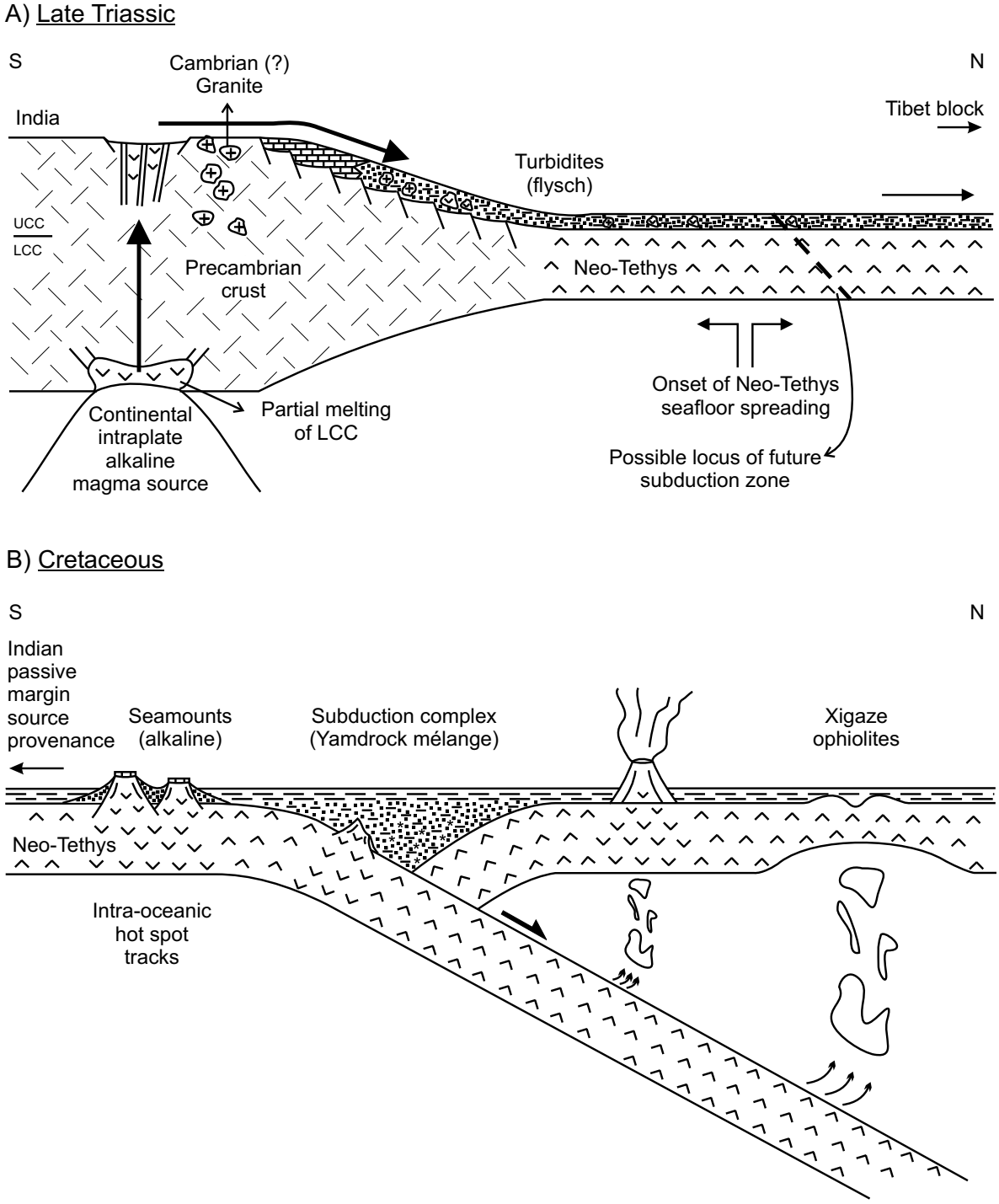

FIG. 4.10 – A) Late Triassic geodynamic situation at the time of flysch deposition ; B) Cretaceous geodynamic situation at the time of intra-oceanic subduction and Yamdrock mélange deposition. Not to scale. The geodynamic setting of the ophiolites is greatly simplified and is shown solely to illustrate the initial spatial distribution between the now adjacent units. UCC = Upper Continental Crust, LCC = Lower Continental Crust.

Ziabrev et al., 2003). Structural and tectonostratigraphic features of the Yamdrock mélange recall its formation within an intra-oceanic subduction complex (Mercier et al., 1984, Searle et al., 1987 ; Aitchison et al, 2000), and the unit has been interpreted to consist mostly of material off-scraped from the down-going Tethyan slab (Chang, 1984 ; Ziabrev et al., 2001) (Fig. 4.10B). Our results indicate that this material represents Indian continental passive margin deposits, including deeper-water radiolarites, that were transported on the growing Neo-Tethys ocean floor. According to paleomagnetic (Pozzi et al., 1984 ; Abrajevitch, 2002) and tomographic (Van der Voo et al., 1999) investigations, the subduction zone that generate the Xigaze ophiolites and the Yamdrock mélange subduction complex was located at equatorial to low northern latitudes at least 1000-1500 km south of Asia's margin and about 2000 km north of India's margin. The turbidite deposits would thus have travelled some 2000 km to the north on the growing Neo-Tethys ocean floor, a scenario observed in modern oceanic basins. Moreover, the Yamdrock mlange contains remnants of alkaline seamounts (e.g. Mercier et al., 1984 ; Searle et al., 1987 ; Liu and Einsele, 1999 ; Aitchison et al., 2000) of intra-oceanic intraplate geochemical affinity (Dupuis et al., 2003 ; 2004). These alkaline seamounts were thus probably derived from the same intraplate alkaline magma source that generated the mafic dykes, now as blocks within the Triassic flysch, and which evolved from continental to oceanic after the rifting event. Albanian and Greek ophiolitic sequences of the Mesozoic Tethys ocean are also thrust over a sub-ophiolitic mélange, which has similar geological characteristics than the Yamdrock mélange (Bortolotti et al., 2004). The origin of both mélanges is probably a multi-stage process, with sedimentary (deposition in an accretionary wedge) and tectonic (progressive obduction onto the Indian continental margin) events.

Implications for Himalayan geology

Several isotopic studies have been conducted on rocks of the Himalayan Series, including the YZSZ (e.g. compilation by Najman et al., 2000), but few trace element data are available for sedimentary rocks of the same area. Nevertheless, we were able to correlate our geochemical data with clastic metasedimentary rocks of greywacke composition from Garhwal Himalaya (Ahmad et al., 2000). As discussed previously, plots of immobile-element ratios can discriminate between clastic units derived from contrasting source regions, and such plots remain robust during high-grade metamorphism. Using such immobile-element ratios (Fig. 4.11), sandstones and shales from the Yamdrock mélange and Triassic flysch correlate especially well with metasedimentary rocks from the High Himalayan (HH) Crystalline Series and Outer Lesser Himalayan (OLH) Series. Except for the Munsiari and Ramgarh Groups which have developed metamorphism up to garnet grade (Ahmad et al., 2000), there is also a good correlation with

metasedimentary rocks from the Inner Lesser Himalayan (ILH) Series. Usually, a linear array in the Zr/Al_2O_3-TiO_2/Zr space (Fig. 4.11B) is defined by sediments of variable size fractions derived from the same source area ; the array is caused by the differences in hydraulic behavior between minerals containing Zr and those containing Al_2O_3-TiO_2 (Fralick and Kronberg, 1997). The main differences observed for our rocks, i.e. displacement towards the Sc pole (Fig. 4.11A) and towards higher TiO_2/Zr ratios (Fig. 4.11B), may be attributed to the mafic contribution detected in the geochemistry of the studied rocks.

Sedimentary rocks of the Yamdrock mélange and the Triassic flysch also correlate well with shales and sandstones of the Cretaceous Tianba flysch (Fig. 4.11), located to the south of the YZSZ, i.e. just southeast of our study area (Zhu, 2003). In agreement with detrital zircon analyses, paleocurrent data and paleontological data (Myrow et al., 2003), the uniformity in sedimentary rocks from the Mesozoic Yamdrock mélange, the Triassic flysch, and the Cretaceous Tianba flysch, which altogether cover a large spatial area and a large time span, as well as the good correlation with distinct lithotectonic units of the Himalaya, all tend to support the 'continuous margin' model. According to this model, all three main lithotectonic zones, the Greater, Lesser and Tethyan Himalaya, represent different proximal-to-distal parts of an ancient passive margin of northern India (Brookfield, 1993 ; Searle, 1986 ; Corfield and Searle, 2000). It appears that element and isotope geochemistry give complementary information about the tectonic setting, source and depositional history of sedimentary rocks, and that conclusions must not be drawn on limited data.

4.7 Conclusion

The geochemical signature of sandstones, red shales and black shales of the Yamdrock mélange and flysch units lying immediately south of the YZSZ, in southern Tibet, do not present significant variations between the different rock types and geological units, and are concordant with a continental passive margin setting. Shales have CIA (average of 72.5 ± 6) typical of shales around the world, which suggests, in addition with important fractionation between Rb and Sr, that moderate to strong weathering occurred in their source areas. Greywackes have undergone higher erosion rates, rapid sedimentation, and therefore weak to moderate chemical weathering (average CIA of 51.5 ± 3.5). Despite this fairly important chemical weathering, the whole-rock chemical signature of both sandstones and shales was not affected by significant sedimentary recycling nor heavy-mineral accumulation. REE patterns indicate that the Neo-Tethyan turbidites mostly derive from a felsic old upper continental crust (UCC) source. Slight

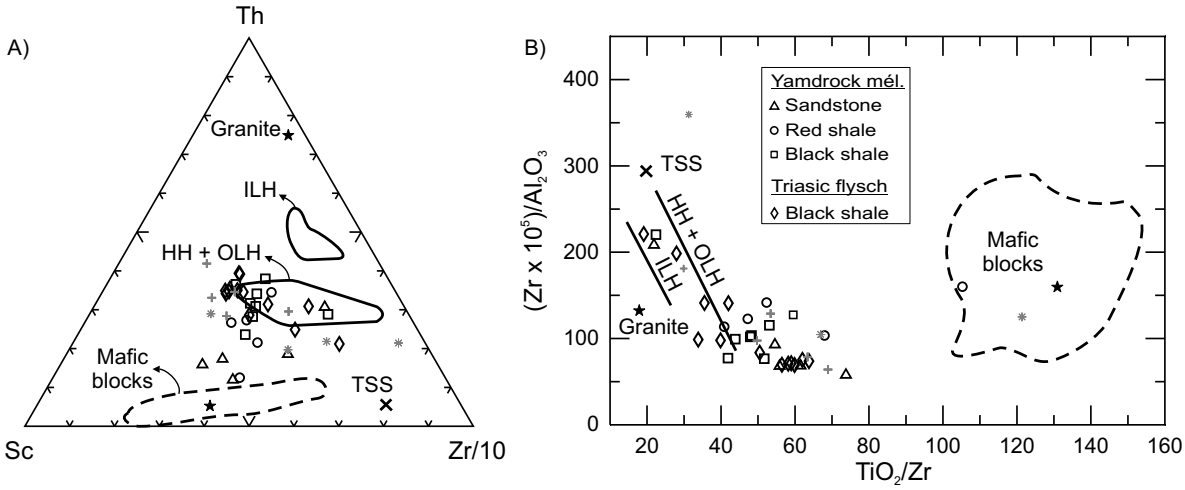

FIG. 4.11 – A) Th-Sc-Zr ternary plot for sandstones and shales of the Yamdrock mélange and Triassic flysch (after Bhatia and Crook, 1986). B) $(Zr \times 10^5)/Al_2O_3$ ratio diagram for the same data set (after Fralick and Kronberg, 1997). Grey crosses and asterisks represent shales and sandstones, respectively, of the Tianba flysch, southern Tibet (Zhu, 2003). Clastic metasedimentary rocks of greywacke composition from Garhwal Himalaya (Ahmad et al., 2000) are shown for comparison. TSS, Tethyan Sedimentary Series ; HH, Higher Himalaya crystalline series ; ILH and OLH, Inner and Outer Lesser Himalaya series, respectively. Dashed fields represent mafic blocs from de Yamdrock mélange with average value represented by the star (Dupuis et al., 2003 ; 2004).

positive Ti anomalies, with respect to the UCC, in addition with characteristic element ratios, indicate a mafic contribution to the source. This mafic contribution most probably comes from mafic blocks of enriched intraplate geochemical affinity found in the sedimentary units. Thus, the sedimentary rocks outcropping south of the YZSZ were derived from the old Indian continental crust, including remnants of migmatitic granite batholiths and intraplate mafic blocks. The results of this study are in agreement with the formation of all Himalayan lithotectonic units along a continuous passive margin of Northern India.

Acknowledgments

We would like to thank the funding organization (NSERC/Grant no. 1253 to R.H.) for financial support of the Tibet project. The first author also thanks the NSERC (scholarship PGS B) and FQRNT for financial support. We are also thankful to M. Choquette for microprobe analyses and to R. Gosselin for ICP-AES and ICP-MS analyses. We are grateful to Marc Richer La Flèche for fruitful discussion during preparation of an early version of the manuscript. The manuscript has further benefited from critical comments by A.J. Barber, A. Yin, J.C. Aitchison, K. Condie, and Y. Najman.

Chapitre 5

Assemblages minéralogiques et histoire P-T

Dans ce chapitre, les paragenèses principales des roches ultramafiques et mafiques des trois unités géologiques à l'étude sont présentées et discutées en terme des histoires P-T qui en découlent. La superposition métamorphique est répandue mais incomplète, tant pour les lithologies ultramafiques que mafiques, ce qui permet de définir une histoire géologique complète. Tous les numéros de courbes subséquemment mentionnés font référence à la Fig. 5.1 qui représente un diagramme composite P-T de réactions pour les roches ultramafiques et mafiques.

5.1 Roches ultramafiques

L'antigorite est le polymorphe de serpentine le plus commun dans les péridotites du mélange ophiolitique (voir Chapitre 3). L'antigorite est en fait la phase la plus stable sous les conditions P-T qui accompagnent la serpentinisation des roches ultramafiques (Bucher et Frey, 1994). Son domaine de stabilité s'étend de 250 à 550°C à une pression relativement basse dans le système *MSH* (ex. Winkler, 1967 ; Bucher et Frey, 1994). Au-dessus de 550°C, elle est instable et est remplacée par de la forstérite et du talc (courbe #4). Au-dessous de 250°C, elle est transformée en chrysotile (courbe #1). La formation de magnétite, souvent à partir de spinelle primaire, est associée à la serpentinisation, les polymorphes de serpentine étant incapable d'accommoder tout le fer présent dans l'olivine et l'orthopyroxène. Le diopside, lorsque présent, a été partiellement rééquilibré à des températures variant de 800°C à <500°C (Fig. 5.2). Selon Bucher

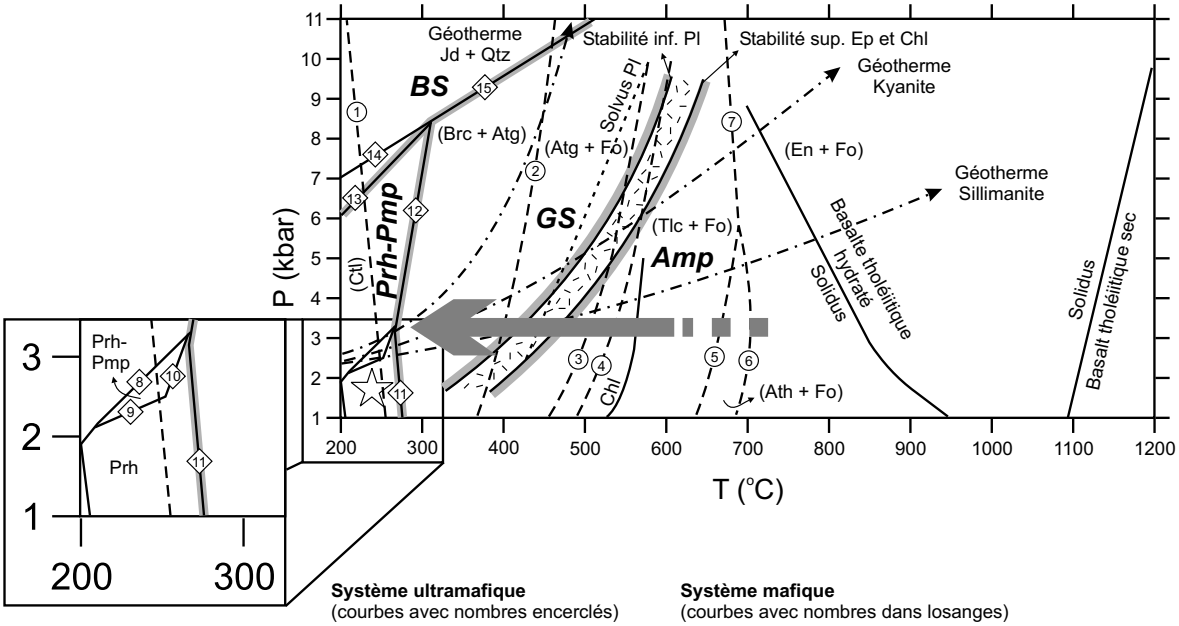

Système ultramafique
(courbes avec nombres encerclés)

1 17 Ctl = Atg + 3 Brc
2 Atg + 20 Brc = 34 Fo + 51 H_2O
3 Atg + 8 Di = 18 Fo + 4 Tr + 27 H_2O
4 Atg = 18 Fo + 4 Tlc + 27 H_2O
5 9 Tlc + 4 Fo = 5 Ath + 4 H_2O
6 Ath + Fo = 9 En + H_2O
7 Tlc + Fo = 5 En + H_2O

Système mafique
(courbes avec nombres dans losanges)

8 20 Pmp + 3 Act + 6 Qtz = 43 Prh + 7 Chl + 2 H_2O
9 6 Lmt + 17 Prh + 2 Chl = 10 Pmp + 21 Qtz + 14 H_2O
10 5 Pmp + 3 Qtz = 7 Prh + 3 Zo + Chl + 5 H_2O
11 5 Prh + Chl + 2 Qtz = 4 Zo + Act + 6 H_2O
12 25 Pmp + 2 Chl + 29 Qtz = 7 Act + 43 Zo + 67 H_2O
13 Act + 10 Ab + 2 Chl = 2 Lws + 5 Gln
14 13 Ab + 3 Chl + 1 Qtz = 5 Gln + 3 Pg + 4 H_2O
15 6 Act + 50 Ab + 9 Chl = 25 Gln + 6 Zo + 7 Qtz + 14 H_2O

FIG. 5.1 – Diagramme P-T de réactions composite pour les roches ultramafiques et mafiques (d'après Huot et al., 2002). Les lignes tiretées avec des nombres encerclés définissent les champs de stabilité pour les assemblages minéralogiques des roches ultramafiques dans un système CMASH à $P_{\mathrm{H_2O}} = P_{\mathrm{total}}$. Les assemblages stables sont écrits entre parenthèses. De la même façon, les lignes continues avec des nombres dans des losanges correspondent aux roches mafiques. Les faciès métamorphiques sont séparés par des lignes grises épaisses : SB = schistes bleus, Prh-Pmp = prehnite-pumpellyite, SV = schistes verts, Amp = amphibolites. Les géothermes et les courbes de réactions sont tirés de Bucher et Frey (1994), sauf les exceptions suivantes. La courbe de solvus du plagioclase de température maximale est tracée de données fournies par Maruyama et al. (1982). La région hachurée représente la zone de transition schistes verts-amphibolites de Murayuma et al. (1983). La courbe de chlorite (limite de stabilité inférieure vs supérieure) est tirée de Liou et al. (1974). Les courbes des solidus hydraté et sec proviennent de Yoder et Tilley (1962). La flèche grise indique l'évolution du métamorphisme rétrograde intra-océanique de faible P/T enregistré dans les péridotites du manteau supérieur et les roches mafiques du mélange ophiolitique, avant le démembrement tectonique (Huot et al., 2002). Les conditions P-T prévalant lors de la formation du mélange ophiolitique sont représentées par l'étoile vide (Huot et al., 2002). Ab = albite, Act = actinote, Atg = antigorite, Ath = anthophyllite, Brc = brucite, Chl = chlorite, Ctl = chrysotile, Di = diopside, En = enstatite, Ep = épidote, Fo = forstérite, Gln = glaucophane, Jd = jadéite, Lmt = laumonite, Lws = lawsonite, Pg = paragonite, Pl = plagioclase, Pmp = pumpellyite, Prh = prehnite, Qtz = quartz, Tlc = talc, Tr = trémolite, Zo = zoïsite.

et Frey (1994), le diopside est la phase calcique stable (dans le système *CMSH*) à des températures inférieures à 520°C et 500°C le long des géothermes de la kyanite et de la sillimanite, respectivement, en l'absence de CO_2 (courbe #3). L'orthopyroxène, lui aussi partiellement rééquilibré, donne des températures variant de 1100° à 500°C.

Le chrysotile et le talc tardifs observés localement dans les serpentinites, ainsi que dans la matrice cisaillée (Huot et al., 2002), pourraient représenter une altération de basses températures dans le faciès à prehnite-pumpellyite (courbe #1). Ces veinules de talc pourraient aussi être dues à l'interaction de l'antigorite avec un fluide contenant du CO_2. Par contre, la présence de spinelles poreux hétérogènes pourrait être en relation avec une telle serpentinisation dans le faciès à prehnite-pumpellyite (Burkhard, 1993). Les paragenèses indiquent donc que les conditions P-T auraient évolué du faciès des schistes verts au faciès à prehnite-pumpellyite. Cependant, le manque de géobaromètres dans ces faciès exclut toute interprétation des pressions avoisinantes prévalant au moment de la serpentinisation.

5.2 Roches mafiques

5.2.1 Mélange ophiolitique

Des observations pétrographiques et de la chimie minérale des roches mafiques du mélange ophiolitique (voir Chapitre 2), il a été déduit que l'amphibole brune alumineuse et titanifère était la première phase à cristalliser et donc probablement d'origine magmatique. Cette amphibole brune n'est généralement pas alcaline (K_2O <0.1 % poids), contrairement à la majorité des amphiboles magmatiques (ex. Mével, 1988 ; Coogan et al., 2001). Cependant, cette composition semble être plus reliée à la composition primitive du magma qu'à la nature du fluide (igné vs métamorphique). De plus, leur contenu en chlore de moins de 0,15 %poids est trop faible pour provenir d'un fluide océanique (Vanko, 1986 ; Mével, 1988). Une diabase particulière, 2002-BUM-03, contient de l'amphibole brune prismatique qui présente des contenus particulièrement élevés en TiO_2 (2,8-3,2 %poids) et K_2O (1-1,2 %poids), lesquels semblent plus typiques d'amphiboles se développant dans des ophiolites sur le plancher océanique ou sous l'influence de fluides ignés (Tribuzio et al., 2000). Les résultats semi-quantitatifs obtenus de deux thermomètres (Holland et Blundy, 1994 ; Ernst et Liu, 1998) donnent des températures maximales entre 850 et 950°C. De telles températures, si métamorphiques, tomberaient dans le champ des granulites à pyroxènes (Bucher et Frey, 1994). Cependant, le clinopyroxène, principalement de l'augite (Fig. 5.2), montre une composition chimique

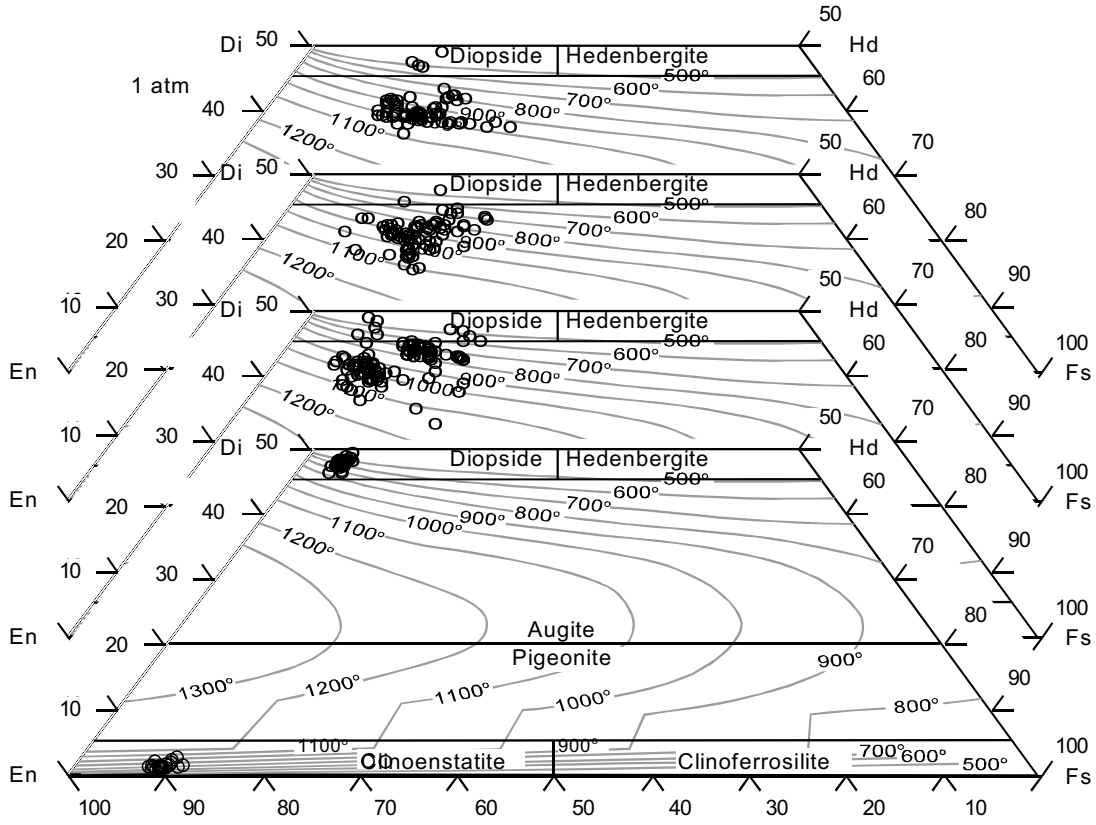

FIG. 5.2 – Composition et température du clinopyroxeène projetées dans le quadrilatère Di-En-Hd-Fs. De l'avant à l'arrière, on aperçoit les roches ultramafiques du mélange ophiolitique et les roches mafiques du mélange ophiolitique, du mélange de Yamdrock et du flysch triasique. Les courbes de température (à 1 atm.) sont tirées de Lindsley (1983) et la nomenclature provient de Morimoto et al. (1989).

clairement magmatique. Les températures élevées données par l'amphibole brune sont donc fort probablement magmatiques.

L'amphibole brune est souvent remplacée en bordure par une hornblende verte moins alumineuse et pauvre en Ti. Cette paragenèse suggère un remplacement rétrograde en présence d'eau. Dans les roches ne contenant pas d'amphibole brune primaire, la hornblende verte remplace généralement le clinopyroxène. Le clinopyroxène suit lui-même une tendance rétrograde : il passe de l'augite magmatique de température initiale avoisinant 1100°C au diopside rééquilibré à des températures inférieures à 500^oC (Fig. 5.2). De façon générale, les roches mafiques du mélange ophiolitique sont aussi composées de plagioclase calcique et d'albite, parfois coexistants, d'actinote, de chlorite et d'un peu de clinozoïsite, ce qui suggère une diminution de la température du faciès des amphibolites à la zone de transition schistes verts-amphibolites (zone hachurée sur la Fig. 5.1). La limite de stabilité supérieure de cette zone de transition, définie par Liou et al. (1974), Apted et Liou (1983) et Maruyama et al. (1983), est d'environ 450-550°C pour des conditions P/T faibles et moyennes, respectivement. Selon Liou et al. (1974) et Liou et Ernst (1979), la présence d'assemblages minéralogiques de transition schistes verts-amphibolites dans des roches basaltiques est indicatrice d'un métamorphisme de très basses P/T. L'absence de minéraux indicateurs de hautes pressions comme le glaucophane, la lawsonite et le grenat (courbes 13 à 15), ou leurs pseudomorphes, exclut toutes conditions P-T le long des géothermes de la jadéite + quartz et de la kyanite. Par ailleurs, certaines roches grossièrement grenues contiennent des amphiboles ferromagnésiennes (gédrite et anthophyllite) en plus des amphiboles calciques (hornblende et actinote), une paragenèse caractéristique des amphibolites de basses pressions, le long du géotherme de la sillimanite (Bucher et Frey, 1994). Puisque l'anthophyllite se retrouve souvent en bordure de l'amphibole brune, elle représente probablement une phase métamorphique précoce qui a cristallisée alors que le magma était encore chaud.

Toutes ces caractéristiques restreignent l'emplacement général du mélange ophiolitique à un environnement de P/T relativement faibles, i.e. le long du géotherme de la sillimanite. La pression métamorphique de départ est estimée inférieure à 4 kbar pour des températures excédant 550°C, conditions sous lesquelles la chlorite est instable (Liou et al., 1974 ; Apted et Liou, 1983 ; Bucher et Frey, 1994). L'état de transition a été atteint lorsque les conditions P-T ont été abaissées à 450°C et 3 kbar (Maruyama et al., 1983 ; Bucher et Frey, 1994). Les paragenèses subséquentes incluent le remplacement partiel à complet du plagioclase calcique, de la hornblende verte et de l'ilménite par l'albite, l'actinote, la titanite, la chlorite et rarement l'épidote. La chlorite, entre autres, donnent des températures variant approximativement de 300° à presque 175°C, calculées selon le géothermomètre de Cathelineau et Nieva (1985). La rareté des carbonates suggèrent que les fluides hydrothermaux étaient pauvres en CO_2.

Le dernier événement métamorphique est représenté par la prehnite abondante, présente autant dans des veines recoupant tous les assemblages métamorphiques qu'en tant que phase secondaire post-déformation remplaçant partiellement à complètement la minéralogie précédente, particulièrement dans les roches rodingitisées (Huot et al., 2002). Des conditions environnantes inférieures à 280°C et 3 kbar (courbe #11) sont nécessaires à la formation de la prehnite aux dépens de l'actinote et de la zoïsite (Bucher et Frey, 1994). Une fois de plus, la présence de prehnite et l'absence de minéraux indicateurs de hautes pressions excluent toutes conditions élevées de P/T. Dans l'ensemble, il semble que l'assemblage magmatique primitif ait été remplacé par des paragenèses rétrogrades successives, alors que les roches mafiques refroidissaient sous des conditions aqueuses. En d'autres mots, les roches mafiques du mélange ophiolitique ont probablement enregistré le régime thermique refroidissant d'une ride océanique (Huot et al., 2002).

5.2.2 Unités sédimentaires

Les assemblages minéralogiques des roches mafiques du mélange de Yamdrock et du flysch triasique sont plus restreints (voir Chapitre 2). Le clinopyroxène est généralement non amphibolitisé, le plagioclase est complètement albitisé, l'ilménite est partiellement remplacée par de la titanite et la chlorite est omniprésente. Cette paragenèse indique que ces roches ont subi un métamorphisme restreint au faciès des schistes verts. Le clinopyroxène a enregistré des températures variant généralement de 1100°C à 700-600°C, seuls quelques diopsides rééquilibrés sont présents (Fig. 5.2). Certaines roches gabbroïques, provenant typiquement des régions voisines de Zisong et Pazuo/Pazhong, contiennent de l'amphibole brune en faible quantité (<10 %vol.), se retrouvant en bordure du clinopyroxène ou formant de petits cristaux automorphes souvant associés à de l'apatite (Fig. 2.2C). La faible abondance de cette amphibole, la couleur brune, la forme automorphe souvent bien développée et l'association avec l'apatite suggèrent toutes que la hornblende dans les roches mafiques des unités sédimentaires sont d'origine magmatique. Quelques aiguilles d'actinote remplacent partiellement la hornblende, en accord avec un métamorphisme au faciès des schistes verts.

L'albite et les phases titanifères (ilménite et titanite) sont grandement remplacées par la séricite et le leucoxène, respectivement. Cette réaction tardive, de même que les veines et les amygdules secondaires de chlorite, d'épidote, d'albite, de quartz et de carbonates, particulièrement abondantes dans les roches du mélange de Yamdrock, sont probablement le résultat d'un métamorphisme/métasomatisme hydrothermal pénétrant, mais de faible intensité. La chlorite donne des températures calculées variant approximativement de 300° à <200°C, passant du faciès des schistes verts au faciès prehnite-

pumpellyite. Quelques roches montrent même un remplacement rétrograde partiel de la chlorite par la pumpellyite bleu-vert (aucune prehnite n'est cependant observée). Les laves du mélange de Yamdrock étant dérivées d'atolls océaniques néo-téthysiens, il semble que ces roches aient été grandement affectées par du métamorphisme/métasomatisme hydrothermal de plancher océanique.

Chapitre 6

Conclusion

6.1 Discussion - modèle géodynamique global

De toutes les conclusions tirées de l'étude des blocs ignés (plus ou moins métamorphisés) provenant des trois principales unités géologiques sous-jacentes aux séquences ophiolitiques de la ZSYZ (i.e. le mélange ophiolitique, le mélange de Yamdrock et le flysch triasique), la plus évidente et la plus fondamentale est que ces dernières ont enregistré des histoires géodynamiques foncièrement différentes. D'ailleurs, les unités sédimentaires comportent de nombreuses similitudes à prime abord, mais aussi des différences remarquables. Un modèle global de l'évolution tectonique paléozoïque à mésozoïque de l'orogène himalayen qui illustre l'environnement tectonique de formation de chacune de ces unités et des blocs qu'elles contiennent (Fig. 6.1) sera discuté dans cette section.

Tout d'abord, il est important de définir la composition du socle archéen commun de l'Inde et du bloc (terrane) de Lhasa. Au Cambrien-Ordovicien précoce (Fig. 6.1 1), une subduction vers le sud sous le nord du supercontinent Gondwana a résulté en une grande production de magma calco-alcalin et la formation de batholites granitiques dans la croûte continentale. Ces batholites ont été démembrés et érodés au cours des temps géologiques, mais des fragments ont été préservés dans la croûte continentale indienne et dans le Bloc de Lhasa. L'ère paléozoïque a, par la suite, été principalement marquée par l'ouverture successive des océans Paléo- et Méso-Téthys (Fig. 6.1 2), aujourd'hui représentés par des sutures situées plus au nord du Tibet (ex. Sengör, 1984).

Au Trias tardif (Fig. 6.1 3), le Bloc de Lhasa s'est détaché de l'Inde suite à un épisode de distension continentale, marquant l'ouverture de la Néo-Téthys (Gansser, 1980 ; Gaetani et Garzanti, 1991). La distension continentale a probablement résulté de

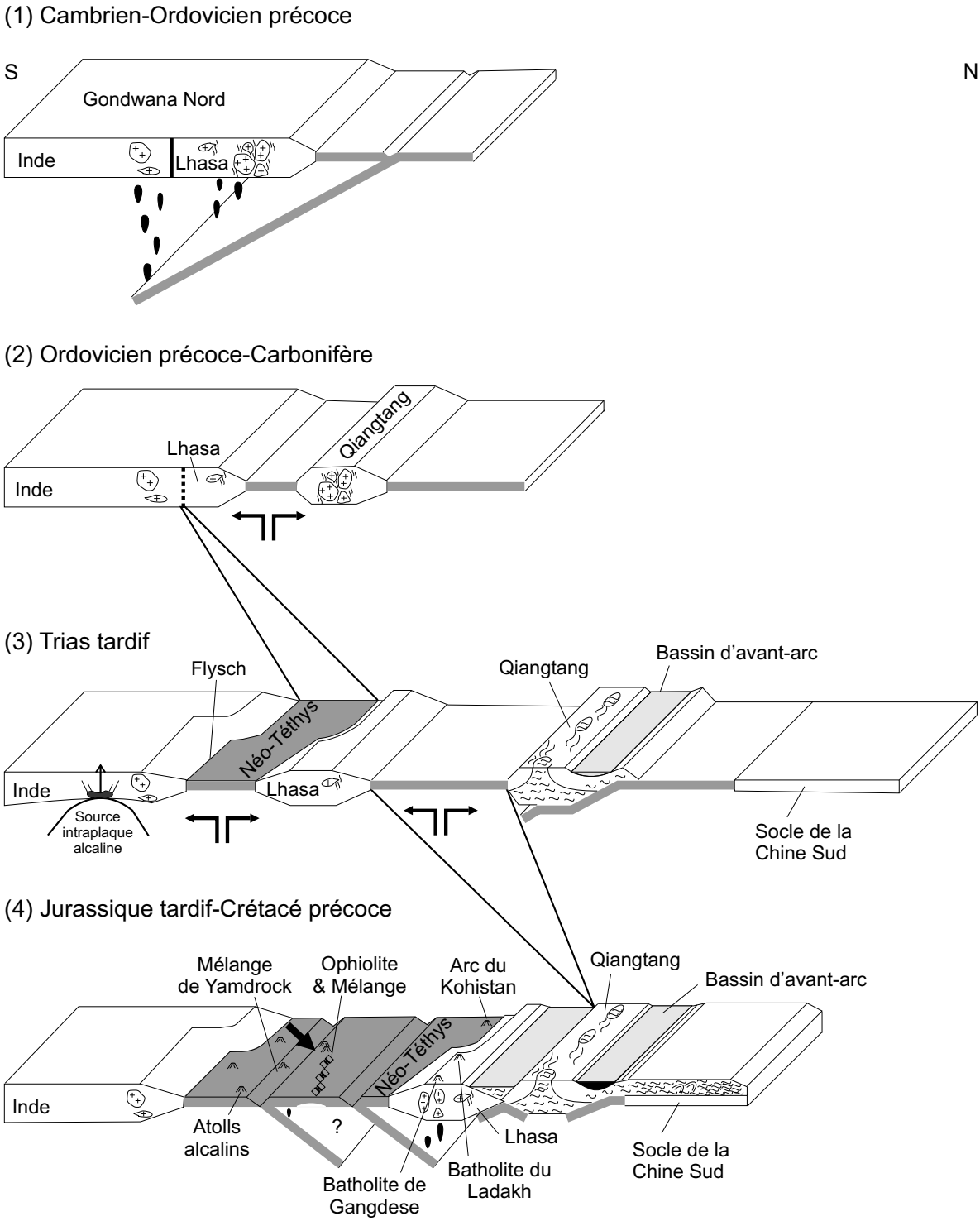

FIG. 6.1 – Modèle d'évolution tectonique paléozoïque-mésozoïque de l'orogène himalayen. Les environnements tectoniques de formation distincts des unités géologiques sous-jacentes aux ophiolites de la ZSYZ y sont illustrés. (1) Cambrien-Ordovicien précoce : subduction sous le Gondwana Nord et magmatisme calco-alcalin ; (2) Ordovicien précoce-Carbonifère : ouverture de l'océan Méso-Téthys séparant le Bloc de Qiangtang du continent indien ; (3) Trias tardif : ouverture de l'océan Néo-Téthys séparant le Bloc de Lhasa du continent indien, magmatisme intraplaque sous le continent indien et dépôt du flysch sur la marge passive indienne ; (4) Jurassique tardif-Crétacé précoce : magmatisme intraplaque intra-océanique, subduction intra-océanique générant les ophiolites et accrétion du mélange de Yamdrock dans le complexe de subduction.

la remontée d'une source magmatique qui a créé un amincissement et un effondrement de la croûte continentale indienne. Le magma a ainsi pu pénétrer la croûte continentale et les batholites granitiques démembrés, en en assimilant une partie le long de fractures. En refroidissant, il a formé des intrusions gabbroïques et diabasiques en grande quantité. L'érosion de la marge nord de l'Inde a par la suite mis à nu et érodé ces roches intrusives dont des fragments métriques ont été incorporés, de concert avec des fragments granitiques cambro-ordoviciens, dans les dépôts de turbidites du flysch triasique. Ce mode de formation proposé pour les blocs mafiques retrouvés dans le flysch est corroboré par la pétrologie, la chimie minérale et la lithogéochimie de ces roches mafiques. Premièrement, le fort fractionnement des TR et l'enrichissement relatif en Ti (Figs. 2.3A et 2.8), indiquent que les roches mafiques sont effectivement dérivées d'une source mantellique enrichie de type intraplaque. Deuxièmement, la présence de quartz interstitiel, le léger enrichissement en TR légères, par rapport à une signature purement intraplaque, et l'appauvrissement anomalique en Nb-Ta (Fig. 2.8), indiquent que ces roches mafiques ont été contaminées par une composante felsique évoluée. La modélisation ACF (assimilation et cristallisation fractionnée), effectuée en utilisant une composition de départ de type $\sim$ *OIB* et un contaminant de composition granitique, a permis de reproduire la signature géochimique *double* des roches mafiques incorporées au flysch triasique et ce, pour un facteur d'assimilation généralement de 0.05, ne dépassant pas 0.3 (Fig. 2.11).

Les roches sédimentaires encaissantes se sont déposées le long de la marge passive indienne nord sur le plancher océanique néo-téthysien grandissant. Leur caractéristiques géochimiques indiquent d'ailleurs une source au niveau d'une croûte continentale supérieure ancienne (Figs. 4.6 et 4.9), donc felsique. Cependant, de légers enrichissements en Ti et Sc indiquent une contribution mafique, laquelle provient vraisemblablement de l'érosion des intrusions gabbroïques enrichies en Ti. La croûte continentale indienne archéenne, comprenant des batholites granitiques calco-alcalins et des intrusions mafiques intraplaques démembrées, semble donc être la source des roches sédimentaires du flysch triasique. Un bloc granitique de composition très évoluée, retrouvé dans le flysch, est considéré comme un témoin de ces batholites calco-alcalins démembrés.

Au Mésozoïque moyen à tardif, l'Océan Néo-Téthys était bien développé et la source magmatique intraplaque enrichie était alors située sous une croûte océanique. La remontée du magma formait des atolls de nature alcaline sur le plancher océanique néo-téthysien. Ces roches mafiques, majoritairement des laves coussinées, n'ont donc pas été affectées par des processus de contamination continentale. Par contre, elles ont été grandement affectées par du métamorphisme/métasomatisme hydrothermal de plancher océanique. Au Crétacé, la Néo-Téthys disparaissait à son tour le long d'au moins trois zones de subduction, deux intra-océaniques et l'autre de type andine (ex. Aitchi-

son et al., 2000 ; Wang et al., 2000 ; Mahéo et al., 2000 ; 2004 ; Hébert et al., 2004 ; Guilmette et al., en préparation). Cette dernière a généré le batholite du Gangdese et c'est dans son bassin d'avant-arc que se sont déposés les sédiments du Groupe de Xigaze, au nord de la ZSYZ. Comme nous allons le voir, les zones de subduction intra-océaniques, plus au sud, nous intéressent tout particulièrement. En arrivant dans la fosse de subduction, les atolls océaniques ont été démembrés et partiellement incorporés, de même que les plates-formes carbonatées les recouvrant, aux sédiments pélagiques accumulés dans le complexe de subduction. Ce complexe de subduction est aujourd'hui représenté par le mélange de Yamdrock. Les blocs mafiques contenus dans ce mélange montrent une signature géochimique de type intraplaque enrichie (Figs. 2.7 et 2.11), plus spécifiquement de type îles océaniques alcalines (*OIB*), en accord avec le scénario proposé. Les roches sédimentaires encaissantes du mélange de Yamdrock montrent des caractéristiques géochimiques tout à fait similaires à celles du flysch triasique. Les sédiments du Yamdrock proviendraient donc d'une même source continentale indienne et auraient été transportées sur le plancher océanique néo-téthysien.

A l'ouest de la zone de suture, le mélange du Sud Ladakh semble posséder une histoire géologique similaire. En effet, ce mélange contient des calcaires permiens, triasiques et crétacés (Reuber et al., 1992 ; Colchen, 1999), ainsi que plusieurs roches volcaniques alcalines associées (ex. Mahéo et al., 2004). De plus, une analogie peut être faite entre la zone de suture dans son ensemble et le point chaud de la Réunion. En effet, les laves du Mélange de Yamdrock corrèlent bien avec les laves d'îles volcaniques récentes situées dans l'Océan indien (Peng et al., 1994 ; Peng et Mahoney, 1995), alors que les roches gabbroïques du flysch triasique corrèlent bien avec les roches mafiques des Trapps de Deccan et de Panjal, à l'ouest de l'Inde (Searle et al., 1987 ; Mahoney et al., 2002), lesquelles sont généralement associées à l'initiation sous-continentale du point chaud. De telles associations ont aussi été faites pour les roches volcaniques alcalines du mélange du Sud Ladakh (voir Mahéo et al., 2004). Sur la base de la géochimie isotopique de roches volcaniques de la zone de suture téthysienne du Pakistan, Mahoney et al. (2002) ont démontré que le point chaud de la Réunion était actif au Crétacé tardif, avant la formation des Trapps de Deccan. Ce point chaud pouvait-il déjà exister au début du Mésozoïque ?

Les zones de subduction intra-océaniques semblent aussi être à l'origine des roches mafiques et ultramafiques du mélange ophiolitique. En effet, les caractéristiques pétrologiques et géochimiques de ces roches démontrent clairement qu'elles se sont initialement formées dans un environnement de supra-subduction intra-océanique. La majorité des roches mafiques montrent des profils de TR typiques des *MORB* et de légères anomalies négatives en Nb-Ta et Ti (Fig. 2.6). Ces éléments sont généralement conservés dans la plaque de subduction plus vieille et sont donc appauvris dans les fluides résultant de

la déshydratation de cette plaque lors de la subduction. Les roches mafiques du mélange ophiolitique représentent donc des roches de croûte océanique affectées par une composante de subduction. Certaines roches montrent des signatures d'arcs intra-océaniques caractérisées par des TR légères très enrichies et des anomalies négatives en Nb-Ta et Ti prononcées. Plusieurs roches ultramafiques montrent des profils de TR en forme de «U »plus ou moins bien développée (Fig. 3.9). Ces profils sont caractéristiques d'interactions entre des résidus mantelliques appauvris en TR et un magma enrichi en TR légères. La composition du spinelle et une fugacité de l'oxygène entre QFM+1 et QFM suggèrent aussi que les péridotites du mélange ophiolitique ont subi différents processus en plusieurs étapes dans un environnement complexe de supra-subduction.

Toutes ces caractéristiques géochimiques rappellent celles des roches mafiques et ultramafiques des systèmes d'arcs intra-océaniques modernes de Tonga-Kermadec (Turner et al., 1997 ; Regelous et al., 1997 ; Ewart et al., 1998), de Izu-Bonin-Mariannes (Hawkesworth et al., 1977 ; Elliott et al., 1997 ; Taylor et Nesbitt, 1998 ; Pearce et al., 1999), et des Îles Sandwich Sud (Hole et al., 1984 ; Pearce et al., 1995 ; 2000). De plus, les paragenèses des roches mafiques et ultramafiques du mélange ophiolitique indiquent que celles-ci ont enregistré un métamorphisme rétrograde, du faciès des amphibolites au faciès à prehnite-pumpellyite, sous des conditions aqueuses de faible P/T. Un tel régime thermique est caractéristique d'une zone d'expansion intra-océanique de faible profondeur, comme une ride en milieu océanique ou dans un bassin d'arrière-arc.

Des conclusions similaires ayant été tirées pour les massifs ophiolitiques directement sus-jacents (Hébert et al., 2000 ; 2001 ; 2003 ; Dubois-Côté, 2004 ; Dubois-Côté et al., 2003 ; 2005 ; voir certaines figures représentatives présentées à l'annexe F), il apparaît que le mélange ophiolitique résulte effectivement de la désagrégation des ophiolites de la ZSYZ. Les données géochronologiques disponibles indiquent que le système de subduction intra-océanique duquel proviennent probablement les ophiolites et le mélange ophiolitique de la ZSYZ était actif au moins du Jurassique tardif à la fin du Crétacé précoce (Girardeau et al., 1984 ; Göpel et al., 1984 ; Miller et al., 2003 ; Zyabrev et al., 1999 ; Ziabrev et al., 2003 ; Aitchison et al., 2003 ; Guilmette and Hébert, 2003), ce qui correspond au modèle géodynamique proposé. La première zone de subduction intra-océanique (177-152 Ma) a généré des ophiolites de types tholéiitique, calco-alcaline et boninitique, alors que la deuxième zone de subduction (130-120 Ma) impliquait des ophiolites d'arc et d'arrière-arc. Le mélange ophiolitique semble donc résulter du remaniement tectonique des ophiolites de la seconde subduction, i.e. la plus jeune. Quelques blocs calco-alcalins provenant de la première subduction, principalement localisés dans la région de Zedong/Jinlu, ont pu être incorporés lors de la formation du mélange. Les ophiolites du Sud Ladakh, dont l'âge (130-110 Ma) correspond d'ailleurs à la seconde subduction, ont aussi été affectées par un événement métasomatique dans une zone de

supra-subduction (Mahéo et al., 2004). Cependant, leur signature géochimique est plus caractéristique d'un arc intra-océanique tholéiitique que d'un bassin d'arrière-arc. La subduction oblique vers le NNE pourrait expliquer la distribution des ophiolites d'arc du Sud Ladakh plus à l'ouest et des ophiolites d'arrière-arc de la ZSYZ à l'est.

6.2 Conclusion générale

Les données pétrologiques et géochimiques présentées dans cette thèse ont permis de déterminer la pétrogenèse de roches mafiques, ultramafiques et sédimentaires provenant de trois unités géologiques au sud des ophiolites de la ZSYZ, soit le mélange ophiolitique, le mélange de Yamdrock et le flysch triasique. Bien qu'ayant toutes une origine associée au bassin océanique néo-téthysien, ces unités se sont formées dans trois environnements tectoniques distincts.

Les roches mafiques du mélange ophiolitique sont caractérisées par des signatures géochimiques (chimie minérale et lithogéochimie) qui suggèrent qu'elles se soient formées dans un environnement de supra-subduction intra-océanique. En particulier, la majorité des roches mafiques sont appauvries en TR légères et présentent de légères anomalies négatives en Nb-Ta et Ti, ce qui suggère que ces roches se sont formées dans un bassin d'arrière-arc, comme les roches mafiques du Bassin de Lau. Quelques roches plus vieilles sont plutôt enrichies en TR légères et présentent d'importantes anomalies négatives en Nb-Ta et Ti, une signature typique d'un arc intra-océanique.

Les roches ultramafiques possèdent aussi des caractéristiques géochimiques qui suggèrent une origine dans un environnement de supra-subduction. Bien que ces caractéristiques soient plus variables, les péridotites peuvent tout de même être subdivisées en trois groupes. Les lherzolites et harzburgites à Cpx correspondent à des péridotites abyssales fertiles avec des profils lisses appauvris en TR légères. Les harzburgites transitionnelles correspondent à des péridotites abyssales appauvries ou de zone de supra-subduction, les TR montrant un appauvrissement continu des TR lourdes aux TR médianes et un léger enrichissement des TR légères résultant d'interactions avec un magma. Les harzburgites et dunites montrent des profils en forme de U caractéristiques d'interactions entre des résidus mantelliques appauvris en TR et un magma enrichi en TR légères. La modélisation de la fusion fractionnée, en accord avec les Mg# et Cr# du spinelle, indique que les harzburgites à Cpx pourraient être les résidus de 5-15% de fusion, les harzburgites transitionnelles de 15-23% et les harzburgites et dunites de 22-29%. Le système arc-bassin de Sandwich Sud est considéré un analogue moderne de l'environnement géodynamique initial.

A première vue, le mélange de Yamdrock et le flysch triasique montrent plusieurs caractéristiques géochimiques semblables. Cependant, un examen plus détaillé permet de relever des différences importantes. Tout d'abord, les deux unités possédent une matrice sédimentaire composée principalement de turbidites de marge passive. La lithogéochimie des roches sédimentaires indique aussi une source commune dérivée de la croûte continentale supérieure felsique ancienne de la marge nord de l'Inde. Par ailleurs, une contribution mafique, provenant probablement de l'érosion des blocs mafiques d'affinité intraplaque retrouvés dans les unités sédimentaires, a produit de légers enrichissements en Ti et Sc. Cependant, ces unités sont d'âges différents, ce qui influence fortement l'interprétation de leur environnement de déposition. Les turbidites du flysch triasique se sont déposées le long de la marge passive indienne nord lors de l'ouverture de l'Océan Néo-Téthys, alors que celles du mélange de Yamdrock, contenant des cherts à radiolaires d'eaux profondes, se sont plutôt déposées sur le plancher océanique néo-téthysien en expansion et dans la fosse de subduction.

Les blocs mafiques incorporés dans ces unités sédimentaires semblent tous dériver d'une source mantellique intraplaque enrichie similaire au point chaud de la Réunion aujourd'hui situé dans l'océan Indien. Par contre, ici encore, bien que non connu de façon précise, l'âge distinct des deux unités joue un rôle important dans la pétrogenèse des roches mafiques. Pour le mélange de Yamdrock, les roches sont enrichies en TR légères. Ces roches sont d'affinité intraplaque océanique (de type *OIB*) et proviennent de la désagrégation d'atolls océaniques néo-téthysiens dans le complexe de subduction intra-océanique. Pour le flysch triasique, les roches sont très enrichies en TR légères et présentent de légères anomalies négatives en Nb-Ta et Ti. Ces roches sont similaires aux roches volcaniques des Trapps de Deccan (Inde) et sont interprétées comme étant dérivées d'une source mantellique intraplaque continentale, avec assimilation crustale résultant de la dislocation de la Plaque indienne lors de l'ouverture du Néo-Téthys. La modélisation ACF (assimilation et cristallisation fractionnée) suggère que ces roches aient assimilé en moyenne environ 5% de roches granitiques démembrées de la croûte continentale indienne.

Toutes ces caractéristiques géochimiques montrent une bonne corrélation avec celles des ophiolites et mélanges associés du Sud Ladakh, lesquels correspondent au prolongement vers l'ouest de la ZSYZ. Elles auront permis d'étendre l'évolution tectonique du bassin néo-téthysien à tout le Mésozoïque. Des comparaisons peuvent aussi être faites avec les unités himalayennes plus au sud. La géochimie isotopique effectuée sur ces mêmes roches permettrait d'appuyer nos conclusions et de raffermir les liens entre les différentes unités géologiques associées à l'orogène himalayen.

Bibliographie

[1] Abrajevitch, A., 2002. *Paleomagnetism of the Dazhuqu Terrane. Yarlung Zangbo Suture Zone, Southern Tibet*. M.Phil. Thesis, University of Hong Kong.

[2] Ahmad, T., Harris, N., Bickle, M., Chapman, H., Bunbury, J., Prince, C., 2000. Isotopic constraints on the structural relationships between the Lesser Himalayan Series and the High Himalayan Crystalline Series, Garhwal Himalaya. *Geological Society of America Bulletin*, 112, 467-477.

[3] Aitchison, J.C., Badengzhu, Davis, A.M., Liu, J., Luo, H., Malpas, J., McDermid, I., Wu, H., Ziabrev, S., Zhou, M.F., 2000. Remnants of a Cretaceous intra-oceanic subduction system within the Yarlung-Zangbo suture (southern Tibet). *Earth and Planetary Science Letters*, 183, 231-244.

[4] Aitchison, J.C., Davis, A.M., Abrajevitch, A.V., Ali, J.R., Badengzhu, Liu, J., Luo, H., McDermid, I., Ziabrev, S., 2003. Stratigraphic and sedimentological constraints on the age and tectonic evolution of the Neotethyan ophiolites along the Yarlung Tsangpo suture zone, Tibet. In : Dylek, Y., Robinson, P.T. (Éds.), *Ophiolites in Earth History. Geological Society of London Special Publications*, 218, 147-164.

[5] Allan, J.F., 1994. Cr-spinel in depleted basalts from the Lau basin back-arc : petrogenetic history from Mg-Fe crystal-liquid exchange. In : Hawkins, J., Parson, L., Allan, J.F., et al., *Proceedings of the Ocean Drilling Program, Scientific Results*, College Station, Texas, 135, 565-583.

[6] Allègre, C.J., Coutillot, V., Tapponnier, P. et al. (32), 1984. Structure and evolution of the Himalaya-Tibet orogenic belt. *Nature*, 307, 17-22.

[7] Apted, M.J., Liou, J.G., 1983. Phase relations among greenschist, epidote-amphibolite, and amphibolite in a basaltic system. *American Journal of Science*, 283, 328-354.

[8] Arai, S., 1992. Chemistry of chromian spinel in volcanic rocks as a potential guide to magma chemistry. *Mineralogical Magazine*, 56, 173-184.

[9] Armijo, R., Tapponnier, P., Han, T., 1989. Late Cenozoic right-lateral strike-slip faulting in southern Tibet. *Journal of Geophysical Research*, 94, 2787-2838.

[10] Armijo, R., Tapponnier, P., Mercier, J.L., Han, T., 1986. Quaternary extension in Southern Tibet : Field observations and ectonic implications. *Journal of Geophysical Research*, 91, 13803-13872.

[11] Bau, M., 1991. Rare-earth element mobility during hydrothermal and metamorphic fluid-rock interactions and the significance of the oxidation state of Eu. *Chemical Geology*, 93, 219-230.

[12] Beck, R.A., Burbank, D.W., Sercombe, W.J., Riley, G.W., Barndt, J.K., 1995. Stratigraphic evidence for an early collision between northwest India and Asia. *Nature*, 373, 55-58.

[13] Beck, R.A., Burbank, W., Sercombe, W.J., Khna, A.M., Lawrence, R.D., 1996. Late Cretaceous ophiolite obduction and Paleocene India-Asia collision in the westernmost Himalaya. *Geodimamica Acta*, 9, 114-144.

[14] Bédard, J.H., 1994. A procedure for calculating the equilibrium distribution of trace elements among the minerals of cumulate rocks, and the concentration of trace elements in the coexisting liquids. *Chemical Geology*, 118, 143-153.

[15] Bhatia, M.R., Crook, K.A.W., 1986. Trace element characteristics of graywackes and tectonic setting discrimination of sedimentary basin. *Contributions to Mineralogy and Petrology*, 92, 181-193.

[16] Blatt, H., Middletown, G.V., Murray, R.C., 1980. *Origin of sedimentary rocks*. Prenctice-Hall Inc., Englewood Cliffs, N.J.

[17] Bodinier, J.L., Dupuy, C., Vernières, J., 1988b. Behaviour of trace elements during upper mantle metasomatism : evidences from the Lherz massif. *Chemical Geology*, 70, 152.

[18] Bodinier, J.L., Vasseur, G., Vernières, J., Dupuy, C., Fabriès, J., 1990. Mechanisms of mantle metasomatism : geochemical evidence from the Lherz orogenic peridotite. *Journal of Petrology*, 31, 597-628.

[19] Bortolotti, V., Chiari, M., Marucci, M., Marroni, M., Pandolfi, L., Principi, G., Saccani, E., 2004. Comparison among the Albanian and Greek ophiolites : In search of constraints for the evolution of the Mesozoic Tethyan ocean. *Ofioliti*, 29, 19-35.

[20] Brookfield, M.E., 1993. The Himalayan passive margin from Precambrian to Cretaceous times. *Sedimentary Geology*, 84, 1-35.

[21] Bucher, K., Frey, M., 1994. *Petrogenesis of Metamorphic Rocks : Complete revision of Winkler's Textbook*, 6^e éd., Springer-Verlag, Berlin, 318 p.

[22] Burg, J.P., Chen, G.M., 1984. Tectonics and structural zonation of southern Tibet, China. *Nature*, 311, 219-223.

[23] Burg, J.P., Leyreloup, A., Girardeau, J., Chen, G.M., 1987. Structure and metamorphism of a tectonically thickened continental crust ; the Yalu Zangbo suture

zone (Tibet). *Philosophical Transactions of the Royal Society of London*, A, 321, 67-86.

[24] Cabanis, B., Lecolle, M., 1989. Le diagramme La/10-Y/15-Nb/8 : un outil pour la discrimination des séries volcaniques et la mise en évidence des processus de mélange et/ou de contamination crustale. *Comptes Rendus de l'Académie des Sciences Série II*, 309, 2023-2029.

[25] Campbell, I.H., 1998. The mantle's chemical strucutre : insights from the melting products of mantle plumes. In : Jackson, I. (Éd.), *The Earth's Mantle : Composition, Structure, and Evolution*. Cambridge University Press, 259-310.

[26] Cannat, M., Chatin, F., Whitechurch, H., Ceuleneer, G., 1997. Gabbroic rocks trapped in the upper mantle at the Mid-Atlantic Ridge. In : Karson, J.A., Cannat, M., Miller, D.J., Elthon, D. (Éds.), *Proceedings of the Ocean Drilling Program, Scientific Results*, 153, College Station, Texas, 243-264.

[27] Cathelineau, M., Nieva, D., 1985. A chlorite solid solution geothermometer ; the Los Azufres (Mexico) geothermal system. *Contributions to Mineralogy and Petrology*, 93, 235-244.

[28] Chang, C., 1984. Les caractéristiques tectoniques et l'évolution de la zone de suture du Yarlung-Zangbo. In : Mercier, J.L., Li, G.C. (Éds.), *Mission franco-chinoise au Tibet 1980 : Étude géologique et géophysique de la croûte terrestre et du manteau supérieur du Tibet et de l'Himalaya*. Éditions du Centre National de la Recherche Scientifique, Paris, France, pp. 341-350.

[29] Cloos, M., 1982. Flow melanges : Numerical modeling and geologic constraints on their origin in the Franciscan subduction complex, California. *Geological Society of America Bulletin*, 93, 330-345.

[30] Cloos, M., 1984. Flow melanges and the structural evolution of accretionary wedges. In : Raymond, L.A. (Éd.), *Melanges : Their Nature, Origin, and Significance, Geological Society of America Special Paper*, 198, 71-79.

[31] Colchen, M., 1999. Ophiolitic melanges of the Ladakh Indus suture zone, a key to understanding the geodynamic evolution of the Indian and Tibetan Tethyan margin. In : *14^{th} Himalaya-Karakorum-Tibet workshop abstracts. Terra Nostra*, 99, 28.

[32] Constantin, M., 1999. Gabbroic intrusions and magmatic metasomatism in harzburgites from the Garret transform fault : implications for the nature of the mantle-crust transition at fast spreading ridges. *Contributions to Mineralogy and Petrology*, 136, 111-130.

[33] Constantin, M., Hékinian, R., Ackermand, D., Stoffers, P., 1995. Mafic and ultramafic intrusions into upper mantle peridotites from fast spreading centers of the Easter Microplate (South East Pacific). In : Vissers, R.L.M. and Nicolas, A. (Éds.), *Mantle and lower crust exposed in oceanic ridges and ophiolites*, 71-120.

[34] Coogan, L.A., Wilson, R.N., Gillis, K.M., MacLeod, C.J., 2001. Near-solidus evolution of oceanic gabbros : Insights from amphibole geochemistry. *Geochimica et Cosmochimica Acta*, 65, 4339-4357.

[35] Corfield, R.I., Searle, M.P., 2000. Crustal shortening estimates across the north Indian continental margin, Ladakh, NW India. In : Khan, M.A., Treloar, P.J., Searle, M.P., Jan, M.Q. (Éds.), *Tectonics of the Nanga Parbat Syntaxis and the Western Himalaya, Geological Society of London Special Publications*, 170, 395-410.

[36] Corfield, R.I., Searle, M.P., Pederson, R.B., 2001. Tectonic setting and obduction history of the Spontang ophiolite, Ladakh Himalaya, NW India. *Journal of Geology*, 109, 715-736.

[37] Coulon, C., Maluski, H., Bollinger, C., Wang, S., 1986. Mesozoic and Cenozoic volcanic rocks from central and southern Tibet ; ^{39}Ar-^{40}Ar dating, petrological characteristics and geodynamical significance. *Earth and Planetary Science Letters*, 79, 281-302.

[38] Crichton, J.G., Condie, K.C., 1993. Trace elements as source indicators in cratonic sediments : a case study from the Early Proterozoic Libby Creek Group, southeastern Wyoming. *Journal of Geology*, 101, 319-332.

[39] Davis, A.M., Aitchison, J.C., Badengzhu, Luo, H., Zyabrev, S., 2002. Paleogene island arc collision-related conglomerates, Yarlung-Tsangpo suture zone, Tibet. *Sedimentary Geology*, 150, 247-273.

[40] de Sigoyer, J., Chavagnac, V., Blichert-Toft, J., Villa, I.M., Luais, B., Guillot, S., Cosca, M., Mascle, G., 2000. Dating the Indian continental subduction and collisional thickening in the Northwest Himalaya ; multichronology of the Tso Marari eclogites. *Geology*, 28, 487-490.

[41] DeCelles, P.G., Gehrels, G.E., Quade, J., LaReau, B., Spurlin, M., 2000. Tectonic implications of U-Pb zircon ages of the Himalayan orogenic belt in Nepal. *Science*, 288, 497-499.

[42] Dick, H.J.B., Bullen, T., 1984. Chromian spinel as a petrogenetic indicator in abyssal and alpine-type peridotites and spatially associated lavas. *Contributions to Mineralogy and Petrology*, 86, 54-76.

[43] Dubois-Côté, V., 2004. *Pétrologie et géochimie des ophiolites de la Zone de Suture du Yarlung Zangbo (ZSYZ), Tibet : Implications géodynamiques*. Mémoire de maîtrise, Université Laval, 231 p.

[44] Dubois-Côté, V., Hébert, R., Dupuis, C. Wang, C.S., Li, Y.L., Dostal, J., 2005. Petrological and geochemical evidence for the origin of the Yarlung Zangbo ophiolites, southern Tibet. *Chemical Geology*, 214, 265-286.

[45] Dubois-Côté, V., Hébert, R., Wang, C.S., Li, Y.L., Dostal, J., 2003. Petrology and geochemistry of Yarlung Zangbo Suture Zone (YZSZ) ophiolites, Tibet : Geodynamic implications. *GAC-MAC-SEG Joint Annual Meeting Abstracts (Vancouver)*, 28, 188.

[46] Duncan, R.A., Richards, M.A., 1991. Hotspots, mantle plumes, flood basalts, and true polar wander. *Reviews in Geophysics*, 29, 31-50.

[47] Dupuis, C., Hébert, R., Huot, F., Wang, C.S., Li, Y.L., Li, Z.J., 2003. Petrology and geochemistry of Tethysian Jurassic and Triassic provinces related to the Yarlung Zangbo Suture Zone (YZSZ), Tibet. In : *18th Himalaya-Karakorum-Tibet workshop abstracts*, 38-40.

[48] Dupuis, C., Hébert, R., Wang, C.S., Li, Y.L., Li, Z.J., 2004. Petrology and geochemistry of Tethyan mélange and flysch units adjacent to the Yarlung Zangbo Suture Zone (YZSZ), Southern Tibet. *AOS Transactions AGU*, 85, Joint Assembly Supplements, Abstract V43A-06.

[49] Dürr, S.B., 1996. Provenance of Xigaze fore-arc basin clastic rocks (Cretaceous South Tibet). *Geological Society od America Bulletin*, 108, 669-684.

[50] Edwards, S.J., Malpas, J., 1996. Melt-peridotite interactions in shallow mantle at the East Pacific Rise : evidence from ODP Site 895 (Hess Deep). *Mineralogical Magazine*, 60, 191-206.

[51] Edwards, S.J., Falloon, T.J., Malpas, J., Pederson, R.B., 1996. A review of the petrology of harzburgites at Hess Deep and Garrett Deep : implications for mantle processes beneath segments of the East Pacific Rise. In : MacLeod, C.J., Tyler, P.A., Walker C.L. (Éds), *Tectonic, hydrothermal and biological segmentation of Mid Ocean Ridges, Geological Society of London Special Publications*, 118, 143-156.

[52] Einsele, G., Liu, B., Dürr, S., Frisch, W., Liu, G., Luterbacher, H.P., Ratschbacher, L., Ricken, W., Wendt, J., Wetzel, A., Yu, G., Zheng, H., 1994. The Xigaze forearc basin ; evolution and facies architecture (Cretaceous, Tibet). *Sedimentary Geology*, 90, 1-2.

[53] Elliott, B., Plank, T., Zindler, A., White, W., Bourdon, B., 1997. Element transport from slab to volcanic front at the Mariana arc. *Journal of Geophysical Research Letters*, 102, 14991-15019.

[54] Ernst, W.G., Liu, J., 1998. Experimental phase-equilibrium study of Al- and Ti-contents of calcic amphibole in MORB-A semiquantitative thermobarometer. *American mineralogist*, 83, 952-969.

[55] Ewart, A., Bryan, W.B., Chappel, B.W., Rudnick, R.L., 1994a. Regional geochemistry of the Lau-Tonga arc and backarc systems. In : Hawkins, J.W., Parson, L.M., Allan, J.F., et al. (Éds.). *Proceedings of the Ocean Drilling Program, Scientific Results*, 135, College Station, Texas, 385-425.

[56] Ewart, A., Hergt, J.M., Hawkins, J.W., 1994b. Major element, trace element, and isotope (Pb, Sr, and Nd) geochemistry of site 839 basalts and basaltic andesites : Implications for arc volcanism. In : Hawkins, J.W., Parson, L.M., Allan, J.F., et al. (Éds.). *Proceedings of the Ocean Drilling Program, Scientific Results*, 135, College Station, Texas, 519-531.

[57] Ewart, A., Collerson, K.D., Regelous, M., Wendt, J.I., Niu, Y., 1998. Geochemical evolution within the Tonga-Kermadec-Lau Arc-Back-arc systems : the role of varying mantle wedge composition in space and time. *Journal of Petrology*, 39, 331-368.

[58] Foucault, A., Raoult, J.F., 2000. *Dictionnaire de géologie, 5^e édition*, Masson Sciences, Dunod, Paris.

[59] Fralick, P.W., Kronberg, B.I., 1997. Geochemical discrimination of clastic sedimentary sources. *Sedimentary Geology*, 113, 111-124.

[60] France-Lanord, C., Derry, L., Michard, A., 1993. Evolution of the Himalaya since Miocene time : isotopic and sedimentological evidence from the Bengal Fan. In : Treloar, P.J., Searle, M.P. (Éds), *Himalayan Tectonis. Geological Society of London Special Publication*, 7, 603-621.

[61] Gaetani, M., Garzanti, E., 1991. Multicyclic history of the northern India continental margin (northwestern Himalaya). *American Association of Petroleum Geologist Bulletin*, 75, 1427-1446.

[62] Galy, A., France-Lanord, C., Derry, L., 1996. The Late Oligocene-Early Miocene Himalayan belt constraints deduced from isotopic compositions of Early Miocene tubidites in the Bengal Fan. *Tectonophysics*, 260, 109-118.

[63] Gansser, A., 1974. The ophiolitic mélange, a world-wide problem on Tethyan examples. *Eclogea Geologicae Helvetiae*, 67, 479-507.

[64] Gansser, A., 1980. The significance of the Himalayan suture zone. *Tectonophysics*, 62, 37-53.

[65] Garcia, D., Fonteilles, M., Moutte, J., 1994. Sedimentary fractionation between Al, Ti, and Zr and the genesis of strongly peraluminous granites. *Journal of Geology*, 102, 411-422.

[66] Girardeau, J., Marcoux, J., Zao, Y., 1984. Lithologic and tectonic environment of the Xigaze ophiolite (Yarlung Zangbo suture zone, Southern Tibet, China) : kinematics of its emplacement. *Eclogea Geologicae Helvetiae*, 77, 153-170.

[67] Girardeau, J., Mercier, J.-C.C., Wang, X., 1985. Petrology of the mafic rocks of the Xigaze ophiolites , Tibet : Implications for the genesis of the oceanic lithosphere. *Contributions to Mineralogy and Petrology*, 90, 309-321.

[68] Girardeau, J., Mercier, J.-C.C., Zao, Y., 1985b. Structure of the Xigaze ophiolite, Yarlung Zangbo suture zone, southern Tibet, China : Genetic implications. *Tectonics*, 4, 267-288.

[69] Gnoss, E., Khan, M., Mahmood, K., Khan, A.S., Shafique, N.A., Villa, I.M., 1998. Bela oceanic lithosphere assemblage and its relation to the Réunion hotspot. *Terra Nova*, 10, 90-95.

[70] Gnoss, E., Khan, M., Mahmood, K., Villa, I.M., Khan, A.S., 2000. Age and tectonic setting of the Ras Koh ophiolite, Pakistan. *Acta Mineralogica Pakistanica*, 11, 105-118.

[71] Göpel, C., Allègre, C.J., Xu, R.-H., 1984. Lead isotopic study of the Xigaze ophiolite (Tibet) : the problem of the relationship between magmatites (gabbros, dolerites, lavas) and tectonites (harzburgites). *Earth and Planetary Science Letters*, 69, 301-310.

[72] Grove, T.L., Kinzler, R.J., 1986. Petrogenesis of andesites. *Annual Reviews in Earth and Planetary Sciences*, 14, 417-454.

[73] Gruau, G., Bernard-Griffiths, J., Lécuyer, C., 1998. The origin of U-shaped patterns in ophiolite peridotites : assessing the role of secondary alteration and melt/rock reaction. *Geochimica et Cosmochimica Acta*, 62, 3545-3560.

[74] Guillot, S., Pêcher, A., de Sigoyer, J., Mascle, G., 1999. Transition from continental subduction to collision during the India-Asia convergence. *EUG X Terra Abtract*, 4, 52-53.

[75] Guilmette, C., Hébert, R., 2003. Occurrence of high-grade metabasites in the Buma and Bainang ophiolitic mélanges along the Yarlung Tsangpo Suture Zone, South Tibet : A dismembered dynamothermal sole ?. In : *18^{th} Himalaya-Karakorum-Tibet workshop abstracts*, 54-55.

[76] Guilmette, C., Hébert, R., Dupuis, C., Wang, C.S., Li, Z.J., en préparation. Petrology, geochemistry and geochronology of amphibolite blocks from the ophiolitic mélange beneath the Xigaze ophiolites, Tibet : Implications for the evolution of Neo-Tethys.

[77] Harrison, T.M., Copeland, P., Kidd, W.S.F., Yin, A., 1992. Rising Tibet. *Science*, 255, 1663-1670.

[78] Harrison, T.M., Yin, A., Grove, M., Lovera, O.M., 2000. The Zedong window : a record of superposed Tertiary convergence in southeastern Tibet. *Journal of Geophysical Research*, 105, 19211-19230.

[79] Hawkesworth, C.J., O'Nions, R.K., Pankhurst, R.J., Hamilton, P.J., Evensen, N.M., 1977. A geochemical study of island-arc and back-arc tholeiites from the Scotia Sea. *Earth and Planetary Science Letters*, 26, 253-262.

[80] Hawkins, J.W., 2003. Geology of supra-subduction zones-Implications for the origin of ophiolites. In : Dilek, Y. and Newcomb, S. (Éds.), *Ophiolite concept and the evolution of geological thought. Geological Society of America Special Papers*, 373, 227-268.

[81] Hawkins, J.W., Allan, J.F., 1994. Petrologic evolution of Lau Basin sites 834 through 839. In : Hawkins, J.W., Parson, L.M., Allan, J.F., et al. (Éds.). *Proceedings of the Ocean Drilling Program, Scientific Results*, 135, College Station, Texas, 427-470.

[82] Hawkins, J.W., Melchior, J.T., 1985. Petrology of Mariana Trough and Lau Basin basalts. *Journal of Geophysical Research*, 90, 11431-11468.

[83] Hébert, R., Dupuis, C., Guilmette, C., Dubois-Côté, V., Huot, F., Wang, C.S., Li, Y.L., Li, Z.J., Liu, Z.F., 2004. The Yarlung Zangbo Suture Zone ophiolites Tibet : A report on a five-year assessment project. *32nd International Geological Congress (Florence, Italie)*, Abstracts Vol., part 1, abs. 13-17, p. 92.

[84] Hébert, R., Huot, F., Wang, C.S., Liu, Z.F., 2003. Yarlung Zangbo ophiolites (Southern Tibet) revisited : Geodynamic implications from the mineral record. In : Dylek, Y., Robinson, P.T. (Éds.), *Ophiolites in Earth History. Geological Society of London Special Publications*, 218, 165-190.

[85] Hébert, R., Varfalvy, V., Huot, F., Wang, C.S., Liu, Z.F., 2000. Yarlung Zangbo ophiolites, southern Tibet revisited. In : *15^{th} Himalaya-Karakorum-Tibet workshop abstracts. Earth Science Frontiers*, 7, 124-126.

[86] Hébert, R., Wang, C.S., Varfalvy, V., Huot, F., Beaudoin, G., Dostal, J., 2001. Yarlung Zangbo Suture Ophiolites and their suprasubduction zone setting. In : *16^{th} Himalaya-Karakorum-Tibet workshop abstracts. Journal of Asian Earth Sciences*, 19, 27-28.

[87] Hietanen, A., 1974. Amphibole pairs, epidote minerals, chlorite, and plagioclase in metamorphic rocks, northern Sierra Nevada, California. *American Mineralogist*, 59, 22-40.

[88] Hirose, K., Kawamoto, T., 1995. Hydrous partial melting of lherzolite at 1 Gpa : the effect of H_2O on the genesis of basaltic magmas. *Earth and planetary Science Letters*, 133, 463-473.

[89] Hodges, K.V., 2000. Tectonics of the Himalaya and southern Tibet from two perspectives. *Geological Society of America Bulletin*, 112, 324-350.

[90] Hole, M.J., Saunders, A.D., Marriner, G.F., Tarney, J., 1984. Subduction of pelagic sediments : implications for the origin of Ce-anomalous basalts from the Mariana Islands. *Journal of the Geological Society of London*, 141, 453-472.

[91] Holland, T., Blundy, J., 1994. Non-ideal interactions in calcic amphiboles and their bearing on amphibole-plagioclase thermometry. *Contributions to Mineralogy and Petrology*, 116, 433-447.

[92] Houlé, M., 2000. Pétrologie et métallogénie du Complexe de Menarik, Baie James, Québec, Canada. Mémoire de maîtrise, Université Laval, 245p.

[93] Huot, F., Hébert, R., Varfalvy, V., Beaudoin, G., Wang, C.S., Liu, Z.F., Cotten, J., Dostal, J., 2002. The Beimarang mélange (southern Tibet) brings additional constraints in assessing the origin, metamorphic evolution and obduction processes of the Yarlung Zangbo ophiolite. *Journal of Asian Earth Sciences*, 21, 307-322.

[94] Huyghe, P., Galy, A., Mugnier, J.L., France-Lanord, C., 2001. Propagation of the thrust system and erosion in the Lesser Himalaya : Geochemical and sedimentological evidence. *Geology*, 29, 1007-1010.

[95] Ishii, T., Robinson, P.T., Maekawa, H., Fiske, M., 1992. Petrological studies from diapiric serpentinite seamounts in the Izu-Ogazawara-Mariana forearc, Leg 125. In : Fryer, P., Pearce, J.A., Stocking, L.B., *et al.* (Éds.), *Proceedings of the Ocean Drilling Program, Scientific Results*, 125, College Station, Texas, 445-485.

[96] Jaeger, J.-J., Courtillot, V., Tapponnier, P., 1989. Paleontological view of the ages of the Deccan Traps, the Cretaceous/Tertiary boundary and the India-Asia collision. *Geology*, 17, 316-319.

[97] Jarosewich, E., Nelen, J.A., Norberg, J.A., 1980. Reference samples for electron microprobe analysis. *Geostandards Newsletter*, 4, 43-47.

[98] Johnson, K.T.M., Dick, H.J.B., Shimizu, N., 1990. Melting in the oceanic upper mantle : an ion microprobe study of diopsides in abyssal peridotites. *Journal of Geophysical Research*, 95, 2661-2678.

[99] Kearey, P., Vine, F.J., 1996. *Global Tectonics (second edition)*. Blackwell Science Ltd, London, 333 p.

[100] Kelemen, P.B., Shimizu, N., Salters, V.J.M., 1995. Extraction of mid-ocean ridge basalt from the upwelling mantle by focused flow of melt in dunite channels. *Nature*, 375, 747-753.

[101] Klootwijk, C.T., Conaghan, P.J., Nazirullah, R., de Jong, K.A., 1994. Further paleomagnetic data from Chitral (Eastern Hindukush) : evidence for an early India-Asia contact. *Tectonophysics*, 237, 1-25.

[102] Klootwijk, C.T., Gee, J.S., Peirce, H.W., Smith, G.M., McFadden, P.L., 1992. An early India-Asia contact : Paleomagnetic constraints from Ninetyeast Ridge, ODP Leg 121. *Geology*, 20, 395-398.

[103] La Flèche M.R., Camiré, G., 1996. Geochemistry and provenance of metasedimentary rocks from the Archean Golden Pond sequence (Casa Berardi mining district, Abitibi sub province). *Canadian Journal of Earth Sciences*, 33, 676-690.

[104] La Flèche, M.R., Camiré, G., Jenner, G.A., 1998. Geochemistry of post-Acadian, Carboniferous continental intraplate basalts from the Maritimes Basin, Magdalen Islands, Québec, Canada. *Chemical Geology*, 148, 115-136.

[105] Land, S.L., Milliken, K.L., McBride, E.F., 1987. Diagenetic evolution of Cenozoic sandstones, Gulf of Mexico sedimenatry basin. *Sedimentary Geology*, 50, 195-225.

[106] Leake, B.E., Wooley, A.R., Arps, C.E.S. et al. (19), 1997. Nomenclature of amphiboles : report of the subcommittee on amphiboles of the International Mineralogical Association Commission on new minerals and mineral names. *Mineralogical Magazine*, 61, 295-321.

[107] Lee, T.Y., Lawver, L.A., 1995. Cenozoic plate reconstruction of Southeast Asia. *Tectonophysics*, 251, 85-138.

[108] Le Fort, P., 1996. Evolution of the Himalaya. In : Yin, A., Harison, T.M. (Éds.), *The Tectonic Evolution of Asia*. New York, Cambridge University Press, 95-106.

[109] Lin, B., 1984. Les strates du Permien inférieur et la faune coralienne dans la région centre-sud du Tibet. In : Mercier, J.L., Li, G.C. (Éds.), *Mission franco-chinoise au Tibet 1980 : Étude géologique et géophysique de la croûte terrestre et du manteau supérieur du Tibet et de l'Himalaya*. Éditions du Centre National de la Recherche Scientifique, Paris, France, 77-107.

[110] Lindsley, D.H., 1983. Pyroxene thermometry. *American Mineralogist*, 68, 477-493.

[111] Liou, J.G., Ernst, W.G., 1979. Oceanic ridge metamorphism of the East Taiwan ophiolite. *Contributions to Mineralogy and Petrology*, 68, 335-348.

[112] Liou, J.G., Kuniyoshi, S., Ito, K., 1974. Experimental studies of the phase relations between greenschist and amphibolite in a basaltic system. *American Journal of Science*, 274, 613-632.

[113] Liu, G., Einsele, G., 1996. Various types of olistostromes in a closing ocean basin, Tethyan Himalaya (Cretaceous, Tibet). *Sedimentary Geology*, 104, 203-226.

[114] Liu, G., Einsele, G., 1999. Jurassic sedimentary facies and paleogeography of the former Indian passive margin in southern Tibet. *Geological Society of America Special Paper*, 328, 75-108.

[115] Mahéo, G., Bertrand, H., Guillot, S., Mascle, G., Pêcher, A., Picard, C., de Sigoyer, J., 2000. Témoins d'un arc immature téthysien dans les ophiolites du Sud Ladakh (NW Himalaya, Inde). *Comptes Rendus de l'Académie des Sciences II (paris)*, 330, 289-295.

[116] Mahéo, G., Bertrand, H., Guillot, S., Villa, I.M., Keller, F., Capiez, P., 2004. The South Ladakh ophiolites (NW Himalaya, India) : an intra-oceanic theoleiitic arc origin with implication for the closure of the Neo-Tethys. *Chemical Geology*, 203, 273-303.

[117] Mahoney, JJ., Duncan, R.A., Khan, W., Gnos, E., McCormick, G.R., 2002. Cretaceous volcanic rocks of the South Tethyan suture zone, Pakistan : implications for the Réunion hotspot and Deccan Traps. *Earth and Planetary Science Letters*, 203, 295-310.

[118] Malpas, J., Zhou, M.F., Robinson, P.T., Reynolds, P.H., 2003. Geochemical and geochronological constraints on the origin and emplacement of the Yarlung Zangbo

ophiolites, Southern Tibet. In : Dilek, Y. and (Éds.), *Ophiolites in Earth History, Geological Society of London Special Publications*, 218, 191-206.

[119] Maruyama, S., Liou, J.G., Suzuki, K., 1982. The peristerite gap in low-grade metamorphic rocks. *Contributions to Mineralogy and Petrology*, 81, 268-276.

[120] Maruyama, S., Suzuki, K., Liou, J.G., 1983. Greenschist-amphibolite transition equilibria at low pressures. *Journal of Petrology*, 24, 583-604.

[121] Matsuoka, A., Kobayashi, K., Takei, M., Nagahashi, Yang, Q., T., Wang, Y., Takei, M., Zeng, Q.G., 2001. Early Middle Jurassic (Aalenian) radiolarian fauna from the Xialu chert in the Yarlung Zangbo Suture Zone, southern Tibet. In : Metcalfe, I., Smith, J.M.B., Morwood, M., Davidson, I. (Éds.), *Faunal and Floral Migrations and Evolution in SE Asia-Australia*. Balkema, Rotterdam, 105-110.

[122] Matsuoka, A., Yang, Q., Kobayashi, K., Takei, M., Nagahashi, T., Zeng, Q., Wang, Y., 2002. Jurassic-Cretaceous radiolarian biostratigraphy and sedimentary environments of the Ceno-Tethys : records from the Xialu Chert in the Yarlung-Zangbo Suture Zone, southern Tibet. *Journal of Asian Earth Sciences*, 20, 277-287.

[123] Matte, P., Mattauer, M., Olivet, J.M., Griot, D.A., 1997. Continental subduction beneath Tibet and the Himalayan orogen : a review. *Terra Nova*, 9, 264-270.

[124] McCulloch, M.T., Bennett, V.C., 1994. Progressive growth of the Earth's continental crust and depleted mantle : Geochemical constraints. *Geochimica et Cosmochimica Acta*, 58, 4717-4738.

[125] McDermid, I., Aitchison, J.C., Badengzhu, Davis, A.M., Liu, J.B., Luo, H., Wu, H., Ziabrev, S.V., 2000. Zedong Terrane, A Mid Cretaceous Intra-Oceanic Arc, South Tibet. In : *15^{th} Himalaya-Karakorum-Tibet workshop abstracts. Earth Science Frontiers*, 7, 265.

[126] McDermid, I.R.C., Aitchison, J.C., Badengzhu, Davis, A.M., 2001. The Zedong Terrane : An Intra-Oceanic Magmatic Arc Assemblage, Tibet. In : *16^{th} Himalaya-Karakorum-Tibet workshop abstracts. Journal of Asian Earth Sciences*, 19, 44.

[127] McDermid, I.R.C,, Aitchison, J.C., Davis, A.M., Harrison, T.M., Grove, M., 2002. The Zedong Terrane : A Late Jurassic Intra-Oceanic Magmatic Arc within the Yarlung-Tsangpo Suture Zone, Southeastern Tibet. *Chemical Geology*, 187, 267-277.

[128] McDonough, W.F., Frey, F.A., 1989. Rare earth elements in upper mantle rocks. In : Lipin, B.R. and McKay, G.A. (Éds.), *Geochemistry and Mineralogy of rare earth elements. Reviews in Mineralogy*, 21, 99-145.

[129] Mckenzie, D., O'Nions, R.K., 1991. Partial melt distributions from inversion of rare earth element concentrations. *Journal of Petrology*, 32, 1021-1091.

[130] McLennan, S.M., 1989. Rare earth elements in sedimenatry rocks : Influence of provenance and sedimenatry processes. *Mineralogical Society of America, Reviews in Mineralogy*, 21, 169-200.

[131] McLennan, S.M., 2001. Relationships between the trace element composition of sedimentary rocks and upper continental crust. *Geochemistry, Geophysics, Geosystems - G^3*, 2, paper 2000GC000109.

[132] McLennan, S.M., Hemming, S., McDaniel, D.K., Hanson, G.N., 1993. Geochemical approaches to sedimentation, provenance, and tectonics. *Geological Society of America Special Papers*, 284, 21-40.

[133] McLennan, S.M., Taylor, S.R., 1991. Sedimentary rocks ans crustal evolution : Tectonic settings and secular trends. *Journal of Geology*, 99, 1-21.

[134] McLennan, S.M., Taylor, S.R., McCulloch, M.T., Maynard, J.B., 1990. Geochemical and Nd-Sr isotopic compositions of deep-sea turbidites : Crustal evolution and and plate tectonic association. *Geochimica Cosmochimica Acta*, 54, 2015-2050.

[135] Mercier, J.L., *et al.* (29), 1984. La collision Inde-Asie côté Tibet. In : Mercier, J.L., Li, G.C. (Éds.), *Mission franco-chinoise au Tibet 1980 : Étude géologique et géophysique de la croûte terrestre et du manteau supérieur du Tibet et de l'Himalaya*. Éditions du Centre National de la Recherche Scientifique, Paris, France, 341-350.

[136] Meschede, M., 1986. A method of discriminating between different types of mid-ocean ridge basalts and continental tholeiites with the Nb-Zr-Y diagram. *Chemical Geology*, 56, 207-218.

[137] Mével, C., 1988. Metamorphism in oceanic layer 3, Gorringe Bank, Eastern Atlantic. *Contributions to Mineralogy and Petrology*, 100, 496-509.

[138] Miller, C., Thoeni, M., Frank, W., Schuster, R., Melcher, F., Meisel, T., Zanetti, A., 2003. Geochemistry and tectonomagmatic affinity of the Yungbwa Ophiolite, SW Tibet. *Lithos*, 66, 155-172.

[139] Molnar, P., Tapponnier, P., 1975. Cenozoic tectonics of Asia : effects of a continental collision. *Science*, 189, 419-426.

[140] Morey, G.B., Setterholm, D.R., 1997. Rare earth elements in weathering profiles and sediments of Minnesota ; implications for provenance studies. *Journal of Sedimentary Research*, 67, 105-115.

[141] Morimoto, N., Fabries, J., Ferguson, A.K., Ginzburg, I.V., Ross, M., Seifert, F.A., Zussman, J., 1989. Nomenclature of pyroxenes. *Canadian Mineralogist*, 27, 143-156.

[142] Mullen, E.D., 1983. $MnO/TiO_2/P_2O_5$: a minor element discriminant for basaltic rocks of oceanic environments and its implications for petrogenesis. *Earth and Planetary Science Letters*, 62, 53-62.

[143] Myrow, P.M., Hughes, N.C., Paulsen, T.S., Williams, I.S., Parcha, S.K., Thompson, K.R., Bowring, S.A., Peng, S.C., Ahluwalia, A.D., 2003. Integrated tectonostratigraphic analysis of the Himalaya and implications for its tectonic reconstruction. *Earth and Planetary Science Letters*, 212, 433-441.

[144] Najman, Y., Bickle, M., Chapman, H., 2000. Early Himalayan exhumation : isotopic constraints from the Indian foreland basin. *Terra Nova*, 12, 28-34.

[145] Nesbitt, H.W., Young, G.M., 1982. Early Proterozoic climates and plate motions inferred from major element chemistry of lutites. *Nature*, 299, 715-717.

[146] Nesbitt, H.W., Young, G.M., 1989. Formation and diagenesis of weathering profiles. *Journal of Geology*, 97, 129-147.

[147] Nicolas, A., 1989. Xigaze and Trinity ophiolites-plagioclase lherzolite massifs : the lherzolite ophiolite type. In : *Structures of Ophiolites and Dynamic of Oceanic Lithosphere*. Kluwer Academic Publishers, Dordrecht, The Neterlands, 91-105.

[148] Nicolas, A., Girardeau, J., Marcoux, J., Dupré, B., Wang, X.B., Cao, Y.G., Zeng, H.X., Xiao, X.C., 1981. The Xigaze ophiolite (Tibet) : a peculiar oceanic lithosphere. *Nature*, 294, 414-417.

[149] Nielsen, R.L., 1988. A model for the simulation of combined major and trace element liquid lines of descent. *Geochimica et Cosmochimica Acta*, 52, 27-38.

[150] Nielsen, R.L., 1990. Simulation of igneous differentiation processes. In : Nicholls, J. and Russell, J.K. (Éds.), *Modern Methods of igneous petrology ; understanding magmatic processes. Reviws in Mineralogy*, 24, 65-105.

[151] Niu, Y., 1997. Mantle melting and melt extraction processes beneath ocean ridges : evidence from abyssal peridotites. *Journal of Petrology*, 38, 1047-1074.

[152] Ohr, M., Halliday, A.N., Peacor, D.R., 1991. Sr and Nd isotopic evidence for ponctuated clay diagenesis, Texas Gulf Coast. *Earth and Planetary Science Letters*, 105, 110-126.

[153] Patriat, P., Achache, J., 1984. India-Eurasia collision chronology has implications for crustal shortening and driving mechanism of plates. *Nature*, 311, 615-621.

[154] Pearce, J.A., 1982. Trace element characteristics of lavas from destructive plate boundaries. In : Thorpe, R.S. (Éd.), *Andesites*. Wiley, Chichester, 525-548.

[155] Pearce, J.A., 1996. A User's Guide to Basalt Discrimnation Diagrams. In : Wyman, D.A. (Éd.), *Trace Element Geochemistry of Volcanic Rocks : Apllications for Massive Sulphide Exploration. Geological Association of Canada, Short Course Notes*, 12, 79-113.

[156] Pearce, J.A., 2003. Supra-subduction zone ophiolites : The search for modern analogues. In : Dilek, Y. and Newcomb, S. (Éds.), *Ophiolite concept and the evolution of geological thought. Geological Society of America Special Papers*, 373, 269-293.

[157] Pearce, J.A., Baker, P.E., Harvey, P.K., Luff, I.W., 1995. Geochemical evidence for subduction fluxes, mantle melting and fractional crystallization beneath the South Sandwich island arc. *Journal of Petrology*, 36, 1073-1109.

[158] Pearce, J.A., Barker, P.F., Edwards, S.J., Parkinson, I.J., Leat, P.T., 2000. Geochemistry and tectonic significance of peridotites from the South Sandwich arc-basin system, South Atlantic. *Contributions to Mineralogy and Petrology*, 139, 36-53.

[159] Pearce, J.A., Cann, J.R., 1973. Tectonic setting of basic volcanic rocks determined using trace element analyses. *Earth and Planetary Science Letters*, 19, 290-300.

[160] Pearce, J.A., Gale, G.H., 1977. Identification of ore-deposition environment from trace element geochemistry of associated igneous host rocks. *Geological Society of London Special Publications*, 7, 14-24.

[161] Pearce, J.A., Kempton, P.D., Nowell, G.M., Noble, S.R., 1999. Hf-Nd element and isotope perspective on the nature and provenance of mantle and subduction components in Western Pacific arc-basin systems. *Journal of Petrololy*, 40, 1579-1611.

[162] Pearce, J.A., Norry, M.J., 1979. Petrogenetic implications of Ti, Zr, Y and Nb variations in volcanic rocks. *Contributions to Mineralogy and Petrology*, 69, 33-47.

[163] Pearce, J.A., Parkinson, I.J., 1993. Trace element models for mantle melting : application to volcanic arc petrogenesis. In : Pritchard, H.M., Alabaster, T., Harris, N.B.W., and Neary, C.R. (Éds), *Magamtic proceses and plate tectonics. Geological Society of London Special Publications*, 76, 373-403.

[164] Pederson, R.B., Serale, M.P., Corfield, R.I., 2001. U-Pb zircon ages for the Spontang Ophiolite, Ladakh Himalaya. *Journal of the Geological Society of London*, 158, 513-520.

[165] Peng, Z.X., Mahoney, J.J., 1995. Drillhole lavas from the northwestern Deccan Traps, and the evolution of Réunion hotspot mantle. *Earth and Planetary Science Letters*, 134, 169-185.

[166] Peng, Z.X., Mahoney, J.J., Hooper, P., Harris, C., Beane, J., 1994. A role for lower continental crust in flood basalt genesis ? Isotopic and incompatible element study of the lower six formations of the western Deccan Traps. *Geochimica et Cosmochimica Acta*, 58, 267-288.

[167] Pettijohn, F.J., Potter, P.E., Siever, R., 1973. *Sand and Sandstone*. Springer-Verlag, New York.

[168] Pini, G.A., 1999. *Tectonosomes and olistostromes in the argille scagliose of the Northern Apennines, Italy. Geological Society of America Special Paper*, 335, 70 p.

[169] Plank, T., Langmuir, C.H., 1998. The geochemical composition of subducting sediment and its consequences for the ccrust and mantle. *Chemical Geology*, 145, 325-394.

[170] Pozzi, J.P., Westphal, M., Girardeau, J., Besse, J., Zhou, Y.X., Chen, X.Y., Xing, L.S., 1984. Paleomagnetism of the Xigaze ophiolite and flysch (Yarlung Zangbo

suture zone, southern Tibet) : latitude and direction of spreading. *Earth and Planetary Science Letters*, 70, 383-394.

[171] Prinzhofer, A., Allègre, J.C., Bao, P.S., Wang, X.B., 1984. Magmatism in the southern Tibet ophiolite : Trace element constraints. *International Symposium on the Geology of the Himalayas, Chengdu, China*.

[172] Ratschbacher, L., Frisch, W., Liu, G., Chen, C., 1994. Distributed deformation in southern and western Tibet during and after India-Asia collision. *Journal of Geophysical Research*, 99, 19817-19945.

[173] Raymond, L.A., 1984. Classification of melanges. In : Raymond (Éd.), *Melanges ; their nature, origin and significance. Geological Society of America Special Paper* 198, 7-20.

[174] Regelous, M., Collerson, K.D., Ewart, A., Wendt, J.I., 1997. Trace element transport rates in subduction zones : evidence from Th, Sr and Pb isotope data for Tonga-Kermadec arc lavas. *Earth and Planetary Science Letters*, 150, 291-302.

[175] Reuber, I., Colchen, M., Mevel, C., 1992. The Spontang ophiolite, ophiolitic mélanges of the Zanskar, NW Himalaya, tracing the evolution of the closing Tethys in the Upper Cretaceous to the Early Tertiary. *Himalayan Orogen and Global Tectonics*, Oxford and IBH Publishing Co. Pub. Ltd., New Delhi, India, 235-264.

[176] Rice, J.M., 1983. Metamorphism of rodingites : Part I. Phase relations in a portion of the system CaO-MgO-Al_2O_3-CO_2-H_2O. *American Journal of Sciences*, 283, 121-150.

[177] Robinson, D.M., DeCelles, P.G., Patchett, P.J., Garzione, C.N., 2001. The kinematic evolution of the Nepalese Himalaya interpreted from Nd isotopes. *Earth and Planetary Science Letters*, 192, 507-521.

[178] Robertson, A., 2000. Formation of mélanges in the Indus Suture Zone, Ladakh Himalaya bu successive subduction-related, collisional, post-collisional processes during Late Mesozoic-Late Tertiary time. In : Khan, M.A., Treolar, P.J., Searle, M.P., Jan, Q. (Éds.), *Tectonics of the Nangat Parbat Syntaxis and the Western Himalaya. Geological Society of London Special Publications*, 170, 333-374.

[179] Robertson, A., Degnan, P., 1994. The Dras arc Complex : lithofacies and reconstruction of a Late Cretaceous oceanic volcanic arc in the Indus Suture Zone, Ladakh Himalaya. *Sedimentary Geology*, 92, 117-145.

[180] Rowley, D.B., 1996. Age of initiation of collision between India and Asia : a review of stratigraphic data. *Earth and Planetary Science Letters*, 145, 1-13.

[181] Rowley, D.B., 1998. Minimum age of initiation of collision between India and Asia north of Everest based on the subsidence history of the Zhephure Mountain section. *Journal of Geology*, 106, 229-235.

[182] Sachan, H.K., 2001. Supra-subduction origin of the Nidar ophiolitic sequence, Indus Suture Zone, Ladakh, India : Evidence from mineral chemistry of upper mantle rocks. *Ofioliti*, 26, 23-32.

[183] Saleeby, J.B., 1984. Tectonic significance of serpentinite mobility and ophiolitic melange. In : Raymond, L.A. (Éd.), *Melanges : Their Nature, Origin, and Significance, Geological Society of America Special Paper*, 198, 153-168.

[184] Searle, M.P., 1986. Structural evolution and sequence of thrusting in the Himalayan, Tibetan-Tethys and Induc suture zones of Zanskar and Ladakh, Western Himalaya. *Journal of Structural Geology*, 8, 923-936.

[185] Searle, M.P., Windley, B.F., Coward, M.P., Cooper, D.J.W., Rex, A.J., Rex, D., Li, T.D., Xiao, X.C., Jan, M.Q., Thakur, V.C., Kumar, S., 1987. The closing of Tethys and the tectonics of the Himalaya. *Geological Society of America Bulletin*, 98, 678-701.

[186] Sengör, A.M.C., 1984. The Cimmeride orogenic system and the tectonics of Eurasia. *Geological Society of America Special Paper*, 195, 88 p.

[187] Shackleton, R.M., 1981. Structure of southern Tibet : Report on a traverse from Lhasa to Khatmandu organized by Academia Silica. *Journal of Structural Geology*, 3, 97-105.

[188] Shervais, J.W., 1982. Ti-V plots and the petrogenesis of modern and ophiolitic lavas. *Earth and Planetary Science Letters*, 59, 101-118.

[189] Sobolev, A.V., Danyushevsky, L.V., 1994. Petrology and geochemistry of boninites from the north termination of the Tonga Trench : Constraints on the generation conditions of primary high-Ca boninite magmas. *Journal of Petrology*, 35, 1183-1212.

[190] Stakes, D.S., Franklin, J.M., 1994. Petrology of igneous rocks at Middle Valley, Juan de Fuca Ridge. In : Mottl, M.J., Davis, E.E., Fisher, A.T., et al. (Éds.), *Proceedings of the Ocean Drilling Program, Scientific Results*, 139, College Station, Texas, 79-102.

[191] Sun, S.S., 1980. Lead isotopic study of young volcanic rocks from mid-ocean ridges, ocean islands and island arcs. *Philosophical Transactions of the Royal Society of London*, 297, 409-445.

[192] Sun, S.S., McDonough, W.F., 1989. Chemical and isotopic systematics of oceanic basalts : Implications for mantle composition and processes. *Geological Society of London Special Publications*, 42, 313-345.

[193] Tapponnier, P., Mercier, J.L., Proust, F. et al. (27), 1981a. The Tibetan side of the India-Eurasia collision. *Nature*, 294, 405-410.

[194] Tapponnier, P., Mercier, J.L., Armijo, R., Han, T., Zhou, J., 1981b. Field evidence for an active normal faulting in Tibet. *Nature*, 294, 410-414.

[195] Taylor, R.N., Nesbitt, R.W., 1998. Isotopic characteristics of subduction fluids in an intra-oceanic setting, Izu-Bonin Arc, Japan. *Earth and Planetary Science Letters*, 164, 79-98.

[196] Taylor, S.R., McLennan, S.M., 1985. *The continental crust : its composition and evolution. An examination of the geological record preserved in sedimentary rocks.* Blackwell, Oxford.

[197] Thiéblemont, D., Chèvremont, P., Castaing, C., Triboulet, C., Feybesse, J.-L., 1994. La discrimination géotectonique des roches magmatiques basiques par les éléments traces. Réévaluation d'après une base de données et application à la chaîne panafricaine du Togo. *Geodinamica Acta (Paris)*, 7, 139-157.

[198] Tomlinson, K.Y. and Condie, K.C., 2001. Archean mantle plumes : Evidence from greenstone belt geochemistry. In : Ernst, R.E. and Buchan, K.L. (Éds.), *Mantle Plumes : Their Identification Through Time. Geological Society of America Special Papers*, 352, 341-357.

[199] Totten, M.W., Blatt, H., 1993. Alterations in the non-clay-mineral fraction of pelitic rocks across the diagenetic low-grade metamorphic transition, Ouachita Mountains, Oklahoma and Arkansas. *Journal of Sedimentary Petrology*, 63, 899-908.

[200] Tribuzio, R., Tiepolo, M., Thirlwall, M.F., 2000. Origin of titanian pargasite in gabbroic rocks from the Northern Apennine ophiolites (Italy) : insights into the late-magmatic evolution of a MOR-type intrusive sequence. *Earth and Planetary Science Letters*, 176, 281-293.

[201] Turner, S., Hawkesworth, C., Rogers, N., Bartlett, J., Worthington, T., Hergt, J., Pearce, J., Smith, I., 1997. ^{238}U-^{230}Th disequilibria, magma petrogenesis, and flux rates beneath the depleted Tonga-Kermadec island arc. *Geochimica et Cosmochimica Acta*, 61, 4855-4884.

[202] van der Laan, S.R., Arculus, R.J., Pearce, J.A., Murton, B.J., 1992. Petrography, mineral chemistry, and phase relations of the basement boninite series of site 786, Izu-Bonin forearc. In : Fryer, P., Pearce, J.A., Stokking, L.B., et al. (Éds.), *Proceedings of the Ocean Drilling Program, Scientific Results*, 125, College Station, Texas, 171-201.

[203] Van der Voo, R., Spakman, W., Bijwaard, H., 1999. Tethyan subducted slab under India. *Earth and Planetary Science Letters*, 171, 7-20.

[204] Vanko, D.A., 1986. High-chlorine amphiboles from oceanic rocks : Product of highly-saline hydrothermal fluids ?. *American Mineralogist*, 71, 51-59.

[205] Wang, C., Liu, Z., Hébert, 2000. The Yarlung-Zangbo paleo-ophiolite, southern Tibet : implications for the dynamic evolution of the Yarlung-Zangbo Suture Zone. *Journal of Asian Earth Sciences*, 18, 651-661.

[206] Wang, X.B., Xiao, X.C., Cao, Y.G., Zheng, H.X. 1984. Geological map of the ophiolite zone along the middle Yarlung Zangbo River, Xizang (Tibet). *2nd Geological and Geophysical brigade of geological Bureau of the Tibet Autonomous Region*, Publishing House of Surveying and Mapping, Beijing, P.R. China.

[207] Willems, H., Zhou, Z., Zhang, B., Grafe, K.-U., 1996. Stratigraphy of the Upper Cretaceous and Lower Tertiary strata in the Tethyan Himalayas of Tibet (tingri area, China). *Geologische Rundschau*, 85, 723-754.

[208] Winchester, J.A., Floyd, P.A., 1977. Geochemical discrimination of diferent magma series and their differentiation products using immmobile elements. *Chemical Geology*, 20, 325-343.

[209] Winkler, H.G.F., 1967. *Petrogenesis of Metamorphic Rocks*. Springer-Verlag, New York, 237 p.

[210] Wintsch, R.P., Kvale, C.M., 1994. Differential mobility of elements in burial diagenesis of siliciclastic rocks. *Journal of Sedimentary Petrology*, 64, 349-361.

[211] Wood, D.A., 1980. The application of a Th-Hf-Ta diagram to problems of tectonomagmatic classification and to establishing the nature of crustal contamination of basaltic lavas of the British Tertiary Volcanic Province. *Earth and Planetary Science Letters*, 50, 11-30.

[212] Wu, H.R., 1993. Upper Jurassic and Lower Cretaceous radiolarians of Xialu chert, Yarlung Zangbo ophiolite belt, southern Tibet. In : Blueford, J.R. and Murchey, B.L. (Éds.), *Radiolaria of Giant and Subgiant Fields of Asia, Nazarov Memorial Volume. Micropaleontological Special Paper*, 6, 115-136.

[213] Wu, H., Deng, W., 1979. Basic geological features of the Yarlung Zangbo ophiolite belt, Xisang, China. In : Panayiotou, A. (Éd.), *Proceedings of the International Ophiolite Symposium in Cyprus*, Nicosia, Cyprus, 462-472.

[214] Xiao, X.C., 1984. Les ophiolites de Xigaze au Tibet méridional et quelques problèmes tectoniques les concernant. In : Mercier, J.L., Li, G.C. (Éds.), *Mission franco-chinoise au Tibet 1980 : Étude géologique et géophysique de la croûte terrestre et du manteau supérieur du Tibet et de l'Himalaya.* Éditions du Centre National de la Recherche Scientifique, Paris, France, 167-188.

[215] Yin, A., Harrison, T.M., 2000. Geologic evolution of the Himalayan-Tibetan orogen. *Annual Reviews in Earth and Planetary Sciences*, 28, 211-280.

[216] Yin, A., Harisson, T.M., Ryerson, F.J., Wenji, C., Kidd, W.S.F., Copeland, P., 1994. Tertiary structural evolution of the Gangdese thrust system, southeastern Tibet. *Journal of Geophysical Research*, 99, 18175-18201.

[217] Yoder, H.S. Jr., Tilley, C.E., 1962. Origin of basalt magmas : an experimental study of natural and synthetic rock systems. *Journal of Petrology*, 3, 342-532.

[218] Zhou, M.F., Robinson, P.T., Malpas, J. et al., 1996. Podiform chromitites in the Luobusa ophiolite (southern Tibet) ; implications for melt-rock interaction and chromite segregation in the upper mantle. *Journal of Petrology*, 37, 3-21.

[219] Zhu, B., 2003. Sedimentology, petrography, and tectonic significance of Cretaceous to Lower Tertiary deposits in the Tingri-Gyangtse area, southern Tibet. Thèse de doctorat, State University of New York at Albany, 213p.

[220] Ziabrev, S.V., Aitchison, J.C., Abrajevitch, A.V., Badengzhu, Davis, A.M., Luo, H., 2003. Precise radiolarian age constraints on the timing of ophiolite generation and sedimentation in the Dazuqu terrane, Yarlung-Tsangpo suture zone, Tibet. *Journal of the Geolological Society of London*, 160, 591-599.

[221] Ziabrev, S.V., Aitchison, J.C., Abrajevitch, A.V., Badengzhu, Davis, A.M., Luo, H., 2004. Bainang Terrane, Yarlung-Tsangpo suture, southern Tibet (Xizang, China) : a record of intra-Neotethyan subductin-accretion processes preserved on the roof of the world. *Journal of the Geolological Society of London*, 161, 1-17.

[222] Ziabrev, S.V., Aitchison, J.C., Badengzhu, Davis, A.M., Luo, H., Liu, J.B., 2001. More about the missing Tethys : Bainang terrane Tibet. In : *16^{th} Himalaya-Karakorum-Tibet workshop abstracts. Journal of Asian Earth Sciences*, 19, 82-83.

[223] Ziabrev, S.V., Aitchison, J.C., Badengzhu, Davis, A.M., Luo, H., Liu, J.B., McDermid, I., Malpas, J., 2000. Oceanic deposits in the Yarlung-Tsangpo suture zone : Structural setting, radiolarian ages and their tectonic implications. In : *15^{th} Himalaya-Karakorum-Tibet workshop abstracts. Earth Science Frontiers*, 7, 118.

[224] Zyabrev, S.V., Aitchison, J.C., Badengzhu, Davis, A.M., Luo, H., Liu, J.B., 2000. Tethyan relics in the Yarlung-Tsangpo suture, Tibet : Structural setting, radiolarian ages and their tectonic significance. *Ninth Meeting of the International Association of Radiolarian Paleontologists INTERRAD 2000, Program with Abstracts*, 72.

[225] Zyabrev, S.V., Aitchison, J.C., Badengzhu, Davis, A.M., Luo, H., Malpas, J., 1999. Radiolarian biostratigraphy of supra-ophiolite sequences in the Xigaze area, Yarlung Tsangpo suture, Southern Tibet (preliminary report). *Radiolaria*, 17, 13-19.

Annexe A

Localisation géographique des roches analysées

Les échantillons sont énumérés au tableau A.1 et localisés sur la carte géologique détaillée jointe à la thèse (Fig. A.1).

TAB. A.1 – Provenance géographique et nomenclature des roches échantillonnées.

Région O à E (Fig. 1.2)	2001	2002
Buma	2001-LHA-16 à 28	2002-BUM-01 à 12
Lhabuxi		2002-LHA-01 à 10
Lhazexian	2001-LHA-29 à 32	2002-LHA-11 à 14
Beilie	2001-LHA-10 à 15, 32 à 39	2002-BEL-01 à 04
Nord de Lhazequ	2001-LHA-08 et 09	
Xiadamei	2001-LHA-01 à 07	2002-XIA-01, 04 et 05
Mamidhuorong		2002-MAM-01 à 07
Liuqu		2002-LIU-01 à 07, 09, 11 et 12
Ouest de Zisong		2002-MAS-01 à 05
Zisong	2001-ZIS-01 à 10	2002-ZIS-01 à 12
Jiding	2001-JID-01 à 05	
Pazuo, Pazhong		2002-PAZ-01 à 10
Qumei		2002-QUM-01 à 15
Beimarang	2001-BEI-01 à 12	
Qunrang	2001-QUN-02 à 05	
Dayu		2002-DAY-01 à 08
Luobusa (Bainang)		2002-LUS-03 et 04
Baigang	2001-BAG-01 à 05	2002-BAG-01 à 08
Dazhuqu		2002-DAZ-01 à 08
Rembu		2002-REM-01 à 11
Jinlu (Zedong)	2001-JNL-01	
Zedong	2001-ZED-01 à 03	

Annexe B

Données pétrographiques

TAB. B.1: Pourcentages modaux des roches mafiques du mélange ophiolitique.

		Minéraux primaires					**Minéraux secondaires**												
Échantillon	**Roche**	**Mtx**	**Pl**	**Ol**	**Cpx**	**Hbl**	**Hbl**	**Act**	**Trm**	**Chl**	**Pmp**	**Ep**	**Prh**	**Qtz**	**Ap**	**Crb**	**Tlc**	**Ttn**	**Ilm**	**Mag**	**Op**
2001-LHA-16	Gabbro		40		15		40			3				x					2		
2001-LHA-18	Gabbro		30		5		50	x		3			10						2		
2002-BUM-06	Gabbro		59		15					20							1 v	5			
2002-BUM-09	Gabbro		58		x		30	10											2		
2002-MAM-07	Microgabbro		53		5		30			10								2	x		
2002-LIU-06	Gabbro grenu		52		10	35 ts													3		
2002-LIU-07	Gabbro folié		62				30							5					3		
2002-LIU-09	Gabbro folié		57				30							10					3		
2002-QUM-01	Microgabbro		63					30					5 v						2		
2002-QUM-03	Gabbro		58					36					2 v	2 v					2		
2002-QUM-12	Microgabbro porph.		75	3	20														2		
2002-QUM-15	Gabbro grenu		47		20	20 ts		10		x											
2002-QUM-15	Gabbro fin		80		20			x													
2001-JID-02	Gabbro		50		20					20		3	2							5	
2001-JID-03	Gabbro		35				30		20	10									5		
2001-JID-05	Gabbro		47		40		10												3		
2001-BEI-03	Gabbro							20		12		3	60						5		
2001-BEI-04	Gabbro		40		10		40	x		2			5						3		
2001-BEI-12	Gabbro bréchifié						20			18			60						2		
2002-DAY-07	Microgabbro		53					30					15 v						2		
2002-LUS-04	Gabbro		49					48											3		
2002-BAG-06	Gabbro rodingitisé	87	10		3					3											
2002-BAG-08	Leucogabbro	60			22		8			7			3 ?								
2002-DAZ-02	Gabbro		58			10	25	x		3			2 v						2		
2002-DAZ-07	Gabbro folié		21				65	5		3 v				3 v	1			2			
2002-DAZ-08	Gabbro cataclastique		46		10		35			5					1	1		2			
2001-LHA-17	Diabase		27		20		25			25								3	x		
2001-LHA-19	Diabase		45		20			x				30 v									
2001-LHA-20	Diabase		38					20		40						1 v	1				
2002-BUM-03	Diabase		73			20				1		1				1		5			
2001-LHA-38	Diabase							60		30								10			
2002-MAM-06	Diabase		65				30	x					2 v					3			
2002-LIU-01	Diabase	84	2					5 v		2				5 v				2			

Tab. B.1: suite

		Minéraux primaires					Minéraux secondaires													
Échantillon	**Roche**	**Mtx**	**Pl**	**Ol**	**Cpx**	**Hbl**	**Hbl**	**Act**	**Trm**	**Chl**	**Pmp**	**Ep**	**Prh**	**Qtz**	**Ap**	**Crb**	**Tlc**	**Ttn**	**Ilm**	**Mag**	**Op**
2002-LIU-02	Diabase porphyrique		61				30					5 v	v	1				3			
2002-LIU-03	Diabase porphyrique		65 a				25						v	5 v				3			
2002-LIU-04	Diabase porphyrique		52	10	35													3			
2002-QUM-02	Diabase porphyrique		62	3	20					10			2 v								
2002-QUM-04	Diabase		66		25					5			1 v					x	3		
2002-QUM-08	Diabase		64	2	20					10			1 v								
2001-JID-01	Diabase		50					20		20		5								5	
2001-BEI-10	Diabase		55					40					2						3		
2002-BAG-07	Diabase		56				30		10					2					2		
2002-DAZ-03	Diabase		61				30			2				5 v					2		
2001-BEI-01	Basalte porphyritique		50		5			30		x											
2001-BEI-09	Basalte	34						40					24 v								
Conglomérat de Liuqu																					
2001-BEI-06	Gabbro		45				20	25		3									7		
2001-BEI-08	Gabbro folié		35				55	5					1 v						5		
2002-QUM-06	Diabase		53			40											5	1	1		
Zedong																					
2001-JNL-01	Diabase porphyrique	62	10					15				2	1		x					10	
2001-ZED-01	Basalte porphyritique	45			15	25								5 v						10	
2001-ZED-01	Xénolite		42				50			5										3	

Mtx = matrice non déterminée, Pl = plagioclase, Ol = olivine, Cpx = clinopyroxène Hbl = hornblende, Ts = tschermakite, Act = actinote, Trm = trémolite, Chl = chlorite, Pmp = pumpellyite, Ep = Épidote, Prh = prehnite, Qtz = quartz, Ap = apatite, Crb = carbonates, v = veines (en totalité ou en partie), a = amygdules (en totalité ou en partie), Tlc = talc, Ttn = titanite, Ilm = ilménite, Mag = magnétite, Hem = hématite, Op = minéraux opaques non déterminés, Spl = spinelle, Pr = pyrite.

TAB. B.2: Pourcentages modaux des roches mafiques du mélange de Yamdrock.

		Minéraux primaires				Minéraux secondaires													
Échantillon	**Roche**	**Mtx**	**Pl**	**Ol**	**Cpx**	**Hbl**	**Hbl**	**Act**	**Trm**	**Chl**	**Pmp**	**Ep**	**Prh**	**Qtz**	**Ap**	**Crb**	**Tlc**	**Ttn**	**Ilm**	**Mag**	**Op**
Zones serp.																					
2002-LHA-04	Microgabbro		67		30			x		10								3			
2002-LHA-06	Gabbro	44	35				10	x		5 v		1 v				3 v				2	
2001-LHA-13	Gabbro		45				45	x	x				8 v					2			
2002-LHA-03	Basalte mylonitisé		69					5		5				10 v		10 v					1
2001-LHA-15	Basalte		30		20					10 v		v		20 v							20
Zones mafiques																					
2002-BAG-03	Gabbro cataclastique		60		10					25								5			
2002-BAG-04	Gabbro porphyrique		55		25					15								5	x		
2002-MAM-01	Diabase porphyrique	35	49							3 v		4 v		3 v		5 v		1			
2002-MAM-02	Diabase	40	39		10					6 v				3 v		1 v		3			
2002-MAM-05	Diabase porphyrique	66	20		2					5				2				5			
2002-BAG-01	Diabase porphyrique		50			20				24								3	3		
2002-REM-11	Basalte amygdalaire		40							2 a				2 a		21 a					35
mél. Yamdrock																					
2001-LHA-10	Microgabbro		30							30				10				30 rt			
2001-LHA-12	Microgabbro porph.	50	30		10					3 v		7 v									
2001-LHA-33	Gabbro		60					30		8						2		5			
2001-BAG-04	Microgabbro		40		27	3				20									10		
2001-LHA-11	Diabase		25							25				5		25		20 rt			
2001-LHA-36	Diabase	30	38							10 v		7 v		7 v		8 v					
2001-BAG-02	Diabase		40		10									10		20			20		
2001-BAG-02	Lave porphyrique		55		10					10								5	20		
2001-BAG-03	Diabase porphyrique		30		22					25								23	x		
2002-BUM-11	Basalte amygdalaire	55	5							10 a				4 v		11 v				15 v	
2001-LHA-35	Basalte	36	13		3					4				10		21					13
2001-LHA-37	Basalte amygdalaire		60							a						20 a		20			
2001-LHA-09	Basalte amygdalaire		35							v a		20 v		v a		15 a v		10	20		

Tab. B.2: suite

		Minéraux primaires				Minéraux secondaires												
Échantillon	**Roche**	**Mtx**	**Pl**	**Ol**	**Cpx**	**Hbl**	**Hbl**	**Act**	**Trm**	**Chl**	**Pmp**	**Ep**	**Prh**	**Qtz**	**Ap**	**Crb**	**Tlc**	**Ttn**	**Ilm**	**Mag**	**Op**
2001-LHA-01	Basalte porphyritique	22	23		22					8		12 v		11 v		1 v				1 hem	
2001-LHA-02	Basalte	30	25		20					4 v		1 v		15 v							5
2001-LHA-05	Basalte porphyritique	10	18		14					30 v		5 v		15 v		5 v					3
2002-XIA-01	Basalte amygdalaire	34	9		4 a					43 v				4 v		4 v				2	
2002-XIA-04	Basalte porphyritique		23		32					6 v				5 v		4 v					30
2001-ZIS-08	Basalte		37		8					30		7 v		5		5		8	x		
2001-ZIS-09	Basalte amygdalaire		52		10					11						17 a v		10	x		
2001-ZIS-10	Basalte porphyritique		34		9	2				21 v		2 v		14 v		1 v		8	9		
2001-BAG-01	Basalte porphyritique		27		27					20 v		5 v		3 v				18	x		
2001-BAG-05	Basalte porphyritique		30		30					29		1						x	10		
2002-REM-06	Basalte amygdalaire	64	5							21 a				4 a		5 a					1
2002-REM-07	Basalte amygdalaire	50	x							1 a				12 a v		19 a v				18 b	
2002-REM-08	Basalte amygdalaire	30	35		3					30				1 a		1a					

Mêmes abréviations qu'au Tab. B.1.

Tab. B.3: Pourcentages modaux des roches mafiques du flysch triasique.

		Minéraux primaires				Minéraux secondaires														
Échantillon	**Roche**	**Mtx**	**Pl**	**Ol**	**Cpx**	**Hbl**	**Hbl**	**Act**	**Trm**	**Chl**	**Pmp**	**Ep**	**Prh**	**Qtz**	**Ap**	**Crb**	**Tlc**	**Ttn**	**Ilm**	**Mag**	**Op**
Zones mafiques																					
2001-ZIS-03	Gabbro		25		35					20				8	2			5	5		
2001-ZIS-04	Gabbro		50		10	x		2		10	x			10	x			x	8		
2001-ZIS-05	Gabbro		30		25					25				9	1				10		
2001-ZIS-06	Gabbro porphyrique		43		7					25				20	x				5		
2002-ZIS-05	Gabbro	35			28	2				20				7				8	x		
2002-ZIS-05A	Gabbro - bordure	33	30		2	x				20	x			10 v				5	x		
2002-ZIS-07	Gabbro	35			20					30				10				x	5		
2002-ZIS-08	Gabbro (porph.)		65		10	5		x		5				10	x				5	x	
2002-ZIS-09	Gabbro		63		10	x				10	2			10	x			5	x		
2002-ZIS-10	Gabbro		70		3	5				9	x			10				3	x		
2002-ZIS-11	Gabbro (porph.)		72		10					10				5					3		

Tab. B.3: suite

		Minéraux primaires				Minéraux secondaires												
Échantillon	**Roche**	**Mtx**	**Pl**	**Ol**	**Cpx**	**Hbl**	**Hbl Act**	**Trm**	**Chl**	**Pmp**	**Ep**	**Prh**	**Qtz**	**Ap**	**Crb**	**Tlc**	**Ttn**	**Ilm**	**Mag**	**Op**
2002-PAZ-01	Diabase porphyrique		70		10	10			2				3				5	x		
2002-PAZ-06	Diabase		55		20	x	10		5				6				5	x		
2002-MAS-02	Diabase		40						12 v				8 v		30			10		pr
2002-MAS-03	Diabase porphyrique		30						13				3		45				2	7
2001-ZIS-01	Diabase		75						10				10					5		
2002-ZIS-06	Diabase	44	30						3	5			10	x			5	3		
2002-PAZ-05	Basalte	55	x						20				2		20		3	x	x	
2002-PAZ-07	Basalte amygdalaire	25	30		20				20 a									5		
2002-MAS-04	Basalte amygdalaire		70						19 a				3 a					5	a	
2001-ZIS-02	Basalte amygdalaire		55			3			25				10		2 a			5		
Flysch																				
2001-QUN-03	Granite	30	18			2 in							10			5 phl			15	
2001-LHA-29A	Gabbro		30						25				x		40					5 pr
2001-LHA-29B	Gabbro		15						50						20		15 ru			
2001-LHA-30	Gabbro		5						15				30		30 a		20	x		
2001-LHA-31	Gabbro porphyrique		30				62										8			
2002-LHA-12	Gabbro	20	10						30						40		20			
2002-LHA-13	Gabbro		35						35				5		20					5
2001-LHA-32	Diabase		25						35						30					10
2001-ZIS-07	Diabase		60		20				15									5		
2002-PAZ-02	Basalte ?								40 v				3		52 v			5		pr
2002-PAZ-09	Basalte	50							20				3		21			5	1 hem	
2002-DZU-01	Basalte amygdalaire		40						29 a				10 a		24 a					1

Mêmes abréviations qu'au Tab. B.1.

TAB. B.4: Pourcentages modaux des roches ultramafiques du mélange ophiolitique.

		Minéraux primaires				Minéraux Secondaires									
Échantillon	**Roche**	**Ol**	**Opx**	**Cpx**	**Spl**	**Bst**	**Atg**	**Srp**	**v**	**Tlc**	**Mgt**	**Hm**	**Hbl**	**Act**	**Ch**	**Crb**
Mélange ophiolitique																
2001-LHA-27	Harzburgite serp.				3	20	62			5 v	10					
2001-LHA-28	Dunite à chromite serp.				5		74			1 v	20					
2002-BUM-02	Harzburgite serp.	20	10	2 in	5	5	53	5								
2002-BUM-08	Lherzolite serp.	7	20	10	3		55	5								
2001-LHA-39	Harzburgite serp.				3	30	67									
2001-LHA-06	Harzburgite serp.				10	30	40				20					
2001-LHA-07	Harzburgite serp.					40	50				10					
2002-LIU-05	Harzburgite serp.					10	85				5					
2002-LIU-11	Harzburgite serp.					25	70				5					
2002-QUM-07	Harzburgite serp.				2	20	73				5					
2002-QUM-11	Harzburgite serp.				2	10	78				10					
2002-QUM-13	Harzburgite serp.				3	20	75	2			x					
2002-QUM-14	Harzburgite serp.	10	15	in	3		72									
2001-JID-04	Harzburgite serp.				2	15	75				5	3				
2001-BEI-02	Harzburgite serp.				5	20	67	5				3				
2001-BEI-11	Harzburgite serp.				5	20	75									
2002-LUS-03	Lherzolite serp.			5	3	10	82									
2002-BAG-05	Harzburgite serp.				3	10	80	5		2 v						
2002-DAZ-01	Harzburgite serp.				5	30	65									
2002-DAZ-04	Harzburgite serp.					20	30			40 ?	10	x				
Zones serp.																
2002-LHA-05	Amph. Peridotite										2 tn		30	60		
2002-LHA-07	Carb. Peridotite										2				3	95 (v)
2002-LHA-08	Harzburgite serp.					30	55	5		5 (v)	5 v					
2001-LHA-08	Harzburgite serp.				5	20	35			35					5	
2002-DAY-04	Harzburgite serp.					20	72			3	5					
2002-DAY-05	Carb. Serp. Peridotite						30				10					60
2002-DAY-06	Lherzolite serp.				3	15	82									
2002-DAY-08	Dunite à chromite serp.						80	15			5 cm					
2002-REM-09	Harzburgite serp.			2 in	10	18	65	5			x					

Tab. B.4: suite

		Minéraux primaires				Minéraux Secondaires								
Échantillon	**Roche**	**Ol**	**Opx**	**Cpx**	**Spl**	**Bst**	**Atg**	**Srp v**	**Tlc**	**Mgt**	**Hm**	**Hbl**	**Act**	**Ch**	**Crb**
Zedong															
2001-ZED-02	Harzburgite	60	27	3 in	5			5							
2001-ZED-03	Harzburgite	65	20	in	3			12							

Ol = olivine, Opx = orthopyroxène, Cpx = clinopyroxène, Spl = spinelle, Bst = bastite, Atg = antigorite, Srp v = veines de serpentine, Tlc = talc, Mgt = magnétite, Hm = hématite, Hbl = hornblende, Act = actinote, Ch = chlorite, Carb = carbonates, ch = chloritisé, in = inclusion, v = veines, (v) veines et matrice

Annexe C

Données de chimie minérale

$$\text{An} = \frac{\text{Ca}}{\text{Ca} + \text{Na} + \text{K}} \qquad \text{Ab} = \frac{\text{Na}}{\text{Ca} + \text{Na} + \text{K}} \qquad \text{Or} = \frac{\text{K}}{\text{Ca} + \text{Na} + \text{K}}$$

$$\text{Wo} = \frac{\text{Ca}}{\text{Ca} + \text{Mg} + \text{Fe}} \qquad \text{En} = \frac{\text{Mg}}{\text{Ca} + \text{Mg} + \text{Fe}} \qquad \text{Fs} = \frac{\text{Fe}^{2+}}{\text{Ca} + \text{Mg} + \text{Fe}}$$

$$\text{Fo} = \frac{\text{Mg}}{\text{Mg} + \text{Fe}^{2+}} \qquad \text{Fa} = \frac{\text{Fe}^{2+}}{\text{Mg} + \text{Fe}^{2+}}$$

$$\text{Mg\#} = \frac{\text{Mg}}{\text{Mg} + \text{Fe}^{2+}} \qquad \text{Cr\#} = \frac{\text{Cr}}{\text{Cr} + \text{Al}}$$

L'aluminium au site tétrahédrique des amphiboles (Al^{iv}) est calculé par le programme Excel PROBAMPH selon la méthode de calcul de Leake et al. (1997).

TAB. C.1: Composition chimique (% poids) des feldspaths des roches mafiques du mélange ophiolitique.

		SiO_2	Al_2O_3	MgO	CaO	FeO	Na_2O	K_2O	Total	An	Ab	Or
Gabbro	lha16-p20	68.75	20.48		0.34	0.45	11.82	0.07	101.91	0.02	0.98	0.00
	lha16-p21	69.16	20.29		0.24	0.00	11.80	0.04	101.53	0.01	0.99	0.00
	lha16-p22	69.84	20.35		0.24	0.02	11.90	0.08	102.42	0.01	0.98	0.00
	lha16-p23	69.59	20.34		0.36	0.04	12.16	0.08	102.57	0.02	0.98	0.00
	lha18-p17	71.30	20.29		0.13	0.00	10.39	0.04	102.15	0.01	0.99	0.00
	lha18-p18	71.92	20.41		0.21	0.00	10.91	0.03	103.48	0.01	0.99	0.00
	lha18-p19	71.72	20.55		0.51	0.07	10.39	0.05	103.29	0.03	0.97	0.00
	lha18-p20	72.53	20.49		0.14	0.06	10.94	0.04	104.20	0.01	0.99	0.00
	lha13-p12	68.77	20.53		0.28	0.03	12.14	0.06	101.81	0.01	0.98	0.00
	lha13-p13	68.83	20.43		0.20	0.04	12.02	0.07	101.58	0.01	0.99	0.00
	lha13-p14	68.78	20.37		0.19	0.06	12.09	0.06	101.55	0.01	0.99	0.00
	lha13-p15	69.77	20.34		0.11	0.02	11.92	0.09	102.25	0.01	0.99	0.01
	lha13-p16	69.18	20.44		0.21	0.03	11.86	0.11	101.83	0.01	0.98	0.01
	lha13-p17	68.77	20.36		0.12	0.04	12.22	0.06	101.57	0.00	0.99	0.00
	lha13-p18	69.29	20.40		0.14	0.08	12.27	0.05	102.23	0.01	0.99	0.00
	lha13-p19	68.39	20.87		0.50	0.09	11.89	0.15	101.89	0.02	0.97	0.01
	2liu6-p2	67.83	17.58	0.01	0.04	0.02	11.70	0.01	97.19	0.00	1.00	0.00
	2liu6-p4	62.14	21.91	0.01	5.39	0.18	8.78	0.13	98.53	0.25	0.74	0.01
	2liu7-ab15	67.63	18.62	0.00	0.03	0.03	12.26	0.01	98.57	0.00	1.00	0.00
	2liu7-ab16	66.53	18.29	0.01	0.04	0.02	12.20	0.01	97.10	0.00	1.00	0.00
	2liu9-p3	67.92	18.74	0.00	0.24	0.06	11.83	0.01	98.80	0.01	0.99	0.00
	2liu9-p4	67.06	18.63	0.00	0.22	0.00	12.06	0.01	97.98	0.01	0.99	0.00
	2liu9-p5	67.21	18.50	0.00	0.19	0.15	11.94	0.01	98.00	0.01	0.99	0.00
	2qum12-p10	46.47	30.25		15.54	0.48	2.77	0.03	95.54	0.76	0.24	0.00
	2qum12-p14	47.55	31.27		16.42	0.33	2.21	0.00	97.78	0.80	0.20	0.00
	2qum12-p15	46.50	31.98		17.19	0.39	1.84	0.01	97.90	0.84	0.16	0.00
	2qum15-p7	46.52	30.15		15.36	0.09	3.06	0.00	95.18	0.74	0.26	0.00
	2qum15-p13	54.14	27.18		11.34	0.14	5.40	0.03	98.23	0.54	0.46	0.00
	2qum15-p14	53.54	26.96		11.57	0.22	5.12	0.04	97.44	0.55	0.44	0.00
	2qum15a-p20	52.56	27.87	0.03	12.17	0.30	4.84	0.08	97.85	0.58	0.42	0.00
	2qum15a-p21	3.18	28.29	0.01	12.21	0.21	4.95	0.05	98.90	0.58	0.42	0.00
	2qum15a-p22	52.18	25.77	0.00	11.08	0.14	5.54	0.06	94.77	0.52	0.47	0.00
	2qum15a-p24	52.29	26.09	0.26	10.83	0.11	5.43	0.08	95.08	0.52	0.47	0.00
	2qum15a-p25	52.72	26.20	0.00	10.72	0.15	5.70	0.06	95.54	0.51	0.49	0.00
	2lus4-p1	50.28	29.83		13.35	0.53	3.59	0.48	98.06	0.65	0.32	0.03

Tab. C.1: Feldspaths- mélange ophiolitique (suite)

		SiO_2	Al_2O_3	MgO	CaO	FeO	Na_2O	K_2O	Total	An	Ab	Or
	2lus4-p4	50.38	29.61		14.28	0.58	3.60	0.17	98.62	0.68	0.31	0.01
	2lus4-p5	51.25	29.75		14.01	0.62	3.83	0.01	99.48	0.67	0.33	0.00
	2lus4-p6	50.77	30.32		14.71	0.76	3.53	0.02	100.11	0.70	0.30	0.00
	2lus4-p10	53.27	29.69		12.03	0.56	4.56	0.27	100.60			
	2lus4-p11	52.24	29.69		12.77	0.75	4.30	0.03	99.98			
	2lus4-p19	51.26	30.92		14.06	0.51	3.70	0.02	100.71			
	2daz2-p14	68.47	18.81	0.00	0.43	0.45	11.69	0.01	99.86	0.02	0.98	0.00
	2daz2-p20	60.48	22.69	0.01	5.99	0.22	8.38	0.14	97.91	0.28	0.71	0.01
	2daz2-p21	64.79	19.63	0.01	2.55	0.19	10.16	0.31	97.65	0.12	0.86	0.02
	2daz8-p9	69.13	19.24	0.09	0.04	0.15	11.95	0.06	100.67	0.00	1.00	0.00
Diabase	lha17-p16	71.84	20.35		0.08	0.02	11.25	0.03	103.56	0.00	0.99	0.00
	lha17-p17	69.87	20.30		0.09	0.00	11.45	0.03	101.74	0.00	0.99	0.00
	lha17-p18	70.71	20.45		0.10	0.03	11.48	0.03	102.79	0.00	0.99	0.00
	lha17-p19	71.10	20.37		0.09	0.02	10.35	0.02	101.94	0.00	0.99	0.00
	lha17-p20	71.22	20.18		0.05	0.01	11.29	0.03	102.78	0.00	1.00	0.00
	2bum3-p7	51.61	28.21	0.04	13.11	0.52	3.88	0.22	97.59	0.64	0.34	0.01
	2bum3-p8	52.61	26.89	0.04	11.88	0.42	4.67	0.25	96.75	0.58	0.41	0.01
	2bum3-p14	57.66	25.36	0.01	8.30	0.37	6.57	0.51	98.77	0.40	0.57	0.03
	2bum3-p15	58.21	24.80	0.02	7.76	0.35	6.90	0.55	98.59	0.37	0.60	0.03
	2liu2-p9	68.91	19.82		0.35	0.10	11.83	0.05	101.06	0.02	0.98	0.00
	2liu2-p10	67.77	20.17		1.06	0.03	11.58	0.01	100.63	0.05	0.95	0.00
	2liu3-p1	65.83	18.88	0.01	0.58	0.06	11.30	0.05	96.70	0.03	0.97	0.00
	2liu3-p2	65.71	18.58	0.02	0.50	0.16	11.52	0.04	96.52	0.02	0.98	0.00
	2liu3-p16	65.37	18.79	0.01	0.49	0.24	11.58	0.05	96.54	0.02	0.97	0.00
	2liu4-p14	62.69	20.48	0.03	2.55	0.15	10.49	0.08	96.48	0.12	0.88	0.00
	2liu4-p15	64.70	20.34	0.02	2.51	0.13	10.47	0.08	98.24	0.12	0.88	0.00
	jid1-p9	69.71	20.52		0.42	0.06	11.28	0.08	102.07	0.02	0.98	0.00
	jid1-p10	70.25	20.46		0.29	0.11	11.65	0.08	102.85	0.01	0.98	0.00
	jid1-p11	69.03	20.18		0.23	0.07	11.39	0.07	100.96	0.01	0.98	0.00
	jid1-p12	69.61	20.33		0.33	0.12	11.24	0.06	101.68	0.02	0.98	0.00
	2lha6-ab9	67.99	17.96	0.01	0.01	0.10	11.97	0.03	98.07	0.00	1.00	0.00
Basalte	2lha3-ab6	69.17	18.16	0.01	0.05	0.07	12.04	0.03	99.53	0.00	1.00	0.00
	2lha3-p7	67.70	17.80	0.07	0.15	0.11	11.55	0.10	97.47	0.01	0.99	0.01
	2lha3-p8	68.02	18.29	0.02	0.39	0.12	11.82	0.06	98.71	0.02	0.98	0.00
	2lha3-p9	66.53	18.41	0.02	0.34	0.06	11.63	0.08	97.07	0.02	0.98	0.00

Tab. C.1: Feldspaths- mélange ophiolitique (suite)

		SiO_2	Al_2O_3	MgO	CaO	FeO	Na_2O	K_2O	Total	An	Ab	Or
	2lha3-p10	68.71	18.15	0.00	0.03	0.03	11.98	0.05	98.96	0.00	1.00	0.00
	2lha3-p11	67.44	17.89	0.01	0.36	0.12	11.81	0.10	97.72	0.02	0.98	0.00

Tab. C.2: Composition chimique (% poids) des feldspaths des roches mafiques du mélange de Yamdrock.

		SiO_2	Al_2O_3	MgO	CaO	FeO	Na_2O	K_2O	Total	An	Ab	Or
Gabbro	2bag3-kf3	62.09	16.34	0.01	0.00	0.11	0.22	15.47	94.24	0.00	0.02	0.98
	2bag3-p3	68.71	18.41	0.02	0.22	0.05	11.87	0.06	99.33	0.01	0.99	0.00
	2bag3-p4	67.64	18.03	0.01	0.43	0.06	11.79	0.05	98.01	0.02	0.98	0.00
	2bag3-p5	68.46	18.36	0.01	0.38	0.10	11.90	0.06	99.27	0.02	0.98	0.00
	2bag3-p6	64.52	17.22	0.01	0.02	0.12	0.18	15.79	97.87	0.00	0.02	0.98
	2bag3-p7	67.65	18.38	0.01	0.52	0.05	11.59	0.16	98.35	0.02	0.97	0.01
	2mam1-p1	66.07	18.48	0.75	0.13	0.98	11.74	0.04	98.19	0.01	0.99	0.00
	2mam1-ab10	67.96	18.85	0.02	0.07	0.12	12.14	0.05	99.21	0.00	0.99	0.00
	2mam2-p8	68.09	19.61		0.33	0.16	11.77	0.03	99.98	0.01	0.98	0.00
	2mam2-p9	67.90	19.80		0.65	0.05	11.75	0.02	100.17	0.03	0.97	0.00
	2mam2-p10	66.02	19.24		0.51	0.08	11.80	0.04	97.69	0.02	0.97	0.00
	2mam2-p11	67.91	19.46		0.49	0.07	11.90	0.01	99.83	0.02	0.98	0.00
	2mam5-p2	67.51	18.34	0.01	0.03	0.19	12.11	0.03	98.21	0.00	1.00	0.00
	2mam5-p3	67.25	18.35	0.03	0.06	0.21	11.92	0.16	97.99	0.00	0.99	0.01
	2mam5-p4	66.09	18.11	0.00	0.09	0.09	12.06	0.07	96.50	0.00	0.99	0.00
	2bag1-p2	68.95	18.50	0.02	0.14	0.13	11.76	0.20	99.69	0.01	0.98	0.01
	2bag1-p3	64.98	19.70	0.31	0.09	1.01	10.02	1.81	97.93	0.00	0.89	0.11
	2bag1-p7	66.89	18.29	0.00	0.27	0.24	11.95	0.04	97.68	0.01	0.99	0.00
	lha10-p1	70.05	20.31		0.02	0.10	11.79	0.05	102.32	0.00	1.00	0.00
	lha10-p2	70.40	20.27		0.04	0.06	11.97	0.04	102.77	0.00	1.00	0.00
	lha10-p3	70.04	20.26		0.04	0.05	11.93	0.04	102.37	0.00	1.00	0.00
	lha10-p4	69.75	20.45		0.10	0.13	11.76	0.02	102.21	0.00	0.99	0.00
	lha10-p5	67.79	19.90		0.08	0.06	12.05	0.04	99.93	0.00	0.99	0.00
	lha33-p9	68.52	20.71		0.04	0.17	11.90	0.02	101.36	0.00	1.00	0.00
	lha33-p10	68.31	20.50		0.03	0.05	11.27	0.02	100.18	0.00	1.00	0.00
	lha33-p11	68.50	20.50		0.08	0.06	11.84	0.02	101.00	0.00	0.99	0.00
	lha33-p12	68.02	20.58		0.07	0.02	11.79	0.03	100.51	0.00	0.99	0.00
Diabase	bag3-p12	65.52	20.65		0.40	0.05	11.91	0.08	98.61	0.02	0.98	0.00

Tab. C.2: Feldspaths - mélange de Yamdrock (suite)

		SiO_2	Al_2O_3	MgO	CaO	FeO	Na_2O	K_2O	Total	An	Ab	Or
	bag3-p13	66.33	20.59		0.16	0.06	12.07	0.07	99.27	0.01	0.99	0.00
	bag3-p15	67.14	21.12		0.51	0.12	11.57	0.08	100.54	0.02	0.97	0.00
Basalte	lha1-p4	66.15	20.80		0.45	1.24	11.05	0.68	100.38	0.02	0.94	0.04
	lha1-p28	63.58	20.69		0.51	1.43	11.01	0.57	97.78	0.02	0.94	0.03
	lha5-p20	66.84	20.21		0.23	0.21	11.89	0.05	99.42	0.01	0.99	0.00
	lha5-p21	67.59	20.52		0.18	0.06	12.01	0.06	100.42	0.01	0.99	0.00
	lha5-p22	67.24	20.27		0.18	0.12	11.97	0.06	99.84	0.01	0.99	0.00
	lha5-p34	65.01	20.69		0.18	0.31	11.73	0.22	98.14	0.01	0.98	0.01
	2xia1-p6	66.98	18.79	0.00	0.35	0.12	11.71	0.06	98.01	0.02	0.98	0.00
	2xia1-p7	67.30	19.11	0.06	0.34	0.18	11.54	0.39	98.91	0.02	0.96	0.02
	2xia1-p8	67.68	19.02	0.04	0.28	0.22	11.83	0.04	99.11	0.01	0.99	0.00
	2xia1-p10	67.05	18.64	0.00	0.29	0.11	11.87	0.05	98.01	0.01	0.98	0.00
	2xia1-p11	67.87	19.03	0.00	0.23	0.13	11.65	0.06	98.98	0.01	0.99	0.00
	2xia4-p5	67.15	19.50	0.02	0.78	0.25	11.18	0.34	99.21	0.04	0.94	0.02
	2xia4-p11	64.98	19.51	0.16	0.33	0.82	9.87	1.51	97.18	0.02	0.89	0.09
	2xia4-p12	67.83	18.38	0.00	0.57	0.23	11.60	0.08	98.70	0.03	0.97	0.00
	2xia4-p13	67.31	18.85	0.04	0.45	0.49	11.20	0.61	98.95	0.02	0.95	0.03
	2xia4-p14	65.84	20.01	0.23	0.36	0.95	10.03	1.57	98.98	0.02	0.89	0.09
	2rem8-p1	69.35	19.60		0.09	0.04	12.19	0.04	101.30	0.00	0.99	0.00
	2rem8-p3	62.75	16.83		5.06	0.27	9.56	0.05	94.52	0.23	0.77	0.00
	2rem8-p4	67.52	19.34		0.14	0.20	11.93	0.06	99.19	0.01	0.99	0.00
	2rem8-p5	68.33	19.19		0.04	0.23	12.13	0.02	99.94	0.00	1.00	0.00
	2rem8-p6	68.33	20.25		0.05	0.17	12.02	0.03	100.84	0.00	1.00	0.00
	2rem8-p11	68.64	19.67		0.16	0.12	11.82	0.06	100.48	0.01	0.99	0.00

Tab. C.3: Composition chimique (% poids) des feldspaths des roches mafiques du flysch triasique.

		SiO_2	Al_2O_3	MgO	CaO	FeO	Na_2O	K_2O	Total	An	Ab	Or
Granite	qun3-kf1	64.87	19.47		0.15	0.08	3.15	11.95	99.66	0.01	0.28	0.71
	qun3-kf2	64.87	19.53		0.16	0.08	3.13	11.99	99.76	0.01	0.28	0.71
	qun3-kf3	64.93	19.44		0.15	0.09	3.02	11.99	99.60	0.01	0.28	0.72
	qun3-kf4	64.79	19.69		0.20	0.02	3.09	12.15	99.94	0.01	0.28	0.71
	qun3-p6	63.03	24.17		4.54	0.18	8.56	0.83	101.30	0.22	0.74	0.05
	qun3-p7	64.40	23.52		3.73	0.14	9.06	0.95	101.80	0.18	0.77	0.05

Tab. C.3: Feldspaths - flysch triasique (suite)

		SiO_2	Al_2O_3	MgO	CaO	FeO	Na_2O	K_2O	Total	An	Ab	Or
	qun3-p8	65.13	19.62		0.15	0.11	3.08	11.85	99.93	0.01	0.28	0.71
	qun3-p9	64.76	23.36		3.61	0.10	8.84	1.03	101.70	0.17	0.77	0.06
	qun3-p10	63.60	23.82		4.13	0.14	8.52	0.91	101.11	0.20	0.75	0.05
	qun3-p11	63.77	23.76		4.27	0.13	8.64	0.89	101.46	0.20	0.75	0.05
	qun3-p12	63.14	24.31		4.66	0.17	8.51	0.78	101.56	0.22	0.73	0.04
	qun3-p13	63.64	23.76		4.09	0.15	8.77	0.88	101.29	0.19	0.76	0.05
	qun3-p14	63.76	23.85		4.17	0.13	8.62	0.86	101.39	0.20	0.75	0.05
Gabbro	zis6-p10	72.63	21.86		0.26	0.03	4.34	0.05	99.15	0.03	0.96	0.01
	2zis5a-p17	66.63	17.61	0.02	0.07	0.07	12.03	0.08	96.52	0.00	0.99	0.00
	2zis5a-p19	65.76	17.04	0.01	0.11	0.03	11.82	0.10	94.85	0.00	0.99	0.01
	2zis8-p16	67.09	17.71	0.01	0.12	0.15	11.70	0.15	96.92	0.01	0.99	0.01
	2zis8-p17	66.98	18.14	0.00	0.20	0.20	11.83	0.12	97.45	0.01	0.98	0.01
	2zis8-p18	67.82	18.04	0.00	0.04	0.30	11.94	0.10	98.25	0.00	0.99	0.01
	2zis10-p17	68.45	18.84	0.00	0.07	0.01	11.91	0.16	99.44	0.00	0.99	0.01
	2zis10-p18	68.43	18.83	0.00	0.09	0.00	11.88	0.12	99.35	0.00	0.99	0.01
	2zis10-p19	67.10	18.16	0.00	0.21	0.03	11.76	0.14	97.40	0.01	0.98	0.01
	2zis10-p20	67.60	18.07	0.02	0.06	0.01	11.83	0.08	97.66	0.00	0.99	0.00
	2zis9-p4	69.07	19.17	0.00	0.06	0.10	11.95	0.15	100.51	0.00	0.99	0.01
	2zis9-p5	69.26	19.13	0.02	0.06	0.46	12.05	0.10	101.08	0.00	0.99	0.00
	2zis9-p6	68.92	19.41	0.01	0.15	0.39	11.90	0.16	100.94	0.01	0.98	0.01
	2zis9-p8	68.99	19.31	0.01	0.12	0.32	11.83	0.09	100.67	0.01	0.99	0.00
	2zis11-p10	68.34	19.37	0.13	0.41	0.37	11.77	0.09	100.47	0.02	0.98	0.00
	2zis11-p11	68.52	19.45	0.00	0.09	0.23	11.90	0.11	100.30	0.00	0.99	0.01
	lha29a-p5	71.33	20.20		0.31	0.19	10.29	0.01	102.33	0.02	0.98	0.00
	lha29a-p6	71.05	20.35		0.10	0.16	10.78	0.01	102.45	0.01	0.99	0.00
	lha29a-p7	71.55	20.13		0.23	0.29	10.21	0.00	102.41	0.01	0.99	0.00
	lha29a-p8	72.21	19.88		0.15	0.15	10.15	0.00	102.54	0.01	0.99	0.00
	lha29a-p9	69.57	20.38		0.22	0.11	11.49	0.01	101.78	0.01	0.99	0.00
	lha29a-p10	71.70	20.35		0.09	0.13	10.85	0.01	103.12	0.00	0.99	0.00
	lha29b-p5	71.93	20.43		0.22	0.18	10.61	0.02	103.39	0.01	0.99	0.00
	lha29b-p6	70.32	20.11		0.14	0.21	11.23	0.01	102.03	0.01	0.99	0.00
	lha29b-p7	70.65	20.39		0.22	0.30	11.18	0.02	102.76	0.01	0.99	0.00
	lha29b-p8	72.07	20.47		0.14	0.26	10.51	0.02	103.47	0.01	0.99	0.00
	lha29b-p9	71.50	20.31		0.14	0.20	10.64	0.04	102.83	0.01	0.99	0.00
	lha31-p15	70.43	20.31		0.89	0.25	11.34	0.05	103.27	0.04	0.96	0.00
	lha31-p23	72.09	19.83		0.20	0.06	10.29	0.04	102.51	0.01	0.99	0.00

Tab. C.3: Feldspaths - flysch triasique (suite)

		SiO_2	Al_2O_3	MgO	CaO	FeO	Na_2O	K_2O	Total	An	Ab	Or
Diabase	2mas3-p2	66.06	17.77	0.27	0.06	0.81	11.26	0.10	96.33	0.00	0.99	0.01
	2mas3-p3	68.33	18.42	0.00	0.07	0.18	12.12	0.03	99.14	0.00	1.00	0.00
	2zis6-p5	67.22	17.75	0.02	0.45	0.09	11.75	0.05	97.33	0.02	0.98	0.00
	2zis6-p6	67.97	17.35	0.00	0.07	0.03	11.94	0.10	97.46	0.00	0.99	0.01
	2zis6-p7	67.17	17.88	0.00	0.09	0.05	11.87	0.10	97.15	0.00	0.99	0.01
	2zis6-p8	68.48	17.97	0.00	0.01	0.05	12.07	0.03	98.62	0.00	1.00	0.00
	2zis6-p11	68.19	17.64	0.00	0.03	0.02	12.02	0.07	97.96	0.00	1.00	0.00
	2zis6-p12	67.92	17.42	0.01	0.05	0.04	12.03	0.18	97.65	0.00	0.99	0.01
Basalte	2paz5-p2	67.28	19.41		0.18	0.11	12.01	0.08	99.08	0.01	0.99	0.00
	2paz5-p3	68.49	19.09		0.14	0.23	11.97	0.07	99.99	0.01	0.99	0.00
	2paz7-p13	67.54	18.92	0.04	0.12	0.33	12.04	0.13	99.11	0.01	0.99	0.01
	2paz7-p14	66.66	18.69	0.02	0.11	0.11	11.88	0.07	97.55	0.00	0.99	0.00
	2paz7-p16	65.75	19.10	0.32	0.08	0.61	10.55	1.54	97.95	0.00	0.91	0.09
	2paz7-p17	67.29	18.61	0.05	0.09	0.22	11.71	0.34	98.30	0.00	0.98	0.02

Tab. C.4: Composition chimique (% poids) des pyroxènes des roches mafiques du mélange ophiolitique.

		SiO_2	TiO_2	Al_2O_3	Cr_2O_3	Fe_2O_3	MgO	CaO	MnO	FeO	Na_2O	Total	Mg#	Wo	En	Fs
Gabbro	lha16-px1	52.79	0.30	2.48	0.30	1.40	17.43	20.94	0.15	4.11	0.27	100.18	0.88	0.43	0.50	0.07
	lha16-px2	52.77	0.33	2.32	0.21	0.68	17.32	20.70	0.12	4.85	0.22	99.53	0.86	0.43	0.50	0.08
	lha16-px3	53.25	0.22	1.24	0.21	1.11	16.75	22.87	0.17	4.05	0.10	100.02	0.88	0.46	0.47	0.06
	lha16-px4	52.29	0.27	2.80	0.66	0.75	17.44	21.17	0.07	3.45	0.23	99.12	0.90	0.44	0.50	0.06
	lha16-px5	52.25	0.26	3.17	0.88	0.41	17.38	21.17	0.07	3.57	0.21	99.38	0.90	0.44	0.50	0.06
	lha16-px55	51.61	0.31	2.19	0.46	0.23	13.21	20.56	0.31	9.85	0.42	99.15	0.70	0.44	0.39	0.16
	lha16-px6	52.73	0.23	2.00	0.73	0.82	16.54	23.05	0.09	3.16	0.21	99.57	0.90	0.47	0.47	0.05
	lha18-px9	53.07	0.15	1.21	0.35	0.55	14.98	21.59	0.31	7.47	0.31	99.98	0.78	0.45	0.43	0.12
	lha18-px10	52.98	0.38	2.59	0.32	0.43	17.44	20.71	0.16	4.76	0.24	100.04	0.87	0.43	0.50	0.08
	2bum6-px1	53.20	0.40	1.90	0.63	1.07	17.77	20.25	0.16	4.85	0.29	100.53	0.87	0.42	0.51	0.08
	2bum6-px2	52.35	0.52	3.00	0.30	2.05	16.89	21.19	0.12	4.39	0.28	101.09	0.87	0.44	0.49	0.07
	2bum6-px3	51.96	0.52	3.06	0.50	1.76	17.24	20.23	0.15	4.58	0.26	100.24	0.87	0.42	0.50	0.07
	2bum6-px4	53.37	0.37	1.77	0.44	1.52	18.61	19.40	0.16	4.92	0.23	100.78	0.87	0.39	0.53	0.08
	2bum6-px5	52.01	0.73	3.18	0.10	2.15	17.00	19.67	0.20	5.88	0.27	101.18	0.84	0.41	0.49	0.10
	2bum6-px11	51.67	0.72	2.32	0.07	2.13	16.09	19.68	0.26	6.98	0.28	100.19	0.80	0.41	0.47	0.11

Tab. C.4: Pyroxènes - mélange ophiolitique (suite)

	SiO_2	TiO_2	Al_2O_3	Cr_2O_3	Fe_2O_3	MgO	CaO	MnO	FeO	Na_2O	Total	Mg#	Wo	En	Fs
2bum9-px1	53.43	0.43	2.08	0.24	1.07	17.33	21.22	0.16	4.93	0.24	101.13	0.86	0.43	0.49	0.08
2bum9-px7	51.96	0.54	3.51	0.39	2.04	16.91	20.54	0.16	4.81	0.26	101.11	0.86	0.43	0.49	0.08
2bum9-px10	53.31	0.46	2.02	0.16	1.63	17.54	20.85	0.16	4.96	0.23	101.32	0.86	0.42	0.50	0.08
2mam7-px1	52.91	0.06	1.19	0.06	2.46	14.75	22.67	0.31	6.80	0.19	101.39	0.79	0.47	0.42	0.11
2liu6-px1	52.37	0.39	1.84	0.01	1.29	14.76	21.63	0.25	7.07	0.35	99.95	0.79	0.45	0.43	0.12
2liu6-px2	52.09	0.44	1.80	0.02	1.66	14.46	22.11	0.21	6.67	0.37	99.84	0.79	0.47	0.42	0.11
2liu6-px3	52.57	0.47	1.91	0.00	1.21	14.77	21.32	0.25	7.76	0.35	100.60	0.77	0.44	0.43	0.13
2liu6-px5	52.38	0.45	1.71	0.01	1.46	14.77	21.78	0.24	7.10	0.32	100.22	0.79	0.46	0.43	0.12
2liu6-px6	52.71	0.40	1.48	0.07	1.36	15.09	21.48	0.24	7.37	0.29	100.49	0.78	0.45	0.44	0.12
2liu6-px8	52.23	0.43	1.92	0.02	1.90	15.01	21.42	0.28	6.75	0.35	100.30	0.80	0.45	0.44	0.11
2liu6-px9	53.25	0.26	1.29	0.08	1.22	15.42	21.83	0.21	7.03	0.26	100.84	0.80	0.45	0.44	0.11
2liu6-px10	52.97	0.40	1.90	0.03	0.87	14.90	21.74	0.20	7.52	0.33	100.87	0.78	0.45	0.43	0.12
2liu6a-px11	51.70	0.59	2.16	0.14	1.57	14.22	21.61	0.26	6.87	0.47	99.59	0.79	0.46	0.42	0.11
2liu6a-px12	51.80	0.58	2.16	0.12	2.65	14.50	21.80	0.27	6.08	0.50	100.46	0.81	0.47	0.43	0.10
2liu6a-px13	51.85	0.49	2.07	0.04	2.40	14.59	22.11	0.27	5.76	0.45	100.02	0.82	0.47	0.43	0.10
2liu6a-px14	51.73	0.55	2.14	0.11	2.66	14.67	21.66	0.26	5.82	0.51	100.10	0.82	0.46	0.44	0.10
2liu6a-px15	52.10	0.43	2.14	0.22	1.86	14.68	22.47	0.22	6.09	0.31	100.51	0.81	0.47	0.43	0.10
jid2-px3	53.63	0.26	2.31	0.18	0.23	18.17	20.57	0.14	4.34	0.24	100.08	0.88	0.42	0.51	0.07
jid2-px8	52.38	0.41	3.25	0.41	0.92	18.07	18.95	0.14	5.13	0.26	99.94	0.86	0.39	0.52	0.08
jid5-px1	51.97	0.18	1.08	0.00	1.32	13.16	20.87	0.32	10.43	0.29	99.63	0.69	0.44	0.39	0.17
jid5-px2	52.32	0.22	1.15	0.00	0.63	13.21	20.88	0.32	10.87	0.27	99.89	0.68	0.44	0.38	0.18
jid5-px3	52.11	0.24	1.10	0.06	0.91	13.17	20.97	0.30	10.62	0.27	99.74	0.69	0.44	0.39	0.17
jid5-px4	51.92	0.21	1.09	0.03	1.54	13.17	20.90	0.35	10.26	0.30	99.79	0.70	0.44	0.39	0.17
jid5-px5	52.43	0.21	1.11	0.04	0.39	13.23	20.98	0.31	10.78	0.28	99.78	0.69	0.44	0.39	0.18
jid5-px6	52.13	0.18	1.08	0.03	1.28	13.22	21.12	0.35	10.20	0.28	99.88	0.70	0.44	0.39	0.17
2qum4-px4	52.77	0.34	3.59	0.43	1.47	17.87	21.14	0.10	3.59	0.17	101.45	0.90	0.43	0.51	0.06
2qum4-px5	53.64	0.17	2.26	0.36	1.83	18.75	21.61	0.12	2.33	0.16	101.23	0.93	0.44	0.53	0.04
2qum4-px6	52.03	0.32	3.52	0.32	2.28	18.07	20.69	0.12	2.97	0.15	100.47	0.92	0.43	0.52	0.05
2qum4-px7	52.35	0.31	3.96	0.51	1.66	18.46	19.93	0.13	3.60	0.15	101.06	0.90	0.41	0.53	0.06
2qum4-px8	52.82	0.32	2.77	0.04	1.90	18.53	18.53	0.20	5.69	0.17	100.96	0.85	0.38	0.53	0.09
2qum4-px10	52.54	0.33	3.73	0.12	1.67	18.59	19.50	0.16	4.19	0.14	100.96	0.89	0.40	0.53	0.07
2qum12-px1	50.83	1.02	3.01	0.04	2.09	14.87	19.48	0.25	8.51	0.32	100.41	0.76	0.42	0.44	0.14
2qum12-px2	52.74	0.43	2.46	0.38	1.35	17.47	19.77	0.19	5.68	0.24	100.71	0.85	0.41	0.50	0.09
2qum12-px3	49.72	1.04	3.12	0.00	2.46	13.95	18.21	0.27	10.49	0.31	99.55	0.70	0.40	0.42	0.18
2qum12-px4	52.35	0.44	2.45	0.27	1.42	16.96	20.59	0.16	5.14	0.24	99.99	0.85	0.43	0.49	0.08
2qum12-px5	51.72	0.65	2.02	0.00	1.67	16.00	16.36	0.34	11.49	0.24	100.49	0.71	0.34	0.47	0.19
2qum12-px6	52.98	0.45	2.47	0.33	1.11	17.34	19.92	0.16	6.06	0.24	101.05	0.84	0.41	0.49	0.10

Tab. C.4: Pyroxènes - mélange ophiolitique (suite)

		SiO_2	TiO_2	Al_2O_3	Cr_2O_3	Fe_2O_3	MgO	CaO	MnO	FeO	Na_2O	Total	Mg#	Wo	En	Fs
	2qum12-px7	54.00	0.42	2.42	0.25	0.00	16.99	20.37	0.17	6.43	0.21	101.26	0.83	0.42	0.48	0.10
	2qum12-px8	52.82	0.39	2.49	0.38	0.96	17.32	19.82	0.18	5.94	0.24	100.55	0.84	0.41	0.50	0.10
	2qum15-px2	52.99	0.38	1.09	0.15	1.31	15.40	21.75	0.22	6.89	0.27	100.45	0.80	0.45	0.44	0.11
	2qum15-px3	52.50	0.48	1.50	0.17	1.13	15.01	21.77	0.19	6.85	0.33	99.93	0.80	0.45	0.44	0.11
	2qum15-px4	53.12	0.36	1.30	0.04	0.56	15.16	22.27	0.19	6.90	0.26	100.16	0.80	0.46	0.43	0.11
	2qum15-px6	53.93	0.19	0.61	0.05	0.18	15.18	22.73	0.23	7.63	0.13	100.84	0.78	0.46	0.42	0.12
	2qum15-px16	52.72	0.37	2.87	0.05	0.00	20.11	2.86	0.44	18.35	0.28	98.06	0.66	0.06	0.62	0.32
	2qum15a-px1	52.08	0.49	1.74	0.06	1.35	14.45	20.95	0.23	8.48	0.30	100.12	0.75	0.44	0.42	0.14
	2qum15a-px2	52.91	0.42	1.26	0.18	0.97	15.15	22.46	0.21	6.30	0.29	100.15	0.81	0.46	0.44	0.10
	2qum15a-px3	52.91	0.40	1.35	0.10	1.39	15.36	21.68	0.24	6.93	0.28	100.64	0.80	0.45	0.44	0.11
	bei4-px11	53.29	0.35	3.49	0.91		14.94	23.14	0.14	3.64	0.39	102.54	0.88	0.49	0.44	0.06
	2lus4-px17	53.11	0.42	2.46	0.06		17.71	20.50	0.17	5.91	0.27	100.70				
	2bag8-px3	52.95	0.32	1.40	0.34	1.86	16.11	24.14	0.13	3.16	0.14	100.54	0.90	0.49	0.46	0.05
	2bag8-px5	53.30	0.25	0.93	0.29	0.92	15.67	24.40	0.13	3.71	0.20	99.80	0.88	0.50	0.44	0.06
	2bag8-px6	52.79	0.36	2.07	0.31	1.40	15.94	23.32	0.14	3.93	0.23	100.49	0.88	0.48	0.46	0.06
	2daz2-px3	51.40	0.45	1.67	0.00	2.41	13.92	19.33	0.40	10.71	0.26	100.53	0.70	0.41	0.41	0.18
	2daz2-px7	51.08	0.47	3.33	0.36	3.12	16.92	20.90	0.16	3.51	0.19	100.03	0.90	0.44	0.50	0.06
	2daz2-px8	51.04	0.48	3.21	0.09	3.02	16.83	20.84	0.16	3.63	0.21	99.50	0.89	0.44	0.50	0.06
	2daz8-px2	52.41	0.28	2.43	0.07	1.11	12.52	22.52	0.37	8.17	0.69	100.56	0.73	0.49	0.38	0.14
	2daz8-px3	51.50	0.36	2.63	0.08	2.35	12.14	22.26	0.35	8.68	0.59	100.94	0.71	0.48	0.37	0.15
	2daz8-px4	50.54	0.45	3.47	0.02	2.39	11.60	21.29	0.33	9.29	0.70	100.06	0.69	0.48	0.36	0.16
	2daz8-px5	51.55	0.33	2.34	0.08	2.14	12.25	22.65	0.34	8.41	0.50	100.59	0.72	0.49	0.37	0.14
	2daz8-px7	51.89	0.27	2.17	0.08	2.74	12.56	22.06	0.37	8.39	0.62	101.14	0.73	0.48	0.38	0.14
	2lha4-px1	52.40	0.57	2.37	0.13	2.29	16.52	21.31	0.19	5.22	0.22	101.21	0.85	0.44	0.48	0.08
	2lha4-px2	52.11	0.60	2.46	0.24	1.97	16.45	21.18	0.18	5.15	0.23	100.55	0.85	0.44	0.48	0.08
	2lha4-px3	52.32	0.57	2.25	0.14	1.88	16.69	20.80	0.18	5.45	0.23	100.50	0.85	0.43	0.48	0.09
	2lha4-px4	52.02	0.50	2.18	0.05	2.45	16.57	20.95	0.15	5.05	0.23	100.17	0.85	0.44	0.48	0.08
	2lha4-px5	52.51	0.48	1.94	0.21	1.84	16.72	21.14	0.13	5.17	0.22	100.37	0.85	0.44	0.48	0.08
Diabase	lha17-px1	52.60	0.32	1.38	0.04	0.66	14.29	21.26	0.20	8.79	0.32	99.86	0.74	0.44	0.41	0.14
	lha17-px2	51.94	0.37	1.77	0.08	0.94	13.88	21.45	0.22	8.57	0.31	99.52	0.74	0.45	0.41	0.14
	lha17-px3	52.44	0.33	1.40	0.06	1.12	14.32	20.75	0.26	9.17	0.31	100.17	0.74	0.43	0.42	0.15
	lha17-px4	52.45	0.34	1.45	0.00	0.87	14.14	21.51	0.26	8.61	0.29	99.94	0.75	0.45	0.41	0.14
	lha17-px5	52.64	0.33	1.40	0.06	0.70	14.19	21.54	0.23	8.78	0.29	100.16	0.74	0.45	0.41	0.14
	lha17-px6	50.95	0.42	3.00	0.97	1.30	13.34	21.51	0.18	7.85	0.41	99.96	0.75	0.47	0.40	0.13
	lha17-px7	51.81	0.30	2.19	0.55	0.99	13.89	21.49	0.20	8.00	0.36	99.84	0.76	0.46	0.41	0.13
	lha17-px8	52.55	0.26	1.29	0.05	1.21	14.44	21.16	0.25	8.50	0.32	100.02	0.75	0.44	0.42	0.14

Tab. C.4: Pyroxènes - mélange ophiolitique (suite)

		SiO_2	TiO_2	Al_2O_3	Cr_2O_3	Fe_2O_3	MgO	CaO	MnO	FeO	Na_2O	Total	Mg#	Wo	En	Fs
	lha17-px9	52.34	0.21	1.80	0.64	0.43	14.48	21.46	0.21	7.78	0.31	99.67	0.77	0.45	0.42	0.13
	lha17-px10	52.53	0.28	1.25	0.03	0.89	14.42	21.26	0.25	8.58	0.28	99.77	0.75	0.44	0.42	0.14
	lha17-px11	50.78	0.28	2.28	0.05	1.65	14.26	19.61	0.22	8.82	0.30	98.25	0.74	0.42	0.43	0.15
	lha17-px26	52.95	0.15	0.73	0.04		14.26	21.83	0.23	9.16	0.20	99.65	0.74	0.45	0.41	0.15
	2liu4-px1	52.26	0.51	2.28	0.15	2.33	17.27	19.92	0.19	5.33	0.24	100.48	0.85	0.41	0.50	0.09
	2liu4-px2	52.75	0.46	2.40	0.41	1.31	17.26	20.90	0.15	4.84	0.21	100.68	0.86	0.43	0.49	0.08
	2liu4-px3	51.35	0.65	2.45	0.00	2.84	16.38	17.63	0.31	8.57	0.29	100.46	0.77	0.37	0.48	0.14
	2liu4-px4	52.21	0.53	2.31	0.07	2.20	17.02	20.14	0.20	5.47	0.24	100.38	0.85	0.42	0.49	0.09
	2liu4-px5	52.37	0.46	2.07	0.27	2.19	17.36	20.50	0.18	4.55	0.23	100.18	0.87	0.43	0.50	0.07
	2liu4-px6	51.74	0.55	2.01	0.15	2.27	16.58	20.29	0.24	5.54	0.23	99.59	0.84	0.43	0.48	0.09
	2liu4-px7	52.68	0.31	1.98	0.55	1.88	18.11	20.19	0.16	3.83	0.24	99.94	0.89	0.42	0.52	0.06
	2liu4-px12	51.23	0.57	3.23	0.72	2.87	16.66	20.61	0.14	4.23	0.28	100.53	0.88	0.44	0.49	0.07
	2qum2-px1	53.07	0.48	2.12	0.10	1.74	17.65	20.27	0.19	5.19	0.23	101.04	0.86	0.41	0.50	0.08
	2qum2-px4	52.84	0.43	2.51	0.36	2.11	17.93	21.16	0.14	3.30	0.23	101.01	0.91	0.43	0.51	0.05
	2qum2-px5	53.41	0.33	2.03	0.23	1.55	17.81	21.13	0.14	4.18	0.22	101.02	0.88	0.43	0.50	0.07
	2qum2-px6	53.35	0.45	1.62	0.03	1.93	17.56	19.82	0.21	6.33	0.21	101.51	0.83	0.40	0.50	0.10
	2qum2-px8	53.14	0.36	2.41	0.43	1.83	17.64	21.56	0.15	3.59	0.23	101.34	0.90	0.44	0.50	0.06
	2qum2-px9	52.16	0.48	3.90	0.32	2.02	17.25	20.72	0.13	4.25	0.24	101.48	0.88	0.43	0.50	0.07
	2qum2-px10	53.72	0.26	1.89	0.15	1.65	19.04	19.98	0.13	4.01	0.17	101.01	0.89	0.40	0.53	0.06
	2qum2-px11	52.75	0.38	2.45	0.40	2.48	17.79	21.35	0.14	3.07	0.24	101.05	0.91	0.44	0.51	0.05
	2qum2-px12	52.29	0.22	3.13	1.08	1.88	18.17	21.32	0.08	2.13	0.17	100.47	0.94	0.44	0.52	0.03
	2qum2-px13	51.67	0.58	2.62	0.00	2.75	16.27	20.48	0.18	5.60	0.28	100.43	0.84	0.43	0.48	0.09
	2qum8-px1	51.82	0.58	3.38	1.12	2.31	16.65	21.52	0.13	3.48	0.35	101.34	0.90	0.45	0.49	0.06
	2qum8-px2	52.59	0.51	2.74	0.61	2.53	17.26	21.36	0.11	3.55	0.33	101.59	0.90	0.44	0.50	0.06
	2qum8-px3	52.43	0.50	2.46	0.47	2.75	17.26	21.73	0.10	3.04	0.30	101.05	0.91	0.45	0.50	0.05
	2qum8-px4	51.84	0.59	3.50	0.17	2.76	17.09	20.10	0.20	4.73	0.30	101.28	0.87	0.42	0.50	0.08
	2qum8-px8	52.77	0.49	2.28	0.31	2.11	17.29	21.26	0.14	4.03	0.28	100.96	0.88	0.44	0.50	0.06
	2qum8-px9	53.10	0.46	2.36	0.27	1.69	17.23	21.44	0.16	4.37	0.26	101.32	0.88	0.44	0.49	0.07
	2qum8-px11	52.21	0.55	2.59	0.01	2.83	17.01	20.61	0.17	4.71	0.28	100.98	0.87	0.43	0.49	0.08
	2qum8-px12	52.48	0.49	2.57	0.02	1.88	17.19	20.28	0.15	5.33	0.24	100.61	0.85	0.42	0.49	0.09
Basalte	zed1-px3	47.64	0.83	7.12	0.00	3.68	12.15	22.86	0.15	5.14	0.32	99.88	0.81	0.52	0.39	0.09
	zed1-px10	52.33	0.15	1.46	0.00	1.48	13.67	22.59	0.65	6.67	0.45	99.43	0.78	0.48	0.41	0.11
	zed1-px11	51.35	0.31	2.16	0.00	2.66	13.59	22.43	0.64	5.81	0.49	99.44	0.81	0.49	0.41	0.10

Tab. C.5: Composition chimique (% poids) des pyroxènes des roches mafiques du mélange de Yamdrock.

		SiO_2	TiO_2	Al_2O_3	Cr_2O_3	Fe_2O_3	MgO	CaO	MnO	FeO	Na_2O	Total	Mg#	Wo	En	Fs
Gabbro	2bag3-px8	51.77	1.22	2.31	0.06	2.22	15.35	20.90	0.27	7.00	0.34	101.45	0.80	0.44	0.45	0.11
	2bag3-px9	50.82	1.25	2.48	0.01	2.82	15.26	20.65	0.24	6.39	0.35	100.26	0.81	0.44	0.45	0.11
	2bag3-px10	48.69	2.04	3.92	0.00	3.14	14.05	20.41	0.26	6.99	0.35	99.83	0.78	0.45	0.43	0.12
	2bag3-px11	51.33	1.18	2.32	0.00	2.55	15.06	20.98	0.23	6.90	0.34	100.89	0.80	0.44	0.44	0.11
	2bag3-px12	51.01	1.18	2.39	0.00	2.63	15.33	20.72	0.25	6.36	0.34	100.21	0.81	0.44	0.45	0.11
	2bag4-px1	51.54	1.00	2.19	0.09	1.82	16.34	19.00	0.22	7.70	0.25	100.13	0.79	0.40	0.48	0.13
	2bag4-px2	51.09	1.18	2.56	0.08	1.95	16.34	18.49	0.21	7.82	0.28	100.00	0.79	0.39	0.48	0.13
	2bag4-px3	50.42	1.23	2.75	0.11	2.84	16.10	18.38	0.26	7.53	0.29	99.91	0.79	0.39	0.48	0.13
	2bag4-px5	51.50	1.06	2.50	0.10	1.38	16.21	18.53	0.20	8.40	0.28	100.15	0.77	0.39	0.47	0.14
	2bag4-px4	51.79	0.98	1.87	0.12	1.38	16.54	17.53	0.28	9.54	0.23	100.25	0.76	0.37	0.48	0.16
	2mam2-px1	48.57	2.13	5.27	0.12	3.28	13.40	21.30	0.19	6.54	0.45	101.25	0.79	0.47	0.41	0.11
	2mam2-px2	48.77	2.15	4.24	0.07	3.50	12.85	21.47	0.23	7.21	0.52	101.02	0.76	0.48	0.40	0.12
	2mam2-px3	48.41	2.10	3.53	0.00	3.84	12.03	20.50	0.32	9.17	0.55	100.46	0.70	0.46	0.38	0.16
	2mam2-px4	48.39	1.93	4.21	0.12	4.09	13.17	21.04	0.25	6.52	0.52	100.25	0.78	0.47	0.41	0.11
	2mam2-px5	47.98	2.19	3.94	0.06	4.93	13.05	21.25	0.24	6.27	0.50	100.41	0.79	0.48	0.41	0.11
	2mam5-px6	49.49	1.38	2.90	0.00	3.68	14.36	19.89	0.25	7.50	0.34	99.78	0.77	0.44	0.44	0.13
	2mam5-px7	51.83	1.15	1.99	0.00	1.23	15.23	19.67	0.26	9.35	0.23	100.93	0.74	0.41	0.44	0.15
	2mam5-px8	51.67	0.98	1.85	0.04	1.84	16.31	18.78	0.26	8.13	0.24	100.13	0.78	0.39	0.47	0.13
	2bag1-px1	50.88	1.21	2.50	0.01	2.45	15.18	20.63	0.21	6.74	0.32	100.13	0.80	0.44	0.45	0.11
	2bag1-px5	48.94	1.87	3.58	0.00	3.49	14.63	19.21	0.28	7.48	0.38	99.84	0.78	0.42	0.45	0.13
	2bag1-px6	50.85	1.25	2.37	0.00	2.42	14.83	20.52	0.28	7.54	0.30	100.36	0.78	0.44	0.44	0.12
	2bag1-px8	50.47	1.71	3.51	0.00	3.00	14.84	20.56	0.23	7.28	0.34	101.93	0.78	0.44	0.44	0.12
	bag4-px6	50.82	1.46	3.16	0.10		14.79	18.24	0.21	10.48	0.36	101.92	0.72	0.39	0.44	0.17
	bag4-px7	52.55	1.21	2.43	0.06		15.00	18.91	0.24	10.15	0.30	103.16	0.72	0.40	0.44	0.17
	bag4-px8	51.77	1.50	2.95	0.12		14.74	19.47	0.20	9.63	0.30	102.90	0.73	0.41	0.43	0.16
	bag4-px11	51.75	1.34	2.76	0.00		14.80	18.63	0.21	10.81	0.31	102.93	0.71	0.39	0.43	0.18
Diabase	bag3-px16	51.23	1.22	2.66	0.12	0.80	15.84	18.74	0.21	8.59	0.28	99.72	0.77	0.39	0.46	0.14
	bag3-px17	51.48	1.13	2.57	0.11	1.00	15.99	18.77	0.20	8.48	0.28	100.02	0.77	0.39	0.47	0.14
	bag3-px18	52.01	0.90	2.18	0.01	0.63	16.54	17.75	0.22	9.32	0.26	99.85	0.76	0.37	0.48	0.15
Basalte	lha1-px1	50.98	1.19	2.94	0.33	0.97	15.65	19.26	0.16	7.72	0.34	99.54	0.78	0.41	0.46	0.13
	lha1-px2	51.17	0.74	3.83	1.28	0.98	16.48	20.97	0.07	4.31	0.26	100.13	0.87	0.44	0.49	0.07
	lha1-px3	51.03	0.77	3.60	0.98	0.92	16.55	20.87	0.06	3.97	0.30	99.14	0.88	0.44	0.49	0.07
	lha1-px5	50.28	1.34	3.47	0.44	1.44	15.48	19.19	0.15	7.46	0.32	99.60	0.79	0.41	0.46	0.13

Tab. C.5: Pyroxènes - mélange de Yamdrock (suite)

	SiO_2	TiO_2	Al_2O_3	Cr_2O_3	Fe_2O_3	MgO	CaO	MnO	FeO	Na_2O	Total	Mg#	Wo	En	Fs
lha1-px6	51.22	1.05	2.63	0.18	0.59	15.84	19.42	0.16	7.54	0.30	98.93	0.79	0.41	0.47	0.12
lha1-px25	49.65	1.62	3.69	0.16	1.71	15.05	19.08	0.20	7.89	0.31	99.38	0.77	0.41	0.45	0.13
lha1-px26	50.61	1.24	3.00	0.36	1.56	15.40	19.65	0.17	7.14	0.35	99.55	0.79	0.42	0.46	0.12
lha1-px27	51.56	1.06	2.05	0.25	0.50	16.12	18.09	0.19	9.31	0.26	99.38	0.76	0.38	0.47	0.15
lha1-px29	50.41	0.70	5.13	0.68	0.00	13.37	20.19	0.21	6.18	0.36	97.24	0.79	0.46	0.43	0.11
lha1-px30	50.61	1.32	2.88	0.33	1.31	15.55	19.03	0.21	8.13	0.27	99.63	0.77	0.40	0.46	0.13
lha5-px7	50.71	0.95	2.88	0.39	1.34	16.05	19.73	0.14	6.19	0.27	98.67	0.82	0.42	0.48	0.10
lha5-px8	50.97	1.10	3.16	0.46	1.16	16.01	19.82	0.13	6.51	0.29	99.62	0.81	0.42	0.47	0.11
lha5-px9	51.14	0.97	2.67	0.26	0.64	15.33	19.28	0.23	7.91	0.40	98.82	0.78	0.41	0.46	0.13
lha5-px23	51.33	1.03	2.66	0.19	0.58	15.80	19.66	0.17	7.51	0.27	99.22	0.79	0.41	0.46	0.12
lha5-px31	51.30	0.98	2.82	0.43	0.95	16.14	19.84	0.13	6.66	0.27	99.51	0.81	0.42	0.47	0.11
lha5-px32	51.71	0.91	2.36	0.40	0.35	16.32	19.66	0.17	7.05	0.24	99.19	0.80	0.41	0.47	0.11
lha5-px33	51.03	0.95	2.58	0.27	1.74	15.60	19.47	0.22	7.42	0.31	99.63	0.79	0.41	0.46	0.12
lha5-px35	51.83	0.80	2.09	0.16	0.37	16.76	18.40	0.19	7.98	0.23	98.83	0.79	0.38	0.49	0.13
2xia1-px1	48.92	1.88	3.87	0.04	3.27	14.19	20.31	0.20	6.84	0.40	99.90	0.79	0.45	0.43	0.12
2xia1-px2	48.04	2.10	4.53	0.11	4.11	14.05	20.11	0.20	6.61	0.37	100.22	0.79	0.45	0.44	0.12
2xia1-px3	48.26	2.09	4.80	0.18	3.63	13.84	20.26	0.25	6.31	0.52	100.13	0.80	0.46	0.43	0.11
2xia1-px4	47.50	2.33	5.16	0.16	3.78	13.67	20.04	0.19	6.81	0.40	100.02	0.78	0.45	0.43	0.12
2xia1-px5	48.22	1.93	4.54	0.13	3.98	14.22	20.28	0.22	6.02	0.39	99.92	0.81	0.45	0.44	0.10
2xia1-px9	46.89	2.63	5.59	0.02	4.73	13.41	20.54	0.21	6.04	0.42	100.48	0.80	0.47	0.42	0.11
2xia4-px1	51.77	1.20	1.72	0.00	2.02	16.41	17.83	0.27	9.35	0.27	100.85	0.76	0.37	0.48	0.15
2xia4-px2	49.76	2.02	2.91	0.01	1.97	13.17	20.26	0.27	9.82	0.38	100.57	0.70	0.44	0.40	0.17
2xia4-px3	48.98	1.95	3.82	0.00	2.81	13.95	20.03	0.24	8.04	0.33	100.13	0.76	0.44	0.42	0.14
2xia4-px4	46.76	2.93	5.23	0.09	4.60	13.62	18.56	0.27	8.32	0.41	100.77	0.75	0.42	0.43	0.15
2xia4-px7	48.96	2.03	3.87	0.04	3.31	13.45	19.65	0.25	8.43	0.55	100.53	0.74	0.44	0.42	0.15
2xia4-px8	48.53	2.41	3.83	0.01	2.74	13.04	20.16	0.22	9.04	0.40	100.38	0.72	0.44	0.40	0.16
zis8-px9	50.06	1.46	4.41	0.03	1.44	15.36	20.33	0.16	5.93	0.35	99.54	0.82	0.44	0.46	0.10
zis8-px39	50.14	1.29	4.73	0.10	1.11	15.68	19.42	0.19	6.37	0.37	99.38	0.81	0.42	0.47	0.11
zis9-px7	46.99	2.41	6.25	0.12	2.15	12.20	21.50	0.28	5.98	0.60	98.49	0.78	0.50	0.39	0.11
zis9-px8	47.97	2.05	4.34	0.00	2.63	12.46	19.27	0.27	9.68	0.51	99.18	0.70	0.44	0.39	0.17
zis10-px4	50.87	0.98	2.82	0.24	2.20	15.92	20.31	0.15	5.62	0.32	99.49	0.84	0.43	0.47	0.09
zis10-px5	49.94	1.45	3.51	0.20	2.17	15.21	19.66	0.18	6.82	0.37	99.50	0.80	0.43	0.46	0.12
zis10-px6	50.50	1.21	3.33	0.09	1.24	15.30	19.59	0.18	7.23	0.35	99.08	0.79	0.42	0.46	0.12
bag2-px5	48.09	1.89	4.41	0.06	1.61	11.72	19.91	0.40	10.60	0.39	99.07	0.66	0.45	0.37	0.19
bag2-px6	49.16	1.43	3.69	0.00	1.77	11.87	20.41	0.39	10.57	0.39	99.67	0.67	0.45	0.37	0.18
bag2-px8	47.90	2.07	5.98	0.12	2.38	14.22	20.04	0.12	6.20	0.38	99.44	0.80	0.45	0.44	0.11

TAB. C.6: Composition chimique (% poids) des pyroxènes des roches mafiques du flysch triasique.

		SiO_2	TiO_2	Al_2O_3	Cr_2O_3	Fe_2O_3	MgO	CaO	MnO	FeO	Na_2O	Total	Mg#	Wo	En	Fs
Gabbro	zis3-px32	50.40	1.53	3.13	0.05	1.38	15.40	19.13	0.18	8.07	0.31	99.57	0.77	0.41	0.46	0.13
	zis3-px33	49.03	1.59	4.16	0.44	2.14	14.54	19.88	0.15	6.76	0.38	99.09	0.79	0.44	0.45	0.12
	zis3-px34	50.76	1.37	3.10	0.08	1.38	15.85	19.02	0.20	7.57	0.33	99.65	0.79	0.40	0.47	0.13
	zis3-px35	50.53	1.39	3.25	0.23	1.39	15.57	20.05	0.15	6.67	0.30	99.54	0.81	0.43	0.46	0.11
	zis4-px27	51.06	0.90	2.01	0.04		14.56	18.77	0.31	11.06	0.23	99.02	0.70	0.39	0.43	0.18
	zis4-px29	51.06	0.76	1.67	0.03	1.08	14.16	18.34	0.40	11.49	0.24	99.22	0.69	0.39	0.42	0.19
	zis5-px14	51.39	0.83	1.91	0.00	1.04	14.96	19.24	0.26	9.23	0.30	99.16	0.74	0.41	0.44	0.15
	zis5-px15	50.68	1.08	2.43	0.00	2.03	15.42	18.87	0.26	8.22	0.31	99.30	0.77	0.40	0.46	0.14
	zis5-px16	51.80	0.93	2.33	0.09	1.13	16.01	20.45	0.18	6.58	0.27	99.77	0.81	0.43	0.47	0.11
	zis5-px17	50.95	1.01	2.24	0.02	1.57	15.59	18.89	0.22	8.08	0.33	98.91	0.78	0.40	0.46	0.13
	zis5-px18	51.64	1.01	2.58	0.26	0.79	16.49	19.49	0.15	6.88	0.26	99.58	0.81	0.41	0.48	0.11
	zis5-px20	51.01	1.07	2.48	0.00	1.75	15.38	19.10	0.23	8.46	0.30	99.77	0.76	0.41	0.45	0.14
	zis5-px21	51.28	0.98	2.52	0.14	1.31	16.43	19.15	0.15	6.81	0.30	99.07	0.81	0.40	0.48	0.11
	zis6-px12	49.14	1.67	3.92	0.12	1.63	13.48	22.19	0.15	5.66	0.43	98.39	0.81	0.49	0.41	0.10
	2zis5-px4	52.06	0.92	1.93	0.36	1.79	17.04	19.54	0.20	6.31	0.25	100.38	0.83	0.41	0.49	0.10
	2zis5-px5	50.33	1.31	3.17	0.37	2.62	15.63	20.34	0.17	5.90	0.30	100.15	0.82	0.44	0.47	0.10
	2zis5-px6	51.46	1.01	2.29	0.03	2.82	16.55	19.03	0.24	7.01	0.28	100.72	0.81	0.40	0.48	0.12
	2zis5-px7	50.28	1.39	3.57	0.63	2.74	16.00	19.48	0.17	6.29	0.31	100.85	0.82	0.42	0.48	0.11
	2zis5-px8	51.73	1.02	2.12	0.17	1.97	16.49	19.74	0.16	6.60	0.28	100.30	0.82	0.41	0.48	0.11
	2zis5-px10	51.81	1.09	2.07	0.01	2.23	16.46	19.47	0.22	7.06	0.30	100.71	0.81	0.41	0.48	0.12
	2zis5a-px1	50.34	1.25	2.64	0.00	3.69	14.72	19.65	0.32	8.27	0.28	101.17	0.76	0.42	0.44	0.14
	2zis5a-px2	49.99	1.15	2.35	0.00	3.33	14.39	19.80	0.32	8.15	0.29	99.74	0.76	0.43	0.43	0.14
	2zis5a-px15	50.19	1.01	2.01	0.00	3.77	14.59	19.44	0.31	8.36	0.29	99.95	0.76	0.42	0.44	0.14
	2zis5a-px16	49.90	1.29	2.45	0.00	3.05	14.42	19.60	0.30	8.35	0.29	99.66	0.75	0.42	0.43	0.14
	2zis7-px1	51.86	0.94	2.05	0.01	2.16	16.12	19.00	0.22	8.30	0.27	100.94	0.78	0.40	0.47	0.14
	2zis7-px2	50.75	1.20	2.44	0.04	2.35	15.27	19.87	0.21	7.53	0.29	99.95	0.78	0.42	0.45	0.13
	2zis7-px3	51.18	1.03	2.29	0.00	2.49	15.40	19.14	0.29	8.61	0.27	100.70	0.76	0.40	0.45	0.14
	2zis7-px8	52.04	0.87	1.94	0.18	2.16	16.82	19.54	0.22	6.76	0.22	100.75	0.82	0.41	0.49	0.11
	2zis7-px9	51.24	1.05	2.15	0.00	1.93	15.83	19.26	0.22	7.96	0.25	99.88	0.78	0.41	0.46	0.13
	2zis8-px6	51.64	0.62	1.41	0.01	2.01	13.55	18.56	0.41	12.18	0.39	100.77	0.66	0.40	0.40	0.20
	2zis8-px9	51.21	0.64	1.51	0.01	2.01	13.97	18.59	0.41	11.68	0.22	100.24	0.68	0.39	0.41	0.19
	2zis8-px10	50.34	0.88	2.05	0.00	2.73	13.44	20.99	0.38	8.15	0.35	99.30	0.75	0.46	0.41	0.14
	2zis8-px11	51.07	0.91	1.78	0.04	2.20	14.50	19.39	0.31	9.79	0.23	100.21	0.72	0.41	0.43	0.16
	2zis8-px13	51.10	0.60	1.25	0.00	2.35	13.07	18.46	0.47	13.23	0.22	100.74	0.64	0.39	0.39	0.22
	2zis9-px1	51.73	0.80	1.68	0.00	1.17	14.82	19.07	0.34	10.32	0.23	100.15	0.72	0.40	0.43	0.17

Tab. C.6: Pyroxènes - flysch triasique (suite)

		SiO_2	TiO_2	Al_2O_3	Cr_2O_3	Fe_2O_3	MgO	CaO	MnO	FeO	Na_2O	Total	Mg#	Wo	En	Fs
	2zis9-px10	51.70	0.76	1.65	0.01	2.16	14.80	18.95	0.33	10.46	0.22	101.05	0.72	0.40	0.43	0.17
	2zis10-px6	50.62	0.54	1.07	0.00	2.80	12.17	18.37	0.51	14.27	0.21	100.56	0.60	0.40	0.36	0.24
	2zis10-px7	52.70	0.19	0.52	0.00	1.44	13.98	20.85	0.46	10.23	0.19	100.55	0.71	0.43	0.40	0.17
	2zis10-px13	51.44	0.71	1.34	0.02	1.53	13.83	18.65	0.43	12.09	0.23	100.26	0.67	0.39	0.41	0.20
	2zis10-px14	51.30	0.73	1.57	0.07	2.12	14.34	18.76	0.39	10.94	0.23	100.46	0.70	0.40	0.42	0.18
	2zis10-px15	50.62	0.54	1.15	0.00	1.91	12.42	18.53	0.49	13.73	0.20	99.59	0.62	0.40	0.37	0.23
	2zis11-px5	51.27	1.04	2.16	0.00	2.49	15.33	19.03	0.26	9.18	0.23	100.98	0.75	0.40	0.45	0.15
	2zis11-px6	51.56	0.92	1.74	0.00	2.31	15.65	19.28	0.27	8.70	0.20	100.62	0.76	0.40	0.46	0.14
	2zis11-px7	52.36	0.80	1.50	0.08	2.08	16.73	18.35	0.27	8.81	0.20	101.18	0.77	0.38	0.48	0.14
	2zis11-px8	51.32	1.08	1.94	0.02	2.26	15.38	19.59	0.26	8.58	0.21	100.62	0.76	0.41	0.45	0.14
Diabase	2paz1-px1	51.31	1.04	2.13	0.09	2.49	15.61	19.58	0.24	8.11	0.22	100.82	0.77	0.41	0.46	0.13
	2paz1-px2	51.78	0.94	1.91	0.07	2.30	16.03	19.65	0.25	7.73	0.22	100.87	0.79	0.41	0.46	0.13
	2paz1-px4	51.51	0.91	1.92	0.00	2.29	15.37	19.49	0.23	8.75	0.23	100.70	0.76	0.41	0.45	0.14
	2paz1-px5	51.11	0.77	1.87	0.04	3.52	15.21	19.51	0.27	8.40	0.22	100.94	0.76	0.41	0.45	0.14
	2paz1-px23	51.33	0.90	1.96	0.00	2.64	15.44	19.65	0.25	8.20	0.23	100.59	0.77	0.41	0.45	0.13
	2paz1-px24	51.46	0.89	1.95	0.00	2.52	15.40	19.69	0.24	8.46	0.21	100.82	0.76	0.41	0.45	0.14
	2paz1-px28	50.64	1.04	2.04	0.05		15.46	19.30	0.23	10.46	0.24	99.58				
	2paz6-px2	51.24	1.12	2.51	0.24	2.31	16.22	20.28	0.20	5.90	0.28	100.29	0.83	0.43	0.48	0.10
	2paz6-px3	50.33	1.33	3.01	0.25	3.43	16.00	20.33	0.20	5.32	0.28	100.47	0.84	0.43	0.48	0.09
	2paz6-px5	51.41	1.04	2.50	0.27	2.20	16.30	20.31	0.19	5.96	0.25	100.42	0.83	0.43	0.48	0.10
	2paz6-px11	50.80	1.24	2.71	0.12	3.11	15.94	20.34	0.19	5.84	0.29	100.58	0.83	0.43	0.47	0.10
	2paz6-px19	50.83	1.29	3.01	0.34	2.86	15.98	20.78	0.18	5.39	0.27	100.92	0.84	0.44	0.47	0.09
	2paz6-px21	51.19	1.28	2.72	0.16	2.24	15.91	20.27	0.19	6.50	0.29	100.76	0.81	0.43	0.47	0.11
Basalte	2paz7-px1	47.82	2.64	4.49	0.06	4.03	13.53	20.34	0.20	7.68	0.32	101.11	0.76	0.45	0.42	0.13
	2paz7-px2	48.53	2.19	3.85	0.07	3.45	13.99	19.60	0.21	8.21	0.33	100.42	0.75	0.43	0.43	0.14
	2paz7-px3	47.71	2.24	4.11	0.09	3.90	13.06	19.80	0.25	8.35	0.39	99.90	0.74	0.44	0.41	0.15
	2paz7-px4	47.55	2.43	4.39	0.12	3.54	12.98	20.07	0.22	8.34	0.35	100.00	0.74	0.45	0.40	0.15
	2paz7-px10	47.19	2.98	4.81	0.19	4.03	13.12	20.30	0.21	7.76	0.38	100.95	0.75	0.45	0.41	0.14
	2paz7-px11	50.50	1.61	3.10	0.19	2.32	15.21	19.45	0.24	8.13	0.31	101.06	0.77	0.41	0.45	0.14
	2paz7-px12	49.16	1.44	3.48	0.00	3.24	12.89	20.13	0.28	9.62	0.30	100.55	0.71	0.44	0.39	0.16

TAB. C.7: Composition chimique (% poids) des amphiboles des roches mafiques du mélange ophiolitique.

		SiO_2	TiO_2	Al_2O_3	V_2O_3	Cr_2O_3	MgO	CaO	MnO	FeO	Na_2O	K_2O	H_2O	F	Cl	Total	Al^{iv}
Gabbro	lha16-h33	51.08	0.88	5.77		0.43	18.36	15.00	0.07	5.78	0.92					98.53	0.81
	lha16-h7	48.50	1.39	6.20	0.08	0.07	13.15	10.63	0.29	15.84	1.15	0.10	2.00	0.00	0.15	99.54	0.99
	lha16-h8	48.40	1.34	6.20	0.05	0.05	12.95	10.80	0.28	16.35	1.21	0.12	1.99	0.00	0.17	99.91	1.01
	lha16-h9	49.47	1.36	6.12	0.02	0.06	13.17	10.73	0.29	15.74	1.03	0.11	2.02	0.00	0.14	100.25	0.92
	lha16-h10	48.98	1.38	2.49	0.11	0.01	13.38	10.80	0.23	16.22	1.11	0.10	1.91	0.06	0.15	96.92	0.44
	lha16-h11	48.66	1.39	6.67	0.14	0.01	12.77	10.96	0.24	16.13	1.24	0.10	.01	0.00	0.15	100.48	1.00
	lha16-h12	50.06	1.33	6.25	0.15	0.01	13.04	10.85	0.25	15.78	1.06	0.13	2.03	0.00	0.16	101.09	0.87
	lha16-h13	49.04	1.33	5.96	0.02	0.03	13.09	10.63	0.24	16.11	1.05	0.09	1.87	0.27	0.16	99.88	0.94
	lha16-h14	49.55	1.32	6.00	0.06	0.02	13.48	10.85	0.26	15.47	1.10	0.12	2.00	0.04	0.15	100.41	0.91
	lha16-h15	49.77	1.31	5.86	0.03	0.00	13.37	10.84	0.23	15.84	1.07	0.10	2.02	0.00	0.17	100.60	0.89
	lha16-h16	48.85	1.29	6.22	0.12	0.04	13.31	10.58	0.27	15.83	1.22	0.10	1.96	0.09	0.15	100.03	0.98
	lha16-h17	47.99	1.55	6.87	0.05	0.02	12.70	10.90	0.21	16.20	1.26	0.11	1.99	0.00	0.17	100.01	1.06
	lha16-h18	48.85	1.39	6.34	0.03	0.05	13.51	10.64	0.25	15.97	1.21	0.06	2.02	0.00	0.14	100.45	1.03
	lha18-h1	49.33	1.34	6.12	0.00	0.01	14.12	10.89	0.23	14.84	1.36	0.16	2.00	0.00	0.24	100.62	0.97
	lha18-h2	50.10	1.19	5.76	0.07	0.00	14.77	10.75	0.24	13.81	1.25	0.07	2.04	0.00	0.12	100.16	0.89
	lha18-h3	49.14	1.27	6.09	0.01	0.00	14.01	10.97	0.23	14.80	1.10	0.13	2.02	0.00	0.13	99.89	0.96
	lha18-h4	50.57	1.18	5.52	0.08	0.03	14.80	10.90	0.24	13.93	1.27	0.08	1.98	0.17	0.10	100.84	0.85
	lha18-h5	50.72	1.22	6.13	0.00	0.00	13.57	10.85	0.20	15.43	1.17	0.06	1.97	0.20	0.10	101.60	0.85
	lha18-h6	50.84	0.97	5.28	0.00	0.13	15.57	11.20	0.24	12.58	0.98	0.13	2.06	0.00	0.10	100.08	0.80
	lha18-h7	51.55	0.79	4.87	0.18	0.10	15.96	11.25	0.21	12.61	0.95	0.11	2.03	0.09	0.08	100.79	0.75
	lha18-h8	51.93	0.87	4.92	0.10	0.51	15.47	11.16	0.21	13.36	0.94	0.08	2.03	0.11	0.09	101.78	0.76
	lha18-h11	51.25	1.09	5.24	0.05	0.07	14.12	10.90	0.35	14.86	1.09	0.08	1.99	0.17	0.09	101.33	0.76
	lha18-h12	55.89	0.36	2.78	0.02	0.44	18.81	11.71	0.13	8.77	0.51	0.05	2.16	0.00	0.04	101.67	0.37
	lha18-h13	53.87	0.48	5.84	0.03	0.39	16.23	11.28	0.24	11.93	0.54	0.08	2.16	0.00	0.05	103.11	0.69
	lha18-h14	48.79	0.15	8.59	0.00	0.04	17.08	11.50	0.18	9.69	1.83	0.25	2.06	0.04	0.08	100.27	1.16
	lha18-h15	45.34	0.07	12.38	0.05	0.02	15.92	11.30	0.19	10.36	2.40	0.31	2.03	0.06	0.10	100.52	1.63
	lha18-h16	47.31	0.26	9.71	0.04	0.00	17.24	11.19	0.22	9.41	1.93	0.24	1.95	0.25	0.07	99.81	1.36
	2bum9-a2	50.54	0.37	2.95	0.06	0.41	14.67	11.51	0.21	12.97	0.60	0.04	1.95	0.08	0.06	96.40	0.49
	2bum9-a3	53.83	0.07	1.09	0.03	0.00	17.55	11.59	0.31	12.72	0.21	0.01	2.06	0.04	0.01	99.50	0.18
	2bum9-a4	50.16	0.32	3.01	0.00	0.05	16.02	11.59	0.28	13.89	0.78	0.04	2.01	0.00	0.05	98.18	0.51
	2bum9-a5	48.93	0.30	2.91	0.00	0.08	14.55	10.97	0.25	12.71	0.57	0.04	1.90	0.05	0.07	93.31	0.52
	2bum9-a8	49.89	0.33	3.54	0.06	0.24	15.96	11.21	0.26	14.16	0.57	0.03	2.01	0.00	0.05	98.30	0.60
	lha13-h1	46.04	1.83	10.26	0.05	0.01	11.51	9.82	0.25	17.79	1.16	0.03	2.04	0.00	0.03	100.81	1.48
	lha13-h2	50.66	0.43	8.02	0.10	0.00	14.62	11.41	0.19	12.41	0.78	0.10	2.11	0.00	0.01	100.83	0.90
	lha13-h3	47.00	1.25	10.63	0.09	0.01	12.66	11.08	0.21	14.28	1.21	0.14	2.07	0.00	0.03	100.63	1.32

Tab. C.7: Amphiboles - mélange ophiolitique (suite)

	SiO_2	TiO_2	Al_2O_3	V_2O_3	Cr_2O_3	MgO	CaO	MnO	FeO	Na_2O	K_2O	H_2O	F	Cl	Total	Al^{iv}
lha13-h4	49.63	0.45	8.81	0.07	0.00	14.03	11.35	0.16	13.14	0.91	0.11	2.06	0.07	0.02	100.81	1.02
lha13-h5	53.90	0.52	4.27	0.00	0.04	16.18	11.08	0.24	12.59	0.46	0.05	2.12	0.00	0.02	101.47	0.56
lha13-h6	45.61	1.89	11.03	0.10	0.02	12.13	10.98	0.20	14.52	1.24	0.15	2.03	0.02	0.04	99.95	1.44
lha13-a7	50.84	0.60	7.05	0.12	0.00	15.62	10.94	0.20	11.59	0.74	0.14	2.09	0.00	0.02	99.95	0.87
lha13-a8	54.93	0.30	3.11	0.07	0.44	17.98	12.27	0.12	9.34	0.25	0.03	2.08	0.13	0.00	101.05	0.39
lha13-a9	54.50	0.18	3.03	0.07	0.69	17.81	10.85	0.16	10.54	0.29	0.02	2.04	0.17	0.01	100.35	0.48
lha13-a10	49.61	0.45	8.87	0.10	0.07	14.47	11.45	0.18	12.47	0.88	0.12	2.10	0.00	0.02	100.78	1.04
lha13-a11	51.76	0.41	6.68	0.04	0.00	15.43	11.32	0.20	11.90	0.76	0.08	2.11	0.00	0.01	100.69	0.77
2mam7-a2	49.95	0.60	5.37	0.05	0.05	16.32	11.60	0.22	12.83	0.95	0.03	1.97	0.18	0.09	100.19	0.89
2mam7-h3	47.93	1.79	7.36	0.13	0.10	14.09	11.55	0.23	14.03	1.52	0.05	2.02	0.04	0.14	100.97	1.15
2mam7-h4	48.62	1.49	6.49	0.16	0.34	14.75	11.25	0.22	13.92	1.33	0.04	2.03	0.07	0.05	100.75	1.09
2mam7-a5	51.68	0.64	4.38	0.09	0.02	16.25	11.60	0.24	12.38	0.81	0.03	2.04	0.03	0.13	100.31	0.71
2mam7-h7	47.96	1.47	6.54	0.08	0.15	14.17	11.40	0.23	13.33	1.34	0.04	1.99	0.07	0.07	98.81	1.02
2liu6-h7	42.91	3.01	10.73	0.15	0.17	13.89	11.22	0.16	12.63	2.51	0.05	2.01	0.03	0.03	99.49	1.76
2liu6-h11	43.03	3.32	10.71	0.14	0.05	13.99	10.98	0.18	12.60	2.50	0.04	1.93	0.21	0.02	99.69	1.77
2liu6-h12	42.49	3.28	10.54	0.11	0.07	14.26	11.11	0.15	2.28	2.51	0.04	1.95	0.12	0.02	98.94	1.80
2liu6-h14	43.04	3.32	10.86	0.21	0.07	14.03	10.92	0.15	12.89	2.55	0.03	1.96	0.17	0.02	100.22	1.80
2liu6-h15	41.82	3.29	10.72	0.23	0.10	13.83	10.95	0.14	12.95	2.50	0.05	1.96	0.09	0.02	98.64	1.85
2liu6a-a1	53.26	0.41	2.88		0.05	16.50	12.13	0.15	12.09	0.40					97.86	0.46
2liu6a-h5	42.17	3.19	10.83	0.12	0.02	14.01	11.19	0.15	12.18	2.58	0.06	1.97	0.07	0.04	98.57	1.81
2liu6a-h6	42.48	3.32	10.69	0.07	0.02	13.89	11.10	0.16	12.73	2.67	0.04	1.97	0.08	0.03	99.25	1.80
2liu6a-h7	42.51	3.41	10.70	0.22	0.01	13.89	11.14	0.16	12.22	2.65	0.04	1.98	0.06	0.03	99.02	1.77
2liu6a-h8	43.27	3.39	10.75	0.07	0.08	13.84	11.05	0.14	12.74	2.67	0.04	1.97	0.14	0.03	100.18	1.75
2liu6a-h9	43.17	3.46	10.87	0.00	0.03	13.78	11.06	0.15	12.85	2.64	0.04	1.96	0.17	0.02	100.21	1.77
2liu6a-h16	41.60	3.22	10.31	0.23	0.21	13.78	11.21	0.16	12.96	2.46	0.07	1.92	0.13	0.04	98.29	1.80
2liu7-a1	49.81	0.59	5.63	0.06	0.06	13.47	11.21	0.35	16.24	0.71	0.09	1.97	0.15	0.03	100.36	0.87
2liu7-a2	49.88	0.48	4.93	0.03	0.08	14.43	11.10	0.30	15.48	0.59	0.08	2.04	0.00	0.02	99.44	0.83
2liu7-a3	50.60	0.40	3.62	0.06	0.08	15.01	11.23	0.35	14.31	0.43	0.05	2.00	0.04	0.02	98.20	0.62
2liu7-a4	50.54	0.28	5.01	0.03	0.13	15.48	10.94	0.33	14.28	0.43	0.07	1.80	0.55	0.02	99.87	0.83
2liu7-a5	48.42	0.75	6.50	0.08	0.00	13.17	11.16	0.40	16.25	0.88	0.10	1.95	0.15	0.04	99.84	1.02
2liu7-h7	44.40	1.71	9.09	0.04	0.01	10.67	10.92	0.34	19.09	1.29	0.16	1.91	0.13	0.10	99.85	1.48
2liu7-h9	43.69	1.39	8.66	0.03	0.03	10.12	10.68	0.34	19.97	1.27	0.12	1.87	0.10	0.13	98.38	1.47
2liu7-h10	44.22	1.31	8.42	0.13	0.00	10.37	11.09	0.33	19.56	1.14	0.16	1.95	0.00	0.07	98.74	1.41
2liu7-h11	44.05	1.15	8.42	0.15	0.02	10.41	10.93	0.35	19.68	1.18	0.15	1.86	0.16	0.07	98.57	1.43
2liu7-h12	41.66	0.99	9.90	0.06	0.00	11.16	9.00	0.30	21.20	1.00	0.13	1.82	0.19	0.06	97.48	1.71
2liu9-a2	43.84	1.08	8.80	0.08	0.06	10.10	10.82	0.36	19.64	1.31	0.23	1.94	0.00	0.07	98.31	1.44
2liu9-h6	39.02	0.88	11.68	0.14	0.00	11.26	7.51	0.30	23.64	0.76	0.12	1.89	0.00	0.05	97.23	2.03

Tab. C.7: Amphiboles - mélange ophiolitique (suite)

	SiO_2	TiO_2	Al_2O_3	V_2O_3	Cr_2O_3	MgO	CaO	MnO	FeO	Na_2O	K_2O	H_2O	F	Cl	Total	Al^{iv}
2liu9-h8	42.71	1.83	9.17	0.08	0.01	9.69	10.80	0.34	20.43	1.31	0.28	1.93	0.00	0.07	98.64	1.60
2liu9-h9	44.59	1.17	8.71	0.00	0.00	10.35	11.01	0.38	19.89	1.21	0.22	1.95	0.03	0.07	99.58	1.42
2liu9-h11	42.72	1.91	9.24	0.02	0.00	9.71	10.73	0.39	20.20	1.35	0.11	1.92	0.00	0.10	98.40	1.60
2liu9-h12	45.23	1.04	8.96	0.08	0.08	10.12	10.87	0.35	19.67	1.25	0.23	1.95	0.07	0.05	99.95	1.35
2liu9-h13	45.73	1.11	8.23	0.04	0.01	10.69	10.93	0.35	19.23	1.12	0.20	1.97	0.03	0.07	99.67	1.29
jid3-a6	55.48	0.37	1.07	0.08	0.00	17.76	8.83	0.32	12.92	0.64	0.04	2.03	0.15	0.02	99.69	0.17
jid3-a7	54.80	0.68	1.43	0.05	0.03	17.11	9.99	0.26	12.66	0.90	0.07	2.01	0.18	0.03	100.21	0.23
jid3-a8	46.50	2.39	9.62	0.00	0.00	15.10	10.75	0.18	11.65	2.69	0.01	1.87	0.44	0.02	101.22	1.43
jid3-a9	45.65	1.79	9.97	0.00	0.00	14.73	10.88	0.20	12.17	2.93	0.02	1.94	0.24	0.04	100.54	1.48
jid3-a10	49.28	0.11	5.65	0.07	0.02	18.64	7.71	0.18	14.05	0.54	0.10	1.81	0.50	0.03	98.68	0.89
jid3-a11	54.26	0.23	2.33	0.03	0.04	16.59	8.66	0.24	14.48	1.27	0.11	1.81	0.57	0.06	100.68	0.38
jid3-a12	48.12	0.22	7.49	0.06	0.81	16.54	10.58	0.18	10.52	2.70	0.19	1.95	0.15	0.18	99.69	1.15
jid3-a13	56.34	0.03	2.92	0.00	0.02	20.26	9.85	0.16	11.01	0.30	0.02	2.19	0.00	0.01	103.12	0.46
jid3-a14	53.64	0.20	5.34	0.00	0.00	16.90	12.01	0.09	10.22	0.72	0.02	2.14	0.00	0.03	101.29	0.57
jid3-a15	57.14	0.08	1.94	0.00	0.07	19.22	12.38	0.07	8.14	0.19	0.01	2.15	0.06	0.01	101.45	0.18
jid3-a16	58.21	0.00	0.59	0.00	0.06	20.51	12.25	0.09	6.44	0.08	0.00	2.17	0.00	0.01	100.41	0.03
jid3-a17	52.86	0.41	5.14	0.00	0.11	16.79	11.79	0.12	10.52	0.65	0.01	2.01	0.22	0.03	100.66	0.63
jid5-h7	47.41	1.74	4.15	0.15	0.10	12.55	11.07	0.23	15.80	1.61	0.14	1.82	0.26	0.10	97.13	0.74
jid5-h8	46.92	1.77	8.13	0.07	0.05	12.50	10.99	0.23	16.13	1.63	0.11	1.91	0.24	0.10	100.76	1.24
jid5-h9	47.94	1.60	7.90	0.06	0.02	12.48	10.96	0.20	16.15	1.62	0.11	2.01	0.05	0.10	101.20	1.13
jid5-h10	47.43	1.76	7.99	0.08	0.00	12.23	10.99	0.20	15.68	1.73	0.11	2.02	0.00	0.10	100.33	1.13
jid5-h11	47.14	1.86	8.40	0.18	0.09	12.22	10.89	0.20	16.40	1.77	0.12	1.92	0.23	0.09	101.52	1.24
jid5-h12	48.22	1.81	8.25	0.18	0.08	12.29	11.02	0.17	15.61	1.63	0.12	2.05	0.00	0.11	101.54	1.10
jid5-h13	54.14	0.20	2.39	0.01	0.05	15.20	11.52	0.44	13.95	0.28	0.04	2.05	0.06	0.06	100.36	0.34
jid5-h14	47.74	1.80	8.29	0.09	0.10	12.01	11.08	0.19	16.40	1.73	0.12	1.95	0.18	0.12	101.79	1.16
2qum1-a1	53.71	0.30	2.50	0.04	0.03	17.86	12.93	0.14	9.77	0.22	0.02	2.10	0.00	0.02	99.61	0.40
2qum1-a2	50.46	0.31	5.00	0.09	0.72	16.08	11.09	0.18	13.68	0.39	0.02	2.06	0.00	0.04	100.14	0.83
2qum1-a5	52.50	0.49	3.95	0.02	0.04	16.37	11.41	0.17	13.13	0.39	0.03	1.99	0.18	0.09	100.75	0.65
2qum1-a6	51.03	0.93	5.46	0.17	0.00	15.24	12.45	0.22	12.52	0.41	0.01	2.08	0.00	0.05	100.56	0.75
2qum1-a7	53.61	0.39	2.44	0.15	0.02	16.80	12.24	0.18	12.76	0.17	0.00	2.09	0.02	0.03	100.88	0.40
2qum1-a10	55.37	0.05	0.79	0.08	0.00	16.41	12.66	0.17	13.40	0.04	0.00	2.10	0.02	0.01	101.08	0.13
2qum3-h1	53.05	0.39	3.55	0.05	0.47	16.46	12.47	0.19	11.95	0.26	0.02	2.04	0.11	0.06	101.07	0.55
2qum3-h4	54.23	0.29	2.45	0.11	0.06	16.93	12.29	0.25	12.12	0.17	0.01	2.11	0.00	0.03	101.06	0.40
2qum3-h5	52.71	0.37	3.11	0.01	0.25	16.40	12.61	0.19	11.99	0.20	0.02	2.08	0.00	0.03	99.97	0.51
2qum3-h6	52.04	0.30	3.30	0.00	0.56	15.59	12.58	0.24	13.00	0.25	0.01	1.96	0.22	0.06	100.11	0.56
2qum3-a10	54.48	0.25	2.09	0.03	0.29	17.53	12.68	0.18	10.99	0.13	0.01	2.11	0.00	0.03	100.79	0.34
2qum3-a11	53.58	0.29	2.82	0.04	0.45	16.79	12.67	0.16	11.19	0.17	0.01	2.03	0.13	0.04	100.38	0.43

Tab. C.7: Amphiboles - mélange ophiolitique (suite)

	SiO_2	TiO_2	Al_2O_3	V_2O_3	Cr_2O_3	MgO	CaO	MnO	FeO	Na_2O	K_2O	H_2O	F	Cl	Total	Al^{iv}
2qum3-a13	53.57	0.32	2.87	0.03	0.08	16.77	11.75	0.20	12.77	0.26	0.02	2.08	0.05	0.03	100.76	0.47
2qum15-a5	53.28	0.11	2.86	0.00	0.01	15.68	15.22	0.24	10.14	0.26	0.00	2.09	0.00	0.00	99.89	0.36
2qum15-h9	52.18	0.45	2.76	0.00	0.00	16.41	11.77	0.37	12.00	0.41	0.04	2.04	0.03	0.03	98.49	0.47
2qum15-h10	49.30	1.48	5.11	0.06	0.00	16.89	10.91	0.23	11.35	0.94	0.02	1.98	0.11	0.10	98.45	0.86
2qum15-h11	49.65	1.60	5.67	0.10	0.06	16.56	10.72	0.18	11.74	0.95	0.03	2.05	0.00	0.10	99.40	0.94
2qum15-a15	52.05	1.08	4.20	0.04	0.00	17.27	10.39	0.26	11.89	0.68	0.03	2.08	0.00	0.08	100.02	0.69
2qum15-a17	54.37	0.34	1.64	0.00	0.04	20.10	3.30	0.45	17.47	0.28	0.03	2.09	0.00	0.04	100.13	0.24
2qum15-a19	53.75	0.43	1.77	0.05	0.09	20.37	2.55	0.45	18.20	0.26	0.02	2.00	0.17	0.05	100.15	0.30
2qum15-a23	53.49	0.35	2.30	0.04	0.05	19.99	2.74	0.48	18.30	0.22	0.02	2.06	0.04	0.04	100.13	0.36
2qum15-a25	50.35	0.83	4.52	0.12	0.00	17.84	10.57	0.21	11.73	0.51	0.09	2.04	0.02	0.08	98.92	0.75
2qum15-a26	53.10	0.27	2.07	0.01	0.00	19.43	7.13	0.41	14.12	0.18	0.02	2.06	0.03	0.02	98.83	0.35
2qum15-a27	54.43	0.26	1.44	0.01	0.07	20.56	1.97	0.47	18.46	0.24	0.01	2.07	0.04	0.02	100.04	0.22
2qum15a-a6	53.42	0.13	1.09	0.00	0.07	21.63	1.09	0.47	18.44	0.18	0.00	2.05	0.02	0.03	98.61	0.18
2qum15a-a7	52.51	0.21	1.97	0.00	0.06	20.14	4.83	0.41	16.07	0.35	0.03	2.02	0.08	0.04	98.71	0.34
2qum15a-a8	48.67	1.52	5.48	0.07	0.03	16.48	11.09	0.22	11.71	0.96	0.04	2.01	0.02	0.10	98.40	0.92
2qum15a-a9	53.43	0.34	1.43	0.01	0.01	20.42	2.22	0.47	18.83	0.23	0.01	2.05	0.02	0.05	99.51	0.24
2qum15a-a10	52.65	0.27	2.29	0.00	0.00	20.25	1.98	0.50	18.70	0.22	0.01	2.05	0.03	0.03	98.97	0.39
2qum15a-a11	53.40	0.27	1.32	0.06	0.00	20.79	1.92	0.44	18.53	0.17	0.02	2.00	0.13	0.03	99.08	0.22
2qum15a-a15	50.79	0.58	4.20	0.10	0.07	17.64	11.02	0.24	11.14	0.70	0.03	2.04	0.00	0.09	98.63	0.70
2qum15a-h16	49.21	1.39	5.48	0.03	0.05	16.63	11.12	0.21	11.58	0.92	0.03	1.94	0.20	0.10	98.88	0.92
2qum15a-h17	53.10	0.31	1.32	0.00	0.01	20.89	1.54	0.50	19.22	0.17	0.02	2.05	0.03	0.03	99.16	0.22
2qum15a-a18	53.51	0.09	1.24	0.00	0.03	20.40	3.26	0.55	17.58	0.16	0.01	2.06	0.00	0.02	98.90	0.21
2qum15a-a19	53.27	0.08	1.28	0.00	0.03	18.32	9.70	0.32	13.68	0.15	0.00	2.05	0.04	0.01	98.91	0.21
2qum15a-a23	50.90	0.34	1.65	0.08	0.04	20.68	2.51	0.45	18.07	0.18	0.02	1.97	0.08	0.03	97.00	0.29
2qum15a-a26	49.74	0.25	4.45	0.09	0.00	19.99	4.75	0.38	15.84	0.35	0.03	2.03	0.00	0.05	97.93	0.76
bei3-a7	52.82	0.64	4.27	0.09	0.00	14.12	11.21	0.30	14.74	0.63	0.06	2.08	0.00	0.04	101.02	0.53
bei3-a8	54.32	0.55	3.69	0.08	0.16	15.29	11.80	0.24	13.01	0.46	0.04	2.12	0.02	0.02	101.77	0.41
bei3-a9	52.48	0.65	4.13	0.09	0.61	14.71	11.74	0.20	12.52	0.54	0.08	2.01	0.13	0.04	99.94	0.49
bei3-a10	53.75	0.65	3.66	0.15	0.03	15.07	11.81	0.25	13.11	0.43	0.04	2.10	0.02	0.02	101.08	0.34
bei3-a11	54.36	0.39	3.01	0.13	0.21	15.33	11.60	0.27	12.96	0.42	0.04	2.10	0.00	0.02	100.85	0.42
bei4-h6	52.10	0.63	4.77	0.15	0.00	14.03	11.19	0.25	15.10	0.63	0.12	2.07	0.00	0.05	101.09	0.63
bei4-h7	52.41	0.51	5.32	0.10	0.00	14.22	10.99	0.24	15.11	0.77	0.08	2.02	0.16	0.03	101.97	0.68
bei4-h8	50.38	0.68	7.22	0.12	0.01	13.57	11.16	0.19	14.91	0.93	0.16	2.04	0.09	0.05	101.50	0.90
bei4-h9	49.95	0.93	6.43	0.09	0.03	13.24	10.85	0.27	15.32	0.79	0.16	2.00	0.11	0.05	100.20	0.87
bei4-h10	52.82	0.66	4.27	0.07	0.00	14.83	9.23	0.32	16.43	0.58	0.13	2.08	0.00	0.07	101.49	0.69
bei4-a12	54.97	0.37	3.36	0.10	1.15	17.75	12.51	0.08	8.48	0.34	0.03	2.12	0.06	0.01	101.31	0.38
bei4-a13	54.38	0.40	3.50	0.01	1.12	17.66	12.41	0.09	8.56	0.41	0.06	2.13	0.00	0.03	100.76	0.42

Tab. C.7: Amphiboles - mélange ophiolitique (suite)

	SiO_2	TiO_2	Al_2O_3	V_2O_3	Cr_2O_3	MgO	CaO	MnO	FeO	Na_2O	K_2O	H_2O	F	Cl	Total	Al^{iv}
bei4-a14	57.30	0.10	1.53	0.00	0.11	18.73	12.88	0.10	8.32	0.15	0.03	2.17	0.00	0.01	101.44	0.10
bei6-a1	50.22	1.26	5.83	0.15	0.03	13.83	11.52	0.24	14.50	0.98	0.08	1.96	0.22	0.04	100.86	0.83
bei6-a2	54.08	0.59	3.70	0.05	0.00	15.14	11.36	0.30	13.92	0.62	0.04	2.07	0.11	0.03	101.99	0.47
bei6-a3	54.86	0.28	3.29	0.03	0.00	15.92	11.95	0.25	12.54	0.48	0.04	2.10	0.06	0.02	101.81	0.36
bei6-a4	52.38	0.78	4.87	0.00	0.00	14.87	11.80	0.29	12.71	0.81	0.06	2.02	0.15	0.03	100.76	0.58
bei6-a5	54.44	0.34	3.62	0.10	0.00	16.04	11.98	0.26	12.22	0.51	0.04	2.13	0.00	0.01	101.68	0.42
bei6-a6	53.52	0.37	3.68	0.00	0.00	15.29	11.11	0.32	13.90	0.68	0.05	2.03	0.13	0.04	101.11	0.50
bei6-a7	53.91	0.31	3.94	0.04	0.08	15.11	11.44	0.28	13.85	0.58	0.05	2.11	0.00	0.03	101.72	0.48
bei6-h8	44.20	2.70	9.80	0.02	0.00	10.31	11.06	0.27	17.47	1.85	0.18	1.91	0.16	0.08	100.01	1.47
bei6-h9	51.19	0.76	5.73	0.00	0.00	13.94	11.35	0.28	14.94	0.91	0.09	2.08	0.00	0.05	101.31	0.77
bei6-h10	50.83	0.75	6.36	0.10	0.03	13.14	11.49	0.26	15.54	1.11	0.12	2.02	0.13	0.04	101.91	0.80
bei6-h11	50.78	0.83	5.40	0.21	0.02	13.36	11.38	0.24	15.27	0.92	0.10	2.05	0.02	0.05	100.62	0.72
bei8-h1	46.61	2.19	8.95	0.06	0.03	10.94	10.97	0.30	17.46	1.37	0.11	2.03	0.00	0.06	101.07	1.27
bei8-h2	47.71	0.62	8.90	0.07	0.02	11.26	11.28	0.25	16.79	1.18	0.15	1.96	0.14	0.04	100.35	1.09
bei8-h3	45.64	2.48	9.84	0.11	0.01	10.36	10.92	0.23	17.42	1.62	0.08	1.98	0.11	0.04	100.83	1.36
bei8-h4	49.51	0.80	7.40	0.09	0.01	12.73	11.20	0.28	16.15	1.07	0.10	2.02	0.09	0.04	101.47	0.97
bei8-h5	44.39	1.84	10.53	0.14	0.00	10.59	9.90	0.25	18.82	1.28	0.12	1.90	0.21	0.05	100.00	1.58
bei8-h6	49.38	0.84	7.54	0.00	0.04	12.39	11.05	0.27	16.55	1.01	0.11	2.06	0.00	0.04	101.28	0.98
bei8-h7	45.22	2.13	9.56	0.12	0.00	10.78	11.08	0.24	17.71	1.41	0.17	2.01	0.00	0.05	100.47	1.41
bei8-h8	48.97	0.92	7.69	0.04	0.00	12.24	11.19	0.25	16.21	1.09	0.12	2.05	0.00	0.05	100.81	0.98
bei8-h88	47.81	0.71	7.86	0.12	0.03	11.92	11.21	0.25	16.51	1.08	0.11	2.02	0.00	0.03	99.67	1.05
bei8-h9	51.61	0.51	4.87	0.06	0.02	14.42	11.15	0.31	14.74	0.68	0.04	2.07	0.00	0.03	100.51	0.69
bei8-a10	51.31	0.54	6.02	0.09	0.29	13.82	11.33	0.23	14.40	0.76	0.08	2.03	0.11	0.03	101.01	0.74
bei8-a10	50.77	0.60	5.95	0.01	0.34	13.84	11.38	0.26	14.48	0.78	0.07	2.07	0.00	0.03	100.59	0.78
bei8-a11	53.04	0.43	5.02	0.02	0.00	14.42	11.25	0.27	14.31	0.69	0.06	2.09	0.04	0.02	101.65	0.58
bei8-a12	55.74	0.18	2.60	0.05	0.02	16.04	10.95	0.29	13.94	0.33	0.03	2.14	0.00	0.02	102.34	0.35
bei8-a13	52.14	0.48	5.22	0.00	0.04	14.54	11.16	0.29	14.59	0.77	0.05	2.10	0.00	0.02	101.40	0.70
bei8-h18	44.63	1.65	10.77	0.12	0.04	10.81	10.25	0.24	18.82	1.29	0.10	2.02	0.00	0.04	100.76	1.60
bei8-h19	48.55	1.03	7.94	0.11	0.03	12.00	11.07	0.28	16.77	1.19	0.11	2.05	0.00	0.04	101.17	1.05
bei8-h20	41.28	0.64	10.69	0.13	0.01	12.54	6.54	0.23	21.39	0.66	0.06	1.89	0.05	0.02	96.12	1.69
bei12-h1	43.52	3.13	11.07	0.12	0.03	12.39	10.63	0.17	15.02	2.26	0.06	2.03	0.00	0.03	100.45	1.72
bei12-h2	44.89	3.11	11.14	0.03	0.00	12.33	10.77	0.19	15.14	2.12	0.06	2.03	0.07	0.02	101.89	1.63
bei12-h3	45.85	2.59	10.08	0.00	0.04	12.56	10.70	0.21	15.19	1.80	0.04	2.00	0.11	0.04	101.20	1.47
bei12-h4	45.69	2.20	9.34	0.12	0.01	12.25	10.44	0.24	16.11	1.70	0.04	2.03	0.00	0.03	100.16	1.42
bei12-h5	46.41	2.42	9.22	0.11	0.01	12.25	10.30	0.26	16.28	1.73	0.04	1.97	0.14	0.06	101.18	1.38
bei12-h6	45.21	2.90	10.59	0.15	0.01	12.31	10.43	0.21	15.54	2.22	0.07	2.06	0.00	0.03	101.74	1.57
bei12-h7	43.78	3.03	10.96	0.09	0.00	12.03	10.50	0.22	15.71	2.11	0.07	2.03	0.00	0.05	100.56	1.69

Tab. C.7: Amphiboles - mélange ophiolitique (suite)

	SiO_2	TiO_2	Al_2O_3	V_2O_3	Cr_2O_3	MgO	CaO	MnO	FeO	Na_2O	K_2O	H_2O	F	Cl	Total	Al^{iv}
bei12-h8	54.96	0.44	2.77	0.00	0.00	17.43	11.56	0.15	11.35	0.39	0.06	2.11	0.06	0.02	101.27	0.41
bei12-h9	44.93	3.25	10.72	0.05	0.00	13.04	10.38	0.18	14.65	2.63	0.06	2.02	0.11	0.02	102.02	1.64
bei12-h10	46.07	2.57	10.06	0.06	0.01	12.55	10.36	0.22	15.28	1.70	0.05	2.06	0.00	0.03	101.01	1.46
bei12-h11	51.36	0.84	5.53	0.00	0.00	14.18	10.38	0.28	15.25	0.90	0.03	2.08	0.00	0.04	100.86	0.79
bei12-h12	54.92	0.35	3.30	0.07	0.05	16.28	12.06	0.22	10.99	0.32	0.03	2.13	0.00	0.01	100.72	0.30
2day7-a1	49.16	1.00	3.86	0.11	0.00	13.97	9.52	0.41	18.05	0.67	0.13	1.97	0.03	0.08	98.97	0.65
2day7-a2	49.87	0.79	3.10	0.01	0.01	14.86	8.05	0.49	19.05	0.51	0.06	2.00	0.00	0.05	98.83	0.52
2day7-a3	50.58	0.66	4.12	0.01	0.00	13.95	9.95	0.42	17.59	0.61	0.10	2.02	0.03	0.04	100.07	0.69
2day7-a4	49.39	0.56	5.58	0.11	0.00	12.94	11.33	0.30	16.70	0.84	0.09	2.00	0.06	0.05	99.94	0.86
2day7-a9	51.38	0.63	3.83	0.08	0.02	14.53	11.53	0.29	14.86	0.51	0.05	2.02	0.07	0.03	99.81	0.64
2day7-a10	50.99	0.44	3.83	0.08	0.03	14.44	11.45	0.31	15.18	0.49	0.06	2.04	0.00	0.03	99.35	0.65
2day7-a11	52.13	0.35	2.62	0.10	0.14	15.45	11.90	0.27	14.12	0.32	0.04	2.04	0.02	0.03	99.54	0.44
2day7-a16	47.48	0.67	5.72	0.04	0.05	13.66	10.51	0.34	17.59	0.68	0.08	1.99	0.00	0.04	98.85	0.97
2day7-a20	50.68	0.75	4.02	0.03	0.01	13.88	11.36	0.31	15.68	0.59	0.12	2.03	0.00	0.05	99.50	0.68
2day7-a21	51.26	0.43	3.85	0.05	0.00	14.46	11.35	0.30	16.18	0.48	0.07	2.05	0.00	0.04	100.52	0.65
2lus4-a8	51.10	0.52	5.78	0.07	0.49	17.77	12.33	0.12	8.96	0.96	0.01	2.10	0.00	0.05	100.26	0.84
2lus4-a9	49.83	0.67	4.26	0.02	0.00	13.61	9.95	0.29	17.57	1.03	0.18	1.96	0.05	0.15	99.56	0.72
2lus4-a12	52.48	0.40	3.52	0.00	0.01	15.91	12.60	0.20	12.05	0.56	0.03	2.03	0.10	0.03	99.92	0.49
2lus4-a13	50.65	0.37	5.45	0.08	0.56	14.70	11.70	0.22	13.55	1.07	0.05	2.04	0.08	0.02	100.52	0.78
2lus4-a18	55.72	0.12	1.23	0.10	0.13	18.49	13.04	0.15	9.58	0.19	0.02	2.13	0.00	0.01	100.92	0.20
2lus4-a18a	50.57	0.50	5.29	0.06	0.23	14.41	12.13	0.22	13.28	0.92	0.07	2.06	0.00	0.03	99.75	0.71
2lus4-a20	45.55	0.12	10.87	0.09	0.00	13.00	12.03	0.15	13.66	1.76	0.16	1.97	0.11	0.07	99.54	1.37
2lus4-a21	45.07	0.18	11.60	0.06	0.00	13.84	12.35	0.14	13.06	1.89	0.18	2.04	0.00	0.07	100.47	1.53
2lus4-a22	44.19	0.28	12.11	0.02	0.00	14.04	12.36	0.13	12.29	2.08	0.18	2.03	0.00	0.08	99.78	1.62
2lus4-a24	56.50	0.00	2.15	0.00	0.06	20.70	12.50	0.14	5.38	0.30	0.02	2.12	0.10	0.01	99.96	0.23
2lus4-a25	57.66	0.00	0.66	0.02	0.05	22.30	11.95	0.14	4.83	0.17	0.01	2.16	0.03	0.01	99.98	0.11
2bag8-a4	52.51	0.41	3.15	0.02	0.41	20.85	12.39	0.12	5.48	0.57	0.03	2.04	0.12	0.03	98.11	0.52
2bag8-a7	51.38	0.48	3.45	0.00	0.31	17.06	16.26	0.18	7.82	0.65	0.02	2.08	0.00	0.04	99.72	0.58
2bag8-a8	45.60	1.65	8.27	0.00	0.42	15.66	11.02	0.19	11.75	1.56	0.05	2.01	0.02	0.05	98.24	1.40
2bag8-a9	45.44	1.63	8.51	0.02	0.25	15.34	11.01	0.20	12.10	1.58	0.06	2.01	0.00	0.05	98.21	1.44
2bag8-h11	45.25	1.59	8.70	0.09	0.49	15.19	11.22	0.20	11.55	1.51	0.07	2.00	0.00	0.08	97.92	1.43
2bag8-h12	45.62	1.55	8.44	0.11	0.57	15.37	11.17	0.19	12.28	1.54	0.05	2.01	0.04	0.05	98.98	1.43
2bag8-h13	49.42	0.93	5.03	0.00	0.34	17.12	11.40	0.17	11.14	0.91	0.04	2.03	0.04	0.05	98.61	0.84
2daz2-a4	53.43	0.07	0.64	0.06	0.01	15.65	12.31	0.15	14.29	0.10	0.01	2.02	0.04	0.00	98.80	0.11
2daz2-h5	42.09	2.08	10.26	0.00	0.01	9.53	9.82	0.34	20.58	2.23	0.04	1.91	0.06	0.05	99.00	1.74
2daz2-h9	41.45	1.96	10.49	0.04	0.00	10.30	9.49	0.32	20.12	2.10	0.04	1.93	0.01	0.05	98.30	1.83
2daz2-h10	41.52	2.34	10.27	0.02	0.05	10.00	10.02	0.30	20.50	2.25	0.04	1.92	0.05	0.04	99.31	1.79

Tab. C.7: Amphiboles - mélange ophiolitique (suite)

		SiO_2	TiO_2	Al_2O_3	V_2O_3	Cr_2O_3	MgO	CaO	MnO	FeO	Na_2O	K_2O	H_2O	F	Cl	Total	Al^{iv}
	2daz2-a11	44.23	0.25	8.01	0.35	0.09	10.60	11.54	0.23	19.30	0.88	0.20	1.92	0.03	0.02	97.64	1.32
	2daz2-a15	47.67	0.28	5.11	0.11	0.24	12.80	11.28	0.30	16.81	0.83	0.11	1.98	0.00	0.00	97.51	0.90
	2daz2-a16	49.26	0.39	4.78	0.15	0.00	13.37	11.62	0.24	16.57	0.60	0.08	2.02	0.00	0.00	99.07	0.82
	2daz2-h17	42.48	1.60	9.87	0.00	0.00	9.44	9.86	0.40	21.57	1.57	0.04	1.91	0.05	0.06	98.85	1.71
	2daz2-h18	40.47	2.22	10.00	0.00	0.03	9.53	9.81	0.29	20.71	2.21	0.05	1.86	0.08	0.06	97.30	1.79
	2daz2-a18	46.09	0.32	6.23	0.19	0.00	11.80	11.10	0.32	18.59	0.85	0.15	1.95	0.00	0.01	97.60	1.10
	2daz2-a19	50.32	0.14	3.30	0.07	0.07	14.06	11.88	0.26	15.50	0.47	0.08	1.96	0.10	0.02	98.23	0.57
	2daz7-h1	52.87	0.08	3.03	0.09	0.01	14.72	12.69	0.28	13.94	0.35	0.04	2.07	0.00	0.00	100.16	0.39
	2daz7-h2	45.84	1.11	9.39	0.12	0.08	11.67	11.81	0.30	16.08	1.45	0.06	2.03	0.00	0.00	99.93	1.30
	2daz7-a3	52.62	0.11	3.13	0.00	0.09	14.72	12.51	0.29	14.09	0.38	0.02	2.07	0.00	0.01	100.02	0.44
	2daz7-h4	44.96	1.49	10.75	0.07	0.10	11.36	11.55	0.27	15.40	1.67	0.07	2.01	0.04	0.00	99.72	1.42
	2daz7-a5	51.23	0.05	4.84	0.10	0.02	13.98	12.47	0.24	14.35	0.53	0.10	2.00	0.13	0.00	100.04	0.60
	2daz7-a6	44.57	1.37	10.69	0.15	0.09	11.81	11.15	0.29	15.96	1.43	0.06	2.02	0.00	0.01	99.59	1.52
	2daz7-h8	45.79	1.35	10.44	0.11	0.00	11.63	11.59	0.26	15.43	1.52	0.07	2.04	0.00	0.02	100.24	1.35
	2daz7-h9	45.14	1.35	10.42	0.03	0.00	11.82	11.53	0.25	15.47	1.78	0.06	1.98	0.09	0.01	99.92	1.42
	2daz8-h1	44.98	1.81	10.44	0.15	0.05	11.66	11.18	0.24	15.43	1.96	0.07	2.02	0.01	0.01	99.99	1.44
	2daz8-h11	43.94	1.99	10.42	0.05	0.00	11.69	10.86	0.31	16.87	2.22	0.05	2.02	0.00	0.00	100.43	1.62
	2daz8-h12	44.20	2.15	10.59	0.08	0.08	11.30	10.94	0.29	16.61	2.16	0.07	2.02	0.00	0.01	100.49	1.57
	2daz8-h13	44.13	2.12	10.77	0.00	0.10	11.28	10.94	0.31	16.28	2.13	0.07	2.02	0.00	0.02	100.17	1.57
	2daz8-h14	45.38	1.69	9.99	0.09	0.08	11.80	10.91	0.30	16.34	1.95	0.06	1.95	0.18	0.01	100.74	1.44
	2daz8-h18	44.86	2.08	10.59	0.06	0.00	11.77	10.97	0.27	16.40	2.03	0.06	2.01	0.07	0.00	101.17	1.55
	2lha6-a1	50.59	0.30	4.24	0.10	0.04	13.52	11.23	0.29	17.05	0.39	0.04	2.03	0.00	0.03	99.85	0.72
	2lha6-a2	51.36	0.22	3.65	0.08	0.05	14.22	11.18	0.31	16.20	0.41	0.04	2.03	0.04	0.02	99.81	0.62
	2lha6-a3	53.72	0.38	2.06	0.08	0.04	17.31	10.86	0.25	13.13	0.28	0.05	2.08	0.00	0.07	100.32	0.34
	2lha6-a4	53.20	0.03	0.62	0.02	0.00	13.63	11.72	0.56	16.25	0.63	0.04	2.01	0.02	0.00	98.73	0.11
	2lha6-a5	50.95	0.14	3.34	0.00	0.02	14.34	11.76	0.24	16.03	0.34	0.07	2.02	0.01	0.03	99.29	0.57
	2lha6-a6	53.84	0.23	1.90	0.02	0.01	17.17	12.04	0.32	12.16	0.18	0.03	2.09	0.00	0.02	100.01	0.32
	2lha6-a10	48.27	1.47	6.06	0.02	0.08	16.24	11.33	0.17	12.17	1.32	0.04	1.98	0.10	0.12	99.36	1.02
Diabase	lha17-h12	49.24	1.73	7.20	0.12	0.06	14.36	11.08	0.19	14.26	1.41	0.08	2.08	0.00	0.07	101.87	1.08
	lha17-h13	47.33	1.69	7.27	0.15	0.03	14.27	10.92	0.17	14.40	1.15	0.06	1.99	0.07	0.08	99.59	1.21
	lha17-h14	52.49	0.41	4.75	0.06	0.00	16.20	11.16	0.20	12.97	0.71	0.04	1.94	0.33	0.05	101.30	0.71
	lha17-h15	49.42	0.72	6.73	0.08	0.00	15.68	9.83	0.19	13.84	0.65	0.03	2.00	0.11	0.05	99.33	1.06
	2bum3-a1	39.17	2.99	12.66	0.07	0.00	14.14	11.80	0.10	11.83	2.29	1.13	1.80	0.38	0.02	98.36	2.17
	2bum3-a2	40.99	2.93	12.32	0.07	0.14	13.74	11.88	0.12	11.95	2.38	1.07	1.80	0.44	0.03	99.86	1.97
	2bum3-a3	40.02	3.04	12.12	0.00	0.04	14.29	11.79	0.08	11.73	2.34	1.12	1.81	0.37	0.02	98.76	2.07
	2bum3-a4	40.60	2.76	12.15	0.08	0.07	13.81	11.25	0.04	10.98	2.20	1.17	1.78	0.41	0.01	97.31	1.92

Tab. C.7: Amphiboles - mélange ophiolitique (suite)

	SiO_2	TiO_2	Al_2O_3	V_2O_3	Cr_2O_3	MgO	CaO	MnO	FeO	Na_2O	K_2O	H_2O	F	Cl	Total	Al^{iv}
2bum3-a9	41.26	3.09	12.10	0.00	0.01	13.45	11.85	0.11	12.63	2.20	1.04	1.86	0.32	0.02	99.92	1.94
2bum3-a10	39.62	3.16	12.38	0.00	0.01	13.11	11.78	0.11	12.79	2.28	1.04	1.71	0.55	0.02	98.57	2.08
2mam6-a1	51.58	0.70	4.03	0.04	0.01	14.80	11.90	0.22	15.04	0.47	0.08	2.04	0.04	0.10	101.04	0.67
2mam6-a2	55.07	0.04	0.65	0.00	0.06	15.14	12.84	0.25	14.38	0.16	0.03	2.09	0.00	0.00	100.71	0.11
2mam6-a3	53.14	0.18	2.00	0.06	0.28	15.30	11.86	0.22	14.85	0.22	0.02	1.98	0.18	0.01	100.30	0.34
2mam6-a4	52.39	0.17	3.39	0.01	0.16	15.04	12.06	0.24	14.05	0.41	0.01	2.07	0.00	0.03	100.01	0.52
2mam6-a5	51.41	0.46	3.02	0.11	0.01	15.23	11.95	0.26	14.81	0.34	0.04	1.99	0.07	0.10	99.79	0.51
2liu2-a1	51.09	0.24	3.30	0.08	0.35	13.90	10.65	0.31	17.50	0.33	0.01	2.01	0.05	0.04	99.85	0.55
2liu2-a2	48.44	0.32	5.47	0.07	0.51	14.00	9.41	0.33	18.64	0.32	0.01	2.01	0.00	0.02	99.54	0.91
2liu2-a3	51.03	0.40	3.98	0.06	0.22	13.22	10.73	0.34	17.58	0.57	0.01	1.98	0.11	0.05	100.28	0.67
2liu2-a4	49.44	0.77	5.01	0.06	0.35	12.58	10.58	0.35	18.38	0.86	0.04	1.96	0.12	0.08	100.56	0.85
2liu2-a5	50.18	0.44	4.30	0.09	0.02	13.90	9.98	0.36	18.08	0.37	0.01	2.01	0.03	0.03	99.80	0.72
2liu2-a6	49.64	0.44	3.78	0.13	0.09	14.00	10.54	0.29	17.48	0.44	0.02	2.00	0.00	0.05	98.89	0.64
2liu2-a7	51.94	0.42	3.31	0.07	0.06	14.14	10.66	0.34	17.17	0.48	0.01	2.05	0.00	0.05	100.70	0.55
2liu3-a3	49.14	0.39	4.42	0.07	0.13	14.07	10.35	0.35	17.11	0.31	0.03	1.99	0.01	0.05	98.40	0.75
2liu3-a4	43.39	0.28	8.49	0.04	0.07	13.69	7.74	0.37	20.40	0.29	0.03	1.93	0.00	0.03	96.74	1.47
2liu3-a6	42.51	0.26	7.99	0.07	0.07	14.25	7.79	0.38	19.77	0.26	0.02	1.89	0.04	0.03	95.31	1.43
2liu3-a7	43.96	0.17	10.11	0.14	0.11	13.72	7.70	0.41	21.87	0.22	0.02	1.99	0.02	0.05	100.47	1.62
2liu3-a8	48.68	0.02	19.57	0.02	0.05	7.07	0.39	0.26	15.83	6.03	0.04	2.08	0.09	0.00	100.12	1.37
2liu3-a9	46.04	0.19	5.58	0.13	0.02	14.30	9.07	0.38	18.16	0.25	0.02	1.93	0.00	0.05	96.11	0.97
2liu3-a10	40.42	0.19	9.58	0.08	0.15	13.76	6.19	0.47	21.75	0.21	0.02	1.78	0.19	0.04	94.81	1.73
2liu3-a13	52.15	0.16	2.98	0.00	0.12	15.31	11.56	0.25	14.03	0.33	0.01	2.04	0.03	0.02	98.98	0.50
2liu3-a14	46.61	0.20	6.19	0.09	0.14	13.93	8.85	0.40	19.30	0.32	0.02	1.91	0.14	0.02	98.11	1.05
jid1-a1	50.85	0.18	3.83	0.06	0.00	11.39	11.37	0.45	18.55	0.76	0.04	1.97	0.04	0.10	99.60	0.52
jid1-a2	55.55	0.05	2.48	0.05	0.04	14.67	12.46	0.84	12.46	0.16	0.00	2.11	0.00	0.00	100.88	0.12
jid1-a3	55.38	0.03	2.21	0.00	0.00	16.28	11.88	0.64	10.91	0.20	0.05	2.03	0.15	0.01	99.77	0.17
jid1-a4	52.99	0.31	3.41	0.04	0.03	13.36	10.96	0.26	16.68	0.85	0.03	2.05	0.00	0.10	101.08	0.46
jid1-a5	51.73	0.14	3.97	0.08	0.00	9.39	11.52	0.61	20.54	0.55	0.04	1.96	0.09	0.09	100.70	0.38
jid1-a6	53.36	0.33	3.25	0.01	0.00	14.43	11.74	0.50	14.53	0.55	0.03	2.07	0.00	0.06	100.85	0.42
jid1-a7	54.44	0.22	2.80	0.00	0.00	14.17	11.99	0.52	14.43	0.46	0.04	2.09	0.00	0.04	101.18	0.27
jid1-a8	54.31	0.40	2.97	0.12	0.05	14.17	11.77	0.56	13.48	0.44	0.02	2.08	0.00	0.06	100.44	0.24
2qum6-a1	51.59	0.09	2.96	0.01	0.00	14.89	12.80	0.10	14.80	0.29	0.00	2.05	0.00	0.00	99.57	0.51
2qum6-a2	46.74	1.18	6.72	0.18	0.06	14.41	11.47	0.21	14.86	0.78	0.10	1.99	0.00	0.09	98.77	1.15
2qum6-a3	47.73	1.31	6.40	0.00	0.04	13.90	11.10	0.22	15.58	1.10	0.09	1.92	0.18	0.11	99.66	1.09
2qum6-a5	48.98	1.24	6.18	0.08	0.00	14.46	11.06	0.23	15.21	0.80	0.09	1.99	0.09	0.09	100.50	1.03
2qum6-a6	46.40	1.72	7.72	0.12	0.02	13.10	11.24	0.22	16.02	1.34	0.14	1.93	0.16	0.12	100.23	1.29
2qum6-a7	48.40	1.37	6.50	0.10	0.00	13.85	11.08	0.22	15.69	1.10	0.10	1.93	0.20	0.10	100.63	1.09

Tab. C.7: Amphiboles - mélange ophiolitique (suite)

		SiO_2	TiO_2	Al_2O_3	V_2O_3	Cr_2O_3	MgO	CaO	MnO	FeO	Na_2O	K_2O	H_2O	F	Cl	Total	Al^{iv}
	2qum6-a8	49.09	1.31	6.04	0.04	0.00	14.11	11.12	0.18	15.47	1.03	0.08	2.01	0.06	0.09	100.61	1.01
	2bag7a-a2	53.68	0.46	3.17	0.05	0.16	18.29	12.59	0.13	8.87	0.64	0.02	2.12	0.01	0.01	100.21	0.47
	2bag7a-a3	49.30	0.42	5.91	0.05	0.19	16.47	11.49	0.17	11.81	1.07	0.12	2.01	0.10	0.01	99.10	0.98
	2bag7a-a4	52.65	0.02	3.21	0.00	0.00	19.42	11.70	0.15	8.90	0.64	0.02	2.10	0.00	0.00	98.81	0.53
	2bag7a-a5	53.34	0.11	2.86	0.00	0.02	19.03	12.08	0.16	8.81	0.64	0.02	2.07	0.07	0.00	99.22	0.47
	2bag7a-a6	55.38	0.00	0.58	0.00	0.03	22.56	12.54	0.16	4.67	0.17	0.01	2.13	0.00	0.00	98.25	0.10
	2bag7a-a7	54.93	0.00	1.99	0.05	0.06	20.21	12.40	0.16	7.22	0.42	0.01	2.08	0.10	0.01	99.64	0.33
	2bag7b-a1	44.59	3.26	9.44	0.15	0.11	15.79	10.04	0.18	9.95	2.57	0.04	1.96	0.15	0.03	98.26	1.58
	2bag7b-a2	55.91	0.01	0.74	0.01	0.04	22.48	12.66	0.11	4.21	0.21	0.01	2.14	0.00	0.01	98.53	0.12
	2bag7b-a3	56.17	0.02	1.77	0.00	0.00	20.57	12.57	0.11	5.75	0.44	0.01	2.12	0.07	0.00	99.60	0.22
	2bag7b-a4	51.02	0.12	5.60	0.00	0.01	18.69	12.51	0.12	7.69	1.21	0.04	2.10	0.00	0.00	99.12	0.80
	2daz3-a1	46.87	1.15	6.43	0.06	0.00	8.47	8.92	0.43	24.82	0.92	0.03	1.88	0.15	0.10	100.23	1.11
	2daz3-a2	49.09	1.22	4.53	0.09	0.00	10.93	8.99	0.50	22.55	0.60	0.13	1.98	0.05	0.02	100.68	0.76
	2daz3-a3	49.75	0.31	4.36	0.05	0.05	13.08	10.13	0.31	18.24	0.99	0.09	1.96	0.11	0.01	99.43	0.74
	2daz3-a4	49.45	1.56	4.59	0.11	0.02	11.47	11.44	0.28	17.97	0.98	0.09	2.00	0.04	0.02	100.03	0.73
	2daz3-a5	50.68	0.19	4.32	0.11	0.00	12.29	10.28	0.31	18.44	1.12	0.10	1.97	0.13	0.01	99.93	0.67
	2daz3-a8	49.98	0.24	4.48	0.13	0.00	11.57	10.78	0.33	19.22	1.11	0.06	2.01	0.01	0.01	99.93	0.70
	2daz3-a9	46.91	1.37	6.57	0.06	0.00	9.93	9.53	0.47	22.20	0.74	0.03	1.97	0.00	0.07	99.85	1.13
	2lha3-a1	52.28	0.06	0.37	0.11	0.05	13.62	10.34	0.26	15.31	0.98	0.03	1.95	0.00	0.07	95.43	0.07
	2lha3-a2	53.74	0.04	0.41	0.09	0.01	15.10	11.05	0.25	13.89	0.73	0.04	2.01	0.00	0.05	97.39	0.07
	2lha3-a3	53.00	0.03	1.83	0.18	0.03	14.91	10.05	0.27	16.00	0.81	0.04	2.05	0.00	0.00	99.19	0.31
	jnl1-a1	53.23	0.07	1.64		0.02	13.85	11.76	1.67	15.48	0.04					97.77	0.28
	jnl1-a2	52.80	0.07	2.48		0.02	14.20	12.04	1.54	14.23	0.10					97.47	0.39
	jnl1-a3	54.75	0.09	1.23		0.00	16.59	12.25	1.49	10.72	0.09					97.19	0.20
	jnl1-a4	52.60	0.06	2.59		0.08	14.31	12.24	1.40	14.05	0.09					97.42	0.40
	jnl1-a5	54.55	0.05	1.26		0.00	15.92	12.56	1.30	12.16	0.06					97.88	0.21
	jnl1-a6	53.92	0.05	1.38		0.04	15.30	12.42	1.34	12.76	0.06					97.30	0.23
	jnl1-a7	56.18	0.09	1.36		0.00	20.61	12.08	0.44	6.70	0.15					97.61	0.22
	jnl1-a8	54.00	0.05	1.42		0.00	15.80	12.30	1.35	12.30	0.05					97.33	0.24
	jnl1-a9	54.14	0.13	2.00		0.02	15.86	11.69	1.38	12.34	0.10					97.68	0.33
	jnl1-a10	53.81	0.19	2.19		0.00	16.24	12.20	1.02	11.36	0.08					97.09	0.32
	jnl1-a11	50.12	0.74	5.53		0.00	16.45	11.63	0.55	10.88	0.18					96.08	0.86
	jnl1-a12	53.69	0.09	2.15		0.00	16.17	11.53	1.57	12.43	0.14					97.76	0.36
	jnl1-a13	53.96	0.23	2.12		0.00	16.68	12.01	0.98	11.34	0.14					97.46	0.35
Basalte	zed1-h2	43.48	1.77	12.61	0.08	0.02	12.61	11.54	0.20	12.53	1.77	1.14	2.03	0.00	0.03	99.81	1.03

Tab. C.7: Amphiboles - mélange ophiolitique (suite)

		SiO_2	TiO_2	Al_2O_3	V_2O_3	Cr_2O_3	MgO	CaO	MnO	FeO	Na_2O	K_2O	H_2O	F	Cl	Total	Al^{iv}
	zed1-a4	41.02	1.89	14.51	0.01	0.00	13.46	12.15	0.11	11.40	2.17	1.36	1.95	0.17	0.03	100.23	1.20
	zed1-a5	50.92	0.41	9.03	0.11	0.06	16.78	11.39	0.17	9.48	1.28	0.25	2.05	0.20	0.03	102.16	2.10
	zed1-a6	49.31	0.51	9.56	0.07	0.20	16.64	10.74	0.21	9.79	1.54	0.28	2.11	0.00	0.07	101.00	1.97
	zed1-h7	40.13	1.94	14.39	0.07	0.03	12.69	11.97	0.14	12.87	2.23	1.22	1.97	0.06	0.06	99.76	1.89
	zed1-h8	41.77	1.87	13.69	0.08	0.07	14.53	12.12	0.10	10.76	2.17	1.25	2.05	0.00	0.02	100.48	2.00
	zed1-a9	41.49	1.84	12.12	0.08	0.00	12.77	11.50	0.35	14.12	2.14	1.10	1.96	0.07	0.05	99.57	2.02
	zed1-a13	41.52	2.12	13.99	0.05	0.00	14.19	12.15	0.12	10.86	2.18	1.14	2.01	0.07	0.02	100.43	2.06
	zed1-a14	40.85	1.75	13.91	0.06	0.07	14.63	12.12	0.11	10.69	2.18	1.24	2.03	0.00	0.03	99.68	1.66

Tab. C.8: Composition chimique (% poids) des amphiboles des roches mafiques du mélange de Yamdrock.

		SiO_2	TiO_2	Al_2O_3	V_2O_3	Cr_2O_3	MgO	CaO	MnO	FeO	Na_2O	K_2O	H_2O	F	Cl	Total	Al^{iv}
Gabbro	2bag1-a11	50.43	0.25	1.86	0.05	0.03	13.30	10.86	0.40	17.87	0.87	0.16	1.97	0.01	0.05	98.10	0.32
	2bag1-a12	50.85	0.61	2.09	0.02	0.05	15.33	10.19	0.38	15.77	0.96	0.18	1.82	0.39	0.06	98.69	0.35
	2bag1-a13	48.87	3.00	2.05	0.01	0.00	13.77	12.16	0.33	14.90	0.80	0.16	1.83	0.33	0.04	98.24	0.36
	2bag1-a16	50.55	0.66	2.56	0.00	0.00	14.29	10.76	0.38	16.53	1.13	0.21	1.70	0.62	0.08	99.47	0.44
	2bag1-a17	49.03	0.63	2.41	0.11	0.01	13.67	9.35	0.39	18.90	1.37	0.33	1.39	1.17	0.12	98.88	0.42
	2bag1-a18	49.42	0.80	2.83	0.03	0.00	15.94	10.44	0.32	14.86	1.04	0.23	1.71	0.59	0.07	98.28	0.48
	lha33-a5	54.03	0.30	3.23	0.09	0.07	14.42	11.26	0.20	14.33	0.74	0.02	2.09	0.02	0.01	100.79	0.35
	lha33-a6	51.78	0.30	4.67	0.13	0.00	14.30	10.72	0.26	15.11	0.93	0.03	1.93	0.29	0.01	100.46	0.66
	lha33-a8	53.22	0.47	2.76	0.09	0.00	12.29	10.87	0.30	17.77	0.55	0.10	1.98	0.14	0.05	100.58	0.33
	bag4-h2	49.63	1.04	4.44	0.00	0.00	10.23	10.41	0.24	21.60	1.21	0.37	1.82	0.29	0.24	101.50	0.76
	bag4-h3	49.88	0.61	3.95	0.07	0.05	10.76	9.43	0.30	21.99	1.18	0.28	1.95	0.00	0.22	100.68	0.67
	bag4-h4	48.80	1.03	6.12	0.02	0.00	9.28	11.74	0.19	19.32	1.16	0.52	1.92	0.09	0.21	100.39	0.72

Tab. C.9: Composition chimique (% poids) des amphiboles des roches mafiques du flysch triasique.

		SiO_2	TiO_2	Al_2O_3	V_2O_3	Cr_2O_3	MgO	CaO	MnO	FeO	Na_2O	K_2O	H_2O	F	Cl	Total	Al^{iv}
Gabbro	zis6-a11	55.65	0.03	28.65	0.00	0.00	0.04	11.29	0.00	0.37	4.71	0.53	2.34	0.00	0.01	103.60	0.86
	2zis5-a11	46.59	1.02	4.80	0.15	0.00	12.96	10.09	0.28	18.93	1.98	0.65	0.94	2.06	0.27	100.71	0.83
	2zis5-a12	49.70	0.22	2.55	0.08	0.01	8.42	10.06	0.32	25.71	0.76	0.29	1.79	0.23	0.24	100.36	0.45
	2zis5a-a3	44.73	1.36	5.17	0.04	0.00	10.38	10.33	0.46	20.50	1.97	0.73	0.85	2.10	0.29	98.90	0.93
	2zis5a-a4	45.03	1.12	4.83	0.00	0.03	10.96	9.95	0.49	21.00	1.99	0.64	0.86	2.09	0.29	99.28	0.86

Tab. C.9: Amphiboles - flysch triasique (suite)

		SiO_2	TiO_2	Al_2O_3	V_2O_3	Cr_2O_3	MgO	CaO	MnO	FeO	Na_2O	K_2O	H_2O	F	Cl	Total	Al^{iv}
	2zis5a-a5	46.75	0.34	2.84	0.00	0.00	6.59	9.12	0.58	29.69	1.01	0.24	1.75	0.13	0.34	99.37	0.51
	2zis5a-a6	44.24	1.44	5.53	0.11	0.04	10.37	10.19	0.42	21.14	2.09	0.77	0.88	2.03	0.35	99.58	0.99
	2zis5a-a7	44.20	1.47	5.42	0.00	0.00	10.50	10.41	0.38	20.91	1.94	0.67	0.97	1.83	0.35	99.04	0.97
	2zis7-a10	49.81	0.44	2.90	0.08	0.04	10.65	10.87	0.17	20.34	0.68	0.24	1.72	0.48	0.08	98.49	0.51
	2zis8-h1	43.08	1.07	5.80	0.02	0.00	6.99	9.43	0.52	26.87	2.16	0.85	0.68	2.31	0.41	100.19	1.06
	2zis8-h3	44.02	1.05	5.03	0.01	0.00	8.18	9.47	0.55	26.07	2.06	0.79	0.68	2.39	0.32	100.62	0.90
	2zis8-h4	42.25	1.17	5.98	0.00	0.00	7.40	9.54	0.51	26.20	2.27	0.86	0.54	2.59	0.40	99.70	1.10
	2zis8-h14	43.34	0.94	5.72	0.06	0.00	6.95	10.00	0.48	26.29	2.16	0.90	0.58	2.52	0.42	100.38	1.05
	2zis8-a20	42.42	0.54	5.56	0.00	0.00	8.26	9.53	0.46	25.08	2.15	0.82	0.68	2.26	0.41	98.16	1.03
	2zis10-h1	45.67	1.05	5.33	0.07	0.02	8.71	9.86	0.36	24.20	2.14	0.72	0.92	1.97	0.35	101.37	0.95
	2zis10-h2	44.71	1.17	5.35	0.11	0.00	8.44	9.81	0.32	24.25	2.18	0.74	1.04	1.67	0.34	100.12	0.96
	2zis10-h4	44.18	1.39	5.58	0.01	0.03	8.66	9.66	0.39	24.12	2.22	0.73	0.75	2.27	0.36	100.34	1.00
	2zis10-h5	42.64	1.50	5.75	0.00	0.03	8.20	9.73	0.40	25.05	2.21	0.82	0.72	2.20	0.45	99.70	1.05
	2zis10-h8	43.30	1.12	5.75	0.07	0.00	6.66	9.39	0.49	27.03	2.22	0.90	0.57	2.53	0.46	100.48	1.05
	2zis10-a9	48.04	0.28	1.77	0.00	0.00	6.29	4.13	0.77	35.07	0.83	0.10	1.68	0.33	0.20	99.46	0.33
	2zis10-h12	42.75	1.49	6.14	0.00	0.00	7.84	9.98	0.33	25.13	2.22	0.82	0.76	2.16	0.43	100.06	1.12
	lha31-h1	44.38	1.82	9.60	0.22	0.08	7.89	40.87	0.31	21.17	1.66	0.87	1.81	0.11	0.48	101.27	1.36
	lha31-h2	53.65	0.05	3.10	0.05	0.00	12.03	11.94	0.31	17.08	0.38	0.10	2.03	0.07	0.02	100.79	0.23
	lha31-h3	50.42	0.12	5.21	0.13	0.03	10.76	11.74	0.47	18.36	0.67	0.21	2.03	0.00	0.00	100.14	0.59
	lha31-a4	54.38	0.04	2.23	0.06	0.39	13.63	12.23	0.30	14.87	0.27	0.08	2.06	0.04	0.00	100.56	0.18
	lha31-a5	52.38	0.03	3.34	0.07	0.42	13.13	12.14	0.28	15.75	0.38	0.09	1.98	0.15	0.01	100.16	0.41
	lha31-a6	52.31	0.04	4.05	0.00	0.23	13.08	12.21	0.31	15.09	0.55	0.14	2.06	0.00	0.01	100.08	0.42
	lha31-a7	54.07	0.01	2.29	0.00	0.00	13.71	12.33	0.31	15.30	0.23	0.07	2.08	0.00	0.00	100.40	0.21
	lha31-a8	51.11	0.07	3.18	0.00	0.76	12.81	12.17	0.31	15.93	0.39	0.12	1.95	0.15	0.00	98.94	0.47
	lha31-a9	51.86	0.06	2.95	0.05	0.54	12.92	12.23	0.33	15.48	0.37	0.11	2.01	0.04	0.00	98.94	0.36
	lha31-a10	53.02	0.04	2.09	0.05	0.12	12.87	12.21	0.33	16.10	0.24	0.07	2.04	0.00	0.00	99.18	0.22
	lha31-a11	52.31	0.02	2.68	0.05	0.00	12.45	12.21	0.32	17.33	0.28	0.09	2.04	0.00	0.00	99.78	0.34
	lha31-a12	53.13	0.02	1.94	0.01	0.06	13.45	12.26	0.32	15.95	0.25	0.06	2.02	0.06	0.00	99.51	0.25
	lha31-a14	54.31	0.00	0.72	0.02	0.00	13.28	12.35	0.34	16.23	0.19	0.06	1.95	0.13	0.14	99.72	0.05
	lha31-a15	52.62	0.03	2.38	0.00	0.02	13.83	12.29	0.35	15.30	0.30	0.08	1.86	0.38	0.01	99.44	0.33
	lha31-a17	50.70	0.05	6.16	0.04	0.00	9.91	9.09	0.23	14.41	1.64	0.30	1.93	0.00	0.15	94.61	0.27
	lha31-a18	54.17	0.05	2.25	0.00	0.03	13.47	12.22	0.30	15.26	0.32	0.09	1.97	0.22	0.00	100.35	0.17
	lha31-a19	54.22	0.04	2.45	0.09	0.09	13.35	11.89	0.26	15.26	0.25	0.10	2.03	0.09	0.02	100.13	0.18
Diabase	2paz1-h8	47.23	1.02	5.18	0.00	0.00	12.15	10.35	0.34	18.94	1.83	0.75	1.34	1.22	0.28	100.64	0.90
	2paz1-h9	47.28	1.38	5.32	0.08	0.03	12.61	10.45	0.26	17.55	2.00	0.74	0.87	2.24	0.26	101.07	0.92
	2paz1-a25	47.60	1.35	5.32	0.05	0.00	13.10	10.52	0.25	17.19	1.98	0.66	0.96	2.09	0.25	101.32	0.92

Tab. C.9: Amphiboles - flysch triasique (suite)

	SiO_2	TiO_2	Al_2O_3	V_2O_3	Cr_2O_3	MgO	CaO	MnO	FeO	Na_2O	K_2O	H_2O	F	Cl	Total	Al^{iv}
2paz1-a26	46.73	1.31	5.12	0.00	0.00	12.75	10.22	0.31	18.36	2.08	0.70	0.80	2.36	0.28	101.02	0.89
2paz6-a6	52.83	0.08	1.67	0.02	0.04	12.24	10.51	0.31	20.14	0.54	0.12	1.94	0.15	0.07	100.67	0.28
2paz6-a8	51.07	0.17	1.92	0.06	0.00	11.52	8.77	0.43	22.72	0.97	0.13	1.96	0.00	0.12	99.84	0.33
2paz6-h12	47.25	1.31	5.44	0.03	0.02	13.28	10.81	0.20	16.94	1.99	0.77	1.26	1.44	0.27	101.00	0.94
2paz6-a17	52.48	0.08	1.67	0.02	0.00	11.55	10.25	0.32	21.68	0.50	0.15	1.97	0.07	0.09	100.82	0.28
2zis6-a13	50.44		5.15			15.95	11.42		12.96	1.36	0.05				97.33	0.80

Tab. C.10: Composition chimique (% poids) de la chlorite des roches mafiques du mélange ophiolitique.

		SiO_2	TiO_2	Al_2O_3	Cr_2O_3	MgO	CaO	MnO	FeO	NiO	CuO	Na_2O	H_2O	Total
Gabbro	2bum6-ch6	27.46	0.00	16.31	0.00	16.67	0.02	0.47	26.22	0.04	0.00	0.01	11.22	98.43
	2bum6-ch7	27.98	0.00	14.66	0.01	15.77	0.11	0.37	28.00	0.00	0.00	0.05	11.08	98.01
	2mam7-ch8	32.41	0.03	17.50	0.01	31.27	0.07	0.17	7.74	0.00	0.00	0.01	12.78	101.97
	2mam7-ch9	32.37	0.01	16.80	0.01	31.41	0.10	0.13	7.18	0.00	0.07	0.00	12.64	100.71
	2liu6-ch18	29.57	0.05	18.28	0.06	19.60	1.05	0.37	19.02	0.02	0.03	0.14	11.85	100.06
	2liu6a-ch17	31.22	0.20	15.70	0.09	19.34	1.88	0.29	18.94			0.16	12.13	100.00
	2liu9-ch1	28.00	0.00	15.83	0.06	13.97	0.19	0.19	29.76	0.00	0.00	0.04	11.15	99.18
	2qum4-ch1	29.31	0.01	16.43	0.00	19.82	0.17	0.24	21.59	0.02	0.12	0.01	11.63	99.36
	2qum4-ch2	30.04	0.02	16.04	0.00	19.76	0.24	0.28	22.37	0.02	0.00	0.01	11.75	100.53
	2qum4-ch13	29.92	0.01	16.93	0.01	20.44	0.13	0.24	21.98	0.00	0.00	0.01	11.91	101.56
	2qum12-ch11	27.48	0.09	16.56	0.01	14.49	0.17	0.26	29.62	0.05	0.08	0.03	11.25	100.08
	2qum12-ch12	27.87	0.00	16.97	0.00	14.69	0.12	0.24	29.56	0.04	0.00	0.02	11.37	100.89
	2qum13a-ch15	32.45	0.16	15.87	0.00	26.39	1.54	0.19	12.37	0.06	0.02	0.03	12.41	101.49
	2qum13a-ch16	30.93	0.07	15.34	0.02	23.12	0.82	0.27	16.60	0.19	0.00	0.05	11.89	99.29
	2qum15-ch1	30.11	0.00	16.81	0.01	24.81	0.12	0.13	15.85	0.08	0.00	0.00	12.04	99.96
	2qum15-ch24	34.09	0.09	15.18	0.00	21.13	1.79	0.31	16.87	0.00	0.00	0.08	10.39	100.00
	2qum15-ch28	29.45	0.08	17.81	0.05	19.76	1.39	0.37	17.37	0.06	0.08	0.13	11.70	98.24
	2qum15a-ch4	30.09	0.02	16.90	0.07	24.50	0.25	0.16	16.10	0.09	0.09	0.00	12.05	100.31
	2qum15a-ch5	30.42	0.00	15.74	0.03	23.94	1.09	0.14	15.02	0.06	0.07	0.04	11.86	98.41
	jid2-ch1	28.41	0.01	17.96	0.00	18.24	0.07	0.27	23.28	0.02	0.00	0.05	11.62	99.93
	jid2-ch2	28.29	0.05	17.81	0.00	18.30	0.08	0.29	23.88	0.04	0.00	0.04	11.63	100.42
	jid2-ch4	28.88	0.01	16.76	0.00	18.25	0.04	0.30	23.51	0.01	0.00	0.02	11.53	99.30
	2bag8-ch1	32.31	0.01	15.52	0.21	25.33	0.31	0.17	14.16	0.09	0.04	0.01	12.21	100.37
	2daz2-ch12	29.97	0.00	14.34	0.01	18.58	0.28	0.27	22.54	0.00	0.00	0.03	11.34	97.35
	2daz7-ch10	31.98	0.02	14.70	0.06	17.54	0.54	0.24	24.15	0.00	0.06	0.06	11.76	101.12

Tab. C.10: Chlorite - mélange ophiolitique (suite)

		SiO_2	TiO_2	Al_2O_3	Cr_2O_3	MgO	CaO	MnO	FeO	NiO	CuO	Na_2O	H_2O	Total
	2daz7-ch12	27.85	0.00	18.28	0.02	17.50	0.03	0.27	24.75	0.01	0.00	0.00	11.57	100.28
	2daz8-ch8	27.43	0.00	17.86	0.03	14.77	0.06	0.33	28.22	0.04	0.00	0.02	11.35	100.09
	2lha4-ch6	28.48	0.00	15.73	0.03	16.73	0.04	0.35	26.85	0.03	0.00	0.03	11.36	99.62
	2lha4-ch7	27.77	0.02	16.81	0.00	17.50	0.01	0.35	25.68	0.03	0.06	0.00	11.41	99.64
	2lha6-ch7	29.91	0.00	15.12	1.21	21.97	0.07	0.31	19.46	0.05	0.06	0.02	11.78	99.95
	2lha6-ch11	27.29	0.01	16.03	0.04	15.30	0.03	0.61	27.23	0.07	0.00	0.01	11.07	97.67
	2bag3-ch2	27.46	0.02	15.05	0.00	9.75	0.51	0.29	34.78	0.00	0.12	0.02	10.80	98.81
	2bag4-ch6	28.81	0.00	15.92	0.00	12.34	0.29	0.17	31.23	0.06	0.00	0.02	11.21	100.04
	2bag4-ch7	28.19	0.00	15.19	0.00	12.28	0.26	0.16	31.68	0.04	0.08	0.02	11.01	98.91
Diabase	lha17-ch23	30.31	0.00	16.90	0.07	17.84	0.35	0.18	22.75	0.03	0.09	0.02	11.73	100.31
	lha17-ch24	30.18	0.00	16.52	0.05	17.74	0.34	0.19	22.92	0.02	0.11	0.02	11.67	100.12
	lha17-ch25	30.60	0.01	16.68	0.11	17.63	0.40	0.15	23.07	0.05	0.16	0.05	11.77	100.94
	2liu3-ch5	27.08	0.07	17.71	0.00	13.56	0.56	0.43	28.47	0.00	0.13	0.01	11.19	99.20
	2liu4-ch8	28.34	0.03	16.40	0.00	12.79	0.33	0.25	29.97	0.06	0.10	0.02	11.18	99.47
	2liu4-ch9	28.64	0.00	15.23	0.04	13.66	0.12	0.29	30.87	0.03	0.08	0.04	11.22	100.22
	2liu4-ch13	28.75	0.05	15.93	0.01	13.70	0.23	0.26	30.35	0.02	0.02	0.01	11.31	100.64
	2qum2-ch15	29.46	0.00	17.60	0.06	17.05	0.30	0.33	24.75	0.02	0.00	0.02	11.72	101.31
	2qum8-ch5	26.99	0.01	17.66	0.00	13.56	0.10	0.29	31.15	0.00	0.08	0.01	11.30	101.14
	2daz3-ch2	26.05	0.08	19.72	0.07	14.89	0.05	0.21	27.80	0.00	0.10	0.02	11.39	100.38
	2daz3-ch10	25.53	0.07	19.15	0.01	14.18	0.09	0.19	28.26	0.00	0.05	0.03	11.15	98.68
	2mam1-ch6	27.83	0.02	17.88	0.10	19.16	0.03	0.37	23.12	0.05	0.00	0.01	11.63	100.19
	2mam1-ch7	28.59	0.00	17.54	0.08	19.16	0.16	0.34	22.61	0.04	0.06	0.02	11.68	100.27
	2mam2-ch7	27.41	0.01	17.94	0.04	18.40	0.05	0.55	24.05	0.03	0.06	0.01	11.54	100.11
	2mam2-ch13	27.89	0.00	18.04	0.00	18.09	0.06	0.50	24.56	0.04	0.00	0.02	11.63	100.81
	2mam5-ch5	27.97	0.04	15.06	0.01	11.83	0.42	0.46	31.99			0.04	11.76	100.00
	2mam5-ch11	26.87	0.00	16.50	0.00	11.13	0.11	0.65	33.69	0.03	0.11	0.01	11.01	100.11
	2mam5-ch12	29.74	0.00	14.97	0.00	11.65	0.35	0.51	31.56			0.02	10.93	100.00
	2bag1-ch4	28.86	2.16	14.24	0.00	15.78	0.43	0.72	26.24	0.00	0.00	0.06	11.37	99.84
	2bag1-ch14	28.32	4.44	13.11	0.00	14.49	1.94	0.57	25.92	0.03	0.12	0.03	11.35	100.32
Basalte	2lha3-ch4	27.76	0.00	16.91	0.00	16.88	0.06	0.31	26.55	0.03	0.06	0.03	11.41	99.99
	2lha3-ch5	32.64	0.05	14.68	0.03	22.14	0.36	0.19	18.77	0.01	0.07	0.04	12.05	101.03

Tab. C.11: Composition chimique (% poids) de la chlorite des roches mafiques du mélange de Yamdrock.

		SiO_2	TiO_2	Al_2O_3	Cr_2O_3	MgO	CaO	MnO	FeO	NiO	CuO	Na_2O	H_2O	Total
Diabase	lha11-ch5	27.55	0.01	19.65	0.05	15.55	0.09	0.20	26.08	0.00	0.00	0.02	11.59	100.82
	lha11-ch6	27.68	0.00	18.64	0.01	16.07	0.02	0.19	25.86	0.03	0.00	0.00	11.49	100.00
	lha11-ch7	28.07	0.02	18.43	0.00	16.63	0.03	0.16	25.80	0.00	0.04	0.01	11.60	100.80
	lha11-ch8	27.83	0.04	19.41	0.05	16.00	0.12	0.14	25.36	0.00	0.03	0.01	11.61	100.64
	lha11-ch9	27.97	0.01	19.37	0.01	15.96	0.13	0.11	25.16	0.02	0.21	0.02	11.63	100.91
Basalte	2xia1-ch12	30.04	0.01	13.63	0.05	17.42	0.13	0.15	26.74	0.00	0.00	0.02	11.38	99.57
	2xia1-ch13	28.48	0.00	15.61	0.02	14.01	0.39	0.30	29.83	0.00	0.06	0.05	11.24	99.98
	2xia4-ch9	25.85	0.02	15.63	0.00	8.49	0.03	0.60	38.05	0.00	0.13	0.02	10.67	99.48
	2xia4-ch10	26.53	0.00	16.10	0.01	9.25	0.23	0.47	36.45	0.00	0.00	0.02	10.84	99.90
	2rem8-ch7	28.05	0.03	20.86	0.07	20.07	0.03	0.22	19.58	0.03	0.00	0.01	11.96	100.89
	2rem8-ch12	28.18	0.05	20.15	0.00	20.64	0.06	0.28	19.68	0.06	0.17	0.00	11.97	101.23
	2rem8-ch13	27.92	0.08	20.96	0.05	19.39	0.07	0.25	19.20	0.00	0.11	0.03	11.86	99.91

Tab. C.12: Composition chimique (% poids) de la chlorite des roches mafiques du flysch triasique.

		SiO_2	TiO_2	Al_2O_3	Cr_2O_3	MgO	CaO	MnO	FeO	NiO	CuO	Na_2O	H_2O	Total
Gabbro	zis4-ch26	26.40	0.00	16.55	0.00	8.77	0.21	0.34	35.71	0.02	0.00	0.02	10.76	98.77
	2zis5-ch9	28.72	0.10	15.82	0.03	13.21	0.45	0.16	29.58	0.00	0.00	0.05	11.20	99.31
	2zis5a-ch12	27.70	0.00	13.50	0.00	9.63	0.34	0.27	36.06	0.00	0.00	0.03	10.66	98.18
	2zis5a-ch14	26.33	0.01	15.15	0.00	9.46	0.30	0.28	35.27	0.00	0.04	0.03	10.60	97.46
	2zis7-ch4	27.91	0.00	16.79	0.00	12.64	0.28	0.19	30.28	0.00	0.04	0.04	11.15	99.30
	2zis8-ch2	27.32	0.46	14.23	0.01	8.74	0.75	0.34	37.45	0.00	0.00	0.02	10.79	100.10
	2zis8-ch5	31.17	0.07	12.27	0.00	8.22	1.44	0.39	36.86	0.04	0.03	0.17	11.08	101.75
	2zis8-ch7	27.54	0.01	13.56	0.00	7.74	0.24	0.35	39.07	0.01	0.02	0.02	10.61	99.16
	2zis8-ch19	26.67	0.00	15.02	0.00	8.59	0.29	0.32	37.24	0.00	0.00	0.03	10.66	98.81
	2zis9-ch2	30.91	0.08	15.70	0.02	8.19	2.58	0.35	32.33	0.00	0.08	0.30	11.34	101.89
	2zis9-ch9	26.82	0.00	16.29	0.00	8.69	0.22	0.30	37.69	0.00	0.00	0.02	10.91	100.93
	2zis10-ch3	27.56	0.02	14.43	0.00	9.84	0.25	0.29	35.81	0.00	0.04	0.03	10.78	99.06
	2zis10-ch11	27.23	0.01	14.87	0.01	8.83	0.39	0.33	35.46	0.00	0.04	0.00	10.65	97.82
	2zis11-ch1	29.67	1.94	14.03	0.02	12.19	0.39	0.23	31.04	0.01	0.00	0.02	11.29	100.82
	2zis11-ch2	29.02	0.04	13.85	0.00	13.01	0.42	0.31	31.69	0.00	0.01	0.02	11.07	99.43
	lha29a-ch9	25.90	0.05	21.00	0.21	15.79	0.06	0.13	24.94	0.08	0.00	0.02	11.48	99.79
	lha29a-ch10	26.41	0.06	20.79	0.19	16.01	0.00	0.14	24.65	0.03	0.00	0.00	11.54	100.00

Tab. C.12: Chlorite - flysch triasique (suite)

		SiO_2	TiO_2	Al_2O_3	Cr_2O_3	MgO	CaO	MnO	FeO	NiO	CuO	Na_2O	H_2O	Total
	lha29a-ch11	25.84	0.04	22.41	0.39	15.27	0.02	0.07	25.00	0.01	0.00	0.01	11.63	100.80
	lha29b-ch14	25.18	0.02	22.45	0.02	14.14	0.00	0.19	26.60	0.00	0.00	0.02	11.46	100.27
	lha29b-ch15	26.40	0.03	20.14	0.07	15.53	0.00	0.14	26.13	0.02	0.00	0.01	11.46	100.00
Diabase	2paz1-ch10	30.02	0.01	14.81	0.03	14.11	0.96	0.19	28.54	0.00	0.00	0.03	11.34	100.04
	2paz1-ch11	28.29	0.02	16.97	0.06	13.85	0.32	0.18	28.99	0.00	0.06	0.01	11.32	100.07
	2paz1-ch14	29.85	0.03	14.24	0.10	16.21	0.13	0.19	28.19	0.00	0.10	0.02	11.41	100.47
	2paz1-ch21	26.80	0.02	17.83	0.00	13.30	0.08	0.21	30.61	0.01	0.00	0.01	11.21	100.08
	2paz6-ch7	30.31	0.00	16.02	0.00	15.08	0.45	0.12	26.93	0.03	0.00	0.04	11.53	100.50
	2paz6-ch9	32.17	0.03	13.41	0.02	16.24	1.13	0.16	26.37	0.06	0.01	0.05	11.63	101.27
	2paz6-ch14	26.83	0.00	18.14	0.00	14.20	0.03	0.16	29.23	0.04	0.00	0.01	11.27	99.91
	2paz6-ch16	26.89	0.08	19.20	0.00	14.03	0.17	0.17	28.67	0.00	0.09	0.01	11.41	100.72
	2paz6-ch18	27.02	0.00	19.03	0.01	14.14	0.05	0.17	29.39	0.01	0.00	0.01	11.44	101.27
	2mas3-ch4	27.40	0.02	17.04	0.00	13.64	0.09	0.12	29.00	0.04	0.06	0.02	11.12	98.56
	2mas3-ch5	27.99	0.05	16.22	0.00	14.78	0.06	0.16	28.89	0.00	0.01	0.03	11.24	99.42
	2zis6-ch2	29.33	0.02	17.31	0.00	6.56	6.44	0.16	30.17	0.00	0.18	0.07	11.27	101.52
	2zis6-ch3	26.40	0.00	14.81	0.00	9.06	0.03	0.29	37.39	0.00	0.07	0.02	10.63	98.70
	2zis6-ch4	26.43	0.01	15.31	0.00	8.54	0.32	0.24	36.43	0.03	0.00	0.08	10.61	98.00
	lha32-ch2	25.00	0.05	19.82	0.07	11.82	0.01	0.25	31.62	0.04	0.00	0.01	11.12	100.03
	lha32-ch4	24.63	0.07	19.82	0.00	11.39	0.00	0.24	32.33	0.03	0.00	0.00	11.03	99.63
	lha32-ch6	25.00	0.07	19.92	0.00	11.89	0.01	0.23	31.50	0.00	0.00	0.01	11.16	100.48
Basalte	2paz5-ch7	27.75	0.03	19.53	0.04	14.34	0.06	0.31	26.88	0.02	0.00	0.00	11.51	100.46
	2paz7-ch5	26.97	0.04	17.75	0.00	12.35	0.09	0.25	31.25	0.01	0.06	0.02	11.16	99.95
	2paz7-ch6	26.74	0.00	17.20	0.00	12.55	0.12	0.25	31.75	0.01	0.00	0.02	11.10	99.75
	2paz7-ch7	26.19	0.01	17.59	0.00	12.07	0.15	0.25	31.05	0.00	0.00	0.02	10.95	98.29
	2paz7-ch8	26.15	0.01	17.88	0.00	11.95	0.08	0.25	30.95	0.00	0.00	0.03	10.96	98.25
	2paz7-ch9	25.91	0.02	17.86	0.00	12.09	0.02	0.28	31.82	0.02	0.03	0.00	11.00	99.04

Tab. C.13: Composition chimique (% poids) de l'olivine des roches ultramafiques du mélange ophiolitique.

		SiO_2	Al_2O_3	Cr_2O_3	MgO	CaO	MnO	FeO	NiO	ZnO	Total	Fo	Fa
Cpx-harzburgite	2bum2-ol1	41.44	0.01	0.00	49.77	0.01	0.12	10.71	0.42	0.00	102.48	89.2	10.8
	2bum2-ol2	40.91	0.00	0.02	49.11	0.02	0.17	10.43	0.41	0.00	101.06	89.4	10.6
	2bum2-ol3	41.32	0.01	0.00	49.44	0.01	0.11	10.27	0.45	0.03	101.63	89.6	10.4

Tab. C.13: Olivine - mélange ophiolitique (suite)

		SiO_2	Al_2O_3	Cr_2O_3	MgO	CaO	MnO	FeO	NiO	ZnO	Total	Fo	Fa
	2bum2-ol4	41.05	0.00	0.00	49.19	0.01	0.15	10.43	0.36	0.00	101.20	89.4	10.6
	2bum2-ol15	40.96	0.01	0.00	49.65	0.00	0.03	10.47	0.39	0.01	101.50	89.4	10.6
	2bum8-ol7	40.99	0.02	0.06	49.81	0.01	0.12	10.17	0.43	0.00	101.61	89.7	10.3
	2bum8-ol8	40.96	0.02	0.02	49.67	0.03	0.11	10.24	0.40	0.00	101.45	89.6	10.4
	2bum8-ol9	40.99	0.01	0.01	49.84	0.00	0.16	10.14	0.46	0.00	101.60	89.8	10.2
	2bum8-ol10	40.98	0.00	0.00	49.74	0.01	0.18	10.19	0.41	0.00	101.52	89.7	10.3
	2bum8-ol12	41.07	0.00	0.02	50.12	0.01	0.09	10.02	0.42	0.01	101.76	89.9	10.1
	zed2-ol6	41.60	0.00	0.02	50.05	0.02	0.09	9.22	0.42	0.01	101.43	90.6	9.4
	zed2-ol7	41.30	0.01	0.00	50.22	0.00	0.17	9.15	0.40	0.00	101.24	90.7	9.3
	zed2-ol8	41.49	0.02	0.00	50.27	0.02	0.11	9.16	0.44	0.06	101.57	90.7	9.3
	zed2-ol9	41.34	0.02	0.04	49.94	0.02	0.12	9.21	0.39	0.00	101.08	90.6	9.4
	zed2-ol10	41.37	0.01	0.02	49.88	0.01	0.07	9.32	0.36	0.00	101.03	90.5	9.5
	zed3-ol1	41.26	0.00	0.03	49.91	0.00	0.17	9.27	0.37	0.00	101.01	90.6	9.4
	zed3-ol2	41.50	0.00	0.00	49.89	0.02	0.12	9.05	0.38	0.02	100.97	90.8	9.2
	zed3-ol3	41.37	0.00	0.00	49.81	0.01	0.13	9.22	0.39	0.05	100.99	90.6	9.4
Harzburgite	2qum14-ol7	41.11	0.00	0.00	50.54	0.01	0.07	9.08	0.43	0.00	101.24	90.8	9.2
	2qum14-ol8	40.88	0.03	0.00	50.60	0.03	0.17	9.04	0.38	0.01	101.14	90.9	9.1
	2qum14-ol9	40.96	0.01	0.04	50.80	0.03	0.11	9.08	0.37	0.00	101.39	90.9	9.1
	2qum14-ol10	41.42	0.00	0.00	50.36	0.03	0.15	9.19	0.38	0.00	101.52	90.7	9.3
	2qum14-ol11	41.39	0.01	0.05	50.35	0.02	0.16	8.97	0.34	0.00	101.28	90.9	9.1
Gabbronorite	2qum13a-ol1	40.53	0.01	0.02	46.81	0.04	0.12	14.07	0.42	0.00	102.03	85.6	14.4
	2qum13a-ol2	40.39	0.01	0.03	46.40	0.02	0.22	14.32	0.38	0.04	101.81	85.2	14.8
	2qum13a-ol3	40.64	0.01	0.00	46.39	0.01	0.18	13.86	0.39	0.00	101.49	85.6	14.4

Tab. C.14: Composition chimique (% poids) des pyroxènes des roches ultramafiques du mélange ophiolitique.

		SiO_2	TiO_2	Al_2O_3	Cr_2O_3	Fe_2O_3	MgO	CaO	MnO	FeO	Na_2O	Total	Mg#	Wo	En	Fs
Cpx-harzburgite	2bum2-opx5	55.43	0.09	4.41	0.44	0.31	32.82	0.65	0.14	6.71	0.04	101.03	0.90	0.01	0.88	0.11
	2bum2-opx6	55.24	0.08	4.37	0.45	0.35	32.41	1.41	0.14	6.13	0.06	100.64	0.90	0.03	0.87	0.10
	2bum2-opx7	55.61	0.07	4.16	0.31	0.01	32.70	0.79	0.14	6.99	0.02	100.80	0.90	0.02	0.88	0.11
	2bum2-cpx8	51.54	0.26	5.29	0.84	2.14	16.48	22.28	0.05	0.74	0.68	100.31	0.89	0.47	0.48	0.04
	2bum2-opx9	54.40	0.05	5.68	0.76	0.76	32.21	1.18	0.14	5.81	0.05	101.04	0.91	0.02	0.88	0.10
	2bum2-cpx10	52.53	0.33	4.58	0.53	0.76	16.35	22.75	0.06	1.89	0.62	100.39	0.87	0.48	0.48	0.04

Tab. C.14: Pyroxènes - mélange ophiolitique (suite)

		SiO_2	TiO_2	Al_2O_3	Cr_2O_3	Fe_2O_3	MgO	CaO	MnO	FeO	Na_2O	Total	Mg#	Wo	En	Fs
	2bum2-opx11	53.97	0.17	5.33	0.72	0.81	28.86	5.71	0.12	5.01	0.18	100.87	0.91	0.11	0.80	0.09
	2bum2-cpx12	52.66	0.26	4.74	0.73	0.70	16.55	22.15	0.07	2.05	0.69	100.61	0.86	0.47	0.49	0.04
	2bum2-cpx13	52.32	0.27	5.06	0.69	0.85	16.03	22.67	0.07	1.81	0.71	100.47	0.86	0.48	0.47	0.04
	2bum2-opx14	54.78	0.09	4.90	0.56	0.74	32.57	0.99	0.13	5.97	0.04	100.76	0.91	0.02	0.88	0.10
	2bum2-cpx14	51.41	0.40	5.67	0.85	1.52	15.44	23.17	0.07	1.09	0.75	100.36	0.87	0.50	0.46	0.04
	2bum8-cpx1	51.62	0.27	6.04	1.22	1.36	15.73	22.74	0.04	1.17	0.77	100.96	0.88	0.49	0.47	0.04
	2bum8-opx2	54.61	0.06	5.73	0.92	0.66	32.60	0.77	0.14	5.94	0.04	101.48	0.91	0.01	0.88	0.10
	2bum8-opx3	56.56	0.03	3.36	0.53	0.49	33.99	0.61	0.15	6.00	0.03	101.75	0.91	0.01	0.89	0.09
	2bum8-opx4	53.60	0.21	5.62	0.91	0.73	26.97	8.34	0.08	4.19	0.27	100.92	0.91	0.17	0.75	0.08
	2bum8-opx11	55.71	0.10	3.94	0.56	1.19	33.37	0.87	0.14	5.77	0.04	101.68	0.91	0.02	0.88	0.10
	2bum8-cpx13	51.60	0.28	5.99	1.09	1.24	15.59	22.70	0.08	1.41	0.78	100.75	0.86	0.49	0.47	0.04
	2bum8-cpx14	51.42	0.23	6.25	1.26	1.20	15.48	22.50	0.08	1.78	0.74	100.93	0.86	0.49	0.46	0.05
	2bum8-cpx15	51.57	0.27	6.08	1.19	1.21	15.69	22.41	0.05	1.48	0.80	100.73	0.86	0.48	0.47	0.04
	2bum8-cpx16	51.65	0.24	6.39	1.19	0.97	15.45	22.56	0.04	1.72	0.82	101.02	0.86	0.49	0.47	0.04
	2rem9-cpx1	52.87	0.20	4.28	0.73	0.47	16.46	22.65	0.08	1.87	0.67	100.26	0.87	0.48	0.48	0.04
	2rem9-cpx2	52.80	0.28	4.33	0.79	1.42	16.37	23.27	0.08	0.95	0.73	101.00	0.88	0.49	0.48	0.04
	2rem9-cpx3	53.32	0.23	3.80	0.58	0.74	16.83	22.92	0.05	1.71	0.62	100.79	0.88	0.48	0.49	0.04
	2rem9-cpx4	53.06	0.20	3.86	0.69	1.42	16.70	23.35	0.05	0.76	0.68	100.75	0.89	0.48	0.48	0.03
	2rem9-cpx5	53.00	0.28	4.18	0.74	1.21	16.77	22.93	0.06	1.23	0.66	101.07	0.88	0.48	0.48	0.04
	zed2-opx1	55.02	0.05	4.48	0.73	1.34	33.52	0.74	0.09	4.90	0.01	100.96	0.93	0.01	0.89	0.09
	zed2-opx2	55.41	0.09	4.30	0.56	0.81	33.50	0.71	0.07	5.42	0.03	100.98	0.92	0.01	0.89	0.09
	zed2-opx3	54.98	0.06	4.98	0.68	0.45	33.16	0.61	0.11	5.62	0.02	100.76	0.92	0.01	0.90	0.09
	zed2-opx4	55.58	0.09	4.02	0.54	0.80	33.66	0.63	0.12	5.49	0.01	101.02	0.92	0.01	0.89	0.09
	zed2-cpx5	51.50	0.27	5.63	1.29	0.43	15.80	23.12	0.04	1.75	0.47	100.35	0.91	0.49	0.47	0.04
	zed3-cpx4	52.83	0.13	3.26	0.64	0.24	17.12	23.52	0.04	2.06	0.12	99.96	0.94	0.48	0.48	0.04
	zed3-cpx5	52.10	0.17	4.22	1.03	0.28	16.55	23.53	0.04	2.07	0.15	100.14	0.94	0.49	0.48	0.04
	zed3-opx6	55.22	0.06	4.29	0.71	0.47	33.32	0.55	0.13	5.73	0.01	100.59	0.92	0.01	0.89	0.09
	zed3-opx7	55.02	0.04	4.15	0.82	1.34	33.67	0.42	0.09	5.08	0.01	100.67	0.93	0.01	0.90	0.09
	zed3-opx8	55.28	0.05	4.17	0.69	0.81	33.62	0.47	0.10	5.36	0.01	100.69	0.92	0.01	0.90	0.09
	zed3-opx9	55.45	0.08	4.05	0.67	0.38	33.53	0.54	0.07	5.69	0.01	100.59	0.92	0.01	0.90	0.09
Harz. + dunite	2qum13-cpx1	54.45	0.02	1.49	0.60	1.21	18.17	24.60	0.08	0.83	0.07	101.50	0.97	0.48	0.49	0.03
	2qum13-cpx11	55.18	0.00	1.39	0.80	0.95	18.66	24.31	0.05	1.19	0.08	102.59	0.97	0.47	0.50	0.03
	2qum14-opx5	56.62	0.03	2.25	0.66	1.17	34.72	0.69	0.14	4.81	0.00	101.09	0.93	0.01	0.90	0.09
	2qum14-cpx5	53.28	0.02	2.62	1.14	0.64	17.39	24.23	0.06	1.50	0.03	100.92	0.98	0.48	0.48	0.03
	2qum14-opx6	56.64	0.01	2.23	0.59	0.69	34.32	1.11	0.10	5.01	0.01	100.70	0.93	0.02	0.90	0.08
	2qum14-cpx6	53.55	0.05	2.15	0.74	0.97	17.56	24.35	0.10	1.38	0.02	100.86	0.97	0.48	0.48	0.03

Tab. C.14: Pyroxènes - mélange ophiolitique (suite)

		SiO_2	TiO_2	Al_2O_3	Cr_2O_3	Fe_2O_3	MgO	CaO	MnO	FeO	Na_2O	Total	Mg#	Wo	En	Fs
	2qum14-opx12	56.72	0.00	2.46	0.80	0.32	34.25	0.74	0.15	5.65	0.00	101.09	0.92	0.01	0.90	0.09
	2qum14-cpx13	52.85	0.05	2.69	1.04	1.28	17.58	23.92	0.06	1.03	0.04	100.53	0.98	0.48	0.49	0.03
	2qum14-opx14	56.72	0.03	2.27	0.82	0.84	34.58	0.68	0.12	5.22	0.00	101.28	0.93	0.01	0.90	0.09
	2qum14-cpx15	53.31	0.06	2.53	0.99	1.35	17.47	24.61	0.07	0.91	0.03	101.33	0.98	0.49	0.48	0.03
	2qum14-cpx16	52.83	0.01	2.97	1.23	1.12	17.25	24.36	0.06	1.08	0.02	100.92	0.99	0.49	0.48	0.03
Gabbronorite	2qum13a-cpx7	53.47	0.19	0.84	0.08	0.57	23.90	1.03	0.41	19.63	0.03	100.14	0.68	0.02	0.66	0.31
	2qum13a-cpx8	54.15	0.22	0.83	0.06	0.70	24.91	1.09	0.36	18.79	0.00	101.09	0.70	0.02	0.68	0.30
	2qum13a-cpx9	54.90	0.36	1.25	0.20	0.00	15.69	22.27	0.16	6.81	0.24	101.87	0.76	0.45	0.44	0.11
	2qum13a-cpx10	53.42	0.36	1.18	0.42	0.80	16.14	22.55	0.15	5.15	0.27	100.43	0.82	0.45	0.45	0.09
	2qum13a-cpx11	53.02	0.37	1.37	0.04	0.46	14.65	21.62	0.22	8.38	0.29	100.42	0.73	0.44	0.42	0.14
	2qum13a-cpx12	52.82	0.35	1.25	0.17	1.00	15.05	21.81	0.21	7.36	0.25	100.25	0.76	0.44	0.42	0.13
	2qum13a-cpx13	52.50	0.39	1.41	0.13	1.46	14.71	21.52	0.23	8.06	0.23	100.63	0.74	0.43	0.41	0.15
	2qum13a-cpx14	52.81	0.38	1.39	0.11	1.04	14.86	21.59	0.20	7.87	0.28	100.53	0.74	0.44	0.42	0.14

Tab. C.15: Composition chimique (% poids) du spinelle des roches ultramafiques du mélange ophiolitique.

		SiO_2	TiO_2	Al_2O_3	Cr_2O_3	Fe_2O_3	MgO	CaO	MnO	FeO	ZnO	Na_2O	Total	Mg#	Cr#
Cpx-harzburgite	2bum8-sp5	0.03	0.04	53.76	14.72	1.37	19.03	0.00	0.00	11.35	0.25	0.00	100.54	0.75	0.16
	2bum8-sp17	0.02	0.03	53.10	15.67	1.75	19.21	0.00	0.00	11.25	0.15	0.00	101.19	0.75	0.17
	2bum8-sp18	0.02	0.07	52.90	15.33	2.32	19.07	0.01	0.00	11.40	0.21	0.01	101.33	0.75	0.16
	2bum8-cr18	1.02	0.08	1.36	12.15	54.34	1.44	0.01	0.04	29.12	0.05	0.01	99.61	0.08	0.86
	2lha8-sp1	0.62	0.16	12.30	44.11	8.71	2.20	0.02	0.80	27.84	1.35	0.04	98.13	0.12	0.71
	lha6-ma1	0.58	0.03	0.02	0.02	69.13	1.13	0.02	0.07	29.39			100.38	0.06	0.38
	lha6-ma2	0.29	0.08	0.01	0.01	68.72	0.07	0.00	0.08	30.90			100.16	0.00	0.40
	lha6-ma3	0.29	0.06	0.00	0.14	68.17	0.18	0.00	0.00	30.59			99.44	0.01	1.00
	lha6-ma4	0.85	0.05	0.04	0.12	67.86	0.69	0.00	0.05	29.80			99.49	0.04	0.65
	lha6-ma5	0.07	0.04	0.00	0.28	68.33	0.06	0.01	0.00	30.79			99.60	0.00	0.99
	lha7-ma1	0.30	0.10	0.02	0.11	68.43	0.36	0.00	0.10	30.31			99.74	0.02	0.83
	lha7-ma2	1.02	0.07	0.00	0.11	68.34	0.75	0.00	0.02	30.05			100.38	0.04	1.00
	lha7-ma3	0.47	0.07	0.01	0.08	67.82	0.29	0.00	0.06	30.26			99.07	0.02	0.81
	lha7-ma4	0.12	0.10	0.01	0.09	67.16	0.07	0.00	0.00	30.19			97.77	0.00	0.86
	lha7-ma5	0.27	0.06	0.04	0.08	68.40	0.25	0.00	0.09	30.44			99.65	0.01	0.59
	2daz4-ma2	0.11	0.02	0.01	0.10	69.06	0.03	0.00	0.01	31.08			100.46	0.00	0.84
	2rem9-ma3	0.55	0.01	0.05	0.22	68.82	0.62	0.02	0.09	29.92			100.28	0.04	0.76

Tab. C.15: Spinelle - mélange ophiolitique (suite)

		SiO_2	TiO_2	Al_2O_3	Cr_2O_3	Fe_2O_3	MgO	CaO	MnO	FeO	ZnO	Na_2O	Total	Mg#	Cr#
	2rem9-ma7	0.08	0.05	0.01	0.32	68.79	0.09	0.00	0.09	30.95			100.42	0.01	0.94
	zed2-sp11	0.03	0.05	48.93	19.83	1.28	18.71	0.00	0.00	10.92	0.15	0.03	99.92	0.75	0.21
	zed2-sp12	0.02	0.04	50.41	18.13	1.36	18.53	0.00	0.00	11.50	0.23	0.00	100.22	0.74	0.19
	zed2-sp13	0.02	0.04	50.08	18.34	1.66	18.50	0.00	0.00	11.55	0.20	0.01	100.40	0.74	0.20
	zed2-sp14	0.03	0.06	49.12	18.98	1.75	18.64	0.00	0.00	11.06	0.16	0.00	99.80	0.75	0.21
	zed2-sp15	0.03	0.06	49.96	18.51	1.36	18.47	0.00	0.00	11.50	0.19	0.01	100.08	0.74	0.20
	zed3-sp11	0.00	0.05	44.02	23.06	2.72	16.91	0.00	0.00	12.86	0.15	0.01	99.79	0.70	0.26
	zed3-sp12	0.02	0.06	43.66	23.11	2.89	16.70	0.00	0.00	13.12	0.12	0.01	99.69	0.69	0.26
	zed3-sp13	0.03	0.05	43.75	23.70	2.44	17.22	0.00	0.00	12.29	0.15	0.02	99.65	0.71	0.27
	zed3-sp14	0.02	0.03	44.89	21.84	3.19	17.24	0.00	0.00	12.55	0.14	0.00	99.90	0.71	0.25
	zed3-sp15	0.03	0.06	43.29	23.71	2.83	16.86	0.00	0.00	12.81	0.17	0.00	99.76	0.70	0.27
Harz. trans.	bei11-sp1	0.01	0.04	30.27	36.18	4.00	13.24	0.00	0.00	16.47	0.21	0.00	100.43	0.59	0.44
	bei11-sp2	0.00	0.06	30.77	35.91	3.42	13.24	0.00	0.00	16.43	0.19	0.01	100.03	0.59	0.44
	bei11-sp3	0.04	0.02	31.08	35.17	3.75	13.26	0.00	0.00	16.42	0.17	0.02	99.94	0.59	0.43
	bei11-sp4	0.12	0.02	29.88	36.78	3.73	12.82	0.02	0.00	17.05	0.24	0.03	100.70	0.57	0.45
	bei11-sp5	0.03	0.03	28.98	37.39	4.11	12.70	0.00	0.00	17.11	0.24	0.01	100.60	0.57	0.46
	2lus3-sp1	0.01	0.04	36.46	31.92	2.27	15.44	0.00	0.00	14.18	0.13	0.01	100.45	0.66	0.37
	2lus3-sp2	0.01	0.01	37.56	30.39	2.23	15.36	0.00	0.00	14.28	0.20	0.01	100.04	0.66	0.35
	2lus3-sp3	0.02	0.01	37.18	30.85	2.20	15.30	0.00	0.00	14.33	0.21	0.00	100.10	0.66	0.36
	2bag5-sp1	0.02	0.13	10.59	50.65	6.93	3.91	0.00	0.00	27.11	0.54	0.02	99.89	0.20	0.76
	2bag5-sp2	0.03	0.09	18.82	44.78	4.88	6.03	0.00	0.00	25.29	0.66	0.03	100.59	0.30	0.61
	2bag5-cr3	0.62	0.20	4.33	52.76	10.07	2.62	0.01	0.00	27.83	0.47	0.02	98.92	0.14	0.89
Harz. part.	lha39-sp1	0.03	0.02	28.57	40.44	1.58	14.25	0.01	0.00	14.46	0.05	0.03	99.44	0.64	0.49
	lha39-sp2	0.05	0.02	28.67	40.85	1.28	14.77	0.00	0.00	13.61	0.14	0.03	99.42	0.66	0.49
	lha39-sp3	0.02	0.03	28.40	41.12	1.15	14.67	0.00	0.00	13.74	0.11	0.00	99.25	0.66	0.49
	lha39-sp4	0.71	0.01	28.18	40.58	1.37	14.64	0.25	0.00	13.54	0.14	0.00	99.41	0.66	0.49
	2day4-cr1	1.71	1.06	0.83	26.21	39.02	2.13	0.14	4.41	23.10	0.48	0.02	99.11	0.14	0.96
	2day4-cr2	1.53	0.63	1.63	24.79	40.33	2.07	0.02	3.68	24.52	0.29	0.00	99.47	0.13	0.91
Harz. + dunite	lha27-sp1	0.01	0.05	16.06	47.68	5.95	7.90	0.00	0.00	22.18	0.02		100.14	0.39	0.67
	lha27-sp3	0.03	0.00	26.91	42.91	1.73	13.50	0.00	0.00	15.76	0.00		101.08	0.60	0.52
	lha27-ma4	0.80	0.01	0.00	1.96	65.32	0.27	0.00	0.00	30.32			98.68	0.02	1.00
	lha28-sp1	0.04	0.08	30.94	37.91	2.47	14.77	0.00	0.00	14.36	0.01		100.78	0.65	0.45
	lha28-sp2	0.01	0.05	31.20	37.81	2.58	15.19	0.00	0.00	13.88	0.00		100.82	0.66	0.45
	lha28-sp3	0.03	0.06	30.17	38.02	2.80	14.59	0.00	0.00	14.43	0.00		100.21	0.64	0.46

Tab. C.15: Spinelle - mélange ophiolitique (suite)

		SiO_2	TiO_2	Al_2O_3	Cr_2O_3	Fe_2O_3	MgO	CaO	MnO	FeO	ZnO	Na_2O	Total	Mg#	Cr#
	lha28-sp4	0.04	0.07	30.33	38.23	0.00	12.56	0.00	0.00	16.84	0.01		98.15	0.57	0.46
	lha28-ma11	0.02	0.00	0.02	2.17	67.58	0.07	0.00	0.00	31.27			101.19	0.00	0.99
	2liu5-sp1	0.03	0.02	29.62	39.08	2.81	14.56	0.00	0.00	14.56	0.12	0.01	100.81	0.64	0.47
	2liu5-sp2	0.02	0.04	29.10	38.23	3.69	14.22	0.00	0.00	14.74	0.14	0.02	100.20	0.63	0.47
	2liu5-sp3	0.20	0.02	29.93	37.16	4.56	14.46	0.01	0.00	14.88	0.17	0.01	101.39	0.63	0.45
	jid4-sp1	0.01	0.02	29.00	38.32	3.44	13.26	0.00	0.00	16.35	0.10	0.01	100.51	0.59	0.47
	jid4-sp2	0.03	0.01	25.82	40.88	3.51	11.62	0.00	0.00	18.16	0.28	0.00	100.31	0.53	0.52
	jid4-sp3	0.04	0.02	25.72	39.75	3.83	10.12	0.01	0.00	20.33	0.28	0.01	100.12	0.47	0.51
	jid4-sp4	0.00	0.02	29.27	37.84	3.19	13.31	0.00	0.00	16.04	0.22	0.00	99.88	0.60	0.46
	2qum7-sp1	0.04	0.04	33.81	35.83	2.05	15.65	0.00	0.00	13.68	0.18	0.00	101.27	0.67	0.42
	2qum7-sp2	0.01	0.04	33.03	36.38	1.35	15.37	0.00	0.00	13.57	0.11	0.02	99.87	0.67	0.42
	2qum7-sp3	0.01	0.03	31.88	37.98	1.94	15.79	0.00	0.00	13.00	0.11	0.03	100.76	0.68	0.44
	2qum7-sp4	0.02	0.02	34.34	35.34	2.01	15.89	0.00	0.00	13.38	0.12	0.00	101.12	0.68	0.41
	2qum7-sp5	0.03	0.04	33.49	35.91	2.13	15.44	0.00	0.00	13.91	0.13	0.01	101.09	0.66	0.42
	2qum11-sp1	0.00	0.08	33.90	33.96	2.37	14.28	0.00	0.00	15.43	0.16	0.01	100.17	0.62	0.40
	2qum11-sp2	0.02	0.09	31.67	36.29	2.48	14.31	0.00	0.00	14.96	0.16	0.02	100.00	0.63	0.43
	2qum11-sp3	0.02	0.13	31.95	37.15	2.67	15.05	0.00	0.00	14.37	0.15	0.01	101.49	0.65	0.44
	2qum11-sp4	0.03	0.12	30.82	37.79	3.44	14.58	0.00	0.00	14.94	0.24	0.03	101.98	0.63	0.45
	2qum11-sp5	0.04	0.14	31.84	36.67	2.41	14.89	0.00	0.00	14.18	0.24	0.00	100.41	0.65	0.44
	2qum11-sp6	0.06	0.12	31.86	36.76	2.64	14.64	0.00	0.00	14.87	0.14	0.00	101.10	0.64	0.44
	2qum13-sp1	0.03	0.04	20.84	47.32	3.26	12.51	0.00	0.00	16.10	0.16	0.00	100.26	0.58	0.60
	2qum13-sp2	0.04	0.03	21.02	46.69	2.53	11.60	0.00	0.00	17.26	0.13	0.00	99.30	0.54	0.60
	2qum13-sp3	0.03	0.01	19.58	48.76	2.98	12.24	0.00	0.00	16.26	0.13	0.01	99.98	0.57	0.63
	2qum13-sp4	0.03	0.00	19.52	48.02	3.24	11.56	0.00	0.00	17.23	0.08	0.01	99.68	0.54	0.62
	2qum13-sp5	0.01	0.02	19.39	49.21	2.66	12.13	0.00	0.00	16.38	0.14	0.00	99.93	0.57	0.63
	2qum14-sp1	0.03	0.01	32.55	36.02	2.01	14.69	0.00	0.00	14.51	0.20	0.01	100.02	0.64	0.43
	2qum14-sp2	0.05	0.04	28.92	40.80	1.34	14.82	0.00	0.00	13.77	0.12	0.01	99.84	0.66	0.49
	2qum14-sp3	0.03	0.02	29.33	40.14	2.09	14.80	0.00	0.00	14.04	0.20	0.01	100.65	0.65	0.48
	2qum14-sp4	0.00	0.02	28.89	40.98	1.93	14.82	0.00	0.00	14.05	0.13	0.01	100.83	0.65	0.49
	2day6-sp1	0.02	0.04	30.82	37.04	3.09	13.75	0.00	0.00	15.90	0.24	0.01	100.92	0.61	0.45
	2day6-sp2	0.02	0.02	30.35	37.81	2.91	13.55	0.00	0.00	16.23	0.18	0.02	101.09	0.60	0.46
	2day6-sp3	0.02	0.01	30.50	37.54	2.19	13.62	0.00	0.00	15.79	0.18	0.01	99.85	0.61	0.45
	2day8-cr1	0.01	0.08	24.46	44.59	2.03	12.39	0.00	0.00	16.97	0.18	0.02	100.73	0.57	0.55
	2day8-cr2	0.01	0.08	22.27	47.24	1.63	12.13	0.00	0.00	17.04	0.14	0.00	100.55	0.56	0.59
	2day8-ma3	0.08	0.08	0.01	2.85	67.94	0.11	0.00	0.00	31.86			102.92	0.01	1.00
Diabase	2qum8-sp16	0.08	0.20	28.65	37.89	4.16	13.30	0.01	0.00	16.32	0.05	0.01	100.67	0.59	0.47

Tab. C.15: Spinelle - mélange ophiolitique (suite)

	SiO_2	TiO_2	Al_2O_3	Cr_2O_3	Fe_2O_3	MgO	CaO	MnO	FeO	ZnO	Na_2O	Total	Mg#	Cr#
2qum8-sp17	0.08	0.19	28.60	39.59	3.71	16.28	0.01	0.00	11.49	0.13	0.02	100.08	0.72	0.48
2qum8-sp18	0.11	0.23	29.10	38.92	4.37	16.52	0.01	0.00	11.54	0.02	0.01	100.82	0.72	0.47

Annexe D

Données de lithogéochimie

Tab. D.1: Composition chimique (éléments majeurs en % poids) des roches mafiques du mélange ophiolitique.

		SiO_2	TiO_2	Al_2O_3	$Fe_2O_3^T$	MnO	MgO	CaO	Na_2O	K_2O	P_2O_5	Total	P.A.F.
Gabbro	2001-LHA-16	49.67	1.06	16.11	10.01	0.17	7.19	12.57	2.91	0.12	0.08	*99.89*	3.02
	2001-LHA-18	57.42	0.38	18.90	3.60	0.07	2.62	10.79	6.08	0.04	0.03	*99.94*	1.99
	2001-LHA-18	57.42	0.38	19.04	3.62	0.07	2.56	10.67	6.11	0.06	0.03	*99.96*	1.99
	2002-BUM-06	52.40	1.26	15.22	10.74	0.18	7.01	7.85	5.05	0.07	0.11	*99.88*	3.18
	2002-MAM-07	45.52	0.64	14.15	8.39	0.18	16.82	13.69	0.46	0.03	0.04	*99.91*	5.36
	2002-LIU-07	51.02	1.31	16.91	10.99	0.17	4.69	8.37	6.11	0.18	0.12	*99.86*	3.11
	2002-LIU-09	52.60	1.18	17.10	9.83	0.16	4.09	7.85	6.79	0.19	0.11	*99.91*	2.70
	2002-LIU-09	52.32	1.19	17.06	10.00	0.16	4.09	8.01	6.77	0.20	0.11	*99.91*	2.65
	2001-JID-01	56.01	1.04	14.55	9.49	0.22	7.33	5.44	5.74	0.10	0.08	*100.01*	2.34
	2001-JID-02	51.05	0.92	16.00	8.88	0.17	9.12	9.30	3.56	0.92	0.08	*100.00*	3.56
	2001-JID-03	51.74	1.05	13.77	10.38	0.17	11.27	7.45	2.07	2.03	0.09	*100.02*	2.94
	2001-JID-05	52.37	0.69	14.98	9.44	0.15	6.88	20.65	0.54	0.03	0.08	*105.82*	3.00
	2002-QUM-01	59.30	0.43	15.35	8.62	0.12	8.33	8.84	3.56	0.75	0.05	*105.33*	3.42
	2002-QUM-03	50.58	0.60	11.43	8.13	0.15	8.04	9.33	4.54	0.03		*92.84*	1.48
	2002-QUM-04	51.33	1.20	15.78	8.90	0.15	8.18	10.31	3.95	0.11	0.04	*99.95*	3.69
	2002-QUM-12	46.84	1.11	15.79	11.06	0.18	6.27	9.95	3.65	0.62	0.08	*95.55*	2.75
	2001-BEI-03	45.19	1.15	16.99	9.03	0.14	7.86	19.17	0.25	0.02	0.08	*99.89*	5.02
	2001-BEI-04	53.33	0.82	16.46	8.35	0.14	7.34	8.70	4.30	0.35	0.07	*99.87*	2.46
	2001-BEI-06	51.71	0.93	16.37	8.20	0.16	8.91	9.76	3.33	0.43	0.06	*99.87*	3.56
	2001-BEI-12	48.36	0.69	14.89	7.73	0.14	8.54	19.14	0.30	0.02	0.05	*99.87*	3.36
	2002-LUS-04	50.22	0.82	16.06	7.71	0.12	7.63	14.25	2.52	0.08	0.06	*99.48*	3.20
	2002-BAG-08	48.79	0.20	19.47	4.80	0.09	8.61	14.92	2.24	0.74		*99.85*	4.38
	2002-DAZ-02	55.91	0.95	16.42	9.37	0.14	5.42	5.30	6.21	0.05	0.14	*99.92*	2.52

Tab. D.1: Roches mafiques - mélange ophiolitique (suite)

		SiO_2	TiO_2	Al_2O_3	$Fe_2O_3^T$	MnO	MgO	CaO	Na_2O	K_2O	P_2O_5	Total	P.A.F.
	2002-DAZ-07	50.56	1.41	14.07	11.14	0.17	8.46	10.30	3.50	0.18	0.11	*99.89*	1.98
	2002-DAZ-08	49.58	1.84	13.48	12.36	0.19	7.67	10.93	3.62	0.05	0.15	*99.87*	2.53
	2002-LHA-04	52.09	1.21	15.55	10.96	0.17	7.62	7.26	4.72	0.22	0.10	*99.91*	3.43
	2002-LHA-06	58.01	0.93	15.59	8.77	0.19	5.73	3.32	7.22	0.04	0.09	*99.90*	2.33
	2001-LHA-13	54.21	0.76	14.52	9.10	0.15	8.39	7.98	4.24	0.48	0.07	*99.87*	2.29
Diabase	2001-LHA-17	49.12	1.02	15.93	10.32	0.17	8.12	11.77	3.30	0.13		*99.87*	3.71
	2001-LHA-19	53.16	1.21	15.67	9.44	0.12	5.38	9.47	5.28	0.06	0.09	*99.87*	3.24
	2001-LHA-20	54.24	1.12	14.90	8.69	0.15	6.40	9.49	4.62	0.16	0.11	*99.88*	2.39
	2002-BUM-03	61.25	0.91	17.25	4.57	0.06	1.84	5.07	4.85	3.31	0.42	*99.52*	2.09
	2001-LHA-38	36.59	1.49	23.00	13.23	0.20	8.65	16.54	0.04		0.13	*99.87*	7.31
	2002-MAM-06	45.07	1.16	15.59	9.86	0.19	8.60	19.05	0.28	0.03	0.09	*99.92*	4.08
	2002-LIU-01	54.21	1.73	16.09	12.55	0.19	3.97	6.66	4.33	0.04	0.15	*99.89*	3.29
	2002-LIU-02	53.93	1.10	16.28	10.48	0.19	5.57	8.31	3.55	0.42	0.10	*99.93*	2.88
	2002-LIU-03	54.91	1.39	16.12	11.36	0.19	5.09	5.84	4.84	0.06	0.12	*99.93*	3.08
	2002-LIU-04	50.48	1.30	15.36	11.22	0.18	6.90	9.57	4.48	0.09	0.10	*99.67*	2.62
	2002-QUM-02	50.45	1.06	15.88	10.29	0.17	8.04	9.81	3.77	0.33	0.08	*99.88*	3.53
	2002-QUM-08	50.44	1.18	15.79	10.97	0.18	7.45	9.21	4.32	0.24	0.10	*99.87*	3.35
	2001-BEI-10	55.10	0.79	14.86	7.59	0.14	6.42	10.44	4.50	0.03	0.05	*99.92*	2.12
	2002-BAG-07	52.73	0.54	15.68	7.30	0.13	7.76	11.29	4.28	0.06	0.11	*99.88*	2.46
	2002-DAZ-03	55.70	1.16	15.05	11.74	0.17	4.15	5.69	5.96	0.20	0.09	*99.90*	1.32
Basalte	2001-BEI-01	45.10	1.08	16.09	9.71	0.21	10.41	16.81	0.34	0.03	0.08	*99.87*	4.66
	2001-BEI-07	50.68	1.18	12.45	10.49	0.23	14.01	8.51	2.04	0.17	0.07	*99.83*	5.34

Tab. D.1: Roches mafiques - mélange ophiolitique (suite)

		SiO_2	TiO_2	Al_2O_3	$Fe_2O_3^T$	MnO	MgO	CaO	Na_2O	K_2O	P_2O_5	Total	P.A.F.
	2001-BEI-09	51.76	1.03	13.38	8.18	0.15	10.15	12.39	2.71	0.04	0.08	*99.87*	2.72
	2001-LHA-15	49.18	1.05	17.79	11.62	0.17	9.69	5.53	4.26	0.43	0.09	*99.81*	4.96
	2001-JNL-01	57.58	0.85	17.35	7.00	0.21	4.13	4.79	4.08	3.39	0.38	*99.74*	2.06
	2001-ZED-01	51.91	0.84	17.41	9.80	0.19	4.69	7.90	3.99	2.85	0.43	*100.01*	1.84

Tab. D.2: Composition chimique (éléments majeurs en % poids) des roches mafiques du mélange de Yamdrock.

		SiO_2	TiO_2	Al_2O_3	$Fe_2O_3^T$	MnO	MgO	CaO	Na_2O	K_2O	P_2O_5	Total	P.A.F.
Gabbro	2002-BAG-03	49.52	3.73	12.62	14.90	0.24	5.57	7.75	3.90	1.15	0.46	*99.83*	3.23
	2002-BAG-04	47.60	3.20	12.56	15.60	0.22	7.15	9.47	2.76	0.94	0.31	*99.81*	2.35
	2001-LHA-10	45.67	4.99	17.89	17.18	0.14	8.10	1.93	3.42	0.02	0.49	*99.83*	5.91
	2001-LHA-33	44.24	1.51	18.21	11.90	0.21	8.26	13.54	1.88	0.02	0.11	*99.87*	5.45
	2001-BAG-04	49.10	3.56	14.46	14.18	0.20	5.09	8.09	4.20	0.59	0.35	*99.82*	2.27
Diabase	2002-MAM-01	49.65	1.21	16.92	11.00	0.17	6.38	9.85	4.24	0.35	0.10	*99.87*	3.85
	2002-MAM-02	50.10	2.58	16.23	11.82	0.23	7.67	5.58	5.14	0.24	0.28	*99.87*	3.69
	2002-MAM-05	49.48	4.00	13.05	15.66	0.32	5.32	6.65	4.45	0.40	0.48	*99.81*	2.71
	2002-BAG-01	48.08	3.92	12.66	16.97	0.30	5.87	6.51	4.39	0.66	0.50	*99.87*	2.27
	2001-LHA-11	49.99	2.98	15.32	12.73	0.16	6.84	9.64	1.78	0.03	0.36	*99.84*	6.89
	2001-LHA-36	49.04	2.98	14.74	16.01	0.25	5.03	7.13	4.13	0.04	0.45	*99.80*	3.87
	2001-BAG-02	48.72	3.41	14.00	13.63	0.33	6.18	7.87	4.28	0.91	0.49	*99.83*	3.93
	2001-BAG-03	48.71	3.71	13.61	15.42	0.20	5.18	8.13	4.39	0.13	0.35	*99.82*	2.40

Tab. D.2: Roches mafiques - mélange de Yamdrock (suite)

		SiO_2	TiO_2	Al_2O_3	$Fe_2O_3^T$	MnO	MgO	CaO	Na_2O	K_2O	P_2O_5	Total	P.A.F.
Basalte	2002-REM-11	47.53	2.07	17.24	12.78	0.18	1.92	9.02	4.12	3.06	1.92	*99.85*	7.20
	2002-BUM-11	50.21	2.11	14.58	12.72	0.21	6.35	10.00	3.39	0.12	0.19	*99.88*	6.78
	2001-LHA-35	50.97	1.71	15.26	8.21	0.11	5.05	13.96	4.12	0.16	0.29	*99.85*	5.69
	2001-LHA-37	45.61	4.94	16.13	16.79	0.44	5.99	5.63	3.58	0.01	0.68	*99.80*	5.19
	2001-LHA-09	49.30	3.75	14.79	16.54	0.29	6.58	4.48	3.61	0.03	0.43	*99.80*	4.96
	2001-LHA-01	48.47	3.93	13.07	14.88	0.18	4.87	8.64	2.76	2.50	0.50	*99.81*	2.63
	2001-LHA-02	49.91	4.13	13.06	14.79	0.18	4.50	8.84	3.70	0.12	0.56	*99.80*	3.77
	2001-LHA-05	49.80	2.98	13.99	13.72	0.16	6.01	7.94	4.52	0.33	0.30	*99.75*	4.63
	2002-XIA-01	46.87	4.29	14.70	15.70	0.13	5.83	7.04	4.47	0.24	0.50	*99.79*	5.12
	2002-XIA-04	47.60	4.30	12.79	17.02	0.21	4.41	8.21	4.17	0.44	0.59	*99.75*	2.36
	2001-ZIS-08	48.41	1.97	16.44	14.26	0.21	6.98	6.86	4.50	0.04	0.19	*99.86*	3.75
	2001-ZIS-09	48.06	1.64	17.03	9.91	0.17	5.33	14.04	3.30	0.02	0.31	*99.82*	5.02
	2001-ZIS-10	47.44	4.73	12.68	16.68	0.22	6.36	7.54	2.90	0.65	0.57	*99.78*	3.76
	2001-BAG-01	49.50	2.30	13.72	14.15	0.20	6.67	9.14	3.76	0.08	0.29	*99.81*	2.57
	2001-BAG-05	50.13	2.25	13.61	14.54	0.28	6.76	8.03	3.77	0.13	0.30	*99.80*	2.68
	2002-REM-06	47.75	4.13	18.10	17.38	0.10	5.15	2.43	2.13	1.63	1.04	*99.84*	5.36
	2002-REM-08	47.15	3.08	18.94	11.54	0.13	10.44	3.32	3.11	1.56	0.59	*99.86*	5.80

TAB. D.3: Composition chimique (éléments majeurs en % poids) des roches mafiques du flysch triasique.

		SiO_2	TiO_2	Al_2O_3	$Fe_2O_3^T$	MnO	MgO	CaO	Na_2O	K_2O	P_2O_5	Total	P.A.F.
Granite	2001-QUN-03	64.99	0.39	16.70	2.24	0.04	0.97	2.73	3.77	7.20	0.28	*99.31*	3.34
	2001-QUN-03	65.68	0.39	16.46	2.22	0.04	0.94	2.67	3.70	7.00	0.28	*99.37*	3.34
Gabbro	2001-ZIS-03	49.41	3.01	14.92	12.82	0.17	5.93	8.80	2.14	2.17	0.37	*99.74*	3.15
	2001-ZIS-04	57.82	1.77	15.75	9.03	0.14	2.04	5.12	4.75	2.79	0.57	*99.78*	1.77
	2001-ZIS-05	51.47	2.24	15.24	10.45	0.16	6.36	9.95	2.53	1.07	0.26	*99.72*	3.03
	2001-ZIS-06	58.07	1.97	14.52	9.35	0.13	4.15	6.85	2.55	1.92	0.31	*99.82*	2.95
	2002-ZIS-05	48.98	3.08	14.74	13.12	0.17	5.77	9.65	2.51	1.42	0.40	*99.85*	3.38
	2002-ZIS-07	53.65	2.31	14.86	11.37	0.15	4.85	7.78	3.00	1.46	0.36	*99.80*	2.94
	2002-ZIS-08	58.56	2.10	12.93	11.75	0.18	2.25	5.81	3.16	2.37	0.66	*99.79*	1.92
	2002-ZIS-09	56.62	2.05	15.72	9.83	0.13	2.35	6.36	3.98	2.33	0.39	*99.77*	2.11
	2002-ZIS-10	54.78	2.14	15.43	11.06	0.17	2.19	5.76	4.74	2.69	0.78	*99.74*	2.67
	2002-ZIS-11	57.16	1.92	14.41	9.76	0.12	4.26	7.05	3.27	1.59	0.32	*99.86*	2.80
	2001-LHA-29A	48.79	1.49	15.13	13.34	0.21	7.07	11.09	2.55	0.03	0.10	*99.80*	11.45
	2001-LHA-29B	47.36	1.63	16.37	14.81	0.19	7.24	8.78	3.33	0.02	0.11	*99.83*	10.08
	2001-LHA-30	53.05	3.21	13.76	12.65	0.14	6.24	8.06	2.39		0.39	*99.88*	9.00
	2001-LHA-31	49.11	1.45	14.96	13.53	0.21	7.00	10.56	2.87	0.05	0.11	*99.85*	2.24
	2002-LHA-13	45.83	1.60	16.18	14.98	0.21	7.44	10.42	3.05	0.03	0.13	*99.87*	11.01
Diabase	2002-PAZ-01	56.97	1.93	14.44	9.57	0.14	4.79	7.24	2.61	1.83	0.30	*99.82*	3.01
	2002-PAZ-06	50.21	2.60	14.50	12.41	0.16	6.80	9.23	2.60	0.95	0.34	*99.80*	3.28
	2002-MAS-02	54.05	4.21	13.79	12.95	0.13	4.76	5.00	3.98	0.26	0.62	*99.76*	7.16
	2002-MAS-03	51.09	4.37	14.20	12.83	0.18	5.08	6.99	4.29	0.11	0.64	*99.78*	7.73

Tab. D.3: Roches mafiques - flysch triasique (suite)

		SiO_2	TiO_2	Al_2O_3	$Fe_2O_3^T$	MnO	MgO	CaO	Na_2O	K_2O	P_2O_5	Total	P.A.F.
	2001-ZIS-01	51.23	3.11	15.59	12.94	0.13	6.94	5.25	3.06	0.86	0.39	*99.50*	6.18
	2002-ZIS-06	70.15	0.44	13.96	3.10	0.04	0.57	8.39	3.03	0.12	0.07	*99.87*	2.35
	2001-LHA-32	51.32	3.80	12.78	14.69	0.18	4.05	7.04	3.70	1.47	0.55	*99.60*	5.33
	2001-ZIS-07	51.12	2.79	14.60	12.19	0.17	6.06	6.97	4.44	1.17	0.33	*99.83*	2.64
Basalte	2002-PAZ-05	50.26	3.24	15.46	13.86	0.16	6.40	6.47	2.73	0.82	0.41	*99.82*	8.51
	2002-PAZ-07	50.46	3.11	14.23	11.72	0.16	5.55	9.56	4.37	0.32	0.37	*99.85*	2.49
	2001-ZIS-02	49.22	3.08	15.43	14.53	0.15	7.74	6.27	2.71	0.17	0.39	*99.69*	6.12
	2002-PAZ-09	52.13	2.77	14.61	12.38	0.19	6.47	10.04	0.54	0.40	0.34	*99.87*	9.60
	2002-PAZ-09	51.58	2.80	14.57	12.76	0.19	6.41	10.29	0.54	0.40	0.34	*99.87*	9.46
	2002-DZU-01	42.51	3.16	16.55	15.81	0.30	4.18	12.00	4.10	0.76	0.47	*99.82*	11.56

TAB. D.4: Composition chimique (éléments traces en ppm) des roches mafiques du mélange ophiolitique.

	Cr	V	Y	Zr	Nb	La	Ce	Pr	Nd	Sm	Eu	Gd	Tb	Dy	Ho	Er	Tm	Yb	Lu	Hf	Ta	Th	U
2001-LHA-16	178.4	238.5	23.7	58.6	0.95	2.04	6.83	1.17	6.57	2.32	0.96	3.32	0.57	4.10	0.87	2.62	0.37	2.46	0.37	1.54	0.06	0.06	<0.02
2001-LHA-18	36.6	96.6	19.6	150.7	0.90	3.59	9.35	1.30	5.91	1.72	0.63	2.37	0.42	2.94	0.64	2.00	0.30	2.09	0.33	3.60	0.09	0.62	0.28
2001-LHA-18	37.5	92.6	19.8	118.8	0.91	3.39	9.07	1.24	5.72	1.75	0.62	2.27	0.42	2.69	0.68	1.90	0.30	2.14	0.33	3.06	0.10	0.55	0.26
2002-BUM-06	170.0	265.4	31.5	89.5	1.14	2.74	9.48	1.56	8.61	3.02	1.25	4.15	0.75	4.76	1.17	3.19	0.47	3.18	0.47	2.15	0.09	0.09	0.04
2002-MAM-07	271.0	160.6	18.2	38.3	0.32	1.10	4.18	0.81	4.53	1.65	0.68	2.31	0.42	2.62	0.63	1.72	0.26	1.73	0.24	0.99	0.02		
2002-LIU-07	35.9	279.2	36.8	109.5	1.39	3.09	10.69	1.76	9.35	3.31	1.22	4.45	0.80	5.16	1.28	3.54	0.54	3.58	0.52	2.43	0.10	0.10	0.05
2002-LIU-09	36.2	241.8	35.4	108.5	1.35	3.59	11.36	1.85	9.65	3.28	1.22	4.48	0.82	5.18	1.26	3.52	0.53	3.61	0.51	2.61	0.11	0.20	0.09
2002-LIU-09	34.0	237.9	32.4	98.3	1.31	3.45	11.03	1.78	9.53	3.17	1.18	4.40	0.81	5.10	1.24	3.47	0.52	3.55	0.52	2.60	0.11	0.20	0.09
2001-JID-01	37.1	251.2	22.4	57.4	0.53	1.78	5.67	0.92	5.61	2.11	0.71	3.13	0.60	4.07	0.86	2.54	0.38	2.44	0.38	1.83	0.03	0.22	0.06
2001-JID-02	210.5	228.7	21.1	53.0	0.46	1.83	6.12	0.96	5.76	2.00	0.94	3.09	0.57	3.85	0.82	2.39	0.36	2.38	0.36	1.63	0.03	0.05	0.04
2001-JID-03	449.7	211.1	24.8	74.5	0.70	2.24	7.36	1.17	7.01	2.45	0.91	3.56	0.66	4.43	0.95	2.75	0.42	2.68	0.41	2.33	0.05	0.13	0.05
2001-JID-05	111.0	236.3	25.7	54.2	1.15	1.79	6.24	1.16	6.49	2.40	0.95	3.53	0.60	4.29	0.92	2.66	0.38	2.47	0.37	1.39	0.07		
2002-QUM-01	203.5	200.1	18.1	41.5	0.26	0.85	3.56	0.68	3.97	1.57	0.60	2.18	0.43	2.70	0.66	1.80	0.27	1.81	0.26	1.11	0.02		0.02
2002-QUM-03	664.6	170.4	15.1	22.3	0.21	0.93	3.27	0.60	3.49	1.40	0.48	1.94	0.36	2.34	0.56	1.47	0.22	1.41	0.20	0.64	0.01		
2002-QUM-04	140.2	217.9	17.1	34.0	0.36	1.03	3.71	0.64	3.66	1.40	0.58	2.05	0.39	2.66	0.64	1.83	0.27	1.86	0.27	0.93	0.03		0.02
2002-QUM-12	101.2	291.3	31.7	76.9	1.05	2.29	7.78	1.34	7.41	2.80	1.05	3.75	0.70	4.48	1.08	2.90	0.46	3.03	0.43	1.90	0.08	0.08	0.04
2001-BEI-03	159.0	220.2	26.4	81.0	0.80	2.12	7.93	1.42	7.85	2.73	0.89	3.77	0.64	4.49	0.95	2.71	0.38	2.49	0.37	1.96	0.05	0.11	0.02
2001-BEI-04	267.6	197.4	22.2	62.9	0.77	1.82	6.07	1.06	5.84	2.09	0.83	2.96	0.51	3.64	0.79	2.30	0.33	2.16	0.32	1.72	0.11	0.12	0.05
2001-BEI-06	122.4	216.3	22.4	60.2	0.73	1.81	6.26	1.13	6.18	2.21	0.93	3.06	0.52	3.76	0.80	2.35	0.33	2.14	0.32	1.56	0.07	0.06	0.02
2001-BEI-12	380.1	173.7	19.4	51.3	0.63	1.39	5.19	0.88	4.73	1.75	0.73	2.43	0.41	2.77	0.65	1.79	0.25	1.72	0.25	1.24	0.03	0.08	0.04
2002-LUS-04	243.6	203.1	18.7	59.1	0.57	1.68	6.08	1.02	5.74	1.98	0.82	2.78	0.48	3.01	0.76	2.00	0.31	2.02	0.29	1.46	0.05	0.06	0.03
2002-BAG-08	626.3	91.8	6.3	9.3	0.10	0.37	1.36	0.25	1.50	0.59	0.32	0.83	0.16	1.06	0.25	0.68	0.10	0.73	0.10	0.33	0.01		
2002-DAZ-02	51.2	179.4	33.8	108.6	1.33	2.70	8.70	1.55	8.61	3.25	0.90	4.41	0.80	5.14	1.22	3.42	0.50	3.31	0.47	2.50	0.11	0.12	0.06
2002-DAZ-07	215.5	316.6	39.5	90.5	1.01	2.44	9.03	1.63	9.62	3.59	1.38	4.84	0.89	5.80	1.40	3.85	0.56	3.87	0.54	2.17	0.07	0.05	0.03
2002-DAZ-08	217.7	363.5	53.2	133.9	1.70	3.71	13.50	2.41	13.47	4.91	2.03	6.67	1.20	7.64	1.82	4.97	0.74	4.88	0.71	2.97	0.11	0.06	0.03
2002-LHA-04	115.7	283.3	32.5	80.4	1.09	2.88	9.35	1.59	8.46	2.97	0.96	4.03	0.74	4.83	1.18	3.27	0.48	3.26	0.46	1.99	0.09	0.09	0.09
2002-LHA-06	266.0	214.9	24.6	106.0	4.72	11.30	26.44	3.39	14.17	3.46	1.06	3.85	0.64	3.90	0.92	2.46	0.38	2.55	0.36	2.62	0.35	4.01	0.79
2001-LHA-13	385.4	218.8	20.7	59.8	0.84	1.83	5.77	1.00	5.54	1.89	0.67	2.76	0.47	3.53	0.75	2.26	0.33	2.17	0.34	1.44	0.05	0.08	0.03

Tab. D.4: Roches mafiques - mélange ophiolitique (suite)

	Cr	V	Y	Zr	Nb	La	Ce	Pr	Nd	Sm	Eu	Gd	Tb	Dy	Ho	Er	Tm	Yb	Lu	Hf	Ta	Th	U
2001-LHA-17	247.4	273.1	16.4	16.1	0.48	0.65	2.36	0.50	3.19	1.37	0.87	2.12	0.39	2.86	0.60	1.80	0.25	1.66	0.24	0.52	0.03		
2001-LHA-19	43.1	264.9	28.5	77.5	1.21	2.75	8.58	1.47	8.15	2.82	1.18	4.12	0.69	4.98	1.04	3.18	0.44	2.86	0.42	1.96	0.11	0.09	0.13
2001-LHA-20	266.3	231.9	26.4	72.0	1.10	2.49	8.50	1.52	8.27	2.76	1.00	3.97	0.67	4.86	1.03	3.00	0.44	2.80	0.42	1.92	0.08	0.10	0.06
2002-BUM-03	11.1	92.9	9.2	133.3	5.42	60.24	131.58	15.72	61.63	9.51	2.14	5.34	0.51	1.92	0.34	0.77	0.10	0.63	0.09	3.75	0.37	22.32	5.70
2001-LHA-38	181.5	317.3	36.6	98.4	1.38	2.71	9.17	1.67	8.96	3.05	1.25	4.45	0.74	5.45	1.17	3.43	0.48	3.11	0.45	2.32	0.10	0.09	0.03
2002-MAM-06	207.8	230.7	24.7	67.6	1.04	2.19	7.61	1.30	7.36	2.70	1.05	3.66	0.67	4.25	1.00	2.80	0.41	2.71	0.38	1.88	0.08	0.09	0.04
2002-LIU-01		390.7	37.6	111.6	1.39	2.62	10.28	1.74	10.01	3.53	1.21	4.93	0.90	5.70	1.40	3.93	0.60	3.99	0.57	2.72	0.10	0.10	0.06
2002-LIU-02	41.7	253.1	24.4	67.5	0.86	2.23	7.67	1.32	7.35	2.57	0.95	3.53	0.66	4.17	1.01	2.88	0.42	2.92	0.42	1.93	0.07	0.07	0.04
2002-LIU-03	18.9	289.0	28.9	85.0	0.94	2.46	8.80	1.48	8.11	2.87	0.90	4.02	0.75	4.87	1.20	3.39	0.52	3.45	0.52	2.42	0.09	0.09	0.05
2002-LIU-04	176.4	285.5	28.3	74.2	1.04	2.59	9.00	1.52	8.44	2.97	1.23	4.16	0.75	4.76	1.14	3.19	0.46	3.16	0.46	2.17	0.08	0.09	0.05
2002-QUM-02	256.8	245.2	25.1	61.0	0.76	2.11	7.19	1.25	6.91	2.50	0.98	3.45	0.63	4.08	0.97	2.65	0.40	2.71	0.39	1.66	0.06	0.07	0.03
2002-QUM-08	192.0	263.7	27.8	73.9	1.04	2.40	8.27	1.45	7.98	2.86	1.09	3.99	0.73	4.61	1.10	3.10	0.46	3.04	0.44	2.00	0.08	0.09	0.04
2001-BEI-10	97.2	190.9	19.2	52.1	0.57	1.26	4.66	0.76	4.51	1.59	0.61	2.36	0.39	2.91	0.60	1.90	0.26	1.60	0.25	1.29	0.03		
2002-BAG-07	406.2	107.8	28.5	84.5	0.61	2.72	9.42	1.63	9.05	2.94	1.11	3.79	0.68	4.24	1.01	2.78	0.41	2.72	0.39	2.07	0.05	0.07	0.03
2002-DAZ-03		322.8	26.6	75.6	1.21	2.65	8.43	1.39	7.71	2.62	0.99	3.66	0.66	4.33	1.01	2.77	0.42	2.92	0.42	1.88	0.09	0.10	0.04
2001-BEI-01	129.2	238.2	27.4	72.1	0.94	2.50	7.94	1.35	7.37	2.55	1.15	3.64	0.61	4.41	0.95	2.75	0.38	2.56	0.37	1.66	0.07	0.46	0.06
2001-BEI-07	325.9	313.8	23.0	66.3	0.90	1.90	6.64	1.13	6.09	2.14	0.83	3.02	0.49	3.62	0.78	2.26	0.33	2.12	0.33	1.72	0.08	0.11	0.04
2001-BEI-09	251.0	213.4	25.2	75.7	1.03	2.09	7.55	1.31	7.18	2.49	1.06	3.50	0.58	3.99	0.88	2.55	0.36	2.30	0.35	1.86	0.07	0.08	0.02
2001-LHA-15	361.0	230.0	20.8	53.7	3.60	2.36	7.01	1.09	5.63	1.91	0.83	2.85	0.50	3.73	0.81	2.41	0.35	2.26	0.34	1.41	0.23	0.36	0.24
2001-JNL-01	55.9	167.5	17.4	134.0	6.05	22.01	48.29	6.03	23.96	4.52	1.41	3.94	0.50	3.00	0.57	1.56	0.22	1.37	0.21	2.92	0.38	5.05	1.33
2001-ZED-01	111.3	276.0	20.8	83.2	5.31	19.68	37.72	4.17	18.14	3.92	1.35	4.37	0.63	3.96	0.78	2.30	0.32	2.27	0.34	2.48	0.30	5.05	1.45

TAB. D.5: Composition chimique (éléments traces en ppm) des roches mafiques du mélange de Yamdrock.

	Cr	V	Y	Zr	Nb	La	Ce	Pr	Nd	Sm	Eu	Gd	Tb	Dy	Ho	Er	Tm	Yb	Lu	Hf	Ta	Th	U
2002-BAG-03	26.8	393.2	44.1	245.8	39.59	28.88	66.01	8.78	38.24	9.04	2.84	9.18	1.37	7.79	1.69	4.35	0.60	3.82	0.56	5.73	2.64	3.42	0.94
2002-BAG-04	117.9	391.5	36.7	214.1	23.55	19.98	49.91	6.83	30.28	7.37	2.40	7.64	1.16	6.42	1.44	3.54	0.49	3.13	0.42	5.03	1.64	2.24	0.67
2001-LHA-10	226.5	403.9	49.7	349.3	24.92	30.96	76.05	10.18	45.47	10.86	4.02	11.16	1.59	9.83	1.77	4.76	0.63	3.82	0.54	8.33	1.52	6.20	1.30
2001-LHA-33	168.7	281.6	34.3	102.3	1.45	3.17	10.43	1.79	9.93	3.42	1.59	5.00	0.85	6.12	1.30	3.80	0.54	3.60	0.53	2.49	0.10	0.09	0.04
2001-BAG-04	57.6	372.5	44.9	275.0	32.43	21.02	53.76	7.13	32.15	7.63	2.23	8.50	1.18	7.65	1.39	3.98	0.50	3.37	0.44	5.82	1.75	2.84	0.76
2002-MAM-01	332.6	234.2	23.9	65.8	1.21	2.22	7.67	1.32	7.41	2.61	0.99	3.51	0.66	4.13	0.97	2.68	0.41	2.66	0.38	1.86	0.10	0.10	0.09
2002-MAM-02	124.2	373.8	42.6	173.7	6.62	6.58	20.10	3.17	16.53	5.25	1.52	6.67	1.22	7.71	1.87	5.17	0.78	5.28	0.76	4.55	0.49	0.65	0.24
2002-MAM-05	18.5	404.8	35.8	254.8	37.96	26.37	65.67	8.76	37.56	8.58	2.50	8.58	1.30	7.12	1.53	3.87	0.55	3.55	0.50	6.88	2.92	4.95	1.36
2002-BAG-01	28.8	399.8	39.2	250.9	36.58	27.47	65.45	8.58	37.86	8.84	2.68	9.00	1.37	7.57	1.66	4.14	0.58	3.73	0.51	6.64	2.68	3.55	0.99
2001-LHA-11	199.6	257.6	33.9	262.9	15.56	20.28	50.14	6.77	30.48	7.19	2.60	7.34	1.04	6.41	1.16	3.09	0.43	2.53	0.37	5.66	0.94	4.18	0.87
2001-LHA-36	30.6	378.2	44.8	264.6	49.67	31.01	67.25	8.19	33.66	7.26	2.42	7.88	1.16	7.72	1.51	4.31	0.61	3.77	0.54	5.38	2.69	4.48	1.05
2001-BAG-02	40.0	325.0	49.7	310.6	53.48	35.93	78.16	9.73	42.32	8.18	2.88	8.97	1.31	7.54	1.58	4.02	0.56	3.32	0.49	6.27	2.94	4.72	1.43
2001-BAG-03	75.4	391.5	49.0	333.5	33.25	26.75	64.23	7.89	36.49	8.39	2.46	9.63	1.24	8.50	1.46	4.38	0.53	3.66	0.49	6.66	1.90	3.45	0.94
2002-REM-11	344.8	126.6	47.8	167.0	14.56	14.51	32.77	5.10	25.42	7.13	2.36	8.42	1.33	7.51	1.75	4.80	0.69	4.69	0.70	3.52	1.00	1.33	0.63
2002-BUM-11	79.1	312.1	33.4	146.7	11.58	10.11	26.19	3.63	17.17	4.82	1.73	5.65	0.95	5.46	1.21	3.10	0.43	2.79	0.39	3.37	0.72	1.12	0.66
2001-LHA-35	313.2	219.4	22.8	126.1	23.07	16.11	33.27	4.39	18.45	4.09	1.41	4.50	0.65	4.33	0.85	2.38	0.32	2.02	0.30	2.74	1.36	2.00	0.58
2001-LHA-37	21.1	462.5	57.4	410.9	60.76	31.14	77.56	10.73	47.36	11.52	3.72	12.26	1.67	10.30	1.89	5.28	0.70	4.28	0.62	8.60	3.54	6.25	1.77
2001-LHA-09	47.8	443.4	44.1	271.9	35.37	23.49	59.14	7.70	32.85	7.72	2.24	8.37	1.24	8.13	1.58	4.32	0.59	3.62	0.52	5.91	2.01	3.45	0.92
2001-LHA-01	69.9	381.3	47.4	330.5	46.79	29.40	69.75	9.57	40.38	9.38	2.81	9.72	1.39	8.72	1.65	4.50	0.59	3.67	0.53	6.94	2.69	5.19	1.44
2001-LHA-02	15.7	377.2	53.2	338.0	46.24	34.41	79.42	10.59	45.48	10.36	3.43	10.82	1.52	9.65	1.83	4.89	0.67	4.14	0.58	7.21	2.58	4.98	1.33
2001-LHA-05	178.7	331.8	34.1	211.2	26.60	18.96	44.15	5.94	26.34	6.22	2.09	6.67	0.98	6.20	1.17	3.19	0.42	2.57	0.36	4.62	1.51	2.76	0.78
2002-XIA-01	41.0	431.6	44.4	291.0	44.21	29.52	72.27	9.46	40.77	9.66	3.06	9.55	1.38	7.43	1.57	3.89	0.52	3.37	0.45	6.20	2.84	4.17	1.15
2002-XIA-04	24.9	419.3	54.3	346.0	46.53	35.30	82.96	10.98	47.87	11.22	3.38	11.35	1.74	9.53	2.05	5.21	0.73	4.62	0.64	8.21	3.27	5.00	1.43
2001-ZIS-08	241.7	243.6	39.8	147.0	8.31	7.59	19.86	2.95	14.79	4.52	1.49	5.81	0.89	6.15	1.22	3.86	0.48	3.22	0.48	2.94	0.47	0.89	0.28
2001-ZIS-09	225.1	243.3	31.4	146.2	27.30	15.79	32.22	4.06	16.33	4.14	1.41	4.97	0.74	5.07	1.03	3.10	0.41	2.72	0.40	3.13	1.53	2.66	0.68
2001-ZIS-10	38.0	417.2	49.5	307.1	46.47	33.31	80.65	11.08	48.19	11.03	3.29	11.25	1.62	10.11	1.92	5.16	0.69	4.33	0.61	7.98	2.88	5.44	1.47

Tab. D.5: Roches mafiques - mélange de Yamdrock (suite)

	Cr	V	Y	Zr	Nb	La	Ce	Pr	Nd	Sm	Eu	Gd	Tb	Dy	Ho	Er	Tm	Yb	Lu	Hf	Ta	Th	U
2001-BAG-01	109.5	373.2	47.2	190.0	24.98	15.87	40.56	5.13	21.55	5.72	1.77	6.69	0.99	6.77	1.40	4.12	0.58	3.74	0.55	3.74	1.30	2.05	0.55
2001-BAG-05	104.3	361.7	39.8	172.4	23.82	15.17	35.18	4.39	20.26	4.70	1.59	5.92	0.92	5.93	1.27	3.58	0.51	3.23	0.51	3.55	1.33	2.07	0.56
2002-REM-06	111.2	269.0	38.4	371.7	70.79	55.66	122.42	14.56	57.13	11.15	3.51	10.06	1.39	7.13	1.49	3.49	0.46	2.84	0.38	7.44	4.93	5.96	1.64
2002-REM-08	201.3	235.8	36.7	259.4	48.86	26.18	58.50	7.73	33.62	8.06	2.90	7.87	1.19	6.31	1.31	3.21	0.44	2.84	0.39	5.36	3.20	3.93	1.18

Tab. D.6: Composition chimique (éléments traces en ppm) des roches mafiques du flysch triasique.

	Cr	V	Y	Zr	Nb	La	Ce	Pr	Nd	Sm	Eu	Gd	Tb	Dy	Ho	Er	Tm	Yb	Lu	Hf	Ta	Th	U
01-QUN-03	47.5	40.6	12.5	213.3	10.01	135.70	264.44	26.67	92.62	12.38	2.48	6.93	0.61	2.59	0.45	0.93	0.12	0.69	0.10	5.12	0.61	83.11	12.53
01-QUN-03	33.1	33.6	13.3	225.7	10.88	136.23	264.64	28.18	94.84	13.00	2.86	9.02	0.76	2.49	0.43	0.96	0.12	0.80	0.11	4.93	0.66	71.38	10.89
01-ZIS-03	104.1	286.0	38.9	304.2	23.52	26.97	57.31	7.38	34.18	7.44	2.70	7.72	1.13	6.70	1.33	3.43	0.46	2.86	0.39	6.26	1.38	5.67	1.23
01-ZIS-04		124.5	52.8	411.0	30.53	49.19	107.84	13.36	56.03	11.70	3.32	11.59	1.54	9.48	1.79	4.89	0.66	3.98	0.60	9.86	1.89	16.33	2.88
01-ZIS-05	92.0	218.2	42.7	393.6	23.27	47.64	105.05	12.60	48.07	10.15	2.37	9.39	1.28	7.96	1.47	4.25	0.56	3.61	0.53	9.42	1.54	18.89	2.80
01-ZIS-06	53.1	178.7	28.7	234.3	16.72	21.83	49.07	6.31	26.59	6.19	1.96	6.22	0.85	5.24	0.98	2.70	0.35	2.24	0.32	6.15	1.08	6.32	1.34
02-ZIS-05	99.4	292.6	38.8	276.2	20.88	29.48	68.59	8.91	38.66	8.87	3.13	8.84	1.28	6.95	1.47	3.66	0.51	3.25	0.45	6.54	1.46	5.39	1.22
02-ZIS-07	53.8	251.9	38.9	295.5	20.38	35.51	80.51	10.25	42.65	9.33	2.84	8.86	1.31	6.93	1.48	3.72	0.52	3.32	0.47	7.11	1.44	9.47	1.74
02-ZIS-08		125.7	66.8	509.6	36.20	68.56	154.56	19.22	79.02	17.00	4.03	15.80	2.26	11.83	2.55	6.38	0.90	5.63	0.77	12.05	2.44	19.52	3.39
02-ZIS-09		185.7	46.6	396.2	25.80	43.81	100.08	12.36	49.93	10.79	3.06	10.30	1.49	7.98	1.73	4.33	0.62	4.07	0.56	9.37	1.82	14.07	2.44
02-ZIS-10		144.2	61.3	497.1	31.76	64.09	141.87	17.34	73.01	15.59	4.35	14.30	2.11	11.13	2.40	6.10	0.84	5.36	0.75	12.46	2.34	18.90	3.32
02-ZIS-11	56.7	183.2	40.2	349.5	20.10	45.76	103.80	12.32	49.93	10.23	2.48	9.24	1.36	7.26	1.61	4.11	0.58	3.74	0.54	9.13	1.58	17.92	2.74
1-LHA-29A	171.2	314.8	28.4	78.0	2.20	3.84	10.67	1.74	9.42	3.16	1.26	4.41	0.75	5.38	1.11	3.28	0.46	2.98	0.43	2.07	0.13	0.86	0.17
1-LHA-29B	174.8	347.9	30.5	88.2	2.51	4.31	11.48	1.94	10.27	3.45	1.11	4.94	0.79	5.65	1.15	3.42	0.48	3.03	0.43	2.27	0.15	0.93	0.18
01-LHA-30	33.0	265.2	34.8	269.8	22.75	25.49	57.99	7.74	33.29	7.48	2.30	7.67	1.08	6.84	1.23	3.47	0.46	2.69	0.38	5.94	1.39	5.46	1.20
01-LHA-31	167.2	330.9	30.9	85.0	2.33	4.31	12.06	1.96	10.40	3.55	1.43	4.96	0.82	5.83	1.20	3.51	0.49	3.16	0.46	2.28	0.17	0.96	0.19
02-LHA-13	201.6	355.4	32.1	87.7	2.43	4.28	12.73	1.96	10.54	3.47	1.30	4.78	0.83	5.20	1.23	3.34	0.47	3.17	0.47	2.31	0.17	0.90	0.19
02-PAZ-01	74.8	185.0	36.4	315.0	18.83	42.34	95.62	11.47	45.88	9.41	2.33	8.73	1.25	6.61	1.47	3.79	0.53	3.54	0.49	8.38	1.52	15.66	2.51

Tab. D.6: Roches mafiques - flysch triasique (suite)

	Cr	V	Y	Zr	Nb	La	Ce	Pr	Nd	Sm	Eu	Gd	Tb	Dy	Ho	Er	Tm	Yb	Lu	Hf	Ta	Th	U
02-PAZ-06	139.1	264.3	28.8	220.1	16.26	22.20	52.21	6.71	30.05	7.03	2.30	6.86	1.04	5.64	1.22	3.02	0.43	2.75	0.39	6.13	1.30	4.93	1.10
02-MAS-02	65.1	292.0	41.1	352.9	37.94	35.08	83.92	11.10	48.91	11.26	3.72	10.68	1.49	7.66	1.59	3.81	0.51	3.03	0.41	8.36	2.73	3.55	0.95
02-MAS-03	65.3	290.1	39.4	352.2	38.00	34.91	84.80	11.07	48.77	11.41	3.80	10.49	1.51	7.70	1.61	3.74	0.50	3.02	0.42	8.36	2.75	3.54	0.93
01-ZIS-01	114.3	284.9	39.8	316.3	25.31	27.60	65.67	8.46	34.88	8.17	2.62	8.65	1.10	6.90	1.25	3.35	0.47	2.71	0.41	6.53	1.34	6.45	1.40
02-ZIS-06	19.6	22.2	51.7	740.5	21.73	57.71	129.15	14.97	59.10	12.00	1.98	11.22	1.75	9.76	2.22	5.90	0.87	5.73	0.84	20.20	2.23	23.37	4.42
01-LHA-32	13.7	316.7	41.1	336.0	28.58	30.44	74.08	9.95	44.67	10.38	3.28	10.34	1.39	8.75	1.59	4.24	0.55	3.30	0.47	7.91	1.92	3.98	1.07
01-ZIS-07	60.8	272.0	37.1	276.9	21.27	25.41	59.10	7.90	31.96	7.72	2.25	7.84	1.07	6.50	1.19	3.33	0.41	2.76	0.37	5.82	1.24	5.93	1.17
02-PAZ-05	104.4	297.8	36.7	278.0	21.16	27.13	64.00	8.25	36.01	8.20	2.46	8.14	1.21	6.50	1.37	3.45	0.48	3.09	0.43	6.36	1.44	4.92	1.09
02-PAZ-07	106.9	304.7	39.5	281.1	21.96	26.74	62.52	8.22	35.95	8.41	2.81	8.46	1.25	6.73	1.43	3.60	0.48	3.14	0.45	6.58	1.45	4.94	1.07
01-ZIS-02	104.0	289.7	37.4	307.1	24.18	25.31	58.23	7.56	32.73	7.60	2.41	8.16	1.03	6.87	1.18	3.56	0.43	2.80	0.37	6.55	1.31	5.39	1.32
02-PAZ-09	68.9	257.9	35.4	272.5	20.74	28.63	64.97	8.32	35.53	8.01	2.66	7.86	1.14	6.10	1.27	3.25	0.46	2.95	0.41	6.35	1.40	6.24	1.25
02-PAZ-09	57.4	257.0	33.1	255.3	19.68	26.23	60.38	7.84	32.90	7.45	2.49	7.26	1.08	5.76	1.25	3.11	0.43	2.81	0.38	5.92	1.34	6.00	1.20
02-DZU-01	298.5	199.5	29.2	227.5	45.28	14.80	33.36	4.58	21.20	5.63	1.89	5.90	0.84	4.67	1.02	2.67	0.39	2.48	0.35	5.07	3.02	2.92	1.10

TAB. D.7: Composition chimique (éléments majeurs (% poids) et métaux de transition (ppm)) des roches ultramafiques du mélange ophiolitique.

		SiO_2	TiO_2	Al_2O_3	Fe_2O_3	MnO	MgO	CaO	Na_2O	K_2O	*Total*	P.A.F.	Sc	Cr	V	Ni	Sr	Y	Zr	Ba
Cpx-hz	2002-BUM-02	46.31	0.06	3.26	6.68	0.15	39.07	3.94	0.15	0.03	*99.64*	10.4	15.7	2672	79	1804	4.6	2.68	0.41	1.8
	2002-BUM-08	44.71	0.06	2.69	7.80	0.12	41.21	2.80	0.13	0.00	*99.52*	10.88	13.0	2677	66	1676	2.4	2.17	0.41	1.1
	2002-LHA-08	46.05	0.02	1.76	11.38	0.06	39.83	0.10	0.10	0.03	*99.33*	11.84	10.8	2323	50	1855	7.1	0.76	0.16	1.8
	2002-LHA-08	45.86	0.02	1.76	10.86	0.06	40.16	0.10	0.08	0.00	*98.91*	11.87	10.9	2361	50	1878	7.4	0.99	2.38	1.7
	2001-LHA-06	44.88	0.04	2.81	10.19	0.19	40.20	1.04	0.02	0.00	*99.36*	14.35	15.1	3346	65	2740	5.3	1.85	1.09	12.2
	2001-LHA-07	45.26	0.05	2.39	8.05	0.15	42.83	0.63	0.00	0.00	*99.35*	14.39	15.4	2955	60	2190	2.9	1.77	0.54	1.9
	2002-DAZ-01	45.91	0.03	1.68	8.56	0.12	43.79	0.13	0.00	0.02	*100.22*	13.65	10.0	2592	47	1905	3.1	0.87	0.28	1.6
	2002-DAZ-04	44.43	0.05	2.01	11.82	0.15	40.04	0.67	0.09	0.00	*99.27*	15.22	12.0	2521	59	1982	3.4	1.87	0.3	6.9
	2002-REM-09	42.31	0.05	2.16	12.96	0.15	40.02	1.45	0.10	0.00	*99.20*	12.07	11.8	2863	58	1996	1.2	1.52	0.55	
	2001-ZED-02	44.33	0.03	1.94	8.53	0.12	43.39	1.61	0.09	0.00	*100.04*	1.91	11.0	2570	47	1610		1	1	2
	2001-ZED-03	43.88	0.02	1.77	8.48	0.12	42.83	1.86	0.09	0.00	*99.06*	3.01	12.0	2570	56	1240		0.9	1	4
Trans.	2002-LIU-11	44.18	0.02	1.32	9.95	0.13	44.02	0.07	0.23	0.23	*100.15*	13.08	11.3	2577	52	1881	2.1	0.67	0.46	1.3
	2001-BEI-02	45.73	0.01	1.32	9.24	0.11	43.39	0.06	0.06	0.00	*99.91*	13.43	10.3	2281	44	2070	2.6	0.69	0.4	4.9
	2001-BEI-11	46.11	0.01	1.10	8.99	0.12	43.05	0.10	0.07	0.00	*99.55*	13.51	10.6	2606	46	2037	6.9	0.43	0.56	2.2
	2002-LUS-03	44.94	0.01	1.37	9.25	0.13	41.12	2.21	0.06	0.00	*99.08*	13.49	14.1	3025	65	1772	1.2	0.51	0.29	
	2002-BAG-05	46.08	0.01	1.69	8.14	0.10	43.59	0.07	0.05	0.00	*99.73*	13.13	9.2	2777	48	1919	5.2	0.32	0.19	1.6
Part.	2001-LHA-39	46.53	0.01	0.85	8.08	0.09	44.26	0.13	0.05	0.00	*99.99*	12.95	8.9	2334	34	2016	5	0.45	0.69	11.5
	2002-DAY-04	46.00	0.02	1.71	7.08	0.12	44.13	0.26	0.11	0.00	*99.43*	14.72	9.5	3315	45	2357	1.2	0.81	0.21	
Hz + dunite	2001-LHA-27	44.22	0.01	1.00	9.64	0.13	45.17	0.01	0.03	0.00	*100.20*	12.75	10.5	2882	48	2169	1.1	0.15	0.35	
	2001-LHA-28	43.32	0.01	0.81	11.73	0.09	44.00	0.03	0.00	0.00	*99.99*	12.14	4.4	4157	36	2437			0.25	
	2002-LIU-05	45.59	0.01	0.87	7.10	0.06	45.44	0.09	0.08	0.00	*99.24*	13.45	8.7	2451	39	1873	24	0.28	0.85	1.3
	2001-JID-04	45.45	0.01	0.80	6.89	0.09	45.39	0.03	0.05	0.00	*98.70*	13.13	7.5	1915	33	1898	4.6	0.35	0.14	
	2002-QUM-07	45.79	0.01	0.85	8.59	0.16	44.60	0.22	0.07	0.00	*100.28*	13.82	6.3	4084	35	2171	1.3	0.16	0.73	1.4
	2002-QUM-11	44.41	0.01	0.83	9.57	0.07	44.60	0.08	0.00	0.08	*99.64*	13.29	9.9	2946	42	1986	2.2	0.16	0.41	1.5

Tab. D.7: Roches ultramafiques - mélange ophiolitique (suite)

	SiO_2	TiO_2	Al_2O_3	Fe_2O_3	MnO	MgO	CaO	Na_2O	K_2O	*Total*	P.A.F.	Sc	Cr	V	Ni	Sr	Y	Zr	Ba
2002-QUM-13	45.68	0.00	0.65	9.00	0.13	43.41	0.39	0.10	0.00	*99.37*	13.75	7.9	2726	37	1896		0.11	0.32	1.6
2002-QUM-14	42.49	0.01	0.81	8.70	0.12	46.23	0.90	0.11	0.00	*99.37*	11.06	7.2	2098	28	2023		0.23	1.33	
2002-DAY-08B	47.47	0.01	0.44	6.61	0.08	44.57	0.07	0.12	0.00	*99.36*	13.18	3.6	2820	14	2044	2.4			2.5

Tab. D.8: Composition chimique (terres rares en ppm) des roches ultramafiques du mélange ophiolitique.

		La	Ce	Pr	Nd	Sm	Eu	Gd	Tb	Dy	Ho	Tm	Yb	Lu
Cpx-hz	2002-BUM-02			0.008	0.112	0.149	0.059	0.274	0.045	0.451	0.095	0.049	0.35	0.055
	2002-BUM-08			0.007	0.103	0.118	0.05	0.249	0.043	0.374	0.085	0.045	0.269	0.031
	2002-LHA-08	0.043	0.118	0.015	0.131	0.051	0.04	0.098	0.021	0.142	0.042	0.028	0.193	0.027
	2002-LHA-08	0.018	0.086	0.014	0.051	0.059	0.041	0.085	0.016	0.142	0.037	0.019	0.158	0.021
	2001-LHA-06	0.026	0.019	0.011	0.093	0.105	0.033	0.214	0.037	0.271	0.072	0.034	0.216	0.023
	2001-LHA-07		0.017	0.009	0.074	0.089	0.031	0.181	0.04	0.282	0.072	0.032	0.245	0.024
	2002-DAZ-01	0.038	0.05	0.016	0.095	0.067	0.023	0.118	0.02	0.144	0.038	0.023	0.159	0.028
	2002-DAZ-04	0.056	0.027	0.013	0.164	0.122	0.043	0.211	0.043	0.331	0.079	0.043	0.261	0.04
	2002-REM-09	0.03	0.078	0.014	0.114	0.082	0.043	0.187	0.037	0.301	0.063	0.036	0.27	0.04
	2001-ZED-02	0.046	0.105	0.014	0.083	0.051	0.02	0.096	0.021	0.173	0.045	0.022	0.201	0.027
	2001-ZED-03	0.018	0.036	0.007	0.047	0.042	0.015	0.076	0.015	0.131	0.034	0.02	0.164	0.028
Trans.	2002-LIU-11	0.04	0.085	0.01	0.05	0.017	0.012	0.063	0.009	0.116	0.026	0.019	0.139	0.017
	2001-BEI-02	0.078	0.098	0.016	0.072	0.036	0.012	0.046	0.009	0.087	0.026	0.013	0.117	0.012
	2001-BEI-11	0.015	0.015	0.005	0.034	0.012		0.013	0.005	0.03	0.009	0.009	0.091	0.02
	2002-LUS-03		0.031		0.024	0.01	0.003	0.031	0.007	0.06	0.02	0.013	0.106	0.019
	2002-BAG-05		0.023	0.005		0.008	0.061	0.012	0.006	0.03	0.012	0.009	0.076	0.009
Part.	2001-LHA-39	0.064	0.157	0.024	0.123	0.043	0.038	0.05	0.009	0.062	0.014	0.007	0.063	0.007
	2002-DAY-04	0.138	0.031	0.031	0.211	0.083	0.025	0.154	0.025	0.168	0.037	0.018	0.141	0.016

Tab. D.8: Roches ultramafiques - mélange ophiolitique (suite)

		La	Ce	Pr	Nd	Sm	Eu	Gd	Tb	Dy	Ho	Tm	Yb	Lu
Hz + dunite	2001-LHA-27	0.086	0.165	0.019	0.077	0.024	0.004	0.027	0.005	0.03	0.009	0.006	0.053	0.008
	2001-LHA-28	0.093	0.146	0.018	0.091	0.026	0.007	0.025	0.003	0.024	0.006	0.003	0.041	
	2002-LIU-05	0.058	0.128	0.026	0.127	0.036	0.007	0.027	0.004	0.038	0.011	0.009	0.061	0.014
	2001-JID-04	0.072	0.103	0.014	0.064	0.024	0.011	0.017	0.004	0.02	0.006	0.004	0.047	
	2002-QUM-07			0.005	0.037	0.023	0.006	0.022	0.004	0.029	0.011	0.007	0.056	0.015
	2002-QUM-11	0.023	0.067	0.007	0.045	0.019	0.008	0.014	0.003	0.024	0.007	0.004	0.05	0.017
	2002-QUM-13				0.031	0.016	0.006	0.009	0.002	0.018	0.006	0.003	0.058	0.009
	2002-QUM-14					0.007	0.003		0.001	0.021	0.007	0.005	0.041	0.016
	2002-DAY-08B	0.016	0.027	0.005	0.023	0.024	0.003		0.002	0.017	0.004	0.003	0.025	0.013

Tab. D.9: Composition chimique (éléments majeurs (% poids) et métaux de transition (ppm)) des roches sédimentaires du mélange de Yamdrock.

		SiO_2	TiO_2	Al_2O_3	$Fe_2O_3^T$	MnO	MgO	CaO	Na_2O	K_2O	P_2O_5	P.A.F.	*Total*	Sc	Cr	V	Rb	Sr	Y	Zr
Grès	LHA-01	80.86	0.30	6.66	2.88	0.05	0.79	6.01	1.13	1.19	0.08	5.75	*97.70*	4.8	38	33	61.25	107	15.56	139.08
	BEL-02	60.99	0.71	16.67	7.02	0.09	3.20	4.05	6.77	0.23	0.17	5.11	*99.09*	16.0	86	145	9.02	201	17.04	96.59
	BEL-03	61.53	0.72	17.14	6.99	0.08	3.29	2.95	6.58	0.47	0.17	4.46	*98.40*	15.7	86	144	21.93	174	15.75	117.70
	DAZ-06	63.81	0.80	15.59	7.71	0.11	3.52	2.18	5.25	0.77	0.17	4.28	*98.99*	17.1	34	172	35.32	157	19.71	145.04
	REM-01	21.15	0.49	4.24	3.00	0.06	0.84	68.28	0.67	0.81	0.19	35.32	*100.56*	4.8		49	12.25	1538	13.73	62.79
	REM-05	74.05	0.43	11.29	7.04	0.04	1.22	1.25	4.04	0.39	0.16	2.43	*97.69*	5.0	105	90	12.73	38	7.47	77.04
A. rouge	BUM-10	71.40	0.64	13.88	6.01	0.13	2.14	0.63	2.04	2.97	0.09	3.14	*99.25*	11.6	67	87	135.95	58	24.83	157.68
	XIA-05	74.10	0.77	10.95	7.06	0.16	1.75	0.56	0.45	3.85	0.26	3.51	*98.24*	14.1	55	125	117.75	23	24.93	113.39
	MAM-04	77.36	1.25	7.44	8.05	0.19	2.64	0.63	0.84	1.49	0.05	3.51	*99.97*	13.1	44	112	40.94	14	17.89	119.10
	ZIS-12	85.92	0.49	6.60	3.86	0.14	0.84	0.17	0.48	1.42	0.04	2.17	*98.24*	8.5	27	51	55.19	21	11.63	93.54
	BAG-02	78.68	0.52	9.08	5.21	0.03	1.72	0.57	0.04	3.96	0.12	2.53	*99.34*	11.5	49	60	110.29	15	23.15	111.53

TAB. D.9: Roches sédimentaires - mélange de Yamdrock (suite)

		SiO_2	TiO_2	Al_2O_3	$Fe_2O_3^T$	MnO	MgO	CaO	Na_2O	K_2O	P_2O_5	P.A.F.	*Total*	Sc	Cr	V	Rb	Sr	Y	Zr
A. noire	BUM-12	62.07	0.68	13.87	6.87	0.26	2.90	9.18	0.95	2.82	0.13	13.62	*100.68*	13.5	66	100	118.77	157	28.89	141.27
	LHA-10	63.66	0.79	18.00	5.28	0.09	2.14	4.28	0.24	4.84	0.17	9.79	*99.18*	14.1	82	114	211.87	107	30.73	178.48
	BEL-01	84.32	0.51	10.09	1.71	0.00	0.51	0.16	0.50	2.04	0.06	2.48	*97.67*	9.4	50	66	115.04	249	9.64	104.45
	BEL-04	59.75	0.90	22.78	8.39	0.05	2.34	0.32	0.96	4.26	0.08	5.63	*98.71*	21.0	122	165	240.00	121	45.69	174.42
	MAM-03	69.29	1.10	14.58	7.70	0.20	2.46	0.29	0.12	4.00	0.07	4.22	*99.18*	19.4	83	162	161.03	15	31.50	185.61
	QUM-10	61.82	1.06	17.20	13.48	0.12	1.97	0.35	0.47	3.17	0.19	4.28	*99.26*	19.5	106	155	176.87	82	36.72	198.27
	DAZ-05	65.38	0.62	19.03	5.32	0.04	2.03	0.56	3.05	3.79	0.08	6.10	*98.62*	13.5	44	99	175.89	37	19.52	147.07
	REM-10	80.26	0.49	9.81	3.24	0.02	1.58	0.63	1.24	2.55	0.10	2.43	*97.32*	7.3	57	55	122.26	30	23.90	216.07

TAB. D.10: Composition chimique (éléments majeurs (% poids) et métaux de transition (ppm)) des roches sédimentaires du flysch triasique.

		SiO_2	TiO_2	Al_2O_3	$Fe_2O_3^T$	MnO	MgO	CaO	Na_2O	K_2O	P_2O_5	P.A.F.	*Total*	Sc	Cr	V	Rb	Sr	Y	Zr
A. noire	LHA-11	61.00	1.02	24.30	7.19	0.15	1.08	0.16	1.65	3.25	0.06	5.24	*99.11*	19.8	111	168	206.11	144	33.04	173.25
	LHA-14	69.00	0.73	17.65	6.83	0.05	1.74	0.11	1.26	2.45	0.04	3.94	*98.93*	17.1	106	139	158.84	481	15.97	124.83
	LHA-14	69.03	0.73	17.68	6.92	0.05	1.75	0.11	1.24	2.29	0.04	3.92	*98.04*	17.0	105	136	142.55	478	16.42	122.41
	PAZ-03	65.19	0.85	18.33	8.76	0.06	2.01	0.17	1.03	3.41	0.05	4.84	*98.49*	18.0	120	148	181.32	66	26.44	137.66
	PAZ-04	66.54	0.86	18.35	8.22	0.07	1.67	0.54	1.12	2.32	0.07	5.99	*99.89*	17.8	140	149	165.77	215	32.06	135.20
	PAZ-08	82.56	0.32	9.65	3.74	0.03	1.18	0.13	0.24	2.06		2.49	*98.61*	9.5	54	81	121.09	125	14.58	95.24
	MAS-01	80.97	0.42	10.71	3.60	0.05	1.05	0.35	0.50	2.21	0.04	3.14	*98.88*	11.3	49	78	121.74	52	40.01	104.65
	MAS-05	73.72	0.60	14.28	5.68	0.05	1.66	0.14	0.78	2.93	0.04	3.50	*98.24*	14.0	73	125	151.32	34	23.75	119.25
	ZIS-02	83.76	0.53	8.91	3.44	0.00	0.58	0.18	0.87	1.54	0.07	3.43	*98.20*	9.8	63	71	82.42	73	20.27	125.54
	DAY-01	56.95	0.95	24.15	8.12	0.09	1.55	0.06	1.48	5.54	0.06	6.49	*99.23*	19.5	117	150	284.97	82	87.28	168.06
	DAY-02	76.48	0.54	12.75	4.61	0.04	1.07	0.24	2.09	1.96	0.15	2.55	*99.02*	9.1	38	55	104.55	50	27.88	281.57
	DAY-03	71.92	0.83	16.65	5.99	0.04	0.50	0.15	0.88	2.77	0.13	5.11	*97.27*	13.4	63	93	141.00	150	31.08	234.91
	DZU-03	73.29	0.60	10.65	5.77	0.20	2.43	3.62	1.14	1.98	0.13	6.69	*99.74*	9.4	63	71	109.51	43	25.83	211.42

Tab. D.11: Composition chimique (éléments traces en ppm) des roches sédimentaires du mélange de Yamdrock.

	Nb	Cs	La	Ce	Pr	Nd	Sm	Eu	Gd	Tb	Dy	Ho	Er	Tm	Yb	Lu	Hf	Ta	Th	U
LHA-01	5.70	3.62	18.43	35.42	4.05	14.70	2.84	0.60	2.68	0.41	2.38	0.53	1.44	0.22	1.51	0.22	3.52	0.53	8.29	1.63
BEL-02	3.90	0.57	12.89	27.66	3.54	14.54	3.17	0.83	3.02	0.47	2.67	0.62	1.70	0.25	1.75	0.26	2.49	0.29	4.85	1.36
BEL-03	5.03	1.16	14.25	30.67	3.85	15.42	3.27	0.90	2.95	0.42	2.33	0.54	1.49	0.23	1.61	0.24	2.89	0.34	5.77	1.48
DAZ-06	5.51	2.70	15.37	34.09	4.12	16.74	3.51	0.89	3.37	0.52	3.05	0.71	1.92	0.29	1.97	0.30	3.43	0.39	4.30	1.02
REM-01	9.79	0.50	9.43	21.58	2.87	12.63	2.90	0.67	2.77	0.41	2.31	0.50	1.23	0.18	1.10	0.17	1.41	0.60	1.08	0.25
REM-05	3.61	0.70	20.41	31.97	3.40	12.27	2.34	0.57	2.06	0.26	1.30	0.27	0.70	0.10	0.70	0.11	1.91	0.21	2.90	0.82
BUM-10	11.65	7.87	35.51	73.53	8.54	31.54	5.87	1.20	5.08	0.76	4.24	0.94	2.58	0.39	2.68	0.39	4.28	1.02	14.41	2.48
XIA-05	14.25	4.15	32.90	95.39	8.31	32.73	6.86	1.45	6.22	0.86	4.53	1.01	2.71	0.41	2.72	0.40	2.73	1.04	9.26	1.04
MAM-04	17.23	1.42	14.21	35.09	3.58	14.52	3.29	0.97	3.24	0.50	2.90	0.64	1.75	0.25	1.67	0.24	2.76	1.23	3.58	0.50
ZIS-12	11.45	1.28	14.15	39.32	3.55	13.10	2.49	0.58	2.21	0.32	1.83	0.43	1.16	0.18	1.23	0.18	2.17	0.82	4.90	0.67
BAG-02	16.35	2.19	30.04	80.27	7.22	27.31	5.04	1.03	4.70	0.70	3.79	0.84	2.18	0.33	2.17	0.32	2.78	1.00	8.51	1.24
BUM-12	13.64	9.33	30.14	66.84	7.30	28.07	5.65	1.12	5.19	0.77	4.13	0.94	2.44	0.34	2.30	0.34	3.10	0.87	10.86	1.88
LHA-10	14.02	13.34	42.77	91.40	10.19	38.08	7.15	1.36	6.27	0.95	5.26	1.18	3.16	0.47	3.12	0.46	4.86	1.28	19.54	3.31
BEL-01	14.08	6.26	27.18	81.03	6.49	23.30	3.21	0.39	2.05	0.24	1.27	0.32	1.01	0.18	1.29	0.20	2.34	0.91	10.27	1.28
BEL-04	23.79	12.82	59.82	136.29	14.48	54.27	8.98	1.56	7.51	1.12	6.60	1.54	4.11	0.58	3.86	0.56	4.04	1.48	22.11	2.41
MAM-03	23.14	7.98	39.03	106.15	9.59	36.34	6.74	1.41	5.92	0.85	4.77	1.09	2.99	0.43	2.88	0.42	4.16	1.47	11.72	1.82
QUM-10	24.39	5.15	45.90	130.49	10.67	39.51	7.61	1.65	7.08	1.00	5.58	1.26	3.33	0.47	3.30	0.48	4.69	1.64	18.20	1.39
DAZ-05	12.15	13.08	7.58	14.33	1.81	7.08	1.64	0.34	1.92	0.33	2.12	0.57	1.86	0.31	2.39	0.39	3.43	1.06	12.59	2.77
REM-10	10.04	6.15	28.47	57.62	6.71	24.52	4.58	0.81	4.04	0.61	3.58	0.83	2.25	0.34	2.33	0.32	5.35	0.87	11.70	2.13

Tab. D.12: Composition chimique (éléments traces en ppm) des roches sédimentaires du flysch triasique.

	Nb	Cs	La	Ce	Pr	Nd	Sm	Eu	Gd	Tb	Dy	Ho	Er	Tm	Yb	Lu	Hf	Ta	Th	U
LHA-11	27.04	10.91	55.68	127.41	13.39	49.03	8.90	1.71	7.43	1.01	5.23	1.18	3.23	0.48	3.34	0.48	4.07	1.85	23.91	2.41
LHA-14	18.72	5.86	33.77	79.89	7.92	28.94	5.41	1.15	4.46	0.58	2.90	0.57	1.32	0.19	1.31	0.21	2.65	1.16	15.33	1.48

Tab. D.12: Roches sédimentaires - flysch triasique (suite)

	Nb	Cs	La	Ce	Pr	Nd	Sm	Eu	Gd	Tb	Dy	Ho	Er	Tm	Yb	Lu	Hf	Ta	Th	U
LHA-14	17.99	4.48	33.33	78.69	7.83	28.74	5.40	1.15	4.35	0.58	2.86	0.57	1.36	0.19	1.33	0.21	2.67	1.16	15.68	1.48
PAZ-03	20.62	3.51	42.05	102.11	9.78	36.01	6.71	1.32	5.80	0.79	4.16	0.90	2.39	0.35	2.37	0.35	3.00	1.29	17.82	2.01
PAZ-04	20.59	7.36	45.77	108.28	10.86	40.03	7.03	1.31	5.96	0.85	4.59	1.05	2.73	0.39	2.54	0.37	2.94	1.25	16.67	2.16
PAZ-08	9.90	4.12	17.38	38.22	4.26	15.86	2.92	0.59	2.60	0.36	1.92	0.43	1.18	0.17	1.22	0.19	2.04	0.63	7.62	0.95
MAS-01	12.60	8.42	37.59	74.57	9.07	34.69	6.24	0.93	5.81	0.91	5.41	1.28	3.33	0.48	3.00	0.41	2.19	0.75	11.50	1.05
MAS-05	15.75	5.88	33.56	78.45	7.81	28.32	4.47	0.76	3.64	0.53	3.17	0.78	2.16	0.33	2.18	0.31	2.73	1.04	13.98	1.50
ZIS-02	14.90	3.93	23.45	55.02	5.40	19.60	3.41	0.65	3.01	0.43	2.48	0.61	1.66	0.24	1.65	0.25	2.74	0.92	10.22	1.40
DAY-01	23.67	13.78	60.68	135.69	15.08	57.42	11.37	2.29	11.95	1.98	11.95	2.77	7.29	0.97	5.88	0.79	4.03	1.68	23.60	2.23
DAY-02	10.81	4.59	26.25	60.12	7.04	27.07	5.42	1.10	5.12	0.75	4.08	0.92	2.46	0.36	2.43	0.35	5.94	0.72	10.02	2.39
DAY-03	13.62	7.11	32.73	73.99	8.61	32.87	6.30	1.22	5.03	0.73	4.30	1.02	2.85	0.42	2.94	0.43	5.29	0.93	12.21	2.94
DZU-03	13.22	5.30	30.22	64.76	7.21	26.39	4.93	0.90	4.49	0.69	3.85	0.88	2.39	0.35	2.40	0.34	4.69	0.97	13.65	2.85

Annexe E

Synthèse des résultats obtenus à partir de diagrammes discriminants

Tab. E.1 – Nature des magmas selon divers diagrammes.

		Mél. oph.	Mél. Yamdrock	Flysch
Irvine & Baragar, 1971	Na2O+K2O vs SiO2	Tholéiitique	Alcalin + tholeiitic	Tholéiitique
Pearce & Cann, 1973	Y/Nb	Tholéiitique	Alcalin WPB	Alcalin WPB
Winchester & Floyd, 1976	P2O5 vs Zr	Tholéiitique	Tholéiitique	Tholéiitique
Winchester & Floyd, 1976	TiO2 vs Zr/(P2O5 E4)	Tholéiitique	Alcalin	Tholéiitique (+ alcalin)
Floyd & Winchester, 1975	Nb/Y vs Zr/(P2O5E4)	Tholéiitique	Tholéiitique	Tholéiitique

TAB. E.2 – Synthèse des résultats des diagrammes discriminants - Mélange ophiolitique.

		VAB			MORB		WPB		
		CAB	IAT	BABB	N-MORB	E-MORB	WPT	WPAB	OIB
Pearce & Gale, 1977	Zr/Y vs Ti/Y	X	X		X				
Pearce, 1982	Ti/Y vs Nb/Y	X	X		X				
Pearce, 1982	Ti vs Zr	X	X		X				
Pearce & Cann, 1973	Ti vs Zr	X	X		X				
Pearce & Norry, 1979	Zr/Y vs Zr	X	X		X				
Pearce, 1982	Cr vs Y	X	X		X		X	X	X
Shervais, 1982	V vs Ti	X	X	X	X				
Pearce & Cann, 1973	Zr-Ti/100-Y×3	X	X		X				
Wood, 1980	Th-Hf/3-Ta		X		X				
Cabanis & Lecolle, 1989	La/10-Y/15-Nb/8		X		X				
Meschede, 1986	Zr/4-2Nb-Y	X	X		X				
Mullen, 1983	10MnO-TiO2-10P2O5		X		X				
Thiéblemont et al., 1994	$(Tb/Ta)_N$ vs $(Th/Ta)_N$			X	X				
Tomlinson & Condie, 2001	Th/Ta vs La/Yb				X				
Pearce, 1996	Roche/MORB			X					

VAB = volcanic-arc basalt (basalte d'arc volcanique), *CAB = calk-alkaline basalt* (basalte calco-alcalin), *IAT = island-arc tholeiite* (tholéiite d'arc), *BABB = back-arc basin basalt* (basalte de bassin d'arrière-arc), *MORB = mid-ocean ridge basalt* (basalte de dorsale médio-océanique), *N-MORB = MORB* normal, *E-MORB = MORB* enrichi, *WPB*, *WPT* et *WPAB = within plate basalt, tholeiite and alkaline basalt* (basalte, tholéiite et basalte alcalin intraplaque), *OIB = ocean island basalt* (basalte d'île océanique).

Tab. E.3 – Synthèse des résultats des diagrammes discriminants - Mélange de Yamdrock.

		VAB			MORB		WPB		
		CAB	IAT	BABB	N-MORB	E-MORB	WPT	WPAB	OIB
Pearce & Gale, 1977	Zr/Y vs Ti/Y						X	X	X
Pearce, 1982	Ti/Y vs Nb/Y						X	X	X
Pearce, 1982	Ti vs Zr						X	X	X
Pearce & Cann, 1973	Ti vs Zr						X	X	X
Pearce & Norry, 1979	Zr/Y vs Zr						X	X	X
Pearce, 1982	Cr vs Y				X	X	X	X	X
Shervais, 1982	V vs Ti							X	X
Pearce & Cann, 1973	Zr-Ti/100-Y×3						X	X	X
Wood, 1980	Th-Hf/3-Ta					X		X	
Cabanis & Lecolle, 1989	La/10-Y/15-Nb/8					X		X	
Meschede, 1986	Zr/4-2Nb-Y						X	X	
Mullen, 1983	10MnO-TiO2-10P2O5								X
Thiéblemont et al., 1994	$(Tb/Ta)_N$ vs $(Th/Ta)_N$							X	X
Tomlinson & Condie, 2001	Th/Ta vs La/Yb								X
Pearce, 1996	Roche/MORB							X	

Mêmes abréviations qu'au Tab. E.2.

Tab. E.4 – Synthèse des résultats des diagrammes discriminants - Flysch triasique.

		VAB			MORB		WPB		
		CAB	IAT	BABB	N-MORB	E-MORB	WPT	WPAB	OIB
Pearce & Gale, 1977	Zr/Y vs Ti/Y	X	X		X	X	X	X	X
Pearce, 1982	Ti/Y vs Nb/Y				X	X	X	X	X
Pearce, 1982	Ti vs Zr						X	X	X
Pearce & Cann, 1973	Ti vs Zr						X	X	X
Pearce & Norry, 1979	Zr/Y vs Zr						X	X	X
Pearce, 1982	Cr vs Y				X	X	X	X	X
Shervais, 1982	V vs Ti							X	X
Pearce & Cann, 1973	Zr-Ti/100-Y×3	X					X	X	X
Wood, 1980	Th-Hf/3-Ta	X							
Cabanis & Lecolle, 1989	La/10-Y/15-Nb/8	X						X	
Meschede, 1986	Zr/4-2Nb-Y						X	X	
Mullen, 1983	10MnO-TiO2-10P2O5								X
Thiéblemont et al., 1994	$(Tb/Ta)_N$ vs $(Th/Ta)_N$	X						X	X
Tomlinson & Condie, 2001	Th/Ta vs La/Yb	X	X						
Pearce, 1996	Roche/MORB	X						X	

Mêmes abréviations qu'au Tab. E.2.

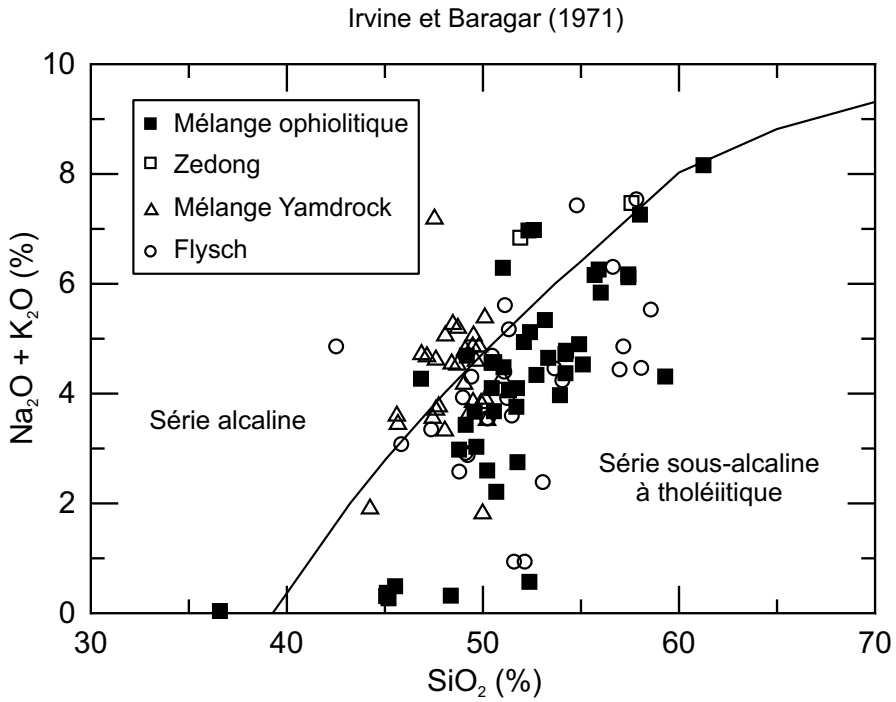

FIG. E.1 – Diagramme discriminant $Na_2O + K_2O$ vs. SiO_2 de Irvine et Barager (1971). La légende s'applique aussi aux Figs. E.2 à E.18.

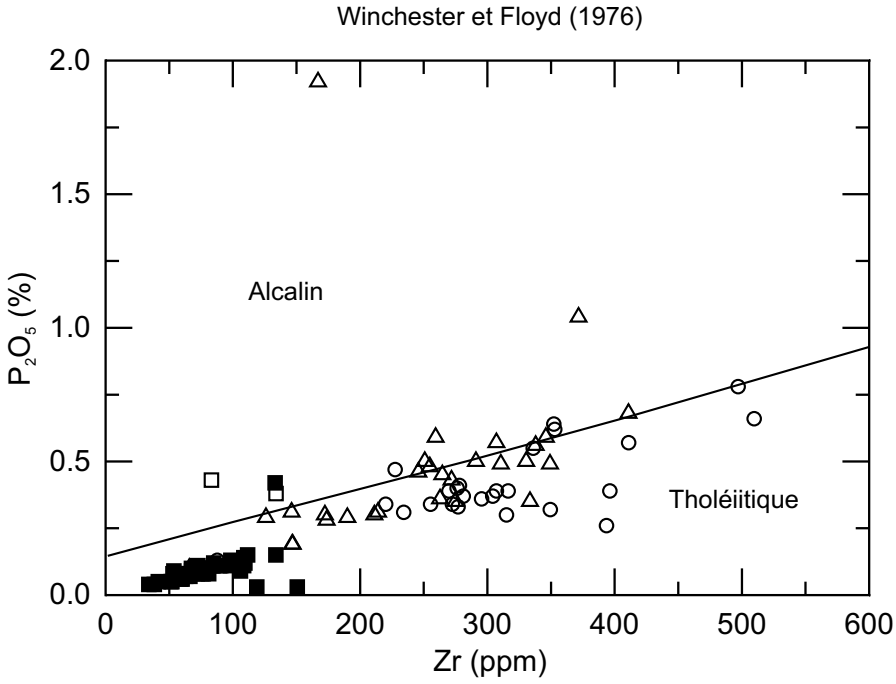

FIG. E.2 – Diagramme discriminant P_2O_5 vs. Zr de Winchester et Floyd (1976).

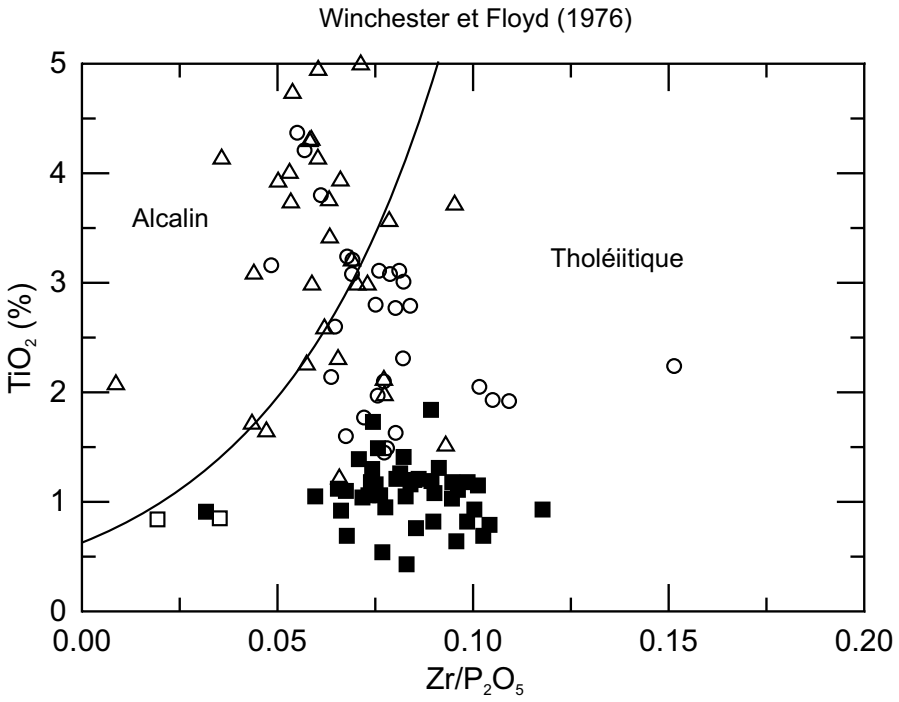

FIG. E.3 – Diagramme discriminant TiO_2 vs. Zr/P_2O_5 de Winchester et Floyd (1976).

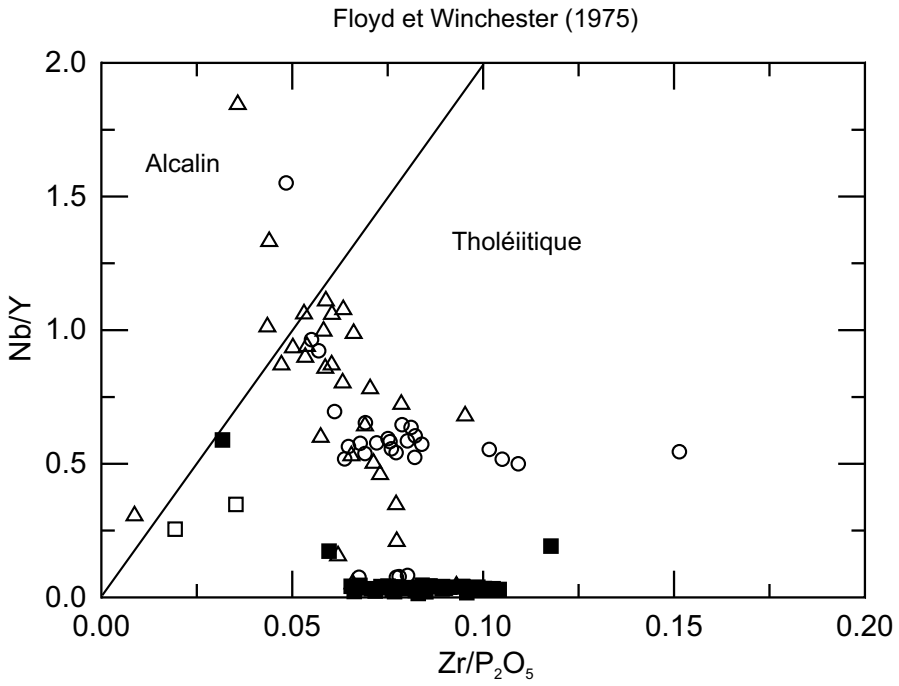

FIG. E.4 – Diagramme discriminant Nb/Y vs. Zr/P_2O_5 de Floyd et Winchester (1975).

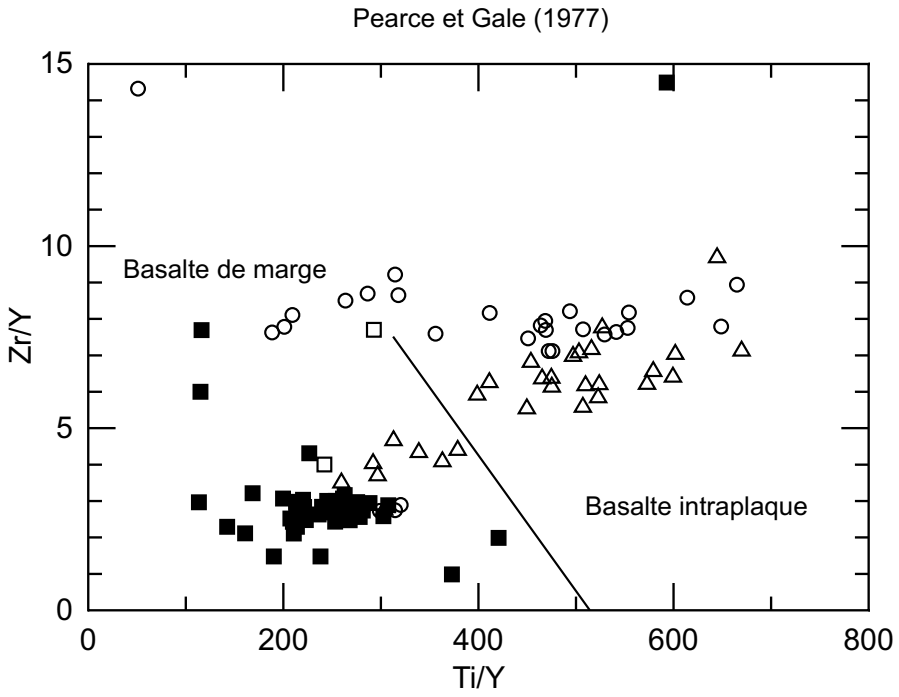

FIG. E.5 – Diagramme discriminant Zr/Y vs. Ti/Y de Pearce et Gale (1977).

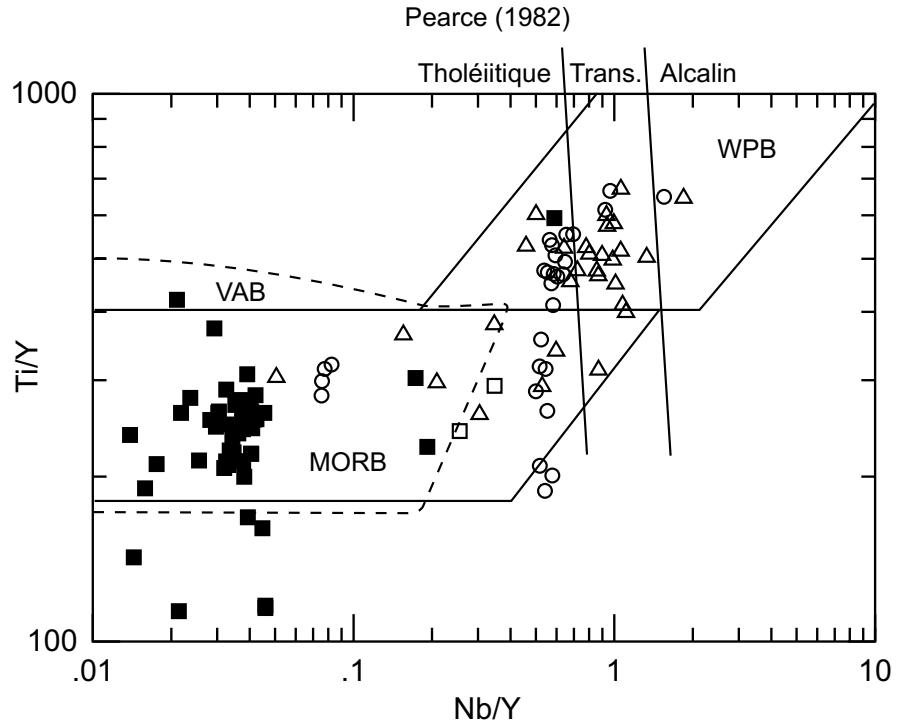

FIG. E.6 – Diagramme discriminant Ti/Y vs. Nb/Y de Pearce (1982).

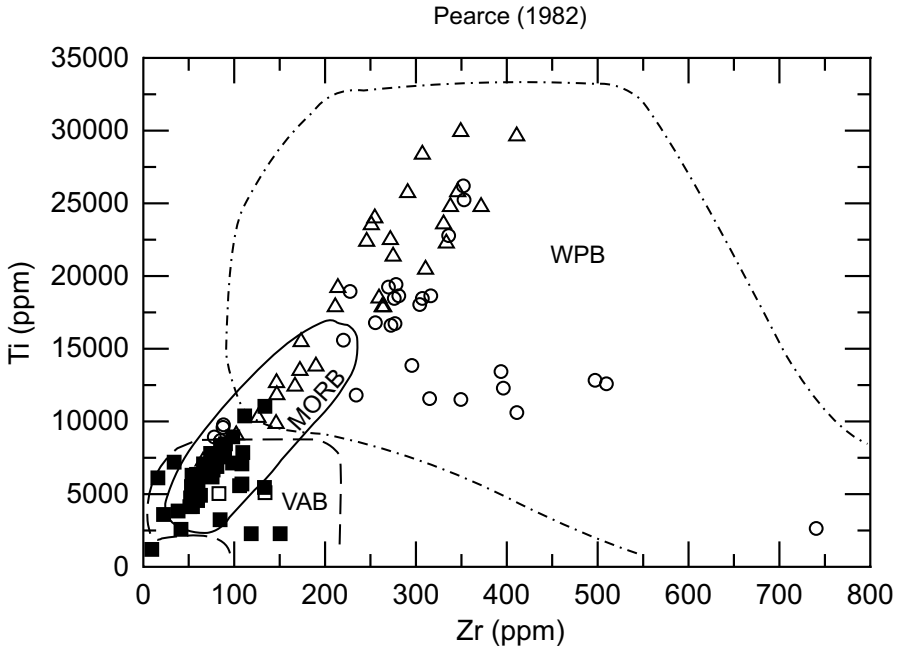

FIG. E.7 – Diagramme discriminant Ti vs. Zr de Pearce (1982).

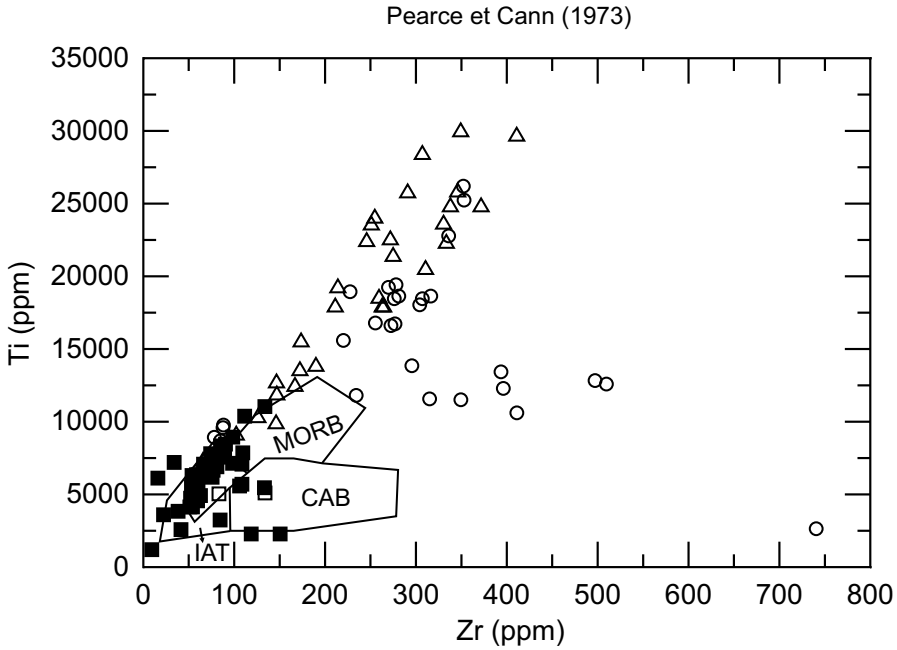

FIG. E.8 – Diagramme discriminant Ti vs. Zr de Pearce et Cann (1973).

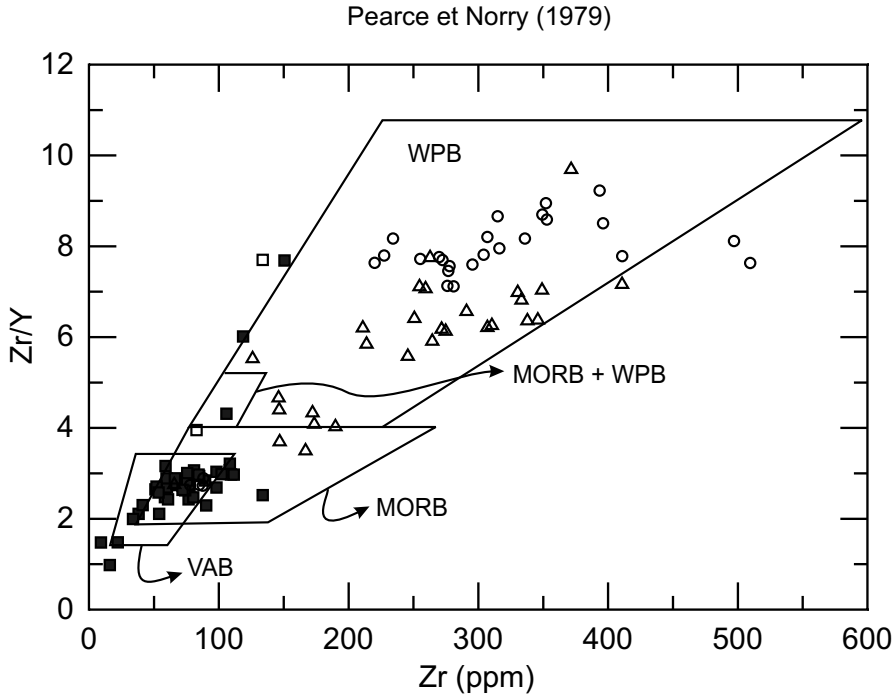

FIG. E.9 – Diagramme discriminant Zr/Y vs. Zr de Pearce et Norry (1979).

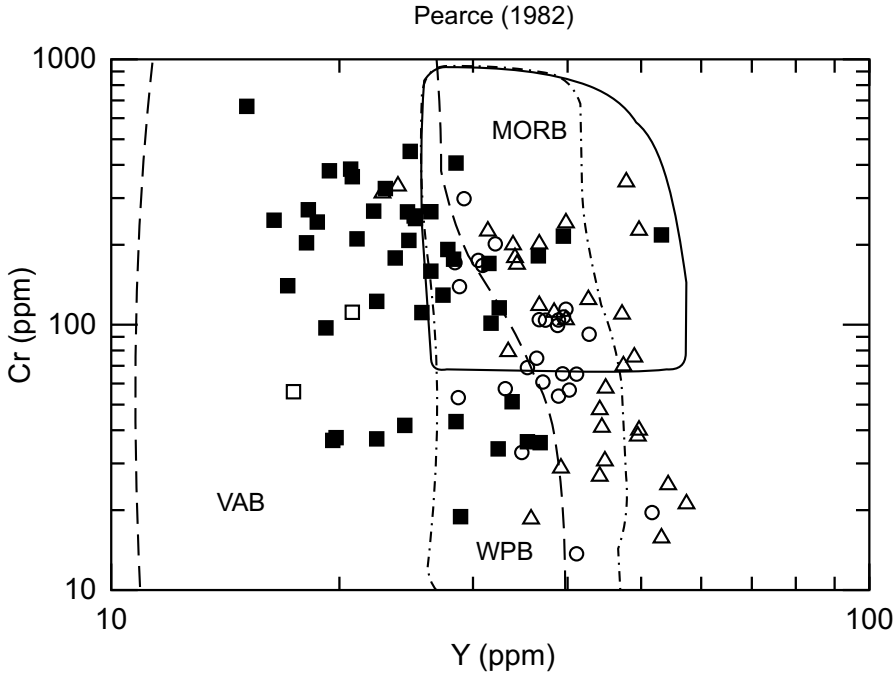

FIG. E.10 – Diagramme discriminant Cr vs. Y de Pearce (1982).

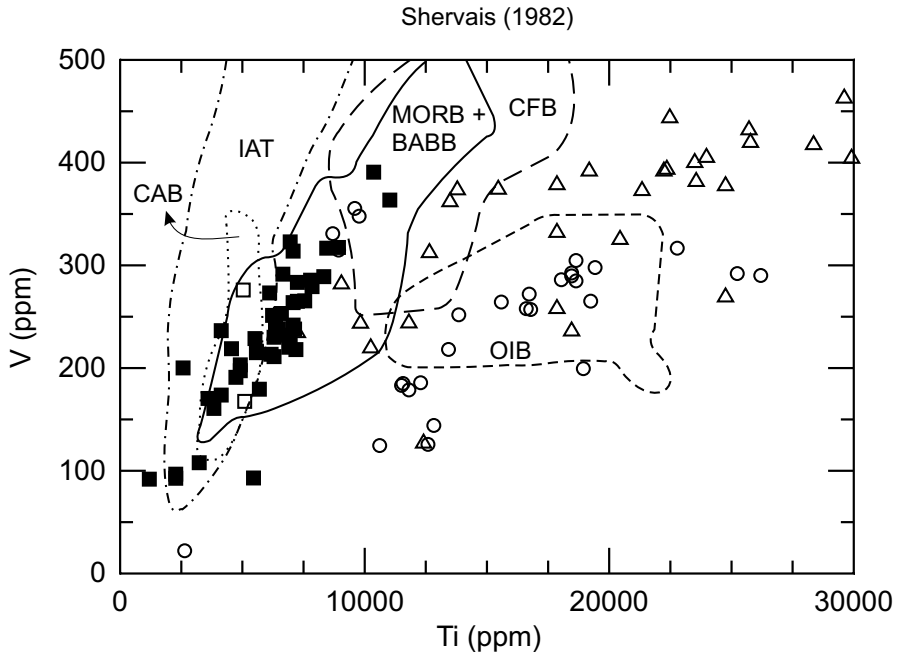

FIG. E.11 – Diagramme discriminant V vs. Ti de Shervais (1982).

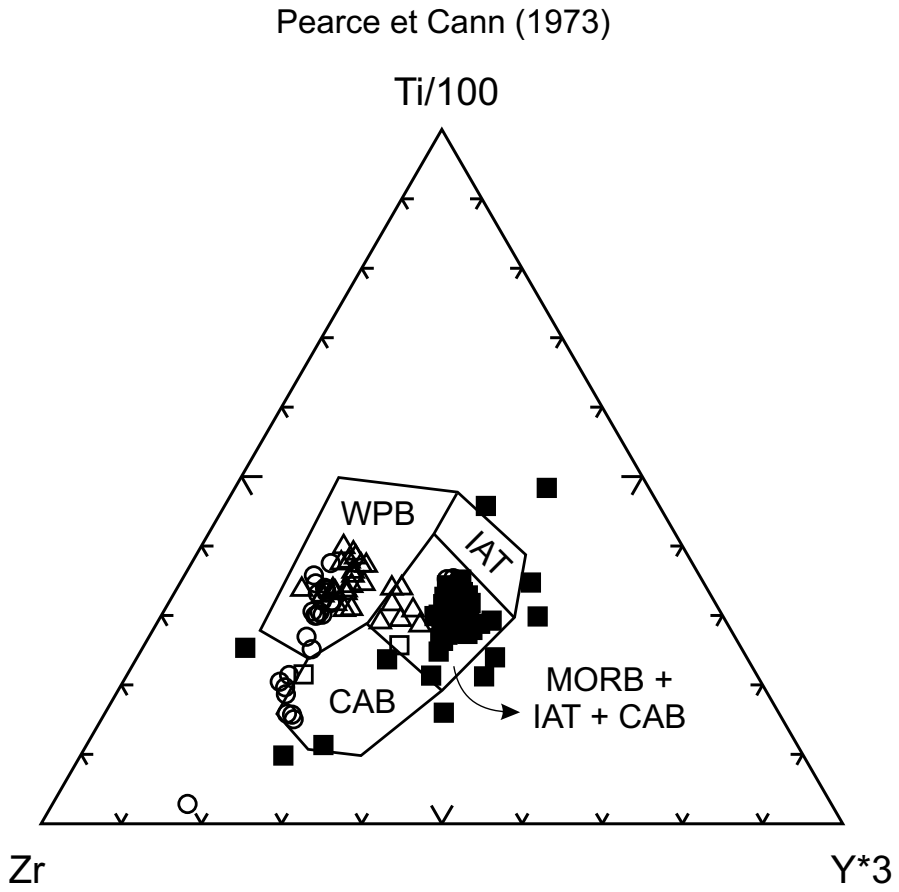

FIG. E.12 – Diagramme discriminant ternaire Zr-Ti-Y de Pearce et Cann (1973).

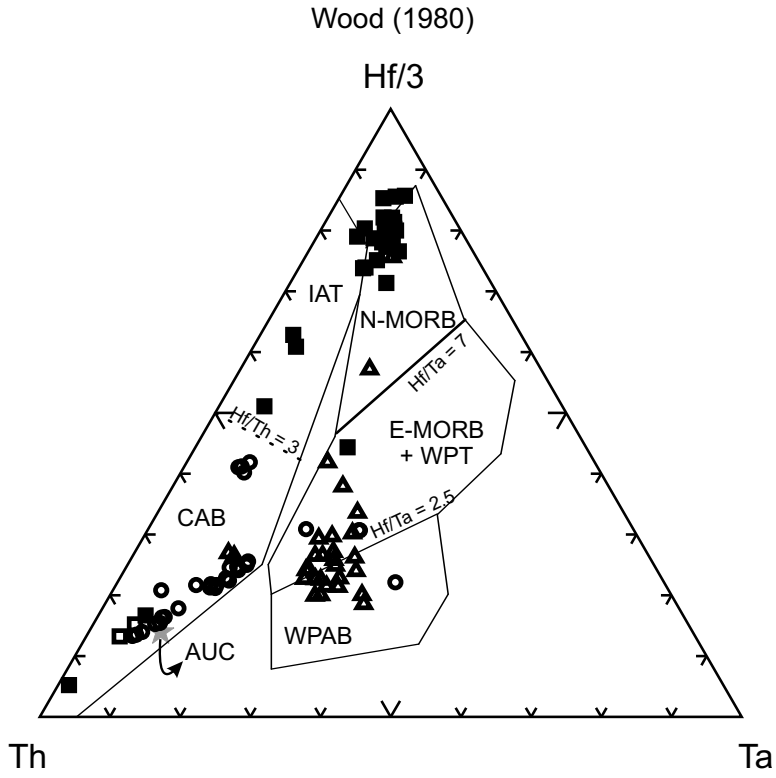

FIG. E.13 – Diagramme discriminant ternaire Th-Hf-Ta de Wood (1980).

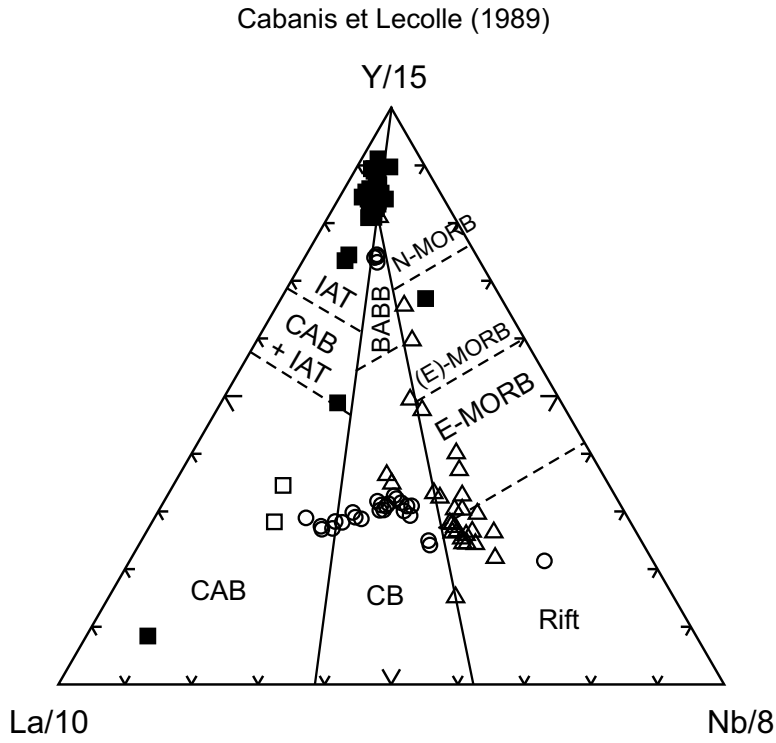

FIG. E.14 – Diagramme discriminant ternaire La-Y-Nb de Cabanis et Lecolle (1989).

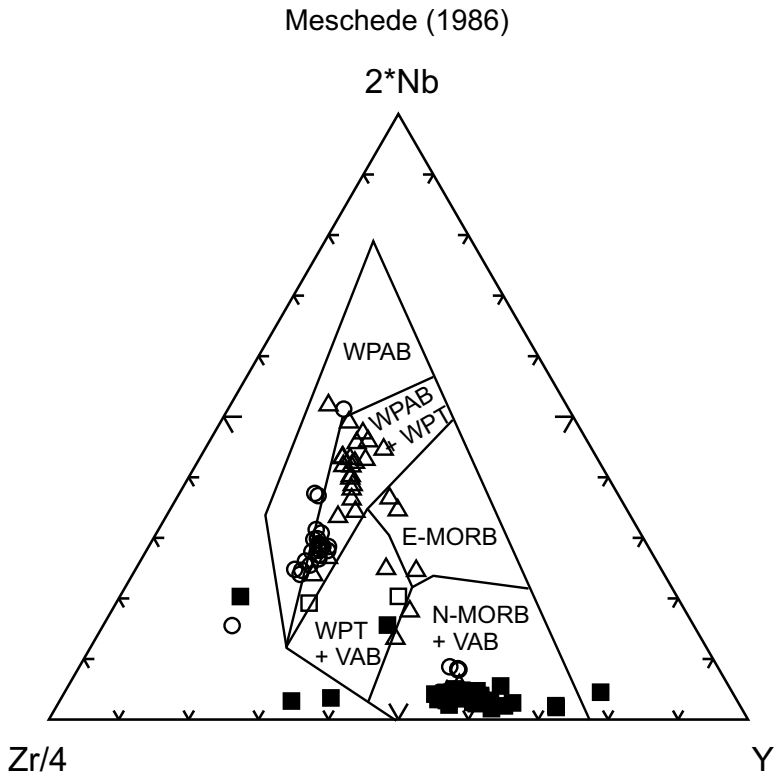

FIG. E.15 – Diagramme discriminant ternaire Zr-Nb-Y de Meschede (1986).

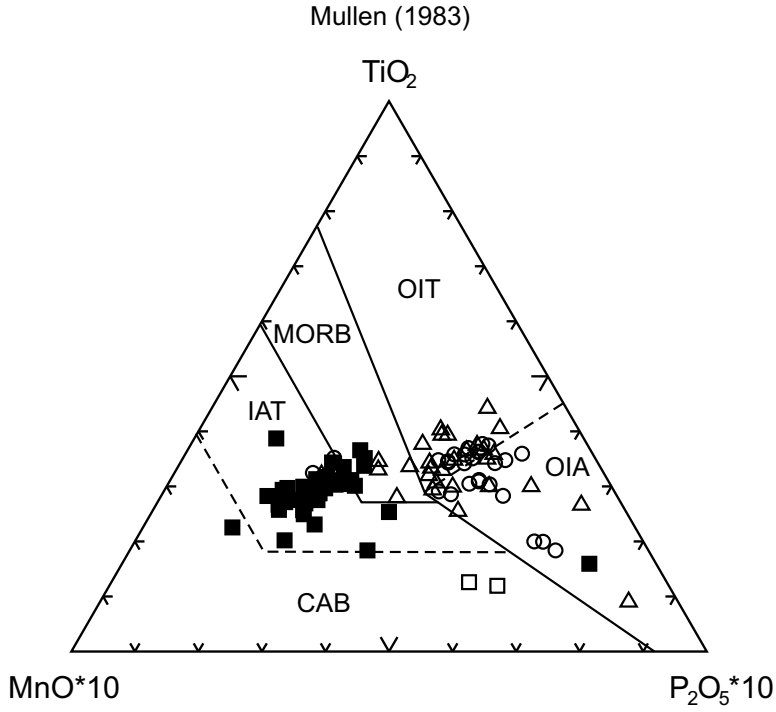

FIG. E.16 – Diagramme discriminant ternaire MnO-TiO_2-P_2O_5 de Mullen (1983).

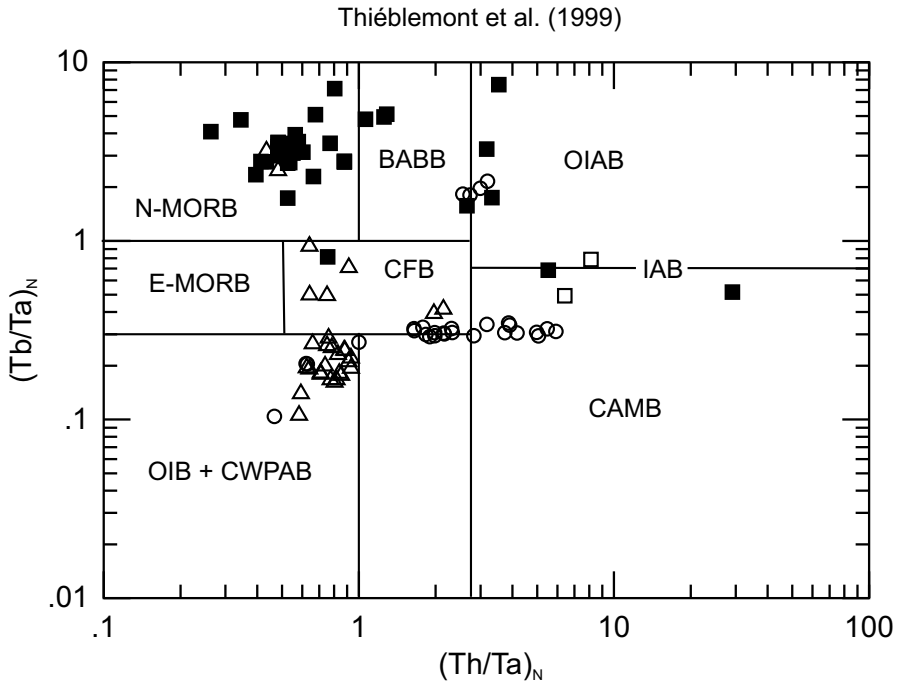

FIG. E.17 – Diagramme discriminant $(Tb/Ta)_N$ vs. $(Th/Ta)_N$ de Thiéblemont et al. (1994).

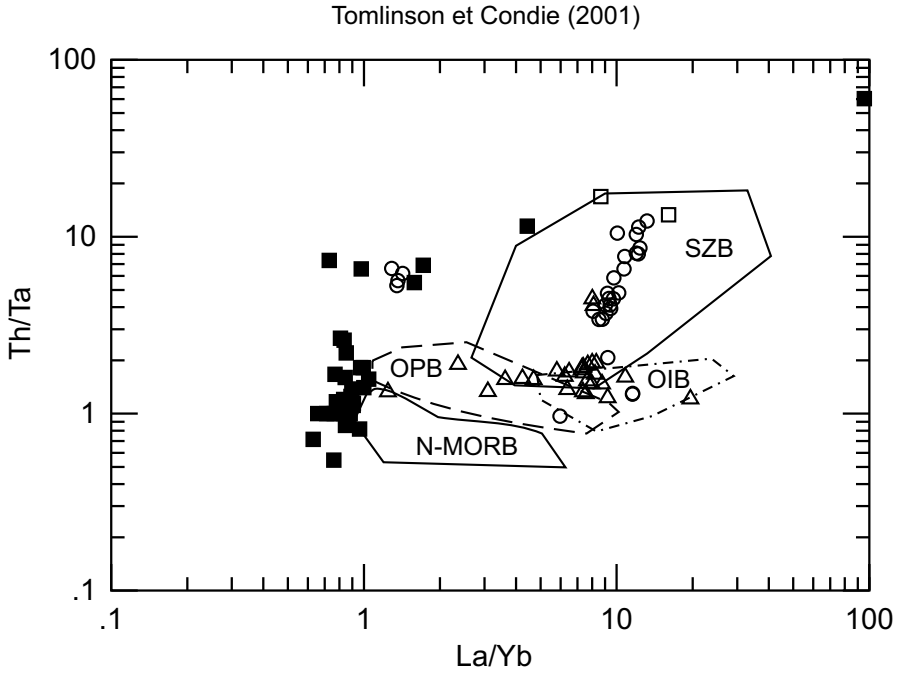

FIG. E.18 – Diagramme discriminant Th/Ta vs. La/Yb de Tomlinson et Condie (2001).

Annexe F

Comparaison de résultats géochimiques représentatifs avec les séquences ophiolitiques

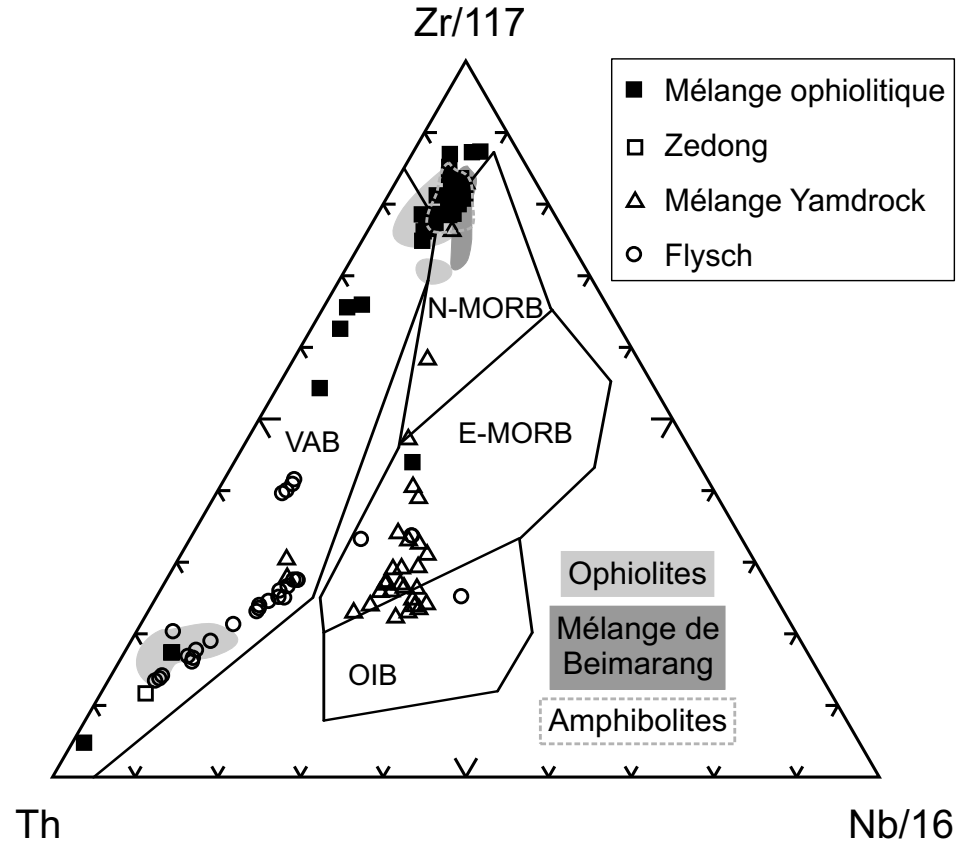

FIG. F.1 – Diagramme discriminant ternaire Th-Zr-Nb de Wood (1980) pour les roches mafiques. A des fins comparatives, les champs des ophiolites (Dubois-Côté et al., 2004 ; 2005), du mélange ophiolitique de Beimarang (Huot et al., 2002) et des amphibolites du mélange ophiolitique (Guilmette et al., en préparation) sont repésentés.

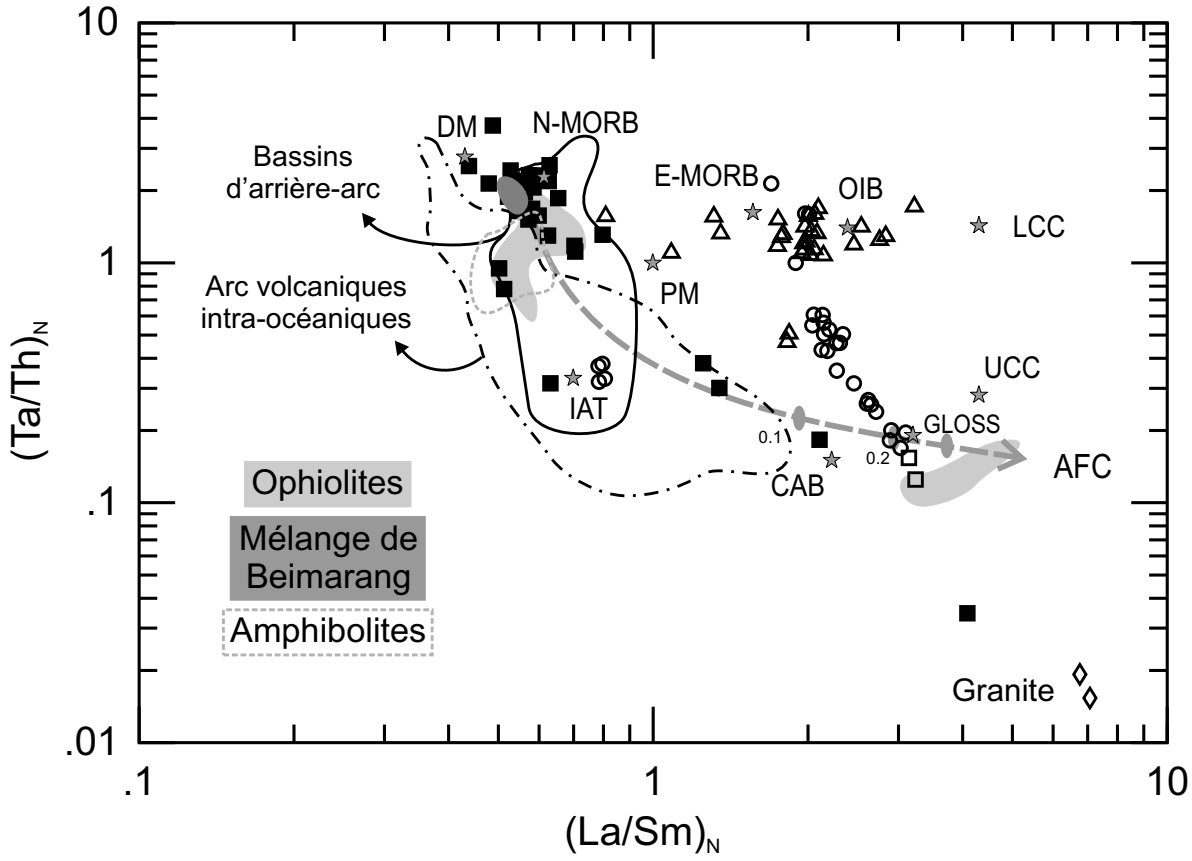

FIG. F.2 – $(Ta/Th)_N$ vs. $(La/Sm)_N$ pour les roches mafiques de toules les unités géologiques de la ZSYZ. A des fins comparatives, les champs des ophiolites (Dubois-Côté et al., 2004 ; 2005), du mélange ophiolitique de Beimarang (Huot et al., 2002) et des amphibolites du mélange ophiolitique (Guilmette et al., en préparation) sont repésentés. DM de Mckenzie et O'Nions (1991) excepté for Ta et Th de Chauvel et al. (1992). PM, N-MORB, E-MORB and OIB de Sun and McDonough (1989). IAT et CAB de Sun (1980). LCC de Weaver et Tarney (1984). UCC de Taylor et McLennan (1981). GLOSS (sédiment subducté global) de Plank et Langmuir (1998). FC = cristallisation fractionnée et AFC = assimilation et cristallisation fractionnée. Le champ noir continu délimite les compositions basaltiques des bassins d'arrière-arc de Lau et de l'arc de Tonga (Ewart et al., 1994a ; 1994b). Le champ noir en tireté et pointillé délimite les compositions basaltiques à andésitiques d'îles particulières d'arc intra-océaniques : l'arc de Tonga-Kermadec (Turner et al., 1997 ; Regelous et al., 1997 ; Ewart et al., 1998), l'arc de Izu-Bonin-Mariannes (Hawkesworth et al., 1977 ; Elliott et al., 1997 ; Taylor et Nesbitt, 1998 ; Pearce et al., 1999), et l'arc de Sandwich Sud (Hole et al, 1984 ; Pearce et al., 1995). La légende est la même qu'à la Fig. F.1.

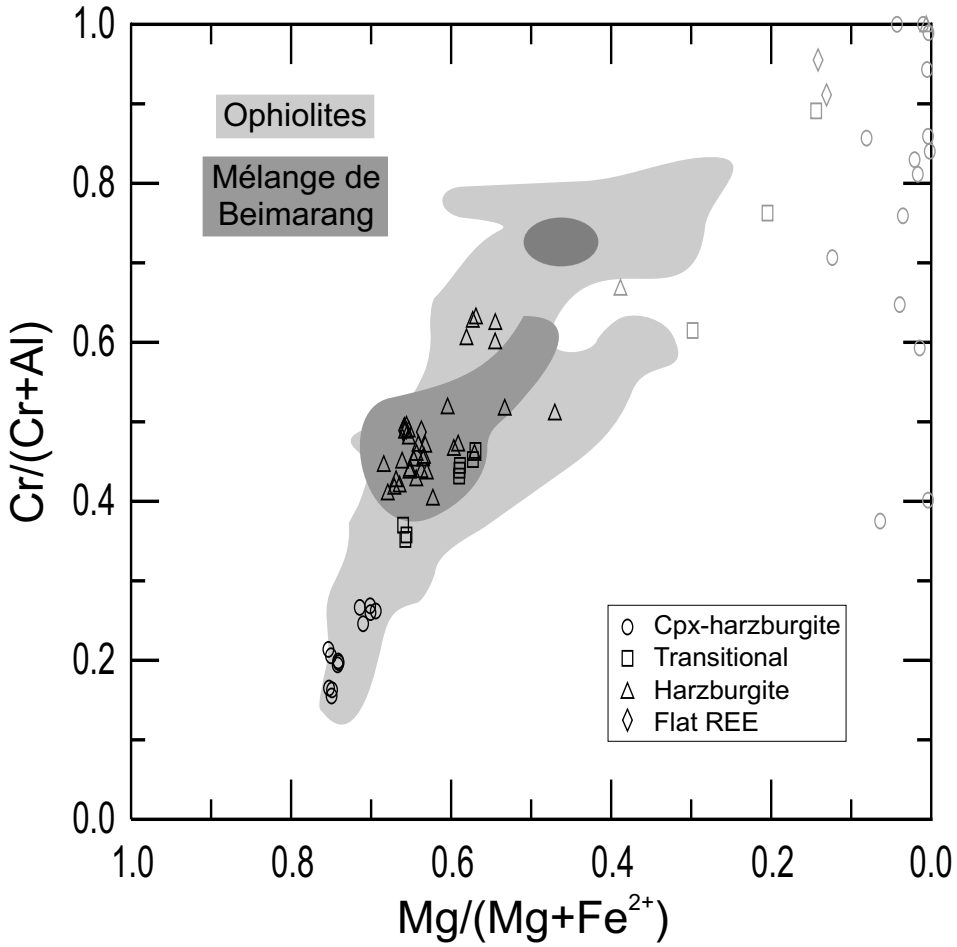

FIG. F.3 – Cr# vs. Mg# pour les spinelles des roches ultramafiques du mélange ophiolitique et des ophiolites. A des fins comparatives, les champs des ophiolites (Dubois-Côté et al., 2004 ; 2005) et du mélange ophiolitique de Beimarang (Huot et al., 2002) sont repésentés.

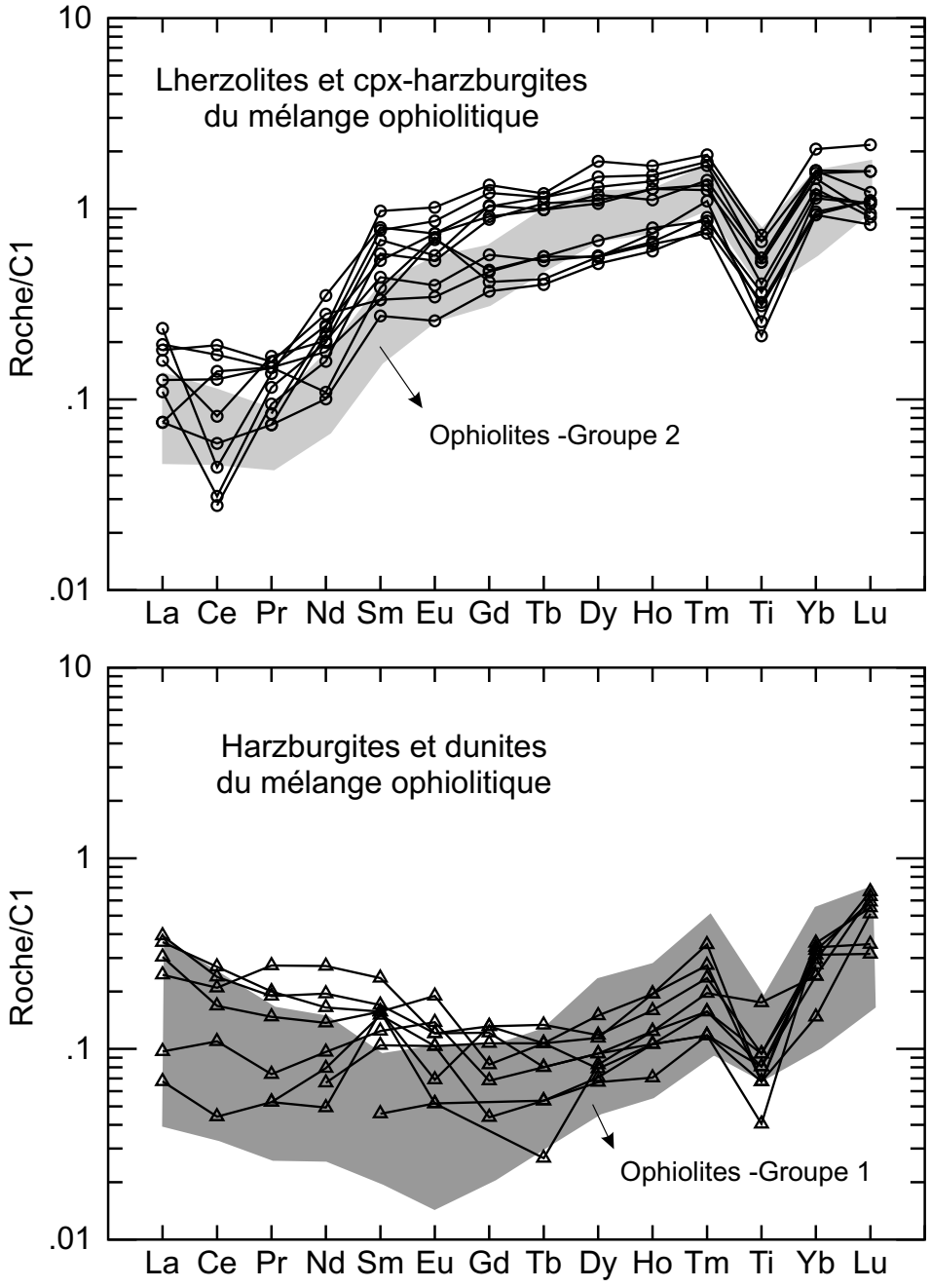

FIG. F.4 – Patrons des terres rares + Ti des roches ultramafiques du mélange ophiolitique et des ophiolites. A des fins comparatives, les champs des ophiolites (Dubois-Côté et al., 2004 ; 2005) sont repésentés.

Annexe G

Résultats de diverses modélisations pétrologiques

TAB. G.1: Modélisation des processus ACF ayant mené à la composition chimique des roches mafiques du flysch triasique pour un facteur d'assimilation de 0 (éléments majeurs en % poids et métaux de transition en ppm).

%ACF	SiO_2	TiO_2	Al_2O_3	Fe_2O_3	FeO	MnO	MgO	CaO	Na2O	K2O	P2O5	Cr	Ni	Co	Sc	V	Zn	Rb	Sr	Y	Zr
0.2	50.14	2.33	13.87	1.70	11.39	0.20	6.76	9.27	3.81	0.08	0.30	110.02	72.11	39.31	43.40	373.02	93.11	2.14	346.05	47.24	190.01
2.2	50.18	2.38	13.71	1.73	11.49	0.20	6.66	9.27	3.83	0.08	0.31	111.37	66.25	39.77	44.15	379.96	94.52	2.18	345.64	48.14	193.69
4.2	50.22	2.42	13.55	1.76	11.60	0.20	6.55	9.28	3.85	0.08	0.31	112.75	60.63	40.24	44.92	387.17	95.97	2.22	345.12	49.08	197.50
6.2	50.29	2.47	13.44	1.80	11.67	0.21	6.37	9.31	3.88	0.08	0.32	113.85	53.16	40.62	45.70	394.63	97.31	2.26	345.54	50.05	201.45
8.2	50.36	2.52	13.33	1.84	11.74	0.21	6.18	9.34	3.91	0.09	0.32	114.95	46.23	41.00	46.51	402.39	98.70	2.30	345.89	51.06	205.57
10.2	50.40	2.57	13.15	1.88	11.85	0.21	6.06	9.36	3.93	0.09	0.33	116.40	41.61	41.52	47.37	410.51	100.31	2.35	345.03	52.12	209.88
12.2	50.48	2.63	13.04	1.92	11.92	0.21	5.86	9.40	3.96	0.09	0.34	117.50	35.59	41.92	48.25	418.94	101.79	2.40	345.19	53.22	214.36
14.2	50.55	2.68	12.92	1.96	11.98	0.21	5.66	9.45	3.98	0.09	0.35	118.59	30.09	42.34	49.16	427.73	103.33	2.45	345.27	54.37	219.04
16.2	50.62	2.74	12.80	2.00	12.04	0.21	5.45	9.50	4.01	0.09	0.35	119.66	25.14	42.76	50.10	436.92	104.92	2.50	345.26	55.57	223.93
18.2	50.67	2.81	12.61	2.05	12.15	0.22	5.31	9.54	4.03	0.09	0.36	121.15	21.89	43.34	51.12	446.56	106.77	2.55	343.82	56.83	229.07
20.2	50.74	2.87	12.48	2.09	12.21	0.22	5.09	9.60	4.05	0.10	0.37	122.19	17.82	43.79	52.15	456.62	108.49	2.61	343.55	58.14	234.44
22.2	50.78	2.94	12.28	2.14	12.32	0.22	4.95	9.65	4.07	0.10	0.38	123.69	15.19	44.40	53.26	467.19	110.49	2.66	341.71	59.52	240.09
24.2	50.86	3.01	12.15	2.19	12.36	0.22	4.72	9.73	4.09	0.10	0.39	124.65	11.97	44.88	54.39	478.25	112.35	2.73	341.13	60.98	246.01
26.2	50.81	3.08	12.12	2.23	12.54	0.22	4.61	9.57	4.14	0.10	0.40	96.07	9.98	44.69	53.53	487.35	114.48	2.79	342.10	62.23	251.86
28.2	50.75	3.14	12.03	2.26	12.75	0.22	4.53	9.43	4.17	0.11	0.41	76.16	8.53	44.72	53.03	497.31	116.84	2.86	341.62	63.58	258.09
30.2	50.74	3.22	12.02	2.30	12.89	0.22	4.36	9.32	4.22	0.11	0.42	58.47	6.66	44.56	52.46	507.72	119.04	2.94	342.63	65.01	264.64
32.2	50.71	3.29	11.93	2.35	13.06	0.23	4.23	9.23	4.25	0.11	0.43	46.72	5.33	44.64	52.27	519.16	121.49	3.02	342.14	66.55	271.63
34.2	50.65	3.37	11.91	2.38	13.26	0.23	4.10	9.05	4.30	0.11	0.45	31.75	4.17	44.40	51.31	530.12	124.04	3.10	342.58	68.05	278.84
36.2	50.57	3.46	11.81	2.43	13.50	0.23	4.01	8.91	4.34	0.12	0.46	22.28	3.35	44.40	50.74	542.18	126.89	3.19	341.33	69.69	286.55
38.2	50.53	3.55	11.71	2.48	13.68	0.23	3.86	8.81	4.37	0.12	0.47	16.27	2.53	44.46	50.52	555.50	129.74	3.28	340.22	71.49	294.81
40.2	50.43	3.64	11.61	2.52	13.94	0.23	3.76	8.66	4.41	0.12	0.49	10.49	1.96	44.45	49.91	568.92	132.90	3.38	338.39	73.31	303.48
42.2	50.40	3.74	11.59	2.57	14.10	0.23	3.56	8.52	4.46	0.13	0.51	6.23	1.32	44.21	49.23	583.13	135.88	3.49	338.33	75.24	312.69
44.3	50.46	3.80	11.44	2.61	14.20	0.23	3.44	8.49	4.49	0.13	0.53	0.07	0.95	43.76	49.37	558.75	135.43	3.61	335.64	77.16	323.32
46.4	51.15	3.59	11.55	2.57	13.66	0.23	3.33	8.47	4.59	0.14	0.55	0.00	0.63	39.62	48.31	394.36	118.62	3.75	339.32	77.07	333.45
48.4	51.56	3.49	11.57	2.56	13.41	0.23	3.22	8.41	4.67	0.14	0.57	0.00	0.42	37.12	47.42	315.45	109.64	3.89	339.67	77.78	344.29
50.4	52.09	3.37	11.68	2.53	13.05	0.23	3.06	8.30	4.78	0.15	0.59	0.00	0.25	34.10	45.86	241.95	99.52	4.05	342.03	78.24	355.93

TAB. G.1: Modélisation ACF - facteur d'assimilation de 0

%ACF	SiO_2	TiO_2	Al_2O_3	Fe_2O_3	FeO	MnO	MgO	CaO	Na2O	K2O	P2O5	Cr	Ni	Co	Sc	V	Zn	Rb	Sr	Y	Zr
52.4	52.63	3.24	11.72	2.51	12.70	0.23	2.94	8.23	4.86	0.15	0.62	0.00	0.16	31.38	44.71	182.41	89.84	4.22	342.04	78.76	368.56
54.5	53.21	3.10	11.76	2.48	12.32	0.23	2.81	8.16	4.96	0.16	0.65	0.00	0.09	28.67	43.44	134.52	80.39	4.40	341.59	79.22	382.12
56.5	53.85	2.95	11.82	2.44	11.90	0.23	2.68	8.07	5.06	0.17	0.68	0.00	0.05	25.97	42.04	96.67	71.21	4.60	340.61	79.60	396.73
58.7	54.38	2.85	11.79	2.43	11.62	0.23	2.54	7.97	5.15	0.18	0.71	0.00	0.03	23.85	40.74	72.81	64.52	4.83	336.00	80.57	413.91
60.7	55.13	2.69	11.87	2.38	11.11	0.23	2.38	7.87	5.26	0.19	0.75	0.00	0.01	21.19	39.06	49.30	55.83	5.08	333.37	80.76	431.15
62.7	55.83	2.54	11.82	2.34	10.67	0.23	2.27	7.82	5.34	0.20	0.79	0.00	0.01	19.02	37.97	33.49	48.49	5.33	326.35	81.19	449.88
64.9	56.60	2.40	11.95	2.29	10.20	0.22	2.03	7.61	5.49	0.21	0.84	0.00	0.00	16.68	35.50	22.88	42.21	5.65	321.06	81.71	472.02
67.0	57.35	2.27	11.84	2.25	9.77	0.22	1.91	7.55	5.56	0.22	0.90	0.00	0.00	14.83	34.37	15.07	36.38	5.99	307.39	82.56	497.14
69.1	58.34	2.08	11.83	2.16	9.15	0.22	1.76	7.46	5.66	0.23	0.93	0.00	0.00	12.73	32.94	8.84	29.85	6.36	295.54	80.94	522.44
71.1	59.38	1.95	11.83	2.09	8.66	0.22	1.60	7.23	5.76	0.25	0.87	0.00	0.00	11.05	31.53	5.48	25.10	6.76	281.21	74.75	550.59
73.1	60.56	1.79	11.84	2.00	8.09	0.21	1.43	6.98	5.87	0.27	0.79	0.00	0.00	9.37	29.94	3.16	20.52	7.23	264.47	68.03	582.03
75.2	61.78	1.67	11.77	1.93	7.60	0.21	1.24	6.70	5.94	0.29	0.71	0.00	0.00	7.94	28.43	1.83	16.90	7.79	239.88	61.49	621.80
77.4	63.14	1.53	11.70	1.82	6.98	0.20	1.02	6.45	6.02	0.31	0.65	0.00	0.00	6.49	26.03	0.95	13.44	8.45	213.90	56.08	667.50
79.5	64.66	1.37	11.45	1.70	6.28	0.20	0.88	6.35	6.01	0.34	0.58	0.03	0.00	5.18	25.20	0.41	9.98	9.20	178.21	50.13	721.09
81.6	66.19	1.26	11.15	1.58	5.68	0.19	0.72	6.24	5.94	0.38	0.49	-0.01	0.00	4.17	24.49	0.19	7.60	10.06	140.42	44.13	784.41
83.6	67.66	1.18	10.75	1.49	5.17	0.19	0.54	6.18	5.79	0.42	0.44	-0.09	0.00	3.39	23.94	0.09	6.00	11.03	102.87	40.47	860.85
85.6	69.27	1.10	10.03	1.38	4.65	0.19	0.45	6.45	5.45	0.47	0.37	0.12	0.00	2.78	24.51	0.04	4.50	12.16	66.60	36.47	955.47
87.6	71.29	1.00	9.14	1.24	3.98	0.19	0.34	6.84	4.97	0.54	0.27	5.76	0.00	2.19	24.58	0.01	3.20	13.58	39.54	31.82	1075.12
89.7	73.03	1.09	7.61	1.29	4.02	0.20	0.24	7.42	4.08	0.63	0.14	-17.14	0.00	2.14	26.98	0.01	3.16	15.37	17.58	28.92	1258.74

TAB. G.2: Modélisation des processus ACF ayant mené à la composition chimique des roches mafiques du flysch triasique pour un facteur d'assimilation de 0 (éléments traces en ppm).

%ACF	Nb	Cs	Ba	La	Ce	Nd	Sm	Eu^{2+}	Eu^{3+}	Gd	Dy	Ho	Er	Tm	Yb	Lu	Hf	Ta	Pb	Th	U
0.2	24.98	0.26	84.37	15.87	40.56	21.55	5.72	1.77	0.00	6.69	6.77	1.40	4.12	0.58	3.74	0.55	3.74	1.30	3.77	2.05	0.55
2.2	25.47	0.27	85.73	16.15	41.31	21.95	5.83	1.76	0.00	6.82	6.90	1.43	4.20	0.59	3.81	0.56	3.81	1.33	3.83	2.09	0.56
4.2	25.97	0.27	87.14	16.45	42.09	22.36	5.94	1.76	0.00	6.95	7.03	1.45	4.28	0.60	3.88	0.57	3.89	1.35	3.89	2.13	0.57

TAB. G.2: Modélisation ACF - facteur d'assimilation de 0

%ACF	Nb	Cs	Ba	La	Ce	Nd	Sm	Eu^{2+}	Eu^{3+}	Gd	Dy	Ho	Er	Tm	Yb	Lu	Hf	Ta	Pb	Th	U
6.2	26.49	0.28	88.63	16.75	42.90	22.79	6.06	1.76	0.00	7.09	7.17	1.48	4.37	0.61	3.96	0.58	3.97	1.38	3.95	2.18	0.58
8.2	27.03	0.28	90.18	17.07	43.75	23.24	6.18	1.76	0.00	7.23	7.32	1.51	4.45	0.63	4.04	0.59	4.05	1.41	4.02	2.22	0.60
10.2	27.60	0.29	91.75	17.40	44.63	23.71	6.31	1.76	0.00	7.38	7.47	1.54	4.55	0.64	4.12	0.61	4.14	1.44	4.09	2.27	0.61
12.2	28.18	0.29	93.42	17.75	45.54	24.19	6.44	1.76	0.00	7.54	7.63	1.58	4.64	0.65	4.21	0.62	4.23	1.47	4.16	2.32	0.62
14.2	28.80	0.30	95.16	18.11	46.50	24.70	6.58	1.76	0.00	7.70	7.79	1.61	4.74	0.67	4.30	0.63	4.32	1.50	4.24	2.37	0.63
16.2	29.44	0.31	96.97	18.49	47.51	25.23	6.72	1.76	0.00	7.87	7.96	1.65	4.85	0.68	4.39	0.64	4.42	1.54	4.32	2.42	0.65
18.2	30.12	0.31	98.80	18.88	48.55	25.79	6.87	1.75	0.00	8.05	8.14	1.68	4.96	0.70	4.49	0.66	4.52	1.57	4.40	2.48	0.66
20.2	30.82	0.32	100.77	19.30	49.65	26.37	7.03	1.75	0.00	8.24	8.33	1.72	5.07	0.71	4.59	0.67	4.63	1.61	4.48	2.54	0.68
22.2	31.57	0.33	102.76	19.73	50.80	26.98	7.20	1.74	0.00	8.44	8.53	1.76	5.19	0.73	4.70	0.69	4.74	1.65	4.57	2.60	0.70
24.2	32.35	0.34	104.91	20.18	52.01	27.62	7.37	1.74	0.00	8.64	8.74	1.81	5.32	0.75	4.81	0.71	4.86	1.69	4.66	2.66	0.71
26.2	33.19	0.35	107.29	20.66	53.25	28.24	7.53	1.75	0.00	8.81	8.88	1.83	5.40	0.76	4.88	0.72	4.95	1.73	4.77	2.73	0.73
28.2	34.07	0.36	109.73	21.16	54.56	28.90	7.71	1.74	0.00	8.99	9.03	1.86	5.49	0.77	4.96	0.73	5.05	1.78	4.88	2.80	0.75
30.2	35.00	0.37	112.36	21.69	55.95	29.60	7.89	1.75	0.00	9.19	9.19	1.90	5.58	0.79	5.04	0.74	5.15	1.82	5.00	2.88	0.77
32.2	35.98	0.38	115.05	22.25	57.41	30.34	8.08	1.75	0.00	9.40	9.38	1.93	5.69	0.80	5.14	0.75	5.27	1.88	5.12	2.96	0.79
34.2	37.03	0.39	117.97	22.84	58.94	31.10	8.28	1.75	0.00	9.60	9.54	1.96	5.77	0.81	5.22	0.76	5.37	1.93	5.25	3.05	0.81
36.2	38.13	0.40	120.96	23.46	60.56	31.90	8.49	1.75	0.00	9.82	9.72	2.00	5.88	0.83	5.31	0.78	5.49	1.99	5.38	3.14	0.84
38.2	39.30	0.41	124.12	24.12	62.29	32.78	8.72	1.74	0.00	10.06	9.93	2.04	6.00	0.84	5.42	0.79	5.63	2.05	5.53	3.24	0.86
40.2	40.56	0.42	127.46	24.82	64.11	33.68	8.95	1.74	0.00	10.31	10.13	2.08	6.11	0.86	5.51	0.81	5.76	2.11	5.68	3.34	0.89
42.2	41.89	0.44	131.13	25.57	66.07	34.65	9.20	1.74	0.00	10.57	10.33	2.11	6.22	0.87	5.62	0.82	5.90	2.18	5.84	3.45	0.92
44.3	43.38	0.45	135.18	26.44	68.35	35.81	9.51	1.72	0.00	10.91	10.63	2.17	6.39	0.90	5.77	0.84	6.08	2.25	6.02	3.58	0.95
46.4	44.85	0.47	140.10	27.43	70.92	37.10	9.84	1.74	0.00	11.26	10.92	2.23	6.55	0.92	5.91	0.86	6.22	2.32	6.24	3.72	0.99
48.4	46.42	0.49	144.93	28.42	73.51	38.40	10.18	1.75	0.00	11.61	11.21	2.28	6.71	0.94	6.05	0.88	6.38	2.39	6.46	3.86	1.03
50.4	48.14	0.51	150.43	29.53	76.37	39.80	10.54	1.76	0.00	11.98	11.48	2.34	6.86	0.96	6.17	0.90	6.54	2.47	6.71	4.02	1.07
52.4	49.98	0.53	156.20	30.72	79.46	41.34	10.93	1.77	0.00	12.39	11.81	2.40	7.03	0.99	6.33	0.92	6.72	2.56	6.97	4.19	1.11
54.5	51.96	0.56	162.43	32.00	82.82	43.00	11.36	1.77	0.00	12.83	12.15	2.46	7.21	1.01	6.49	0.95	6.91	2.65	7.25	4.38	1.16
56.5	54.10	0.59	169.20	33.41	86.48	44.79	11.82	1.76	0.00	13.30	12.51	2.53	7.41	1.04	6.65	0.97	7.11	2.75	7.55	4.59	1.21
58.7	56.61	0.62	176.67	34.99	90.64	46.83	12.35	1.74	0.00	13.83	12.91	2.60	7.62	1.07	6.84	1.00	7.36	2.87	7.89	4.82	1.27
60.7	59.16	0.65	184.74	36.68	95.05	48.98	12.89	1.73	0.00	14.38	13.32	2.68	7.83	1.10	7.02	1.02	7.59	2.98	8.25	5.07	1.34
62.7	61.88	0.69	193.01	38.47	99.80	51.31	13.50	1.70	0.00	15.00	13.79	2.76	8.08	1.13	7.24	1.05	7.86	3.11	8.62	5.34	1.41
64.9	65.21	0.73	203.22	40.62	105.40	53.97	14.16	1.67	0.00	15.64	14.20	2.83	8.28	1.16	7.40	1.08	8.14	3.26	9.08	5.67	1.49

Tab. G.2: Modélisation ACF - facteur d'assimilation de 0

%ACF	Nb	Cs	Ba	La	Ce	Nd	Sm	Eu^{2+}	Eu^{3+}	Gd	Dy	Ho	Er	Tm	Yb	Lu	Hf	Ta	Pb	Th	U
67.0	68.88	0.78	213.73	42.98	111.70	57.04	14.96	1.61	0.00	16.45	14.81	2.94	8.60	1.20	7.68	1.12	8.50	3.42	9.55	6.04	1.58
69.1	72.62	0.83	225.09	45.16	117.10	59.23	15.41	1.53	0.00	16.88	15.13	3.01	8.80	1.23	7.89	1.15	8.84	3.59	10.05	6.43	1.68
71.1	76.88	0.89	237.43	46.35	118.53	58.10	14.64	1.37	0.00	16.05	14.54	2.93	8.67	1.22	7.89	1.15	9.22	3.78	10.60	6.87	1.79
73.1	81.66	0.95	251.19	47.56	119.69	56.61	13.76	1.21	0.00	15.09	13.85	2.84	8.48	1.21	7.86	1.15	9.64	3.99	11.21	7.38	1.92
75.2	87.69	1.04	267.14	48.91	120.93	54.88	12.80	1.02	0.00	14.06	13.10	2.73	8.28	1.19	7.84	1.15	10.19	4.26	11.91	8.01	2.08
77.4	94.62	1.14	285.13	50.87	123.98	54.22	12.20	0.85	0.00	13.42	12.67	2.68	8.23	1.20	7.94	1.17	10.82	4.57	12.69	8.76	2.27
79.5	102.64	1.25	304.13	52.81	126.72	53.14	11.47	0.65	0.00	12.66	12.18	2.62	8.19	1.21	8.07	1.19	11.57	4.92	13.50	9.66	2.49
81.6	112.19	1.40	324.06	54.49	128.33	51.17	10.51	0.47	0.00	11.66	11.49	2.54	8.06	1.21	8.16	1.21	12.46	5.34	14.34	10.72	2.76
83.6	123.67	1.56	344.57	57.06	132.79	50.79	10.04	0.32	0.00	11.17	11.19	2.52	8.11	1.23	8.39	1.25	13.55	5.86	15.18	11.98	3.07
85.6	137.74	1.78	364.75	59.67	137.30	50.10	9.49	0.19	0.00	10.65	10.96	2.53	8.29	1.28	8.80	1.32	14.94	6.49	15.94	13.59	3.46
87.6	155.63	2.05	387.83	62.47	141.73	48.83	8.77	0.10	0.00	9.97	10.68	2.54	8.52	1.34	9.35	1.41	16.73	7.30	16.76	15.69	3.98
89.7	183.26	2.45	410.28	65.27	145.62	46.58	7.80	0.04	0.00	9.02	10.14	2.52	8.70	1.40	9.96	1.52	19.53	8.60	17.48	18.67	4.70

Tab. G.3: Modélisation des processus ACF ayant mené à la composition chimique des roches mafiques du flysch triasique pour un facteur d'assimilation de 0.05 (éléments majeurs en % poids et métaux de transition en ppm).

%ACF	SiO_2	TiO_2	Al_2O_3	Fe_2O_3	FeO	MnO	MgO	CaO	Na2O	K2O	P2O5	Cr	Ni	Co	Sc	V	Zn	Rb	Sr	Y	Zr
0.2	50.14	2.33	13.87	1.70	11.39	0.20	6.76	9.27	3.81	0.08	0.30	110.02	72.11	39.31	43.40	373.02	93.11	2.14	346.05	47.24	190.01
2.2	50.20	2.37	13.71	1.73	11.48	0.20	6.65	9.26	3.83	0.09	0.31	111.29	66.20	39.74	44.11	379.61	94.47	2.45	346.69	48.11	193.72
4.2	50.26	2.42	13.55	1.76	11.58	0.20	6.54	9.26	3.85	0.10	0.31	112.58	60.55	40.18	44.84	386.44	95.87	2.77	347.23	49.01	197.56
6.2	50.34	2.46	13.45	1.80	11.64	0.21	6.35	9.29	3.88	0.11	0.32	113.60	53.06	40.52	45.57	393.49	97.16	3.10	348.72	49.94	201.52
8.2	50.43	2.51	13.34	1.83	11.69	0.21	6.16	9.32	3.91	0.12	0.32	114.60	46.11	40.87	46.33	400.81	98.48	3.45	350.16	50.90	205.65
10.2	50.52	2.56	13.24	1.87	11.75	0.21	5.96	9.35	3.94	0.12	0.33	115.59	39.71	41.22	47.11	408.42	99.85	3.81	351.54	51.91	209.94
12.2	50.58	2.61	13.06	1.91	11.84	0.21	5.83	9.36	3.95	0.13	0.34	116.93	35.45	41.71	47.95	416.36	101.43	4.18	351.66	52.95	214.42
14.2	50.67	2.67	12.95	1.95	11.89	0.21	5.62	9.40	3.98	0.15	0.35	117.90	29.97	42.08	48.80	424.60	102.89	4.56	352.86	54.04	219.08
16.2	50.76	2.72	12.83	1.99	11.94	0.21	5.40	9.44	4.01	0.16	0.35	118.84	25.02	42.46	49.68	433.18	104.39	4.97	353.98	55.18	223.93
18.2	50.83	2.78	12.65	2.04	12.03	0.21	5.27	9.47	4.02	0.17	0.36	120.19	21.78	42.98	50.62	442.15	106.14	5.39	353.65	56.36	229.02

TAB. G.3: Modélisation ACF - facteur d'assimilation de 0.05

%ACF	SiO_2	TiO_2	Al_2O_3	Fe_2O_3	FeO	MnO	MgO	CaO	Na2O	K2O	P2O5	Cr	Ni	Co	Sc	V	Zn	Rb	Sr	Y	Zr
20.2	50.92	2.84	12.53	2.08	12.07	0.22	5.04	9.52	4.05	0.18	0.37	121.08	17.73	43.38	51.57	451.49	107.75	5.82	354.54	57.60	234.31
22.2	50.98	2.91	12.34	2.13	12.16	0.22	4.90	9.56	4.06	0.19	0.38	122.42	15.12	43.94	52.59	461.27	109.63	6.28	353.83	58.89	239.87
24.2	51.08	2.97	12.21	2.18	12.19	0.22	4.66	9.62	4.09	0.20	0.39	123.22	11.92	44.35	53.62	471.48	111.36	6.76	354.43	60.25	245.67
26.2	51.06	3.03	12.20	2.21	12.35	0.22	4.55	9.46	4.13	0.22	0.40	94.62	9.95	44.11	52.67	479.69	113.35	7.27	356.63	61.39	251.38
28.2	51.04	3.09	12.19	2.24	12.51	0.22	4.43	9.28	4.17	0.23	0.41	70.80	8.20	43.85	51.71	488.23	115.41	7.80	358.76	62.59	257.37
30.2	51.04	3.16	12.11	2.28	12.65	0.22	4.29	9.18	4.21	0.25	0.42	57.24	6.67	43.87	51.41	498.04	117.57	8.35	359.64	63.93	263.79
32.2	51.04	3.23	12.03	2.32	12.80	0.22	4.15	9.08	4.24	0.26	0.43	45.52	5.35	43.88	51.10	508.31	119.83	8.94	360.35	65.33	270.54
34.2	51.00	3.30	11.95	2.36	12.99	0.22	4.06	8.92	4.27	0.28	0.44	33.10	4.40	43.82	50.41	518.54	122.32	9.55	360.50	66.74	277.55
36.2	50.97	3.38	11.93	2.39	13.17	0.22	3.93	8.74	4.32	0.30	0.46	21.50	3.40	43.50	49.33	528.71	124.77	10.21	362.00	68.15	284.84
38.2	50.96	3.46	11.85	2.44	13.33	0.22	3.78	8.63	4.36	0.32	0.47	15.54	2.59	43.48	48.96	540.49	127.35	10.89	362.07	69.75	292.72
40.2	50.93	3.54	11.84	2.47	13.51	0.22	3.63	8.43	4.41	0.34	0.48	8.99	1.91	43.11	47.81	551.64	130.03	11.62	363.11	71.28	300.83
42.2	50.89	3.63	11.68	2.53	13.70	0.22	3.51	8.35	4.42	0.36	0.50	6.65	1.49	43.36	47.83	565.28	133.06	12.38	360.90	73.12	309.73
44.2	51.07	3.63	11.68	2.54	13.68	0.22	3.38	8.22	4.48	0.38	0.52	0.01	1.08	41.89	46.80	517.04	129.80	13.25	362.42	74.21	318.70
46.3	51.61	3.49	11.81	2.51	13.29	0.22	3.24	8.12	4.57	0.40	0.53	0.00	0.71	38.56	45.40	397.86	117.77	14.17	367.03	74.42	328.36
48.3	52.07	3.39	11.84	2.50	13.01	0.22	3.13	8.04	4.64	0.43	0.55	0.01	0.51	36.04	44.37	317.57	108.61	15.14	368.90	74.87	338.35
50.5	52.73	3.21	11.91	2.46	12.53	0.22	3.01	7.98	4.73	0.46	0.58	0.00	0.36	32.72	43.16	227.99	95.90	16.27	371.77	74.88	349.53
52.6	53.20	3.12	11.97	2.44	12.26	0.22	2.85	7.83	4.82	0.49	0.60	0.01	0.25	30.36	41.55	182.52	88.69	17.48	373.04	75.51	361.74
54.6	54.02	2.89	12.04	2.37	11.63	0.22	2.75	7.81	4.91	0.53	0.63	0.00	0.20	26.95	40.46	118.94	75.22	18.76	375.11	74.96	373.40
56.7	54.49	2.82	12.11	2.36	11.39	0.22	2.58	7.63	5.01	0.57	0.66	0.01	0.14	24.94	38.61	95.76	69.77	20.10	374.42	75.65	387.08
58.8	55.15	2.67	12.09	2.32	10.96	0.22	2.48	7.57	5.07	0.60	0.69	0.00	0.13	22.63	37.56	67.78	61.43	21.54	370.97	75.78	401.14
60.8	55.86	2.52	12.18	2.27	10.49	0.21	2.32	7.43	5.17	0.65	0.72	0.00	0.11	20.23	35.80	47.54	53.81	23.15	369.34	75.71	415.82
62.9	56.56	2.39	12.20	2.22	10.06	0.21	2.16	7.28	5.26	0.70	0.76	0.00	0.10	18.09	34.08	33.26	47.23	24.95	363.27	75.96	433.44
64.9	57.39	2.22	12.31	2.15	9.51	0.21	1.98	7.12	5.37	0.75	0.80	0.01	0.08	15.79	32.02	21.85	40.29	26.83	358.93	75.59	450.47
67.0	58.31	2.03	12.33	2.07	8.89	0.20	1.84	7.03	5.46	0.81	0.84	0.01	0.09	13.63	30.49	13.26	33.33	28.96	350.06	75.03	469.04
69.0	58.90	1.97	12.32	2.04	8.62	0.20	1.65	6.80	5.53	0.87	0.89	0.01	0.07	12.34	28.51	10.19	30.46	31.15	336.17	75.80	490.75
71.1	60.18	1.77	12.41	1.93	7.91	0.20	1.49	6.52	5.64	0.95	0.80	0.00	0.07	10.30	26.79	5.60	24.21	33.84	323.77	67.54	513.35
73.3	61.31	1.63	12.39	1.84	7.39	0.19	1.33	6.24	5.71	1.03	0.74	0.02	0.07	8.79	25.15	3.40	20.09	36.90	302.19	61.36	540.62
75.5	62.47	1.50	12.37	1.75	6.83	0.19	1.15	5.96	5.77	1.13	0.69	0.00	0.06	7.38	23.34	2.03	16.43	40.27	276.06	56.35	570.64
77.5	63.81	1.32	12.30	1.62	6.15	0.18	1.02	5.73	5.80	1.23	0.60	0.01	0.08	6.02	22.09	1.07	12.61	43.87	247.62	48.91	600.15

Tab. G.3: Modélisation ACF - facteur d'assimilation de 0.05

%ACF	SiO_2	TiO_2	Al_2O_3	Fe_2O_3	FeO	MnO	MgO	CaO	Na2O	K2O	P2O5	Cr	Ni	Co	Sc	V	Zn	Rb	Sr	Y	Zr
79.6	65.35	1.15	12.32	1.46	5.37	0.17	0.79	5.40	5.87	1.36	0.54	-0.01	0.05	4.64	18.68	0.54	9.42	48.16	218.46	42.70	636.53
81.8	66.90	0.99	12.17	1.30	4.62	0.16	0.64	5.19	5.83	1.51	0.46	-0.01	0.06	3.58	16.75	0.30	6.84	52.92	176.95	36.34	677.10
83.8	68.42	0.85	11.98	1.14	3.91	0.15	0.48	5.01	5.74	1.68	0.41	-0.01	0.05	2.70	15.49	0.20	4.93	58.09	131.23	31.76	723.04
85.9	70.07	0.75	11.76	0.97	3.26	0.13	0.30	4.75	5.59	1.88	0.30	0.01	0.01	2.02	14.39	0.18	3.65	63.96	90.26	25.13	776.04
88.0	71.20	0.73	11.09	0.93	3.02	0.13	0.22	4.88	5.14	2.12	0.28	-1.24	0.04	1.82	14.47	0.27	3.39	69.98	48.83	23.98	852.06
90.1	72.43	0.77	10.29	0.92	2.93	0.13	0.13	5.00	4.54	2.41	0.19	-20.32	-0.05	1.75	15.00	0.42	3.54	77.01	25.37	20.72	948.64

Tab. G.4: Modélisation des processus ACF ayant mené à la composition chimique des roches mafiques du flysch triasique pour un facteur d'assimilation de 0.05 (éléments traces en ppm).

%ACF	Nb	Cs	Ba	La	Ce	Nd	Sm	Eu^{2+}	Eu^{3+}	Gd	Dy	Ho	Er	Tm	Yb	Lu	Hf	Ta	Pb	Th	U
0.2	24.98	0.26	84.37	15.87	40.56	21.55	5.72	1.77	0.00	6.69	6.77	1.40	4.12	0.58	3.74	0.55	3.74	1.30	3.77	2.05	0.55
2.2	25.45	0.27	89.67	16.27	41.53	22.02	5.84	1.76	0.00	6.81	6.90	1.43	4.20	0.59	3.81	0.56	3.81	1.32	3.86	2.16	0.57
4.2	25.94	0.29	95.15	16.69	42.54	22.51	5.96	1.76	0.00	6.94	7.02	1.45	4.27	0.60	3.88	0.57	3.89	1.35	3.96	2.27	0.59
6.2	26.44	0.30	100.85	17.12	43.59	23.02	6.08	1.77	0.00	7.07	7.16	1.48	4.35	0.61	3.95	0.58	3.97	1.38	4.06	2.39	0.62
8.2	26.96	0.32	106.76	17.58	44.68	23.54	6.21	1.77	0.00	7.20	7.30	1.51	4.44	0.62	4.02	0.59	4.05	1.40	4.17	2.51	0.64
10.2	27.50	0.33	112.88	18.05	45.81	24.09	6.34	1.77	0.00	7.34	7.44	1.54	4.53	0.64	4.10	0.60	4.14	1.43	4.28	2.64	0.66
12.2	28.07	0.35	119.18	18.53	46.99	24.66	6.48	1.77	0.00	7.49	7.59	1.57	4.62	0.65	4.18	0.61	4.23	1.46	4.39	2.77	0.69
14.2	28.66	0.37	125.77	19.04	48.22	25.25	6.63	1.77	0.00	7.64	7.75	1.60	4.71	0.66	4.27	0.63	4.32	1.49	4.51	2.91	0.72
16.2	29.27	0.38	132.61	19.57	49.50	25.87	6.78	1.77	0.00	7.80	7.91	1.64	4.81	0.68	4.36	0.64	4.42	1.53	4.63	3.06	0.74
18.2	29.91	0.40	139.66	20.11	50.83	26.51	6.94	1.76	0.00	7.97	8.08	1.67	4.91	0.69	4.45	0.65	4.52	1.56	4.75	3.21	0.77
20.2	30.58	0.42	147.05	20.69	52.22	27.19	7.10	1.76	0.00	8.14	8.26	1.71	5.02	0.71	4.54	0.67	4.63	1.60	4.89	3.36	0.80
22.2	31.28	0.44	154.67	21.28	53.67	27.89	7.28	1.75	0.00	8.32	8.45	1.75	5.13	0.72	4.64	0.68	4.74	1.63	5.02	3.53	0.83
24.2	32.02	0.46	162.70	21.91	55.20	28.63	7.46	1.75	0.00	8.51	8.64	1.79	5.25	0.74	4.75	0.70	4.86	1.67	5.16	3.70	0.87
26.2	32.81	0.49	171.29	22.57	56.76	29.34	7.62	1.76	0.00	8.66	8.77	1.81	5.32	0.75	4.81	0.70	4.95	1.71	5.33	3.88	0.90
28.2	33.64	0.51	180.29	23.26	58.40	30.09	7.80	1.76	0.00	8.82	8.89	1.83	5.39	0.76	4.87	0.71	5.04	1.76	5.49	4.07	0.94

Tab. G.4: Modélisation ACF - facteur d'assimilation de 0.05

%ACF	Nb	Cs	Ba	La	Ce	Nd	Sm	Eu^{2+}	Eu^{3+}	Gd	Dy	Ho	Er	Tm	Yb	Lu	Hf	Ta	Pb	Th	U
30.2	34.50	0.54	189.59	23.98	60.12	30.89	7.99	1.76	0.00	9.00	9.05	1.86	5.48	0.77	4.95	0.73	5.14	1.80	5.66	4.27	0.98
32.2	35.42	0.56	199.33	24.74	61.94	31.73	8.19	1.76	0.00	9.18	9.22	1.90	5.58	0.78	5.04	0.74	5.26	1.85	5.84	4.49	1.02
34.2	36.38	0.59	209.55	25.53	63.83	32.60	8.39	1.76	0.00	9.37	9.37	1.93	5.66	0.80	5.11	0.75	5.37	1.90	6.03	4.71	1.06
36.2	37.40	0.62	220.45	26.37	65.83	33.50	8.60	1.76	0.00	9.55	9.51	1.95	5.74	0.81	5.18	0.76	5.48	1.95	6.24	4.94	1.10
38.2	38.48	0.65	231.75	27.26	67.95	34.48	8.83	1.76	0.00	9.77	9.70	1.99	5.84	0.82	5.27	0.77	5.61	2.01	6.44	5.19	1.15
40.2	39.63	0.68	243.85	28.19	70.17	35.47	9.05	1.76	0.00	9.97	9.84	2.01	5.92	0.83	5.34	0.78	5.72	2.06	6.67	5.46	1.20
42.2	40.83	0.72	256.21	29.17	72.54	36.57	9.31	1.74	0.00	10.22	10.06	2.06	6.04	0.85	5.45	0.80	5.87	2.13	6.89	5.73	1.25
44.2	42.08	0.76	270.64	30.27	75.16	37.76	9.59	1.75	0.00	10.46	10.25	2.09	6.14	0.86	5.54	0.81	6.01	2.19	7.16	6.05	1.31
46.3	43.45	0.80	286.19	31.53	78.16	39.12	9.91	1.76	0.00	10.75	10.48	2.13	6.26	0.88	5.64	0.82	6.14	2.25	7.47	6.38	1.37
48.3	44.84	0.84	302.30	32.81	81.22	40.52	10.23	1.77	0.00	11.05	10.72	2.18	6.39	0.90	5.76	0.84	6.29	2.32	7.77	6.73	1.44
50.5	46.40	0.90	321.06	34.31	84.80	42.16	10.61	1.78	0.00	11.39	11.01	2.23	6.54	0.92	5.89	0.86	6.45	2.39	8.13	7.14	1.52
52.6	48.13	0.95	340.93	35.88	88.55	43.84	11.00	1.78	0.00	11.73	11.25	2.28	6.67	0.93	6.00	0.88	6.62	2.47	8.50	7.58	1.60
54.6	49.73	1.01	361.89	37.53	92.52	45.66	11.42	1.78	0.00	12.12	11.57	2.34	6.84	0.96	6.15	0.90	6.78	2.54	8.89	8.04	1.69
56.7	51.69	1.07	383.56	39.28	96.70	47.51	11.84	1.77	0.00	12.48	11.82	2.38	6.96	0.97	6.25	0.91	6.97	2.63	9.31	8.53	1.78
58.8	53.64	1.14	406.56	41.15	101.23	49.56	12.32	1.75	0.00	12.92	12.16	2.44	7.14	1.00	6.40	0.93	7.17	2.72	9.74	9.07	1.88
60.8	55.72	1.21	432.26	43.18	106.09	51.71	12.81	1.74	0.00	13.33	12.46	2.49	7.28	1.02	6.53	0.95	7.37	2.82	10.21	9.65	1.99
62.9	58.22	1.30	460.49	45.52	111.73	54.21	13.39	1.70	0.00	13.83	12.80	2.56	7.45	1.04	6.67	0.97	7.62	2.93	10.75	10.32	2.11
64.9	60.66	1.39	490.09	47.91	117.48	56.72	13.95	1.68	0.00	14.30	13.11	2.61	7.59	1.06	6.79	0.99	7.84	3.04	11.30	11.01	2.24
67.0	63.26	1.49	522.73	50.58	123.95	59.58	14.61	1.63	0.00	14.87	13.52	2.68	7.80	1.09	6.96	1.01	8.09	3.15	11.90	11.80	2.39
69.0	66.38	1.60	555.47	53.35	130.67	62.47	15.26	1.56	0.00	15.40	13.82	2.73	7.93	1.11	7.07	1.03	8.38	3.29	12.51	12.64	2.54
71.1	69.70	1.73	595.86	54.50	130.99	60.22	14.13	1.39	0.00	14.24	12.97	2.60	7.66	1.08	6.96	1.01	8.68	3.44	13.25	13.65	2.73
73.3	73.66	1.88	639.73	56.06	132.51	58.72	13.27	1.21	0.00	13.33	12.29	2.50	7.45	1.06	6.89	1.01	9.05	3.61	14.04	14.84	2.94
75.5	78.02	2.05	686.51	58.07	135.38	58.06	12.70	1.04	0.00	12.69	11.78	2.42	7.28	1.05	6.84	1.00	9.46	3.80	14.87	16.16	3.19
77.5	82.32	2.23	734.53	59.08	134.86	55.21	11.51	0.85	0.00	11.49	10.90	2.29	7.00	1.02	6.72	0.99	9.86	3.99	15.69	17.59	3.45
79.6	87.68	2.46	790.38	61.00	136.80	53.62	10.69	0.68	0.00	10.67	10.32	2.20	6.83	1.01	6.72	0.99	10.35	4.21	16.65	19.35	3.77
81.8	93.59	2.72	845.64	62.40	137.19	51.08	9.67	0.50	0.00	9.65	9.59	2.09	6.62	0.99	6.69	0.99	10.92	4.46	17.53	21.41	4.14
83.8	100.24	3.03	898.42	64.45	139.78	49.84	9.05	0.34	0.00	8.98	9.06	2.01	6.45	0.98	6.66	0.99	11.55	4.74	18.33	23.75	4.56
85.9	108.13	3.39	951.72	64.16	134.95	44.50	7.45	0.20	0.00	7.40	7.78	1.79	5.92	0.92	6.37	0.96	12.28	5.08	19.07	26.55	5.05
88.0	118.93	3.84	982.45	67.12	141.43	45.18	7.37	0.10	0.00	7.30	7.78	1.82	6.07	0.95	6.64	1.00	13.45	5.59	19.23	30.03	5.66

Tab. G.4: Modélisation ACF - facteur d'assimilation de 0.05

%ACF	Nb	Cs	Ba	La	Ce	Nd	Sm	Eu^{2+}	Eu^{3+}	Gd	Dy	Ho	Er	Tm	Yb	Lu	Hf	Ta	Pb	Th	U
90.1	132.97	4.40	1010.78	67.36	139.42	41.38	6.28	0.05	0.00	6.24	6.99	1.70	5.85	0.94	6.68	1.02	14.95	6.26	19.25	34.42	6.43

Tab. G.5: Modélisation des processus ACF ayant mené à la composition chimique des roches mafiques du flysch triasique pour un facteur d'assimilation de 0.1 (éléments majeurs en % poids et métaux de transition en ppm).

%ACF	SiO_2	TiO_2	Al_2O_3	Fe_2O_3	FeO	MnO	MgO	CaO	Na2O	K2O	P2O5	Cr	Ni	Co	Sc	V	Zn	Rb	Sr	Y	Zr
0.2	50.14	2.33	13.87	1.70	11.39	0.20	6.76	9.27	3.81	0.08	0.30	110.02	72.11	39.31	43.40	373.02	93.11	2.14	346.05	47.24	190.01
2.2	50.21	2.37	13.72	1.73	11.47	0.20	6.65	9.26	3.83	0.10	0.31	111.21	66.16	39.71	44.07	379.26	94.42	2.72	347.74	48.07	193.75
4.2	50.29	2.41	13.56	1.76	11.56	0.20	6.53	9.25	3.85	0.11	0.31	112.42	60.47	40.12	44.75	385.72	95.77	3.32	349.33	48.93	197.61
6.2	50.39	2.46	13.46	1.80	11.60	0.20	6.34	9.27	3.88	0.13	0.32	113.34	52.96	40.43	45.44	392.36	97.00	3.94	351.88	49.82	201.59
8.2	50.49	2.50	13.36	1.83	11.65	0.21	6.13	9.29	3.91	0.14	0.32	114.25	46.00	40.74	46.14	399.24	98.27	4.58	354.39	50.74	205.73
10.2	50.60	2.55	13.25	1.87	11.69	0.21	5.93	9.31	3.93	0.16	0.33	115.13	39.59	41.06	46.88	406.38	99.57	5.25	356.86	51.70	210.01
12.2	50.68	2.60	13.09	1.91	11.77	0.21	5.80	9.31	3.95	0.18	0.34	116.36	35.32	41.50	47.66	413.82	101.08	5.93	358.03	52.69	214.49
14.2	50.79	2.65	12.98	1.94	11.81	0.21	5.58	9.35	3.98	0.20	0.35	117.22	29.85	41.83	48.44	421.51	102.45	6.65	360.33	53.72	219.11
16.2	50.90	2.70	12.87	1.98	11.84	0.21	5.36	9.38	4.01	0.22	0.35	118.04	24.91	42.16	49.25	429.50	103.87	7.39	362.55	54.79	223.93
18.2	50.98	2.76	12.69	2.03	11.92	0.21	5.22	9.39	4.02	0.24	0.36	119.25	21.69	42.64	50.12	437.84	105.53	8.16	363.29	55.91	228.96
20.2	51.10	2.81	12.58	2.07	11.94	0.21	4.99	9.44	4.05	0.26	0.37	120.00	17.65	42.98	51.00	446.49	107.03	8.97	365.28	57.07	234.19
22.2	51.18	2.87	12.39	2.11	12.01	0.21	4.84	9.46	4.06	0.28	0.38	121.18	15.06	43.48	51.93	455.52	108.80	9.80	365.64	58.28	239.65
24.2	51.31	2.93	12.34	2.15	12.01	0.21	4.57	9.50	4.09	0.30	0.39	116.29	11.49	43.63	52.52	464.51	110.28	10.67	368.71	59.50	245.27
26.2	51.30	2.99	12.27	2.19	12.17	0.22	4.49	9.34	4.12	0.33	0.40	93.28	9.93	43.55	51.84	472.29	112.25	11.59	370.69	60.59	250.92
28.2	51.31	3.04	12.27	2.22	12.31	0.22	4.36	9.16	4.17	0.35	0.41	69.51	8.19	43.24	50.79	479.93	114.16	12.55	373.98	61.67	256.75
30.2	51.33	3.10	12.20	2.25	12.42	0.22	4.23	9.05	4.20	0.38	0.42	56.29	6.67	43.20	50.40	488.76	116.16	13.55	375.99	62.90	262.98
32.2	51.32	3.17	12.12	2.29	12.59	0.22	4.13	8.89	4.23	0.41	0.43	42.04	5.59	43.09	49.66	497.47	118.36	14.60	377.46	64.11	269.42
34.2	51.36	3.23	12.13	2.32	12.69	0.22	3.95	8.75	4.28	0.44	0.44	30.21	4.23	42.79	48.85	506.54	120.37	15.70	380.68	65.38	276.17
36.2	51.35	3.30	12.05	2.36	12.86	0.22	3.85	8.58	4.31	0.47	0.45	21.02	3.45	42.65	48.04	515.97	122.75	16.86	381.68	66.69	283.24
38.2	51.33	3.37	11.98	2.40	13.04	0.22	3.74	8.41	4.34	0.50	0.46	14.12	2.77	42.50	47.22	525.81	125.24	18.07	382.38	68.05	290.67

Tab. G.5: Modélisation ACF - facteur d'assimilation de 0.1

%ACF	SiO_2	TiO_2	Al_2O_3	Fe_2O_3	FeO	MnO	MgO	CaO	Na2O	K2O	P2O5	Cr	Ni	Co	Sc	V	Zn	Rb	Sr	Y	Zr
40.2	51.35	3.45	11.91	2.44	13.17	0.22	3.59	8.29	4.37	0.53	0.48	9.82	2.11	42.41	46.73	536.67	127.68	19.34	383.22	69.54	298.57
42.2	51.39	3.53	11.91	2.47	13.26	0.22	3.38	8.14	4.42	0.57	0.49	5.93	1.47	42.03	45.83	547.46	130.04	20.69	385.63	71.03	306.79
44.2	51.58	3.52	11.85	2.49	13.23	0.22	3.29	8.02	4.45	0.61	0.51	0.01	1.17	40.81	45.08	500.92	126.88	22.21	386.54	71.98	315.29
46.4	52.21	3.35	12.00	2.45	12.77	0.22	3.14	7.92	4.55	0.65	0.53	0.01	0.79	37.22	43.53	373.89	113.55	23.85	392.86	71.87	324.45
48.6	52.67	3.26	11.99	2.44	12.51	0.21	3.04	7.82	4.61	0.70	0.55	0.01	0.61	34.88	42.50	300.82	105.15	25.67	394.42	72.34	334.69
50.7	53.37	3.08	12.16	2.38	11.99	0.21	2.87	7.70	4.71	0.75	0.57	0.01	0.42	31.38	40.65	216.20	92.67	27.63	400.63	72.02	344.82
52.9	53.87	2.98	12.16	2.37	11.70	0.21	2.76	7.58	4.77	0.81	0.59	0.01	0.34	29.19	39.40	170.77	85.22	29.70	400.70	72.42	356.21
55.0	54.62	2.80	12.26	2.31	11.17	0.21	2.62	7.48	4.86	0.87	0.61	0.01	0.27	26.13	37.82	118.39	74.12	31.93	403.38	72.04	367.58
57.0	55.25	2.66	12.33	2.27	10.75	0.21	2.48	7.35	4.94	0.93	0.64	0.00	0.24	23.74	36.19	87.60	66.24	34.24	404.28	71.91	379.07
59.1	55.97	2.51	12.43	2.21	10.25	0.20	2.33	7.21	5.03	0.99	0.67	0.00	0.20	21.23	34.43	61.50	57.94	36.69	404.48	71.54	391.36
61.2	56.65	2.38	12.46	2.16	9.84	0.20	2.18	7.05	5.11	1.07	0.70	0.01	0.18	19.12	32.69	44.24	51.34	39.41	400.10	71.53	405.81
63.4	57.35	2.25	12.50	2.11	9.41	0.20	2.02	6.88	5.19	1.15	0.73	0.01	0.17	17.12	30.83	31.57	45.34	42.42	394.05	71.44	421.14
65.5	58.22	2.07	12.53	2.03	8.81	0.20	1.89	6.77	5.26	1.23	0.77	0.00	0.17	14.91	29.29	19.82	37.96	45.53	386.68	70.68	436.14
67.6	59.11	1.91	12.61	1.95	8.24	0.19	1.71	6.57	5.35	1.33	0.81	0.01	0.16	12.87	27.13	12.66	32.03	49.16	376.86	70.01	453.60
69.8	60.06	1.76	12.69	1.86	7.68	0.18	1.51	6.32	5.44	1.44	0.83	0.00	0.13	11.01	24.87	8.04	26.92	53.13	364.35	67.96	472.31
71.8	61.09	1.61	12.75	1.77	7.14	0.18	1.35	6.03	5.51	1.55	0.77	0.01	0.12	9.46	23.14	5.07	22.53	57.14	349.15	61.89	490.60
73.8	62.21	1.46	12.83	1.67	6.56	0.17	1.19	5.71	5.59	1.67	0.70	0.00	0.11	7.98	21.25	3.10	18.51	61.51	330.56	55.49	509.99
76.0	63.43	1.31	12.85	1.55	5.96	0.17	1.02	5.37	5.64	1.82	0.63	0.00	0.09	6.59	19.34	1.85	14.90	66.73	302.95	48.93	533.42
78.1	64.78	1.12	12.84	1.39	5.19	0.16	0.89	5.16	5.67	1.98	0.57	-0.01	0.12	5.20	17.87	0.94	10.96	72.12	272.57	42.97	554.84
80.1	65.97	1.01	12.84	1.28	4.66	0.15	0.69	4.77	5.69	2.15	0.51	0.01	0.07	4.22	15.80	0.67	8.95	77.93	233.79	37.72	582.14
82.3	67.52	0.83	12.78	1.09	3.84	0.14	0.55	4.52	5.67	2.36	0.44	-0.01	0.09	3.13	13.65	0.38	6.22	84.70	191.17	31.36	609.47
84.4	68.88	0.72	12.66	0.95	3.25	0.13	0.40	4.23	5.58	2.59	0.36	0.00	0.08	2.42	12.28	0.32	4.74	91.52	141.92	25.46	640.46
86.4	70.24	0.61	12.52	0.79	2.65	0.11	0.25	3.96	5.44	2.85	0.30	0.21	0.02	1.81	10.92	0.30	3.60	98.62	95.92	21.13	674.19
88.6	71.47	0.54	12.10	0.68	2.22	0.11	0.18	3.93	5.10	3.16	0.24	-24.52	0.08	1.49	10.44	0.33	3.00	106.01	53.13	17.37	718.95

TAB. G.6: Modélisation des processus ACF ayant mené à la composition chimique des roches mafiques du flysch triasique pour un facteur d'assimilation de 0.1 (éléments traces en ppm).

%ACF	Nb	Cs	Ba	La	Ce	Nd	Sm	Eu^{2+}	Eu^{3+}	Gd	Dy	Ho	Er	Tm	Yb	Lu	Hf	Ta	Pb	Th	U
0.2	24.98	0.26	84.37	15.87	40.56	21.55	5.72	1.77	0.00	6.69	6.77	1.40	4.12	0.58	3.74	0.55	3.74	1.30	3.77	2.05	0.55
2.2	25.44	0.28	93.60	16.39	41.76	22.09	5.84	1.77	0.00	6.80	6.89	1.42	4.19	0.59	3.80	0.56	3.82	1.32	3.90	2.23	0.58
4.2	25.91	0.30	103.13	16.93	42.99	22.66	5.97	1.76	0.00	6.92	7.01	1.45	4.27	0.60	3.87	0.57	3.89	1.35	4.03	2.41	0.61
6.2	26.39	0.33	113.00	17.49	44.28	23.24	6.10	1.77	0.00	7.04	7.14	1.48	4.34	0.61	3.94	0.58	3.97	1.37	4.17	2.61	0.65
8.2	26.89	0.35	123.20	18.08	45.61	23.84	6.24	1.77	0.00	7.17	7.28	1.50	4.42	0.62	4.01	0.59	4.06	1.40	4.31	2.81	0.68
10.2	27.41	0.38	133.75	18.68	46.99	24.47	6.38	1.78	0.00	7.30	7.41	1.53	4.51	0.63	4.08	0.60	4.14	1.43	4.46	3.01	0.72
12.2	27.95	0.41	144.60	19.30	48.42	25.12	6.52	1.77	0.00	7.44	7.56	1.56	4.59	0.65	4.16	0.61	4.23	1.46	4.61	3.23	0.76
14.2	28.52	0.43	155.90	19.95	49.90	25.79	6.68	1.78	0.00	7.58	7.71	1.59	4.68	0.66	4.24	0.62	4.33	1.49	4.77	3.45	0.79
16.2	29.10	0.46	167.60	20.62	51.45	26.50	6.84	1.78	0.00	7.73	7.86	1.62	4.78	0.67	4.32	0.63	4.43	1.52	4.94	3.68	0.84
18.2	29.71	0.49	179.65	21.32	53.05	27.22	7.00	1.77	0.00	7.88	8.02	1.66	4.87	0.69	4.41	0.65	4.53	1.55	5.11	3.92	0.88
20.2	30.34	0.52	192.23	22.05	54.73	27.98	7.17	1.77	0.00	8.04	8.19	1.69	4.97	0.70	4.50	0.66	4.63	1.59	5.28	4.17	0.92
22.2	31.01	0.55	205.19	22.80	56.47	28.77	7.35	1.76	0.00	8.21	8.37	1.73	5.08	0.71	4.59	0.67	4.74	1.62	5.46	4.43	0.97
24.2	31.70	0.59	218.90	23.59	58.28	29.59	7.53	1.77	0.00	8.38	8.54	1.76	5.18	0.73	4.68	0.69	4.85	1.66	5.66	4.71	1.02
26.2	32.44	0.62	233.17	24.42	60.15	30.40	7.71	1.77	0.00	8.52	8.66	1.79	5.25	0.74	4.74	0.69	4.94	1.70	5.86	5.00	1.07
28.2	33.22	0.66	248.21	25.28	62.09	31.24	7.89	1.78	0.00	8.65	8.77	1.81	5.31	0.75	4.80	0.70	5.03	1.74	6.08	5.30	1.12
30.2	34.03	0.70	263.73	26.18	64.13	32.13	8.08	1.78	0.00	8.81	8.92	1.84	5.39	0.76	4.87	0.71	5.14	1.78	6.31	5.61	1.17
32.2	34.88	0.74	279.93	27.11	66.26	33.05	8.28	1.78	0.00	8.97	9.05	1.86	5.46	0.77	4.93	0.72	5.24	1.82	6.54	5.94	1.23
34.2	35.77	0.78	297.07	28.10	68.50	34.01	8.48	1.78	0.00	9.13	9.18	1.89	5.53	0.78	5.00	0.73	5.35	1.87	6.79	6.29	1.29
36.2	36.71	0.83	314.79	29.13	70.83	35.02	8.70	1.78	0.00	9.30	9.32	1.91	5.61	0.79	5.06	0.74	5.46	1.92	7.04	6.65	1.35
38.2	37.70	0.88	333.34	30.21	73.28	36.06	8.92	1.77	0.00	9.48	9.46	1.94	5.68	0.80	5.13	0.75	5.58	1.97	7.31	7.04	1.42
40.2	38.74	0.93	352.80	31.34	75.87	37.18	9.16	1.77	0.00	9.67	9.63	1.97	5.77	0.81	5.21	0.76	5.71	2.02	7.59	7.44	1.49
42.2	39.85	0.98	373.55	32.55	78.60	38.35	9.41	1.77	0.00	9.86	9.78	2.00	5.85	0.82	5.28	0.77	5.83	2.08	7.89	7.87	1.56
44.2	40.97	1.04	396.62	33.88	81.62	39.64	9.68	1.76	0.00	10.08	9.96	2.03	5.95	0.84	5.36	0.78	5.97	2.13	8.22	8.35	1.65
46.4	42.21	1.10	422.05	35.41	85.09	41.14	10.01	1.78	0.00	10.34	10.16	2.07	6.05	0.85	5.45	0.80	6.09	2.19	8.61	8.86	1.74
48.6	43.57	1.18	449.78	37.06	88.86	42.76	10.36	1.78	0.00	10.62	10.39	2.11	6.17	0.87	5.56	0.81	6.25	2.26	9.01	9.44	1.83
50.7	44.95	1.25	479.96	38.83	92.87	44.47	10.71	1.79	0.00	10.89	10.59	2.14	6.27	0.88	5.64	0.82	6.38	2.32	9.47	10.06	1.94

Tab. G.6: Modélisation ACF - facteur d'assimilation de 0.1

%ACF	Nb	Cs	Ba	La	Ce	Nd	Sm	Eu^{2+}	Eu^{3+}	Gd	Dy	Ho	Er	Tm	Yb	Lu	Hf	Ta	Pb	Th	U
52.9	46.48	1.34	511.12	40.69	97.12	46.28	11.10	1.78	0.00	11.19	10.83	2.19	6.39	0.90	5.74	0.84	6.55	2.39	9.92	10.72	2.05
55.0	48.01	1.43	544.73	42.69	101.67	48.21	11.51	1.78	0.00	11.51	11.07	2.23	6.51	0.91	5.85	0.85	6.71	2.46	10.42	11.42	2.17
57.0	49.56	1.52	579.24	44.71	106.25	50.13	11.91	1.78	0.00	11.81	11.28	2.27	6.61	0.93	5.93	0.86	6.87	2.53	10.92	12.15	2.30
59.1	51.23	1.62	615.75	46.89	111.21	52.21	12.35	1.77	0.00	12.13	11.51	2.30	6.72	0.94	6.02	0.88	7.03	2.60	11.45	12.93	2.43
61.2	53.19	1.73	655.54	49.33	116.80	54.54	12.84	1.74	0.00	12.50	11.76	2.35	6.83	0.95	6.12	0.89	7.24	2.69	12.04	13.81	2.58
63.4	55.28	1.85	699.02	51.96	122.83	57.03	13.36	1.70	0.00	12.88	12.00	2.39	6.94	0.97	6.21	0.90	7.45	2.79	12.67	14.78	2.75
65.5	57.29	1.98	743.55	54.70	129.15	59.67	13.92	1.65	0.00	13.30	12.30	2.44	7.08	0.99	6.33	0.92	7.65	2.88	13.31	15.79	2.92
67.6	59.68	2.13	794.87	57.85	136.38	62.61	14.52	1.60	0.00	13.72	12.55	2.48	7.18	1.00	6.41	0.93	7.88	2.98	14.05	16.97	3.12
69.8	62.27	2.29	850.19	60.80	142.65	64.63	14.81	1.51	0.00	13.84	12.55	2.47	7.18	1.00	6.42	0.93	8.12	3.09	14.85	18.27	3.34
71.8	64.84	2.46	904.77	62.21	143.68	63.00	13.95	1.36	0.00	12.97	11.87	2.37	6.94	0.98	6.29	0.92	8.36	3.20	15.63	19.60	3.56
73.8	67.59	2.65	962.99	63.47	144.07	60.88	12.97	1.20	0.00	11.98	11.08	2.24	6.64	0.94	6.13	0.89	8.61	3.32	16.45	21.07	3.81
76.0	70.90	2.88	1029.67	64.82	144.31	58.44	11.91	1.01	0.00	10.92	10.23	2.10	6.31	0.91	5.94	0.87	8.92	3.46	17.37	22.85	4.11
78.1	73.87	3.12	1095.51	66.42	145.57	56.83	11.14	0.84	0.00	10.15	9.64	2.00	6.09	0.88	5.83	0.86	9.20	3.58	18.25	24.73	4.42
80.1	77.76	3.39	1161.78	67.69	145.66	54.40	10.19	0.66	0.00	9.19	8.81	1.86	5.73	0.84	5.59	0.82	9.56	3.75	19.14	26.85	4.76
82.3	81.60	3.72	1232.56	68.78	145.11	51.52	9.16	0.49	0.00	8.21	8.08	1.74	5.47	0.81	5.49	0.81	9.92	3.90	20.00	29.42	5.19
84.4	86.02	4.08	1291.94	68.52	140.97	46.94	7.80	0.32	0.00	6.95	7.04	1.56	5.01	0.76	5.19	0.77	10.33	4.08	20.66	32.20	5.64
86.4	90.81	4.49	1340.88	68.90	139.25	43.88	6.89	0.19	0.00	6.06	6.28	1.42	4.65	0.72	4.95	0.74	10.78	4.28	21.11	35.34	6.14
88.6	97.02	5.00	1361.91	68.49	136.30	40.34	5.95	0.10	0.00	5.19	5.59	1.31	4.37	0.69	4.83	0.73	11.46	4.56	20.94	39.32	6.77

Tab. G.7: Modélisation des processus ACF ayant mené à la composition chimique des roches mafiques du flysch triasique pour un facteur d'assimilation de 0.2 (éléments majeurs en % poids et métaux de transition en ppm).

%ACF	SiO_2	TiO_2	Al_2O_3	Fe_2O_3	FeO	MnO	MgO	CaO	Na2O	K2O	P2O5	Cr	Ni	Co	Sc	V	Zn	Rb	Sr	Y	Zr
0.2	50.14	2.33	13.87	1.70	11.39	0.20	6.76	9.27	3.81	0.08	0.30	110.02	72.11	39.31	43.40	373.02	93.11	2.14	346.05	47.24	190.01
2.2	50.24	2.37	13.72	1.73	11.45	0.20	6.64	9.24	3.83	0.11	0.31	111.05	66.07	39.65	43.98	378.56	94.33	3.26	349.83	48.00	193.81
4.2	50.35	2.41	13.57	1.76	11.52	0.20	6.51	9.22	3.85	0.14	0.31	112.09	60.31	40.00	44.58	384.27	95.58	4.41	353.50	48.79	197.72
6.2	50.48	2.44	13.48	1.79	11.54	0.20	6.30	9.23	3.88	0.17	0.32	112.83	52.75	40.24	45.18	390.12	96.70	5.60	358.14	49.59	201.73

Tab. G.7: Modélisation ACF - facteur d'assimilation de 0.2

%ACF	SiO_2	TiO_2	Al_2O_3	Fe_2O_3	FeO	MnO	MgO	CaO	Na2O	K2O	P2O5	Cr	Ni	Co	Sc	V	Zn	Rb	Sr	Y	Zr
8.2	50.62	2.48	13.38	1.82	11.56	0.20	6.09	9.23	3.91	0.20	0.32	113.55	45.76	40.48	45.79	396.15	97.85	6.82	362.73	50.42	205.88
10.2	50.76	2.53	13.29	1.86	11.58	0.21	5.87	9.24	3.93	0.24	0.33	114.24	39.33	40.73	46.42	402.38	99.01	8.08	367.29	51.28	210.16
12.2	50.87	2.57	13.13	1.89	11.63	0.21	5.73	9.23	3.95	0.27	0.34	115.25	35.06	41.09	47.09	408.84	100.38	9.38	370.52	52.17	214.61
14.2	51.02	2.61	13.03	1.93	11.64	0.21	5.51	9.24	3.97	0.30	0.34	115.88	29.60	41.34	47.75	415.48	101.61	10.72	374.89	53.09	219.19
16.2	51.17	2.66	12.94	1.97	11.64	0.21	5.28	9.26	4.00	0.34	0.35	116.47	24.69	41.59	48.44	422.34	102.86	12.11	379.19	54.04	223.93
18.2	51.28	2.71	12.77	2.01	11.69	0.21	5.13	9.26	4.01	0.38	0.36	117.43	21.49	41.97	49.17	429.47	104.33	13.54	381.93	55.02	228.85
20.2	51.44	2.76	12.67	2.04	11.69	0.21	4.90	9.28	4.04	0.42	0.37	117.91	17.50	42.22	49.90	436.83	105.65	15.03	385.98	56.04	233.94
22.2	51.59	2.81	12.57	2.08	11.68	0.21	4.66	9.31	4.06	0.46	0.37	118.32	14.01	42.47	50.65	444.44	106.99	16.56	389.93	57.10	239.22
24.2	51.69	2.86	12.46	2.12	11.73	0.21	4.51	9.26	4.08	0.50	0.38	109.00	11.81	42.61	50.80	451.59	108.56	18.16	393.21	58.11	244.59
26.2	51.76	2.90	12.41	2.15	11.81	0.21	4.37	9.13	4.11	0.54	0.39	91.04	9.88	42.48	50.28	458.21	110.17	19.82	397.48	59.06	250.04
28.2	51.81	2.95	12.42	2.17	11.91	0.21	4.24	8.94	4.15	0.59	0.40	67.38	8.16	42.08	49.07	464.22	111.81	21.55	402.81	59.94	255.57
30.2	51.85	3.00	12.36	2.20	12.04	0.21	4.15	8.76	4.18	0.63	0.41	51.37	6.94	41.88	48.19	470.82	113.62	23.34	406.42	60.90	261.37
32.2	51.93	3.05	12.31	2.23	12.11	0.21	4.00	8.63	4.21	0.68	0.42	40.53	5.63	41.72	47.62	478.08	115.38	25.21	410.15	61.94	267.48
34.2	51.98	3.10	12.32	2.26	12.21	0.21	3.86	8.43	4.25	0.73	0.43	27.15	4.48	41.26	46.31	484.64	117.16	27.16	414.94	62.89	273.67
36.2	52.02	3.16	12.27	2.29	12.34	0.21	3.75	8.24	4.28	0.78	0.44	18.88	3.69	41.02	45.35	491.87	119.16	29.18	417.73	63.93	280.19
38.2	52.11	3.21	12.29	2.32	12.39	0.21	3.55	8.08	4.32	0.84	0.45	12.39	2.73	40.57	44.31	499.34	120.92	31.29	422.48	64.99	286.97
40.2	52.19	3.27	12.24	2.35	12.46	0.21	3.39	7.94	4.35	0.90	0.47	8.62	2.11	40.36	43.63	507.62	122.89	33.49	425.12	66.16	294.14
42.2	52.23	3.33	12.19	2.39	12.58	0.21	3.28	7.75	4.38	0.96	0.48	5.16	1.69	40.05	42.54	515.59	125.08	35.78	426.66	67.28	301.50
44.3	52.55	3.29	12.24	2.38	12.42	0.20	3.14	7.59	4.43	1.02	0.49	0.00	1.27	38.19	41.19	454.84	119.89	38.33	431.57	67.68	309.11
46.3	53.08	3.16	12.30	2.35	12.07	0.20	3.03	7.48	4.49	1.09	0.51	0.01	0.99	35.54	39.96	361.43	110.00	41.01	436.97	67.58	316.80
48.4	53.70	3.01	12.38	2.31	11.62	0.20	2.91	7.38	4.55	1.17	0.52	0.02	0.78	32.59	38.61	272.65	98.79	43.94	442.71	67.24	324.97
50.4	54.24	2.89	12.45	2.28	11.27	0.20	2.79	7.25	4.61	1.25	0.54	0.02	0.66	30.22	37.20	215.73	90.52	46.99	447.23	67.05	333.07
52.4	54.78	2.78	12.52	2.24	10.91	0.20	2.66	7.12	4.67	1.33	0.56	0.01	0.54	27.91	35.74	168.54	82.54	49.91	449.93	66.86	341.62
54.6	55.57	2.58	12.64	2.17	10.33	0.19	2.52	7.00	4.75	1.42	0.58	0.02	0.45	24.85	34.05	115.82	71.34	53.45	454.62	66.06	350.83
56.7	56.16	2.47	12.75	2.13	9.96	0.19	2.35	6.79	4.83	1.52	0.60	0.01	0.37	22.67	31.96	89.87	64.94	57.16	456.83	65.78	360.83
58.7	56.80	2.34	12.77	2.08	9.54	0.19	2.25	6.67	4.88	1.62	0.62	0.02	0.39	20.68	30.69	66.29	57.93	60.93	455.12	65.33	370.43
60.7	57.49	2.20	12.87	2.02	9.07	0.18	2.10	6.50	4.95	1.72	0.64	0.01	0.33	18.52	28.83	47.58	51.03	64.66	454.03	64.64	380.42
62.7	58.24	2.05	12.99	1.95	8.57	0.18	1.94	6.31	5.02	1.83	0.67	0.02	0.31	16.41	26.83	33.27	44.47	68.94	453.06	63.72	390.52
64.7	58.98	1.90	13.03	1.88	8.07	0.18	1.82	6.17	5.07	1.94	0.69	0.00	0.30	14.58	25.36	22.66	38.39	73.09	445.25	62.90	401.40
66.9	59.72	1.78	13.10	1.81	7.63	0.17	1.65	5.94	5.13	2.08	0.72	0.00	0.27	12.90	23.32	16.07	33.71	77.99	435.63	62.13	413.73

Tab. G.7: Modélisation ACF - facteur d'assimilation de 0.2

%ACF	SiO_2	TiO_2	Al_2O_3	Fe_2O_3	FeO	MnO	MgO	CaO	Na2O	K2O	P2O5	Cr	Ni	Co	Sc	V	Zn	Rb	Sr	Y	Zr
68.9	60.58	1.61	13.16	1.71	7.04	0.17	1.52	5.78	5.19	2.21	0.75	0.00	0.27	11.12	21.65	10.09	28.09	82.93	424.08	60.79	425.16
71.1	61.48	1.48	13.26	1.63	6.54	0.16	1.33	5.47	5.25	2.37	0.74	0.02	0.23	9.59	19.45	6.79	24.05	88.61	409.39	57.42	438.50
73.1	62.44	1.35	13.35	1.53	6.03	0.15	1.19	5.16	5.31	2.52	0.68	0.05	0.24	8.25	17.71	4.51	20.33	94.38	392.70	51.70	450.72
75.1	63.49	1.21	13.45	1.41	5.46	0.15	1.04	4.83	5.36	2.69	0.62	0.04	0.20	6.90	15.89	2.83	16.62	100.40	371.84	45.63	463.25
77.1	64.58	1.04	13.45	1.29	4.84	0.14	0.93	4.61	5.38	2.87	0.57	0.01	0.21	5.66	14.61	1.61	12.93	106.55	340.95	40.63	475.96
79.2	65.59	0.94	13.48	1.18	4.35	0.13	0.77	4.25	5.40	3.08	0.53	0.00	0.19	4.71	12.77	1.18	10.77	113.48	303.80	35.89	491.27
81.4	66.82	0.79	13.56	1.03	3.70	0.12	0.60	3.87	5.42	3.31	0.47	0.00	0.14	3.62	10.78	0.78	8.15	121.12	262.47	30.48	505.64
83.5	68.10	0.65	13.65	0.87	3.03	0.11	0.42	3.46	5.43	3.56	0.42	-0.03	0.04	2.66	8.78	0.57	6.03	129.08	216.46	24.94	519.52
85.6	69.33	0.53	13.62	0.71	2.42	0.09	0.29	3.14	5.37	3.83	0.35	0.00	0.04	1.97	7.46	0.44	4.41	136.75	162.13	19.55	532.77
87.6	70.42	0.43	13.57	0.57	1.90	0.08	0.17	2.84	5.27	4.12	0.31	-0.15	-0.03	1.47	6.20	0.44	3.43	143.81	109.13	15.83	546.63
89.8	71.52	0.37	13.48	0.45	1.46	0.06	0.06	2.49	5.09	4.46	0.23	85.44	-0.11	1.12	5.13	0.52	2.96	150.69	60.31	11.22	564.50

Tab. G.8: Modélisation des processus ACF ayant mené à la composition chimique des roches mafiques du flysch triasique pour un facteur d'assimilation de 0.2 (éléments traces en ppm).

%ACF	Nb	Cs	Ba	La	Ce	Nd	Sm	Eu^{2+}	Eu^{3+}	Gd	Dy	Ho	Er	Tm	Yb	Lu	Hf	Ta	Pb	Th	U
0.2	24.98	0.26	84.37	15.87	40.56	21.55	5.72	1.77	0.00	6.69	6.77	1.40	4.12	0.58	3.74	0.55	3.74	1.30	3.77	2.05	0.55
2.2	25.41	0.30	101.44	16.63	42.20	22.24	5.86	1.77	0.00	6.79	6.88	1.42	4.19	0.59	3.80	0.56	3.82	1.32	3.97	2.37	0.60
4.2	25.84	0.34	118.98	17.42	43.89	22.95	6.00	1.77	0.00	6.89	7.00	1.45	4.25	0.60	3.86	0.57	3.90	1.35	4.17	2.69	0.66
6.2	26.29	0.38	137.06	18.23	45.64	23.68	6.14	1.77	0.00	7.00	7.11	1.47	4.32	0.61	3.92	0.58	3.98	1.37	4.38	3.03	0.71
8.2	26.75	0.42	155.65	19.06	47.44	24.44	6.29	1.78	0.00	7.11	7.24	1.49	4.39	0.62	3.98	0.59	4.06	1.40	4.60	3.38	0.77
10.2	27.23	0.47	174.80	19.92	49.30	25.22	6.45	1.79	0.00	7.22	7.36	1.52	4.47	0.63	4.05	0.59	4.15	1.42	4.83	3.74	0.83
12.2	27.73	0.51	194.43	20.81	51.21	26.02	6.61	1.78	0.00	7.34	7.49	1.55	4.55	0.64	4.12	0.60	4.24	1.45	5.06	4.11	0.89
14.2	28.24	0.56	214.74	21.73	53.20	26.85	6.77	1.79	0.00	7.46	7.63	1.57	4.62	0.65	4.19	0.61	4.34	1.47	5.29	4.50	0.95
16.2	28.77	0.61	235.68	22.68	55.25	27.71	6.94	1.79	0.00	7.59	7.77	1.60	4.71	0.66	4.26	0.62	4.43	1.50	5.54	4.89	1.02
18.2	29.32	0.66	257.14	23.65	57.37	28.60	7.12	1.79	0.00	7.72	7.91	1.63	4.79	0.67	4.33	0.64	4.53	1.53	5.79	5.31	1.08
20.2	29.89	0.71	279.42	24.67	59.56	29.52	7.31	1.79	0.00	7.85	8.06	1.66	4.88	0.69	4.41	0.65	4.64	1.56	6.05	5.73	1.15

TAB. G.8: Modélisation ACF - facteur d'assimilation de 0.2

%ACF	Nb	Cs	Ba	La	Ce	Nd	Sm	Eu^{2+}	Eu^{3+}	Gd	Dy	Ho	Er	Tm	Yb	Lu	Hf	Ta	Pb	Th	U
22.2	30.48	0.77	302.42	25.72	61.84	30.48	7.50	1.79	0.00	7.99	8.21	1.69	4.97	0.70	4.49	0.66	4.75	1.60	6.31	6.18	1.23
24.2	31.10	0.82	326.19	26.80	64.18	31.44	7.69	1.79	0.00	8.12	8.35	1.72	5.05	0.71	4.56	0.67	4.85	1.63	6.59	6.64	1.30
26.2	31.75	0.88	350.97	27.93	66.60	32.43	7.87	1.79	0.00	8.24	8.46	1.74	5.11	0.72	4.62	0.68	4.94	1.66	6.89	7.11	1.38
28.2	32.43	0.94	376.85	29.10	69.09	33.42	8.06	1.80	0.00	8.35	8.54	1.76	5.15	0.72	4.65	0.68	5.03	1.70	7.20	7.61	1.46
30.2	33.13	1.01	403.44	30.31	71.68	34.46	8.25	1.80	0.00	8.46	8.65	1.78	5.20	0.73	4.70	0.69	5.12	1.73	7.51	8.13	1.54
32.2	33.87	1.07	430.99	31.57	74.38	35.55	8.46	1.80	0.00	8.59	8.76	1.80	5.27	0.74	4.75	0.70	5.23	1.77	7.84	8.67	1.63
34.2	34.64	1.14	459.87	32.87	77.17	36.65	8.66	1.81	0.00	8.70	8.85	1.81	5.31	0.75	4.79	0.70	5.32	1.81	8.19	9.23	1.72
36.2	35.44	1.22	489.54	34.23	80.07	37.80	8.88	1.80	0.00	8.83	8.95	1.83	5.36	0.75	4.83	0.71	5.42	1.85	8.54	9.82	1.82
38.2	36.27	1.29	520.77	35.65	83.11	39.01	9.10	1.81	0.00	8.95	9.05	1.85	5.41	0.76	4.88	0.71	5.53	1.90	8.92	10.43	1.92
40.2	37.14	1.37	552.85	37.13	86.28	40.27	9.34	1.80	0.00	9.10	9.17	1.87	5.47	0.77	4.93	0.72	5.65	1.94	9.30	11.07	2.02
42.2	38.06	1.46	586.20	38.66	89.56	41.56	9.58	1.79	0.00	9.23	9.27	1.89	5.51	0.77	4.97	0.73	5.76	1.99	9.70	11.74	2.13
44.3	39.01	1.55	623.54	40.38	93.24	43.01	9.85	1.80	0.00	9.39	9.39	1.91	5.57	0.78	5.02	0.73	5.88	2.04	10.15	12.48	2.25
46.3	39.95	1.64	662.80	42.20	97.16	44.58	10.15	1.80	0.00	9.56	9.53	1.93	5.64	0.79	5.08	0.74	5.99	2.08	10.62	13.26	2.37
48.4	40.95	1.75	705.58	44.19	101.43	46.28	10.47	1.81	0.00	9.75	9.69	1.96	5.71	0.80	5.14	0.75	6.11	2.13	11.14	14.10	2.51
50.4	41.94	1.86	749.83	46.21	105.75	47.97	10.78	1.81	0.00	9.93	9.82	1.98	5.77	0.81	5.19	0.76	6.23	2.17	11.67	14.98	2.65
52.4	43.00	1.97	791.97	48.21	110.07	49.68	11.10	1.80	0.00	10.12	9.96	2.00	5.83	0.82	5.24	0.76	6.35	2.22	12.19	15.84	2.79
54.6	44.14	2.09	843.07	50.60	115.19	51.69	11.47	1.81	0.00	10.33	10.12	2.03	5.90	0.83	5.30	0.77	6.47	2.27	12.81	16.86	2.95
56.7	45.40	2.23	896.07	53.05	120.42	53.69	11.83	1.80	0.00	10.51	10.22	2.04	5.93	0.83	5.32	0.77	6.61	2.33	13.45	17.94	3.13
58.7	46.55	2.37	948.93	55.51	125.75	55.76	12.22	1.77	0.00	10.72	10.38	2.07	6.00	0.84	5.38	0.78	6.75	2.38	14.07	19.05	3.30
60.7	47.82	2.51	1001.36	58.02	131.14	57.83	12.59	1.75	0.00	10.92	10.49	2.08	6.04	0.84	5.40	0.79	6.88	2.44	14.71	20.15	3.48
62.7	49.07	2.66	1061.16	60.77	137.02	60.04	12.99	1.73	0.00	11.11	10.58	2.09	6.06	0.85	5.41	0.79	7.01	2.49	15.42	21.40	3.68
64.7	50.42	2.82	1117.69	63.54	143.08	62.37	13.42	1.69	0.00	11.35	10.73	2.12	6.12	0.85	5.46	0.79	7.16	2.55	16.10	22.65	3.87
66.9	51.96	3.01	1183.69	66.70	149.89	64.90	13.87	1.63	0.00	11.56	10.81	2.12	6.13	0.85	5.46	0.79	7.32	2.62	16.88	24.11	4.11
68.9	53.37	3.20	1249.25	69.90	156.87	67.52	14.34	1.57	0.00	11.79	10.94	2.14	6.17	0.86	5.49	0.80	7.47	2.67	17.65	25.60	4.34
71.1	55.08	3.41	1323.75	72.43	161.17	68.00	14.15	1.46	0.00	11.47	10.59	2.07	6.00	0.84	5.37	0.78	7.64	2.75	18.53	27.32	4.61
73.1	56.66	3.64	1397.71	73.64	161.24	65.78	13.20	1.31	0.00	10.58	9.87	1.95	5.70	0.80	5.18	0.75	7.79	2.81	19.39	29.08	4.89
75.1	58.30	3.88	1472.87	74.52	160.31	62.98	12.14	1.15	0.00	9.62	9.06	1.82	5.36	0.76	4.95	0.72	7.95	2.88	20.26	30.95	5.18
77.1	59.91	4.13	1544.51	75.84	160.97	61.29	11.42	0.99	0.00	8.96	8.53	1.73	5.15	0.74	4.83	0.70	8.11	2.94	21.06	32.93	5.49
79.2	61.90	4.42	1621.63	76.95	160.74	58.92	10.55	0.82	0.00	8.14	7.80	1.60	4.81	0.69	4.58	0.67	8.30	3.02	21.91	35.22	5.84
81.4	63.79	4.75	1702.04	77.79	159.59	56.01	9.57	0.65	0.00	7.25	6.99	1.45	4.42	0.64	4.28	0.63	8.46	3.09	22.79	37.78	6.23

Tab. G.8: Modélisation ACF - facteur d'assimilation de 0.2

%ACF	Nb	Cs	Ba	La	Ce	Nd	Sm	Eu^{2+}	Eu^{3+}	Gd	Dy	Ho	Er	Tm	Yb	Lu	Hf	Ta	Pb	Th	U
83.5	65.65	5.11	1777.55	77.81	156.24	52.03	8.41	0.49	0.00	6.23	6.06	1.27	3.95	0.58	3.92	0.58	8.60	3.15	23.58	40.56	6.65
85.6	67.41	5.50	1831.28	76.42	149.69	46.81	7.07	0.32	0.00	5.14	5.14	1.11	3.50	0.53	3.58	0.53	8.74	3.21	24.01	43.56	7.09
87.6	69.23	5.91	1858.08	75.55	145.57	43.20	6.17	0.20	0.00	4.37	4.44	0.97	3.12	0.47	3.27	0.49	8.90	3.27	24.06	46.72	7.55
89.8	71.73	6.41	1848.69	70.71	131.39	35.32	4.55	0.10	0.00	3.14	3.34	0.76	2.53	0.40	2.79	0.42	9.13	3.38	23.55	50.53	8.10

Tab. G.9: Modélisation des processus ACF ayant mené à la composition chimique des roches mafiques du flysch triasique pour un facteur d'assimilation de 0.3 (éléments majeurs en % poids et métaux de transition en ppm).

%ACF	SiO_2	TiO_2	Al_2O_3	Fe_2O_3	FeO	MnO	MgO	CaO	Na2O	K2O	P2O5	Cr	Ni	Co	Sc	V	Zn	Rb	Sr	Y	Zr
0.2	50.14	2.33	13.87	1.70	11.39	0.20	6.76	9.27	3.81	0.08	0.30	110.02	72.11	39.31	43.40	373.02	93.11	2.14	346.05	47.24	190.01
2.2	50.27	2.36	13.73	1.73	11.43	0.20	6.62	9.23	3.83	0.12	0.31	110.89	65.98	39.59	43.90	377.87	94.24	3.79	351.90	47.93	193.87
4.2	50.41	2.40	13.58	1.76	11.47	0.20	6.49	9.20	3.85	0.17	0.31	111.77	60.15	39.88	44.42	382.84	95.39	5.49	357.63	48.64	197.83
6.2	50.58	2.43	13.50	1.79	11.47	0.20	6.27	9.19	3.88	0.21	0.32	112.33	52.55	40.05	44.92	387.91	96.40	7.23	364.32	49.37	201.87
8.2	50.75	2.47	13.41	1.82	11.47	0.20	6.05	9.18	3.90	0.26	0.32	112.87	45.53	40.23	45.44	393.11	97.43	9.02	370.95	50.11	206.03
10.2	50.92	2.50	13.32	1.85	11.46	0.20	5.82	9.17	3.93	0.31	0.33	113.36	39.09	40.40	45.96	398.46	98.47	10.85	377.52	50.88	210.31
12.2	51.07	2.54	13.17	1.88	11.49	0.20	5.67	9.14	3.95	0.36	0.34	114.17	34.82	40.69	46.53	403.98	99.71	12.74	382.70	51.67	214.73
14.2	51.24	2.58	13.09	1.92	11.48	0.20	5.44	9.14	3.97	0.41	0.34	114.59	29.37	40.87	47.08	409.63	100.79	14.67	389.03	52.48	219.26
16.2	51.42	2.62	13.00	1.95	11.46	0.20	5.21	9.15	3.99	0.46	0.35	114.95	24.49	41.03	47.65	415.44	101.88	16.66	395.27	53.31	223.93
18.2	51.58	2.66	12.85	1.99	11.48	0.21	5.05	9.13	4.01	0.51	0.36	115.68	21.31	41.33	48.25	421.45	103.19	18.71	399.86	54.18	228.75
20.2	51.76	2.70	12.76	2.02	11.45	0.21	4.81	9.13	4.03	0.56	0.36	115.92	17.36	41.49	48.85	427.61	104.32	20.81	405.78	55.06	233.71
22.2	51.95	2.74	12.67	2.06	11.41	0.20	4.56	9.15	4.05	0.62	0.37	116.08	13.91	41.64	49.46	433.95	105.47	22.98	411.57	55.98	238.82
24.2	52.08	2.79	12.58	2.09	11.44	0.20	4.41	9.07	4.07	0.68	0.38	106.61	11.75	41.69	49.46	439.77	106.83	25.22	416.62	56.83	244.00
26.2	52.17	2.82	12.60	2.11	11.50	0.20	4.28	8.87	4.11	0.74	0.39	80.54	9.83	41.23	48.17	444.24	108.20	27.55	423.93	57.53	249.09
28.2	52.28	2.86	12.56	2.13	11.55	0.20	4.13	8.73	4.14	0.80	0.40	65.55	8.15	41.00	47.48	449.57	109.61	29.94	429.79	58.34	254.47
30.2	52.36	2.90	12.52	2.16	11.63	0.20	4.03	8.54	4.16	0.87	0.41	49.72	6.96	40.71	46.47	454.64	111.16	32.41	435.03	59.10	259.96
32.2	52.48	2.94	12.48	2.18	11.68	0.20	3.87	8.39	4.19	0.93	0.42	39.04	5.67	40.46	45.74	460.24	112.63	34.96	440.34	59.94	265.69
34.2	52.57	2.98	12.50	2.20	11.74	0.20	3.73	8.18	4.23	1.00	0.42	25.97	4.54	39.92	44.30	465.08	114.11	37.61	446.71	60.68	271.45

TAB. G.9: Modélisation ACF - facteur d'assimilation de 0.3

%ACF	SiO_2	TiO_2	Al_2O_3	Fe_2O_3	FeO	MnO	MgO	CaO	Na2O	K2O	P2O5	Cr	Ni	Co	Sc	V	Zn	Rb	Sr	Y	Zr
36.2	52.67	3.02	12.53	2.23	11.80	0.20	3.58	7.95	4.27	1.07	0.43	16.49	3.59	39.36	42.83	470.00	115.62	40.35	452.80	61.42	277.39
38.2	52.79	3.07	12.50	2.25	11.83	0.20	3.42	7.80	4.29	1.15	0.44	11.93	2.84	39.06	42.04	476.01	117.19	43.18	457.18	62.31	283.72
40.2	52.88	3.12	12.46	2.28	11.91	0.20	3.30	7.60	4.32	1.22	0.46	7.54	2.33	38.69	40.86	481.64	118.92	46.10	460.42	63.13	290.15
42.2	53.00	3.17	12.44	2.31	11.93	0.20	3.14	7.45	4.34	1.30	0.47	5.12	1.83	38.36	40.02	487.96	120.55	49.13	463.84	64.04	296.92
44.3	53.41	3.10	12.51	2.29	11.70	0.19	3.00	7.28	4.39	1.39	0.48	0.01	1.40	36.31	38.51	421.88	114.42	52.52	470.48	64.10	303.76
46.3	53.95	2.98	12.58	2.25	11.33	0.19	2.88	7.16	4.44	1.48	0.49	0.01	1.13	33.75	37.16	336.39	104.95	55.99	477.07	63.76	310.47
48.4	54.49	2.85	12.66	2.22	10.95	0.19	2.76	7.03	4.50	1.57	0.51	0.03	0.93	31.30	35.74	266.95	96.10	59.58	482.91	63.38	317.33
50.4	55.08	2.72	12.75	2.17	10.55	0.19	2.64	6.89	4.55	1.67	0.52	0.02	0.79	28.83	34.23	207.48	87.25	63.35	488.26	62.89	324.39
52.4	55.67	2.59	12.83	2.13	10.15	0.18	2.52	6.75	4.61	1.77	0.54	0.02	0.68	26.48	32.65	160.46	79.08	67.25	492.67	62.35	331.59
54.5	56.29	2.46	12.93	2.07	9.72	0.18	2.38	6.59	4.66	1.88	0.55	0.02	0.59	24.16	30.99	121.65	71.09	71.34	496.33	61.70	338.97
56.5	56.92	2.33	13.03	2.02	9.30	0.18	2.25	6.43	4.72	1.99	0.57	0.01	0.53	22.00	29.27	92.06	63.88	75.56	498.77	61.00	346.49
58.5	57.58	2.19	13.14	1.96	8.85	0.17	2.11	6.25	4.78	2.11	0.58	0.00	0.47	19.86	27.47	68.05	56.85	79.99	500.30	60.17	354.17
60.5	58.23	2.06	13.17	1.90	8.41	0.17	2.00	6.11	4.82	2.24	0.60	0.02	0.50	18.00	26.09	49.73	50.44	84.73	497.80	59.35	362.02
62.5	58.94	1.92	13.29	1.83	7.93	0.17	1.85	5.92	4.88	2.37	0.62	0.00	0.45	16.02	24.16	35.48	44.24	89.55	496.46	58.27	369.95
64.6	59.62	1.80	13.36	1.76	7.50	0.16	1.70	5.71	4.93	2.50	0.64	0.01	0.38	14.32	22.28	25.81	39.19	94.75	488.78	57.40	379.29
66.6	60.37	1.66	13.42	1.68	7.00	0.16	1.59	5.54	4.96	2.65	0.66	0.00	0.42	12.63	20.74	17.53	33.70	100.17	480.74	56.13	387.47
68.8	61.12	1.53	13.51	1.60	6.53	0.15	1.42	5.30	5.02	2.81	0.69	0.04	0.34	11.06	18.74	12.20	29.25	105.89	467.94	54.91	397.13
70.8	61.95	1.38	13.59	1.50	5.96	0.14	1.29	5.12	5.05	2.97	0.71	0.00	0.36	9.49	17.10	7.80	24.41	111.85	454.94	53.22	405.28
72.8	62.81	1.26	13.67	1.41	5.51	0.14	1.17	4.83	5.09	3.14	0.66	0.00	0.36	8.27	15.54	5.37	20.94	117.86	437.89	48.09	413.92
74.8	63.73	1.13	13.77	1.30	5.00	0.13	1.03	4.52	5.13	3.32	0.60	0.00	0.33	7.03	13.91	3.52	17.45	124.21	417.73	42.68	422.34
77.0	64.64	1.01	13.81	1.20	4.52	0.13	0.90	4.21	5.16	3.51	0.56	0.00	0.28	5.95	12.29	2.40	14.59	131.04	385.99	38.38	432.35
79.1	65.60	0.89	13.87	1.09	4.02	0.12	0.76	3.89	5.17	3.73	0.52	0.00	0.25	4.92	10.65	1.65	11.96	138.31	350.75	33.87	441.92
81.3	66.63	0.76	13.95	0.96	3.46	0.11	0.61	3.55	5.19	3.96	0.48	0.00	0.20	3.91	8.96	1.13	9.43	145.90	310.73	29.14	450.73
83.4	67.68	0.64	14.03	0.82	2.90	0.10	0.46	3.18	5.19	4.20	0.43	0.00	0.13	3.03	7.28	0.85	7.34	153.59	265.37	24.36	458.78
85.6	68.82	0.51	14.13	0.66	2.29	0.08	0.31	2.79	5.20	4.47	0.38	0.00	0.02	2.18	5.63	0.61	5.34	161.46	216.25	19.34	464.60
87.7	69.78	0.42	14.12	0.54	1.83	0.07	0.21	2.48	5.13	4.74	0.33	-0.10	-0.03	1.68	4.60	0.57	4.23	168.20	158.95	15.04	470.89
89.8	70.85	0.31	14.13	0.39	1.29	0.06	0.11	2.17	5.06	5.03	0.27	-1.72	-0.12	1.15	3.60	0.40	2.95	174.48	105.51	10.60	472.45

TAB. G.10: Modélisation des processus ACF ayant mené à la composition chimique des roches mafiques du flysch triasique pour un facteur d'assimilation de 0.3 (éléments traces en ppm).

%ACF	Nb	Cs	Ba	La	Ce	Nd	Sm	Eu^{2+}	Eu^{3+}	Gd	Dy	Ho	Er	Tm	Yb	Lu	Hf	Ta	Pb	Th	U
0.2	24.98	0.26	84.37	15.87	40.56	21.55	5.72	1.77	0.00	6.69	6.77	1.40	4.12	0.58	3.74	0.55	3.74	1.30	3.77	2.05	0.55
2.2	25.38	0.32	109.25	16.87	42.64	22.38	5.87	1.77	0.00	6.78	6.87	1.42	4.18	0.59	3.79	0.56	3.82	1.32	4.04	2.51	0.62
4.2	25.78	0.37	134.70	17.90	44.78	23.24	6.03	1.77	0.00	6.87	6.98	1.44	4.24	0.60	3.85	0.57	3.90	1.34	4.31	2.97	0.70
6.2	26.20	0.43	160.82	18.95	46.98	24.12	6.19	1.78	0.00	6.96	7.09	1.46	4.30	0.61	3.90	0.57	3.99	1.37	4.60	3.45	0.77
8.2	26.62	0.49	187.57	20.03	49.24	25.02	6.35	1.79	0.00	7.05	7.20	1.49	4.37	0.61	3.96	0.58	4.07	1.39	4.89	3.95	0.85
10.2	27.06	0.56	214.98	21.14	51.56	25.94	6.52	1.80	0.00	7.15	7.31	1.51	4.43	0.62	4.01	0.59	4.16	1.41	5.18	4.45	0.93
12.2	27.51	0.62	242.98	22.28	53.94	26.90	6.69	1.80	0.00	7.25	7.43	1.53	4.50	0.63	4.07	0.60	4.25	1.44	5.48	4.97	1.02
14.2	27.97	0.69	271.79	23.46	56.39	27.88	6.87	1.80	0.00	7.35	7.55	1.56	4.57	0.64	4.14	0.61	4.35	1.46	5.80	5.51	1.10
16.2	28.45	0.75	301.35	24.66	58.91	28.88	7.05	1.81	0.00	7.45	7.67	1.58	4.64	0.65	4.20	0.62	4.44	1.49	6.12	6.06	1.19
18.2	28.94	0.82	331.51	25.90	61.50	29.92	7.24	1.80	0.00	7.56	7.80	1.61	4.71	0.66	4.26	0.62	4.54	1.52	6.44	6.63	1.28
20.2	29.45	0.90	362.63	27.17	64.18	30.99	7.43	1.81	0.00	7.68	7.93	1.63	4.79	0.67	4.33	0.63	4.64	1.54	6.77	7.22	1.37
22.2	29.97	0.97	394.59	28.49	66.93	32.09	7.63	1.81	0.00	7.79	8.07	1.66	4.87	0.68	4.40	0.64	4.75	1.57	7.12	7.83	1.47
24.2	30.52	1.05	427.44	29.83	69.75	33.20	7.83	1.81	0.00	7.90	8.18	1.68	4.93	0.69	4.45	0.65	4.85	1.60	7.48	8.45	1.57
26.2	31.10	1.13	461.74	31.23	72.63	34.30	8.02	1.82	0.00	7.97	8.24	1.69	4.96	0.70	4.48	0.66	4.93	1.63	7.85	9.10	1.67
28.2	31.69	1.21	496.76	32.66	75.61	35.45	8.22	1.82	0.00	8.06	8.33	1.71	5.01	0.70	4.52	0.66	5.02	1.66	8.24	9.77	1.78
30.2	32.30	1.29	532.80	34.14	78.67	36.62	8.42	1.82	0.00	8.15	8.41	1.72	5.04	0.71	4.55	0.67	5.11	1.69	8.63	10.46	1.89
32.2	32.93	1.38	569.91	35.66	81.84	37.84	8.63	1.82	0.00	8.24	8.50	1.74	5.09	0.71	4.59	0.67	5.21	1.73	9.04	11.18	2.00
34.2	33.59	1.47	608.54	37.24	85.09	39.07	8.83	1.83	0.00	8.32	8.56	1.75	5.11	0.72	4.61	0.67	5.30	1.76	9.47	11.92	2.12
36.2	34.28	1.57	648.42	38.86	88.45	40.32	9.04	1.83	0.00	8.40	8.61	1.76	5.13	0.72	4.62	0.68	5.39	1.80	9.91	12.69	2.24
38.2	34.98	1.67	689.11	40.54	91.95	41.66	9.27	1.83	0.00	8.50	8.70	1.77	5.17	0.72	4.66	0.68	5.50	1.84	10.35	13.49	2.36
40.2	35.72	1.77	731.05	42.27	95.53	43.01	9.50	1.82	0.00	8.58	8.76	1.78	5.19	0.73	4.68	0.68	5.60	1.87	10.81	14.31	2.49
42.2	36.48	1.87	774.37	44.07	99.28	44.42	9.74	1.82	0.00	8.69	8.85	1.80	5.23	0.73	4.71	0.69	5.71	1.91	11.29	15.17	2.63
44.3	37.26	1.99	823.42	46.09	103.48	46.01	10.01	1.82	0.00	8.79	8.93	1.81	5.26	0.74	4.74	0.69	5.81	1.95	11.83	16.12	2.78
46.3	38.01	2.11	873.31	48.17	107.80	47.65	10.29	1.83	0.00	8.92	9.03	1.82	5.30	0.74	4.77	0.70	5.91	1.99	12.39	17.09	2.93
48.4	38.78	2.24	924.70	50.31	112.25	49.33	10.58	1.83	0.00	9.04	9.12	1.84	5.34	0.75	4.80	0.70	6.01	2.02	12.96	18.10	3.09
50.4	39.57	2.37	978.47	52.55	116.91	51.08	10.87	1.83	0.00	9.16	9.21	1.85	5.37	0.75	4.82	0.70	6.11	2.06	13.56	19.16	3.25

TAB. G.10: Modélisation ACF - facteur d'assimilation de 0.3

%ACF	Nb	Cs	Ba	La	Ce	Nd	Sm	Eu^{2+}	Eu^{3+}	Gd	Dy	Ho	Er	Tm	Yb	Lu	Hf	Ta	Pb	Th	U
52.4	40.38	2.51	1033.80	54.86	121.71	52.87	11.17	1.83	0.00	9.28	9.29	1.86	5.40	0.75	4.84	0.71	6.21	2.09	14.17	20.25	3.43
54.5	41.21	2.65	1091.52	57.27	126.72	54.72	11.48	1.82	0.00	9.39	9.36	1.87	5.42	0.76	4.86	0.71	6.32	2.13	14.82	21.41	3.60
56.5	42.06	2.80	1150.70	59.75	131.85	56.61	11.79	1.81	0.00	9.51	9.42	1.88	5.43	0.76	4.86	0.71	6.42	2.17	15.47	22.60	3.79
58.5	42.93	2.96	1212.48	62.33	137.21	58.56	12.11	1.80	0.00	9.62	9.47	1.88	5.44	0.76	4.86	0.71	6.52	2.21	16.16	23.85	3.98
60.5	43.78	3.13	1277.38	65.06	142.92	60.66	12.46	1.77	0.00	9.74	9.56	1.89	5.46	0.76	4.88	0.71	6.63	2.24	16.86	25.20	4.19
62.5	44.69	3.30	1343.56	67.84	148.68	62.71	12.79	1.74	0.00	9.84	9.58	1.89	5.44	0.76	4.86	0.70	6.74	2.28	17.59	26.58	4.41
64.6	45.76	3.49	1413.05	70.84	154.97	64.95	13.15	1.70	0.00	9.96	9.61	1.89	5.43	0.75	4.84	0.70	6.86	2.33	18.36	28.08	4.64
66.6	46.65	3.69	1485.01	73.91	161.40	67.25	13.53	1.65	0.00	10.07	9.65	1.89	5.42	0.75	4.83	0.70	6.97	2.37	19.13	29.65	4.88
68.8	47.76	3.90	1559.47	77.16	168.21	69.60	13.90	1.59	0.00	10.17	9.64	1.87	5.38	0.75	4.78	0.69	7.09	2.41	19.95	31.33	5.14
70.8	48.64	4.12	1636.19	80.48	175.19	72.03	14.28	1.52	0.00	10.27	9.65	1.87	5.34	0.74	4.74	0.68	7.19	2.44	20.77	33.07	5.40
72.8	49.66	4.35	1711.71	81.45	174.71	69.65	13.35	1.38	0.00	9.48	8.98	1.75	5.06	0.71	4.55	0.66	7.30	2.49	21.58	34.86	5.68
74.8	50.65	4.59	1789.68	82.15	173.40	66.80	12.34	1.22	0.00	8.64	8.25	1.63	4.75	0.67	4.33	0.63	7.39	2.52	22.41	36.76	5.97
77.0	51.83	4.86	1868.30	83.42	173.83	64.97	11.62	1.07	0.00	8.00	7.67	1.52	4.48	0.63	4.14	0.60	7.52	2.57	23.24	38.90	6.29
79.1	52.95	5.16	1948.69	84.44	173.47	62.69	10.81	0.91	0.00	7.29	7.03	1.41	4.17	0.60	3.91	0.57	7.63	2.61	24.06	41.20	6.63
81.3	53.98	5.47	2027.39	85.06	172.01	59.84	9.90	0.75	0.00	6.52	6.32	1.28	3.82	0.55	3.64	0.53	7.72	2.64	24.85	43.66	7.00
83.4	54.94	5.81	2099.25	84.96	168.72	56.15	8.85	0.59	0.00	5.68	5.53	1.13	3.42	0.50	3.31	0.48	7.79	2.67	25.54	46.25	7.38
85.6	55.65	6.17	2163.33	83.90	163.00	51.39	7.64	0.44	0.00	4.76	4.66	0.96	2.96	0.43	2.93	0.43	7.80	2.68	26.13	49.01	7.77
87.7	56.40	6.54	2191.22	81.24	154.01	45.60	6.34	0.29	0.00	3.83	3.85	0.81	2.54	0.38	2.60	0.38	7.85	2.70	26.21	51.85	8.18
89.8	56.63	6.94	2192.24	76.69	140.76	38.39	4.89	0.17	0.00	2.86	2.97	0.64	2.07	0.32	2.21	0.33	7.81	2.68	25.94	54.88	8.59

TAB. G.11: Modélisation des processus ACF ayant mené à la composition chimique des roches calco-alcalines du mélange ophiolitique pour un facteur d'assimilation de 0.05 (éléments majeurs en % poids et métaux de transition en ppm).

%ACF	SiO_2	TiO_2	Al_2O_3	Fe_2O_3	FeO	MnO	MgO	CaO	Na2O	K2O	P2O5	Cr	Ni	Co	Sc	V	Zn	Rb	Sr	Y	Zr
0.2	51.16	1.09	16.56	1.16	8.25	0.17	7.41	10.90	3.00	0.12	0.09	181.83	69.67	36.16	38.51	244.13	53.84	0.86	93.13	24.20	59.88
2.2	51.22	1.11	16.23	1.18	8.41	0.18	7.54	10.82	3.00	0.13	0.09	185.41	71.08	36.88	39.22	248.71	54.97	0.94	92.85	24.68	61.17
4.2	51.27	1.14	15.89	1.21	8.57	0.18	7.69	10.74	3.01	0.13	0.10	189.12	72.56	37.63	39.95	253.46	56.14	1.02	92.54	25.18	62.50
6.2	51.32	1.16	15.54	1.23	8.73	0.19	7.84	10.66	3.01	0.14	0.10	192.98	74.08	38.40	40.72	258.39	57.36	1.11	92.20	25.70	63.89
8.2	51.37	1.18	15.18	1.26	8.91	0.19	8.00	10.57	3.01	0.14	0.10	196.99	75.67	39.21	41.51	263.52	58.63	1.20	91.83	26.25	65.33
10.2	51.44	1.21	14.88	1.29	9.06	0.19	8.07	10.52	3.01	0.15	0.10	200.68	74.85	39.93	42.31	268.81	59.85	1.29	91.68	26.81	66.82
12.2	51.57	1.23	14.77	1.31	9.12	0.20	7.86	10.55	3.03	0.15	0.10	202.99	66.88	40.34	43.07	274.16	60.81	1.39	92.28	27.38	68.33
14.2	51.68	1.26	14.58	1.34	9.22	0.20	7.74	10.56	3.05	0.16	0.11	205.86	61.56	40.88	43.88	279.78	61.91	1.49	92.60	27.98	69.92
16.2	51.82	1.29	14.46	1.38	9.29	0.20	7.53	10.60	3.07	0.16	0.11	208.24	54.36	41.31	44.70	285.59	62.93	1.60	93.18	28.60	71.56
18.2	51.94	1.32	14.27	1.41	9.39	0.20	7.40	10.61	3.09	0.17	0.11	211.24	49.56	41.87	45.57	291.69	64.11	1.71	93.46	29.25	73.29
20.2	52.08	1.35	14.14	1.44	9.45	0.21	7.17	10.66	3.11	0.17	0.12	213.68	43.14	42.32	46.46	298.01	65.20	1.83	94.02	29.93	75.08
22.2	52.21	1.38	13.94	1.48	9.55	0.21	7.04	10.67	3.13	0.18	0.12	216.81	38.89	42.92	47.41	304.66	66.47	1.95	94.24	30.64	76.97
24.2	52.37	1.41	13.80	1.52	9.62	0.21	6.79	10.73	3.15	0.19	0.12	219.28	33.27	43.40	48.37	311.56	67.65	2.07	94.77	31.38	78.93
26.2	52.50	1.44	13.58	1.56	9.72	0.21	6.65	10.75	3.16	0.19	0.12	222.52	29.57	44.04	49.40	318.84	69.02	2.20	94.93	32.16	81.00
28.2	52.67	1.48	13.44	1.60	9.78	0.22	6.39	10.82	3.18	0.20	0.13	225.01	24.76	44.54	50.45	326.42	70.29	2.34	95.42	32.97	83.16
30.2	52.85	1.52	13.29	1.64	9.84	0.22	6.12	10.88	3.20	0.21	0.13	227.45	20.43	45.05	51.55	334.37	71.61	2.48	95.88	33.83	85.42
32.2	52.99	1.56	13.05	1.69	9.94	0.22	5.95	10.93	3.22	0.22	0.14	230.78	17.64	45.75	52.73	342.78	73.15	2.63	95.91	34.73	87.82
34.2	53.03	1.59	13.03	1.72	10.10	0.22	5.84	10.74	3.26	0.22	0.14	199.78	15.66	45.57	51.62	349.73	74.73	2.80	96.96	35.52	90.23
36.2	53.11	1.63	12.94	1.75	10.25	0.23	5.70	10.63	3.29	0.23	0.14	181.02	13.63	45.69	51.27	357.67	76.39	2.97	97.65	36.41	92.81
38.2	53.15	1.67	12.84	1.79	10.44	0.23	5.62	10.45	3.32	0.24	0.15	157.99	12.26	45.73	50.51	365.67	78.22	3.15	98.28	37.31	95.53
40.2	53.23	1.72	12.74	1.82	10.60	0.23	5.47	10.33	3.35	0.25	0.15	140.54	10.52	45.84	50.11	374.43	80.05	3.34	98.94	38.29	98.42
42.2	53.27	1.76	12.64	1.86	10.81	0.23	5.38	10.14	3.38	0.26	0.16	119.65	9.34	45.87	49.29	383.27	82.07	3.54	99.51	39.29	101.47
44.2	53.35	1.81	12.53	1.90	10.98	0.24	5.21	10.01	3.41	0.27	0.16	104.24	7.87	45.97	48.87	393.00	84.10	3.75	100.11	40.38	104.73
46.2	53.40	1.86	12.51	1.94	11.18	0.24	5.06	9.78	3.46	0.29	0.17	81.88	6.62	45.68	47.51	402.35	86.21	3.98	101.13	41.45	108.15
48.2	53.49	1.92	12.40	1.99	11.36	0.24	4.88	9.64	3.49	0.30	0.17	68.84	5.44	45.74	47.03	413.19	88.46	4.23	101.68	42.66	111.85

Tab. G.11: Modélisation ACF - facteur d'assimilation de 0.05

%ACF	SiO_2	TiO_2	Al_2O_3	Fe_2O_3	FeO	MnO	MgO	CaO	Na2O	K2O	P2O5	Cr	Ni	Co	Sc	V	Zn	Rb	Sr	Y	Zr
50.2	53.54	1.98	12.28	2.03	11.61	0.24	4.77	9.43	3.52	0.31	0.18	54.00	4.66	45.72	46.06	424.17	90.96	4.49	102.09	43.90	115.78
52.2	53.63	2.04	12.16	2.08	11.80	0.25	4.57	9.28	3.56	0.33	0.19	43.67	3.74	45.77	45.54	436.38	93.48	4.76	102.53	45.27	120.02
54.2	53.68	2.11	12.03	2.13	12.06	0.25	4.45	9.05	3.59	0.34	0.20	32.16	3.14	45.72	44.49	448.77	96.30	5.06	102.78	46.66	124.55
56.2	53.78	2.18	11.90	2.19	12.27	0.25	4.24	8.89	3.62	0.36	0.20	24.35	2.45	45.74	43.88	462.62	99.14	5.38	103.05	48.21	129.45
58.2	53.84	2.26	11.88	2.23	12.52	0.25	4.03	8.61	3.67	0.38	0.21	14.81	1.88	45.24	42.17	475.98	102.15	5.73	103.78	49.71	134.68
60.2	53.95	2.35	11.75	2.29	12.73	0.26	3.80	8.44	3.70	0.40	0.22	10.25	1.41	45.21	41.52	491.84	105.38	6.10	103.88	51.48	140.43
62.2	53.99	2.44	11.60	2.35	13.04	0.26	3.63	8.18	3.73	0.42	0.23	5.87	1.13	45.04	40.23	508.00	109.04	6.51	103.62	53.28	146.62
64.2	54.11	2.54	11.46	2.42	13.27	0.26	3.38	8.00	3.76	0.44	0.24	3.58	0.83	44.96	39.50	526.40	112.76	6.95	103.41	55.32	153.43
66.2	54.12	2.65	11.17	2.50	13.65	0.26	3.26	7.77	3.75	0.47	0.26	2.02	0.74	45.20	38.74	546.24	117.29	7.43	101.90	57.50	160.87
68.2	54.24	2.77	11.02	2.57	13.89	0.26	2.99	7.59	3.77	0.50	0.27	1.06	0.55	45.07	37.90	567.93	121.68	7.96	101.19	59.89	169.08
70.2	54.67	2.75	10.87	2.60	13.87	0.27	2.83	7.41	3.79	0.53	0.29	0.01	0.50	42.75	36.73	481.71	116.35	8.57	100.47	61.43	177.71
72.4	55.62	2.58	10.94	2.57	13.37	0.26	2.59	7.21	3.87	0.57	0.31	0.00	0.35	37.68	34.47	326.76	101.39	9.33	101.00	62.13	187.83
74.4	56.69	2.35	10.83	2.53	12.80	0.26	2.46	7.14	3.91	0.61	0.33	0.00	0.35	33.05	33.19	202.54	85.27	10.13	100.05	62.53	198.08
76.4	57.88	2.13	10.87	2.46	12.13	0.26	2.23	6.96	3.98	0.66	0.35	-0.01	0.32	28.28	30.81	122.16	70.86	11.04	99.66	62.65	209.23
78.6	59.02	1.95	10.79	2.43	11.62	0.26	2.00	6.72	4.02	0.72	0.38	0.01	0.26	24.47	28.34	77.13	60.35	12.11	97.20	63.33	223.03
80.6	60.51	1.69	10.68	2.34	10.80	0.26	1.82	6.59	4.04	0.79	0.41	0.01	0.28	20.21	26.23	39.57	47.19	13.31	94.18	63.08	236.98
82.7	61.83	1.54	10.57	2.29	10.27	0.25	1.53	6.27	4.05	0.86	0.45	0.00	0.19	17.12	23.09	24.53	39.97	14.70	89.27	63.67	254.54
84.8	63.48	1.34	10.26	2.21	9.57	0.24	1.32	6.06	3.99	0.96	0.50	0.00	0.20	14.09	19.79	12.82	31.86	16.38	82.51	63.95	274.82
86.8	65.78	1.07	10.13	2.05	8.53	0.23	1.06	5.62	3.97	1.07	0.40	0.00	0.18	10.71	16.94	5.57	22.98	18.36	75.42	55.64	295.43
88.9	68.34	0.84	9.79	1.88	7.51	0.22	0.78	5.17	3.84	1.21	0.33	-0.04	0.06	7.89	13.81	2.47	16.27	20.82	63.47	49.45	322.27
91.0	71.37	0.59	9.09	1.67	6.37	0.21	0.59	4.86	3.53	1.39	0.25	0.01	0.12	5.58	11.52	1.15	10.58	23.80	47.04	42.52	352.60
93.1	75.07	0.41	8.49	1.40	5.05	0.17	0.23	4.13	3.21	1.62	0.13	155.05	-0.16	3.51	7.24	0.81	6.84	27.49	30.50	33.28	388.68

TAB. G.12: Modélisation des processus ACF ayant mené à la composition chimique des roches calco-alcalines du mélange ophiolitique pour un facteur d'assimilation de 0.05 (éléments traces en ppm).

%ACF	Nb	Cs	Ba	La	Ce	Nd	Sm	Eu^{2+}	Eu^{3+}	Gd	Dy	Ho	Er	Tm	Yb	Lu	Hf	Ta	Pb	Th	U
0.2	0.97	0.09	6.02	2.08	6.98	6.71	2.37	0.98	0.00	3.39	4.19	0.89	2.68	0.38	2.51	0.38	1.57	0.06	1.78	0.06	0.00
2.2	1.00	0.10	7.01	2.15	7.17	6.86	2.42	0.97	0.00	3.46	4.27	0.91	2.73	0.38	2.56	0.39	1.61	0.06	1.82	0.07	0.00
4.2	1.03	0.10	8.03	2.22	7.36	7.01	2.47	0.97	0.00	3.53	4.36	0.92	2.78	0.39	2.61	0.39	1.64	0.07	1.87	0.08	0.00
6.2	1.06	0.11	9.08	2.30	7.57	7.18	2.53	0.96	0.00	3.61	4.45	0.94	2.84	0.40	2.67	0.40	1.68	0.07	1.93	0.09	0.01
8.2	1.09	0.12	10.18	2.37	7.78	7.34	2.58	0.95	0.00	3.68	4.54	0.96	2.90	0.41	2.72	0.41	1.72	0.07	1.98	0.10	0.01
10.2	1.13	0.12	11.31	2.45	8.00	7.52	2.64	0.95	0.00	3.76	4.64	0.98	2.96	0.42	2.78	0.42	1.76	0.07	2.03	0.11	0.01
12.2	1.16	0.13	12.50	2.53	8.23	7.70	2.70	0.95	0.00	3.84	4.74	1.00	3.03	0.42	2.84	0.43	1.80	0.07	2.09	0.12	0.01
14.2	1.20	0.14	13.73	2.62	8.46	7.88	2.76	0.95	0.00	3.93	4.84	1.02	3.09	0.43	2.90	0.44	1.85	0.08	2.15	0.13	0.02
16.2	1.23	0.15	15.01	2.71	8.71	8.08	2.83	0.96	0.00	4.02	4.95	1.04	3.16	0.44	2.96	0.45	1.89	0.08	2.22	0.15	0.02
18.2	1.27	0.15	16.33	2.80	8.97	8.28	2.89	0.96	0.00	4.11	5.06	1.06	3.23	0.45	3.03	0.46	1.94	0.08	2.28	0.16	0.02
20.2	1.31	0.16	17.72	2.90	9.24	8.49	2.96	0.96	0.00	4.21	5.18	1.08	3.30	0.46	3.10	0.47	1.99	0.08	2.35	0.17	0.02
22.2	1.35	0.17	19.16	3.00	9.52	8.72	3.04	0.96	0.00	4.31	5.30	1.11	3.38	0.47	3.17	0.48	2.04	0.09	2.43	0.19	0.03
24.2	1.40	0.18	20.66	3.11	9.82	8.95	3.12	0.96	0.00	4.42	5.43	1.13	3.46	0.48	3.25	0.49	2.09	0.09	2.50	0.20	0.03
26.2	1.45	0.19	22.22	3.22	10.12	9.19	3.20	0.96	0.00	4.53	5.56	1.16	3.55	0.49	3.33	0.50	2.15	0.09	2.58	0.21	0.03
28.2	1.49	0.20	23.87	3.34	10.45	9.45	3.28	0.96	0.00	4.64	5.70	1.19	3.64	0.51	3.41	0.51	2.21	0.10	2.66	0.23	0.04
30.2	1.55	0.21	25.58	3.46	10.79	9.71	3.37	0.97	0.00	4.77	5.85	1.22	3.73	0.52	3.49	0.52	2.27	0.10	2.75	0.25	0.04
32.2	1.60	0.22	27.37	3.59	11.14	10.00	3.46	0.96	0.00	4.90	6.00	1.25	3.83	0.53	3.59	0.54	2.33	0.10	2.83	0.26	0.04
34.2	1.66	0.23	29.30	3.72	11.51	10.27	3.55	0.97	0.00	5.00	6.11	1.27	3.90	0.54	3.65	0.55	2.38	0.11	2.93	0.28	0.05
36.2	1.72	0.24	31.30	3.86	11.91	10.57	3.65	0.97	0.00	5.12	6.24	1.29	3.98	0.55	3.72	0.56	2.45	0.11	3.04	0.30	0.05
38.2	1.78	0.26	33.42	4.02	12.32	10.88	3.75	0.98	0.00	5.25	6.37	1.31	4.05	0.56	3.79	0.57	2.51	0.12	3.15	0.32	0.06
40.2	1.85	0.27	35.65	4.17	12.75	11.21	3.85	0.98	0.00	5.38	6.51	1.34	4.14	0.57	3.88	0.58	2.57	0.12	3.26	0.35	0.06
42.2	1.92	0.29	38.00	4.34	13.21	11.55	3.96	0.98	0.00	5.51	6.65	1.37	4.23	0.58	3.95	0.59	2.64	0.12	3.38	0.37	0.07
44.2	2.00	0.30	40.49	4.52	13.70	11.92	4.08	0.99	0.00	5.66	6.80	1.40	4.32	0.59	4.04	0.61	2.72	0.13	3.51	0.39	0.07
46.2	2.08	0.32	43.16	4.71	14.22	12.31	4.20	0.99	0.00	5.80	6.94	1.42	4.40	0.60	4.12	0.62	2.79	0.13	3.65	0.42	0.08
48.2	2.17	0.34	45.96	4.91	14.77	12.72	4.34	0.99	0.00	5.97	7.11	1.45	4.50	0.62	4.21	0.63	2.88	0.14	3.80	0.45	0.08
50.2	2.27	0.36	48.94	5.12	15.36	13.16	4.48	1.00	0.00	6.14	7.27	1.48	4.60	0.63	4.30	0.64	2.97	0.15	3.95	0.48	0.09

Tab. G.12: Modélisation ACF - facteur d'assimilation de 0.05

%ACF	Nb	Cs	Ba	La	Ce	Nd	Sm	Eu^{2+}	Eu^{3+}	Gd	Dy	Ho	Er	Tm	Yb	Lu	Hf	Ta	Pb	Th	U
52.2	2.37	0.38	52.11	5.35	15.99	13.63	4.63	1.00	0.00	6.32	7.46	1.52	4.72	0.64	4.41	0.66	3.06	0.15	4.11	0.51	0.10
54.2	2.47	0.40	55.50	5.60	16.66	14.12	4.78	1.00	0.00	6.51	7.64	1.55	4.82	0.66	4.51	0.67	3.16	0.16	4.29	0.55	0.10
56.2	2.59	0.42	59.12	5.86	17.39	14.66	4.96	0.99	0.00	6.72	7.85	1.58	4.94	0.67	4.62	0.69	3.27	0.17	4.47	0.58	0.11
58.2	2.72	0.45	63.08	6.14	18.16	15.22	5.13	1.00	0.00	6.92	8.02	1.61	5.04	0.69	4.71	0.70	3.38	0.18	4.68	0.62	0.12
60.2	2.86	0.48	67.28	6.45	19.01	15.85	5.33	1.00	0.00	7.15	8.25	1.65	5.18	0.70	4.84	0.72	3.51	0.19	4.90	0.67	0.13
62.2	3.01	0.51	71.82	6.78	19.92	16.50	5.53	0.99	0.00	7.39	8.46	1.69	5.30	0.72	4.95	0.74	3.65	0.19	5.13	0.72	0.14
64.2	3.17	0.54	76.74	7.14	20.92	17.24	5.77	0.98	0.00	7.67	8.72	1.74	5.45	0.74	5.08	0.76	3.80	0.21	5.38	0.77	0.15
66.2	3.35	0.58	81.96	7.53	22.00	18.02	6.01	0.97	0.00	7.96	8.99	1.78	5.60	0.76	5.23	0.78	3.96	0.22	5.65	0.83	0.16
68.2	3.55	0.62	87.80	7.96	23.19	18.89	6.29	0.95	0.00	8.29	9.27	1.83	5.76	0.78	5.38	0.80	4.14	0.23	5.95	0.89	0.17
70.2	3.76	0.66	94.61	8.46	24.57	19.88	6.60	0.94	0.00	8.65	9.60	1.89	5.94	0.80	5.54	0.83	4.33	0.24	6.29	0.96	0.19
72.4	4.01	0.72	102.86	9.08	26.28	21.11	6.98	0.94	0.00	9.08	9.95	1.94	6.13	0.82	5.70	0.85	4.52	0.26	6.74	1.05	0.21
74.4	4.26	0.78	111.48	9.73	28.10	22.44	7.40	0.93	0.00	9.57	10.39	2.02	6.37	0.85	5.93	0.88	4.73	0.27	7.19	1.15	0.23
76.4	4.54	0.85	121.43	10.47	30.12	23.87	7.84	0.92	0.00	10.05	10.77	2.08	6.56	0.88	6.09	0.91	4.94	0.29	7.70	1.26	0.25
78.6	4.88	0.93	132.63	11.33	32.50	25.55	8.35	0.90	0.00	10.62	11.19	2.14	6.77	0.90	6.28	0.93	5.21	0.31	8.29	1.38	0.28
80.6	5.22	1.03	145.20	12.28	35.17	27.42	8.93	0.86	0.00	11.26	11.69	2.22	7.03	0.93	6.50	0.97	5.48	0.33	8.93	1.53	0.31
82.7	5.66	1.14	159.23	13.37	38.21	29.49	9.55	0.81	0.00	11.90	12.06	2.27	7.18	0.95	6.62	0.98	5.81	0.35	9.66	1.70	0.34
84.8	6.16	1.28	175.79	14.71	42.01	32.12	10.37	0.74	0.00	12.81	12.75	2.38	7.52	0.99	6.93	1.03	6.21	0.38	10.49	1.91	0.38
86.8	6.69	1.44	195.08	15.49	43.20	31.36	9.63	0.62	0.00	11.83	11.81	2.22	7.16	0.95	6.74	1.00	6.58	0.41	11.46	2.16	0.43
88.9	7.37	1.65	217.38	16.64	45.58	31.57	9.29	0.48	0.00	11.28	11.13	2.10	6.86	0.92	6.57	0.98	7.06	0.45	12.58	2.48	0.50
91.0	8.14	1.92	241.64	17.87	48.04	31.49	8.81	0.32	0.00	10.63	10.46	1.99	6.62	0.89	6.46	0.97	7.60	0.49	13.71	2.89	0.58
93.1	9.09	2.27	269.31	18.88	49.25	29.61	7.65	0.18	0.00	9.02	8.56	1.63	5.53	0.75	5.55	0.83	8.20	0.53	15.01	3.42	0.68

TAB. G.13: Modélisation des processus ACF ayant mené à la composition chimique des roches calco-alcalines du mélange ophiolitique pour un facteur d'assimilation de 0.1 (éléments majeurs en % poids et métaux de transition en ppm).

%ACF	SiO_2	TiO_2	Al_2O_3	Fe_2O_3	FeO	MnO	MgO	CaO	Na2O	K2O	P2O5	Cr	Ni	Co	Sc	V	Zn	Rb	Sr	Y	Zr
0.2	51.16	1.09	16.56	1.16	8.25	0.17	7.41	10.90	3.00	0.12	0.09	181.83	69.67	36.16	38.51	244.13	53.84	0.86	93.13	24.20	59.88
2.2	51.23	1.11	16.23	1.18	8.40	0.18	7.54	10.82	3.00	0.13	0.09	185.31	71.09	36.87	39.19	248.58	55.01	1.00	93.12	24.69	61.25
4.2	51.30	1.14	15.88	1.21	8.56	0.18	7.68	10.73	3.00	0.14	0.10	188.90	72.57	37.60	39.90	253.18	56.23	1.16	93.09	25.20	62.68
6.2	51.37	1.16	15.53	1.23	8.72	0.19	7.82	10.64	3.01	0.14	0.10	192.63	74.10	38.36	40.63	257.95	57.49	1.31	93.04	25.73	64.15
8.2	51.43	1.18	15.17	1.26	8.89	0.19	7.97	10.56	3.01	0.15	0.10	196.51	75.68	39.14	41.39	262.90	58.80	1.47	92.95	26.28	65.68
10.2	51.52	1.21	14.87	1.29	9.03	0.19	8.04	10.50	3.01	0.16	0.10	200.04	74.86	39.85	42.16	267.98	60.06	1.64	93.09	26.84	67.25
12.2	51.66	1.23	14.76	1.31	9.09	0.20	7.83	10.53	3.03	0.16	0.11	202.19	66.90	40.23	42.87	273.12	61.05	1.82	93.98	27.42	68.85
14.2	51.79	1.26	14.57	1.34	9.18	0.20	7.70	10.53	3.05	0.17	0.11	204.89	61.59	40.74	43.64	278.49	62.18	2.00	94.60	28.02	70.53
16.2	51.94	1.28	14.45	1.37	9.24	0.20	7.48	10.56	3.07	0.18	0.11	207.09	54.40	41.14	44.41	284.03	63.24	2.19	95.48	28.64	72.25
18.2	52.08	1.31	14.26	1.41	9.34	0.20	7.35	10.57	3.08	0.19	0.11	209.88	49.63	41.68	45.24	289.84	64.44	2.38	96.06	29.29	74.07
20.2	52.24	1.34	14.14	1.44	9.39	0.21	7.12	10.61	3.10	0.20	0.12	212.11	43.25	42.10	46.06	295.83	65.57	2.58	96.93	29.97	75.94
22.2	52.41	1.37	14.01	1.47	9.45	0.21	6.88	10.65	3.13	0.21	0.12	214.31	37.33	42.53	46.92	302.07	66.73	2.80	97.80	30.67	77.89
24.2	52.56	1.40	13.80	1.51	9.54	0.21	6.73	10.67	3.14	0.22	0.12	217.22	33.45	43.10	47.85	308.63	68.06	3.02	98.31	31.41	79.94
26.2	52.71	1.43	13.58	1.55	9.63	0.22	6.58	10.69	3.15	0.23	0.13	220.18	29.80	43.70	48.81	315.47	69.45	3.24	98.78	32.17	82.09
28.2	52.90	1.46	13.44	1.59	9.68	0.22	6.32	10.74	3.17	0.24	0.13	222.38	25.03	44.16	49.78	322.56	70.74	3.48	99.59	32.97	84.31
30.2	53.06	1.50	13.21	1.63	9.78	0.22	6.16	10.77	3.18	0.25	0.13	225.38	21.94	44.79	50.82	330.02	72.22	3.73	99.97	33.82	86.66
32.2	53.22	1.54	13.13	1.67	9.84	0.22	5.90	10.76	3.21	0.26	0.14	216.28	18.19	44.98	51.12	337.20	73.60	4.00	101.09	34.64	89.06
34.2	53.32	1.57	13.05	1.70	9.97	0.23	5.76	10.65	3.24	0.27	0.14	197.03	16.05	45.06	50.70	344.14	75.18	4.28	102.13	35.46	91.56
36.2	53.38	1.61	12.95	1.73	10.14	0.23	5.68	10.47	3.27	0.29	0.15	173.72	14.62	45.07	49.91	351.10	76.92	4.57	103.12	36.29	94.18
38.2	53.48	1.64	12.86	1.77	10.28	0.23	5.53	10.35	3.29	0.30	0.15	156.09	12.74	45.13	49.46	358.68	78.65	4.88	104.14	37.18	96.94
40.2	53.55	1.68	12.76	1.80	10.46	0.23	5.45	10.16	3.32	0.31	0.15	134.80	11.50	45.13	48.61	366.28	80.54	5.20	105.09	38.08	99.84
42.2	53.66	1.73	12.67	1.84	10.61	0.24	5.29	10.03	3.35	0.33	0.16	118.77	9.89	45.18	48.13	374.58	82.43	5.54	106.07	39.06	102.92
44.2	53.73	1.77	12.65	1.87	10.78	0.24	5.14	9.81	3.39	0.35	0.16	95.66	8.53	44.87	46.77	382.47	84.39	5.90	107.48	40.01	106.12
46.2	53.84	1.82	12.55	1.91	10.93	0.24	4.97	9.67	3.42	0.36	0.17	82.08	7.21	44.90	46.23	391.60	86.45	6.28	108.43	41.09	109.57
48.2	53.92	1.87	12.44	1.95	11.14	0.25	4.86	9.46	3.45	0.38	0.18	66.30	6.35	44.83	45.24	400.76	88.73	6.68	109.26	42.18	113.20

Tab. G.13: Modélisation ACF - facteur d'assimilation de 0.1

%ACF	SiO_2	TiO_2	Al_2O_3	Fe_2O_3	FeO	MnO	MgO	CaO	Na2O	K2O	P2O5	Cr	Ni	Co	Sc	V	Zn	Rb	Sr	Y	Zr
50.2	53.99	1.92	12.33	1.99	11.35	0.25	4.75	9.25	3.48	0.40	0.18	52.44	5.56	44.76	44.22	410.38	91.13	7.11	110.02	43.32	117.06
52.2	54.12	1.98	12.22	2.03	11.52	0.25	4.56	9.09	3.51	0.42	0.19	42.45	4.59	44.74	43.59	421.02	93.53	7.56	110.81	44.57	121.19
54.2	54.25	2.04	12.11	2.08	11.68	0.25	4.36	8.93	3.54	0.44	0.20	33.70	3.76	44.72	42.93	432.28	96.05	8.05	111.54	45.90	125.59
56.2	54.34	2.10	11.99	2.13	11.92	0.26	4.22	8.70	3.56	0.46	0.20	24.20	3.23	44.58	41.76	443.60	98.86	8.56	112.06	47.23	130.27
58.2	54.48	2.17	11.87	2.18	12.09	0.26	4.01	8.53	3.59	0.49	0.21	17.95	2.61	44.51	41.02	456.22	101.68	9.11	112.60	48.70	135.31
60.2	54.58	2.24	11.85	2.22	12.31	0.26	3.80	8.25	3.64	0.51	0.22	10.52	2.08	43.93	39.20	468.19	104.63	9.71	113.62	50.11	140.66
62.2	54.68	2.32	11.72	2.28	12.56	0.26	3.64	7.99	3.66	0.54	0.23	6.40	1.76	43.69	37.90	481.64	107.97	10.35	113.76	51.68	146.45
64.2	54.84	2.41	11.60	2.33	12.74	0.26	3.40	7.81	3.68	0.57	0.24	4.11	1.38	43.54	37.05	496.83	111.33	11.03	113.92	53.44	152.75
66.2	54.91	2.50	11.34	2.40	13.06	0.27	3.28	7.59	3.67	0.61	0.25	2.57	1.29	43.67	36.21	513.05	115.39	11.76	112.79	55.30	159.56
68.2	55.08	2.60	11.21	2.46	13.24	0.27	3.02	7.40	3.68	0.64	0.27	1.57	1.01	43.46	35.33	530.56	119.24	12.57	112.53	57.32	166.98
70.2	55.18	2.71	11.06	2.52	13.52	0.27	2.83	7.13	3.69	0.68	0.28	0.76	0.86	43.07	33.81	548.24	123.62	13.45	111.68	59.33	174.99
72.3	55.86	2.61	10.97	2.52	13.27	0.27	2.67	6.97	3.71	0.73	0.30	0.01	0.76	39.78	32.48	424.43	113.64	14.49	111.46	60.29	183.63
74.3	56.82	2.43	11.00	2.47	12.73	0.27	2.48	6.82	3.77	0.78	0.31	0.00	0.63	35.22	30.68	287.03	98.53	15.62	112.06	60.50	192.32
76.3	57.87	2.22	10.90	2.43	12.18	0.27	2.35	6.73	3.78	0.84	0.33	0.00	0.64	31.09	29.31	183.96	83.87	16.87	111.16	60.68	201.80
78.5	59.02	2.03	10.86	2.38	11.61	0.27	2.14	6.53	3.81	0.90	0.36	0.00	0.59	27.01	27.11	116.94	71.32	18.39	109.82	60.93	213.25
80.6	60.23	1.85	10.80	2.32	11.03	0.26	1.92	6.29	3.83	0.98	0.38	0.05	0.52	23.29	24.62	73.76	60.51	20.07	107.52	61.09	225.85
82.6	61.68	1.60	10.70	2.23	10.24	0.26	1.75	6.14	3.83	1.06	0.41	0.00	0.56	19.45	22.57	40.14	48.24	21.89	104.58	60.53	238.17
84.7	62.97	1.46	10.61	2.17	9.72	0.25	1.48	5.81	3.83	1.16	0.45	0.00	0.37	16.62	19.56	25.97	41.40	23.94	99.55	60.61	253.59
86.8	64.61	1.26	10.34	2.08	8.98	0.24	1.29	5.58	3.76	1.27	0.49	0.00	0.38	13.73	16.43	14.09	33.20	26.39	92.91	60.19	270.74
88.9	66.90	0.98	10.26	1.89	7.87	0.23	1.06	5.17	3.73	1.40	0.40	-0.02	0.31	10.34	13.76	6.13	23.59	29.23	86.29	52.23	287.06
91.0	69.03	0.81	9.95	1.76	7.11	0.22	0.81	4.70	3.59	1.56	0.34	0.00	0.13	8.15	10.96	3.64	18.48	32.46	74.13	47.03	308.51
93.1	71.89	0.57	9.40	1.56	6.01	0.21	0.65	4.31	3.33	1.76	0.21	0.00	0.32	5.91	8.89	1.85	12.38	36.40	58.01	38.01	330.24
95.2	75.01	0.38	8.94	1.30	4.80	0.18	0.35	3.70	3.08	1.99	0.17	-2.55	-0.06	3.91	5.31	1.34	8.33	40.91	41.03	32.23	353.66

TAB. G.14: Modélisation des processus ACF ayant mené à la composition chimique des roches calco-alcalines du mélange ophiolitique pour un facteur d'assimilation de 0.1 (éléments traces en ppm).

%ACF	Nb	Cs	Ba	La	Ce	Nd	Sm	Eu^{2+}	Eu^{3+}	Gd	Dy	Ho	Er	Tm	Yb	Lu	Hf	Ta	Pb	Th	U
0.2	0.97	0.09	6.02	2.08	6.98	6.71	2.37	0.98	0.00	3.39	4.19	0.89	2.68	0.38	2.51	0.38	1.57	0.06	1.78	0.06	0.00
2.2	1.01	0.10	7.90	2.18	7.22	6.88	2.42	0.97	0.00	3.46	4.27	0.90	2.73	0.38	2.56	0.39	1.61	0.06	1.85	0.08	0.00
4.2	1.05	0.11	9.83	2.29	7.48	7.06	2.48	0.97	0.00	3.54	4.36	0.92	2.79	0.39	2.62	0.39	1.65	0.07	1.92	0.10	0.01
6.2	1.09	0.12	11.83	2.39	7.75	7.25	2.54	0.96	0.00	3.61	4.45	0.94	2.84	0.40	2.67	0.40	1.69	0.07	1.99	0.11	0.01
8.2	1.13	0.13	13.90	2.50	8.02	7.44	2.60	0.96	0.00	3.69	4.54	0.95	2.90	0.41	2.73	0.41	1.73	0.07	2.07	0.13	0.02
10.2	1.18	0.14	16.03	2.62	8.31	7.64	2.66	0.95	0.00	3.77	4.64	0.97	2.96	0.41	2.78	0.42	1.78	0.08	2.14	0.15	0.02
12.2	1.22	0.16	18.26	2.74	8.61	7.85	2.72	0.96	0.00	3.86	4.74	0.99	3.03	0.42	2.84	0.43	1.82	0.08	2.23	0.17	0.03
14.2	1.27	0.17	20.56	2.86	8.91	8.06	2.79	0.96	0.00	3.95	4.84	1.01	3.09	0.43	2.90	0.44	1.87	0.08	2.31	0.20	0.03
16.2	1.32	0.18	22.95	2.99	9.23	8.29	2.86	0.96	0.00	4.04	4.95	1.03	3.16	0.44	2.97	0.45	1.92	0.08	2.40	0.22	0.04
18.2	1.37	0.19	25.42	3.12	9.56	8.52	2.93	0.96	0.00	4.13	5.06	1.05	3.23	0.45	3.03	0.46	1.97	0.09	2.50	0.24	0.04
20.2	1.42	0.21	27.99	3.26	9.91	8.76	3.01	0.97	0.00	4.23	5.18	1.07	3.30	0.46	3.10	0.47	2.02	0.09	2.59	0.26	0.05
22.2	1.47	0.22	30.66	3.40	10.27	9.01	3.08	0.97	0.00	4.33	5.30	1.09	3.38	0.46	3.17	0.48	2.07	0.10	2.69	0.29	0.05
24.2	1.53	0.24	33.43	3.55	10.65	9.27	3.17	0.97	0.00	4.44	5.43	1.12	3.46	0.47	3.24	0.49	2.13	0.10	2.80	0.32	0.06
26.2	1.59	0.25	36.30	3.71	11.04	9.55	3.25	0.97	0.00	4.55	5.56	1.14	3.54	0.48	3.32	0.50	2.19	0.10	2.90	0.34	0.06
28.2	1.65	0.27	39.31	3.87	11.45	9.83	3.34	0.97	0.00	4.67	5.70	1.16	3.63	0.50	3.40	0.51	2.25	0.11	3.02	0.37	0.07
30.2	1.72	0.28	42.42	4.04	11.87	10.13	3.43	0.97	0.00	4.79	5.84	1.19	3.72	0.51	3.49	0.52	2.31	0.11	3.13	0.40	0.08
32.2	1.79	0.30	45.72	4.22	12.32	10.44	3.53	0.97	0.00	4.91	5.98	1.22	3.81	0.52	3.56	0.53	2.38	0.12	3.26	0.43	0.08
34.2	1.86	0.32	49.18	4.41	12.79	10.75	3.62	0.98	0.00	5.02	6.10	1.24	3.88	0.53	3.63	0.54	2.44	0.12	3.39	0.47	0.09
36.2	1.94	0.34	52.80	4.60	13.27	11.08	3.72	0.98	0.00	5.14	6.21	1.25	3.95	0.53	3.70	0.55	2.50	0.13	3.53	0.50	0.10
38.2	2.02	0.36	56.59	4.81	13.78	11.42	3.82	0.99	0.00	5.26	6.34	1.28	4.03	0.54	3.77	0.57	2.56	0.13	3.67	0.54	0.11
40.2	2.10	0.38	60.57	5.03	14.32	11.78	3.93	0.99	0.00	5.39	6.46	1.30	4.10	0.55	3.84	0.58	2.63	0.14	3.83	0.58	0.12
42.2	2.19	0.41	64.75	5.25	14.89	12.16	4.04	0.99	0.00	5.52	6.60	1.32	4.19	0.56	3.92	0.59	2.71	0.14	3.99	0.62	0.13
44.2	2.29	0.43	69.20	5.50	15.48	12.55	4.16	1.00	0.00	5.65	6.72	1.34	4.26	0.57	3.99	0.60	2.78	0.15	4.16	0.66	0.14
46.2	2.39	0.46	73.83	5.75	16.12	12.97	4.28	1.00	0.00	5.80	6.88	1.36	4.35	0.58	4.07	0.61	2.86	0.16	4.34	0.71	0.15
48.2	2.50	0.49	78.72	6.02	16.78	13.41	4.41	1.00	0.00	5.95	7.02	1.39	4.43	0.59	4.15	0.62	2.94	0.16	4.53	0.75	0.16
50.2	2.61	0.51	83.89	6.30	17.48	13.87	4.55	1.01	0.00	6.10	7.17	1.41	4.52	0.60	4.23	0.63	3.03	0.17	4.73	0.81	0.17

Tab. G.14: Modélisation ACF - facteur d'assimilation de 0.1

%ACF	Nb	Cs	Ba	La	Ce	Nd	Sm	Eu^{2+}	Eu^{3+}	Gd	Dy	Ho	Er	Tm	Yb	Lu	Hf	Ta	Pb	Th	U
52.2	2.73	0.55	89.36	6.60	18.23	14.37	4.70	1.01	0.00	6.28	7.33	1.44	4.62	0.61	4.32	0.65	3.13	0.18	4.94	0.86	0.18
54.2	2.86	0.58	95.16	6.92	19.03	14.90	4.86	1.01	0.00	6.46	7.51	1.47	4.73	0.62	4.42	0.66	3.23	0.19	5.16	0.92	0.19
56.2	3.00	0.62	101.32	7.26	19.88	15.45	5.02	1.00	0.00	6.64	7.68	1.49	4.82	0.63	4.51	0.68	3.34	0.20	5.39	0.98	0.21
58.2	3.15	0.65	107.88	7.63	20.79	16.05	5.20	1.00	0.00	6.84	7.87	1.52	4.93	0.65	4.61	0.69	3.46	0.21	5.65	1.05	0.22
60.2	3.31	0.70	115.00	8.02	21.75	16.66	5.37	1.01	0.00	7.03	8.02	1.54	5.01	0.66	4.69	0.70	3.57	0.22	5.92	1.12	0.24
62.2	3.49	0.74	122.50	8.44	22.79	17.32	5.57	1.00	0.00	7.24	8.20	1.57	5.11	0.67	4.78	0.71	3.70	0.23	6.21	1.20	0.26
64.2	3.67	0.79	130.55	8.89	23.91	18.05	5.78	0.99	0.00	7.49	8.41	1.60	5.24	0.68	4.89	0.73	3.85	0.24	6.52	1.28	0.28
66.2	3.87	0.84	139.01	9.37	25.12	18.83	6.01	0.98	0.00	7.74	8.64	1.64	5.36	0.70	5.01	0.75	4.00	0.26	6.84	1.38	0.30
68.2	4.09	0.90	148.34	9.89	26.44	19.68	6.26	0.97	0.00	8.02	8.88	1.68	5.50	0.71	5.13	0.77	4.17	0.27	7.20	1.47	0.32
70.2	4.34	0.96	158.42	10.46	27.86	20.57	6.52	0.95	0.00	8.29	9.08	1.70	5.60	0.72	5.23	0.78	4.34	0.29	7.59	1.58	0.34
72.3	4.60	1.03	170.47	11.15	29.58	21.68	6.84	0.95	0.00	8.65	9.38	1.75	5.76	0.74	5.37	0.80	4.53	0.30	8.05	1.71	0.37
74.3	4.86	1.11	183.52	11.89	31.42	22.85	7.18	0.94	0.00	9.01	9.67	1.79	5.91	0.76	5.50	0.82	4.70	0.32	8.56	1.85	0.40
76.3	5.15	1.20	197.62	12.70	33.48	24.17	7.56	0.93	0.00	9.44	10.02	1.84	6.10	0.78	5.68	0.85	4.90	0.34	9.11	2.00	0.44
78.5	5.50	1.31	214.62	13.68	35.93	25.71	8.00	0.91	0.00	9.90	10.36	1.89	6.27	0.79	5.82	0.87	5.13	0.36	9.76	2.19	0.48
80.6	5.89	1.44	233.25	14.76	38.63	27.37	8.47	0.88	0.00	10.37	10.67	1.92	6.41	0.81	5.94	0.88	5.39	0.38	10.48	2.40	0.52
82.6	6.27	1.57	253.13	15.91	41.53	29.16	8.98	0.85	0.00	10.90	11.03	1.97	6.58	0.82	6.09	0.90	5.63	0.40	11.23	2.63	0.57
84.7	6.75	1.72	274.75	17.19	44.75	31.06	9.50	0.80	0.00	11.38	11.23	1.98	6.63	0.83	6.12	0.91	5.93	0.43	12.07	2.89	0.63
86.8	7.27	1.91	299.98	18.75	48.73	33.47	10.19	0.73	0.00	12.08	11.71	2.04	6.84	0.85	6.31	0.94	6.27	0.46	13.01	3.21	0.70
88.9	7.81	2.13	329.03	19.67	50.02	32.74	9.52	0.62	0.00	11.20	10.83	1.89	6.46	0.81	6.07	0.90	6.57	0.49	14.10	3.58	0.78
91.0	8.48	2.39	359.50	20.86	52.21	32.72	9.15	0.50	0.00	10.62	10.08	1.75	6.08	0.76	5.78	0.86	6.97	0.53	15.24	4.02	0.87
93.1	9.19	2.72	393.39	21.66	52.70	30.78	8.05	0.34	0.00	9.27	8.85	1.56	5.55	0.70	5.43	0.81	7.36	0.56	16.42	4.58	0.99
95.2	9.95	3.12	428.55	23.22	55.78	30.93	7.75	0.23	0.00	8.64	7.71	1.32	4.75	0.60	4.67	0.70	7.74	0.60	17.65	5.25	1.13

TAB. G.15: Modélisation des processus ACF ayant mené à la composition chimique des roches calco-alcalines du mélange ophiolitique pour un facteur d'assimilation de 0.2 (éléments majeurs en % poids et métaux de transition en ppm).

%ACF	SiO_2	TiO_2	Al_2O_3	Fe_2O_3	FeO	MnO	MgO	CaO	Na2O	K2O	P2O5	Cr	Ni	Co	Sc	V	Zn	Rb	Sr	Y	Zr
0.2	51.16	1.09	16.56	1.16	8.25	0.17	7.41	10.90	3.00	0.12	0.09	181.83	69.67	36.16	38.51	244.13	53.84	0.86	93.13	24.20	59.88
2.2	51.26	1.11	16.22	1.18	8.40	0.18	7.53	10.81	3.00	0.13	0.09	185.10	71.11	36.84	39.14	248.31	55.09	1.13	93.68	24.71	61.43
4.2	51.36	1.13	15.87	1.21	8.54	0.18	7.66	10.71	3.00	0.14	0.10	188.47	72.59	37.54	39.79	252.63	56.39	1.42	94.20	25.23	63.02
6.2	51.45	1.16	15.52	1.23	8.69	0.19	7.79	10.62	3.00	0.16	0.10	191.96	74.12	38.26	40.47	257.08	57.74	1.71	94.69	25.78	64.67
8.2	51.55	1.18	15.16	1.26	8.85	0.19	7.93	10.52	3.00	0.17	0.10	195.55	75.71	39.01	41.16	261.67	59.12	2.01	95.16	26.34	66.37
10.2	51.68	1.20	14.92	1.28	8.96	0.20	7.89	10.49	3.01	0.18	0.10	198.31	72.44	39.56	41.83	266.32	60.35	2.33	96.11	26.91	68.10
12.2	51.84	1.22	14.74	1.31	9.03	0.20	7.76	10.48	3.03	0.19	0.11	200.63	66.92	40.02	42.49	271.07	61.52	2.65	97.32	27.49	69.88
14.2	52.02	1.25	14.62	1.34	9.08	0.20	7.53	10.50	3.05	0.21	0.11	202.46	59.45	40.36	43.15	275.93	62.60	2.98	98.79	28.10	71.70
16.2	52.18	1.27	14.44	1.37	9.16	0.20	7.40	10.49	3.06	0.22	0.11	204.84	54.50	40.83	43.85	281.01	63.83	3.32	99.96	28.72	73.60
18.2	52.37	1.30	14.31	1.40	9.20	0.21	7.16	10.52	3.08	0.23	0.12	206.65	47.84	41.18	44.55	286.21	64.98	3.68	101.43	29.37	75.55
20.2	52.55	1.32	14.12	1.43	9.28	0.21	7.01	10.52	3.09	0.25	0.12	209.06	43.45	41.67	45.30	291.63	66.28	4.05	102.56	30.04	77.59
22.2	52.75	1.35	13.99	1.47	9.32	0.21	6.77	10.55	3.11	0.26	0.12	210.84	37.61	42.03	46.05	297.20	67.48	4.43	104.00	30.73	79.69
24.2	52.93	1.38	13.79	1.50	9.39	0.22	6.61	10.55	3.12	0.28	0.13	213.27	33.80	42.54	46.85	303.02	68.85	4.82	105.08	31.45	81.88
26.2	53.11	1.41	13.58	1.54	9.47	0.22	6.45	10.56	3.13	0.29	0.13	215.72	30.23	43.06	47.68	309.05	70.27	5.23	106.11	32.20	84.15
28.2	53.33	1.44	13.44	1.57	9.50	0.22	6.19	10.60	3.15	0.31	0.13	217.40	25.53	43.44	48.50	315.26	71.58	5.65	107.49	32.98	86.50
30.2	53.53	1.47	13.22	1.61	9.57	0.23	6.02	10.62	3.16	0.33	0.14	219.83	22.53	43.98	49.38	321.75	73.08	6.09	108.44	33.78	88.95
32.2	53.69	1.50	13.15	1.64	9.65	0.23	5.83	10.54	3.18	0.35	0.14	205.96	19.52	44.04	49.21	327.65	74.54	6.55	110.11	34.55	91.45
34.2	53.82	1.53	13.06	1.67	9.76	0.23	5.68	10.42	3.21	0.36	0.14	187.51	17.40	44.04	48.68	333.49	76.12	7.03	111.75	35.32	94.03
36.2	53.92	1.56	12.98	1.70	9.90	0.23	5.60	10.24	3.23	0.38	0.15	165.48	16.02	43.99	47.79	339.28	77.84	7.53	113.32	36.08	96.71
38.2	54.06	1.59	12.89	1.73	10.01	0.24	5.45	10.11	3.25	0.40	0.15	148.69	14.16	43.97	47.22	345.55	79.53	8.05	114.92	36.91	99.52
40.2	54.17	1.63	12.81	1.76	10.16	0.24	5.35	9.92	3.28	0.43	0.16	128.64	12.96	43.89	46.28	351.75	81.37	8.59	116.46	37.73	102.45
42.2	54.32	1.66	12.80	1.79	10.25	0.24	5.15	9.75	3.31	0.45	0.16	109.11	11.00	43.61	45.24	358.12	83.07	9.16	118.53	38.58	105.50
44.2	54.43	1.70	12.71	1.82	10.41	0.25	5.04	9.56	3.34	0.47	0.17	91.80	9.99	43.49	44.23	364.76	85.04	9.75	120.01	39.46	108.70
46.2	54.59	1.74	12.62	1.85	10.52	0.25	4.87	9.41	3.36	0.50	0.17	79.12	8.66	43.43	43.56	372.03	86.99	10.37	121.53	40.41	112.08
48.2	54.72	1.78	12.52	1.89	10.69	0.25	4.76	9.20	3.38	0.52	0.18	64.45	7.81	43.28	42.48	379.19	89.11	11.03	122.91	41.36	115.60

Tab. G.15: Modélisation ACF - facteur d'assimilation de 0.2

%ACF	SiO_2	TiO_2	Al_2O_3	Fe_2O_3	FeO	MnO	MgO	CaO	Na2O	K2O	P2O5	Cr	Ni	Co	Sc	V	Zn	Rb	Sr	Y	Zr
50.2	54.84	1.82	12.43	1.92	10.85	0.25	4.65	8.99	3.41	0.55	0.19	51.57	7.03	43.12	41.37	386.63	91.33	11.71	124.23	42.34	119.31
52.2	55.02	1.87	12.42	1.95	10.94	0.26	4.41	8.80	3.44	0.58	0.19	40.04	5.75	42.72	40.19	394.34	93.36	12.43	126.24	43.36	123.20
54.2	55.16	1.91	12.32	1.99	11.11	0.26	4.28	8.58	3.46	0.61	0.20	30.35	5.13	42.51	39.00	402.37	95.76	13.18	127.42	44.42	127.30
56.2	55.34	1.96	12.13	2.03	11.26	0.26	4.14	8.44	3.47	0.64	0.21	25.61	4.57	42.68	38.64	411.81	98.28	13.97	127.91	45.63	131.68
58.2	55.49	2.02	12.13	2.06	11.41	0.26	3.95	8.18	3.50	0.67	0.21	16.90	3.85	42.10	36.90	419.99	100.71	14.81	129.61	46.70	136.22
60.2	55.64	2.07	12.02	2.10	11.58	0.27	3.80	7.94	3.52	0.71	0.22	11.62	3.42	41.82	35.60	429.10	103.43	15.70	130.44	47.88	141.06
62.2	55.83	2.13	11.82	2.15	11.73	0.27	3.64	7.80	3.52	0.74	0.23	9.34	3.06	41.95	35.17	439.92	106.30	16.62	130.46	49.26	146.24
64.2	56.05	2.20	11.72	2.19	11.85	0.27	3.42	7.62	3.53	0.78	0.24	6.69	2.56	41.71	34.24	450.64	109.11	17.61	131.15	50.63	151.71
66.2	56.22	2.26	11.61	2.24	12.03	0.27	3.26	7.37	3.54	0.82	0.25	4.06	2.28	41.34	32.76	461.12	112.23	18.66	131.39	51.95	157.49
68.2	56.39	2.33	11.50	2.28	12.21	0.27	3.09	7.12	3.54	0.87	0.26	2.43	2.02	40.93	31.28	472.10	115.51	19.78	131.42	53.32	163.65
70.2	56.57	2.41	11.39	2.32	12.39	0.27	2.91	6.86	3.55	0.92	0.27	1.47	1.76	40.48	29.82	483.64	118.96	20.98	131.20	54.75	170.23
72.2	56.79	2.49	11.18	2.38	12.54	0.28	2.72	6.72	3.52	0.96	0.28	1.28	1.61	40.52	29.26	497.62	122.65	22.23	130.00	56.48	177.34
74.2	57.32	2.45	11.09	2.38	12.39	0.28	2.58	6.55	3.52	1.02	0.29	0.01	1.53	38.37	27.96	425.57	117.15	23.67	129.94	57.28	184.43
76.4	58.16	2.31	11.04	2.35	12.00	0.28	2.42	6.39	3.53	1.09	0.31	0.02	1.32	34.89	26.45	314.25	105.36	25.28	129.76	57.58	192.35
78.4	59.16	2.13	11.09	2.29	11.42	0.27	2.24	6.23	3.56	1.16	0.32	0.01	1.20	30.85	24.56	213.67	91.37	27.02	130.62	57.26	199.85
80.5	60.16	1.98	11.05	2.24	10.93	0.27	2.07	6.04	3.57	1.23	0.34	0.05	1.01	27.44	22.61	148.41	80.25	28.94	129.45	57.21	208.84
82.5	61.30	1.78	10.99	2.17	10.30	0.27	1.93	5.90	3.56	1.31	0.36	0.01	1.10	23.97	21.00	93.81	67.76	30.96	128.07	56.67	217.25
84.6	62.42	1.63	10.95	2.10	9.79	0.27	1.73	5.66	3.56	1.41	0.38	0.00	0.85	21.00	18.68	63.47	58.92	33.21	125.24	56.32	227.40
86.8	63.63	1.46	10.78	2.04	9.23	0.26	1.59	5.47	3.51	1.51	0.41	0.01	0.91	18.33	16.93	40.65	50.18	35.70	120.30	55.90	238.17
88.9	65.04	1.28	10.75	1.93	8.53	0.25	1.37	5.17	3.49	1.62	0.44	0.00	0.63	15.34	14.24	24.70	41.54	38.52	115.87	54.67	249.58
91.0	66.47	1.14	10.56	1.86	8.00	0.25	1.21	4.85	3.42	1.75	0.40	0.00	0.60	13.26	12.28	16.37	35.55	41.52	108.33	51.09	262.07
93.2	68.19	0.96	10.37	1.73	7.27	0.24	1.03	4.50	3.33	1.89	0.35	0.02	0.56	10.93	10.12	9.81	28.65	44.94	99.39	46.65	275.03
95.4	70.27	0.75	10.19	1.57	6.41	0.23	0.84	4.07	3.22	2.06	0.27	0.00	0.32	8.58	7.83	5.65	21.90	48.85	89.01	39.86	288.09
97.5	72.36	0.57	9.78	1.42	5.58	0.22	0.72	3.75	3.02	2.24	0.21	0.00	0.61	6.81	6.35	3.58	16.57	52.94	74.35	34.71	300.84
99.5	74.54	0.43	9.46	1.25	4.76	0.20	0.50	3.27	2.84	2.45	0.18	0.00	0.29	5.21	3.97	2.89	12.96	57.35	59.30	30.17	314.20
101.7	77.35	0.23	8.93	0.99	3.64	0.17	0.37	2.83	2.55	2.70	0.11	0.68	0.34	3.57	2.55	1.68	8.33	62.22	41.93	23.07	320.64

TAB. G.16: Modélisation des processus ACF ayant mené à la composition chimique des roches calco-alcalines du mélange ophiolitique pour un facteur d'assimilation de 0.2 (éléments traces en ppm).

%ACF	Nb	Cs	Ba	La	Ce	Nd	Sm	Eu^{2+}	Eu^{3+}	Gd	Dy	Ho	Er	Tm	Yb	Lu	Hf	Ta	Pb	Th	U
0.2	0.97	0.09	6.02	2.08	6.98	6.71	2.37	0.98	0.00	3.39	4.19	0.89	2.68	0.38	2.51	0.38	1.57	0.06	1.78	0.06	0.00
2.2	1.03	0.11	9.67	2.24	7.34	6.93	2.43	0.97	0.00	3.47	4.28	0.90	2.73	0.38	2.56	0.39	1.62	0.07	1.89	0.09	0.01
4.2	1.09	0.13	13.42	2.41	7.72	7.16	2.50	0.97	0.00	3.55	4.36	0.92	2.79	0.39	2.62	0.39	1.66	0.07	2.00	0.13	0.02
6.2	1.15	0.15	17.27	2.58	8.11	7.40	2.56	0.97	0.00	3.63	4.46	0.93	2.85	0.40	2.67	0.40	1.71	0.07	2.12	0.16	0.02
8.2	1.21	0.17	21.24	2.76	8.51	7.64	2.63	0.96	0.00	3.71	4.55	0.95	2.91	0.40	2.73	0.41	1.76	0.08	2.24	0.20	0.03
10.2	1.27	0.19	25.33	2.94	8.92	7.89	2.70	0.96	0.00	3.80	4.65	0.96	2.97	0.41	2.79	0.42	1.81	0.08	2.36	0.24	0.04
12.2	1.34	0.21	29.55	3.13	9.35	8.15	2.77	0.96	0.00	3.89	4.75	0.98	3.03	0.42	2.84	0.43	1.86	0.09	2.49	0.28	0.05
14.2	1.41	0.23	33.91	3.32	9.79	8.41	2.85	0.97	0.00	3.98	4.86	0.99	3.09	0.42	2.90	0.44	1.91	0.09	2.63	0.32	0.06
16.2	1.48	0.25	38.39	3.52	10.24	8.69	2.93	0.97	0.00	4.07	4.96	1.01	3.16	0.43	2.97	0.45	1.96	0.10	2.77	0.36	0.07
18.2	1.55	0.27	43.03	3.73	10.72	8.97	3.01	0.97	0.00	4.17	5.07	1.03	3.23	0.44	3.03	0.46	2.02	0.10	2.91	0.40	0.08
20.2	1.62	0.30	47.79	3.95	11.20	9.27	3.09	0.97	0.00	4.27	5.19	1.04	3.30	0.44	3.10	0.47	2.08	0.11	3.06	0.44	0.09
22.2	1.70	0.32	52.73	4.17	11.71	9.57	3.17	0.98	0.00	4.37	5.31	1.06	3.38	0.45	3.17	0.48	2.14	0.11	3.21	0.49	0.10
24.2	1.78	0.35	57.82	4.40	12.23	9.89	3.26	0.98	0.00	4.48	5.43	1.08	3.45	0.46	3.24	0.49	2.20	0.12	3.36	0.54	0.11
26.2	1.87	0.37	63.07	4.64	12.77	10.22	3.36	0.98	0.00	4.59	5.56	1.10	3.53	0.47	3.31	0.50	2.26	0.12	3.52	0.59	0.12
28.2	1.95	0.40	68.52	4.88	13.34	10.56	3.45	0.98	0.00	4.71	5.69	1.12	3.62	0.48	3.39	0.51	2.33	0.13	3.69	0.64	0.14
30.2	2.05	0.43	74.13	5.14	13.92	10.91	3.55	0.98	0.00	4.83	5.83	1.14	3.70	0.49	3.47	0.52	2.40	0.14	3.86	0.69	0.15
32.2	2.14	0.46	80.04	5.41	14.52	11.27	3.65	0.99	0.00	4.94	5.95	1.16	3.78	0.49	3.54	0.53	2.47	0.14	4.05	0.75	0.16
34.2	2.24	0.49	86.17	5.68	15.15	11.64	3.75	0.99	0.00	5.05	6.06	1.18	3.84	0.50	3.60	0.54	2.53	0.15	4.24	0.81	0.18
36.2	2.34	0.52	92.55	5.97	15.80	12.02	3.85	1.00	0.00	5.16	6.16	1.19	3.90	0.51	3.66	0.55	2.60	0.16	4.44	0.87	0.19
38.2	2.45	0.55	99.17	6.27	16.48	12.41	3.96	1.00	0.00	5.28	6.28	1.21	3.98	0.51	3.72	0.56	2.67	0.16	4.64	0.93	0.20
40.2	2.57	0.59	106.06	6.58	17.18	12.82	4.07	1.00	0.00	5.40	6.39	1.22	4.04	0.52	3.78	0.57	2.74	0.17	4.86	1.00	0.22
42.2	2.69	0.63	113.30	6.91	17.92	13.25	4.18	1.01	0.00	5.52	6.50	1.23	4.11	0.52	3.84	0.58	2.81	0.18	5.09	1.07	0.24
44.2	2.81	0.67	120.79	7.25	18.68	13.69	4.30	1.02	0.00	5.65	6.62	1.25	4.17	0.53	3.91	0.59	2.89	0.19	5.32	1.14	0.25
46.2	2.94	0.71	128.59	7.61	19.49	14.15	4.43	1.02	0.00	5.78	6.75	1.26	4.25	0.54	3.98	0.60	2.97	0.20	5.57	1.21	0.27
48.2	3.08	0.75	136.73	7.98	20.33	14.63	4.55	1.02	0.00	5.92	6.87	1.28	4.32	0.54	4.04	0.61	3.06	0.21	5.82	1.29	0.29
50.2	3.22	0.79	145.24	8.36	21.21	15.13	4.69	1.02	0.00	6.06	6.99	1.29	4.39	0.55	4.11	0.62	3.15	0.22	6.09	1.38	0.31

Tab. G.16: Modélisation ACF - facteur d'assimilation de 0.2

%ACF	Nb	Cs	Ba	La	Ce	Nd	Sm	Eu^{2+}	Eu^{3+}	Gd	Dy	Ho	Er	Tm	Yb	Lu	Hf	Ta	Pb	Th	U
52.2	3.37	0.84	154.27	8.77	22.13	15.66	4.83	1.03	0.00	6.20	7.12	1.31	4.46	0.56	4.17	0.63	3.24	0.23	6.38	1.47	0.33
54.2	3.53	0.89	163.61	9.20	23.09	16.21	4.97	1.03	0.00	6.35	7.24	1.32	4.53	0.56	4.24	0.63	3.34	0.24	6.67	1.56	0.35
56.2	3.70	0.94	173.24	9.65	24.12	16.80	5.13	1.02	0.00	6.52	7.41	1.34	4.63	0.57	4.33	0.65	3.45	0.25	6.97	1.66	0.37
58.2	3.88	1.00	183.67	10.13	25.18	17.39	5.29	1.03	0.00	6.67	7.52	1.35	4.69	0.57	4.38	0.66	3.55	0.26	7.30	1.76	0.40
60.2	4.07	1.06	194.47	10.62	26.31	18.02	5.45	1.02	0.00	6.84	7.65	1.37	4.76	0.58	4.45	0.67	3.67	0.27	7.64	1.87	0.42
62.2	4.27	1.12	205.63	11.15	27.51	18.70	5.64	1.01	0.00	7.04	7.83	1.39	4.86	0.59	4.55	0.68	3.80	0.29	7.98	1.99	0.45
64.2	4.48	1.19	217.61	11.71	28.78	19.42	5.83	1.01	0.00	7.23	7.99	1.41	4.95	0.60	4.63	0.69	3.93	0.30	8.35	2.11	0.48
66.2	4.71	1.26	230.24	12.29	30.10	20.14	6.01	1.00	0.00	7.41	8.12	1.42	5.02	0.60	4.69	0.70	4.07	0.32	8.75	2.24	0.51
68.2	4.95	1.34	243.61	12.92	31.51	20.91	6.21	0.99	0.00	7.60	8.25	1.43	5.08	0.61	4.75	0.71	4.21	0.33	9.17	2.39	0.54
70.2	5.21	1.42	257.78	13.58	33.01	21.73	6.42	0.98	0.00	7.80	8.38	1.44	5.14	0.61	4.80	0.72	4.36	0.35	9.61	2.54	0.58
72.2	5.48	1.50	272.49	14.28	34.63	22.64	6.66	0.96	0.00	8.05	8.59	1.46	5.26	0.62	4.91	0.73	4.53	0.37	10.07	2.70	0.61
74.2	5.77	1.60	289.52	15.08	36.43	23.62	6.92	0.95	0.00	8.30	8.77	1.48	5.35	0.63	4.99	0.74	4.70	0.39	10.59	2.88	0.66
76.4	6.08	1.71	308.40	15.99	38.50	24.77	7.22	0.94	0.00	8.60	8.98	1.50	5.45	0.63	5.08	0.76	4.87	0.41	11.19	3.08	0.70
78.4	6.39	1.83	328.95	16.94	40.65	25.92	7.51	0.93	0.00	8.87	9.15	1.51	5.52	0.64	5.14	0.77	5.03	0.43	11.84	3.30	0.75
80.5	6.75	1.96	350.98	17.99	43.06	27.22	7.85	0.92	0.00	9.18	9.33	1.52	5.60	0.64	5.20	0.77	5.22	0.45	12.54	3.54	0.81
82.5	7.10	2.10	374.17	19.10	45.58	28.57	8.19	0.89	0.00	9.50	9.54	1.54	5.69	0.65	5.28	0.78	5.40	0.47	13.25	3.80	0.87
84.6	7.51	2.26	399.31	20.31	48.34	30.00	8.55	0.87	0.00	9.80	9.65	1.54	5.70	0.64	5.28	0.78	5.61	0.49	14.05	4.09	0.93
86.8	7.94	2.44	426.42	21.66	51.43	31.62	8.95	0.82	0.00	10.17	9.83	1.54	5.77	0.65	5.33	0.79	5.84	0.52	14.88	4.41	1.01
88.9	8.41	2.64	457.09	23.13	54.75	33.24	9.33	0.78	0.00	10.44	9.82	1.51	5.69	0.63	5.25	0.78	6.07	0.55	15.84	4.78	1.09
91.0	8.93	2.86	488.29	24.19	56.60	33.37	9.12	0.69	0.00	10.10	9.38	1.43	5.47	0.60	5.09	0.75	6.33	0.58	16.79	5.18	1.18
93.2	9.48	3.12	522.83	25.32	58.50	33.36	8.85	0.60	0.00	9.67	8.82	1.33	5.17	0.57	4.85	0.72	6.59	0.61	17.84	5.65	1.28
95.4	10.05	3.42	560.90	26.10	59.04	31.98	8.08	0.49	0.00	8.70	7.82	1.17	4.66	0.51	4.45	0.66	6.83	0.64	18.99	6.18	1.40
97.5	10.60	3.75	596.37	27.07	60.34	31.28	7.59	0.38	0.00	8.07	7.15	1.06	4.31	0.47	4.17	0.62	7.07	0.67	20.00	6.79	1.53
99.5	11.19	4.13	632.08	28.31	62.40	31.00	7.26	0.29	0.00	7.48	6.20	0.89	3.66	0.39	3.54	0.52	7.29	0.70	21.02	7.45	1.68
101.7	11.54	4.58	663.73	28.72	61.90	28.66	6.28	0.18	0.00	6.31	5.01	0.69	2.97	0.31	2.93	0.43	7.32	0.70	21.81	8.25	1.85

TAB. G.17: Modélisation des processus ACF ayant mené à la composition chimique des roches calco-alcalines du mélange ophiolitique pour un facteur d'assimilation de 0.3 (éléments majeurs en % poids et métaux de transition en ppm).

%ACF	SiO_2	TiO_2	Al_2O_3	Fe_2O_3	FeO	MnO	MgO	CaO	Na2O	K2O	P2O5	Cr	Ni	Co	Sc	V	Zn	Rb	Sr	Y	Zr
0.2	51.16	1.09	16.56	1.16	8.25	0.17	7.41	10.90	3.00	0.12	0.09	181.83	69.67	36.16	38.51	244.13	53.84	0.86	93.13	24.20	59.88
2.2	51.29	1.11	16.21	1.18	8.39	0.18	7.52	10.80	3.00	0.14	0.09	184.90	71.12	36.82	39.09	248.05	55.18	1.26	94.23	24.73	61.60
4.2	51.42	1.13	15.86	1.21	8.53	0.18	7.64	10.70	3.00	0.15	0.10	188.05	72.62	37.49	39.69	252.08	56.56	1.68	95.29	25.27	63.36
6.2	51.54	1.15	15.51	1.23	8.67	0.19	7.76	10.59	3.00	0.17	0.10	191.29	74.15	38.18	40.30	256.21	57.98	2.11	96.33	25.82	65.18
8.2	51.67	1.17	15.14	1.26	8.82	0.19	7.88	10.49	3.00	0.19	0.10	194.62	75.73	38.88	40.93	260.46	59.44	2.55	97.33	26.39	67.04
10.2	51.83	1.20	14.90	1.28	8.91	0.20	7.83	10.44	3.01	0.20	0.11	197.09	72.46	39.39	41.53	264.73	60.74	3.00	98.82	26.97	68.94
12.2	52.01	1.22	14.72	1.31	8.98	0.20	7.69	10.43	3.02	0.22	0.11	199.12	66.96	39.81	42.12	269.08	61.97	3.46	100.57	27.57	70.87
14.2	52.22	1.24	14.60	1.34	9.01	0.20	7.46	10.44	3.04	0.24	0.11	200.63	59.52	40.11	42.70	273.50	63.12	3.93	102.58	28.18	72.85
16.2	52.42	1.26	14.42	1.37	9.08	0.21	7.31	10.42	3.05	0.26	0.11	202.67	54.60	40.53	43.32	278.09	64.41	4.42	104.28	28.80	74.90
18.2	52.63	1.28	14.29	1.40	9.11	0.21	7.07	10.44	3.07	0.28	0.12	204.14	48.00	40.83	43.93	282.77	65.60	4.92	106.28	29.45	76.99
20.2	52.84	1.31	14.10	1.43	9.17	0.21	6.91	10.43	3.08	0.29	0.12	206.17	43.67	41.26	44.58	287.63	66.95	5.44	107.93	30.11	79.17
22.2	53.06	1.33	13.98	1.46	9.20	0.22	6.66	10.45	3.10	0.31	0.12	207.56	37.89	41.57	45.22	292.59	68.19	5.97	109.90	30.79	81.39
24.2	53.27	1.36	13.78	1.49	9.26	0.22	6.50	10.44	3.11	0.33	0.13	209.56	34.15	42.01	45.91	297.74	69.60	6.52	111.47	31.50	83.70
26.2	53.49	1.38	13.57	1.52	9.32	0.22	6.34	10.44	3.11	0.36	0.13	211.55	30.65	42.46	46.62	303.05	71.04	7.08	112.99	32.23	86.09
28.2	53.73	1.41	13.44	1.56	9.33	0.23	6.07	10.47	3.13	0.38	0.14	212.78	26.02	42.77	47.31	308.47	72.37	7.66	114.88	32.98	88.53
30.2	53.96	1.44	13.23	1.59	9.39	0.23	5.90	10.47	3.13	0.40	0.14	214.71	23.10	43.23	48.06	314.12	73.88	8.26	116.30	33.76	91.07
32.2	54.15	1.46	13.16	1.62	9.44	0.23	5.70	10.39	3.16	0.42	0.14	200.87	20.15	43.23	47.77	319.13	75.33	8.88	118.48	34.48	93.64
34.2	54.28	1.49	13.08	1.65	9.56	0.24	5.61	10.21	3.18	0.45	0.15	178.64	18.75	43.12	46.82	323.80	76.98	9.53	120.55	35.18	96.27
36.2	54.44	1.52	13.08	1.67	9.63	0.24	5.42	10.05	3.21	0.47	0.15	157.00	16.36	42.84	45.82	328.55	78.49	10.20	123.13	35.90	98.99
38.2	54.58	1.54	13.00	1.69	9.75	0.24	5.32	9.87	3.23	0.50	0.16	137.03	15.14	42.70	44.81	333.46	80.23	10.89	125.17	36.63	101.81
40.2	54.72	1.57	12.92	1.72	9.87	0.24	5.22	9.67	3.25	0.53	0.16	118.52	13.98	42.56	43.79	338.49	82.01	11.61	127.17	37.38	104.74
42.2	54.90	1.60	12.84	1.75	9.96	0.25	5.06	9.53	3.27	0.55	0.17	104.59	12.39	42.46	43.09	343.97	83.75	12.35	129.20	38.19	107.80
44.2	55.05	1.63	12.75	1.77	10.09	0.25	4.96	9.33	3.29	0.58	0.17	88.45	11.40	42.28	42.01	349.29	85.63	13.12	131.11	38.98	110.96
46.2	55.20	1.67	12.67	1.80	10.21	0.25	4.85	9.13	3.31	0.61	0.18	73.85	10.47	42.10	40.92	354.76	87.57	13.92	132.96	39.79	114.24
48.2	55.40	1.70	12.59	1.83	10.30	0.26	4.68	8.98	3.33	0.64	0.18	63.10	9.20	41.96	40.14	360.73	89.46	14.74	134.82	40.67	117.66

TAB. G.17: Modélisation ACF - facteur d'assimilation de 0.3

%ACF	SiO_2	TiO_2	Al_2O_3	Fe_2O_3	FeO	MnO	MgO	CaO	Na2O	K2O	P2O5	Cr	Ni	Co	Sc	V	Zn	Rb	Sr	Y	Zr
50.2	55.56	1.74	12.50	1.86	10.43	0.26	4.56	8.77	3.34	0.68	0.19	51.07	8.43	41.74	38.99	366.51	91.52	15.61	136.53	41.53	121.21
52.2	55.77	1.77	12.42	1.89	10.51	0.26	4.38	8.61	3.36	0.71	0.19	42.43	7.37	41.57	38.16	372.86	93.52	16.50	138.25	42.45	124.92
54.2	55.94	1.81	12.42	1.91	10.62	0.26	4.21	8.36	3.39	0.75	0.20	30.99	6.43	41.04	36.52	378.52	95.56	17.44	140.48	43.29	128.75
56.2	56.12	1.85	12.33	1.94	10.75	0.27	4.08	8.14	3.40	0.78	0.21	23.48	5.85	40.75	35.28	384.81	97.81	18.41	141.92	44.21	132.78
58.2	56.34	1.89	12.25	1.98	10.83	0.27	3.89	7.98	3.42	0.82	0.21	18.47	5.04	40.52	34.39	391.76	99.99	19.42	143.38	45.21	136.99
60.2	56.53	1.93	12.16	2.01	10.95	0.27	3.75	7.75	3.43	0.86	0.22	13.24	4.58	40.19	33.08	398.43	102.38	20.47	144.55	46.17	141.38
62.2	56.72	1.98	12.07	2.04	11.08	0.27	3.61	7.52	3.44	0.90	0.23	9.28	4.15	39.84	31.75	405.31	104.85	21.57	145.56	47.15	145.97
64.2	56.95	2.03	11.90	2.08	11.18	0.28	3.45	7.38	3.43	0.94	0.23	7.71	3.79	39.86	31.23	413.56	107.43	22.71	145.73	48.32	150.83
66.2	57.16	2.08	11.81	2.11	11.31	0.28	3.30	7.15	3.43	0.99	0.24	5.18	3.44	39.46	29.84	420.90	110.07	23.91	146.35	49.34	155.87
68.2	57.37	2.13	11.72	2.14	11.43	0.28	3.15	6.91	3.44	1.04	0.25	3.48	3.10	39.03	28.45	428.48	112.81	25.17	146.75	50.39	161.16
70.2	57.62	2.18	11.55	2.18	11.52	0.28	2.98	6.77	3.41	1.09	0.26	3.01	2.86	39.00	27.85	437.68	115.68	26.48	146.23	51.66	166.77
72.2	57.84	2.24	11.46	2.21	11.64	0.28	2.82	6.54	3.41	1.14	0.27	2.00	2.55	38.50	26.40	445.79	118.62	27.87	146.10	52.75	172.62
74.2	58.13	2.30	11.38	2.25	11.67	0.28	2.59	6.36	3.40	1.19	0.28	1.63	2.09	38.07	25.35	455.01	121.44	29.33	146.05	53.98	178.82
76.2	58.42	2.34	11.20	2.28	11.76	0.28	2.47	6.17	3.37	1.25	0.29	0.13	2.05	37.50	24.26	447.34	122.93	30.89	144.49	55.09	185.39
78.4	59.23	2.21	11.18	2.24	11.35	0.28	2.33	6.02	3.37	1.32	0.30	0.07	1.84	34.25	22.84	336.58	111.10	32.73	144.78	55.07	191.97
80.4	60.17	2.04	11.24	2.18	10.80	0.28	2.17	5.88	3.39	1.40	0.32	0.03	1.66	30.60	21.16	237.48	97.58	34.62	145.93	54.54	198.05
82.5	60.99	1.92	11.10	2.14	10.44	0.28	2.08	5.75	3.36	1.47	0.33	0.01	1.66	28.10	20.04	176.79	88.08	36.58	143.67	54.57	205.26
84.7	61.96	1.78	11.09	2.08	9.94	0.28	1.92	5.56	3.36	1.56	0.35	0.01	1.48	25.08	18.22	124.89	77.73	38.80	142.44	54.09	212.71
86.9	63.08	1.60	11.09	2.00	9.35	0.27	1.75	5.36	3.35	1.65	0.36	0.01	1.25	21.92	16.26	82.74	66.78	41.22	140.79	53.25	220.41
89.0	64.04	1.48	10.94	1.95	8.92	0.27	1.63	5.19	3.30	1.74	0.38	0.02	1.33	19.78	14.85	59.19	59.37	43.63	136.45	52.84	228.50
91.1	65.22	1.32	10.93	1.86	8.33	0.26	1.45	4.95	3.29	1.85	0.40	0.00	1.04	17.12	12.71	39.29	50.94	46.32	132.93	51.63	236.79
93.2	66.27	1.20	10.77	1.80	7.89	0.26	1.32	4.75	3.22	1.96	0.42	0.15	1.04	15.29	11.19	28.15	45.08	49.03	126.57	50.86	245.55
95.4	67.66	1.04	10.65	1.70	7.32	0.25	1.19	4.44	3.15	2.08	0.36	0.04	1.01	13.21	9.60	18.47	38.17	52.14	119.75	46.27	254.46
97.5	69.01	0.91	10.50	1.61	6.78	0.25	1.05	4.13	3.07	2.21	0.32	0.01	0.88	11.45	7.98	12.96	32.81	55.34	111.33	42.68	263.70
99.6	70.57	0.77	10.35	1.50	6.17	0.24	0.91	3.77	2.98	2.36	0.25	0.01	0.72	9.66	6.34	8.92	27.36	58.86	101.84	37.42	272.80
101.7	72.15	0.62	10.17	1.37	5.50	0.22	0.75	3.44	2.87	2.51	0.24	0.03	0.52	7.97	4.68	6.36	22.42	62.51	90.62	34.05	281.54
103.9	73.97	0.47	9.99	1.21	4.75	0.20	0.58	3.04	2.75	2.69	0.19	0.00	0.15	6.31	3.11	4.55	17.69	66.49	78.31	28.81	289.07
105.9	75.75	0.35	9.61	1.08	4.13	0.19	0.49	2.70	2.55	2.87	0.13	0.00	0.37	5.22	2.24	3.81	14.41	70.37	63.04	24.17	295.80
108.0	77.75	0.24	9.35	0.90	3.35	0.16	0.31	2.23	2.38	3.08	0.11	-0.01	-0.22	3.91	1.00	3.07	11.14	74.57	48.44	19.02	299.56

TAB. G.18: Modélisation des processus ACF ayant mené à la composition chimique des roches calco-alcalines du mélange ophiolitique pour un facteur d'assimilation de 0.3 (éléments traces en ppm).

%ACF	Nb	Cs	Ba	La	Ce	Nd	Sm	Eu^{2+}	Eu^{3+}	Gd	Dy	Ho	Er	Tm	Yb	Lu	Hf	Ta	Pb	Th	U
0.2	0.97	0.09	6.02	2.08	6.98	6.71	2.37	0.98	0.00	3.39	4.19	0.89	2.68	0.38	2.51	0.38	1.57	0.06	1.78	0.06	0.00
2.2	1.05	0.12	11.44	2.31	7.46	6.98	2.44	0.98	0.00	3.47	4.28	0.90	2.73	0.38	2.57	0.39	1.62	0.07	1.93	0.11	0.01
4.2	1.12	0.14	16.98	2.54	7.95	7.26	2.51	0.97	0.00	3.56	4.37	0.91	2.79	0.39	2.62	0.39	1.67	0.07	2.09	0.16	0.02
6.2	1.20	0.17	22.65	2.77	8.46	7.54	2.59	0.97	0.00	3.64	4.46	0.92	2.85	0.39	2.67	0.40	1.73	0.08	2.25	0.21	0.04
8.2	1.28	0.20	28.45	3.01	8.98	7.83	2.66	0.96	0.00	3.73	4.56	0.94	2.91	0.40	2.73	0.41	1.78	0.08	2.41	0.26	0.05
10.2	1.37	0.23	34.42	3.26	9.52	8.13	2.74	0.97	0.00	3.82	4.66	0.95	2.97	0.40	2.79	0.42	1.84	0.09	2.58	0.32	0.06
12.2	1.45	0.26	40.54	3.51	10.07	8.44	2.82	0.97	0.00	3.91	4.76	0.96	3.03	0.41	2.85	0.43	1.89	0.09	2.75	0.37	0.07
14.2	1.54	0.28	46.83	3.77	10.64	8.75	2.91	0.97	0.00	4.01	4.87	0.98	3.10	0.42	2.91	0.44	1.95	0.10	2.93	0.43	0.09
16.2	1.63	0.32	53.27	4.04	11.22	9.08	2.99	0.98	0.00	4.10	4.97	0.99	3.16	0.42	2.97	0.45	2.01	0.11	3.11	0.49	0.10
18.2	1.72	0.35	59.89	4.32	11.82	9.41	3.08	0.98	0.00	4.20	5.08	1.01	3.23	0.43	3.03	0.46	2.07	0.11	3.30	0.55	0.12
20.2	1.82	0.38	66.67	4.60	12.43	9.76	3.17	0.98	0.00	4.30	5.20	1.02	3.30	0.43	3.10	0.47	2.13	0.12	3.50	0.61	0.13
22.2	1.92	0.41	73.65	4.90	13.07	10.11	3.26	0.99	0.00	4.41	5.31	1.03	3.37	0.44	3.16	0.47	2.20	0.13	3.69	0.68	0.15
24.2	2.02	0.45	80.79	5.20	13.72	10.47	3.36	0.99	0.00	4.52	5.43	1.05	3.45	0.45	3.23	0.49	2.27	0.13	3.90	0.75	0.16
26.2	2.13	0.48	88.12	5.50	14.40	10.85	3.45	0.99	0.00	4.63	5.56	1.07	3.52	0.45	3.30	0.50	2.34	0.14	4.10	0.82	0.18
28.2	2.24	0.52	95.69	5.82	15.09	11.24	3.56	0.99	0.00	4.75	5.69	1.08	3.60	0.46	3.38	0.51	2.41	0.15	4.32	0.89	0.20
30.2	2.35	0.56	103.44	6.15	15.81	11.64	3.66	0.99	0.00	4.87	5.82	1.10	3.69	0.47	3.45	0.52	2.48	0.16	4.54	0.96	0.21
32.2	2.46	0.60	111.53	6.49	16.54	12.04	3.76	1.00	0.00	4.98	5.93	1.11	3.75	0.47	3.52	0.53	2.55	0.17	4.77	1.04	0.23
34.2	2.59	0.64	119.88	6.84	17.30	12.45	3.87	1.00	0.00	5.08	6.02	1.12	3.81	0.48	3.57	0.53	2.62	0.17	5.01	1.11	0.25
36.2	2.71	0.68	128.56	7.21	18.08	12.86	3.97	1.01	0.00	5.19	6.12	1.13	3.86	0.48	3.62	0.54	2.69	0.18	5.26	1.20	0.27
38.2	2.84	0.73	137.46	7.58	18.89	13.30	4.08	1.02	0.00	5.30	6.22	1.14	3.92	0.48	3.67	0.55	2.76	0.19	5.52	1.28	0.29
40.2	2.98	0.77	146.64	7.97	19.72	13.74	4.19	1.02	0.00	5.41	6.31	1.15	3.98	0.49	3.72	0.56	2.83	0.20	5.79	1.37	0.31
42.2	3.12	0.82	156.11	8.37	20.59	14.21	4.31	1.03	0.00	5.53	6.42	1.16	4.04	0.49	3.79	0.57	2.91	0.21	6.06	1.46	0.33
44.2	3.26	0.87	165.91	8.78	21.48	14.68	4.43	1.03	0.00	5.64	6.53	1.17	4.10	0.50	3.84	0.58	2.99	0.22	6.34	1.55	0.36
46.2	3.42	0.92	176.04	9.21	22.40	15.17	4.55	1.03	0.00	5.76	6.63	1.17	4.16	0.50	3.89	0.58	3.07	0.23	6.63	1.65	0.38
48.2	3.57	0.98	186.51	9.65	23.37	15.68	4.68	1.04	0.00	5.89	6.74	1.19	4.22	0.50	3.96	0.59	3.16	0.24	6.94	1.76	0.40
50.2	3.74	1.03	197.35	10.11	24.36	16.20	4.80	1.04	0.00	6.02	6.85	1.19	4.28	0.51	4.01	0.60	3.25	0.25	7.25	1.86	0.43

TAB. G.18: Modélisation ACF - facteur d'assimilation de 0.3

%ACF	Nb	Cs	Ba	La	Ce	Nd	Sm	Eu^{2+}	Eu^{3+}	Gd	Dy	Ho	Er	Tm	Yb	Lu	Hf	Ta	Pb	Th	U
52.2	3.91	1.09	208.57	10.59	25.40	16.75	4.94	1.04	0.00	6.15	6.97	1.20	4.35	0.51	4.07	0.61	3.34	0.26	7.57	1.97	0.45
54.2	4.09	1.15	220.39	11.09	26.46	17.30	5.07	1.05	0.00	6.27	7.05	1.21	4.39	0.51	4.11	0.62	3.43	0.28	7.92	2.09	0.48
56.2	4.27	1.21	232.47	11.61	27.57	17.88	5.22	1.04	0.00	6.41	7.15	1.21	4.45	0.52	4.16	0.62	3.53	0.29	8.27	2.21	0.51
58.2	4.47	1.28	245.02	12.14	28.74	18.49	5.37	1.04	0.00	6.55	7.27	1.22	4.51	0.52	4.23	0.63	3.64	0.30	8.63	2.34	0.54
60.2	4.67	1.35	258.05	12.70	29.94	19.11	5.52	1.04	0.00	6.69	7.37	1.23	4.56	0.52	4.27	0.64	3.75	0.32	9.00	2.47	0.57
62.2	4.88	1.42	271.59	13.28	31.19	19.75	5.67	1.04	0.00	6.83	7.47	1.23	4.61	0.52	4.32	0.65	3.86	0.33	9.40	2.61	0.60
64.2	5.11	1.50	285.41	13.89	32.52	20.44	5.85	1.03	0.00	7.01	7.62	1.25	4.70	0.53	4.39	0.66	3.99	0.35	9.79	2.75	0.64
66.2	5.34	1.58	300.05	14.52	33.88	21.13	6.01	1.02	0.00	7.15	7.71	1.25	4.74	0.53	4.44	0.66	4.11	0.36	10.21	2.90	0.67
68.2	5.59	1.66	315.32	15.18	35.30	21.85	6.18	1.01	0.00	7.30	7.80	1.25	4.78	0.53	4.47	0.67	4.24	0.38	10.65	3.06	0.71
70.2	5.84	1.75	330.90	15.87	36.81	22.63	6.38	1.00	0.00	7.49	7.95	1.26	4.86	0.53	4.55	0.68	4.38	0.40	11.10	3.23	0.75
72.2	6.12	1.84	347.52	16.59	38.37	23.40	6.56	0.99	0.00	7.65	8.04	1.26	4.89	0.53	4.58	0.68	4.52	0.42	11.58	3.41	0.79
74.2	6.40	1.94	364.94	17.35	40.02	24.24	6.76	0.98	0.00	7.83	8.15	1.26	4.95	0.54	4.62	0.69	4.67	0.44	12.08	3.59	0.83
76.2	6.71	2.05	383.25	18.17	41.80	25.13	6.98	0.96	0.00	8.02	8.27	1.27	5.00	0.54	4.67	0.70	4.83	0.46	12.60	3.80	0.88
78.4	7.03	2.17	405.11	19.12	43.88	26.17	7.23	0.95	0.00	8.24	8.40	1.27	5.06	0.54	4.72	0.70	4.98	0.48	13.23	4.03	0.94
80.4	7.33	2.30	427.69	20.09	45.96	27.19	7.46	0.94	0.00	8.44	8.50	1.27	5.09	0.53	4.74	0.71	5.12	0.50	13.89	4.27	0.99
82.5	7.66	2.43	450.21	21.12	48.22	28.34	7.74	0.92	0.00	8.69	8.66	1.28	5.16	0.54	4.80	0.72	5.28	0.52	14.53	4.52	1.05
84.7	8.02	2.58	475.76	22.24	50.65	29.51	8.01	0.90	0.00	8.91	8.73	1.27	5.17	0.53	4.81	0.71	5.45	0.54	15.27	4.80	1.11
86.9	8.40	2.75	503.44	23.46	53.28	30.75	8.29	0.88	0.00	9.11	8.78	1.25	5.15	0.52	4.78	0.71	5.61	0.56	16.07	5.11	1.19
89.0	8.79	2.92	529.98	24.67	55.94	32.01	8.59	0.84	0.00	9.35	8.86	1.24	5.17	0.52	4.79	0.71	5.79	0.59	16.82	5.43	1.26
91.1	9.20	3.11	559.84	25.99	58.76	33.26	8.85	0.81	0.00	9.50	8.78	1.21	5.07	0.50	4.68	0.69	5.97	0.61	17.68	5.78	1.34
93.2	9.63	3.30	588.49	27.31	61.66	34.55	9.13	0.76	0.00	9.69	8.76	1.18	5.01	0.49	4.62	0.68	6.16	0.64	18.49	6.15	1.42
95.4	10.08	3.53	620.87	28.06	62.47	33.86	8.67	0.68	0.00	9.11	8.16	1.09	4.71	0.46	4.40	0.65	6.35	0.66	19.40	6.57	1.52
97.5	10.55	3.77	653.01	28.97	63.80	33.59	8.37	0.60	0.00	8.68	7.64	1.00	4.42	0.43	4.15	0.62	6.54	0.69	20.29	7.01	1.62
99.6	11.02	4.04	687.12	29.51	63.86	32.20	7.70	0.51	0.00	7.87	6.81	0.88	3.98	0.38	3.79	0.56	6.72	0.71	21.24	7.51	1.73
101.7	11.48	4.32	720.57	30.62	65.76	32.24	7.53	0.44	0.00	7.52	6.23	0.78	3.59	0.34	3.42	0.51	6.88	0.74	22.15	8.03	1.85
103.9	11.90	4.64	754.98	31.20	65.93	30.82	6.89	0.36	0.00	6.70	5.26	0.64	3.00	0.28	2.88	0.43	7.00	0.76	23.08	8.62	1.97
105.9	12.29	4.99	782.18	31.49	65.45	29.07	6.20	0.27	0.00	5.89	4.44	0.52	2.53	0.23	2.45	0.36	7.10	0.77	23.73	9.25	2.11
108.0	12.56	5.37	809.42	31.85	65.16	27.21	5.50	0.20	0.00	4.94	3.23	0.34	1.73	0.15	1.66	0.24	7.09	0.78	24.42	9.94	2.26

TAB. G.19: Résultats de la modélisation de la fusion partielle des roches ultramafiques du mélange ophiolitique.

	C. modal frac. Jonhson et al., 1990	C. n-modal frac. Jonhson et al., 1990	Inc. modal frac. Niu, 1997	Inc. n-modal frac. Niu, 1997
La				
DM	3.34E-01	3.34E-01	3.34E-01	3.34E-01
5%	5.74E-03	4.45E-03	7.19E-03	5.98E-03
10%	7.91E-05	2.36E-05	1.26E-04	5.38E-05
15%	8.53E-07	3.06E-08	1.74E-06	1.83E-07
20%	6.99E-09	3.40E-12	1.86E-08	1.43E-10
25%	4.20E-11	1.72E-18	1.49E-10	9.00E-15
30%	1.78E-13	3.77E-35	8.51E-13	2.91E-21
35%	5.00E-16		3.32E-15	3.77E-36
Ce				
DM	9.30E-01	9.30E-01	9.30E-01	9.30E-01
5%	1.10E-01	9.83E-02	1.34E-01	1.23E-01
10%	1.16E-02	6.88E-03	1.74E-02	1.17E-02
15%	1.07E-03	2.65E-04	2.00E-03	7.02E-04
20%	8.58E-05	4.01E-06	2.02E-04	2.16E-05
25%	5.84E-06	1.12E-08	1.77E-05	2.22E-07
30%	3.30E-07	5.60E-13	1.30E-06	2.83E-10
35%	1.51E-08	3.53E-31	7.92E-08	1.15E-15
Nd				
DM	9.92E-01	9.92E-01	9.92E-01	9.92E-01
5%	2.69E-01	2.44E-01	2.80E-01	2.61E-01
10%	6.81E-02	4.20E-02	7.35E-02	5.32E-02
15%	1.59E-02	4.02E-03	1.79E-02	7.51E-03
20%	3.41E-03	1.20E-04	4.01E-03	5.87E-04
25%	6.60E-04	9.86E-08	8.15E-04	1.55E-05
30%	1.14E-04		1.48E-04	2.64E-08
35%	1.74E-05		2.38E-05	
Sm				
DM	3.78E-01	3.78E-01	3.78E-01	3.78E-01
5%	1.64E-01	1.53E-01	1.67E-01	1.60E-01
10%	6.79E-02	4.91E-02	7.09E-02	5.71E-02
15%	2.67E-02	1.06E-02	2.86E-02	1.60E-02
20%	9.95E-03	1.02E-03	1.09E-02	3.01E-03
25%	3.48E-03	7.16E-06	3.91E-03	2.71E-04
30%	1.13E-03		1.31E-03	3.63E-06
35%	3.37E-04		4.02E-04	

TAB. G.19: Modélisation de fusion partielle

	C. modal frac. Jonhson et al., 1990	C. n-modal frac. Jonhson et al., 1990	Inc. modal frac. Niu, 1997	Inc. n-modal frac. Niu, 1997
Eu				
DM	1.56E-01	1.56E-01	1.56E-01	1.56E-01
5%	7.53E-02	7.11E-02	7.69E-02	7.38E-02
10%	3.50E-02	2.64E-02	3.64E-02	3.02E-02
15%	1.55E-02	6.96E-03	1.66E-02	9.99E-03
20%	6.57E-03	9.22E-04	7.17E-03	2.34E-03
25%	2.63E-03	1.37E-05	2.94E-03	2.91E-04
30%	9.88E-04		1.14E-03	7.09E-06
35%	3.45E-04		4.09E-04	
Gd				
DM	5.50E-01	5.50E-01	5.50E-01	5.50E-01
5%	3.06E-01	2.93E-01	3.16E-01	3.06E-01
10%	1.65E-01	1.35E-01	1.76E-01	1.53E-01
15%	8.58E-02	4.86E-02	9.46E-02	6.50E-02
20%	4.29E-02	1.13E-02	4.90E-02	2.16E-02
25%	2.05E-02	8.80E-04	2.44E-02	4.62E-03
30%	9.32E-03		1.15E-02	3.63E-04
35%	3.99E-03		5.17E-03	1.22E-07
Dy				
DM	7.00E-01	7.00E-01	7.00E-01	7.00E-01
5%	4.60E-01	4.48E-01	4.76E-01	4.66E-01
10%	2.96E-01	2.60E-01	3.17E-01	2.89E-01
15%	1.85E-01	1.30E-01	2.06E-01	1.61E-01
20%	1.13E-01	5.11E-02	1.31E-01	7.67E-02
25%	6.64E-02	1.21E-02	8.05E-02	2.79E-02
30%	3.78E-02	5.53E-04	4.79E-02	5.85E-03
35%	2.06E-02		2.74E-02	1.88E-04
Er				
DM	4.58E-01	4.58E-01	4.58E-01	4.58E-01
5%	2.98E-01	2.90E-01	3.11E-01	3.05E-01
10%	1.89E-01	1.69E-01	2.07E-01	1.89E-01
15%	1.17E-01	8.61E-02	1.34E-01	1.07E-01
20%	7.02E-02	3.59E-02	8.49E-02	5.20E-02
25%	4.08E-02	1.04E-02	5.21E-02	2.00E-02
30%	2.28E-02	1.28E-03	3.09E-02	4.90E-03
35%	1.23E-02	3.91E-07	1.77E-02	3.52E-04

Tab. G.19: Modélisation de fusion partielle

	C. modal frac. Jonhson et al., 1990	C. n-modal frac. Jonhson et al., 1990	Inc. modal frac. Niu, 1997	Inc. n-modal frac. Niu, 1997
Yb				
DM	4.75E-01	4.75E-01	4.75E-01	4.75E-01
5%	3.42E-01	3.37E-01	3.56E-01	3.52E-01
10%	2.42E-01	2.25E-01	2.63E-01	2.48E-01
15%	1.68E-01	1.38E-01	1.91E-01	1.63E-01
20%	1.14E-01	7.51E-02	1.36E-01	9.70E-02
25%	7.55E-02	3.34E-02	9.49E-02	4.94E-02
30%	4.86E-02	1.02E-02	6.45E-02	1.91E-02
35%	3.03E-02	1.13E-03	4.26E-02	3.91E-03
Lu				
DM	7.20E-02	7.20E-02	7.20E-02	7.20E-02
5%	5.42E-02	5.35E-02	5.64E-02	5.57E-02
10%	4.01E-02	3.79E-02	4.36E-02	4.14E-02
15%	2.92E-02	2.52E-02	3.32E-02	2.91E-02
20%	2.08E-02	1.53E-02	2.48E-02	1.89E-02
25%	1.46E-02	8.11E-03	1.82E-02	1.08E-02
30%	9.93E-03	3.40E-03	1.31E-02	5.06E-03
35%	6.58E-03	8.84E-04	9.22E-03	1.54E-03

C. = congruent, Inc. = incongruent ; DM = manteau appauvri de McCulloch et Bennett, 1994 (source lherzolitique asthénosphérique).